# SEISMOTECTONIC EVALUATION

## PHASE II FAULT AND SEISMIC HAZARDS INVESTIGATIONS

## NORTH OF DELTA OFFSTREAM STORAGE
## DWR - INTEGRATED STORAGE INVESTIGATIONS

Prepared for
State of California
The Resources Agency
DEPARTMENT OF WATER RESOURCES

by

William Lettis & Associates, Inc.
1777 Botelho Drive, Suite 262
Walnut Creek, CA 94596

in association with

Lahontan Geosciences
Reno, Nevada
and
URS Corp.
Seattle, Washington

October, 2002

# TABLE OF CONTENTS


Page

EXECUTIVE SUMMARY ..... xiv

Introduction ..... xiv

Structural Geologic Setting of the Sites and Golden Gate Dam Sites ..... xiv

Neotectonic Setting ..... xx

Controlling Seismic Source and Maximum Earthquake Magnitudes ..... xxii

Seismic Ground Motions ..... xxvi

Surface Rupture Hazards ..... xxvii

1.0 INTRODUCTION ..... 1-1

1.1 Purpose ..... 1-1

1.2 Location and Extent of the Study Region ..... 1-1

1.3 Scope of Work ..... 1-1

1.3.1 Literature Review ..... 1-5

1.3.2 Photogeologic Interpretation and Mapping ..... 1-6

1.3.3 Aerial Reconnaissance ..... 1-7

1.3.4 Detailed Field Mapping ..... 1-7

1.3.5 Paleoseismic Trenching ..... 1-8

1.3.6 Dating and Soils Analysis ..... 1-8

1.3.7 Drilling ..... 1-9

1.3.8 Detailed Surveying ..... 1-9

1.3.9 Quantitative Geomorphic Analyses ..... 1-10

1.3.10 Analysis of Seismic Reflection Data ..... 1-10

1.3.11 Structural Geologic Analysis and Construction of Cross Sections ..... 1-11

1.3.12 Numerical Modeling ..... 1-11

1.3.13 Seismicity Analysis ..... 1-12

1.3.14 Analysis of Ground Motions ..... 1-12

1.4 Review of DSOD Criteria ..... 1-13

2.0 GEOLOGIC SETTING ..... 2-1

2.1 Plate Tectonic Evolution of the Northern Coast Ranges and Western Sacramento Valley ..... 2-1

2.2 Modern Plate Tectonic Setting ..... 2-2

**TABLE OF CONTENTS (cont'd)**


2.3 Basement and Crustal Structure ..... 2-5

2.4 Jurassic and Cretaceous Stratigraphy in the Study Region ..... 2-16

2.5 Regional Geomorphic Setting and Late Cenozoic Stratigraphy of the Study Region ..... 2-18

2.6 Quaternary Stratigraphy at the Sites and Golden Gate Dam Sites ..... 2-21

2.6.1 Quaternary Stratigraphy at Golden Gate Dam Site ..... 2-21

2.6.2 Quaternary Stratigraphy at Sites Dam Site ..... 2-25

2.6.3 Trench Stratigraphy ..... 2-27

3.0 NEOTECTONIC CHARACTERIZATION OF GEOLOGIC STRUCTURE ..... 3-1

3.1 Introduction ..... 3-1

3.2 Structural Geologic Setting of the Dam Sites ..... 3-1

3.3 Kinematic Model For Development of Folds and Faults ..... 3-8

3.4 Characterization of Proximal Geologic Structures ..... 3-15

3.4.1 Northeast-Striking Faults In The Vicinity Of The Sites And Golden Gate Dam sites ..... 3-17

3.4.1.1 Fault GG-1 ..... 3-17

3.4.1.2 Fault GG-2 ..... 3-27

3.4.1.3 Fault GG-3 ..... 3-36

3.4.1.4 Fault S-2 ..... 3-52

3.4.2 Salt Lake Fault ..... 3-62

3.4.2.1 Characterization of the Salt Lake Fault ..... 3-62

3.4.2.2 Earthquake History of the Salt Lake Fault ..... 3-83

3.4.2.3 Activity Assessment, Salt Lake Fault ..... 3-86

3.4.3 Fault S-3 ..... 3-88

3.4.4 Great Valley Fault ..... 3-103

3.4.4.1 Funks Segment, Great Valley Thrust Fault ..... 3-106

3.4.4.1.1 Length of the Funks Segment ..... 3-106

3.4.4.1.2 Activity of the Funks Segment ..... 3-106

3.4.4.1.3 Summary and Conclusions ..... 3-116

3.4.4.2 Bear Valley Segment, Great Valley Fault ..... 3-117

3.4.4.2.1 Length of the Bear Valley Segment ..... 3-117

3.4.4.2.2 Activity of the Bear Valley Segment ..... 3-118

**TABLE OF CONTENTS (cont'd)**


3.5 Regional Faults ..... 3-119
3.5.1 San Andreas Fault ..... 3-119
3.5.2 Maacama Fault ..... 3-120
3.5.3 Bartlett Springs Fault ..... 3-121
3.5.4 Stony Creek Fault ..... 3-122
3.5.5 Coast Range Fault ..... 3-124
3.5.6 Green Valley Thrust Fault ..... 3-125
3.5.7 Paskenta Fault ..... 3-126
3.5.8 Rumsey Hills Thrust Fault ..... 3-127
3.5.9 Sweitzer Fault ..... 3-129
3.5.10 Valley Side Fault ..... 3-131
3.5.11 Black Butte Fault ..... 3-132
3.5.12 Corning Fault ..... 3-136
3.6 Cascadia Subduction Zone ..... 3-138
3.6.1 Interplate Sources ..... 3-138
3.6.2 Intraplate Sources ..... 3-145
4.0 SEISMICITY ..... 4-1
4.1 Introduction ..... 4-1
4.2 Historical Seismicity ..... 4-3
4.2.1 Compilation of the Historical Catalog ..... 4-3
4.2.2 Completeness of the Historical Record ..... 4-4
4.2.3 Significant Regional Historical Earthquakes ..... 4-5
4.2.3.1 North Coast Ranges Province ..... 4-7
4.2.3.1.1 March 31, 1898, Sonoma County, $M_L$ 6.2 ..... 4-8
4.2.3.1.2 April 15, 1898, Mendocino County, M 6.5 ..... 4-8
4.2.3.1.3 December 21, 1954, Arcata, M 6.6 ..... 4-8
4.2.3.2 Western Sierra Nevada ..... 4-9
4.2.3.2.1 January 7, 1881, M 5.0 ..... 4-9
4.2.3.2.2 June 6, 1884, M 4.2 ..... 4-9
4.2.3.2.3 February 8, 1940, Chico, $M_L$ 5.7 ..... 4-9
4.2.3.2.4 November 18, 1942, Sterling City, M 4.8 ..... 4-10
4.2.3.3 Coast Ranges – Sierran Block Boundary Zone ..... 4-10
4.2.3.3.1 May 19, 1889, Antioch, M 6 ..... 4-10

## TABLE OF CONTENTS (cont'd)


4.2.3.3.2 April 19 – 30, 1892, Winters-Vacaville, $M_L$ 5.5 – 6.4 ..... 4-11

4.2.3.3.3 October – December, 1943, Maxwell Swarm.... 4-12

4.3 Instrumental Seismicity ..... 4-13

4.3.1 Compilation of the Instrumental Catalog ..... 4-13

4.3.2 Completeness of the Instrumental Catalog..... 4-16

4.3.3 Regional Seismicity, 1970 – 2000..... 4-16

4.3.3.1 Northern Coast Ranges ..... 4-17

4.3.3.1.1 Maacama Fault..... 4-17

4.3.3.1.2 Bartlett Springs Fault Zone..... 4-17

4.3.3.1.3 Green Valley Fault System ..... 4-18

4.3.3.1.4 Gorda Plate..... 4-18

4.3.3.2 Western Sierran MIcroplate..... 4-19

4.3.3.2.1 August 1, 1975, Oroville, $M_L$ 5.7 ..... 4-20

4.3.3.2.2 Red Bluff Region ..... 4-20

4.3.3.2.3 Willows Region ..... 4-22

4.3.4 Seismicity in the Northern Coast Ranges – Sierran Block Boundary Zone, 1970 – 2000 ..... 4-22

4.4 Focal Depths in the Study Region ..... 4-24

4.4.1 Northern Coast Ranges..... 4-24

4.4.1.1 Focal Depths in the High Coast Ranges ..... 4-29

4.4.2 Sierran Microplate..... 4-31

4.4.3 Coast Ranges-Sierran Block Boundary Zone..... 4-33

4.5 Regional Stress Patterns..... 4-33

4.5.1 Characterization of Tectonic Stresses From Focal Mechanisms..... 4-33

4.5.2 Stress Patterns in Northern California..... 4-36

4.5.2.1 Northern Coast Ranges ..... 4-36

4.5.2.2 Gorda Plate..... 4-40

4.5.2.3 Western Sierran Microplate ..... 4-44

4.5.2.4 High Coast Ranges..... 4-50

4.5.2.5 Maxwell ..... 4-50

4.5.2.6 Colusa Region..... 4-50

## TABLE OF CONTENTS (cont'd)


4.6 Relocation of Earthquakes in the Central Sacramento Valley ..... 4-57
4.6.1 Reservoir-Induced Seismicity ..... 4-62
4.6.2 Lake Oroville, Butte County ..... 4-64
4.6.3 Lake Berryessa ..... 4-65
4.6.4 San Luis Reservoir ..... 4-66
4.6.5 Lake Shasta ..... 4-66
4.6.6 Potential for Induced Seismicity in the Vicinity of the Dam Sites ..... 4-67
5.0 SEISMOTECTONICS ..... 5-1
5.1 Introduction ..... 5-1
5.2 Description of Contemporary Seismic Source Domains ..... 5-1
5.2.1 Colusa Domain ..... 5-3
5.2.2 Maxwell Domain ..... 5-3
5.2.3 Willows Area ..... 5-3
5.2.3.1 Willows North Domain ..... 5-4
5.2.3.2 Willows South Domain ..... 5-4
5.2.4 High Coast Ranges Domain ..... 5-4
5.2.5 Bartlett Springs Fault ..... 5-5
5.3 Characterization of Seismogenic Deformation ..... 5-5
5.3.1 Analytical Approach ..... 5-5
5.3.2 Results ..... 5-8
5.3.2.1 Colusa Domain ..... 5-8
5.3.2.2 Maxwell Domain ..... 5-9
5.3.2.3. Willows North and Willows South Domains ..... 5-9
5.3.2.4 High Coast Ranges Domain ..... 5-10
5.3.2.5 Bartlett Springs Fault ..... 5-10
5.4 Discussion ..... 5-10
5.5 Summary ..... 5-14
6.0 EARTHQUAKE HAZARDS ..... 6-1
6.1. Maximum Earthquake Magnitudes ..... 6-1
6.2 Funks Segment, Great Valley Fault System ..... 6-3
6.2.1 Rupture Length ..... 6-3
6.2.2 Rupture Width ..... 6-6

6.2.3 Maximum Earthquake Magnitude, Funks Segment ..... 6-10
6.2.4 Aseismic Hanging Wall Deformation East of the Ramp-Flat Transition, Funks Segment ..... 6-10
6.2.4.1 Modeling Approach ..... 6-11
6.2.4.2 Methodology ..... 6-12
6.2.4.3 Model Results ..... 6-14
6.2.4.4 Conclusions ..... 6-17
6.3 Bear Valley Segment, Great Valley Fault ..... 6-17
6.4 Northeast-Striking Dextral Faults ..... 6-19
6.5 Bartlett Springs Fault ..... 6-19
6.6 Corning Fault ..... 6-22
6.7 The Cascadia Subduction Zone ..... 6-23
6.7.1 Rupture Length ..... 6-23
6.7.2 Rupture Width ..... 6-24
6.7.3 Maximum Earthquake ..... 6-25
6.8 Intraplate Earthquakes in the Gorda Plate ..... 6-26
6.9 Surface Rupture Hazards ..... 6-27
6.9.1 Salt Lake Fault ..... 6-27
6.9.2 Northeast-Striking Dextral Fault ..... 6-28
6.9.2.1 Surface Displacement on a Fraction of Coseisimic Slip on the Funks Segment ..... 6-29
6.9.2.2 Magnitude of Dextral Slip Necessary to Accommodate Tectonic Wedging ..... 6-31
6.9.2.3 Slip Predicted by Elastic Dislocation Models ..... 6-32
6.9.2.3.1 Funks Segment Model Results ..... 6-33
6.9.2.3.2 Bear Valley Segment Model Results ..... 6-34
6.9.2.3.3 Discussion ..... 6-34
6.9.2.4 Conclusions ..... 6-37
7.0 GROUND MOTION ANALYSIS ..... 7-1
7.1 Introduction ..... 7-1
7.2 Computational Approach ..... 7-2
7.2.1 Abrahamson and Silva (1997) ..... 7-3
7.2.2 Sadigh et al. (1997) ..... 7-4

7.3 Selection of Controlling Seismic Source ..... 7-4
7.4 Maximum Earthquake Response Spectra ..... 7-5
7.4.1 Average Response Spectra ..... 7-10
7.4.2 Directivity Connection ..... 7-11
7.5 Summary ..... 7-11
8.0 REFERENCES ..... 8-1

## List Of Appendices

A Analysis of Seismic Reflection Profiles ..... A-1
B Paleoseismic Trenches ..... B-1
C Soil Profiles ..... C-1

## List Of Tables

1 Faults and Geologic Structures Investigated in this Report ..... xv
3-1 Characteristics of Faults in the Vicinity of the Golden Gate and Sites Dam sites ..... 3-16
3-2 Geomorphic Field Descriptions for Fault GG-1 ..... 3-21
3-3 Radiocarbon Dates from Paleoseismic Trenches in the vicinity of the Sites and Golden Gate dam sites ..... 3-25
3-4 Geomorphic and Stratigraphic Field Descriptions for Fault GG-2 ..... 3-28
3-5 Geomorphic and Stratigraphic Field Descriptions for Fault GG-3 ..... 3-38
3-6 Geomorphic and Stratigraphic Field Descriptions for Fault S-2 ..... 3-54
3-7 Position of Carbonate Rinds on Pebbles ..... 3-78
3-8 Geomorphic and Stratigraphic Field Descriptions for Fault S-3 ..... 3-90

5-1 Earthquake Sources, Sites and Golden Gate Dam Sites ..... 5-8

6-1 Maximum Earthquake Parameters for Ground Motion Calculation ..... 6-2

7-1 ME Parameters for Ground-Motion Calculations ..... 7-10

## List of Plates

1 Regional Tectonic Map.....in pocket

## List of Figures

1 Shaded Relief Map Showing Faults in the Vicinity of the Dam Sites..... xvii

2 Cross Section Showing Map-Scale Structures in the Study Area..... xix

3 Site-Source Geometry, Sites Dam Site and the Bear Valley Segment of the Great Valley Fault..... xxiii

4 Neotectonic Characterization of Geologic Structures.....xxv

5 Golden Gate Dam Site—Average of 50th and 84th Percentile Deterministic Response Spectra ..... xxvii

6 Sites Dam Site— Average of 50th and 84th Percentile Deterministic Response Spectra ..... xxix

7 Golden Gate Dam Site – 84th Percentile Deterministic Response Spectra (with and without Directivity) .....xxx

8 Sites Dam Site – 84th Percentile Deterministic Response Spectra (with and without Directivity)..... xxxi

1-1 Location of the Sites and Golden Gate Dam Sites, Northwestern California..... 1-2

1-2 Location of the Sites and Golden Gate Dam Sites, Northwestern Sacramento Valley ..... 1-3

1-3 Major Faults of the San Andreas System, and Faults in the Cascadia Forearc Region..... 1-4

2-1 Oblique Mercator Projection of the Sierra Nevada Microplate ..... 2-4

2-2 Seismic Reflection Profile Showing Thrust Fault Beneath Folds ..... 2-8

2-3 Regional Cross Section (A-A') Through the Northern Coast Ranges, Sacramento Valley, and Western Sierra Nevada Foothills..... 2-10

2-4 Regional East-West Cross Section (B-B') At Latitude 39.75° ..... 2-11

2-5 Regional East-West Cross Section (C-C') At Latitude 40° ..... 2-12

2-6 Model for Evolution of Crustal Structure ..... 2-14

2-7 Stratigraphic Correlation Chart For the Study Region ..... 2-17

## TABLE OF CONTENTS (cont'd)


2-8 Map of Quaternary Deposits and Geomorphic Surfaces Along Lower Funks Creek in Vicinity of Golden Gate Dam Site (Part 1) ..... 2-22

2-9 Map of Quaternary Deposits and Geomorphic Surfaces Along Lower Funks Creek in Vicinity of Golden Gate Dam Site (Part 2) ..... 2-23

2-10 Map of Quaternary Deposits and Geomorphic Surfaces Along Stone Corral Creek in Vicinity of Sites Dam Site ..... 2-26

3-1 Bedrock Structures Near Sites and Golden Gate Dam Sites ..... 3-2

3-2 Cross Section Showing Map-Scale Structures in the Study Area, and Their Relationship To Structures Imaged By Seismic Reflection Profiles ..... 3-5

3-3 Seismic Line SV-12 Across the Boundary Between the Funks and Bear Valley Segments of the Great Valley Fault ..... 3-7

3-4 Kinematic Model For Growth of the Sites Anticline ..... 3-9

3-5 Cross Section A-A' ..... 3-11

3-6 Cross Section B-B' ..... 3-12

3-7 Cross Section C-C' ..... 3-13

3-8 Map of Potentially Significant Bedrock Structures Near the Dam Sites ..... 3-18

3-9 Map of Fault Features Along GG-1 and GG-2 Faults in Vicinity of Golden Gate Dam Site ..... 3-19

3-10 Trench Log of Trench FT-4a, GG-1 Fault ..... 3-20

3-11 Trench Log of Trench FT-4b, GG-1 Fault ..... 3-22

3-12 Trench Log of Trench FT-4c, GG-1 Fault ..... 3-24

3-13 Photograph of Trench FT-3a and FT-3b, GG-2 Fault ..... 3-30

3-14 Trench Log of Trench FT-3a, GG-2 Fault ..... 3-31

3-15 Photograph of GG-2 Fault Exposed in Trench FT-3a ..... 3-32

3-16 Trench Log of Trench FT-3b, GG-2 Fault ..... 3-34

3-17 Trench Log of Trench FT-5 ..... 3-35

3-18 Map of Fault Features Along the GG-3 Fault in Vicinity of the Golden Gate and Sites Dam Sites ..... 3-37

3-19 Cross-Section of Boreholes Across the GG-3 Fault ..... 3-40

3-20 Photograph of Trench-2a ..... 3-41

3-21 Trench Log of Trench FT-2a, GG-3 Fault ..... 3-42

3-22 Trench Log of Trench FT-2b, GG-3 Fault ..... 3-43

3-23 Trench Log of Testpit TPE-1, GG-3 Fault ..... 3-45

3-24 Photograph of GG-3 Fault Exposed in Testpit TPE-1 ..... 3-46

## TABLE OF CONTENTS (cont'd)


3-25 Trench Log of Testpit TPE-2, GG-3 Fault ..... 3-47
3-26 Trench Log of Testpit TPE-3, GG-3 Fault ..... 3-48
3-27 Trench Log of Trench FT-7, GG-3 Fault ..... 3-50
3-28 Conceptual Diagram of Origin of Soil-Filled Bedrock Cracks ..... 3-51
3-29 Map of Fault Features Along the S-2 Fault in the Vicinity of Sites Dam Sites ..... 3-53
3-30 Trench Log of Trench FT-6, S-2 Fault ..... 3-55
3-31 Trench Log of Trench FT-8, S-2 Fault ..... 3-57
3-32 Trench Log of Trench FT-9a, S-2 Fault ..... 3-59
3-33 Trench Log of Trench FT-9b, S-2 Fault ..... 3-61
3-34 Map of Southern Salt Lake Fault near Sites ..... 3-64
3-35 Location Map of Paleoseismic Trenches Across the Salt Lake Fault ..... 3-66
3-36 Photograph of Trench FT- HC-1 Location ..... 3-67
3-37 Trench Log of Trench FT- HC-1, North Wall, Salt Lake Fault ..... 3-68
3-38 Trench Log of Trench FT- HC-1, South Wall, Salt Lake Fault ..... 3-69
3-39 Trench Log of Trench SL-T1, North Wall, Southern Salt Lake fault ..... 3-71
3-40 Trench Log of Trench FT- HC-2, South Wall, Salt Lake Fault ..... 3-74
3-41 Photo of Salt Lake Fault in Trench FT- HC-2, South Wall ..... 3-75
3-42 Trench Log of Trench FT- HC-2, North Wall, Salt Lake Fault ..... 3-76
3-43 Detail of Trench Log of Trench SL-T1, North Wall, Southern Salt Lake Fault ..... 3-82
3-44 Reconstruction of Fault Displacement on Salt Lake Fault in Trench FT-HC-2 ..... 3-84
3-45 Photograph of the S-3 Fault, Sites Quarry ..... 3-89
3-46 Reconstruction of Displacement on the GG-2, GG-3, and S-2 Faults ..... 3-91
3-47 Photograph of S-3 Fault Trench Locations South of Funks Creek ..... 3-93
3-48 Photograph of Trench T1-S3 Looking North Towards Funks Creek ..... 3-94
3-49 Trench Log of Trench T1-S3, North Wall, S-3 Fault ..... 3-95
3-50 Trench Log of Trench T2-S3, North Wall, S-3 Fault ..... 3-97
3-51 Photograph Showing Trenches Across S-3 Fault and Stream Terrace Back Edge ..... 3-99
3-52 Trench Log of Trench T3-S3, North Wall, S-3 Fault ..... 3-100
3-53 Trench Log of Trench T4-S3, North Wall, S-3 Fault ..... 3-101

## TABLE OF CONTENTS (cont'd)


3-54 Structure Contour Map ..... 3-105

3-55 Regional Topographic Residual Map ..... 3-108

3-56 Topographic Map of Stream Terraces and GPS Survey Points Along Hunters Creek ..... 3-111

3-57 Stream Terrace Profile Along Hunters Creek ..... 3-113

3-58 Stream Thalweg Profile of Hunters Creek ..... 3-115

3-59 Detail of Seismic Line 805, Orland Buttes ..... 3-134

3-60 Geologic Evidence for Plate-Boundary Earthquakes on the Cascadia Subduction Zone ..... 3-139

3-61 Southern Edge of the Subducting Gorda Plate ..... 3-142

3-62 Seismicity and Geometry of the Subducted Gorda Plate ..... 3-143

3-63 Site-Source Geometry, Cascadia Subduction Zone and Gorda Plate ..... 3-144

4-1 Seismicity in the Sacramento Valley Region, 1970-2000 ..... 4-2

4-2 Historical Seismicity in the Sacramento Valley Region, 1850-1969 ..... 4-6

4-3 Northern California Seismograph Stations, 1900-1979 ..... 4-14

4-4 Northern California Seismograph Stations, 1980-2000 ..... 4-15

4-5 Seismicity in the Vicinity of the Sites Project, 1970-2000 ..... 4-21

4-6 Cross Section Index ..... 4-25

4-7 Seismicity Section Through 40° North (Section A-A′) ..... 4-26

4-8 Seismicity Section Through Proposed Newville Dam site (Section B-B′) ..... 4-27

4-9 Regional Seismicity Section Through Sites Project (Section C-C′) ..... 4-28

4-10 Distribution of Focal Depths, Northern Coast Ranges Province ..... 4-30

4-11 Distribution of Focal Depths, Western Sierran Block Province ..... 4-32

4-12 Distribution of Focal Depths, CRSB Boundary Zone ..... 4-34

4-13 Stress Orientations from Selected Earthquakes in Northern California ..... 4-37

4-14 Stress Axes from the Maacama Fault Zone, NCSN Dataset, 1970-2000 ..... 4-38

4-15 Stress Axes from the Bartlett Springs Fault Zone, NCSN Dataset, 1970-2000 ..... 4-39

4-16 Stress Axes from the Green Valley Fault System, NCSN Dataset, 1970-2000 ..... 4-41

4-17 Stress Axes from the Gorda Plate, Depth > 15 Kilometers, NCSN Dataset, 1970-2000 ..... 4-42

4-18 Stress Axes from the Red Bluff Region, NCSN Dataset, 1970-2000 ..... 4-45

4-19 Stress Axes from the Lake Oroville Region, NCSN Dataset, 1970-2000 ..... 4-46
4-20 Stress Axes from the Willows Region, NCSN Dataset, 1970-2000 ..... 4-48
4-21 Willows Region, Selected Focal Mechanisms from NCSN Locations..... 4-49
4-22 Stress Axes from the West Tehama County, NCSN Dataset, 1970-2000 ..... 4-51
4-23 West Tehama County, Selected Focal Mechanisms from NCSN Locations..... 4-52
4-24 Stress Axes from the Maxwell Region, NCSN Dataset, 1970-2000 ..... 4-53
4-25 Maxwell Region, Selected Focal Mechanisms from NCSN Locations..... 4-54
4-26 Stress Axes from the Colusa Region, NCSN Dataset, 1970-2000 ..... 4-55
4-27 Colusa Region, Selected Focal Mechanisms from NCSN Locations..... 4-56
4-28 Central Sacramento Valley Southwest-Northeast Seismicity Section..... 4-60
4-29 Central Sacramento Valley North-south Seismicity Section..... 4-61

5-1 Orientation of Principal Strains From Inversions of Earthquake Focal Mechanisms ..... 5-2

6-1 Segment Boundaries of the Great Valley Thrust Fault System ..... 6-4
6-2 Site-Source Geometry: Funks Segment and the Golden Gate Dam Site ..... 6-7
6-3 Site-Source Geometry: Funks Segment and the Sites Dam Site..... 6-8
6-4 Rupture Ratio vs. Magnitude for Thrust- and Reverse-Faulting Earthquakes..... 6-9
6-5 Schematic Diagram Showing Poly 3-D Model Configuration ..... 6-13
6-6 Plan Views of Surface Displacement From Rupture on the Ramp and 1.25 Miles (2 km) of the Flat ..... 6-15
6-7 Vertical Profiles of a Modeled Surface Displacement From Rupture on the Ramp and 1.25 Miles (2 km) of the Flat..... 6-16
6-8 Site-Source Geometry: Bear Valley Segment and the Sites Dam Site ..... 6-20
6-9 Model of Surface Displacements on the Tear Faults From Rupture of the Funks Segment..... 6-35
6-10 Model of Surface Displacements on the Tear Faults From Rupture of the Bear Valley Segment ..... 6-36

7-1 Comparison of Response Spectra for Crustal Sources, Golden Gate Dam Site ..... 7-6
7-2 Comparison of Response Spectra for Crustal Sources, Sites Dam Site..... 7-7

## TABLE OF CONTENTS (cont'd)


7-3 Comparison of Response Spectra, Great Valley Fault and Subduction Zone Sources, Golden Gate Dam Site ..... 7-8

7-4 Comparison of Response Spectra, Great Valley Fault and Subduction Zone Sources, Sites Dam Site ..... 7-9

7-5 Golden Gate Dam Site, California -- 84th-Percentile Deterministic Response Spectra (without Directivity) ..... 7-13

7-6 Sites Dam Site, California -- 84th-Percentile Deterministic Response Spectra (without Directivity) ..... 7-14

7-7 Golden Gate Dam Site, California –Average of 50th and 84th-Percentile Deterministic Response Spectra (without Directivity) ..... 7-15

7-8 Sites Dam Site, California Average of 50th and 84th-Percentile Deterministic Response Spectra (without Directivity) ..... 7-16

7-9 Golden Gate Dam Site, California -- 84th-Percentile Deterministic Response Spectra (with and without Directivity) ..... 7-17

7-10 Sites Dam Site, California -- 84th-Percentile Deterministic Response Spectra (with and without Directivity) ..... 7-18

# EXECUTIVE SUMMARY

## INTRODUCTION

This report presents the results of a seismotectonic evaluation of the northeastern California Coast Ranges and northwestern Sacramento Valley. The purpose of this investigation is to evaluate surface-faulting hazards and maximum levels of strong ground shaking at two sites that are being considered by the California Department of Water Resources (DWR) for the construction of new dams. The proposed dam sites are herein referred to as Sites and Golden Gate, and they are located on Stone Corral Creek and Funks Creek, respectively, about 8 miles (13 km) west of the town of Maxwell in the northwestern Sacramento Valley. All faults and geologic structures investigated in this report are summarized on Table 1.

## STRUCTURAL GEOLOGIC SETTING OF THE SITES AND GOLDEN GATE DAM SITES

The Sites and Golden Gate dam sites are located in stream-cut watergaps within the Venado sandstone member of the Upper Cretaceous Cortina Formation. At the dam sites, the Cortina Formation is part of a homoclinally east-dipping sequence of Mesozoic marine strata in the foothills bordering the eastern Coast Ranges (Figure 1). Directly west of the dam sites, these rocks are folded about the axes of the north-trending Sites anticline and Fruto syncline. East of the dam sites, the strata progressively flatten beneath the western Sacramento Valley margin.

In addition to the folds, numerous faults offset and deform the Mesozoic bedrock strata in the study area. Two primary sets of surface faults are mapped in the vicinity of the dam sites:

**Table E-1** Faults and Geologic Structures Investigated in this Report

| Fault Name | Fault Type | Activity | Seismic Source Characterization | | | | Closest Approach | | Comments |
|---|---|---|---|---|---|---|---|---|---|
| | | | Fault Length | Fault Width | Rupture Area | Maximum Magnitude | Sites | Golden Gate | |
| GG-1 | Right Lateral, Strike Slip | No Holocene Activity | 1.1 mi (1.8 km) | Not a seismic source | | | 3.1 mi (4.1 km) | <0.5 mi (<1 km) | GG-1, GG-2, GG-3 and S-2 are interpreted to be shallow tear faults along Funks/Bear Valley Segment boundary. Conservatively assumed to be sources of aftershocks. Possible surface-rupture hazards. |
| GG-2 | Right Lateral, Strike Slip | No Holocene Activity | 3.7 mi (5.9 km) | Faults GG-2, GG-3 are S-2 are considered potential sources of shallow aftershocks. Maximum earthquake magnitude for these structures is $M_w$ 5.4. | | | 1.7 mi (2.3 km) | <0.5 mi (<1 km) | |
| GG-3 | Right Lateral, Strike Slip | No Holocene Activity | 3.0 mi (4.8 km) | | | | 0.4 mi (0.7 km) | <0.5 mi (<1 km) | |
| S-2 | Right Lateral, Strike Slip | No Holocene Activity | 2.4 mi (3.9 km) | | | | <0.5 mi (<1 km) | 2.2 mi (3.5 km) | |
| Salt Lake Fault | Thrust | Multiple Late Quaternary Surface Ruptures | 12 mi (20 km) | Not a seismic source | | | 1.5 mi (2.4 km) | 1.7 mi (2.7 km) | Interpreted to accommodate triggered, aseismic slip |
| S-3 | Thrust | No Holocene Activity | ≥4.25 mi (6 km) | Not a seismic source | | | 0.9 mi (1.5 km) | 600 ft (200 m) | May accommodate triggered aseismic slip |
| Funks Segment, Great Valley Fault | Blind Thrust | Late Quaternary Activity | 11 mi (17 km) | 14 mi (22 km) | 146 $mi^2$ (374 $km^2$) | $M_w$ 6.6 | 4.0 mi (6.5 km) | 3.6 mi (5.8 km) | Indirect evidence of late Quaternary activity |
| Bear Valley Segment, Great Valley Fault | Blind Thrust | Assumed to be Active | 14.4 mi (23 km) | 14.4 mi (23 km) | 207 $mi^2$ (529 $km^2$) | $M_w$ 6.8 | 4.8 mi (7.7 km) | 4.4 mi (7.0 km) | Conservatively assumed to be active |
| San Andreas Fault | Strike Slip | Active | 650 mi (1,050 km) | Maximum magnitude = $M_w$ 8 (WLA, 1997) | | | 70 mi (113km) | 70 mi (113 km) | Assumes maximum earthquake will rupture 272 mi (435 km) |
| Maacama Fault | Strike Slip | Active | 84 mi (135 km) | Maximum magnitude = $M_w$ 6.5 (WLA, 1997) | | | 45 mi (72 km) | 45 mi (72 km) | Too far from sites to dominate hazard |
| Bartlett Springs Fault | Strike Slip | Active | 70 mi (113 km) | 9.4 mi (15 km) | 117 $mi^2$ (306 $km^2$) | $M_w$ 6.6 | 20 mi (32 km) | 22 mi (32 km) | Maximum rupture length of proximal Coyote Rocks Segment is 11 mi (18 km) |

**Table E-1** Faults and Geologic Structures Investigated in this Report

| Fault Name | Fault Type | Activity | Seismic Source Characterization | | | | Closest Approach | | Comments |
|---|---|---|---|---|---|---|---|---|---|
| | | | Fault Length | Fault Width | Rupture Area | Maximum Magnitude | Sites | Golden Gate | |
| Stony Creek Fault | Thrust (?) | Not Active | 63 mi (100 km) | Not characterized | | | 10 mi (16 km) | 11 mi (18 km) | Interpreted to be a deformed Mesozoic fault |
| Coast Range Fault | Normal | Not Active | Not a continuous fault trace | Not characterized | | | 12.4 mi (20 km) | 12.4 mi (20 km) | Interpreted to be a deformed Mesozoic fault |
| Paskenta Fault | Normal | Not Active | 28 mi (45 km) | Not characterized | | | 25 mi (41 km) | 23 mi (37 km) | Interpreted to be a deformed Mesozoic fault |
| Rumsey Hills Fault | Blind Thrust | Active | 16 mi (25 km) | Not characterized | | | 28 mi (45 km) | 30 mi (49 km) | Too far from dam sites to dominate hazard |
| Sweitzer Fault | Thrust | Active | 11 mi (17 km) | Not a seismic source | | | 28 mi (45 km) | 30 mi (49 km) | May accommodate triggered aseismic slip |
| Valley Side Fault | Thrust/Reverse | Active | 10.5 mi (17 km) | Not a seismic source | | | 16 mi (26 km) | 18.6 mi (30 km) | May accommodate triggered aseismic slip |
| Black Butte Fault | Bedrock Escarpment | Not a Fault | 10.5 mi (17 km) | Not characterized | | | 30 mi (48 km) | 27 mi (44 km) | |
| Southern Reach, Corning Fault | Oblique-Reverse | Active | 13 mi (21 km) | 13 mi (21 km) | 182 $mi^2$ (462 $km^2$) | $M_w$ 6.7 | 20 mi (32 km) | 18 mi (29 km) | Associated with clusters of seismicity |
| Cascadia Subduction Zone | Megathrust Fault | Active | 620mi (1,000 km) | 74.5 mi (120 km) | 46,310 $mi^2$ (120,000 $km^2$) | $M_w$ 9 | 100 mi (160 km) | 100 mi (160 km) | Geologic evidence for giant Cascadia earthquakes |
| Intraplate (Gorda slab) Faults | Probable Strike Slip | Active | Source dimensions not directly observed; maximum magnitude adopted from empirical observations | | | $M_w$ 7.5 | 53 mi (85 km) | 53 mi (85 km) | 1922 Gorda plate earthquake estimated to be $M_s$ 7.6 |

**Table 1** Faults and Geologic Structures Investigated in this Report

| Fault Name | Fault Type | Activity | Seismic Source Characterization | | | | Closest Approach | | Comments |
|---|---|---|---|---|---|---|---|---|---|
| | | | Fault Length | Fault Width | Rupture Area | Maximum Magnitude | Sites | Golden Gate | |
| GG-1 | Right Lateral, Strike Slip | No Holocene Activity | 1.1 mi (1.8 km) | Not a seismic source | | | 3.1 mi (4.1 km) | <0.5 mi (<1 km) | GG-1, GG-2, GG-3 and S-2 are interpreted to be shallow tear faults along Funks/Bear Valley Segment boundary. Conservatively assumed to be sources of aftershocks. Possible surface-rupture hazards. |
| GG-2 | Right Lateral, Strike Slip | No Holocene Activity | 3.7 mi (5.9 km) | Faults GG-2, GG-3 are S-2 are considered potential sources of shallow aftershocks. Maximum earthquake magnitude for these structures is $M_w$ 5.4. | | | 1.7 mi (2.3 km) | <0.5 mi (<1 km) | |
| GG-3 | Right Lateral, Strike Slip | No Holocene Activity | 3.0 mi (4.8 km) | | | | 0.4 mi (0.7 km) | <0.5 mi (<1 km) | |
| S-2 | Right Lateral, Strike Slip | No Holocene Activity | 2.4 mi (3.9 km) | | | | <0.5 mi (<1 km) | 2.2 mi (3.5 km) | |
| Salt Lake Fault | Thrust | Multiple Late Quaternary Surface Ruptures | 12 mi (20 km) | Not a seismic source | | | 1.5 mi (2.4 km) | 1.7 mi (2.7 km) | Interpreted to accommodate triggered, aseismic slip |
| S-3 | Thrust | No Holocene Activity | ≥4.25 mi (6 km) | Not a seismic source | | | 0.9 mi (1.5 km) | 600 ft (200 m) | May accommodate triggered aseismic slip |
| Funks Segment, Great Valley Fault | Blind Thrust | Late Quaternary Activity | 11 mi (17 km) | 14 mi (22 km) | 146 $mi^2$ (374 $km^2$) | $M_w$ 6.6 | 4.0 mi (6.5 km) | 3.6 mi (5.8 km) | Indirect evidence of late Quaternary activity |
| Bear Valley Segment, Great Valley Fault | Blind Thrust | Assumed to be Active | 14.4 mi (23 km) | 14.4 mi (23 km) | 207 $mi^2$ (529 $km^2$) | $M_w$ 6.8 | 4.8 mi (7.7 km) | 4.4 mi (7.0 km) | Conservatively assumed to be active |
| San Andreas Fault | Strike Slip | Active | 650 mi (1,050 km) | Maximum magnitude = $M_w$ 8 (WLA, 1997) | | | 70 mi (113km) | 70 mi (113 km) | Assumes maximum earthquake will rupture 272 mi (435 km) |
| Maacama Fault | Strike Slip | Active | 84 mi (135 km) | Maximum magnitude = $M_w$ 6.5 (WLA, 1997) | | | 45 mi (72 km) | 45 mi (72 km) | Too far from sites to dominate hazard |
| Bartlett Springs Fault | Strike Slip | Active | 70 mi (113 km) | 9.4 mi (15 km) | 117 $mi^2$ (306 $km^2$) | $M_w$ 6.6 | 20 mi (32 km) | 22 mi (32 km) | Maximum rupture length of proximal Coyote Rocks Segment is 11 mi (18 km) |
| Stony Creek Fault | Thrust (?) | Not Active | 63 mi (100 km) | Not characterized | | | 10 mi (16 km) | 11 mi (18 km) | Interpreted to be a deformed Mesozoic fault |

**Table 1** Faults and Geologic Structures Investigated in this Report

| Fault Name | Fault Type | Activity | Seismic Source Characterization | | | | Closest Approach | | Comments |
|---|---|---|---|---|---|---|---|---|---|
| | | | Fault Length | Fault Width | Rupture Area | Maximum Magnitude | Sites | Golden Gate | |
| Coast Range Fault | Normal | Not Active | Not a continuous fault trace | Not characterized | | | 12.4 mi (20 km) | 12.4 mi (20 km) | Interpreted to be a deformed Mesozoic fault |
| Green Valley Thrust Fault and related faults | Thrust | Not Active | 11 mi (17 km) | Not characterized | | | 8 mi (12.5 km) | 9 mi (15 km) | Bedding-parallel thrust fault confined to the upper 3 mi (5 km) of the crust |
| Paskenta Fault | Normal | Not Active | 28 mi (45 km) | Not characterized | | | 25 mi (41 km) | 23 mi (37 km) | Interpreted to be a deformed Mesozoic fault |
| Rumsey Hills Fault | Blind Thrust | Active | 16 mi (25 km) | Not characterized | | | 28 mi (45 km) | 30 mi (49 km) | Too far from dam sites to dominate hazard |
| Sweitzer Fault | Thrust | Active | 11 mi (17 km) | Not a seismic source | | | 28 mi (45 km) | 30 mi (49 km) | May accommodate triggered aseismic slip |
| Valley Side Fault | Thrust/Reverse | Active | 10.5 mi (17 km) | Not a seismic source | | | 16 mi (26 km) | 18.6 mi (30 km) | May accommodate triggered aseismic slip |
| Black Butte Fault | Bedrock Escarpment | Not a Fault | 10.5 mi (17 km) | Not characterized | | | 30 mi (48 km) | 27 mi (44 km) | |
| Southern Reach, Corning Fault | Oblique-Reverse | Active | 13 mi (21 km) | 13 mi (21 km) | 182 $mi^2$ (462 $km^2$) | $M_w$ 6.7 | 20 mi (32 km) | 18 mi (29 km) | Associated with clusters of seismicity |
| Cascadia Subduction Zone | Megathrust Fault | Active | 620mi (1,000 km) | 74.5 mi (120 km) | 46,310 $mi^2$ (120,000 $km^2$) | $M_w$ 9 | 100 mi (160 km) | 100 mi (160 km) | Geologic evidence for giant Cascadia earthquakes |
| Intraplate (Gorda slab) Faults | Probable Strike Slip | Active | Source dimensions not directly observed; maximum magnitude adopted from empirical observations | | | $M_w$ 7.5 | 53 mi (85 km) | 53 mi (85 km) | 1922 Gorda plate earthquake estimated to be $M_s$ 7.6 |

Figure 1

1) Northeast-striking, high-angle faults that obliquely cut the north-striking bedrock units, and consistently displace stratigraphic contacts in a right-lateral strike-slip sense. Specific examples of these structures include the informally named GG-1, GG-2, GG-3 and S-2 faults, all of which pass directly through or near the proposed Sites and Golden Gate dam sites (Figure 1); and

2) North-striking faults that are generally parallel to bedding. The most laterally continuous example of these structures is the east-dipping Salt Lake thrust fault (Figure E-1), which is parallel to, and directly east of, the axis of the Sites anticline. The Salt Lake fault is approximately 0.9 miles (1.4 km) west of the Golden Gate dam site and the southern end of the fault is approximately 0.7 miles (1.15 km) west of the Sites dam site (Figure 1). The fault trace is mapped through a proposed saddle dam site. Another example of a bedding-parallel fault is the informally named east-dipping S-3 fault, which is exposed in the Sites rock quarry just north of Sites road approximately 2000 feet (600 m) east of the Sites dam site (Figure 1).

Based on analysis of seismic reflection data and surface geologic relationships, we interpret that the Fruto syncline, Sites anticline, and surface faults described above are underlain by a blind, west-dipping thrust fault (Figure 2). This structure is informally named the Funks segment of the Great Valley fault (the Great Valley fault is described in the following section). The Funks segment is about 10.6 miles (17 km) long, dips about 27° toward the west beneath the Fruto syncline, and flattens eastward beneath the Sites anticline on seismic reflection profiles. At the latitude of the Sites and Golden Gate dam sites, the Sites anticline is interpreted to be a fault-propagation fold developed above a blind, east-dipping thrust fault that splays upward from the low-angle Funks segment. This east-dipping blind thrust fault and the overlying Sites anticline accommodate shortening of the crustal block above the west-dipping Funks segment (Figure 2). The Salt Lake fault also splays upward from the gently west-dipping part of the Funks segment. The intersection of the Salt Lake fault with the blind Funks segment forms an

Figure 2

east-tapering underthrust tectonic wedge beneath the western valley margin. The S-3 fault is interpreted to be a bedding-parallel thrust fault that has accommodated shearing of the sedimentary rocks during uplift and eastward tilting along the valley margin (Figure 2).

The northeast-striking GG-1, GG-2, GG-3 and S-2 faults are interpreted to be tear faults in the upper crust associated with the southern structural boundary of the Funks segment. Based on analysis of seismic reflection data, we interpret that another distinct segment of the Great Valley fault, here referred to as the Bear Valley segment, is present south of the Funks segment. The Bear Valley segment is about 14 miles (23 km) long and strikes almost due north-south. Based on available reflection seismic data, we interpret that the Bear Valley segment has a constant west dip, in contrast to the ramp-flat geometry of the Funks segment. The hanging wall of the Bear Valley segment appears to be deformed by simple fault-propagation folding rather than tectonic wedging because an east-dipping backthrust similar to the Salt Lake fault has not been recognized or mapped along the entire length of the segment (Brown and Rich, 1961; Rich, 1971).

## NEOTECTONIC SETTING

The Sites-Golden Gate study area is part of a tectonically active boundary between the Pacific plate to the west and the Sierra Nevada-Great Valley ("Sierran") microplate to the east. Geodetic data show that the Pacific plate moves approximately 39 mm/yr toward N30°W, relative to the Sierran microplate (Argus and Gordon, 2001). Because major strike-slip faults of the San Andreas system strike more westerly than average Pacific-Sierran motion north of the San Francisco Bay, there is a small component of convergence resolved across the plate boundary in the northern Coast Ranges. This overall "transpressional" plate motion is accommodated by a combination of active strike-slip and thrust faulting, and over the past several million years has produced uplift of the Coast Ranges.

Ongoing research suggests that transpressional plate motion is accommodated in part by movement on the "Great Valley fault", which is a segmented system of hidden or "blind"

thrust faults beneath the western margin of the Central Valley. The western valley margin has been referred to by previous workers as the "Coast Ranges – Sierran Block Boundary Zone" (CRSBZ), and described as a belt of active crustal shortening driven by impingement of the Sierra Nevada block against the Coast Ranges (Wong and Ely, 1983). The "Great Valley fault", as discussed in this report, is the potentially seismogenic fault that accommodates most of the shortening within the CRSBZ. The Funks and Bear Valley segments, described in the previous section, are the structural segments of the Great Valley fault closest to the Sites and Golden Gate dam sites. Other segments of the Great Valley fault are known or inferred to have generated the 1983 Coalinga and 1892 Winters-Vacaville earthquakes (e.g., O'Connell et al., 2001). Neotectonic investigations have documented evidence for Quaternary growth of folds overlying segments of the Great Valley fault beneath the Rumsey Hills and Dunnigan Hills 27 miles (44 km) south of the Sites and Golden Gate dam sites. Thus, there is a general consensus among the seismotectonic community that the Great Valley fault is an active or potentially active seismic source in the modern transpressional tectonic setting.

Data acquired and analyzed for this study provide indirect evidence for late Quaternary activity of the Funks segment of the Great Valley thrust fault system. These data include:

1) Evidence for late Quaternary surface rupture on the Salt Lake fault from paleoseismic trenching investigations. Specifically, we interpret data from trenches excavated across the fault to indicate that at least one and probably three or more surface ruptures have occurred on the Salt Lake fault in the past 30,000 to 70,000 years. If it is assumed that surface-rupturing events associated with earthquakes on the Funks segment have a regular recurrence, then this evidence strongly suggests that at least one surface-rupturing event probably has occurred in the past 35,000 years. As discussed previously, we interpret that the Salt Lake fault terminates downdip against the Funks segment of the Great Valley fault (Figure 2). If this interpretation is correct, then surface displacement on the Salt Lake fault is derived from slip at depth on the Funks segment. We thus conclude that stratigraphic and structural relations exposed in trenches across the Salt Lake

fault provide indirect evidence of at least one earthquake on the blind Funks segment of the Great Valley fault during the past 35,000 years.

2) Morphometric analysis of regional topography, incorporating GIS analysis of available digital elevation models, shows patterns of topographic residuals coincident with the Sites anticline and Salt Lake thrust fault, and which are consistent with localized late Quaternary uplift above the Funks segment.

3) Morphometric analyses of streams draining eastward across the Coast Ranges foothills, in general, and the Sites anticline, in particular, reveal patterns of localized fluvial incision and channel morphology consistent with active surface uplift above the Funks segment of the Great Valley fault.

We therefore conclude that the Funks segment of the Great Valley thrust system is an active seismic source, according to criteria for fault activity adopted by the Division of Safety of Dams (DSOD, 1995; Fraser, 1997).

Although we did not perform similar investigations of the Bear Valley segment south of the dam sites, we conservatively conclude that this segment also is an active fault because it lies within a recognized zone of late Cenozoic tectonic activity (i.e., the "Coast Ranges-Sierra Block Boundary Zone"), and it lies between the active Funks segment to the north, and the tectonically active Rumsey Hills-Dunnigan Hills region to the south (Unruh and Moores, 1992; Unruh et al., 1995).

## CONTROLLING SEISMIC SOURCE AND MAXIMUM EARTHQUAKE MAGNITUDES

The controlling seismic source for both dam sites is the Bear Valley segment of the Great Valley fault system (Figure 3). The selection of the Bear Valley segment as the controlling seismic source is based on comparison of the response spectrum for a

Figure 3

maximum earthquake on this fault with response spectra for earthquakes on other active seismic sources within a 31-mile (50-km) radius of the dam sites (Chapter 6). The Bear Valley segment of the Great Valley fault is imaged by seismic reflection data as a west-dipping feature in the 3 to 6 mile (5 to 9 km) depth range that juxtaposes east and west-dipping strata against a package of underlying bright, high amplitude, subhorizontal to west-dipping reflectors (Appendix A). Based on analysis of map-scale geologic structures and reflection seismic data, we interpret that the Bear Valley segment is about 14 miles (23 km) long, strikes north-south, and dips about 21° to the west. If the Bear Valley segment maintains a constant dip to the brittle-ductile transition depth at a depth of about 9 miles (15 km), then the total potential rupture width is about 14 miles (23 km). Given a 14 mile (23 km) rupture length and 14 mile (23 km) rupture width, we calculate a rupture area of 207 square miles (529 $km^2$) for the Bear Valley segment of the Great Valley fault. Empirical regression relations in Wells and Coppersmith (1994) give an associated maximum earthquake magnitude of $M_w$ 6.8.

The structural model adopted for this study relates slip on northeast-striking faults (GG-1, GG-2, GG-3 and S-2) that pass through or near the dam sites to differential shortening in the upper crust above the structural boundary between the Funks and Bear Valley segments of the Great Valley fault. We interpret that the northeast-striking faults terminate downward against the Funks segment of the Great Valley fault, and act as tear faults to accommodate greater northeast translation and shortening of the hanging wall block of the Funks segment relative to the Bear Valley segment (Figure 4). Our preferred interpretation is that the GG-1, GG-2, GG-3 and S-2 faults move sympathetically during moderate to large magnitude earthquakes on the Funks thrust ramp, and probably do not behave as independent seismic sources. Elastic dislocation models support this interpretation, and suggest that minor triggered movement also may occur on these faults during earthquakes on the Bear Valley segment.

Although we conclude that the northeast-striking faults are not independent seismic sources, they may be a source of aftershocks following an earthquake on the Funks or Bear Valley segments. We calculate a response spectrum for the largest potential

Figure 4

aftershock at zero distance for comparison with the response spectrum for the controlling event on the Bear Valley segment. Based on our analysis of seismic reflection data, we interpret that the northeast-striking faults are confined to the hanging wall block of the Funks segment and that their maximum rupture depth is about 5 km (Figure 4). The exception is fault GG-1, which has such a short surface trace that we interpret it to have a maximum depth of 2-3 km. From regression relations in Wells and Coppersmith (1994), we calculate an associated range of aftershock magnitudes from $M_w$ 5.3 to $M_w$ 5.4. We conservatively adopt $M_w$ 5.4 as the maximum magnitude for aftershocks on faults GG-2, GG-3, and S-2.

Comparison of response spectra indicates that the zero period ordinate (i.e., peak ground acceleration – PGA) for the maximum aftershock is greater than the PGA for the controlling event on the Bear Valley segment by about 20%. At periods greater that 0.1 second, which is the band of interest for large engineered structures, damped spectral acceleration is significantly higher for the controlling event. The difference in PGA between the two events is not important; dams designed to a maximum earthquake (and higher ground motions at periods greater than 0.1 second) on the Bear Valley segment should not be adversely affected by an aftershock at zero distance (Chapter 6).

**SEISMIC GROUND MOTIONS**

We adopted the following two-step approach for computing response spectra for earthquakes on the Bear Valley segment of the Great Valley fault:

1) Calculate the 84th-percentile, 5%-damped response spectra from the Abrahamson and Silva (1997) and Sadigh et al. (1997) attenuation equations, and average the results: and

2) Modify the resulting response spectrum for fault-rupture directivity effects using the procedure in Somerville et al. (1997), as appropriate.

These spectra are to be used in the design of major dams. The directivity effect evaluated in step 2 of the ground motion analysis impacts the duration of shaking and the amplitude of long period motion. For rupture that is directed toward the site, the ground motion is compressed in time (shorter duration) with larger long period amplitudes. An additional effect of the directivity is that there is a systematic difference in the long period ground motion on the two horizontal components when they are oriented normal and parallel to the fault strike (Somerville et al., 1997). The directivity effect produces an increase in the long period motion on the component that is orthogonal to the fault strike. There also is a corresponding decrease in the component parallel to the fault strike. This increase in the long-period motion on the fault-normal component leads to large long-period pulses in the ground motion in the forward rupture direction.

Average response spectra for the maximum earthquake on the Bear Valley segment were prepared by computing the 50th and 84th percentile level of 5% damped spectral acceleration from the Abrahamson and Silva (1997) and Sadigh et al. (1997) attenuation equations, as described in step 1 above. The pairs of spectra from the Abrahamson and Silva and the Sadigh et al. equations were averaged to produce the $50^{th}$ and $84^{th}$ percentile spectra in Figure 5 (Golden Gate) and Figure 6 (Sites). Modified $84^{th}$ percentile spectra showing directivity effects also are prepared (Figures 7 and 8); these figures also show unmodified $84^{th}$ percentile spectra for comparison.

## SURFACE RUPTURE HAZARDS

### Salt Lake Fault

The Salt Lake fault is mapped by Brown and Rich (1961) as passing through at least one potential saddle dam site. Based on evidence for late Quaternary surface-rupturing events from paleoseismic trenching studies, we conclude that surface rupture may occur on the Salt Lake fault during earthquakes on the Funks segment of the Great Valley thrust fault system. Restoration of faulted contacts in late Quaternary deposits overlying the bedrock surface indicates that about 16 inches (40 cm) of reverse displacement may

Figure 5

Figure 6

Figure 7

Figure 8

occur during a single surface rupturing event on the Salt Lake fault. The subsurface relationships conservatively can be interpreted as evidence that up to 43 inches (110 cm) displacement has occurred during a single event, but we do not favor this interpretation because palinspastic restoration of stratigraphic and structural relations is more reasonably accomplished through a series of smaller displacements. Results from elastic dislocation modeling of triggered, aseismic slip on the Salt Lake fault associated with the maximum earthquake on the Funks segment suggest discrete displacements of about 4.5 inches (11 cm). We conclude that surface displacements on the Salt Lake fault during a moderate to large earthquake on the Funks segment of the Great Valley fault are likely to range from 4.5 inches to 16 inches (11 cm to 40 cm).

**Northeast-Striking Dextral Faults**

Paleoseismic trench investigations for this study document no Holocene surface displacement on the GG-1, GG-2, GG-3 and S-2 faults. Our preferred kinematic model for the structural evolution of the area directly around the dam sites, however, posits that movement on these faults may be related to movement at depth on the blind Funks segment of the Great Valley fault. Given this structural model, our conclusion that the Funks segment is an active seismic source is in apparent contradiction with evidence for no activity of the northeast-striking dextral faults. This apparent contradiction arises in part from poor age constraints on the timing of late Quaternary events on the Funks segment and the northeast-striking faults. Paleoseismic data provide indirect evidence for a minimum of three earthquakes on the Funks segment during the past 30,000 to 70,000 years. It is possible that the last Funks segment earthquake occurred in latest Pleistocene time (i.e., about 10,000 years ago), just prior to deposition of undeformed early Holocene sediments overlying the GG-1, GG-2, GG-3 and S-2 faults, which were exposed in trenches and documented during this investigation. Thus, the oldest deposits available for evaluating activity of the GG-1, GG-2, GG-3 and S-2 faults may post-date the last surface-faulting event on these structures. Alternatively, it is possible that the GG-1, GG-2, GG-3 and S-2 faults are not kinematically related to the Great Valley fault or, if they are that they are not reactivated during every earthquake on the Funks segment.

Given these uncertainties, we conservatively assume that the GG-1, GG-2, GG-3 and S-2 faults may accommodate minor displacement during a moderate to large earthquake on a proximal segment of the Great Valley fault (i.e., the Funks and Bear Valley segments). To assess the potential magnitude of triggered surface displacement, we used three different approaches, which are described as follows:

a. Surface Displacement as a Fraction of Coseismic Slip on the Funks Segment

For this approach, we assume that the ratio of incremental slip on the dextral faults to slip on the Funks segment of the Great Valley thrust system during an earthquake is the same as the ratio of total, cumulative slip on these structures. We estimated cumulative slip through analysis of seismic reflection data and map-scale geologic structure. We assume that 3.3 feet (1 m) of slip may occur on the Funks segment during the maximum earthquake ($M_w$ 6.6). This assumption is consistent with estimates of about 4 feet (1.3 m) for the average coseismic slip during the M 6.7 1994 Northridge earthquake (Wald et al., 1996), which occurred on a blind thrust fault in southern California. With these assumptions, the predicted surface displacements on the northeast-striking faults associated with 3.3 feet (1 m) of slip on the Funks segment are:

Fault GG-1: 0.4 inches ± 0.12 inches (1 cm ± 3 mm)
Fault GG-2: 2 inches ± 0.2 inches (5 cm ± 5 mm)
Fault GG-3: 2.4 inches ± 0.12 inches (6 cm ± 3 mm)
Fault S-2: 0.8 inches ± 0.24 inches (2 cm ± 6 mm)

A more conservative assumption is that the total dextral slip distributed over all of the faults in the previous example instead may be concentrated on a single northeast-striking fault during a given earthquake. The summed dextral displacement on the GG and S faults for 3.3 feet (1.0 m) of coseismic slip on the Funks segment in the previous example is 5.5 inches (14 cm), with a combined uncertainty of about 1 inch (± 2 cm). We attach a low likelihood to this scenario.

b. Magnitude Of Dextral Slip As A Function Of Tectonic Wedging

In this approach, we consider the possibility that dextral slip on the northeast-striking faults accommodates northeast propagation of the tectonic wedge structure created by the intersection of the Salt Lake fault with the blind Funks segment of the Great Valley fault (Figure 2). We assume that the component of coseismic slip on the east-dipping Salt Lake fault resolved in the horizontal plane represents incremental propagation of the tectonic wedge during an earthquake. Dextral slip on the northeast-striking faults accommodates differential propagation of the wedge above the Funks and Bear Valley segments. Based on the analysis and discussion in the previous sections, we assume that the range of likely displacement on the Salt Lake fault is about 4 to 16 inches (11 to 40 cm). We also assume that the fault dips parallel to bedding; mapping by Brown and Rich (1961) indicates that Upper Cretaceous strata adjacent to the Salt Lake fault dip about 60° to 80° in the vicinity of Hunters Creek. The horizontal component of motion accommodated by 4 to 16 inches (11 to 40 cm) of slip on a fault dipping 60° to 80° ranges from about 1 to 8 inches (2 to 20 cm).

This inferred horizontal displacement could be fully accommodated by dextral slip on a single fault, or it could be distributed across faults GG-1, GG-2, GG-3 and S-2. In the former scenario, the maximum displacement is 8 inches (20 cm). For the latter scenario, the simplest model is to assume that slip is distributed equally across the four dextral faults. With this assumption, coseismic slip on each of the four faults could range from about 0.25 inches to 2 inches (0.5 to 5 cm). Alternatively, the slip could be distributed among the four faults in the same proportions as the total dextral slip is distributed, similar to the model discussed in the previous section. For this model, 1 to 8 inches (2 to 20 cm) of total dextral shear is distributed among the faults as follows:

Fault GG-1: about 0.1 inches to 0.6 inches (0.2 to 1.4 cm)
Fault GG-2: about 0.7 inch to 3 inches (0.7 cm to 7 cm)
Fault GG-3: about 0.4 inches to 3.4 inches (0.9 cm to 8.6 cm)
Fault S-2: about 0.2 inches to 1.2 inches (0.3 cm to 3 cm)

The extreme range of surface displacement on the northeast-striking dextral faults thus predicted by this model is about 0.1 inches to 8 inches (0.2 to 20 cm). The high end of this range is based on the assumption that all of the differential east-directed displacement of the tectonic wedge is accommodated by dextral slip on a single northeast-striking fault. We favor distribution of the total wedge displacement across the GG-1, GG-2, GG-3 and S-2 faults, and thus our preferred range of coseismic displacement on an individual fault for this model is about 0.25 inches to 3.4 inches (0.5 to 9 cm).

c. Elastic Dislocation Modeling

In this approach, we use numerical modeling to evaluate potential coseismic slip on the northeast-striking dextral faults. The model assumes that dextral slip on the faults releases elastic strain of the hanging wall block produced by coseismic slip on the blind Funks and Bear Valley segments of the Great Valley thrust fault. All numerical models were scaled to duplicate the geometry and depth of faults and their relative distances as inferred from analysis of geologic maps (Brown and Rich, 1961) and seismic reflection data (Appendix A). We tested a variety of models to assess a range of potential surface displacements on the northeast-striking GG and S faults. The model results consistently indicate that, for a variety of rupture scenarios on the Funks and Bear Valley segments, maximum triggered or sympathetic surface displacement on the GG and S faults is about 2.5 inches (6 cm).

d. Discussion and Conclusions

The two kinematic models that explicitly relate the magnitude of slip on the blind thrust fault to slip on the northeast-striking faults in the hanging wall block both predict up to about 3 inches (about 8 cm) of surface displacement on the GG and S faults. The tectonic wedge model predicts maximum displacements up to about 8 inches (20 cm) if all of the deformation is accommodated by slip on a single fault rather than distributed across several faults. Alternatively, the numerical models based on elastic dislocation theory

predict about 2.5 inches (6 cm) of displacement. Based on these models, therefore, we conclude that maximum surface displacements on the GG and S faults probably will not exceed about 8 inches (20 cm), and are likely to be lower (on the order of about 2.4 to 4 inches (i.e., 6 to 10 cm).

We emphasize that our assumption that the northeast-striking dextral faults may accommodate triggered slip during large earthquakes on proximal segments of the Great Valley fault is conservative, because paleoseismic studies provide positive evidence for no surface-faulting activity on these structures during the Holocene.

# 1.0 INTRODUCTION

## 1.1 PURPOSE

This report presents the results of a seismotectonic evaluation of the northeastern California Coast Ranges and northwestern Sacramento Valley, northern California (Figure 1-1). The purpose of this investigation is to evaluate surface-faulting hazards and maximum levels of earthquake strong ground shaking at two sites that are being considered by the California Department of Water Resources (DWR) for the construction of new dams. The investigation also gathered and evaluated data for assessment of whether or not surface faulting is a "fatal flaw" for these projects. The proposed dam sites are located in water gaps along Stone Corral Creek and Funks Creek west of the town of Maxwell in the northwestern Sacramento Valley (Figure 1-2; Plate 1). The Sites dam site is located on Stone Corral Creek, and the Golden Gate dam site is located on Funks Creek.

## 1.2 LOCATION AND EXTENT OF THE STUDY REGION

The study region straddles the boundary between the northern Coast Ranges and Sacramento Valley (Figure 1-1). This region is part of a broad zone of active deformation comprising the transpressional boundary between the Pacific plate and Sierra Nevada microplate (Figure 1-3) (see Chapter 2). North of the Mendocino fracture zone in northwestern California, plate boundary deformation is characterized by convergence between the Gorda plate and the Sierra Nevada microplate across the Cascadia subduction zone. Major faults and geologic structures in the study region are shown in Plate 1.

## 1.3 SCOPE OF WORK

The seismotectonic evaluation presented in this report is based on analysis of available geologic and seismologic data, supplemented by reconnaissance and detailed

Figure 1-1

Figure 1-2

Figure 1-3

investigations to obtain site-specific data in selected areas of potential fault activity. These investigations included photogeologic interpretation, aerial reconnaissance, quantitative geomorphic analysis, field mapping, drilling, and detailed topographic surveys of selected sites, and analysis of historical and instrumental seismicity. Paleoseismic trenching investigations were conducted to assess late Quaternary activity of several faults that pass through and near the proposed dam sites (Plate 1). In addition, we acquired and reprocessed petroleum industry seismic reflection profiles to assess whether "hidden" or "blind" thrust faults are present beneath the boundary between the eastern Coast Ranges and western Sacramento Valley (Appendix A). Maximum earthquake magnitudes were calculated for active faults in the direct vicinity of the dam sites. Maximum earthquakes also were evaluated for major active faults within about 31 miles (50 km) of the dam sites, and for distant, large-magnitude sources like the Cascadia subduction zone that may generate significant long-period motions at the dam sites. Earthquake magnitudes and proximity to the dam sites were used to determine seismic sources for calculating maximum levels of vibratory ground motion.

Specific analytical approaches incorporated in this study are described in detail in the following sections:

### 1.3.1 Literature Review

We reviewed existing geologic mapping, peer-reviewed literature and unpublished technical reports that characterize the geologic and geotechnical setting of the study area. Of particular importance to this study is the mapping of bedrock stratigraphy and structure by Brown and Rich (1961), which documented several unnamed northeast-striking faults that pass near or through the Sites and Golden Gate dam sites. For this study, we refer to these structures as the GG-1, GG-2, GG-3 and S-2 faults (Plate 1; see Chapter 3). In addition, Brown and Rich (1961) identified and mapped the Sites anticline and Salt Lake fault in Antelope Valley west of the Golden Gate dam site (Plate 1). Subsequent mapping, drilling and trench investigations by the U.S. Bureau of Reclamation and the DWR have provided additional documentation of these structures.

Reports with limited distribution that summarize these investigations were provided to us by DWR for review.

We also reviewed 1:24,000 scale Quaternary geologic mapping of the Sacramento Valley by Helley and Harwood (1985). This mapping identified Quaternary deposits along Stone Corral Creek and Funks Creek in the vicinity of the Sites and Golden Gate dam sites. In addition, Steele (1980) identified, mapped and characterized terraces formed along major streams in the northern part of the study area at a scale of 1:62,500. Although this mapping does not cover the Sites and Golden Gate dam sites, terraces identified by Steele (1980) provide regionally correlative late Quaternary markers for assessing recent fault activity and deformation in the northwestern Sacramento Valley.

We incorporated results from our recent seismic hazard assessment for East Park and Stony Gorge dams (William Lettis & Associates, 1997), which are located west and northwest, respectively, of the present study area. This previous work, performed for the U.S. Bureau of Reclamation, included a thorough review of the existing literature on the stratigraphy, structure and seismotectonics of the northern Coast Ranges and western Sacramento Valley and reconnaissance and detailed mapping of geomorphic surfaces in the project site region (see references cited in WLA, 1997).

### 1.3.2 Photogeologic Interpretation and Mapping

We analyzed and interpreted stereo pairs of aerial photographs to map the location, continuity and length of potentially significant faults in the study area that have surface traces, and to map Quaternary terraces and geomorphic surfaces in the project site area. The aerial photography consisted of 1:7,200-scale color photographs acquired in November, 1998 by DWR, and 1:22,000-scale black-and-white photographs taken by the U.S. Department of Agriculture in 1937. The older photos predate construction of Funks Reservoir (located downstream of the proposed Golden Gate dam site), as well as other post-1937 cultural features that locally obscure geologic and geomorphic field relations.

The aerial photographs were analyzed to assess geomorphic expression of mapped fault traces, cultural modification of potential trench sites, and changes in the location of modern streams and their flood plains. Geomorphic features observed on the photos and used to identify faults included truncated bedding contacts, ponded alluvial basins, deflected drainages, topographic saddles, sidehill benches, vegetation lineaments, scarps, spring lines, closed depressions, and linear drainages. Faults and other geologic features obscured by shadows on the aerial photographs were carefully checked and mapped in the field.

### 1.3.3 Aerial Reconnaissance

We flew fixed-wing aerial reconnaissance to examine mapped faults and lineaments, and to identify potential sites for detailed field study. Our reconnaissance consisted of one low altitude flight over the region during the mid-morning to take advantage of low sun-angle conditions. The reconnaissance focused primarily on the Salt Lake fault and Sites anticline in the vicinity of the Golden Gate and Sites dam sites. We noted geomorphic and geologic features suggestive of potential faulting, including tonal lineaments, scarps, and drainage anomalies for subsequent field investigations. We also noted potential evidence for the absence of late Quaternary activity (e.g., apparently unfaulted fluvial terraces) for further field investigation.

### 1.3.4 Detailed Field Mapping

We performed detailed geologic and geomorphic mapping to locate and characterize faults in the vicinity of the Sites and Golden Gate dam sites, and to identify and map Quaternary deposits and surfaces that overlie the faults. Field mapping was performed using aerial photographs (1:7,200 to 1:22,000 scale) as base maps, typically enlarged to 1:2,400 scale. Detailed site geologic maps also were prepared from DWR topographic base maps with 5-foot contours. Each fault trace was walked out in the field, and all possible sites where faults may be exposed such as stream cuts, landslide scarps, and road cuts were examined. Possible fault-related lineaments and features identified on the aerial photographs were examined in the field and, where confirmed as tectonic features, mapped as such.

Geologic mapping of fluvial terraces and stream deposits along Funks Creek, Stone Corral Creek, and Hunters Creek was conducted to establish and document local late Cenozoic stratigraphy. In addition, we identified and examined field sites with geologic deposits extending across mapped faults to document the presence or absence of late Quaternary deformation. We incorporated field mapping of stream terrace deposits along Hunters Creek in our detailed topographic survey of geomorphic surfaces across the Fruto syncline, Sites anticline, and Salt Lake fault.

### 1.3.5 Paleoseismic Trenching

To assess the activity of faults in the vicinity of the Golden Gate and Sites dam sites (Brown and Rich, 1962; see Plate 1), we excavated thirty-one paleoseismic trenches and test pits at fourteen locations. These locations were selected from areas where DWR previously had secured permission from landowners to conduct geologic investigations. In conjunction with the trench investigations, we conducted additional detailed field mapping of these sites to precisely determine the locations of surface fault traces.

After excavating each trench, we cleaned and examined one or both walls of the exposure. Geologic structure, stratigraphic contacts and lithologic boundaries were flagged, surveyed electronically and logged at scales of approximately 1:20 to 1:40. Selected logs are discussed in detail in the main body of this report. All other paleoseismic trench logs prepared for this study are presented in Appendix B.

### 1.3.6 Dating and Soils Analysis

We used a variety of dating methods and soil analyses to assess the age and stratigraphic correlation of Quaternary units in the region. Samples of detrital and in situ (e.g., burn horizons) charcoal were analyzed by direct radiocarbon analysis. Radiocarbon dates were dendrochronologically corrected to calibrated years according to the procedure of Stuiver and Reimer (1993). The degree of soil development at each site was evaluated via detailed soil profile descriptions to reconstruct the depositional history at each site, provide additional age constraints on deposits, and correlate stratigraphic units among trench sites. These dating methods also were used to estimate timing of most recent

movement on individual faults. Soil profile descriptions from paleoseismic trenches are presented in Appendix C.

### 1.3.7 Drilling

We conducted limited drilling in cooperation with DWR to evaluate depth to bedrock and document alluvial stratigraphy across the GG-1 and GG-3 faults at four locations. The DWR drilled three linear transects, consisting of four borings per transect, across the GG-3 fault in two locations southwest of Funks Creek (in the vicinity of the proposed outlet works for the Golden Gate dam site), and across the GG-1 fault south of Funks Creek see Figure B-1 in Appendix B. We subsequently drilled a series of 12 continuously cored vertical borings across the projected trace of the GG-3 fault 0.2 miles (0.3 km) north of the town of Sites (Figure 1-2).

### 1.3.8 Detailed Surveying

We conducted a detailed topographic survey of geomorphic surfaces along Hunters Creek using radio-beacon corrected Global Positioning Satellite (GPS) survey techniques. The survey included observation points on the unmodified surfaces of fluvial terraces along Hunters Creek, and approximately every 100 feet (30 m) along the stream channel thalweg. Two site control points (CP-1 and CP-2) were established using Rapid Static GPS Observations from National Geodetic Survey (NGS) control stations. The control points are located along Hunters Creek approximately 2.35 miles (3.8 km) apart, and were occupied by a base station with a continuously broadcasting radio beacon. All survey points were recorded within a 1.5 mile (2.4 km) radius from the occupied control points. A total of 5490 survey points were collected in NAD83 primary horizontal coordinates (California Coordinate system, Zone 2) along 7.7 miles (12.4 km) of the stream channel, including all stream bends, and of approximately 5 miles (8 km) of stream terraces parallel to the stream. The survey was used to perform a quantitative geomorphic analysis of the terrace sequence as described below.

### 1.3.9 Quantitative Geomorphic Analyses

We used quantitative geomorphic techniques as part of our assessment of the location, style, rate, and overall pattern of late Quaternary deformation. Late Quaternary fluvial terraces and terrace remnants along major creeks in the study area were mapped via air photo analysis and checked in the field. We surveyed and profiled the stream thalweg and stream terrace remnants along Hunters Creek that extend across the Salt Lake fault, Sites anticline, and Fruto syncline. Changes in terrace surface gradients and stream channel gradients provide a direct means of assessing the presence or absence of Quaternary deformation associated with these structures and, if present, documenting the location, amount and pattern of deformation.

Regional envelope and sub-envelope maps of the northwestern Sacramento Valley (using second-order drainages) were constructed using digital elevation model (DEM) data following methods developed by Strahler (1952) and Stearns (1967). Subtracting the sub-envelope from the envelope provides a topographic residual map that quantifies the relief due to stream incision (surface dissection), which can be interpreted as an indirect measure of tectonic uplift. An interpretive contour map was prepared to show major long-wavelength anomalies in patterns of fluvial incision.

### 1.3.10 Analysis of Seismic Reflection Data

We analyzed and interpreted seismic reflection profiles to infer the location, depth and geometry of blind thrust faults beneath the eastern Coast Ranges piedmont and western Sacramento Valley. The analysis of the reflection data was performed in collaboration with the U.S. Bureau of Reclamation. The data consist of eight east-west-trending lines at a high angle to structural strike, and two regional north-south-trending lines that tie the northern six of the east-west lines together. The data were jointly licensed to DWR and Reclamation for use in evaluating seismic hazards in the study area. The raw seismic reflection data were reprocessed by Dr. Dan O'Connell of the U.S. Bureau of Reclamation to produce a series of depth-migrated sections. These sections were analyzed by WLA to interpret the subsurface structure in the vicinity of the Sites and Golden Gate dam sites. All seismic reflection profiles used in this study are presented

and discussed in detail in Appendix A.

### 1.3.11 Structural Geologic Analysis and Construction of Cross-Sections

Structural geologic analyses were performed to evaluate the presence, geometry and dimensions of blind thrust or reverse faults in the study region. The results of the analysis are synthesized in numerous cross-sections throughout this report. The cross-sections were constructed to develop models for the location, geometry, and dimensions of thrust faults at depth, and to assess interactions between surface faults and blind structures at depth.

The locations of the cross sections were chosen to illustrate the structures in the vicinity of the dam sites. Published geologic maps (e.g., Brown and Rich, 1961; Chuber, 1961) showing the orientation of bedding (strike and dip data) were used to evaluate the location and geometry of map-scale folds. Cross section lines were oriented perpendicular to the strike of bedding to illustrate the geometry of faults and folds with a minimum of geometric distortion. Surface data were compiled on 1:24,000-scale cross sections. Folds larger than several hundred meters in amplitude were identified and projected to about 2 miles (3-4 km) depth using the kink-fold method of Suppe (1983). The cross sections then were reduced to 1:48,000 scale and various models for the deep structure were tested for compatibility with the shallow fold geometry. Final cross sections were prepared at smaller scales for inclusion in this report.

### 1.3.12 Numerical Modeling

Numerical modeling methods were used to analyze the effects of coseismic fault rupture on surface displacements in the region surrounding the main blind thrust fault. Models for the location, geometry, and dimensions of thrust faults were derived from our structural analysis. Modeling was performed using the program Poly3D (Thomas, 1993), a three-dimensional, displacement discontinuity boundary element code that calculates stress, strain, and displacement fields in an isotropic, homogeneous, linear elastic medium. Poly3D has been used by previous workers to assess the mechanical interaction between segmented normal faults (Crider and Pollard, 1998; Maerten et al., 1999;

Willemse et al., 1996), as well as segmented strike-slip faults (Brankman and Aydin, 2000; Lettis et al., 2001).

### 1.3.13 Seismicity Analysis

Historical and instrumentally recorded seismicity in northwestern California was evaluated to identify potential seismic sources capable of generating significant ground motion at the DWR dam sites. The seismicity analysis also focused on characterizing styles of seismogenic faulting in the study region, and estimating the state of upper crustal stress. The boundaries of the seismicity study region were selected to include potential seismic sources within 62 miles (100 km) of the dam sites and to provide sufficient data to evaluate the seismic activity of potentially significant geologic structures. The study region extends from latitudes 38 to 41 degrees north and from longitudes 124 to 121 degrees west. Analyses consisted of: compilation of a catalog of earthquake locations and magnitudes; assessment of significant historical earthquakes; evaluation of focal depths; and calculation of focal mechanisms.

We also used focal mechanisms calculated for this study to evaluate patterns of seismogenic deformation in the eastern Coast Ranges and northern Sacramento Valley. This analysis consisted of inverting groups of seismic P- and T-axes from groups of focal mechanisms to obtain the orientations and relative magnitudes of the principal strains, using the method of Twiss et al. (1991, 1993) and Twiss and Unruh (1998). The inversion results were used to directly interpret whether deformation accommodated by distributed seismicity is characterized by crustal shearing, transtension, transpression, crustal thinning or crustal thickening.

### 1.3.14 Analysis of Ground Motions

For this study, analysis of ground motions was performed according to guidelines adopted by the Department of Water Resource's Division of Safety of Dams (DSOD). A deterministic analysis was performed to develop ground motion response spectra for feasibility level studies, in accordance with DSOD guidelines. The deterministic analysis uses one or more attenuation relationships to provide an estimate of ground motion at the

site based on the largest earthquake that may occur on a fault at the fault's closest approach to the site. The deterministic approach does not consider the rate or probability of earthquake occurrence.

The method to compute the response spectra consisted of the following:

1) Calculate the 84th-percentile, 5%-damped response spectra from the Abrahamson and Silva (1997) and Sadigh et al. (1997) attenuation equations, and average the results; and
2) Modify the resulting response spectrum for fault-rupture directivity effects using the procedure in Somerville et al. (1997).

## 1.4 REVIEW OF DSOD CRITERIA

For this study, assessment of fault activity was performed according to guidelines adopted by the Department of Water Resource's Division of Safety of Dams (DSOD). DSOD (1995; also, Fraser, 1997) defines three categories of seismic sources for dam design or re-evaluation:

**Active Seismic Sources,** which include Holocene-active faults and latest Pleistocene active faults;
Inactive Seismic Sources; and
Conditionally Active Seismic Sources.

**Holocene-active faults** are defined as faults on which surface or subsurface displacement has occurred within the last 11,000 years. Holocene activity is demonstrated by: displacement or deformation of Holocene stratigraphic units; geomorphic evidence of Holocene displacement; well-located zones of seismicity; or documented fault creep.

**Latest Pleistocene-active faults** are defined as faults with no Holocene displacement, but which have produced surface or subsurface displacement of units 11,000 to 35,000 years old or show geomorphic evidence of latest Pleistocene displacement.

**Inactive faults** are defined as faults which have had no surface or subsurface displacement within the last 35,000 years demonstrated by a confidently-located fault trace that is overlain by unbroken geologic materials 35,000 years or older.

**Conditionally active faults** are defined as faults with a displacement history during the last 35,000 years that is not known with sufficient certainty to consider the fault an active or inactive seismic source.

# 2.0 GEOLOGIC SETTING

The study region described in this report straddles the boundary between the Coast Ranges and Sacramento Valley physiographic provinces (Figure 1-1; Plate 1). The Coast Ranges are a mountainous region characterized by north- to northwest-trending ranges and valleys that generally parallel the trend of major tectonic features. The Sacramento Valley is a north-south-trending intermontane basin of very low relief that lies between the Coast Ranges to the west and the Sierra Nevada mountain range to the east. The Klamath Mountains and Cascade Range physiographic provinces bound the study region on the north (Figure 1-1; Plate 1).

## 2.1 PLATE TECTONIC EVOLUTION OF THE NORTHERN COAST RANGES AND WESTERN SACRAMENTO VALLEY

Northwestern California has been part of a tectonically-active plate boundary since Mesozoic time. The oldest rocks exposed in the study area are Upper Jurassic ultramafic rocks consisting of fragments of the Coast Range ophiolite, and Upper Jurassic marine sediments of the Great Valley Group. These rocks have been interpreted, respectively, as the oceanic basement and basin-fill strata of a forearc basin that developed on the North American lithospheric plate above an east-dipping subduction zone (Dickinson and Seely, 1979). The Coast Range ophiolite structurally overlies the Franciscan complex, which is interpreted to be the remnants of an accretionary complex that accumulated and was deformed in a trench above a subducting slab. Collectively, the Great Valley Group, Coast Range ophiolite and Franciscan complex comprise the basement rocks of the northern Coast Ranges.

The present structural relationships between these rocks are the result of over 140 million years of complex deformation along the western margin of the North American lithospheric plate. Moxon (1990) interpreted stratigraphic and structural relations in the northern Sacramento Valley as evidence for late Jurassic to early Cretaceous oblique extension of the ancestral forearc basin. In early to middle Cretaceous time, the Great

Valley forearc basin was shortened or "telescoped" in a roughly east-west direction (Ingersoll, 1978; Dickinson and Seely, 1979). The timing of this deformation generally coincides with an episode of shortening in the ancestral Sierra Nevada mountains to the east, and may be associated with a change in the relative motion between the North American plate and the ancestral Farallon plate to the west (Moxon, 1988). From middle to late Cretaceous time, sedimentation continued relatively uninterrupted in the forearc basin. In the latest Cretaceous to early Tertiary, the western margin of the forearc basin was uplifted and tilted eastward (Moxon and Graham, 1987), beginning a process of progressive northeast-directed contraction of the Coast Ranges and western Great Valley that has continued episodically during the Tertiary and Quaternary (Unruh et al., 1995).

Evolution of the ancestral convergent plate boundary to the modern transpressional plate boundary began with collision of the East Pacific Rise spreading center with the trench at approximately the latitude of south-central California sometime between 29-17 Ma (Atwater, 1970). The collision formed two triple junctions (the Mendocino triple junction to the north and the Rivera triple junction to the south) that migrated away from each other as the East Pacific rise was consumed along the plate boundary. The triple junctions are connected by a dextral transform fault system that increases in length as the triple junctions move in opposite directions, thus progressively changing the western margin of the North American plate from convergent plate margin to a strike-slip fault system (Atwater, 1970). The San Andreas fault and associated right-lateral strike-slip faults in western California presently comprise the transpressional plate boundary fault system in northwestern California (Figure 1-3). The trace of the San Andreas fault directly west of the study area has formed since approximately 6 Ma, during which time the Mendocino triple junction migrated from a latitude near San Francisco northward to its present location opposite Cape Mendocino in northern California (Atwater and Stock, 1998) (Figure 1-3).

## 2.2 MODERN PLATE TECTONIC SETTING

Recent geodetic studies show that relative motion between the Pacific plate and stable North America is not exclusively accommodated by dextral slip along the San Andreas

fault system, but rather is distributed across a 745-mile-wide (1200-km-wide) zone that spans much of the western United States. Major tectonic features within the broad Pacific-North American plate boundary east of the San Andreas system that accommodate this deformation include the Sierra Nevada-Central Valley (i.e., "Sierran") microplate (Argus and Gordon, 1991; Dixon et al. 2000), and the extensional Basin and Range province. The San Andreas fault system in northwestern California accommodates about 75 to 80% of the total relative motion across the entire plate boundary (Argus and Gordon, 2001). The remaining plate motion is accommodated by deformation east of the Sierra Nevada.

Space geodesy indicates that the Sierra Nevada range and most of the Central Valley of California move together as a single, rigid microplate (i.e., the "Sierra Nevada microplate"; Argus and Gordon, 1991; Dixon et al., 2000). The motion of the Sierra Nevada microplate with respect to stable North America is measurably different from the Pacific-North American motion, which indicates that the tectonics of the study area must be analyzed within the framework of the relative motion between the independent Sierran microplate and the Pacific plate.

The role of the Sierra Nevada microplate in the Pacific-North American plate boundary can be readily visualized in a map projection that specifically highlights Sierran-North American motion. Figure 2-1 is an oblique Mercator projection of the western United States about the preferred Euler pole of Dixon et al. (2000) for Sierran-North American motion. In this projection, vertical lines on the map are parallel to the instantaneous motion of the Sierra Nevada with respect to stable North America (i.e., large white arrows). The map shows that a zone of Quaternary faulting borders the eastern Sierra Nevada. This zone is part of a more extensive belt of deformation can be traced continuously from the Gulf of California on the south, to the Cascadia subduction zone on the north. The zone includes the eastern California shear zone (ECSZ) in the Mojave desert, and the Walker Lane belt bordering the eastern Sierra (Figure 2-1). Normal faults and right-lateral strike-slip faults in this zone accommodate northwest motion of the

Figure 2-1

Sierra Nevada with respect to North America. Thrust faults and folds in the northern Sacramento Valley, including the Inks Creek belt fold, Battle Creek fault and Red Bluff fault (Plate 1) may be accommodating shortening at the northern end of the Sierra Nevada microplate as it impinges on the Klamath Mountains (Figure 2-1). Significantly, the San Andreas fault system is oblique to average Sierra Nevada-North American motion, indicating relative motion between the Sierra Nevada mircoplate and the Pacific plate includes a component of convergence resolved across the plate boundary (Figure 2-1).

Analysis of space-geodetic data indicates that relative Sierra Nevada-Pacific plate motion can be described by counterclockwise rotation of 0.930 (+/- 0.227) degrees per million years about an Euler pole located at latitude 46.7°N and longitude 94.6°W (Argus and Gordon, 2001). This pole predicts that active tectonic structures in the northern Coast Ranges and western Sacramento Valley accommodate approximately 39 mm/yr of dextral motion directed toward about N30°W. In general, the strike of the on-shore reach of the San Andreas fault and the Hayward-Rodgers Creek fault both are about N35°W, which is several degrees more westerly than the azimuth trend of Pacific-Sierra Nevada motion. Argus and Gordon (2001) noted that this geometry favors transpressional deformation, which is expressed regionally by late Cenozoic uplift of the Coast Ranges and locally by activity of young folds and thrust faults. The onset of late Cenozoic transpression in western California originally was attributed to a change in the azimuth of Pacific plate motion (Page and Engebretson, 1985; Zoback et al., 1987) beginning approximately 3.9 to 3.4 Ma (Harbert and Cox, 1989). Recent studies incorporating refined global plate motion models find that the major change in Pacific-North American motion, which presumably triggered transpressional deformation in western California, probably began about 6 to 8 Ma (Argus and Gordon, 2001), somewhat earlier than previous estimates.

## 2.3 BASEMENT AND CRUSTAL STRUCTURE

Present structural relations within the basement rocks of the northern Coast Ranges reflect a long history of convergence along the ancestral western North American plate boundary, as well as tectonic processes that affected the forearc region east of the trench

during subduction (Section 2.1). The structural contact between the Franciscan complex and overlying Coast Range ophiolite is the Coast Range fault (Plate 1), the trace of which is about 12.5 miles (20 km) west of the Sites and Golden Gate dam sites. The Coast Range fault originally was interpreted by Bailey et al. (1970) to mark the former position of the Mesozoic-Tertiary subduction zone, and, consequently, the fault was referred to in the literature as the "Coast Range thrust" (Bailey et al., 1970). Subsequent workers (Platt, 1986; Jayko et al., 1987) noted that blueschist-grade Franciscan rocks in the footwall of the Coast Range fault were metamorphosed under lithostatic pressures equivalent to depths of 15.5. to 18.6 miles (25-30 km) or greater, whereas the relatively unmetamorphosed Coast Range ophiolite and Great Valley Group strata in the hanging wall were never buried deeper than their apparent stratigraphic thickness of 7.4 to 9.4 miles (12-15 km). The juxtaposition in metamorphic grade implies that approximately 6.2 to 9.4 miles (10-15 km) of crustal section is missing across the Coast Range fault. Jayko et al. (1987) proposed that the majority of slip on the fault accommodated crustal attenuation rather than crustal shortening, and thus that the term "Coast Range thrust" is a misnomer. For this study, we adopt the convention of Jayko et al. (1987) and refer to the Franciscan-ophiolite structural contact as the “Coast Range fault” (Plate 1).

In addition to crustal attenuation, the three major basement units of the northern Coast Ranges have been deformed by uplift, folding and thrust faulting. Although some of this deformation is very young and probably related to late Cenozoic transpressional plate motion (e.g., Wentworth and Zoback, 1989; Unruh and Moores, 1992), stratigraphic and structural relationships indicate that early Tertiary crustal shortening occurred along the western margin of the ancestral Great Valley forearc basin, during plate convergence and subduction beneath western California. Examples of folds that show evidence for episodic uplift and growth since early Tertiary time include the Rumsey Hills and Dunnigan Hills anticlines in the western Sacramento Valley (Plate 1) (Unruh et al., 1995), and the Coalinga anticline in the western San Joaquin Valley (Meltzer, 1988). Seismic reflection data document that these folds are underlain by blind, west-dipping thrust faults (Wentworth, et al., 1984; Wentworth and Zoback, 1989; Unruh et al., 1995).

Seismic reflection data acquired for this study support the hypothesis that crustal shortening along the northwestern margin of the Sacramento Valley is accommodated in part by movement on blind thrust faults. Figure 2-2 is an east-west reflection profile that extends from the Coast Ranges eastward to the Sacramento Valley at the latitude of the town of Willows, approximately 12.4 miles (20 km) north of the proposed dam sites (i.e., seismic line 001; see Appendix A for location and detailed interpretation). The layered reflectors in the upper 3.1 miles (5 km) of the central and eastern part of the seismic line are marine strata of the Mesozoic Great Valley Group. The layered Great Valley Group rocks are synformally and antiformally folded about the axes of the Fruto syncline and Sites anticline, respectively (Figure 2-2). The folds terminate abruptly downward against a west-dipping interface at a depth of 3.1 to 4.4 miles (5 to 7 km). Below this interface, the structure and patterns of folding expressed by the reflectors is distinctly different. For example, the antiformally folded reflectors of the Sites anticline are juxtaposed across the west-dipping interface against synformally folded reflectors at a depth of about 3.1 to 4.4 miles (5-7 km) (Figure 2-2). These relations indicate that the upper 3.1 to 4.4 miles (5 to 7 km) of the crust in the vicinity of the Sites anticline is deformed in a different manner than the crust beneath the west-dipping interface. We interpret that the interface is a blind, west-dipping thrust fault. The Fruto syncline and Sites anticline are folds that have developed as a consequence of northeast-directed displacement and shortening of the hangingwall block.

Based on analysis of an array of 2-D reflection lines, which includes the seismic profile in Figure 2-2, we interpret that a system of structurally segmented, blind, west-dipping thrust faults underlies the northwestern Sacramento Valley (Appendix A). These faults are the local segments of the Great Valley fault system, which is inferred to underlie the western boundary of the Central Valley (Working Group on California Earthquake Potential, 1996). Movement on these structures has uplifted, tilted and folded the Great Valley Group strata in the vicinity of the Sites and Golden Gate dam sites. The Great Valley fault and related structures are discussed in detail in Chapter 3 of this report. All seismic reflection profiles analyzed for this study are presented and discussed in Appendix A.

Figure 2-2

The modern crustal structure across the northern Coast Ranges and Sacramento Valley is shown by a series of regional cross sections (Figures 2-3, 2-4, and 2-5; see Figure 1-3 for locations of cross sections). The southernmost cross-section (Figure 2-3) is drawn perpendicular to the San Andreas fault system, and passes through the study area between the Sites and Golden Gate dam sites. The crustal block on the west side of the San Andreas fault is the granitic Salinian terrain, which is variously interpreted to be an allocthonous block that collided with the continental margin of North America in Eocene time (Wakabayashi and Moores, 1988), or part of the ancestral Cordilleran Cretaceous plutonic arc that originated at the latitude of Central America and was progressively translated northward to its present location (Page, 1982). Franciscan complex accretionary rocks border the Salinian block to the east and comprise the upper crust of the Coast Ranges. The Franciscan rocks are cut and displaced by strike-slip faults of the San Andreas system. From west to east, the three major strike-slip faults include the San Andreas fault, the Hayward-Rodgers Creek-Maacama fault system, and the Concord-Green Valley-Bartlett Springs fault system (Figure 2-3).

The Coast Range fault is a major structural feature exposed in the eastern Coast Ranges that juxtaposes blueschist facies rocks of the eastern belt Franciscan complex (locally, the South Fork Mountain Schist) against a thin remnant of highly deformed and serpentinized Coast Range ophiolite. Structural relations in the region provide important information on the timing and recency of activity on the Coast Range fault. For example, seismic reflection data presented and analyzed in this report (Figure 2-2; Appendix A) show that the structural contact represented by the Coast Range fault dips eastward, approximately parallel to bedding in the lower Great Valley Group section, and is truncated against a segment of the west-dipping Great Valley fault beneath the eastern Coast Ranges piedmont. The Franciscan complex, Coast Range ophiolite and Great Valley group strata exposed at the surface, as well as the structural contacts between these units, have been faulted and offset from their counterparts in the footwall by slip on the blind Great Valley thrust (Figure 2-2).

Figure 2-3

Figure 2-4

Figure 2-5

A palinspastic forward model for evolution of the structure imaged in seismic line 001 (Appendix A and Figure 2-2) is presented in Figure 2-6. An early phase of structural and stratigraphic development in late Jurassic to mid Cretaceous time was characterized by subsidence and filling of the Great Valley forearc basin above an east-dipping subduction zone. In late Cretaceous, the ophiolitic crust of the forearc region was attenuated and Franciscan blueschist rocks from deep within the subduction complex were exhumed and juxtaposed against the thinned ophiolite and Great Valley Group rocks. Beginning in early Tertiary and continuing episodically during the Cenozoic, the attenuated forearc crust was uplifted, tilted and folded by movement on the Great Valley thrust fault (Figure 2-6). If this model is correct, then crustal attenuation and movement along the Coast Range fault predates regional crustal shortening and movement on the Great Valley fault, and strongly suggests that the Coast Range fault is not a Quaternary-active structure.

The ophiolitic basement beneath the Sacramento Valley thickens eastward, and is interpreted to be an approximately 9.3-mile- (15-km-) thick section of oceanic crust and upper mantle that was obducted eastward in late Jurassic time onto an older Sierran basement terrain (Godfrey et al., 1997). The allocthonous ophiolitic basement is cut by the Corning fault, a sub-vertical to steeply east-dipping structure that underlies the Greenwood anticline and Corning domes in the central Sacramento Valley, and which shows evidence for Quaternary activity (Harwood and Helly, 1987; Section 3.5.11). Godfrey et al. (1997) also interpret an abrupt eastern boundary to the accreted ophiolitic basement terrain (Figure 2-3). Their inferred eastern boundary generally coincides with the Chico monocline on the northeastern margin of the Sacramento Valley, north of the Sutter Buttes (Plate 1). The Chico monocline is interpreted by Harwood and Helley (1987) to be underlain by a steeply east-dipping fault that separates basement rocks of Sierran affinity on the east from ophiolitic basement on the west. We correlate the Chico monocline fault with the eastern tectonic boundary of the accreted ophiolitic terrain of Godfrey et al. (1997).

The crustal structure and major tectonic features in an east-west cross-section at latitude 39.75° north (Figure 2-4; see Figure 1-3 for location) are similar to those shown in the

Figure 2-6

cross-section to the south. However, several differences between the two cross sections reflect the relatively recent passage of the Mendocino triple junction through this latitude in the past 4 Ma (Atwater and Stock, 1998). The "slab window" hypothesis (Dickinson and Snyder, 1979) holds that progressive northward migration of the southern edge of the subducting Gorda plate north of the triple junction creates a "gap" that is filled by upwelling asthenospheric mantle. Seismic tomography studies reveal that the P-wave velocity of the asthenospheric mantle beneath the eastern margin of the Coast Ranges and latitude 39.75° is anomalously low (Benz et al., 1992); this result is interpreted by Benz et al. (1992) to be the seismic expression of upwelling asthenospheric mantle in the "slab window".

West of the low velocity zone in the upper mantle, the Franciscan accretionary complex rocks that form the Coast Ranges basement are underlain by a 3.1 to 6.2-mile- (5- to 10-km-) thick layer of relatively high velocity rock that extends a minimum of 31 miles (50 km) east of the San Andreas fault, and possibly as far as 56 miles (90 km) east (Henstock and Levander, 2000; Figure 2-4). These authors interpret the top of this high velocity body to be a prominent reflector on a single-fold, depth-migrated section developed from seismic refraction shot gathers. The high velocity layer is interpreted to be fragments of the Gorda plate that were underplated to the Coast Ranges prior to or during passage of the Mendocino triple junction and subsequently intruded with small amounts of mafic melt that presumably were generated by opening of the slab window (Henstock and Levander, 2000, and references therein). The top of the high velocity layer is apparently offset down to the east across major strike-slip faults of the San Andreas system (Figure 2-4). Henstock and Levander (2000) interpret these relations as evidence that the strike-slip faults persist as discrete shear zones through the crust into the upper mantle.

At 40°N (Figure 2-5), the southeast-trending southern edge of the Gorda plate projects obliquely beneath the eastern Coast Ranges and western Sacramento Valley. Analyses of late Cenozoic plate motions suggest that the Mendocino triple junction passed through 40°N approximately 2 Ma (Atwater and Stock, 1998). The "slab window" shown to the west of the Gorda plate represents the region that previously was occupied by the

subducting slab, and since the passage of the triple junction presumably has been exposed to upwelling asthenospheric mantle. The moderate east dips of the Maacama and Bartlett Springs faults are determined from the orientations of planar alignments of hypocenters beneath the fault traces. Castillo and Ellsworth (1993) interpreted that the Maacama and Bartlett Springs faults originated as northeast-dipping reverse faults in the forearc region above the subduction zone, and gradually evolved into strike-slip faults as the triple junction migrated northward and the relative plate motion locally changed from convergence to transpression.

## 2.4 JURASSIC AND CRETACEOUS STRATIGRAPHY IN THE STUDY REGION

The foothills region in general, and the Sites and Golden Gate dam sites in particular, are underlain by north-striking marine sandstones and shales of the Jurassic-Cretaceous Great Valley Group (GVG). Outcrops of these strata in the study area originally were mapped by Brown and Rich (1961) and Chuber (1961). Both groups of workers developed different stratigraphic subdivisions of the GVG (Figure 2-7). The easiest GVG unit to identify and correlate between the two maps is the Turonian (Upper Cretaceous) Venado sandstone, which is mapped as Venado Formation by Chuber (1961), and "Unit 8" by Brown and Rich (1961). The Venado sandstone underlies a prominent strike ridge that can be traced continuously across the boundary between the two maps.

Subsequent to the work of Brown and Rich (1961) and Chuber (1961), Dickinson and Rich (1972) proposed a simplified and unified stratigraphy for the GVG based primarily on the lithology of major sandstone units (Figure 2-7). They combined the Upper Jurassic and Lower Cretaceous GVG strata into two units (i.e., the Stony Creek and Lodoga "petrofacies"). The basal (Cenomanian) Upper Cretaceous unit was named the Boxer petrofacies. The Venado sandstone directly overlies the Boxer petrofacies and represents the basal unit of the Turonian-Coniacian Cortina petrofacies. This unit can be traced continuously in the foothills outcrop belt from the Sacramento-San Joaquin Delta region northward to the study area, and it underlies a series of prominent strike ridges

Figure 2-7

including Cortina Ridge and Logan Ridge. The uppermost unit of the GVG in the Dickinson and Rich subdivision is the Campanian-Maastrichtian Rumsey petrofacies (Figure 2-7). Rich (unpublished manuscript) subsequently formalized the descriptions of the petrofacies as "Formations" (for additional discussion and overview, see Ingersoll and Dickinson, 1990). For this study, we adopt the stratigraphy of Dickinson and Rich (1972) and Rich (unpublished manuscript) (Figure 2-7).

Based on analysis of high altitude imagery and aerial photography, the contact between the Stony Creek and Lodoga formations was formally associated by Constenius et al. (2000) with a locally angular "discontinuity" between sandstone strike ridges in the lower Great Valley Group section. The "discontinuity" of Constenius et al. (2000) specifically is associated with the erosional base of a conglomeratic sandstone within the Wintun Formation mapped by Chuber (1961), and is near the base of "Unit 4" mapped by Brown and Rich (1961) (Figure 2-7). The discontinuity, which probably marks an unconformity within the lower Great Valley Group section, was used as a stratigraphic marker in this study for interpretation of seismic reflection data (Appendix A).

## 2.5 REGIONAL GEOMORPHIC SETTING AND LATE CENOZOIC STRATIGRAPHY OF THE STUDY REGION

The Sites and Golden Gate dam sites are located along the margin between the northern Coast Ranges and Central Valley geomorphic provinces (Plate 1). These provinces are separated by a steep north-south-trending range front, including a transitional 15.5-mile-(25-km-) wide zone of low foothills. Several large creeks, including Thomes Creek, Stony Creek, Willow Creek and Funks Creek, flow west to east across the province boundary. These creeks have eroded deep V-shaped canyons within the high ranges of the Coast Ranges, a series of strath terraces and pediments across the low foothills, and they open eastward onto large alluvial fans in the western Sacramento Valley. Differential erosion between less resistant mudstone and more resistant sandstone units in the foothills region, especially north of the Rumsey Hills area, also has formed several prominent broad north-south-trending valleys separated by prominent strike ridges. These valleys are connected by widely-spaced, east-west-trending narrow canyons.

Large dissected alluvial fan complexes of the Pliocene-Pleistocene Tehama Formation underlie the western Sacramento Valley piedmont, and locally bury the Mesozoic strata in the foothills region at the latitude of Orland (Plate 1). The fan deposits form distinctive landforms that radiate eastward from relict fan apices within the foothills, and are best preserved in the northwestern Sacramento Valley east of the town of Orland. Relict fans coalesce eastward, and locally cover a large area of the northwestern Sacramento Valley. These relict fans may have been deposited by the ancestral Stony and Thomes Creeks (Corps of Engineers, 1986). The Tehama Formation also thickens eastward, reaching a total thickness beneath the Sacramento Valley of approximately 2,000 ft (610 m; Earth Science Associates, 1980). The 3.3 Ma Nomlaki Tuff is near the base of the Tehama Formation and forms an important time-stratigraphic marker in the western Sacramento Valley (Helley and Harwood, 1985).

Extensive erosion has occurred in the Coast Range foothills and northwestern Sacramento Valley since deposition of the Tehama Formation ceased approximately 1.0 million years ago (Helley and Harwood, 1985). This erosion was driven by regional tectonic uplift, climatic changes, or a combination of both processes (Steele, 1980). East-west-trending interfluves between small drainages locally are capped by a relict geomorphic surface that may represent either the upper depositional surface of the Tehama Formation, or an erosional pediment surface cut on the Tehama Formation shortly after deposition ceased, or both. This laterally-extensive surface is older than the 0.45-1.0 Ma Red Bluff Formation (Helley and Harwood, 1985), which unconformably overlies the Tehama Formation along the northwestern margin of the Sacramento Valley (Helley and Jaworowski, 1985).

The middle Quaternary Red Bluff Formation is a widespread gravel deposit along the northwestern margin of the Sacramento Valley (Helley and Harwood, 1985; Helley and Jaworowski, 1985). Helley and Jaworowski (1985) interpreted the Red Bluff gravels to be deposits associated with development of a regional pediment during a change in post-Tehama regional hydraulic regimes. Stability of the regional stream base level, possibly caused by impedance of drainage in the southern Sacramento Valley, may have resulted

in widespread pediment formation (Helley and Jaworowski, 1985). Other workers have questioned the interpretation that the Red Bluff Formation represents a pediment surface (Harlan-Miller-Tait, 1983). Regardless of origin, we accept the interpretation that landforms capped by the Red Bluff Formation provide an originally subhorizontal geomorphic datum along the western margin of the Sacramento Valley that can be used to evaluate subsequent tectonic uplift and tilting (Helley and Jaworowski, 1985).

The Orland Buttes rise 295 to 394 feet (90 to 120 m) above the surrounding Tehama and Red Bluff Formations at the confluence of North Stony and Stony Creeks west of the western margin of the Sacramento Valley (Plate 1). The Orland Buttes are capped by the 16 Ma Lovejoy Basalt, which was originally deposited as a subhorizontal basalt flow (Helley and Harwood, 1985) and now is preserved atop a structural hogback ridge (Corps of Engineers, 1986). The Lovejoy Basalt presently dips 4.5° to 6.5° east beneath the western margin of the Sacramento Valley (Corps of Engineers, 1986), and thus provides an upper bound on the amount of east-directed tilting along the northwestern margin of the Sacramento Valley since the mid-Miocene.

The Tehama and Red Bluff Formations generally are absent along the northwestern margin of the Sacramento Valley in the vicinity of the Sites and Golden Gate dam sites. Cretaceous strata of the Great Valley Group exposed in this area are being actively dissected by widely-spaced eastward flowing streams (Helley and Harwood, 1985). Late Quaternary deposits in this region are sparse. Where present, they typically are preserved in north-trending valleys, such as Antelope Valley west of the town of Sites, and as discontinuous terrace and floodplain remnants along major streams.

Although stream terraces are very discontinuous or absent in the mountains west of the Coast Ranges piedmont (Steele, 1980), terraces locally are laterally extensive along creeks draining the foothills region between the Coast Ranges and the western margin of the Sacramento Valley. Terraces are formed on both bedrock surfaces (i.e., erosional "strath" terraces), and on alluvial terrace deposits (i.e., aggradational "fill" terraces). Six regionally-correlative terraces along Stony Creek that are younger than the Red Bluff

Formation provide widespread late Quaternary markers for assessing recent fault activity and deformation in the northwestern Sacramento Valley (Steele, 1980). Steele suggested that these terraces are correlative with extensive east-dipping pediment surfaces within major range-front valleys, including Stony Creek Valley). The pediments typically are gently-sloping erosion surfaces that abut the mountain front along the eastern margin of the Coast Ranges. In contrast to the Red Bluff pediment, these pediments are less extensive and are confined to the foothills area. Pediments developed atop Great Valley Group shale commonly are covered by a thin veneer of locally derived alluvium (Steele, 1980; Helley and Jaworowski, 1985). The 1° to 2° slope of the range-front pediments is greater than the regional stream gradient of ≤1°, implying post-pediment regional uplift and/or eastward tilting.

In the vicinity of the Golden Gate and Sites dam sites, east-flowing streams incised within sandstone, mudstone and shale of the Great Valley Group do not extend westward across the entire Coast Range piedmont. Terraces along these streams are more discontinuous, and less well preserved, than terraces developed along streams incised across the Tehama Formation to the north. Regional correlation of terraces in the vicinity of the dam sites is problematic because they can not be directly tied to pediment surfaces or to terraces mapped farther north by Steele (1980).

## 2.6 QUATERNARY STRATIGRAPHY AT THE SITES AND GOLDEN GATE DAM SITES

Late Quaternary deposits mapped in the vicinity of the dam sites include stream terrace, floodplain, alluvial fan, and colluvial deposits. These deposits primarily are located along major streams (i.e., Stone Corral Creek and Funks Creek) and associated minor tributaries. These deposits and their stratigraphic relations are important for evaluating fault activity, and are discussed in detail in the following sections.

### 2.6.1 Quaternary Stratigraphy at Golden Gate Dam Site

Funks Creek flows within a deep, wide channel inset into broad alluvial plains upstream and downstream of the Golden Gate dam site (Figures 2-8 and 2-9). The dam site is a

Figure 2-8

Figure 2-9

water gap along a sinuous reach of Funks Creek that is deeply incised in the Venado sandstone and other north-south-trending bedrock ridges of Upper Cretaceous Great Valley Group. At the dam site, Funks Creek is narrow, lacks a well-developed floodplain, and locally flows on bedrock. Quaternary sediment exposed along Funks Creek includes slope deposits (colluvium), alluvial fan, terrace, and floodplain deposits (Figures 2-8 and 2-9). Stream terrace and floodplain deposits exposed along the banks of the modern stream channel directly overlie bedrock, or are inset into older Quaternary terrace, alluvial fan or slope deposits.

Five stream terraces (units Qt1 though Qt5) are mapped along Funks Creek (Figures 2-8 and 2-9). Of these deposits, the oldest and topographically highest unit (Qt1) is laterally extensive and underlies broad valleys upstream and downstream of the Golden Gate water gap. The deposits associated with the Qt1 terrace locally are greater than 40 feet (12 m) thick, and are composed of fine-grained sandy silt and silty sand. The deposits typically are overlain by up to 3 feet (1 m) of younger Holocene or historic overbank fluvial deposits. Based on radiocarbon analyses and analysis of soil profile development (described in greater detail below), the underlying Qt1 terrace deposits are late Pleistocene to early Holocene age. Younger deposits (units Qt2 through Qt5) are preserved as inset terraces at bends in Funks Creek, and as isolated fill terrace remnants above the modern floodplain. Field observations and trench exposures reveal that these deposits are composed of bedded silt, sandy silt, fine to coarse sand, and gravel.

Terraces Qt2 through Qt5 represent overbank sediments deposited during large floods on Funks Creek, and probably are historic based on the presence of man-made artifacts in the deposits and lack of soil profile development. Additionally, landowners along Funks Creek report that spring floodwaters locally inundate areas of the uppermost Qt1 surface, indicating that the topographically lower Qt2 through Qt5 surfaces lie within reach of floodwaters associated with large storm events

The modern floodplain is laterally extensive along Funks Creek. Floodplain deposits (unit Qfp; Figures 2-8 and 2-9) and stream channel deposits (unit Qhc) are the youngest

geologic deposits mapped along Funks Creek and locally are inset into terrace and colluvial deposits. Floodplain deposits typically contain beds of sandy gravel and silty sand. Stream channel deposits consist of sandy silt and gravel inset into either the modern floodplain or terrace deposits. The width of the modern stream channel, and thickness of stream deposits, varies along the length of Funks Creek.

### 2.6.2 Quaternary Stratigraphy at Sites Dam Site

Stone Corral Creek has a smaller drainage basin than Funks Creek and a less well-developed series of stream terraces, especially in the vicinity of the Sites dam site. Stream terrace deposits typically are preserved as isolated remnants above the modern stream channel or floodplain. Quaternary deposits exposed along Stone Corral Creek include colluvial, alluvial fan, terrace, floodplain, and stream channel deposits (Figure 2-10). Bedrock is exposed within the stream channel along much of the reach that we mapped in detail.

Four stream terraces (units Qt1-Qt4; Figure 2-10) are present along Stone Corral Creek. These terraces are less well preserved than terraces mapped along Funks Creek, and are not as laterally extensive. With the possible exception of the highest, oldest Qt1 terrace, none of the terraces mapped along Stone Corral Creek are obviously correlative to those mapped along Funks Creek. Stream terrace and floodplain deposits exposed along the banks of Stone Corral Creek have minimal soil development, indicating that these terraces are historic. Field observations indicate that these deposits are composed of silt and fine to coarse sand and gravel.

The modern floodplain (unit Qfp; Figure 2-10) locally is preserved as remnants within bends along Stone Corral Creek and contains beds of sandy gravel and silty sand. Much of the stream bottom along Stone Corral Creek consists of either exposed bedrock or modern stream channel deposits. Stream channel deposits are composed of sandy silt and gravel, typically inset into either the modern floodplain or terrace deposits.

Figure 2-10

### 2.6.3 Trench Stratigraphy

Paleoseismic trenches were excavated within late Quaternary deposits in the vicinity of the Sites dam site, the Golden Gate dam site, and across the Salt Lake fault at Hunters Creek. Trenches at each locality exposed a sequence of colluvial and/or alluvial deposits overlying sandstone, mudstone, and shale of the Great Valley Group. The trenches provide information on the lithology, texture, and structure of the deposits, as well as the degree of weathering and soil profile development, which provides a means of correlating deposits and assessing their relative ages. Deposits exposed in the trenches are discussed in detail in Chapter 3 and trench logs with accompanying detailed stratigraphic descriptions are presented in Appendix B ("Paleoseismic Trenches").

Based on analysis of trench exposures, soil-profile development in the oldest mapped terrace deposits (Qt1) along Stone Corral and Funks Creeks in the vicinity of the dam sites is consistent with an age of early Holocene to latest Pleistocene (i.e., 8 to 15 ka). Soil colors determined in the field with Munsell charts are 10YR hues; no reddening typical of soils formed in older deposits was observed. Although clay content of the late Quaternary deposits is high and clay films locally are present, much of the clay is primary and is not pedogenic. The primary clay has been redistributed to form the observed clay films and structure. There does not seem to be significant clay accumulation in the Bt horizon relative to the C-horizon, nor is there significantly less clay in the A-horizon indicating loss through illuviation. An early Holocene to latest Pleistocene age for these deposits is consistent with the radiocarbon analyses of samples collected from the trenches (see discussions in Chapter 3.0).

The early Holocene to late Pleistocene age estimate for unit Qt1 is consistent with a general climatic model for late Quaternary weathering, erosion, and sedimentation in the Coast Ranges (Lettis, 1982). During the period of full glacial advance in latest Pleistocene time, the combination of increased effective moisture and denser vegetation likely resulted in the accumulation of a thick, weathered mantle on the hillslopes. A change in climate to drier conditions and less vegetation, which is thought to have occurred during the Holocene-Pleistocene transition (Lettis, 1982; Bull, 1991), likely

would precipitate erosion of the weathered mantle, downslope transportation as colluvium, and eventual accumulation of the deposits as alluvium in valley bottoms. Within the vicinity of the Sites and Golden Gate dam sites, deposits along Stone Corral Creek and Funks Creek typically are fine grained, consistent with the expectation that the weathered mantle material was mobilized during the Holocene-Pleistocene climatic transition. In contrast, older terrace deposits preserved along Hunters Creek and Logan Creek to the north typically are clast-supported gravels suggestive of a relatively high-energy environment. This is consistent with the expectation that the wetter Pleistocene climate resulted in higher discharges in Stone Corral and Funks Creek, thus transporting and depositing more coarsely textured sediments.

# 3.0 NEOTECTONIC CHARACTERIZATION OF GEOLOGIC STRUCTURES

## 3.1 INTRODUCTION

We evaluate two major classes of geologic structures as potential seismic hazards at the Sites and Golden Gate dam sites:

Faults with well-defined surface traces that may pose a surface-rupture hazard, a source of strong vibratory ground motion, or both; and

Blind thrust faults, either known or inferred to underlie map-scale folds, which do not pose a surface-rupture hazard but may be a source of strong vibratory ground shaking at the dam sites.

In the following sections (Sections 3.2, 3.3 and 3.4), we first evaluate folds and faults in close proximity to the Sites and Golden Gate dam sites (Figure 3-1). These structures potentially pose the most direct surface-fault rupture and strong ground-motion hazards to engineered structures at these sites. We then evaluate more distant geologic structures as potential sources of strong ground shaking at the dam sites (Sections 3.5 and 3.6).

## 3.2 STRUCTURAL GEOLOGIC SETTING OF THE DAM SITES

The Sites and Golden Gate dam sites are located in watergaps cut into the Upper Cretaceous Venado sandstone by the east-flowing Stone Corral and Funks Creeks, respectively (Figure 1-2). The Venado sandstone member of the Cortina Formation (Section 2.4) is part of a homoclinally east-dipping sequence of Great Valley Group strata in the foothills bordering the eastern Coast Ranges (Sections 2.1 and 2.3). Directly west of the dam sites, Great Valley Group strata are folded about the axes of the north-trending Sites anticline and Fruto syncline (Figure 3-1). East of the dam sites, the strata progressively flatten beneath the western Sacramento Valley margin.

Figure 3-1

In addition to map-scale folds, Cretaceous bedrock units along the Coast Range-Sacramento Valley boundary are deformed by faulting. We recognize two major sets of surface faults in the local vicinity of the dam sites:

Northeast-striking, high-angle faults that obliquely cut across the north-striking bedrock units, and consistently displace stratigraphic contacts in a right-lateral sense. Specific examples of these structures include the informally named GG-1, GG-2, GG-3 and S-2 faults, all of which pass directly through the proposed Sites and Golden Gate dam sites, or are close enough to potentially impact facilities associated with the dams (Figure 3-1); and

North-striking faults that generally are parallel to bedding. The most laterally continuous example of these structures is the Salt Lake thrust fault (Figure 3-1), which is parallel to, and east of, the axis of the Sites anticline. The Salt Lake fault is approximately 0.9 miles (1.4 km) west of the Golden Gate dam site and the southern end of the fault is approximately 1.7 miles (2.7 km) northwest of the Sites dam site (Figure 3-1). The trace of the fault passes through at least one proposed saddle dam site (K. Buer, California Department of Water Resources, personal communication, 2001).

In addition, south of the town of Sites, Brown and Rich (1961) mapped a north-striking, east-side-up fault that lies within the mudstone unit stratigraphically beneath the Venado sandstone. As mapped, this fault locally duplicates stratigraphic contacts in the Cretaceous Great Valley Group and thus is likely a bedding-parallel thrust fault similar to the Salt Lake fault. This unnamed fault is located approximately 0.75 miles (1.2 km) southwest of the Sites dam site (Figure 3-1).

A third example of this class of bedding-parallel faults is the informally named S-3 fault, which is exposed in the Sites rock quarry just north of Sites road approximately 2000 feet (0.6 km) east of the Sites dam site (Figure 3-1).

Based on analysis of seismic reflection data acquired for this study, we interpret that the surface folds and thrust faults shown in Figure 3-1 are related to activity of a system of

segmented blind thrust faults that dip west beneath the eastern Coast Ranges (Section 2.3; Appendix A). Following the U.S. Geological Survey (Working Group on Northern California Earthquake Potential, 1996) and DWR (California Department of Water Resources, 1999), we refer to these structures collectively as the Great Valley fault. The segment of the Great Valley fault closest to the DWR dam sites is informally named the Funks segment (Appendix A). An east-west geologic cross-section drawn parallel to seismic line 798, about 4.4 to 5 miles (7 to 8 km) north of the Golden Gate dam site (Appendix A), shows Funks segment of the Great Valley fault dipping west beneath the western limb of the Fruto syncline (Figure 3-2). Based on structural and stratigraphic relations visible in seismic reflection data (Appendix A), the dip of the thrust fault is interpreted to shallow beneath the axis of the Fruto syncline and extend eastward beneath the Sites anticline and east-dipping strata along the western valley margin as a low-angle detachment (Figure 3-2). The more steeply dipping reach of the thrust fault beneath the Fruto syncline is termed a "ramp", and the steeply dipping reach beneath the Sites anticline to the east is called a "flat".

We interpret the western limb of the Fruto syncline to be the forelimb of a large, east-vergent fault-propagation fold above the ramp in the Funks segment (Figure 3-2). At the latitude of the Sites and Golden Gate dam sites, the Sites anticline is interpreted to be a west-vergent fault-propagation fold developed above a blind, east-dipping thrust fault that is rooted in the flat of the Funks segment east of the ramp. The Salt Lake fault is a west-vergent structure that is antithetic to the Funks segment, and is interpreted to terminate downdip against the gently west-dipping flat (Figure 3-2). The intersection of the Salt Lake fault with the Funks segment forms an east-tapering underthrust tectonic wedge beneath the western Sacramento Valley margin at the latitude of the dam sites.

Both the Sites anticline and Fruto syncline plunge out at or slightly south of the town of Sites (Figure 3-1), indicating that the subsurface fault geometry shown in Figure 3-2 changes south of Sites. We interpret the southward termination of the folds, and the

Figure 3-2

presence of northeast-striking dextral faults such as GG-1, GG-2, GG-3 and S-2, to mark the southern end of the Funks segment and a structural boundary with the Bear Valley segment, which is the segment of the Great Valley fault directly south of the Funks segment (Appendix A).

The boundary between the Funks and Bear Valley segments is imaged by seismic line SV-12, which trends east-west and crosses the boundary obliquely. The Bear Valley segment in the central part of SV-12 (east of the surface trace of fault S-2) is a west-dipping interface in the 3.75 to 5 mile (6 to 8 km) depth range that separates east-dipping reflectors associated with the Great Valley Group above from west-dipping reflectors below (Figure 3-3). The interface between these oppositely dipping reflectors flattens eastward at a depth of about 2.8 miles (4.5 km) beneath the Sacramento Valley. If projected westward, the interface we associate with the Bear Valley segment would intersect the west end of line SV-12 at a depth of about 5.6 miles (9 km). West of the surface trace of fault S-2, the reflector we correlate with the Bear Valley segment is indistinct. There is another west-dipping reflector or interface in the 3.7 to 4.7 mile (6 to 7.5 km) depth range west of fault S-2, however, that juxtaposes east-dipping layered reflectors above against west-dipping reflectors below. We interpret this horizon to be the southern end of the Funks segment. The Funks segment is structurally higher than and separated vertically from the Bear Valley segment by about 1 mile (1.6 km) across the segment boundary.

The subsurface expression of the northeast-striking dextral faults (e.g., S-2) in line SV-12 is poor (Figure 3-3). This is probably due in part to structural complexity and loss of fold near the west end of the line (Appendix A). There is some discontinuity in reflectors beneath the surface trace of Fault GG-3 that may be related to movement on the fault. If this interpretation is correct, then the fault does not appear to cut or extend below the Funks segment of the Great Valley fault. In general, we believe that the simplest interpretation is that the northeast-striking dextral faults are confined to the hanging wall block of the Funks segment and accommodate differential northeast-directed shortening across the segment boundary. The kinematics of differential shortening and involvement

Figure 3-3

of other structures like the Sites anticline and Salt Lake fault are discussed in greater detail in the following section.

## 3.3 KINEMATIC MODEL FOR DEVELOPMENT OF FOLDS AND FAULTS

We propose a sequential model for the development of faults and folds in the vicinity of the DWR dam sites (Figure 3-4). Stratigraphic and structural relations in the Rumsey Hills region about 28 miles (45 km) south of the DWR dam sites (Plate 1) indicate that upper crustal shortening there began in late Cretaceous-early Tertiary time (Unruh et al., 1995). We assume that shortening began in the present study area at about the same time. The earliest phase of deformation was accommodated by development and growth of an east-tapering "tectonic wedge". The flat part of the Funks segment of the Great Valley fault is the basal detachment for the wedge, and the Salt Lake fault forms the roof thrust (Figure 3-4b).

After initial growth of the tectonic wedge (Figure 3-4b), we interpret that the wedge tip "locked" in position north of the latitude of the town of Sites, preventing further significant wedge propagation to the east. Progressive slip on the Funks segment continued, however, and shortening of the hanging wall block was accommodated by development of the blind Sites thrust fault and growth of the overlying Sites anticline (Figure 3-4c). At this stage of structural development, we infer that east- or northeast-directed thrust displacement extended to the point where the Sites thrust fault splays upward from the Funks segment.

After the Sites anticline developed, we interpret that the system again "locked" where the Sites thrust fault intersects the Funks segment (i.e., the "pin" in Figure 3-4d). We think it is likely that slip on the flat section of the Funks segment diminished east of the Fruto syncline axis, such that the majority of slip occurred on the more steeply dipping ramp to the west. If this is correct, then uplift would primarily occur above the ramp, thus preferentially elevating strata west of the Fruto syncline axis relative to the Sites anticline to the east (Figure 3-4d). Because the majority of slip was confined to the ramp, slip primarily was consumed by uplift, tilting and folding of the hanging well block west of

Figure 3-4

the Fruto syncline axis, thus forming the east-facing homocline that underlies the Coast Range foothills and western Sacramento Valley (Figures 3-4d and 3-4e).

The Sites anticline and Fruto syncline abruptly plunge out at the latitude of the town of Sites in the vicinity of the GG-1, GG-2, GG-3 and S-2 faults (Figure 3-1). We interpret that the folds and strike-slip faults are genetically related, and that they primarily accommodate greater northeast-directed shortening of the hanging wall block of the Funks segment relative to hanging wall of the Bear Valley segment to the south. Because the flat part of the Funks thrust fault directly beneath the dams has a lower dip than the Bear Valley segment, the hanging wall of the Funks segment will propagate farther east for a given increment of slip on the thrust fault than the hanging wall of the Bear Valley segment. We interpret that the northeast-striking GG-1, GG-2, GG-3 and S-2 faults accommodate the differential movement between the segments, resulting in relative right-lateral offset. The northeast-striking faults also may accommodate differential north-south shortening represented by the southern termination of the Sites anticline at the town of Sites.

Our interpretation of the subsurface interaction between the northeast-striking faults, and the Fruto syncline and Sites anticline is illustrated by a series of three cross-sections through the study area (Figures 3-5, 3-6 and 3-7; see Figure 3-1 for section locations). Section A-A' (Figure 3-5) is located south of the town of Sites, the Sites anticline and the S-2 fault, and shows the northern end of the Bear Valley segment of the Great Valley fault. It depicts the east-dipping, unnamed thrust fault mapped south of the S-2 fault (Brown and Rich, 1961) as backthrust splaying upward from the blind Bear Valley segment. Section B-B' (Figure 3-6), which is located just north of the town of Sites (Figure 3-1), shows that the southern end of the Sites anticline developed as a fault-propagation fold above a blind, east-dipping thrust fault that splays upward from the flat, consistent with our interpretation of seismic reflection data (Figures 3-2, 3-3). The S-2 fault is depicted as a high-angle fault that accommodates oblique right-lateral motion of the hanging wall block of the thrust fault into the plane of the section (Figure 3-5). The

Figure 3-5

Figure 3-6

Figure 3-7

S-2 fault is interpreted to terminate downward against the Funks segment and form its southern structural boundary. Because cross section B-B' crosses the segment boundary obliquely, we indicate the trajectory of the thrust faults as they extend into and out of the plane of the section (Figure 3-6).

Both the blind Sites thrust fault and the S-2 fault in section B-B' accommodate additional shortening of the upper 3 miles (5 km) of the hanging wall of the Funks segment, relative to the northern end of the Bear Valley segment as shown in section A-A' (Figure 3-5). Evidence for a progressive south-to-north increase in shortening can be seen in the northeast-directed displacement of the 6a/6b contact in the Great Valley Group by a series of northeast-striking dextral faults (labeled "NEF") west of the Fruto syncline axis (Figure 3-1). Between sections A-A' and B-B', the 6a/6b contact is displaced approximately 3150 to 3940 feet (960 to 1200 m) to the northeast across faults NEF-1 and NEF-2 (Figure 3-1). This additional shortening is absorbed, in part, by growth of the Sites anticline and dextral slip on the S-2 fault.

Section C-C' (Figure 3-7) is located north of B-B' at about the latitude of the Golden Gate dam site (Figure 3-1). The amplitude of the Sites anticline is greater in section C-C', implying greater slip on the blind Sites thrust fault and hence greater horizontal shortening of the hanging wall block relative to section B-B' (Figure 3-6). This is consistent with increased northeast-directed displacement of the 6b/6c contact between sections B-B' and C-C', accommodated by dextral slip on faults NEF-3 and NEF-4 (Figure 3-1). The GG-2 and GG-3 faults in section C-C' are depicted as high-angle tear faults that are confined to the hanging wall of the Funks segment of the Great Valley thrust fault.

Comparison of the cumulative northeast-directed displacement of the 6b/6c contact across the "NEF" faults at the latitude of section C-C' with the cumulative dextral displacement of the 7/8 contact across the GG and S faults provides some constraint on the maximum crustal shortening absorbed by the Sites anticline. Total northeast-directed displacement of the 6b/6c contact between sections A-A' and C-C' is about one mile

(1440 m to 1820 m; Figure 3-1). Total northeast-directed displacement of the 7/8 contact across the GG-1, GG-2, GG-3 and S-2 faults is about 0.7 miles (1.1 km) (Figure 3-1). If the Salt Lake fault "locked" prior to growth of the Sites anticline (Figure 3-4), then the Sites anticline may have accommodated about 0.3 miles (0.5 km) of additional horizontal shortening north of the town of Sites, relative to the area crossed by section A-A' south of Sites (Figure 3-3). It is possible that some of the additional 0.3 miles of shortening also was accommodated by reverse slip on the Salt Lake fault.

The implications of this kinematic model for seismic hazards at the DWR dam sites is that the Sites anticline, Salt Lake fault and the GG-1, GG-2, GG-3 and S-2 faults all are genetically related to activity on the underlying Funks segment of the Great Valley fault. The faults and folds are interpreted to collectively accommodate shortening of the hanging wall block at the southern end of the Funks segment. We thus interpret evidence for activity of the surface faults and folds as indirect evidence for activity of the Funks segment.

## 3.4 CHARACTERIZATION OF PROXIMAL GEOLOGIC STRUCTURES

In this section, we characterize folds and faults near the dam sites based on air photo analyses, field mapping and subsurface investigations. These proximal structures include the northeast-striking GG-1, GG-2, GG-3, and S-2 faults, and the north-striking S-3 and Salt Lake faults. Characteristics of these structures are summarized on Table 3-1. Trench and test pit exposures that provide information on the physical morphology of each fault and overlying deposits are summarized. Trench logs with accompanying full descriptions of alluvial and colluvial deposits are provided in Appendix B. Descriptions of soil-stratigraphic relations exposed in the trenches also are included in Appendix B. Detailed soil profile descriptions are provided in Appendix C.

**TABLE 3-1** Characteristics of Faults in Vicinity of Sites/Golden Gate Damsites

| Fault | Fault Length | Sense of Displacement | Fault Separation (Horizontal) | Fault Separation (Vertical) | Fault Width | Nearest Distance to Golden Gate Damsite | Nearest Distance to Sites Damsite | Fault Trenches[a] | Activity[b] |
|---|---|---|---|---|---|---|---|---|---|
| **GG-1** | 3.4 ± 0.1 miles (1.8 ± 0.16 km) | Right-lateral | 246 ± 82 ft (75 ± 25 m) | Unknown | 2 feet (0.6 m) | 0.1 miles (0.2 km) | 1.9 miles (3.0 km) | FT-4a,4b,4c | Holocene deposits unfaulted |
| **GG-2** | 3.7±0.2 miles (6.0 ± 0.3 km) | Right-lateral | 1,312 +196/-98 ft (400 +60/-30 m) | Unknown | 2 feet (0.6 m) | 328 feet (100 m) | 0.9 miles (1.5 km) | FT-3a,3b,5 | Holocene deposits unfaulted |
| **GG-3** | 3.0 ± 0.2 miles (4.8 ± 0.3 km) | Right-lateral | 1,574 ± 65 ft (480 ± 20 m) | Unknown | 2 feet (0.6 m) | 2.7 miles 2.8 (1.8 km) | 0.6 miles (1.0 km) | FT-2a,2b, TPE-1,2,3, FT-7 | Early Holocene deposits unfaulted |
| **S-2** | 2.4 ± 0.1 miles (3.9 ± 0.2 km) | Right-lateral | 558 +164/-180 ft (170 +50/-55 m) | None | 3 feet (1 m) | 1.8 miles (2.9 km) | 0.2 miles (0.3 km) | FT-6, FT-8, FT-9 | Early Holocene deposits unfaulted |
| **S-3** | Unknown | Thrust (east side up?) | Unknown | Unknown | 6 feet (2 m) | Unknown (to be based on fieldwork) | 0.9 miles (1.5 km) | T1-S3, T2-S3, T3-S3, T4-S3, T5-S3, T6-S3 | Older than, and offset by, Faults S-2, GG-3 |
| **Salt Lake fault** | - | Thrust (east side up) | Unknown | >3 m | 2 feet (0.6 m) | 0.9 miles (1.5 km) | 2.0 miles (3.2 km) | HC-FT1,2,3 | Pleistocene gravels offset |

[a] See Appendix B for trench logs and detailed fault descriptions.

[b] Youngest faulted or oldest deposits that cross the fault are given.

### 3.4.1 Northeast-Striking Faults in The Vicinity Of Sites And Golden Gate Dam Sites

#### 3.4.1.1 Fault GG-1

Fault GG-1 is a northeast-striking fault located northwest, or upstream, of the Golden Gate watergap on Funks Creek (Figure 3-8). Fault GG-1 is expressed on aerial photographs as a series of well-defined topographic and vegetation lineaments that coincide with truncated and/or offset north-striking beds of the Great Valley Group. As mapped by Brown and Rich (1961), the GG-1 fault has a total length of 0.4 miles (0.6 km). Based on the presence of truncated bedding (Station 1-1, Figure 3-9; see Table 3-2) and an exposure of faulted bedrock in a stream cut (Station 1-2), we map the fault across Funks Creek, extending further southwest than the map trace of Brown and Rich (1961). Total verified length of the GG-1 fault is 1.1 ± 0.1 miles (1.8 ± 0.16 km). Correlation of displaced stratigraphy near Station 1-4 (Figure 3-9) suggests a maximum right-lateral separation across the fault of 246 ± 82 feet (75 ± 25 m).

**Trench Exposure FT-4a**

The GG-1 fault is best observed in outcrop on a steep hillside north of Funks Creek and west of the Golden Gate water gap (location 1-4, Figure 3-9). Sandstone beds truncated by the fault form a distinct west-facing scarp halfway up the hillside. We excavated Trench FT-4a, a 22-foot-long (7 m), vertical cut in the hillside approximately 100 feet (30 m) downslope of the GG-1 fault lineament, to confirm the presence of the fault and document its morphology (Figure 3-10; Trench FT-4a; Appendix B). The vertical cut exposed a two-foot-wide (0.6 m) zone of faulting in bedrock, overlain by 3 feet (1 m) of unfaulted colluvial slope deposits (Figure 3-10). After an initial assessment, we extended the trench both east and west for a total length of 56 feet (17 m) to assess the full width of the fault zone. We observed no additional bedrock faults or shears in the new exposure. The final log of this trench (Figure 3-10) shows only the original excavation.

Figure 3-8

Figure 3-9

Figure 3-10

**Table 3-2** Geomorphic Field Descriptions for Fault GG-1
(see Figure 3-9 for station locations)

| Station | Geomorphic Field Description |
|---|---|
| 1-1 | Truncated bedding. Linear slope break. |
| 1-2 | Exposure of GG-1 fault (037°/84°NW) within bedrock in small stream. |
| 1-3 | Exposure of GG-1 in fault trench FT 4a (1.5 feet (0.5 m) as a wide shear zone). |
| 1-4 | Truncated bedding within Great Valley Group. Estimated maximum offset of bedding is 246±82 ft (75±25 m) |
| 1-5 | Linear saddle. Truncated bedding. |

### Trench Exposure FT-4b

We sited fault trench FT-4b on the highest, and presumably oldest, fluvial terrace remnant surface north of Funks Creek (Figure 3-9) to determine if the deposits overlying the projection of the fault are offset. Given its similar geomorphic expression and relative topographic position, we interpret that this geomorphic surface is correlative to the broad Qt1 terrace present south of the creek, and thus initially expected the terrace surface to be underlain by fluvial deposits. However, the 79-foot-long (24 m), 13-foot-deep (4 m) trench exposed massive colluvial deposits derived from the slope to the north (Figure 3-11) rather than stream terrace deposits as anticipated. We interpret these relations to indicate that the flat, upper surface of the terrace is graded across colluvium that was deposited near the Qt1 terrace tread-riser transition, and that the colluvium exposed in the trench probably is coeval with Qt1-age fluvial deposits. Due to the instability of the trench walls, we did not enter the excavation and instead prepared a rough log of the exposure from observations from the ground surface above (Figure 3-11). Two distinct colluvial units separated by a sub-horizontal contact crossed the downslope projection of the GG-1 fault. The colluvium, as well as the horizontal contact, exhibited no fault offset or other deformation (Figure 3-11).

Figure 3-11

**Trench Exposure FT-4c**

Trench FT-4c was excavated on terrace Qt2 located approximately 40 feet (12 m) to the south of Trench FT-4a (Figure 3-9). Trench FT-4c was extended 75 feet (23 m) along a N46°W trend sub-parallel to Funks Creek. The trench exposed 16 feet (5 m) of well-bedded stream terrace deposits that extend undeformed across the projected trace of the GG-1 fault (Figure 3-12). Bedrock was not exposed in the trench.

The basal alluvial unit exposed in trench FT-4c (Unit 1; Figure 3-12) consists of sandy gravel with minor clay. The upper contact of this unit is unfaulted and apparently undeformed. This unit is overlain by clay with gray and reddish-brown mottles (Unit 2), and sandy gravel (Unit 3). Interbeds of clay, sand, and gravel within unit 3 pinch out laterally. At the eastern end of the trench (horizontal distance 46 to 53 feet (14-16 m); Figure 3-12), several of the interbeds in unit 3 appear to roll over in an antiformal structure. Charcoal samples from the interbeds provide a calibrated age of 1170 to 1290 AD (Tables 3-1 and 3-3). Unit 4, which overlies the interbeds in unit 3, consists of poorly bedded sand, silt, and clay containing sub-horizontal lenses of coarse, sandy gravel. Radiocarbon analysis of charcoal collected from unit 4 provide a calibrated age of 1520 to 1940 AD (Table 3-3), which is slightly younger and thus stratigraphically consistent with the dates from the underlying unit. The lower contact of unit 4 is clear, planar, and undeformed, providing evidence for no late Holocene surface rupture on the GG-1 fault at this site.

Because bedding within fluvial units and stratigraphic contacts directly above and below the dipping interbeds in unit 3 are undeformed, we conclude that the antiformal geometry of the interbeds in unit 3 is not tectonic in origin. The finely laminated, inclined bedding may be the product of deposition over an existing streamside feature such as a fluvial point bar or sloped channel margin. The warping of the beds also may have been produced by collapse of a cut bank. Alternatively, the beds may have been folded or warped after deposition by tree roots. Excavation of the opposite trench wall revealed

Figure 3-12

**Table 3-3** Radiocarbon Age Estimates for Sites/Golden Gate Trenches

| Field Sample No. | Laboratory Sample No. | Sample material | Stratigraphic Unit | Depth interval (m) | $\delta^{13}C$ (‰) | Lab-reported age ($^{14}$Cyr B.P. at 1σ)[a] | Calibrated age (yr BC/AD at 2σ)[b] |
|---|---|---|---|---|---|---|---|
| ***Trench FT-3a, Fault GG-2*** | | | | | | | |
| GGC-RC1 | CAMS-58038 | charcoal | Colluvium over fractured bedrock | | -25 | 2200 ± 40 | 379-170 BC |
| ***Trench FT-2a, Fault GG-3*** | | | | | | | |
| GGE-RC4 | Beta-133741 | charcoal | Buried soil, south wall trench FT-2 | 2.8 m | -26.2 | 9250 ± 40 | 8600-8310 BC |
| GGE-RC3 | n/a | charcoal | Alluvial silt, south wall trench FT-2 | 2.4 m | n/a | withdrawn from analysis | n/a |
| ***Trench FT-4c, Fault GG-1*** | | | | | | | |
| GGW-RC2 | Beta-133742 | charcoal | Sandy silt alluvium north wall trench FT-4c | 3 m | -22.7 | 240 ± 40 | 1520-1940 AD |
| GGW-RC6 | Beta-133743 | charcoal | Clayey silt alluvium, north wall trench FT-4c | 4.2 m | -23.8 | 800 ± 40 | 1170-1290 AD |
| ***Trench FT-6a, Fault S-2*** | | | | | | | |
| FT6A-RC1 | NZA-10658 | charcoal | Alluvium overlying bedrock | 0.7 m | -25 | 170.1 ± 1% modern | modern |
| FT6A-RC2 | NZA- 10799 | charcoal | Alluvium overlying bedrock | 0.5 m | -25.04 | 164.56 ± 1.18% modern | modern |
| ***Trench FT-7, Fault 99-3*** | | | | | | | |
| FT7-RC3 | n/a | charcoal and unidentifiable humic material | Clayey colluvium overlying bedrock near base of trench | 1.1 m? | n/a | sample too small to analyze | n/a |
| FT7-RC4 | n/a | unidentifiable humic material | Clayey colluvium overlying bedrock, base of trench | 2.5 m | n/a | material dissolved in alkali solution, withdrawn from analysis | n/a |

**Table 3-3** Radiocarbon Age Estimates for Sites/Golden Gate Trenches

| Field Sample No. | Laboratory Sample No. | Sample material | Stratigraphic Unit | Depth interval (m) | $\delta^{13}C$ (‰) | Lab-reported age ($^{14}$Cyr B.P. at 1σ)[a] | Calibrated age (yr BC/AD at 2σ)[b] |
|---|---|---|---|---|---|---|---|
| FT7-RC5 | n/a | unidentifiable humic material | Clayey colluvium overlying bedrock, base of trench | 2.5 m | n/a | material dissolved in alkali solution, withdrawn from analysis | na |
| FT7-RC11 | n/a | unidentifiable humic material | Clayey colluvium overlying bedrock, base of trench | 2.5 m | n/a | material dissolved in alkali solution, withdrawn from analysis | n/a |

[a] Ages reported by radiocarbon laboratory based upon the Libby half life (5568) for $^{14}$C.

[b] Calibrated age ranges before A.D. 1950 according to Stuiver and Reimer (1998) calculated using a lab error multiplier of 1.0 and reported at 2σ.

abundant horizontal tubular voids and roots, consistent with the presence of vegetation and roots in unit 3 subsequent to deposition (Figure 3-12; Appendix B).

**Summary of Trench Exposures, GG-1 Fault**

Three trenches across the GG-1 fault document that the structure is a discrete, well-defined, narrow zone of shearing less than 3 feet (1 m) wide (e.g., Figure 3-10). Based on the presence of unfaulted colluvial deposits in trench FT-4b on the highest, and oldest, remnant surface north of Funks Creek, it is likely that there has been no surface rupture during the Holocene. This interpretation is based on correlation of this geomorphic surface to the broad Holocene Qt1 terrace south of Funks Creek and downstream of the trench site. Late Pleistocene deposits were not encountered in trenches across the GG-1 fault, and thus there are no observations that permit assessment of late Pleistocene (10 - 35 ka) or older Quaternary activity.

### 3.4.1.2 Fault GG-2

Fault GG-2 strikes northeast, sub-parallel to and approximately 0.3 miles (0.5 km) southeast of Fault GG-1 (Figures 3-8 and 3-9). The fault is visible on aerial photographs as a well-defined lineament that truncates north-striking beds of the Great Valley Group. The fault is defined geomorphically by linear bedrock scarps, flowing springs and distinct vegetation changes across the fault (Figure 3-9; Table 3-4). As mapped by Brown and Rich (1961), the GG-2 fault has a length of 3.0 ± 0.2 miles (4.8 ± 0.3 km). Based on our field mapping, however, we believe the southwestern end of the fault does not curve northwestward as mapped by Brown and Rich (1961); instead, we extend the fault southwestward along strike for a total length of 3.7 ± 0.2 miles (6.0 ± 0.3 km). Based on offset of sandstone marker beds within the Great Valley Group, we estimate a maximum right-lateral separation of 1,312 feet (400 +60/-30 m) across the GG-2 fault (Table 3-1).

**Table 3-4** Geomorphic and Stratigraphic Field Descriptions for Fault GG-2
(see Figure 3-9 for station locations)

| Station | Field Description |
|---|---|
| 2-1 | Linear swale within bedrock. Apparent right-lateral offset of bedding. |
| 2-2 | Subtle break in slope (< 2 feet), aligned with linear swale to the northeast. Coincides with truncated bedding. |
| 2-3 | Linear northeast-trending swale. |
| 2-4 | Fault exposure in Trench FT-3a (046°/88°SE). |
| 2-5 | Exposure of fault within bedrock in stream cut. Truncated bedding (oriented 003/75°E), with near-vertical shear plane (oriented 026/58°E). |
| 2-6 | Truncated bedding. |
| 2-7 | Stream exposure of fault in bedrock (045°/70°NW; 035°/70°NW). |
| 2-8 | Truncated bedding. Northwest -facing bedrock scarp. |
| 2-9 | Linear bedrock scarp, coincident with prominent vegetation lineament |

We trenched the GG-2 fault at two separate locations near the Golden Gate dam site where alluvial fan and terrace deposits overlie the mapped trace of the fault (Trenches FT-3a, FT-3b and FT-5; Figure 3-9). Extensive cultural modification from a quarrying operation downstream of the Golden Gate water gap has obscured geomorphic expression of stream terraces at trenches FT-3a and FT-3b. Despite cultural modifications of the landforms and uppermost fluvial deposits, the site for trench FT-3a was selected because this is where the highest, oldest undisturbed terrace deposits are present across the fault. In addition, the U.S. Bureau of Reclamation previously opened a trench across the GG-2 fault at this location (C. Howard, U.S. Bureau of Reclamation, personal communication, 1999), and the FT-3a trench was sited in an attempt to re-excavate the original Bureau of Reclamation trench.

**Trench Exposure FT-3a**

Trench FT-3a was located on a terrace of Funks Creek that crosses the projected trace of the GG-2 fault (Figures 3-9 and 3-13). The FT-3a trench was oriented N35°W and extended 39 feet (12 m) sub-parallel to the base of the adjacent hillslope (Figure 3-14). Trenching initially exposed only road fill and trench spoils from the Bureau of Reclamation trench. We removed the exposed Reclamation trench spoils, re-excavated the uphill portion of the trench, and benched the excavation for safety. As fully excavated, FT-3a exposed 2 to 3 feet (approximately 1 m) of colluvial deposits overlying a well-expressed bedrock exposure of the GG-2 fault (Figure 3-14). The GG-2 fault is a discrete, well-defined, narrow zone of faulting less than 2 feet (0.6 m) wide, with minor secondary shears in the adjacent bedrock (Figure 3-15). We identified three distinct types of bedrock juxtaposed by faults in the trench exposure: (1) bedded sandstone (bedding dips 35°E); (2) massive sandstone; and (3) laminated mudstone (bedding dips 57°E). The main fault plane strikes N46°E and dips 88° to the southeast. Slickensides on the fault plane indicate predominately horizontal (i.e., strike-slip) motion, with minimal dip-slip motion.

The faulted bedrock in trench FT-3a is overlain by unfaulted colluvial deposits (Units 1 through 3; Figure 3-14). The colluvial deposits directly overlying bedrock (Unit 1) consist of brownish yellow poorly-sorted gravel that contains boulders up to 2.5 feet (0.9 m) diameter. These coarse deposits, likely derived locally from the underlying bedrock, are overlain by finer-grained yellowish-brown silty colluvium (Unit 2) containing angular to subangular gravel. Radiocarbon analysis of charcoal collected from Unit 2 provide a calibrated age of 379-170 BC (Table 3-3). Unit 2 is overlain by similar dark yellowish brown silt containing angular clasts and well-developed prismatic soil structure (i.e., unit 3; Figure 3-14). We interpret unit 3 to represent pedogenic alteration and soil profile development on unit 2; thus, unit 2 is the parent material (or C horizon) of the modern soil.

Figure 3-13

Figure 3-14

Figure 3-15

**Trench Exposure FT-3b**

We excavated trench FT-3b across the projection of the GG-2 fault on a terrace located downslope of, and southwest of, the FT-3a trench (Figures 3-9 and 3-13). Trench FT-3b exposed artificial fill and terrace deposits covering a bedrock exposure of the GG-2 fault (Figure 3-16). The GG-2 fault is expressed in this trench as a well-defined zone of faulting less than 3 feet (1 m) wide, with a primary, steeply dipping to subvertical fault, and several west-dipping secondary fault shears (Figure 3-16). The terrace deposits overlying the fault are not sheared or otherwise deformed. No charcoal was recovered from deposits exposed in test pit FT-3b to evaluate their ages directly. Based on the topographic position and lack of soil development, we estimate that these terrace deposits are late Holocene to Historic age.

**Trench Exposure FT-5**

Trench FT-5 was located on the surface of a small alluvial fan deposited by a tributary to Funks Creek, approximately 1,200 feet (366 m) northeast of the FT-3a site (Figure 3-9). Sandstone beds of the Great Valley Group truncated by the GG-2 fault are exposed in a stream cut southwest of the trench site. Trench FT-5 crosses the projection of the fault between the exposure in the stream cut to the southwest, and an exposure of faulted bedrock on the hillslope to the northeast. The alluvial fan surface on which the trench is sited grades to the Qt1 terrace (Figure 2-8), and thus we interpret the fan deposits to be equivalent in age to Qt1.

Trench FT-5 extended 72 feet (22 m) along a N35°W trend and was excavated to the maximum operating depth of the excavating equipment (approximately 15 feet (4.5 m)). Although bedrock is exposed in the ephemeral stream channel to the southwest, no bedrock was exposed at the base of the trench during excavation (Figure 3-17), indicating that several meters of relief must be present on the bedrock surface between the trench and stream cut exposure. We infer that this relief was generated during a prior (latest Pleistocene?) episode of incision of the tributary stream, followed by aggradation and accumulation of at least 15 feet (4.5 m) of interbedded fluvial and colluvial deposits above the base of the channel in bedrock. We do not believe that this relief is due to fault

Figure 3-16

Figure 3-17

offset as the stream is actively cutting into bedrock across the fault and there is no apparent lateral offset of the buried bedrock channel.

Trench FT-5 exposed layered, sub-horizontal deposits with locally inset stream channel deposits. The deposits are not faulted or otherwise deformed. Six distinct units are identified in trench FT-5 (Figure 3-17). The lower four units are interpreted to be colluvial deposits, and are distinguished on the basis of color, texture, clast composition and stratigraphic position. The uppermost units logged in Trench FT-5 (Units 5 and 6) are horizons in the modern soil profile that formed subsequent to the deposition of the underlying parent deposits. In this interpretation, colluvial unit 4 is the deposit or parent material (i.e., the C horizon) in which the modern soil has developed. Unit 5 exhibits pedogenic (soil) alteration that represents the B horizon of the modern soil. The uppermost unit (Unit 6) exhibits pedogenic alteration that represents the A horizon of the modern soil (Soil Profile SP-3; Appendix C).

**Summary of Trench Exposures, GG-2 Fault**

Three trenches at two sites across the GG-2 fault reveal that the structure is a narrow zone of sub-vertical shearing that juxtaposes contrasting Great Valley Group bedrock units. Kinematic indicators from the FT-3a exposure indicate predominantly horizontal (i.e., strike-slip) deformation. Based on the presence of unfaulted alluvial and colluvial deposits in trench FT-5 underlying a fan surface that is graded to the early Holocene Qt1 terrace, we interpret that there has been no surface rupture on the GG-2 fault during the Holocene. Late Pleistocene deposits were not encountered in trenches across the GG-2 fault, and thus there are no observations that permit assessment of late Pleistocene (i.e., 10 - 35 ka) or older Quaternary activity on the GG-2 fault.

### 3.4.1.3 Fault GG-3

Fault GG-3 strikes northeast, sub-parallel to and approximately 0.7 miles (1.1 km) southeast of Fault GG-2 (Figures 3-1 and 3-9). The fault is visible on aerial photographs as a series of well-defined lineaments that extend from near Funks Reservoir southwest to the town of Sites. Fault-related features noted on the aerial photographs, and confirmed

Figure 3-18

by field mapping, include truncated bedding, topographic saddles, sidehill benches, springs, topographic scarps, and vegetation lineaments (Figure 3-18; Table 3-5). The central reach of the fault, located southwest of Funks Creek, coincides with a linear northeast-trending valley (Figures 3-8 and 3-18). As mapped by Brown and Rich (1961), and confirmed by our field mapping, the GG-3 fault has a total length of 3.0 ± 0.2 miles (4.8 ± 0.3 km). Based on offset of a prominent sandstone marker bed within the Great Valley Group, we estimate a maximum right-lateral separation of 1,575 ± 66 feet (480 ± 20 m) across the GG-3 fault (Figure 3-9; Table 3-1).

**Table 3-5** Geomorphic and Stratigraphic Field Descriptions for Fault GG-3
(see Figure 3-18 for station locations)

| Station | Field Description |
|---|---|
| 3-1 | Truncated bedding. Prominent vegetation lineament. |
| 3-2 | Exposure of fault in test pit TPE-1 (N30°E/36°W). |
| 3-3 | Truncated bedding. |
| 3-4 | Spring, truncated bedding |
| 3-5 | Exposure of fault within bedrock in stream cut. Truncated bedding (oriented 003/75°E), with near-vertical shear plane (oriented 026/58°E). |
| 3-6 | Truncated bedding. Fractured bedrock. |

A splay of the GG-3 fault extends east-northeast from the main trace towards Funks Reservoir, approximately 0.1 miles (0.16 km) southwest of Funks Creek (Figures 3-8 and 3-18). This splay is well expressed on aerial photos and confirmed by field observations of truncated sandstone beds (Figure 3-18). Right-lateral offset of correlated marker beds indicates that the splay has a maximum dextral separation of 590 feet (180 ± 20 m). The maximum length of the GG-3 fault splay is 0.3 miles (0.5 km), based on the presence of unfaulted marker beds that cross the northeastern projection of the fault splay in the vicinity of Funks Reservoir.

A total of five trenches and test pits were excavated across the GG-3 fault at two separate sites (Figure 3-18).

**Trench Exposure FT-2a**

Data from four hollow-stem rotary auger boreholes drilled during this study documented a pronounced "step" in the elevation of bedrock beneath an alluvial plain along the projection of the GG-3 fault (Figure 3-19). Trench FT-2a was located to cross the bedrock step (Figure 3-18). The bedrock step is buried by valley fill that we interpret to be correlative with Qt1 terrace deposits (Section 2.6.1).

The FT-2a trench (Figures 3-18 and 3-20) was 72 feet (22 m) long and oriented east-west. We identified five distinct alluvial units (Units 1 through 5) exposed along the entire length of the trench (Figure 3-21). The upper two units (Units 4 and 5) probably represent soil horizons developed on the uppermost alluvial deposit (Unit 3). A radiocarbon age of 9250 + 40 yr from unit 2 (Table 3-3) indicates that the alluvial deposits in the trench are early Holocene in age. The contacts between units logged in the trench are undeformed (Figure 3-21), providing evidence for no Holocene surface faulting on the GG-3 fault.

**Trench Exposure FT-2b**

Trench FT-2a was extended 56 feet (17 m) to the west by excavating FT-2b (Figure 3-22). The primary goal of this additional excavation was to expose and characterize bedrock west of the main step in bedrock revealed by the borehole transect (Figure 3-19), and document the western extent of possible deformation associated with the GG-3 fault zone. FT-2b exposed shallow bedrock west of the projection of the GG-3 fault, thus confirming the east-down step in the bedrock surface inferred from the boreholes. The trench exposed sub-vertical shears within bedrock that may represent the western margin of the GG-3 fault zone (Figure 3-22). Alluvial deposits overlying the bedrock shears were not faulted or otherwise deformed.

Figure 3-19

Figure 3-20

Figure 3-21

Figure 3-22

**Trench Exposures TPE-1, TPE-2, and TPE-3**

Trench FT-2a could not be safely excavated deep enough to expose the GG-3 fault in bedrock due to shallow groundwater conditions. To confirm that trench FT-2a and its extension FT-2b actually crossed the fault, we excavated two short trenches (TPE-1 and TPE-2) across the fault trace along the base of a linear ridge to the northeast (Figure 3-18). TPE-1 (Figure 3-23) exposed a west-dipping fault (N30°E/36°W) in the Cretaceous Great Valley Group (Figure 3-24). TPE-2 exposed a sub-vertical bedrock shear zone partially obscured by a large animal burrow (i.e., krotovina) (Figure 25; Appendix B). The bedrock step beneath the alluvial plain to the southwest documented by the boreholes lies along a line projected between the trace of the GG-3 fault mapped to the southwest and the fault exposures in TPE-1 and TPE-2. We therefore conclude that the undeformed deposits in trench FT-2a overlie the GG-3 fault.

We excavated a third trench (TPE-3) adjacent to TPE-2 (Figure 3-18) to provide an additional exposure of the GG-3 fault, and confirm the presence or absence of another fault or fault splay at the base of the linear ridge. A suspected secondary fault trace was inferred to lie along the slope break at the base of the linear ridge. TPE-3 was oriented N45°W, extended east approximately 125 feet (38 m) from the midpoint of the slope across the base of the hillslope, and exposed east-dipping, interbedded sandstone and mudstone of the Great Valley Group overlain by a thin (1 to 2 feet (0.5 m)) veneer of colluvial deposits (Figure 3-26). Faulted and overturned bedrock near the upper part of the trench, on projection of the fault exposed in nearby TPE-2, likely represents the GG-3 fault trace. TPE-3 exposed unfaulted mudstone bedrock overlain by up 13 feet (4 m) of massive, undeformed alluvium across the base of the ridge (Figure 3-26). We conclude that there is no fault coincident with the slope break along the base of the ridge. Based on these relations, we conclude that fault GG-3 is a single linear fault trace that extends along the hillslope as mapped.

**Trench Exposure FT-7**

Trench FT-7 was sited on the margin of a laterally extensive fluvial terrace mapped as Qt1 (Figure 3-18, also Figure 2-9). The GG-3 fault is expressed as a well-defined tonal

Figure 3-23

Figure 3-24

Figure 3-25

Figure 3-26

and vegetation lineament on the hillside northeast of the trench site, and clearly truncates sandstone beds that crop out along the upper slope above the terrace tread. The trench was 92 feet (28 m) long, oriented N22°W, and exposed thinly-bedded mudstone, siltstone, and sandstone of the Great Valley Group overlain by Quaternary sand, silt, and clay, with scattered subrounded cobbles (Figure 3-27). We interpret the Quaternary deposits to be a mixture of alluvium from Funks Creek and colluvium from the adjacent hillslope. We identified two distinct packages of Quaternary deposits overlying Cretaceous bedrock: a colluvial unit (unit 1) overlain by an alluvial unit (unit 2). Three distinct soil horizons (units 3, 4 and 5) represent the modern soil profile developed on the upper alluvial unit 2.

Weathered sandstone bedrock exposed at the base of Trench FT-7 contains v-shaped cracks or fissures containing soil material that is distinct from the Unit 1 material directly above (e.g., fracture at horizontal distance 14 m; Figure 3-27). The in-filling material is a fine sandy clay loam with distinct reddish clay films, similar to those found coating bedding planes and joints in the adjacent bedrock. Angular fragments of bedrock are supported by the matrix of fines. We do not believe that these fractures are of neotectonic origin, and prefer to interpret the fill as derived from older soil material that once formed a thick layer over the bedrock. We infer that this material was erosionally stripped from the bedrock, leaving only small, protected remnants that had infiltrated bedrock cracks and fissures (Figure 3-28). The present soil profile is developed in Units 1 and 2, and represents less weathering than that of the weathered material found in the bedrock cracks. No shear fabric or other evidence of faulting was observed in the older soil material that fills the cracks in bedrock. Although Trench FT-7 crosses the GG-3 fault, the weathered nature of bedrock precludes unequivocal identification of the fault.

**Summary of Trench Exposures, GG-3 Fault**

Three trenches and three short excavations document that the GG-3 fault is a narrow (less than 2-ft wide), sub-vertical bedrock shear zone. A radiocarbon age of 9250 + 40 yr from the lower part of Trench FT-2 documents that basal alluvial deposits in the trench are

Figure 3-27

Figure 3-28

early Holocene or younger. These sediments extend across the fault and are not faulted or otherwise deformed, thus providing positive evidence for no Holocene surface rupture on the GG-3 fault. Late Pleistocene deposits were not encountered in trenches across the GG-3 fault, and thus, there are no stratigraphic constraints on late Pleistocene (10 – 35 ka) or older Quaternary activity.

#### 3.4.1.4 Fault S-2

The S-2 fault strikes northeast and can be traced for approximately 2.4 ± 0.1 miles (3.9 ± 0.2 km) between Funks Reservoir and the town of Sites (Figures 3-1 and 3-8). We did not identify or observe any fault-related geomorphic or stratigraphic features in Antelope Valley south of Sites that support extending the fault southwest into the valley, as shown on the map by Brown and Rich (1961).

The S-2 fault coincides with a linear series of truncated sandstone beds of the Great Valley Group, and associated topographic saddles and vegetation lineaments (Figure 3-29; Table 3-6). In the vicinity of the Sites dam site, the S-2 fault primarily is distinguished by the presence of juxtaposed bedrock types, fractured bedrock, and side-hill benches and topographic saddles. Based on correlation of offset bedding near the northeastern end of the S-2 fault, maximum right-lateral separation is approximately 558 feet + 164/-180 feet (170 meters + 50/-55 m; Figure 3-8, Table 3-1).

The S-2 fault is overlain by Holocene to historic deposits along Stone Corral Creek (units Qt2 through Qt4, Hfp; see Figure 2-10 and Section 2.6.2). The young age of these deposits renders them unsuitable for evaluating activity of the fault per DSOD criteria. In addition, the instability of the terrace remnants adjacent to the creek, extensive cultural modifications (including road fill), and environmental restrictions made trenching the S-2 fault along Stone Corral Creek logistically impractical. We thus elected to trench alluvial deposits that overlie the S-2 fault at two locations near Funks Reservoir, approximately 1.5 miles (2.4 km) northeast of the Sites dam site (Figures 3-18 and 3-29). Although somewhat distant from the Sites dam site, these locations provide better opportunities to characterize the activity of the S-2 fault than sites along the creek near the dam site.

Figure 3-29

**Table 3-6** Geomorphic and Stratigraphic Field Descriptions for Fault S-2
(see Figure 3-29 for station locations)

| Station | Field Description |
|---|---|
| 2-1 | Truncated bedding; change in strike and dip of bedding across fault. |
| 2-2 | Truncated bedding. |
| 2-3 | Fault-line scarp; possible drag fold in "brown beds" (i.e., marker beds). |
| 2-4 | Truncated bedding. |
| 2-5 | Offset bedrock; scarps in bedrock. Main fault strikes 048°; fault is vertical. |
| 2-6 | Notch in ridge; linear stream drainages along trend of fault. |
| 2-7 | Notch in ridge; distinctive conglomerate bed offset by fault. |

**Trench Exposure FT-6**

Trench FT-6 was 95 feet (29 m) long and extended north-south within fluvial deposits across the projection of truncated sandstone bedding exposed near the top of a small, flat hill (Figure 3-29). The trench exposed Great Valley Group sandstone overlain by up to three feet (1 m) of Quaternary alluvial deposits (Figure 3-30). Yellowish-brown sandstone bedrock exposed in the trench varies from massive with no discernable sedimentary structure, to thinly bedded with some cross beds. Near the center of the trench, at horizontal distance station 16.5 m (see horizontal scale on trench log), a coherent 3 foot wide (1 m) sandstone block is bounded on both sides by faults (Figure 3-30). These faults coincide with the projection of the northeast-striking truncation of sandstone beds exposed 20 feet (6 m) northwest of the FT-6 trench and we interpret the faults to be the S-2 fault zone.

The contact between the bedrock and overlying Quaternary alluvium exposed in the trench is a relatively flat, sub-horizontal surface with minor irregularities. The bedrock

Figure 3-30

surface likely was cut by stream erosion and thus is a buried fluvial 'strath' (stream-cut) surface. This buried strath surface is not offset vertically across the fault, and the overlying deposits are not faulted. The profile characteristics of the soil developed in the alluvium are consistent with an early Holocene age (Appendix C); thus, we interpret that the fault has not been active during the Holocene.

The southeast side of the faulted sandstone block is heavily fractured, and clay gouge is present between discrete shear planes. Wedge-shaped infillings of soil material are present in cracks, crevices and fissures in the bedrock adjacent to and within the fault zone (Figure 3-30). Close inspection of the fill material revealed that the fillings consist of a mixture of pulverized bedrock and alluvium. Based primarily on the lack of shear fabric in this material and the absence of shearing in the overlying deposits, we interpret that the alluvium filled fractures in the bedrock by non-tectonic, soil-forming processes (i.e., the crack-filling deposits are not tectonic fissure-fill deposits; see Figure 3-28 and discussion in Section 3.4.1.3).

**Trench Exposure FT-8**

Trench FT-8 extended 49 feet (15 m), north-south (N5°E), across the projection of the S-2 fault (Figure 3-29). The trench exposed massive sandstone faulted against thinly bedded sandstone and mudstone of the Great Valley Group (Figure 3-31). The bedrock units were pervasively sheared and fractured. The bedrock units were overlain by 5 to 8 feet (1.5-2.5 m) of Quaternary fluvial deposits (Figure 3-31). At the upward termination of the main fault in bedrock, there is a v-shaped opening filled with material similar to that in the overlying fluvial deposits. Based on the lack of shear fabric or other features characteristic of faulting in this material, we interpret that this material was deposited within a pre-existing crack or fracture, similar to the infilling deposits encountered in Trench FT-6 (see discussion above).

The soil development within trench FT-8 is very similar to that within deposits estimated to be of early Holocene age in the Funks Creek area and that within trench FT-6. Based

Figure 3-31

on the stratigraphic setting and overall soil development, we conclude that Unit 4 in trench FT-8, which is unfaulted, is Holocene. At horizontal distance 26 to 29.5 ft (station 8-9 m; Figure 3-31), the contact between bedrock and alluvial unit 1 is near vertical and exhibits about 1.5 ft (0.45 m) of local relief. The origin of the steep contact does not appear to be tectonic due to the lack of shear fabric or gouge along fractures that bound it, and the fact that the bedrock fractures do not extend into the overlying fluvial deposits. Based on the presence of fluvial deposits on the bedrock surface, and the close proximity of the trench to the modern stream channel, we interpret that the vertical surface is the buried edge of a channel margin.

**Trench Exposure FT-9**

Trench FT-9 was extended 80 feet (24.5 m) north-south across the projection of fault S-2 within a broad, flat alluvial Qt1 surface adjacent to Funks Reservoir (Figure 3-29). Trench FT-9 exposed interbedded sandstone, siltstone, and mudstone of the Cretaceous Great Valley Group overlain by bedded Quaternary fluvial deposits (Figure 3-32). The fluvial deposits exhibit stratification and distinct bedding, and overlie a subhorizontal erosional surface on the bedrock. The northern 20 feet (6 meters) of the trench were not logged in detail due to unsafe conditions; major units were logged by dropping a tape from the surface and sighting across to the estimated contacts.

The bedrock surface underlying Quaternary deposits in trench FT-9 is subplanar with minor erosional irregularities (Figure 3-32). As shown on the trench log, the surface has been channeled in the vicinity of horizontal distance 3.3 and 9.9 ft (1 and 3 m), resulting in approximately 0.8 feet (0.25 m) of local erosional relief. Rusty-brown colored clasts of Great Valley Group sandstone, ranging in size from 5-25 cm and probably derived from a local bedrock source, are present on the bedrock surface.

Bedrock exposed in Trench FT-9 is overlain by 12 feet (3.75 m) of fluvial deposits (Units 1-7). Of particular interest is a channel deposit (Unit 4) that contains a distinctive water-lain tephra. The channel deposit appears to be inset into Unit 3 on the west wall of the

Figure 3-32

trench, and it unconformably overlies Unit 1. Unit 4 also was observed on the east trench wall. We interpret the stratigraphic relations in the trench exposure to indicate that it overlies Units 1 and 2b at the bottom of the east wall (Figure 3-33). Units 1 and 2b directly overlie the main traces of the S-2 fault zone (Figure 3-33), and are not faulted. By sighting across the trench, we estimate that the orientation of the channel thalweg containing the ash is 12°/ N20°E. The general trend of the tephra deposit across the trench is N15°E to N25°E. The trends are similar to that of the present course of Funks Creek. This unit crosses the S-2 fault and appears unfaulted.

A sample of the Unit 4 tephra was submitted to Dr. Andrei Sarna-Wojcicki of the USGS for analysis. Dr. Sarna-Wojcicki reported that the sample was contaminated with detrital sediment and contained only about 15% glass shards (A. Sarna-Wojcicki, written communication, 2000), which indicates that the tephra was eroded and transported to the trench location by fluvial processes. Microprobe analysis of the glass shards (USGS sample DWR-FP-9-1, T439-2) indicates that the shard population is relatively homogenous, and thus is not a mixture of several different tephra. Chemically, the volcanic glass of this tephra is similar to tephra layers erupted from the central Cascade Range of Oregon. According to Dr. Sarna-Wojcicki (written communication, 2000), the closest match is to reworked disseminated glass shards found in Holocene (historic) sediments of Grass Lake, in northern California (northeast of Mount Shasta). The Grass Lake shards are found as one of two compositional populations within disturbed sediments, and are probably reworked locally as a consequence of logging (A. Sarna-Wojcicki, written communication, 2000). Both compositional modes in the Grass Lake tephra samples probably are Pleistocene in age. Sarna-Wojcicki and others have identified the one compositional mode in the Grass Lake core as the Olema ash bed, ca. 55-75 ka in age. The chemical composition of the Grass Lake tephra is also similar to the Jefferson Pumice (est. age ~80 ka) and its distal correlatives, but there is no secure match. Despite chemical similarities, Dr. Sarna-Wojcicki (written communication, 2000) cautions that there is no guarantee that the ash sample obtained from trench FT-9 is the same age as the Olema ash bed or the Jefferson Pumice.

Figure 3-33

In summary, the tephra found in trench FT-9 may be correlative with reworked late Pleistocene ashes found in Holocene sediments of Grass Lake in northeastern California. Like the Grass Lake ashes, the tephra in trench FT-9 has been reworked by fluvial processes and thus the *maximum* age of sediments containing the tephra is late Pleistocene; the deposits could be Holocene. The soil profile within trench FT-9 (SP-7 in Appendix C) is very similar to other profiles of soils developed within deposits estimated to be of early Holocene age in the Funks Creek area. Based on the stratigraphic setting and overall soil development (profile SP-7 in Appendix C), we conclude that Unit 4 in trench FT-7, which contains the tephra, is a Holocene deposit.

**Summary of Trench Exposures, S-2 Fault**

The S-2 fault is a narrow (less than 2-ft wide) sub-vertical bedrock shear zone. The fault is overlain by unfaulted Early Holocene colluvial and alluvial deposits. Small packages of colluvial deposits appear to have developed downward into zones of pre-existing sheared rock associated with the fault. We interpret that these infilling deposits accumulated by non-tectonic processes; i.e., they are not tectonic fissure-fill deposits. The stratigraphic and structural relations in the trenches thus provide evidence for no Holocene surface faulting on the S-2 fault. The deposits exposed in the trenches are too young to evaluate late Pleistocene (i.e., 10 ka - 35 ka) or older Quaternary activity of the fault.

### 3.4.2 Salt Lake Fault

#### 3.4.2.1 Characterization of the Salt Lake Fault

The Salt Lake fault is a north-striking fault that can be traced confidently for approximately 12 miles (20 km) from north of Logan Creek to south of Funks Creek, within 1.5 miles (2.4 km) of the Sites dam site and within 1.7 miles (2.7 km) of the Golden Gate dam site (Figures 3-1 and 3-8). The Salt Lake fault passes through at least one proposed Saddle dam site (K. Buer, personal communication, 2000) The fault is visible on aerial photographs as a series of discontinuous topographic features, springs, and vegetation lineaments that coincide with truncated and locally folded strata of the Great Valley Group. The fault has been mapped by Brown and Rich (1961) and DWR

(1978, 1999) on the basis of the bedrock discontinuities (including truncated bedding and shear zones in bedrock), topographic lineaments (including topographic saddles, sidehill benches, and truncated ridges), salt water springs, gas seeps, and sag pond features.

From Salt Lake northward to Logan Creek, the Salt Lake fault coincides with a linear series of disrupted beds of the Great Valley Group, and associated topographic saddles and vegetation lineaments (Plate 1). North of Logan Creek, the fault is covered by deposits of the Pliocene-Pleistocene Tehama Formation (Chuber, 1961). During aerial reconnaissance, we observed that the trace of the Salt Lake fault coincided with a flowing spring near the base of the southern extent of the Tehama Formation outcrops, and that the surface of the Tehama Formation overlying the northward projection of the fault trace appeared to be undeformed. However, we were unable to obtain access to this location to verify our aerial observations in the field.

Brown and Rich (1961) mapped the Salt Lake fault south to the county road in sec. 17, T.17N., R.4W., about 1.5 miles (2.5 km) north of the town of Sites. We trace the Salt Lake fault at least as far south as the town of Sites (Figure 3-34). South of the county road, we map the fault trace through a small north-northeast-trending drainage. We interpret the Salt Lake fault to be offset about 500 ft (160 m) in a right-lateral sense by southwest end of the GG-2 fault, which we project through a developed spring west of the county road in the SW $^1/_4$ of sec. 18, T.17N., R.4W (Figure 3-34). The fault extends south of fault GG-2 through a series of north-south- and NE-SW-trending saddles and troughs along the eastern margins of the low hills centered on the Sites anticline axis. A trench across the map trace of the fault (SL-T1, described in detail below) exposed the eastern margin of a major shear zone within bedrock. South of the trench site, we associate deformed beds of the Boxer Formation exposed in the channel of Stone Corral Creek with the Salt Lake fault. The main trace of the fault is interpreted to coincide with sheared bedding and a perennial saline spring (Figure 3-34).

Figure 3-34

We selected a site on Hunters Creek to excavate paleoseismic trenches across the Salt Lake fault. The trenches were sited approximately 6.4 miles (10.3 km) northeast of the Golden Gate dam site on older terrace deposits of Hunters Creek that cross the fault (Figure 3-35), which is exposed in the north bank of Hunters Creek as folded and faulted bedrock. Although distant from the Golden Gate and Sites dam site the older terrace deposits adjacent to Hunters Creek provide a longer stratigraphic record for characterization of the activity of the Salt Lake fault per DSOD (1995) criteria.

At the Hunters Creek location, we initially excavated a long, shallow trench (FT-HC-1; Figure 3-36) across the inferred trace of the Salt Lake fault to confirm the location of the structure. We observed an abrupt west-side-down step in bedrock during excavation (Figure 3-37), and subsequently deepened the middle reach of the trench to better expose the bedrock step. We concluded that the step in the bedrock surface is associated with the Salt Lake fault. Detailed examination of the trench exposure (Figure 3-38) revealed that stream deposits overlying the fault and associated step in bedrock were warped and possibly deformed. To better assess and document these relations, we excavated an additional trench (Trench FT-HC-2) within thicker gravel deposits of the same stream terrace approximately 30 feet (10 m) to the north of trench FT-HC-1. Based on the presence of faulted Pleistocene gravels in Trench FT-HC-2, and in order to document the presence or absence of fault offset in younger deposits, we excavated an additional trench (Trench FT-HC-3) within a Holocene terrace south of Funks Creek.

Based on our field mapping of the southern end of the Salt Lake fault near Sites, we excavated an additional trench (Trench SL-T1) across the Salt Lake fault northwest of the town of Sites, in the vicinity of the Sites dam site. The purpose of the trench was to confirm the location of the main trace of the Salt Lake fault and, in combination with our geologic mapping and trenching of the topographic saddle to the east, document that the Salt Lake fault, or a related fault strand, does not extend beneath the proposed Sites dam site. Trench SL-T1 was located approximately 0.4 miles (0.6 km) northeast of the town

Figure 3-35

Figure 3-36

Figure 3-37

Figure 3-38

of Sites, north of the main Sites-Maxwell Road across the eastern margin of the fault (Figure 3-34).

At the SL-T1 trench location, the Salt Lake fault is distinguished by the presence of a subtle west-facing scarp adjacent to a north-south-trending topographic swale. To the south, the Salt Lake fault is exposed in the banks of Stone Corral Creek as a broad zone of folded and faulted bedrock at least 500 feet (150 m) wide. The zone of faulted and folded bedrock exposed along Stone Corral Creek is along projection of the scarp and topographic swale at the trench location that likely is the surface expression of the Salt Lake fault.

Based on exposure of a well-developed shear zone in trench SL-T1 (Figure 3-39), coincident with mapped geomorphic surface features northwest of Sites and projection of the exposure of the Salt Lake fault along Stone Corral Creek to the south, we conclude that the main Salt Lake fault is located west of the Sites dam site. Our mapping of the southern end of the Salt Lake fault, and trenching of the topographic saddle north of the Sites dam site (Section B.8; Appendix B) supports our interpretation that the Salt Lake fault, or a related fault strand, does not extend beneath the proposed Sites dam site. Stratigraphic relations exposed in the SL-T1 trench across the southern Salt Lake fault and in all three trenches (FT-HC-1, FT-HC-2, and FT-HC-3) across the Salt Lake fault at Hunters Creek are described below.

**Trench Exposure FT-HC-1**

Bedrock exposed in trench FT-HC-1 consists of vertical to sub-vertical sandstone and mudstone beds in fault contact (N60°E/70°SE) with sheared mudstone and siltstone (Figures 3-37 and 3-38). Within the north wall of trench FT-HC-1, a large, subangular bedrock boulder is bounded by faults (Figure 3-37). Within the south wall of trench FT-HC-1, the bedrock boulder is absent, but a large cast of the southern margin of the boulder is preserved within the trench wall (Figure 3-38). The boulder was deposited on a flat erosional surface cut on sandstone and mudstone and is bounded on the east by a

Figure 3-39

remnant of well-developed soil containing rounded pebbles (Unit 1). Soil development is consistent with a late Pleistocene (?) buried soil (Soil profile SP-9; Appendix C). The soil is faulted and the boulder appears to have been rotated within the fault zone, suggesting fault displacement occurred subsequent to emplacement of the boulder and development of the soil.

One possible origin for the boulder is that it is locally derived from degradation of a fault scarp developed in bedrock (i.e., collapse of the scarp). However, it is also possible that the boulder was deposited within the same pebbly silt stream deposit as that in which the relict soil, located between the boulder and bedrock to the east, is developed.

The bedrock, boulder, and the relict soil all have been eroded to form a sub-horizontal upper strath surface (Figure 3-37). This surface is down-dropped to the west approximately 3 feet (1 m) across the fault. The entire package (bedrock, boulder, and soil) is thrust over coarse, bedded stream gravel (Unit 2). The inferred fault scarp is overlain by a two-foot (0.7 m) thick package of coarse, sandy gravel (Unit 3). The gravel is significantly thicker west of the fault and appears warped across the fault zone. A small colluvial deposit (Unit 4), most likely derived from the underlying Unit 3 gravels, is preserved west of the fault on the warped gravels of Unit 3. Sandy gravel of Unit 5 is not found in the footwall of the fault. In the hanging wall, Unit 5 is overlain by sandy silt of Unit 7, possibly correlative to similar silty sand of Unit 6 in the western portion of the trench. A young stream channel deposit (Unit 8), with minimal soil development, is incised into Units 5 and 7.

Faulted soils and offset stream gravels exposed in Trench FT-HC-1 clearly document late Pleistocne activity on the Salt Lake fault. However, no datable material was obtained from Trench FT-HC-1. Soil profile SP-9 (Appendix C) of the faulted buried soil exhibits a well-developed stage III Bt horizon, suggestive of a late Pleistocene age. More than one surface-rupturing event likely is preserved in the trench stratigraphy based on the presence of the large boulder adjacent to a possible buried fault scarp, inferred rotation of

the boulder subsequent to deposition, and the presence of overlying warped stream gravels.

**Trench Exposure FT-HC-2**

Bedrock exposed in trench FT-HC-2 consists of sub-vertical, interbedded sandstone and mudstone in fault contact (076°/88°SE to 020°/58°E) with sheared mudstone and siltstone (Figures 3-40, 3-41, and 3-42). Bedrock is down-dropped approximately 4.5 ft (1.5 m), forming a buried west-facing scarp. Bedding changes across the fault from interbedded sandstone and mudstone oriented 005°/88°E to predominately mudstone oriented 355°/72°W. Bedrock west of the fault is pervasively sheared and fractured.

The Salt Lake fault is an east-dipping zone of sheared bedrock approximately 1.5 to 3 feet (0.5 to 1 m) wide (Figures 3-40 and 3-42). Within the fault zone, the main fault strand generally dips approximately 60° to 70° to the east. Secondary shears within the fault zone dip 60° to 88° and bound faulted bedrock blocks. The main fault strand is best expressed within the south wall of Trench FT-HC-2 as a well-defined main fault trace with up to 2 inches (5 cm) of fault gouge (Figure 3-40). Small (1-2 cm diameter) rounded stream pebbles from terrace gravels overlying bedrock are incorporated in the fault gouge.

The 4.5 ft (1.5 m) step in bedrock across the Salt Lake fault is overlain by 4.5 to 9 feet (1.5 to 3 m) of late Quaternary fluvial deposits (Figure 3-40). The basal alluvial deposit, Unit 1, consists of carbonate-cemented, clast-supported stream gravels preserved only within the foot wall west of the fault. Unit 1 is in conformable contact with similar, uncemented clayey gravels of Unit 2. On the south wall of Trench FT-HC-2 (Figure 3-40), similar gravels correlated to Unit 2 are preserved within the hanging wall east of the fault. On the north wall of Trench FT-HC-2 (Figure 3-42), it is unclear whether gravels of Unit 2 are preserved within the hanging wall. Unit 1 probably is correlative to Unit 2. The carbonate matrix of Unit 1 may be the result of localized precipitation of carbonate from groundwater ponded atop bedrock against the Salt Lake fault.

Figure 3-40

Figure 3-41

Figure 3-42

Units 1 and 2 are overlain by 1.5 feet (0.5 m) of well-bedded, well-sorted clayey gravel consisting of well-rounded pebbles (Unit 3). Gravel beds within Unit 3 in the hanging wall are back-tilted, coincident with overall eastward tilting of the underlying bedrock strath surface. Gravel beds within Unit 3 in the foot wall are sub-horizontal but progressively become vertical adjacent to the fault zone (Figures 3-40 and 3-42). In the south wall of the trench (Figure 3-39), beds within Unit 3 are rotated to subvertical between two strands of the faults.

Calcium carbonate ($CaCO_3$) coatings on the bottoms of pebbles within fluvial gravels of Unit 3 in the south wall of trench FT-HC-2 (Figure 3-40) provide additional evidence that the gravels have been progressively deformed by the Salt Lake fault. In the relatively undeformed beds located about 3 feet (1 m) west of the fault, 22 of 25 clasts (88%) had bottom coatings at a depth of 93 to 111 inches (237-282 cm) below the ground surface (Table 3-7). The high percentage of bottom coatings is consistent with the preferential precipitation of carbonate, either as part of soil development or groundwater processes, at the bottoms of the pebbles. In the vertically deformed section, adjacent to and within the fault zone, 9 of 25 clasts had left side coatings, 7 had left and bottom coatings, 4 had bottom coatings, 3 had bottom and right side coatings, 1 had a right side coating, and 1 had a coating that covered the top, left side, and the bottom (Table 3-7). The high percentage of carbonate coatings found on the tops and sides of the pebbles in the vertical section near the fault suggest that gravel beds of Unit 3 have been progressively rotated by the fault and that this deformation took place after deposition of the carbonate coatings.

Unit 4 consists of approximately 2 feet (0.75 m) of poorly sorted, moderately bedded fluvial gravel (Figures 3-40 and 3-42). Unit 4, although not as well-bedded as the underlying gravels in Unit 3, is clearly faulted and is thicker in the footwall of the fault than in the hanging wall. Approximately 9 feet (3 m) east of the fault, within the hanging wall, Unit 4 is only about 1.5 feet (0.5 m) thick and appears to have been eroded prior to deposition of the overlying fluvial flood deposits of Units 6 and 7.

**Table 3-7** Position of Carbonate Rinds on Pebbles

Rinds adhered to the sides of the pebbles are assumed to have been rotated from an original bottom-of-pebble position.

| Position of rind on pebble * | Number of pebbles | |
|---|---|---|
| | Deformed section of bed | Undeformed section of bed |
| Bottom | 4 | 22 |
| Left side | 9 | 0 |
| Bottom and left side | 7 | 0 |
| Top, bottom, and left side | 1 | 0 |
| Right side | 1 | 0 |
| Bottom and right side | 3 | 2 |
| All sides | 0 | 1 |
| TOTAL SAMPLED | 25 | 25 |

* As seen in the southwest wall of Trench FT-HC-2, downthrown western side of the Salt Lake fault. Vertical section (deformed section) of gravel bed is located adjacent to the fault plane at 220 to 240 cm depth (see Figure 3-40). Horizontal section of gravel bed is located 1 to 2 meters away from the fault plane at 237 to 282 cm depth.

Unit 5 consists of approximately 1 to 2 feet (0.3 to 0.7 m) of poorly sorted, unbedded clayey gravel similar to that of underlying gravel within Unit 4. Unit 5 is thickest directly west of the projection of the main fault strand (Figures 3-40 and 3-42). Based on the similarity of Unit 4 to the underlying gravels of Unit 3, location adjacent to the fault scarp, and thinning of Unit 4 within the hanging wall east of the fault and foot wall west of the fault, we believe that Unit 4 is a colluvial deposit derived from erosion of the underlying faulted gravels of Unit 4. In the south and north walls of Trench FT-HC-2 (Figures 3-40, 3-41, and 3-42) sheared mudstone and sandstone is thrust over bedded gravel of Units 1, 2, 3, and 4.

Units 6 and 7 are fine-grained overbank deposits consisting of yellowish-brown silt with minor gravel. These units are horizons of the modern soil profile. Unit 6 is exposed from 33 ft (10 m) to the south end of the trench, exhibits a well-developed blocky structure, and has a gradational lower contact. It represents the B-horizon of the modern soil. Unit 7 is exposed from 33 ft (10 m) to the south end of the trench, is gray-brown and characterized by prominent horizontal partings. The lower contact of this unit is gradational over 4 to 6 inches (10-15 cm). This unit represents the A-horizon of the modern soil.

The soil profile within trench FT-HC-2 (SP-11 in Appendix C) is characterized by an upper A-horizon with a massive to granular structure. The Bt horizon is 20 to 54 inches (50-137 cm) thick and is characterized by a prominent blocky structure. Ped faces within the Bt horizon are planar and orthgonal, giving the peds a cube-like blocky structure. This structure is similar to that of Bt horizons described in soil profiles in the Funks Creek area.

The upper modern soil horizons are formed in young deposits, possibly younger than 8-15 ka (J. Sowers. personal communication, 2000), based on similarity of the soils to early Holocene soils dated in the Funks Creek area. It is possible that fault offset of Unit 5 predates the development of the early Holocene soil profile within Units 5 through 7. However, a drop in the abundance of clay films across the projection of the main fault strand through Unit 5 suggests that offset of the deposit post-dates formation of the soil. An alternative explanation for the drop in clay films is that differences in the abundance of clay films reflects changes in the parent gravels juxtaposed across the fault. However, colluvial gravels of Unit 5 are very similar to, and appear to have been derived from, underlying fluvial gravels of Unit 4.

The lower portion of the soil profile within Units 3 and 4, all IIB horizons, are significantly older based on the presence of hard, dense $CaCO_3$ coatings and the presence of distinct to prominent reddish clay films that coat the $CaCO_3$ (Soil Profile 11; Appendix C). Based on the absence of thick clay films typical of 100 ka or older soils (Soil Profile

SP-11; Appendix C), the estimated age of the older gravels ranges from 30 ka to 70 ka (J. Sowers, personal communication, 2000). These late Pleistocene gravels are clearly deformed and faulted by the Salt Lake fault.

**Trench FT-HC-3**

Trench FT-HC-3 was extended east-west across the projection of the Salt Lake fault within a late Holocene terrace located south of Hunters Creek (Figure 3-35). Although excavated to the maximum working depth of the equipment, the trench was not deep enough to expose bedrock and, thus, the Salt Lake fault was not exposed. However, based on projection of exposures of the fault within trenches FT-HC-1 and FT-HC-2, and within bedrock exposed along Hunters Creek, we believe that trench FT-HC-3 crossed the trace of the Salt Lake fault.

Trench FT-HC-3 exposed 9 ft (3 m) of late Holocene fluvial and colluvial deposits (Figure 3-35). The basal colluvial deposit (Unit 1) is a 2.5-foot-thick (0.75 m), hard, very dark brown to dark yellowish brown pebbly clay. The unit contains abundant rounded pebbles, suggesting that the deposits may have a fluvial origin. The basal unit (Unit 1) is overlain by a series of interlapping stream deposits consisting of silt to sandy gravel lenses.

The original stratigraphy of Unit 1 is obscured by pedogenic churning associated with the development of a vertisol within the deposits (see Soil Profile SP-12; Appendix C). Due to the development of deep, vertical soil peds, any original stratigraphic and structural features have been obliterated and, thus, the presence or absence of fault-related deformation cannot be documented within Unit 1. In addition, the degree of soil development within the deposits is suggestive of early to mid-Holocene age (J. Sowers, pers. comm, 2000) (Soil Profile SP-12; Appendix C). The combination of deposits that are too young for evaluation of inactivity of the fault, per DSOD criteria, presence of a vertisol that obscures stratigraphy, and the broad uncertainty on the location of the Salt Lake fault limits the utility of assessing late Quaternary fault activity within Trench FT-HC-3.

**Trench Exposure SL-T1**

Trench SL-T1 was extended 217 feet (66 m) east-west across the eastern margin of the Salt Lake fault (Figure 3-39). The trench exposed mudstone of the Cretaceous Great Valley Group (Figures 3-39 and 3-43). We documented 59 ft (18 m) of intensely sheared and disrupted mudstone at the western end of the trench juxtaposed against over 155 feet (48 m) of relatively intact, north-south trending, east-dipping bedded mudstone exposed in the eastern portion of the trench. Within the shear zone exposed in the western end of the trench, fractures cut bedding, and typically are coated with calcium carbonate (Figure 3-43). Mudstone bedding, where preserved, generally trends north-south and dips east but locally is intensely sheared with vein-infilling evidence for repeated displacement. Unsheared mudstone bedrock west of the fault zone contains minor, bedding-parallel fractures. Based on the well-developed shear zone within bedrock, coincident with geomorphic surface features and projection of the exposure of the fault along Stone Corral Creek to the south, we conclude that the shear zone exposed in trench SL-T1 is the Salt Lake fault shear zone.

With the exception of a thin colluvial soil layer, the trench did not expose late Quaternary stratigraphy. The colluvial deposits extend across the Salt Lake fault zone and are not deformed, faulted, or sheared. However, the colluvial soil is poorly developed and thus the colluvial deposits likely are late Holocene or younger. During our earlier geomorphic mapping of stream terraces along Stone Corral Creek, we did not identify Quaternary deposits of sufficient age for evaluation of fault activity (i.e. DSOD criteria).

**Summary of Trench Exposures, Salt Lake Fault**

Three trenches were excavated across the Salt Lake fault. The trenches show that the fault is a narrow 1- to 2-ft- (0.25 to 0.5 m) wide, east-dipping (60° to 80°) plane. The presence of well-developed clay gouge, rotated pebbles and boulders within the fault zone, stratigraphic correlation of progressively faulted units, and the presence of multiple colluvial wedges provide evidence of repeated incremental displacement on the Salt Lake

Figure 3-43

fault within the late Quaternary. Soil profiles developed in Pleistocene gravels are estimated to be 30,000 to 70,000 years old and are offset and warped by the fault. In combination with our mapping, exposure of a well-developed shear zone in trench SL-T1 indicates that the Salt Lake fault extends south as far as Stone Corral Creek near the town of Sites. However, our field mapping and trench exposures document that the Salt Lake fault is located west of the Sites dam site and does not pose a surface faulting hazard to the dam site.

#### 3.4.2.2 Earthquake History of the Salt Lake Fault

Late Quaternary deposits exposed within trenches at Hunters Creek have been faulted and warped by repeated offset on the Salt Lake fault, producing an upstream-facing scarp in bedrock and overlying fluvial gravels, uplift and erosion of the hanging wall, and a series of colluvial wedge deposits in the foot wall block.

Based on reconstruction of faulted and folded stratigraphic units (Figure 3-44), we document a minimum of one surface rupturing event and interpret at least three events that postdate formation of a bedrock strath surface buried beneath the alluvial deposits. Faulted fluvial gravels exposed at the base of trench FT-HC-2 (Figure 3-40) are late Pleistocene age (30 ka to 70 ka based on Soil Profile SP-11, Appendix C). Based on soil development within upper deposits exposed within trench FT-HC-2 (Figure 3-40), including within an offset colluvial wedge (Unit 5), it is possible that the most recent fault offset occurred during the late Pleistocene to early Holocene (8 to 12 ka).

Restoring the base of Unit 5, offset by the main trace of the Salt Lake fault, requires 1.3 feet (0.4 m) of dip-slip displacement (reconstruction Part B, Note 2; Figure 3-44). Unit 5 is a faulted, poorly sorted gravel deposit preserved on the foot wall side of the fault that is very similar to, and probably derived from, underlying faulted gravels of Unit 4. It is our interpretation that Unit 5 is a colluvial wedge deposit derived from uplift and subsequent erosion of Unit 4 in the hanging wall of the fault. Although the base of Unit 5 is restored

Figure 3-44

by 1.3 feet (0.4 m) of dip-slip displacement, the contacts between underlying stratigraphic units 1, 2, 3, and 4 are not fully restored. In addition, the top of Unit 5 is over-restored (reconstruction Part B, Note 3; Figure 3-44). We interpret the upper part of Unit 5 to represent a younger colluvial wedge derived from faulting of an older colluvial wedge (i.e. the lower part of Unit 5). As discussed previously, it is possible that fault offset of Unit 5 predates the development of the early Holocene soil profile within Units 5 through 7. However, the drop in the abundance of clay films to the west (within the foot wall) across the projection of the main fault strand through Unit 5 strongly suggests that fault offset post-dates soil development within Unit 5.

Restoring the base of Unit 4 requires an additional 1.3 feet (0.4 m) of offset for a total of 2.6 feet (0.8 m) of displacement (reconstruction Part C, Notes 2 and 3; Figure 3-44). This does not fully restore stratigraphic contacts between Units 1, 2, and 3; however, the inferred offset does restore an eroded strath surface developed within Unit 4 (reconstruction Part C, Note 1; Figure 3-44). We infer that the strath surface within Unit 4 probably was developed on a pre-existing fault scarp based on the changes in thickness and apparent warped bedding within Unit 4. This strath surface was offset by subsequent fault displacement (Event 1 shown on reconstruction Part B; Figure 3-44).

Restoring lateral continuity of Unit 2 and the underlying bedrock strath surface, offset by the main trace of the Salt Lake fault, requires an additional 1.3 feet (0.4 m) of offset for a total of 3.9 feet (1.2 m) of cumulative displacement (reconstruction Part D, Notes 1 and 2; Figure 3-44). Lateral continuity of Unit 3 across the fault is not restored, however. Based on the absence of Unit 3 within the hanging wall directly adjacent to the fault, it is likely that Unit 3 was deposited on a strath surface formed after the reconstructed Event 3 (reconstruction D; Figure 3-44), but possibly faulted prior to reconstructed Event 2 (reconstruction C). Thus, it is possible that a record of more than three fault offsets are preserved within trench FT-HC-2.

To summarize, we interpret stratigraphic and structural relations in the trench exposures as evidence for a minimum of three discrete surface-faulting events. The discrete fault

offsets may represent characteristic displacements on the Salt Lake fault of approximately 1.3 feet (0.4 m) during large earthquakes on the main underlying Funks segment of the Great Valley thrust fault. Although we cannot preclude the possibility that the total measured offset along the fault of 3.9 feet (1.2 m) of the bedrock strath surface occurred during a single event, we believe that the presence of multiple scarp-derived colluvial wedges, mismatch of individual units, and presence of well-developed fault gouge are best explained by the occurrence of several discrete faulting events subsequent to formation of the bedrock strath surface.

The development of horizontal, restorable strath surfaces on the alluvial gravels and well-developed buried soils strongly suggests that significant periods of relative stability occurred between faulting events. If this interpretation is correct, then it appears to preclude on-going incremental (i.e. less than 0.4 m) repeated fault offset or creep.

#### 3.4.2.3 Activity Assessment, Salt Lake Fault

Based on evidence for at least one and probably three or more surface-faulting events that have deformed a gravel deposit estimated to be about 30 ka to 70 ka in age, we conclude that the Salt Lake fault likely has been active during the past 35,000 years. The fault should thus be considered active per DSOD criteria (Fraser, 1997).

Although the Salt Lake fault exhibits evidence for multiple late Quaternary surface ruptures, we do not believe that the fault is likely to be an independent source of moderate to large earthquakes. Seismic reflection data analyzed for this study (Appendix A) show that the Salt Lake fault dips east, parallel to bedding in the Great Valley group, and terminates downdip against the Funks segment of the Great Valley fault at a maximum depth of 3.1 miles (5 km) (Figure 3-2). These relations indicate that the Salt Lake fault is confined to the shallow upper crust where little seismic moment is released during earthquakes; the fault does not extend to deeper, higher-strength regions of the crust where significant elastic strain energy accumulates and moderate to large magnitude earthquakes nucleate (Sibson, 1982). We therefore conclude that the Salt Lake fault probably is not capable of storing and releasing significant elastic strain energy.

Our preferred explanation for Quaternary surface rupture is that triggered or sympathetic movement occurs on the Salt Lake fault moves during moderate to large magnitude earthquakes on the underlying Funks segment of the Great Valley fault. Triggered slip on faults from nearby earthquakes is a relatively well-documented phenomenon. For example, triggered aseismic slip was observed on thrust faults in the southwestern Santa Clara Valley following the 1989 Loma Prieta earthquake, which occurred on a blind reverse-oblique fault beneath the Santa Cruz mountains to the southwest (Hitchcock and Kelson, 1999). Triggered, aseismic slip also was documented on the Hilton Creek fault, an active segment of the Sierra Nevada frontal fault system, during a sequence of moderate earthquakes in Long Valley caldera in 1980 that were located north of the fault trace (Taylor et al., 1980).

A more relevant example, and a potential analogue for the Salt Lake fault, is the Nunez fault, which is located along the western margin of the San Joaquin Valley in the Coast Ranges-Sierran Block boundary zone (CRSBZ) and is associated with the Coalinga anticline. The Nunez fault produced localized surface rupture, and possibly several small (M 5) aftershocks in the upper 3.1 miles (5 km) of the crust, following the 1983 M 6.3 Coalinga earthquake on a segment of the Great Valley fault at 6.2 to 8.1 miles (10-13 km) depth (Hart and McJunkin, 1983). Like the Salt Lake fault, the Nunez fault dips east and is antithetic to the west-dipping thrust fault that was the source of the mainshock. The example of the Nunez fault suggests that relatively shallow reverse faults in the CRSBZ may produce localized surface rupture during moderate to large magnitude earthquakes on segments of the underlying Great Valley fault, rather than acting as independent seismic sources.

Using the Nunez fault as an analogue, we infer that the relatively shallow Salt Lake fault may rupture at the surface sympathetically during or following a larger event on the Funks segment of the Great Valley fault at depth. We further test and evaluate this hypothesis in Chapter 5 using numerical models based on elastic dislocation theory. It is possible that the Salt Lake fault may produce some aftershocks following an earthquake

on the Funks segment, but given its shallow depth it is not likely to be a significant, independent seismic source for moderate to large magnitude earthquakes.

### 3.4.3 Fault S-3

The S-3 fault is a bedrock fault exposed in a south-facing wall of the Sites Quarry north of Stone Corral Creek, approximately 0.9 miles (1.5 km) east of the Sites dam site (Figure 3-29). Within the Sites Quarry exposure, the fault is steeply dipping to subvertical (Figure 3-45). The S-3 fault was not recognized or mapped by Brown and Rich (1961). The S-3 fault exposure was first discovered by DWR geologists and subsequently identified and mapped on aerial photographs and in the field during this study.

The S-3 fault strikes parallel to bedding and is coincident with a linear series of prominent sandstone beds of the Great Valley Group. The S-3 fault was recognized and traced in the field by alignment of subtle saddles and other topographic irregularities, the presence of fractured bedrock and carbonate (typically found in the field as 'float'), and local coincidence with animal burrows. The sense of lateral separation, if any, and total vertical displacement across the fault are not known. Fault S-3 can be traced confidently for approximately 2.4 ± 0.1 miles (3.9 ± 0.2 km) between the Sites Quarry and the GG-3 fault (Figure 3-8). The S-3 fault is offset to the northeast by the GG-3 fault (Figure 3-29), and is less confidently traced approximately 3 ± 0.5 miles (4.8 ± 0.8 km) to the north. The S-3 fault appears to be offset to the northeast several hundred feet by the GG-2 fault. The closest approach of the S-3 fault to the Golden Gate dam site is approximately 600 feet (200 m).

Figure 3-45

**Table 3-8** Geomorphic and Stratigraphic Field Descriptions for Fault S-3
(see Figures 3-18 and 3-29 for station locations)

| Station | Field Description |
|---|---|
| S3-1 (Figure 3-29) | Sites Quarry exposure. |
| S3-2 (Figure 3-29) | East-facing scarp. Carbonate float. |
| S3-3 (Figure 3-29) | Drag folds in bedding. Fault offset by S-1 fault. |
| S3-4 (Figure 3-18) | East-facing scarp. Carbonate float. |
| S3-5 (Figure 3-18) | Bedrock shear exposure |
| S3-6 (Figure 3-18) | Spring. Topographic linear depression. Carbonate float. |

The S-3 fault underlies Holocene to historic deposits along Stone Corral Creek south of the Sites Quarry (Figure 3-29). The very young age of these deposits renders them unsuitable for evaluating activity of the fault per DSOD criteria. However, the mapped offset of the S-3 fault by the S-2, GG-3, and GG-2 faults strongly suggests that the S-3 fault is older than these structures. Restoration of lateral slip along the GG-1, GG-2, GG-3, and S-2 faults reconnects offset Great Valley Group marker beds and returns the S-3 fault to a continuous, linear feature (Figure 3-46). The restoration of the S-3 fault strongly suggests that the S-3 fault is an older bedrock fault that predates offset along the GG-2 and 3 and S-2 faults.

Based on trenches across the S-2, GG-3, and GG-2 faults that directly and indirectly document unfaulted early Holocene deposits, these faults have not experienced surface

Figure 3-46

displacement events in the Holocene. The cumulative offset of the S-3 fault by these faults, and localized drag folding of the S-3 fault across the S-2 fault, suggest repeated and incremental offset of the S-3 fault over time. It is therefore probable that surface displacement on the S-3 fault occurred prior to development of the S-2, GG-3, and GG-2 faults and likely significantly predates the 35,000-year DSOD criteria for activity.

We excavated three trenches (FT-T1-S3, FT-T2-S3, and FT-T5-S3; Figures 3-9 and 3-29) across S-3 fault, north of the GG-3 fault. The purpose of these trenches was to confirm the location of the fault and characterize the width of the fault zone. These trenches were excavated within bedrock across the inferred trace of the fault. Trench locations were chosen based on our previous air photo interpretation and field mapping, the presence of a prominent east-facing scarp, and the presence of carbonate float.

In addition, we excavated three additional paleoseismic trenches (FT-T3-S3, FT-T4-S3, and FT-T6-S3; Figures 3-9 and 3-47) within the oldest mapped stream terrace south of Funks Creek. These trenches were excavated to confirm the location of the S-3 fault near the Golden Gate dam site and to evaluate the activity of the S-3 fault, specifically by documenting the presence or absence of vertical and/or horizontal offset of late Quaternary deposits. The trenches exposed the S-3 fault zone in bedrock, the unfaulted back edge of a stream terrace, and overlying unfaulted early Holocene terrace deposits.

**Trench Exposure FT-T1-S3**

Trench FT-T1-S3 was 65 feet (20 m) long, 5 feet (1.5 m) deep, and oriented east-west across the S-3 fault (Figure 3-9). We excavated trench FT-T1-S3 across an east-facing scarp located based on our field mapping (Figure 3-48). The scarp coincides with a resistant east-dipping sandstone bed exposed in the center of the trench (Figure 3-49). The trench exposed the S-3 fault in bedrock, overlain by a thin mantle of unfaulted colluvial deposits. The S-3 fault is expressed as a well-defined zone of bedding-parallel faulting approximately 6 feet (2 m) wide. The fault zone is within east-dipping bedded mudstone bounded by unfaulted, intact interbedded sandstone and mudstone (Figure 3-49). Steeply east-dipping to sub-vertical faults within the S-3 fault zone truncate

Figure 3-47

Figure 3-48

Figure 3-49

bedding.

**Trench Exposure FT-T2-S3**

The FT-T3-S3 trench was 30 feet (10 m) long and oriented east-west across the S-3 fault approximately 0.6 miles (1 km) south of Funks Creek (Figures 3-9 and 3-47). We excavated trench FT-T2-S3 across an east-facing scarp coincident with the mapped trace of the S-3 fault. As in trench FT-T1-S3, the scarp coincides with a resistant east-dipping sandstone bed exposed as a dip slope at the west end of the trench (Figure 3-50). In order to obtain a better exposure of the fault in bedrock, we benched the trench at approximately the 6-foot-depth (2-m-depth) and deepened the trench for a total depth of 9 feet (3 m).

Trench FT-T2-S3 exposed the S-3 fault in bedrock (Figure 3-50). The S-3 fault is expressed as a well-defined zone of bedding-parallel faulting approximately 9 feet (3 m) wide within east-dipping bedded mudstone. Within the S-3 fault zone, locally intense shearing obscures relict mudstone bedding and steeply east-dipping to sub-vertical fault shears truncate beds. Along major shears, well-developed clay fault gouge with abundant calcium carbonate is common. East of the fault zone, mudstone bedrock is relatively intact with minor bedding parallel fractures (Figure 3-50). The intact sandstone bed west of the fault has formed a scarp along much of the mapped trace of the S-3 fault, providing evidence that the S-3 fault is preferentially located within the same stratigraphic horizon along strike.

Within trench FT-T2-S3, the S-3 fault is overlain by unfaulted colluvial deposits. The colluvium is up to 3 feet (1 m) thick and is thickest across the S-3 shear zone where hillslope erosion has preferentially removed less-resistant material present within the shear zone. The colluvium consists of brown silty clay with minor subangular sandstone clasts and has poorly developed soil structure. Above the S-3 shear zone, erosion apparently has undercut mudstone beds, causing these beds to tilt uphill. Alternatively, internal deformation within the fault zone tilted the beds to subhorizontal bedding. These beds have then been exposed by erosional exhumation of the fault zone.

Figure 3-50

**Trench Exposures FT-T3-S3, FT-T4-S3, and FT-T6-S3**

Three trenches (FT-T3-S3, FT-T4-S3, and FT-T6-S3) were excavated across the southern margin of the Qt1 stream terrace south of Funks Creek (Figures 3-9 and 3-47). At this location the back edge of the terrace, cut into bedrock of the Great Valley Group, obliquely crosses the S-3 fault (Figures 3-47 and 3-51). We excavated trenches across the terrace margin in order to document the presence or absence of: (1) vertical offset of terrace deposits that overlie the S-3 fault zone; and (2) horizontal offset of the terrace back edge across the fault.

Trench FT-T3-S3 was 36 feet (11 m) long, up to 5 feet (1.5 m) deep, and oriented east-west across the S-3 fault (Figure 3-9). We excavated trench FT-T3-S3 across an east-facing scarp coincident with the edge of stream terrace Qt1 based on our field mapping (Figure 3-51). The scarp coincides with a resistant east-dipping sandstone bed exposed in western end of the trench (Figure 3-52).

The trench exposed the S-3 fault in bedrock overlain by unfaulted stream terrace deposits, which, in turn, are covered by slope-derived colluvial deposits (Figure 3-52). The S-3 fault is expressed in trench FT-T1-S3 as a well-defined zone of bedding-parallel faulting approximately 4 feet (1.5 m) wide. The fault zone is within east-dipping bedded mudstone bounded by unfaulted, intact interbedded mudstone on the east and resistant sandstone on the west (Figure 3-52). Within the S-3 fault zone, steeply east-dipping shears are primarily bedding parallel although several truncate bedding. The S-3 shear zone and adjacent intact bedrock have been eroded by Funks Creek, forming a horizontal bedrock strath surface covered by stream terrace deposits. At this location, the stepped back edge of the terrace is coincident with the western margin of the S-3 shear zone, although bedded gravels at the base of the terrace are undeformed.

Based on the coincidence of the S-3 fault zone with the back edge of stream terrace Qt1, we decided to excavate trench FT-T4-S3 6 feet (2 m) to the north. Trench FT-T4-S3 (Figure 3-53) was 23 feet (7 m) long, up to 5 feet (1.5 m) deep, and oriented east-west across the S-3 fault. We excavated trench FT-T4-S3 across the edge of stream terrace

Figure 3-51

Figure 3-52

Figure 3-53

Qt1 (Figure 3-51). As in trench FT-T3-S3, the trench expose a resistant east-dipping sandstone bed in western end of the trench and inset terrace deposits of Qt1 (Figure 3-53). In trench FT-T4-S3, the stepped back edge of the terrace is located west of the S-3 shear zone. The stream-cut surface at the base of the terrace crosses the S-3 shear zone, and intact mudstone bedrock west of the fault, with no apparent vertical offset. In addition, bedded gravels at the base of the terrace that cross the fault zone clearly are undeformed.

We excavated FT-T6-S3 across the S-3 fault zone and inferred Qt1 terrace margin. At this location, the back edge of the Qt1 terrace is located east of the S-3 fault. Our intention was to confirm that the terrace back edge was not laterally offset by the S-3 fault. Trench FT-T6-S3 was 49 feet (15 m) long, up to 5 feet (2 m) deep, and oriented east-west across the S-3 fault (Figure 3-9). At this location, however, a topographic swale and associated stream channel deposits, intersects terrace Qt1 within the western portion of the trench. As a result, the stratigraphy within trench FT-T6-S3 is not as clear as in the adjacent trenches (Appendix B). In particular, we were unable to definitely identify the terrace back edge, although we believe that it is located near the center of the trench. If our interpretation is correct, there is no observable lateral offset of the early Holocene Qt1 terrace across the S-3 fault. Alternatively, if the inferred channel associated with the topographic swale is actually the western margin of terrace Qt1, the terrace margin may parallel the fault and we can not definitely preclude lateral offset across the S-3 fault. Our preferred interpretation, supported by our geomorphic mapping of the Qt1 terrace surface, is that there is no offset of the Qt1 terrace across the S-3 fault.

**Summary of Trench Exposures, S-3 Fault**

Six trenches across the S-3 fault reveal that the structure is a narrow, well-defined zone of bedding-parallel shearing. Based on our mapping, and confirmed by trenching, the S-3 fault is preferentially located along strike at, or adjacent to, a stratigraphic contact between resistant sandstone bed(s) and thick mudstone unit within Great Valley Group bedrock. The presence of bedding-parallel shears within ductile mudstone, adjacent to intact sandstone bed bounding, suggest that the S-3 fault primarily has accommodated

layer-parallel shearing.

Trenches across the S-3 fault confirm the mapped offset of the S-3 fault by the GG-3, and GG-2 faults. Based on trenches within early Holocene terrace deposits across the S-3 fault that document the absence of horizontal and vertical fault displacement, the S-3 fault has not experienced surface displacement events in the Holocene. The cumulative offset of the S-3 fault by the GG faults, and localized drag folding of the S-3 fault across the S-2 fault, suggest repeated and incremental offset of the S-3 fault over time.

Our preferred interpretation of the S-3 fault is that it has accommodated layer-parallel shearing of bedding during uplift and eastward tilting of the Great Valley group strata along the western margin of the Sacramento Valley. The majority of shearing on the S-3 fault may have occurred in the early stages of uplift and tectonic wedging during late Cretaceous-early Tertiary time, as discussed in Section 3.3 (see also Figure 3-4a, b). Based on map relations, we interpret that the original trace of the S-3 fault has been offset by the S-2, GG-3 and GG-2 faults, which we infer to have occurred during later growth of the Sites anticline (Figure 3-4c). If this interpretation is correct, and if the S-3 fault remains parallel to bedding downdip, then it is likely that the fault dies out in the upper 2 to 3 mile (3-4 km) depth range as the Great Valley strata flatten eastward beneath the Sacramento Valley (Figure 3-2). Like the Salt Lake fault, the S-3 fault lacks significant rupture area and does not extend deep enough to be an independent source of earthquakes (see discussion, Section 3.4.2.3). In the current tectonic setting, we infer that the S-3 fault is not active but may accommodate minor, aseismic surface displacement during incremental uplift of the Great Valley associated with moderate to large earthquakes on the underlying Great Valley fault. We conclude that the S-3 fault is not an independent seismic source.

### 3.4.4 Great Valley Fault

As discussed in Section 2.3, we interpret that the western edge of the Sacramento Valley is underlain by a system of blind thrust faults that dip west beneath the Coast Ranges. These faults lie within a zone of contractional deformation that Wong and Ely (1983) and

Wong et al. (1988) called the "Coast Ranges-Sierran Block Boundary Zone". Subsequent workers have referred to the system of blind thrust faults within this zone as the "Great Valley fault" (Working Group on Northern California Earthquake Potential, 1996; CDWR, 1999). For convenience, we adopt the latter term for this report, with the understanding that the "Great Valley fault" is a system of geometrically and structurally distinct thrust-fault segments rather than a single continuous fault (Wakabayashi and Smith, 1994; O'Connell and Unruh, 2001). A segment of the Great Valley fault beneath the Coalinga anticline in the western San Joaquin Valley was the source of the M6.5 1983 Coalinga earthquake (Wentworth and Zoback, 1989). Recent investigations by U.S. Bureau of Reclamation (WLA, 1997; O'Connell and Unruh, 2000) have documented evidence for Quaternary activity of segments of the Great Valley fault in the western Sacramento Valley south of the Sites and Golden Gate dam sites. In particular, O'Connell and Unruh (2000) interpreted that the moderate-magnitude 1892 Winters-Vacaville earthquake sequence occurred on a structural segment of the Great Valley fault in the southwestern Sacramento Valley.

We recognize at least five discrete geometric segments of the Great Valley fault system along the northwestern Sacramento Valley margin between the towns of Williams and Orland (Figure 3-54; see Appendix A for additional discussion). From south to north, the segments are informally designated as follows:

- Bear Valley Segment
- Funks Segment
- Willows Segment
- Elk Creek Segment
- Orland Segment

The Funks segment (Figure 3-54), which is the closest segment to the dam sites, exhibits a tectonic wedge geometry; that is, there is a ramp-flat transition beneath the Fruto syncline that has produced some fault-bend folding of the hanging wall block, and backthrusting has occurred along the Salt Lake fault to accommodate underthrusting of

Figure 3-54

the hanging wall block beneath the western Sacramento Valley margin (Figure 3-2; Section 3.3). In contrast, the Bear Valley segment to the south, as well as the Willows, Elk Creek and Orland segments to the north, are characterized by fault-propagation folding; (i.e., displacement on the thrust fault is consumed by folding of the hanging wall block, with no significant backthrusting or wedging at the thrust tip) (Appendix A). The Willows, Elk Creek and Orland segments progressively steepen northward, and the eastern limit of deformation steps abruptly eastward moving north of the boundary between the Elk Creek and Orland segments (Figure 3-54).

### 3.4.4.1 Funks Segment, Great Valley Thrust Fault

#### *3.4.4.1.1 Length of the Funks Segment*

The array of 2-D seismic reflection lines available for this study (Appendix A) indicate that the northern termination of the Funks segment lies between Hunters and Logan Creeks (Figure 3-54) (Appendix A). The southern segment boundary underlies the S-2 fault (Section 3.2). The Funks segment steps down to the Bear Valley segment by about 1 mile (1.6 km) across the southern segment boundary. Total length of the Funks segment measured between its northern and southern terminations is about 11 mi (17 km).

#### *3.4.4.1.2 Activity of the Funks Segment*

The Great Valley fault is a blind thrust fault, and is not exposed at the earth's surface. Standard paleoseismic methods of trenching the fault to assess recency and timing of surface-rupturing events cannot be used to evaluate the activity of the Great Valley fault. Consequently, we use indirect lines of evidence to assess activity, including trenching investigations of secondary faults like the Salt Lake fault that are genetically related to the Great Valley fault, and geomorphic studies of surface uplift and folding related to slip on the fault at depth. Indirect lines of evidence for activity or non-activity of the Funks segment are presented in the following sections.

**Activity of the Salt Lake Fault**

Our model for the origin of surface faults and folds proximal to the DWR dam sites (Section 3.3) links activity of these structures to slip at depth on the Funks segment of the Great Valley fault. In particular, the Salt Lake fault is interpreted to splay upward and derive its slip from the flat part of the Funks segment (Figures 3-2 and 3-3). We therefore interpret paleoseismic evidence for late Quaternary surface rupture on the Salt Lake fault, described in Section 3.4.2, as indirect evidence for late Quaternary activity of the Funks segment.

**Late Quaternary Incision of the Coast Ranges West of Fruto Syncline**

We hypothesize that late Quaternary reverse slip on the Funks segment would produce observable and quantifiable uplift of the hanging wall block. For a given magnitude of slip, we expect greater uplift above the more steeply dipping ramp part of the fault west of the Fruto syncline axis than above the more gently dipping flat to the east (Figure 3-2). To test this hypothesis, we employed quantitative geomorphic analysis to map loci of Quaternary uplift in the vicinity of the Funks segment and assess their relationship to segments of the Great Valley fault.

We prepared a topographic residual map of the eastern Coast Ranges, foothills, and western Sacramento Valley (Figure 3-55) to identify areas of anomalous Quaternary stream incision. If it is assumed that erosional relief is a response to tectonic uplift, then residual maps indirectly document the loci and magnitude of uplift. Residual relief maps are derived from "envelope" and "sub-envelope" maps, using methods developed by Strahler (1952). An envelope map is an interpretation of the pre-incision landscape that is created by interpolating a smooth, continuous surface that connects interfluves and flattish summit surfaces. The sub-envelope map is a smooth, continuous surface formed by interpolating among the thalwegs of second-order drainages, and is interpreted to represent the current level of stream incision. The "residual" relief is derived by subtracting the elevation of the envelope surface from the sub-envelope surface at a point; a residual map is the contoured values of the residuals at many points.

Figure 3-55

We used an algorithm based on work by George Hilley of Arizona State University (pers. comm., G. Hilley, 2000; Hilley and Arrowsmith, 2000) to compute the envelope, subenvelope, and residual surfaces from 30-meter Digital Elevation Models (DEMs). The upper envelope surface is calculated by taking elevations from ridgelines in a landscape, derived from DEM data, and interpolating a gridded surface from these points. The subenvelope surface is calculated by first calculating approximate stream channel bottoms and then interpolating a gridded surface between those points. By subtracting the subenvelope surface from the envelope surface, the erosional relief within drainage basins is quantified. Our computations were performed with the aid of ArcView 3.2 and Surfer 7 running on a Windows NT operating system.

The residual map (Figure 3-55) clearly shows a zone of localized and pronounced fluvial incision above the ramp in the Funks segment. The magnitude of the residual erosional relief is at least 1000 feet (300 m). The localized high incision values also are associated with a pronounced west-side-up step in the topography, where the average surface elevation increases by about 1000 to 1310 feet (300 to 400 m) moving from east to west across the Fruto syncline axis. We attribute both the high residual values and increased surface elevation to localized uplift above the ramp in the Funks segment. In particular, we note that the zone of high residual relief terminates southward at the inferred southern boundary of the Funks segment, consistent with our interpretation of the location of the southern segment boundary (Section 3.4.4.1.1).

For comparison, high residual values of 1000 feet (300 m) or more also are associated with the Rumsey Hills (Figure 3-55), an actively growing anticline associated with a segment of the Great Valley thrust fault system about 28 miles (45 km) south of the DWR dam sites (Plate 1; Section 3.5.7). The correlation of anomalous incision with a well-studied active anticline lends additional confidence to our interpretation that high residual values above the Funks segment are associated with localized Quaternary uplift.

Although we cannot date the timing of the uplift and fluvial incision above the ramp section of the Funks segment, we infer that it occurred during the Quaternary because

incision of the northern Coast Ranges foothills regionally postdates deposition of the 1.0-3.3 Ma Tehama Formation. The deep, narrow morphology of the canyons further suggests that incision is an on-going process in the eastern Coast Ranges and foothills region.

Our tectonic interpretation of high topographic residuals west of the DWR dam sites is reasonable because, unlike streams to the north, the upper reaches of streams in the vicinity of the Golden Gate and Sites dam sites do not extend across the entire foothills region. Stone Corral, Funks, Hunters, and Logan Creeks terminate east of the area of inferred uplift and currently have poorly developed drainage areas. Deep incision across resistant sandstone ridges of the Great Valley Group, however, suggest that these creeks originally were higher energy streams, possibly with larger drainage areas. Uplift above the Funks segment ramp may have disturbed previous drainage patterns in this region. East-west wind gaps within the areas of high topography west of the dam sites, east of Lodoga, are possible evidence of truncation of the upper drainage areas of these streams. In addition, gravels in older terraces preserved along Hunters and Logan Creeks north of the dam sites are well-rounded and of varied lithology. The abundance of well-rounded chert pebbles, volcanic clasts, and other lithologies that are rare in the Great Valley Group (but common in the Franciscan complex) in older terraces suggests significant transport distances and indicates that the drainage basins of major creeks in the area may originally have extended farther west prior to Quaternary uplift above the Funks segment ramp.

**Deformation of Fluvial Terraces along Hunters Creek**

Our kinematic model (Section 3.3) posits that growth of the Sites anticline is a direct result of slip on the Funks segment of the Great Valley fault. We thus interpret activity or non-activity of the fold to provide indirect evidence of activity or non-activity of the Funks segment. To assess Quaternary activity of the Sites anticline and Fruto syncline, we first mapped and surveyed remnants of Quaternary fluvial terraces along Hunters Creek (Figure 3-56). The elevations of terrace remnants, as well as the elevation of the modern channel thalweg, were correlated along the length of Hunters Creek to construct

Figure 3-56

longitudinal profiles of the terraces (Figure 3-57). We assume that the terrace surfaces originally had concave profiles similar to that of the modern Hunters Creek channel. Departures from a concave profile (i.e., local convexities) were compared to the axes of folds and assessed for evidence of activity of the Sites anticline and Fruto syncline (Figure 3-57).

The terrace profiles along Hunters Creek provide good evidence for late Quaternary fold deformation. Terraces diverge from each other over the Sites anticline and converge toward the Fruto syncline axis (Figure 3-57). In particular, the divergence of the highest terraces over Sites anticline represent a major convexity in their longitudinal profiles, which we directly attribute to late Quaternary growth of the Sites anticline.

To more clearly illustrate patterns of terrace deformation, we plotted the height of the T3 (green) and T5 (red) terraces above the modern Hunters Creek channel (bottom graph, Figure 3-57). Because the channel thalweg has a concave shape, plotting the terrace heights above the channel is equivalent to subtracting what we assume to be an original concave geometry from the present terrace profiles, thus more clearly revealing the presence and dimensions of profile convexities. The net or "residual" profiles for both the T3 and T5 terraces show a well-defined antiformal fold over the Sites anticline. The amplitude of the fold in the T5 terrace profile is several times that of the fold in the T3 terrace profile, which we interpret as evidence for progressive growth of the Sites anticline during the Quaternary.

To summarize, we interpret well-defined convexities in longitudinal profiles of fluvial terraces along Hunters Creek as evidence for progressive growth of the Sites anticline in mid (?) to late Quaternary time. We in turn interpret this as indirect evidence for mid- to late Quaternary activity on the underlying Funks segment of the Great Valley fault.

**Morphology of the Hunters Creek Channel**

We used the stream-gradient method of Hack (1973) to evaluate the morphology of the modern Hunters Creek channel, and to assess whether it has been affected by Holocene

Figure 3-57

activity of the Sites anticline. The elevation of the channel thalweg of a graded stream typically decreases in an exponential or logarithmic manner downstream, producing a characteristic concave profile (Hack, 1973; Schumm, 1977). Variations in channel gradient that depart from a convex logarithmic or exponential profile may be related to localized uplift or subsidence. Field studies by Burnett and Schumm (1983), Merritts and Vincent (1989), Bullard and Lettis (1993), and Marple and Talwani (1993) have confirmed that localized changes in stream channel gradient may be associated with areas of tectonic uplift and/or subsidence.

We also used the stream-gradient index Hack (1973) to evaluate variations in channel character. The stream-gradient index (SL), which relates channel gradient to channel length, was defined by Hack (1973) as follows:

$$SL = \Delta H/\Delta L * L \qquad (1)$$

where $\Delta H/\Delta L$ is the channel slope or gradient ($\Delta H$ is the change in elevation of the stream reach and $\Delta L$ is the length of the reach), and L is the total channel length from the stream divide.

The stream-gradient index is a means of quantifying stream power, with higher index values representing stream reaches with greater available power to incise and transport sediment. The stream-gradient index is very sensitive to changes in channel gradient, which generally correspond to differences in bedrock strength, particle size, and load supplied to the stream. Where climatic factors and lithological controls on the fluvial system are constant, and where tectonic activity is suspected, anomalous high values of the stream-gradient index are interpreted to indicate localized uplift (Keller and Pinter, 1996).

The thalweg profile of Hunters Creek is plotted on a semi-log graph in Figure 3-58. Segments of the profile that lie along lines of constant slope are delineated by arrows. Abrupt changes in gradient from one segment to another may represent reaches of the

Figure 3-58

stream affected by tectonic uplift or subsidence. There are several key features on this profile:

The gradient steepens abruptly at point A west of the Fruto syncline axis, possibly representing localized uplift of the channel above the ramp in the Funks segment, and local oversteepening of the channel above the ramp-flat transition.

The inflection in the profile at point B (Figure 3-58) represents an abrupt downstream reduction in channel gradient. Point B coincides with the westward extent of backtilting of the T2 and T5 terraces due to growth of the western limb of the Sites anticline (Figure 3-57). It is possible that the decrease in channel gradient here reflects recent incremental growth of Sites anticline, and local backtilting of the channel on the western limb of the anticline.

The channel gradient abruptly decreases in the reach between points C and D, west of the Salt Lake fault. This region is in the footwall of the fault, and it is downdropped relative to the area east of point D. It is possible that the decrease in channel gradient along this reach reflects ponding of sediment upstream of the Salt Lake fault due to the east-side-up displacement.

To summarize, some of the variations in the gradient of the modern Hunters Creek channel are correlated with patterns of folding and faulting as expressed in mid (?) to late Pleistocene fluvial terraces. We interpret these relations as evidence that the Hunters Creek channel has been affected by Holocene growth of the Sites anticline, and possibly by Holocene movement on the Salt Lake fault.

*3.4.4.1.3 Summary and Conclusions*

The previous section presented several lines of indirect evidence for late Quaternary activity of the Funks segment of the Great Valley fault:

1) The Salt Lake fault has produced multiple late Quaternary surface ruptures (Section 3.4.2);

2) There is localized Quaternary uplift and fluvial incision of the eastern Coast Ranges and foothills region above the ramp in the Funks segment;
3) Mid (?) to late Quaternary fluvial terraces are folded about the axis of the Sites anticline; and
4) The modern channel of Hunters Creek shows evidence of being perturbed by growth of the Sites anticline, and possibly by movement on the Salt Lake fault.

Based on these observations, we conclude that the Funks segment of the Great Valley fault is an active seismic source. This interpretation is consistent with evidence for late Quaternary activity of segments of the Great Valley fault about 28 miles (45 km) south of the DWR dam sites (Unruh and Moores, 1992; Unruh et al., 1995), and is consistent with the style and timing of deformation observed elsewhere in the Coast Ranges-Sierran Block Boundary Zone (Wong et al., 1988).

#### 3.4.4.2 Bear Valley Segment, Great Valley Fault

The Bear Valley segment is the next discrete fault segment of the Great Valley fault south of the Funks segment. The fault is imaged in seismic line SV-12 as a west-dipping reflector south of the S-2 fault that juxtaposes east-dipping strata of the Great Valley Group above against a package of bright, west-dipping reflectors below (Appendix A). The Bear Valley segment flattens abruptly eastward beneath the western Sacramento Valley. The Bear Valley segment also is imaged on line 807 as a west-dipping feature that similarly juxtaposes oppositely dipping reflectors (Appendix A). From preparation of a structure contour map of the Great Valley fault system in the northwestern Sacramento Valley, we interpret that the strike of the Bear Valley segment is about due north-south (Figure 3-54).

##### *3.4.4.2.1 Length of the Bear Valley Segment*

The northern boundary of the Bear Valley segment is interpreted to coincide with the S-2 fault, and is imaged directly by seismic line SV-12 (Appendix A). The southern boundary probably lies south of line 807 and is not imaged directly by seismic reflection

profiles acquired for this study. From inspection of Shell line 806 (published in Constenius et al., 2000), which crosses the southern end of the Wilbur Springs anticline south of line 807, we interpret that the southern boundary of the Bear Valley segment lies between lines 807 and 806. The dip discordance that we interpret to be the thrust fault in line 806 cannot be correlated with the Bear Valley segment without significantly changing the strike of the fault between line 807 and 806. We thus infer that the thrust faults imaged in lines 807 and 806 are two different structures, and that the southern boundary of the Bear Valley segment is located between the two seismic lines near latitude N 39° 07'.

We interpret the location of the segment boundary by assessing variations in patterns of late Cenozoic uplift along the western Valley margin. Notable physiographic changes near latitude N 39° 07' include the northern termination of a range of low hills along the western Sacramento valley margin west-southwest of Williams that are underlain by uplifted and folded Tehama Formation strata, as well as the southern termination of Bear Valley and Antelope Valley. In particular, the abrupt northern termination of the late Cenozoic hills west-southwest of Williams indicates that an abrupt boundary is present at depth in the geologic structures responsible for their uplift. We interpret the northern termination of the hills, which coincides with east-draining Salt Creek, to be the surface expression of the southern Bear Valley segment boundary. We adopt a length of 14.4 miles (23 km) for the Bear Valley segment, which is the distance between the S-2 fault and the northern end of the hills.

*3.4.4.2.2 Activity of the Bear Valley Segment*

We did not perform detailed studies to evaluate activity of the Bear Valley segment of the Great Valley fault. We conservatively assume that this segment is active because it lies between the active Funks segment to the north (Section 3.4.4.1), and the tectonically active Rumsey Hills region to the south (Unruh et al., 1995).

## 3.5 REGIONAL FAULTS

### 3.5.1 San Andreas Fault

The San Andreas fault is the most significant active fault in western California. The fault strikes northwest and can be traced as a continuous, well-defined geomorphic feature for approximately 650 miles (1,050 km) between the Gulf of California in southern California to Pt. Arena on the northern California coast (Figure 1-3). The San Andreas fault extends north of Pt. Arena in the offshore region and terminates in the vicinity of the Mendocino triple junction for a total length of approximately 700 miles (1,200 km). The San Andreas fault accommodates a large part of the approximately 39 mm/yr of distributed Pacific/Sierran plate motion in western California. Paleoseismic studies indicate that the slip rate on the San Andreas fault north of San Francisco is approximately 24 mm/yr (Niemi and Hall, 1992). Based on elastic dislocation modeling of geodetic data, Freymueller et al. (1999) inferred that the slip rate on the northern San Andreas fault is about 15 to 20.5 mm/yr. The closest approach of the San Andreas fault to the Sites and Golden Gate dam sites is 70 miles (113 km).

The San Andreas fault is the source of two M ≈ 8 historic earthquakes in California (the 1857 Fort Tejon earthquake in southern California and the 1906 San Francisco earthquake). The 1906 earthquake ruptured approximately 270 miles (435 km) of the northern San Andreas fault between San Juan Batista to the south, and Shelter Cove to the north. The reach of the San Andreas fault that ruptured in 1906 currently is aseismic or nearly so (Hill et al., 1990). Workers generally interpret the relative lack of seismicity as evidence that the fault is "locked" and presumably accumulating strain for release in a future large-magnitude earthquake (Working Group on Northern California Earthquake Probabilities, 1996).

Based on paleoseismic evidence for repeated Holocene earthquakes and the occurrence of historic events such as the 1906 earthquakes, we conclude that the San Andreas fault is an active seismic source.

### 3.5.2 Maacama Fault

The Maacama fault is an approximately 84-mile (135-km)-long, northwest-striking dextral fault zone that extends northward from several kilometers east of Healdsburg to the area around the town of Laytonville (Figure 1-3). The fault zone is characterized by discontinuous, subparallel strands that locally exhibit anastomozing and en echelon geometry. The fault traces are marked by saddles, springs, closed depressions, shutter ridges, 3.3 to 6.5 ft (1-2 m) high scarps in late Quaternary alluvium, ponded alluvium and possible deformation of cultural features by fault creep (Upp, 1982). Paleoseismic trenches excavated across traces of the fault show evidence for multiple Holocene surface-rupturing events (Upp, 1982). The closest approach of the Maacama fault to the Sites and Golden Gate dam sites is 45 miles (72 km).

Based primarily on variations in the strike of surface traces, Upp (1982) divided the Maacama fault in Mendocino County into four "subzones" ranging from less than 1 km to approximately 15 miles (24 km) in length. Each subzone consists of numerous shorter "segments" that share a common strike. The subzones are separated by 0.3 to 0.6 miles (0.5-1.0 km) gaps or stepovers in the main trace of the fault zone. Upp (1982) argued that the discontinuous nature of Maacama fault may represent an early stage in the development of the structure as a through-going strike-slip fault. The fault appears to die out in the vicinity of the Mendocino triple junction, or join with the Little Salmon thrust fault north of the triple junction. Based on analysis of contemporary seismicity, Castillo and Ellsworth (1993) proposed that the modern strike-slip Maacama fault may have evolved from a pre-existing thrust or reverse fault (i.e., an ancestral trace of the Little Salmon fault) that was active in the forearc region prior to northward passage of the triple junction.

The Maacama fault is associated with a prominent NW-trending zone of seismicity and aligned epicenters that extends southward and encompasses the Healdsburg and Rodgers Creek faults (Hill et al., 1990; Castillo and Ellsworth, 1993) (see Chapter 4). Elastic dislocation modeling of space geodetic data suggests that the secular slip rate on the Maacama fault is about 10-16 mm/yr (Freymueller et al., 1999). Based on the evidence

for Holocene surface rupture and the association of the fault with active seismicity, we conclude that the Maacama fault is an active source of moderate to large magnitude earthquakes.

### 3.5.3 Bartlett Springs Fault

The Bartlett Springs fault is a northwest-striking, 0.6- to 1.9 mile- (1- to 3-km-) wide fault zone in the northern Coast Ranges that extends northward as a series of discontinuous faults and lineaments from an area east of Clear Lake to Round Valley (Plate 1). Total length of the Bartlett Springs fault zone is approximately 70 miles (113 km). Previous workers (dePolo and Ohlin, 1984; Geomatrix Consultants, 1986) recognized that the Bartlett Springs fault zone locally exhibits geomorphic features and stratigraphic relationships indicative of Quaternary activity, including faulting of Holocene deposits. The closest approach of the Bartlett Springs fault zone to the Sites and Golden Gate dam sites is 20 and 22 miles (32 and 35 km), respectively.

The Bartlett Springs fault is similar to the Maacama fault in that it is not characterized by an integrated, well-developed single fault trace. The fault zone is a 1.2- to 1.9-mile- (2- to 3-km-) wide, northwest-trending belt of sheared rock that separates two relatively intact tectonostratigraphic terranes of the Franciscan assemblage (McLaughlin et al., 1989), but individual late Cenozoic lineaments, scarps and other tectonic-geomorphic features within the fault zone typically are diffuse and discontinuous (Plate 1). The Bartlett Springs fault is part of the San Andreas fault system, and thus is likely to have formed within the last 5 million years following northward migration of the Mendocino triple junction (Section 2.1). Consequently, it has not matured into a single through-going fault trace, and has not fully integrated with the Lake Mountain fault zone to the north or the Hunting Creek fault of the Green Valley fault system to the south (Geomatrix Consultants, 1986).

The southern part of the Bartlett Springs fault zone is seismically active. North of Clear Lake, the fault zone is associated with a distinct northwest-trending alignment of microseismicity (Dehlinger and Bolt, 1985; Hill et al., 1990; Castillo and Ellsworth,

1993). Cross sections of hypocenters generally show an east-dipping zone (Chapter 4), and focal mechanisms indicate a mix of right-lateral strike-slip faulting and normal faulting (Chapters 4 and 5).

Based on a detailed interpretation of aerial photographs, and aerial and field reconnaissance, Geomatrix Consultants (1986) concluded that the Bartlett Springs fault zone consists of at least six structural segments that range from 7.5 to 15 miles (12 to 24 km) in length, and which are separated by well-defined boundaries (Plate 1). Of these six segments, evidence for Holocene displacement was observed only on the 11.2-mile- (18-km-) long Coyote Rocks segment, which traverses the Lake Pillsbury basin (Geomatrix Consultants, 1986). This basin may be a tectonic pull-apart basin related to a right en-echelon stepover within the fault zone (McLaughlin and Nilsen, 1982; Geomatrix Consultants, 1986). Analysis of epicentral maps (Hill et al., 1990; Castillo and Ellsworth, 1993) shows that the Coyote Rocks segment generally corresponds with the northern end of seismicity associated with the Bartlett Springs fault zone.

Trenching studies along the Coyote Rocks segment of the Bartlett Springs fault zone reveal evidence for multiple Holocene surface-faulting events (Geomatrix Consultants, 1986). Paleoseismic data at one site suggest that the penultimate event occurred about 3800 $\pm$ 100 yrs BP. The most recent event deforms the modern soil, but occurred prior to settlement of the area some 300 to 1,000 years ago (Geomatrix Consultants, 1986). These data suggest a recurrence interval for surface-faulting events on the order of 2,000 to 3,000 years.

Based on paleoseismic evidence for repeated Holocene surface-rupturing events, and an association with contemporary seismicity, we conclude that the Bartlett Springs fault is an active seismic source.

### 3.5.4 Stony Creek Fault

The Stony Creek fault is the structural contact between the basal Great Valley Group strata and the Coast Range ophiolite (Plate 1). This contact can be traced along strike for

a total distance of approximately 100 km in the northern part of the study area west of the Sites and Golden Gate dam sites (Plate 1). Detailed field studies show that the contact between the ophiolite and the Great Valley strata commonly is marked by a zone of shearing (Earth Science Associates, 1980). Chuber (1961) noted that the trace of the fault locally is marked by perennial saline springs and up to 10 m of black fault gouge. The closest approach of the Stony Creek fault to the Sites and Golden Gate dam sites is 10 miles (16 km) and 11.2 miles (18 km), respectively.

The Stony Creek fault is exposed in numerous accessible stream and road cuts. Earth Science Associates (1980) described or sketched nine exposures of the fault and found that the Stony Creek fault commonly forms a shear zone up to 200 ft (60 m) wide with dips ranging between 30° to 50° east. WLA (1997) analyzed stereo aerial photography and performed aerial and field reconnaissance studies to assess the geomorphic character of the Stony Creek fault between the towns of Stonyford and Paskenta. They observed that the fault generally is expressed on aerial photographs as a vegetation or soil color contrast due to the juxtaposition of Great Valley Group shales against serpentinite of the Coast Range ophiolite. WLA (1997) concluded that the fault trace is subtle and lacks geomorphic features typically associated with active faults.

WLA (1997) also studied exposures of the Stony Creek fault in the field to evaluate Quaternary activity. They found that:

- The fault underlies a broad alluvial terrace several kilometers north of the town of Stonyford that is estimated to be 250 ka by Earth Science Associates (1980). The terrace surface and deposits are not obviously deformed by the fault.

The fault underlies undeformed late Quaternary deposits in Salt Spring Valley 3.7 miles (6 km) north of Stonyford.

The fault underlies an undeformed late Quaternary alluvial terrace (estimated to be about 30 ka) 2.8 miles (4.5 km) north of Stonyford.

The Stony Creek fault was trenched at three locations by Earth Science Associates (1980). The trenches were excavated in Quaternary sediments, typically terrace deposits and/or colluvium interpreted to be 100 ka in age or older, that overlie the fault trace near Stonyford, within Salt Spring Valley and near Thomes Creek. The trenches exposed a bedrock fault separating the Coast Range ophiolite from the Great Valley Group Quaternary deposits overlying the fault were not deformed (Earth Science Associates, 1980).

Based on the results of previous studies by Earth Science Associates (1980) and WLA (1997), we conclude that the Stony Creek fault is not an active seismic source.

### 3.5.5 Coast Range Fault

The Coast Range fault is the structural contact between the Coast Range ophiolite and the Franciscan assemblage (Plate 1), and as such is present throughout large areas of the northern Coast Ranges. Outcrop and map patterns of the Coast Range fault strongly suggest that the fault surface has been folded and deformed by younger structures (Wagner and Bortugno, 1982), and thus is unlikely to behave as a continuous zone of faulting or shearing. The closest approach of the Coast Range fault to both the Sites and Golden Gate dam sites is 12.4 miles (20 km).

From analysis of seismic reflection data performed for this investigation, we interpret that the Coast Range fault originally formed as an east-dipping fault or fault zone that accommodated attenuation of the ancestral forearc region crust (see Section 2.3 and Appendix A). The modern trace of the Coast Range fault has been uplifted, tilted and folded by late Cretaceous to Tertiary contractional deformation along the western Sacramento basin margin (Chapter 2). The fault probably terminates downdip in the upper 6.2 miles (10 km) of the crust against the blind Great Valley fault (Figure 3-2).

Based on analysis of regional geomorphic development and local geomorphic relationships adjacent to the fault, Earth Science Associates (1980) concluded that no movement has occurred on the Coast Range fault since late Pliocene time or earlier.

Evidence for no late Quaternary activity cited by Earth Science Associates (1980) includes the following: (1) no deformation of Holocene and possibly late Pleistocene colluvial deposits that locally overlie the fault trace; and (2) no faulting of late Quaternary deposits exposed in a paleoseismic trench excavated across the fault. WLA (1997) studied aerial photographs of the fault trace and briefly examined it during aerial and field reconnaissance. WLA (1997) concluded that the fault trace is subtle, lacks geomorphic features typically associated with active faults, and concurred with the previous assessment of Earth Science Associates (1980) that the Coast Range fault is not an active seismic source.

### 3.5.6 Green Valley Thrust Fault

The Green Valley fault is the longest of several north-northwest-striking faults near the towns of Stonyford and Lodoga, east of the DWR dam sites (Chuber, 1961; Plate 1). For clarity, only the Green Valley fault is shown on Plate 1. Maximum length of the fault is about 11 miles (17 km). The Green Valley fault and related structures originally were mapped and described by Chuber (1961). Based on map patterns, the Green Valley fault and related structures appear to splay southward from the Stony Creek fault and continue approximately 9 miles (14 km) to the south as a bedding-parallel fault system in the lower part of the Great Valley Group section (Plate 1). The fault traces are marked by gas seeps and perennial saline springs (Chuber, 1961). Despite these field observations, subsequent workers (Rich, unpublished mapping; Blake et al., 1992) have not included the Green Valley faults on compilation maps. The closest approach of the Green Valley fault to the Sites dam site is about 8 miles (12.5 km); the closest approach of the fault to Golden Gate dam site is about 9 miles (15 km).

Chuber (1961) interpreted the Green Valley fault and related structures to be high-angle, west-side down normal faults. He noted, however, that the faults repeat approximately 900 m (3,000 ft) of Upper Jurassic Great Valley Group strata, and that numerous small folds are present in blocks between strands of the fault system; these observations are not consistent with the interpretation of the structures as normal faults. Based on the presence of folds, the repetition of stratigraphic units, and the evidence for regional

crustal shortening in the northern Coast Ranges, WLA (1997) interpreted the Green Valley fault and related structures to be east-dipping, primarily bedding-parallel thrust faults. This interpretation is shown on the kinematic forward model for evolution of the crustal structure in this region in Figure 2-6. The Green Valley fault is interpreted to splay upward from the Stony Creek fault at depth and flatten within the lower Great Valley Group section.

WLA (1997) performed air photo analysis and conducted aerial and field reconnaissance to evaluate evidence for late Quaternary activity of the Green Valley fault and related structures. The faults have no significant geomorphic expression and locally are overlain by undeformed late Quaternary geomorphic surfaces, colluvium and fluvial deposits. Based on these observations, WLA (1997) concluded that the Green Valley thrust fault and related structures are not active. In our structural interpretation (Figure 2-6), the Green Valley fault is rooted at a depth of about 3 miles (5 km), and thus is confined to the shallow upper crust. We conclude that Green Valley fault is not an independent seismic source.

### 3.5.7 Paskenta Fault

The Paskenta fault is a northwest-striking fault or fault zone in the eastern Coast Ranges foothills bordering the northwestern Sacramento Valley (Plate 1). Based on patterns of stratigraphic separation, Jones et al. (1968, 1969) interpreted the Paskenta fault to be a left-lateral strike-slip fault. In contrast, Moxon (1990) observed that because the Paskenta fault is exposed in an uplifted and east-tilted homoclinal section of lower Great Valley Group strata, the stratigraphic and structural relations along the fault are best interpreted by viewing them down-dip on a geologic map. In this reference frame, the Paskenta fault cuts steeply downsection through the lower Great Valley Group strata and soles into or dies out in the serpentinite of the Coast Range ophiolite structurally above the Coast Range fault (Plate 1). Individual stratigraphic units in the lower Great Valley Group are consistently thicker on the north side of the fault than the south side. Moxon (1990) interpreted these relationships as evidence that the Paskenta fault originally was a north-dipping normal fault that was active in the early Cretaceous. This interpretation

also was adopted by Constenius et al. (2000). The fault and associated growth strata subsequently were rotated to a northwest strike in outcrop by uplift and eastward tilting along the western margin of the Sacramento Valley. In the present reference frame, the original down-to-the-north displacement on the fault is viewed as apparent left-lateral offset.

Moxon's interpretation (1990) implies that the Paskenta fault is present in the subsurface of the northern Sacramento Valley as an east-striking, north-dipping fault. In contrast, Harwood and Helley (1987) speculatively linked the Paskenta fault to the north-striking, steeply east-dipping Willows-Corning fault in the subsurface of the Sacramento Valley. Based on structural geologic relationships, WLA (1997) concluded that the Paskenta fault is not connected or directly related to the Willows-Corning fault. Williams (1997) similarly concluded that the Paskenta fault is not linked to the Willows-Corning fault, based on analysis of seismic reflection data. In this current study, we regard the Paskenta and Willows-Corning faults as two separate and unrelated structures.

The Paskenta Fault was investigated in detail by ESA (1980), which concluded that the fault does not deform mid- to late Quaternary fluvial terraces developed by Thomes creek above the map trace. WLA (1997) found that geomorphic profiles of the upper surface of the 1.0-3.4 Ma Tehama Formation, as well as profiles of late Pleistocene terraces along Thomes Creek, show no displacement or warping across the mapped trace of the Paskenta fault. Based on the results of the ESA (1980) and WLA (1997) investigations, we conclude that the Paskenta fault is not an active seismic source. The closest approach of the Paskenta fault to the Sites and Golden Gate dam sites is 25.5 miles (41 km) and 23 miles (37 km), respectively.

### 3.5.8 Rumsey Hills Thrust Fault

The Rumsey Hills anticline is an approximately 15.5-mile- (25-km-) long, north-south-trending, asymmetric west-vergent fold (Plate 1). The anticline is the surface expression of movement on a segment of the Great Valley thrust fault system at depth. Development of the west limb of the fold locally has overturned the unconformable contact between

Cretaceous Great Valley Group Strata and the Pliocene-Pleistocene Tehama Formation (Loewen, 1992). The crest of the fold is relatively broad, and Tehama Formation on the back (eastern) limb of the fold dips 10-30° eastward. Stratigraphic relationships in the northeastern Rumsey Hills show that the Tehama Formation is as young as 0.5-1.0 Ma (Munk, 1992; Unruh et al., 1995). Thus, uplift, folding and local thrust faulting of the Rumsey Hills has occurred since the middle Pleistocene. The closest approach of the axis of the Rumsey Hills anticline to the Sites and Golden Gate dam sites is 28 miles (45 km) and 30.4 miles (49 km), respectively.

Ramirez (1992) interpreted seismic reflection data to show that the Rumsey Hills anticline overlies a blind, east-dipping thrust fault. Slip on this fault, named the Rumsey Hills thrust by Unruh et al. (1995), is responsible for growth of the Rumsey Hills anticline as a fault-propagation fold and for uplift of the physiographic Rumsey Hills. The Rumsey Hills thrust fault is interpreted to splay upward from a blind thrust fault that dips westward beneath the Coast Ranges (Unruh et al., 1995); this west-dipping blind thrust fault is the local segment of the Great Valley fault at the latitude of the Rumsey Hills and Capay Valley. The Rumsey Hills anticline and its relationship to the Great Valley fault, therefore, is similar to the structural model of the Sites anticline discussed in Section 3.3.

WLA (1997) noted flights of uplifted terraces along Cache Creek at the southern end of the Rumsey Hills and in northern Capay Valley, indicating progressive uplift of the Rumsey Hills anticline since deposition of the Tehama Formation ceased. From evidence for late Quaternary uplift and growth of the Rumsey Hills anticline, WLA (1997) concluded that the underlying blind thrust fault is active. Based on construction of balanced cross sections and analysis of Quaternary stratigraphy, Unruh et al. (1995) estimated that the average middle to late Quaternary slip rate on the east-dipping Rumsey Hills thrust fault is approximately 1.0-3.5 mm/yr. Because the Rumsey Hills thrust fault is interpreted to be rooted in the Great Valley fault, we infer that the slip rate on the segment of the Great Valley fault at the latitude of the Rumsey Hills also is 1.0-3.5 mm/yr, or possibly slightly higher.

Based on the evidence for late Pleistocene fold growth discussed above, we conclude that the blind thrust fault beneath the Rumsey Hills is active.

### 3.5.9 Sweitzer Fault

The Sweitzer thrust fault is a northwest-striking, northeast-dipping thrust fault at the base of a steep, west-facing escarpment below the crest of the northern Rumsey Hills (Plate 1). Along with the Rumsey Hills anticline, the Sweitzer fault is part of the surface expression of movement on a segment of the blind Great Valley thrust fault. The Sweitzer fault locally places massive sandstone of the Cretaceous Guinda Formation over the Pliocene-Pleistocene Tehama Formation (Kirby, 1943; Loewen, 1992). Based on stratigraphic relationships exposed on the eastern flank of the Rumsey Hills, Munk (1992) and Unruh et al. (1995) interpreted that the youngest Tehama sediments in this region were deposited between 1 Ma and 500 ka. These relations show that surface faulting on the Sweitzer fault is middle Pleistocene in age or younger. The closest approach of the fault to the Sites and Golden Gate dam sites is 28 miles (45 km) and 30.4 miles (49 km), respectively.

Structural relations visible in seismic reflection profiles indicate that the Sweitzer fault is a bedding-parallel fault that extends eastward and roots in a blind, west-dipping thrust fault beneath the Dunnigan Hills at a depth of approximately 3.1 miles (5 km) (Unruh and Moores, 1992). The deeper blind fault dips west beneath the Rumsey Hills and Capay Valley, and is the local segment of the Great Valley fault at this latitude. The intersection of the east-dipping Sweitzer thrust fault and the west-dipping Great Valley fault forms the tip of an east-tapering tectonic wedge system, similar to the relationship between of the Salt Lake fault and the Funks segment of the Great Valley thrust fault system at the latitude of the dam sites (Section 3.2). The Dunnigan Hills are an anticline that developed in the hanging wall of the Sweitzer fault (Unruh et al., 1995). Quaternary growth of the Dunnigan Hills anticline has deformed the Tehama Formation. Evidence for late Quaternary growth is provided by flights of uplifted middle to late Pleistocene fluvial terraces cut by streams draining eastward across the structure (Munk, 1992), similar to the uplifted and folded terraces of Hunters Creek across the Sites anticline

(Section 3.4.4.2.3). Soil stratigraphic relationships indicate that the highest accordant surfaces mantled by fluvial gravels in the Dunnigan Hills date from ≤ 450 ka (Munk, 1992). These surfaces are approximately 164 to 200 feet (50-60 m) above the channels of modern east-draining streams. If it is assumed that the present relief of the preserved high surface is equivalent to the tectonic uplift of the Dunnigan Hills, then the minimum late Quaternary uplift rate is approximately 0.1 mm/yr (Unruh et al., 1993).

Based on evidence for Quaternary surface faulting along the Sweitzer fault in the western Rumsey Hills, and for late Quaternary uplift of the Dunnigan Hills, Unruh et al. (1993) concluded that the Sweitzer fault is active. They added several caveats to this assessment, however. First, detailed analysis of seismic reflection profiles shows that the tip of the tectonic wedge beneath the Dunnigan Hills has not propagated a significant distance eastward since Eocene time, even though stratigraphic relations record at least two episodes of post-Eocene uplift and folding of the Dunnigan Hills. These relationships suggest that post-Eocene shortening at the wedge tip, including Quaternary deformation, may be accommodated by tectonic thickening and distributed faulting, rather than eastward propagation of the wedge beneath the Dunnigan Hills. Second, the surface trace of the Sweitzer fault appears to be cut by several east-striking tear faults in the northern Rumsey Hills (Loewen, 1992). The tear faults limit the lateral continuity of the fault plane and may represent significant barriers to rupture propagation. Finally, the stratigraphic units repeated by the Sweitzer fault vary from north to south, indicating the presence of lateral ramps that shift displacement on the primary thrust faults up or down within the stratigraphic section (Loewen, 1992). Like the surface tear faults, the lateral ramps may act as rupture barriers.

Given these caveats, Unruh et al. (1993) interpreted that movement on the Sweitzer fault may occur sympathetically with moderate to large-magnitude events on deeper blind thrust faults such as the Great Valley fault, but that the Sweitzer fault probably is not an independent source of moderate to large-magnitude earthquakes because it does not extend to depths where such earthquakes nucleate (Sibson, 1982). Localized surface rupture may occur on the fault, however, similar to the Nunez fault during the 1983

Coalinga earthquake sequence (Hart and McJunkin, 1983). This interpretation of the seismic potential of the Sweitzer fault is analogous to our assessment of the Salt Lake fault (Section 3.4.2.3)

### 3.5.10 Valley Side Fault

The Valley Side fault is a north-south-striking, east-dipping thrust or reverse fault along the eastern Coast Ranges piedmont north of the Rumsey Hills (Plate 1). The Valley Side fault was mapped by Lawton (1956) as three discontinuous sections. The northernmost section is approximately 4.1 miles (6.7 km) in length and generally is coincident with the valley of Spring Creek. The central section is approximately 1.5 miles (2.4 km) long and terminates northward at or near the southern boundary of the Cortina Rancheria reservation. The southern section is approximately 4.7 miles (7.6 km) long. Total length of the Valley Side fault is approximately 10.5 miles (17 km). The southern section juxtaposes the Pliocene-Pleistocene Tehama Formation against Cretaceous Great Valley Group strata (Lawton, 1956), thus indicating that the most recent movement occurred during the middle to late Quaternary. The closest approach of the Valley Side fault to the Sites and Golden Gate dam sites is 16 miles (26 km) and 18.6 miles (30 km), respectively.

Unruh et al. (1994) analyzed 1:13,200-scale black and white aerial photographs acquired in July of 1994 to assess late Quaternary activity of the central and northern segments of the Valley Side fault. They observed that the fault is associated with a north-south-trending line of low hills that lie east of the outcrops of Cretaceous Great Valley Group strata, and that can be traced continuously for approximately 8.7 miles (14 km) along strike. The hills generally are characterized by steep topographic breaks or escarpments on their west sides, and gently east-sloping surfaces on their east sides.

Based on field reconnaissance and detailed mapping, Unruh et al. (1994) interpreted the north-south line of low hills associated with the northern segment of the Valley Side fault to be the result of Quaternary folding or uplift in the hanging wall. In particular, they observed exposures of steeply west-dipping, vertical, and overturned Upper Cretaceous

strata in the bottoms of several small, east-draining streams that cross the hills, consistent with the interpretation that the line of low hills probably represents a small, asymmetric, west-vergent fault-propagation fold. Growth of the fold locally has elevated the Great Valley Group/Tehama contact such that the Cretaceous strata are exposed in east-draining stream channels. Although exposures are sparse, field relationships at a single site in the northeastern corner of the Cortina Rancheria reservation suggest that the fold locally may be breached by an east-dipping thrust or reverse fault that juxtaposes Great Valley Group strata up on the east against the Tehama Formation (Unruh et al., 1994). This interpretation of the field relations is similar to the mapping of the southern segment of the Valley Side fault by Lawton (1956).

Based on the work of Unruh et al. (1994) in the Cortina Rancheria area, and the regional mapping of Lawton (1956), we interpret that the Valley Side fault probably is a bedding-parallel thrust fault in the shale-rich Cretaceous Funks Formation. The Valley Side fault probably dips eastward and may extend to 3.1 to 4.4 miles (5-7 km) depth where it intersects the blind, west-dipping detachment surface, thus forming the roof thrust of a tectonic wedge similar to the Salt Lake fault (Figure 3-2) and the Sweitzer fault (Section 3.5.8). Alternatively, the Valley Side fault may be a flexural slip fault that has accommodated layer-parallel shearing within the Great Valley Group during uplift and tilting of the Coast Range foothills region, similar to our interpretation of the S-3 fault (Section 3.4.3). In both models, the Valley Side fault is too shallowly rooted to be a source of moderate to large earthquakes. We conclude that the fault is not an independent seismic source; however, the Valley Side fault may be a potential surface-rupture hazard, analogous to the shallowly rooted Nunez fault that ruptured sympathetically during the 1983 Coalinga earthquake sequence and locally broke the surface (Hart and McJunkin, 1983).

### 3.5.11 Black Butte Fault

The Black Butte fault is shown as a 10.5-mile- (17-km-) long, northwest-striking fault along the western margin of the Orland Buttes by Jennings and Strand (1960). The mapped fault trace is associated with a prominent west-facing escarpment at the base of

east-dipping Miocene Lovejoy basalt, which underlies the Orland Buttes. Russell (1931) first suggested the presence of a fault at this location to explain the presence of the escarpment and the buttes. Russell (1931) originally mapped the Black Butte fault as displacing late Pliocene-early Pleistocene deposits down to the west. Investigations by Earth Science Associates (1980) and the Corps of Engineers (1986), however, concluded that the topographic escarpment at the Orland Buttes formed by differential erosion of the basalt atop a structural hogback, rather than east-side-up movement on a fault. The closest approach of the western Orland Buttes escarpment to the Sites and Golden Gate dam sites is 30 miles (48 km) and 27.3 miles (44 km), respectively.

Subsurface relations inferred from analysis of seismic reflection profiles support the interpretation that the west-facing Black Butte escarpment is due to differential erosion of an east-tilted basalt, rather than displacement on a west-side-down fault. East-west seismic line 805 passes along the southern margin of the Orland Buttes and images homoclinally east-dipping reflectors beneath the western Sacramento Valley margin (Figure 3-59; see Appendix A for location and detailed interpretation of seismic line 805). The signal/noise ratio in the upper part of line 805 is poor, and thus the upper 0.6 mile (1 km) of the depth-migrated section is muted to enhance reflections in the lower part of the section (Figure 3-47; D. O'Connell, personal communication, 2000). Consequently, the reflector geometry directly beneath the western margin of the Buttes is not visible. Structural relations suggest, however, that the Lovejoy basalt is part of the east-dipping package of reflectors in the upper 3.1 miles (5 km) of the crust that flattens eastward beneath the Sacramento Valley (Figure 3-59). Based on detailed analysis of outcrop relations and well data, the Corps of Engineers (1986) determined that the Lovejoy basalt dips about 6.5° eastward beneath the Sacramento Valley. The basalt flattens eastward, similar to the underlying Great Valley Group reflectors (Figure 3-59).

The east-dipping Great Valley Group reflectors imaged directly beneath the western Orland Buttes escarpment on seismic line 805 are laterally continuous and are not visibly offset by a moderately or steeply dipping fault that displaces the western margin of the

Figure 3-59

Buttes up to the east (Figure 3-59). It is possible that a bedding plane fault is present along the base of the Buttes escarpment that has accommodated layer-parallel shear during uplift and eastward tilting along the western valley margin. If a layer-parallel fault is present, then structural relations visible in line 805 indicate that it must flatten eastward in the upper 0.6 to 1.2 miles (1-2 km) of the crust (Figure 3-59). If this is the case, then the fault is a very shallow upper crustal feature and not capable of being an independent seismic source.

WLA (1997) constructed geomorphic profiles of the modern channel thalweg, the 30 ka Arbuckle terrace, and the 120 ka Perkins terrace along Stony Creek; all of these surfaces extend eastward across the surface trace of the Black Butte fault. The profiles show that the Perkins and Arbuckle terraces maintain steady gradients across the Black Butte fault and are not deformed (WLA, 1997). The results are consistent with field mapping by Earth Science Associates (1980), which indicates that exposures of the Tehama Formation in Hambright Creek are not deformed where they overlie the mapped fault trace.

Based on a review of previous work and analysis of seismic reflection data, we do not find compelling evidence for the presence of a fault along the base of the western Orland Buttes escarpment. It is possible that minor bedding-parallel flexural slip has occurred in the vicinity of the mapped fault trace as a consequence of uplift and eastward tilting. The presence of the Orland Buttes can be entirely explained, however, by eastward tilting in the hanging wall of a blind, west-dipping thrust fault (i.e., the Orland segment of the Great Valley thrust fault system; see Appendix A). The stratigraphic and structural relations shown on Figure 3-59 are most simply explained by post-Lovejoy uplift and eastward tilting along the western margin of the Sacramento Valley associated with fault-propagation folding updip of the blind thrust fault (Appendix A). We conclude that, if present, the Black Butte fault is a shallow, bedding-parallel fault, and thus is not an active, independent seismic source.

### 3.5.12 Corning Fault

The Corning fault is a north-striking, steeply east-dipping reverse fault that underlies the north-central Sacramento Valley (Plate 1) (Harwood and Helley, 1987). The fault is imaged on seismic reflection profiles (Harwood and Helley, 1987; Williams, 1997), but is blind and thus not associated with a discrete surface trace. To the north, the Corning fault intersects or is truncated by the northeast-striking Red Bluff fault (Plate 1) (Harwood and Helley, 1987), an approximately east-west striking, high-angle fault imaged on seismic reflection profiles (Harlan-Miller-Tait Associates, 1984). Near its southern end, the Corning fault is interpreted to turn to a more northwest-southeast strike and either splay off from or terminate against the Willows fault (Harwood and Helley, 1987; Plate 1). The closest approach of the Corning fault to the Sites and Golden Gate dam sites is 20 miles (32 km) and 18 miles (29 km), respectively.

Structure contours on the top of upper Cretaceous strata in the northern Sacramento Valley reveal reverse movement on the Corning fault and antiformal folding of the hanging wall (Harwood and Helley, 1987). The structure contours delineate at least three sets of folds along strike of the fault: (1) an unnamed, south-plunging fold that extends approximately 9.3 miles (15 km) south of the town of Red Bluff; (2) the North and South Corning Domes, near the town of Corning (Plate 1), which extend for a combined north-south distance of approximately 12.4 to 15.5 miles (20-25 km); and (3) the doubly-plunging Greenwood anticline, which is developed along the southern 15.5 to 18.6 miles (25-30 km) reach of the Corning fault (Plate 1). The axis of the Greenwood anticline is flexed along the change in strike of the fault near the intersection with the Willows fault (WLA, 1997).

Quaternary movement on the central reach of the Corning fault is demonstrated by uplift and doming of the 0.45-1.0 Ma Tehama and Red Bluff Formations at the Corning Domes (Harwood and Helley, 1987). Based on the magnitude of closure in structure contours on the base of the folded Tehama Formation, WLA (1997) calculated a long-term average vertical separation rate of approximately 0.036 mm/yr for the underlying Corning fault. If it is assumed that the fault dips 70° to the east, then the corresponding average

Quaternary dip-slip rate on the fault is approximately 0.04 mm/yr (WLA, 1997). A similar analysis of structure contours on the base of the 0.45-1.0 Ma Red Bluff Formation suggests a middle to late Quaternary average slip rate is 0.02 to 0.04 mm/yr. WLA (1997) concluded that the average slip rate on this reach of the Corning fault (approximately 0.02-0.04 mm/yr) has been relatively uniform since at least 3.4 Ma.

To evaluate late Quaternary activity of the Greenwood anticline (i.e., the southern reach of the Corning fault), WLA (1997) constructed a profile of an abandoned fluvial channel that crosses the axis of the structure approximately one kilometer south of Orland. The channel deposits are mapped as the Modesto Formation (12 ka to 26 ka) by Helley and Harwood (1985). The profile of the unnamed channel shows a broad convexity across the axis of the Greenwood anticline with a wavelength of approximately 5 miles (8 km) and maximum amplitude of approximately 3.3 to 6.5 feet (1-2 m). With the assumption that the convexity is a product of tectonic uplift, WLA (1997) estimated that the uplift rate above the Greenwood anticline is approximately 0.04-0.2 mm/yr. The lower value is this range (0.04 mm/yr) is comparable to the average Quaternary uplift rate of the Corning Domes north of the Greenwood anticline (WLA, 1997).

The Corning fault is associated with clusters of background seismicity (Wong et al., 1988). As discussed in Chapters 4 and 5, there is a zone of elevated background seismicity in the north-central Sacramento Valley east of Willows and Orland that has a general north-south trend. Relocated epicenters of the events plot along and near the Greenwood anticline, and seismicity cross sections suggest that some of the events may lie along the down-dip projection of the Corning fault (Section 4.3.3.2.3).

Based on evidence for progressive Quaternary surface folding above the Corning fault, including possible antiformal folding of a late Pleistocene (Modesto-ages) channel deposit across the Greenwood anticline, as well as a possible association with contemporary seismicity, we conclude that the Corning fault is an active seismic source.

## 3.6 CASCADIA SUBDUCTION ZONE

This section characterizes two classes of potential seismic sources associated with the southern Cascadia subduction: (1) an "interplate" source, which is the subduction zone megathrust fault between the subducting Gorda plate and the overlying crust of the Sierran microplate; and (2) "intraplate" sources, which are seismogenic faults within the Gorda slab.

### 3.6.1 Interplate Sources

Geological investigations (Atwater et al., 1995; Nelson et al., 1995), geophysical modeling (Fluck et al., 1997; Hyndman and Wang, 1995), and historical tsunami records from Japan (Satake et al., 1996) provide the basis for the current scientific consensus that the Cascadia subduction zone (CSZ) has the potential to generate earthquakes that may rupture the entire 1,000-km length of the plate boundary. Geological evidence for repeated great earthquakes on the CSZ includes: (1) stratigraphic relations in estuaries that document repeated episodes of sudden submergence of forests and tidal marshes; (2) seismically triggered turbidites in submarine channels; (3) liquefaction caused by strong shaking; and (4) tsunamis generated by dislocation of the seafloor (Atwater et al., 1995) (Figure 3-60).

The most recent great earthquake on the Cascadia subduction zone is estimated to have occurred about 300 years ago, based on analyses of tree rings from fossil spruce and cedar trees at Cascadia estuaries, as well as radiocarbon dating of fossil trees and marsh herbs interpreted to have been killed by earthquake-induced subsidence (Jacoby et al., 1995; Nelson et al., 1995; Yamaguchi et al., 1997). These data are consistent with the interpretation of Satake et al. (1996) that a large tsunami, which struck Japan on the evening of 26 January 1700, was triggered by an earthquake that ruptured 560 to 621 miles (900-to-1000) km of the Cascadia plate boundary. Paleoseismic data indicate that earthquakes of this size may recur on average every 500 to 600 years (Atwater and Hemphill-Haley, 1997; Goldfinger et al., 2001). Therefore, on the basis of this evidence and upon geophysical modeling that supports a $M_w$ 9 capability for the CSZ (Fluck et al.,

Figure 3-60

1997; Hyndman and Wang, 1995), we conclude that the northern California portion of the CSZ will likely be involved in a future great plate-boundary earthquake (Figure 3-60).

The 1992 $M_w$ 7 to 7.2 Cape Mendocino earthquake was the first well-recorded historical seismic event to release significant strain within the subduction complex of the Cascadia margin (Murray et al., 1996; Oppenheimer et al., 1993; Velasco et al., 1994). Based on observations of dead marine intertidal organisms above the normal elevation range of their habitats following the earthquake, the maximum coseismic uplift was estimated to be 4.6 feet (1.4 m) (Carver et al., 1994). The focal mechanism and aftershock distribution indicate rupture of a northeast-dipping thrust plane located 25 km southeast of Cape Mendocino at 10 km depth (Murray et al., 1996). Within uncertainty, the slip vector derived from inversion of geodetically determined coseismic surface displacements (16 feet, or 4.9 m, directed 250°±10°N) is parallel to the relative plate convergence direction between the North America and Juan de Fuca plates (240.6°N; Murray et al., 1996). Based on the shallow depth of the 1992 earthquake (about 8 km above the top of the Gorda-North America plate interface), Verdonck and Zandt (1994) suggested that the 1992 event was an intraplate earthquake caused by low-angle thrust faulting within the subduction complex of the upper plate, rather than rupture of the actual subduction zone megathrust fault. However, Oppenheimer (19993) interpreted the focal mechanism and distribution of aftershocks to be consistent with nearly pure reverse slip on the plate interface striking N10°W and dipping 13° to the east-northeast.

Evidence for repeated uplift of wave-cut platforms in the Cape Mendocino region indicate that the southern North America-Gorda plate boundary has produced large to great earthquakes over the last 7,000 years. Merritts (1996) evaluated the uplift and pattern of deformation of ancient marine strandlines along the southern CSZ and found evidence for larger amounts of incremental uplift (about 8.2 feet) (2.5 m) than the 1992 earthquake, suggesting that great earthquakes ($M_w > 8$) may have ruptured the southern portion of the plate boundary in the last 7000 years in addition to Cape Mendocino-type events.

To summarize, recent geologic studies have documented evidence for Holocene earthquakes that probably ruptured the full 560- to 621-mile (900- to 1000-km) length of the Cascadia subduction zone. We conclude that the subduction zone megathrust fault in northern California will be involved in future great earthquakes to rupture the Cascadia convergent margin. We also conclude that faults within the accretionary complex above the subduction zone also may be a source of large ($M_W$ 7 or greater) earthquakes, similar to the 1992 Cape Mendocino earthquake.

The closest approach of the potential Cascadia earthquake rupture plane to the Sites and Golden Gate dam sites is a function of: (1) the dip of the plate interface; (2) the downdip extent of the coseismic rupture surface; and (3) the position of the southern edge of the subducting Gorda plate (Figure 3-61). We calculate the closest approach from estimates of the minimum depth to coseismic rupture on the plate interface, as well as the horizontal distance to the southern edge of the Gorda plate. Beaudoin et al. (1996) estimate an ~11° dip for the Gorda slab from wide-angle reflection profiles acquired during the Mendocino triple junction seismic experiment. This estimate agrees well with the 10° to 14° dip of the Gorda plate estimated by Smith et al. (1993) based on seismicity (Figure 3-61). The down-dip extent of the seismic rupture surface has been estimated by Hyndman and Wang (1995) and Fluck et al. (1997) based on dislocation modeling of geodetic data and thermal constraints (Figure 3-61 and 3-62). The three-dimensional dislocation model developed by Fluck et al. (1997) predicts a 35-km wide locked zone and a 21.7-mile- (35-km-) wide transition zone for the northern California portion of the CSZ based on geodetic data from central Oregon. The transition zone is downdip of the interseismic locked portion of the fault where maximum coseismic rupture is expected but above the free-slip portion of the fault where no coseismic displacement occurs. The lower limits of the locked and transition zones are constrained by maximum temperatures predicted by numerical thermal models of the fault of 350°C and 450°C, respectively (Hyndman and Wang, 1995). To estimate the maximum coseismic rupture area, Fluck et al. (1997) assumed that both the locked and transition zones are involved in the rupture. From these estimates of the dip of the subduction zone and depth range of brittle

Figure 3-61

Figure 3-62

Figure 3-63

behavior, we therefore estimate that the minimum depth to the southeastern-most edge of the rupture zone is 12.4 miles (20 km) (Figure 3-63a).

The horizontal distance to the southern edge of the subducting Gorda plate is inferred from estimates of the plate geometry beneath northwestern California. Beaudoin et al. (1996) traced the Gorda slab 93 miles (150 km) eastward from the Cascadia margin based on seismic reflection and refraction data. Other studies have delineated the southern edge of the Gorda plate using gravity anomalies (Jachens and Griscom, 1983), the northern progression of late Cenozoic volcanic activity in the Coast Ranges (Wilson, 1989), local earthquake travel times (Verdonck and Zandt, 1994), and seismic profiling and gravity (Beaudoin et al., 1998) (Figure 3-63a). Beaudoin et al. (1998) located the southern edge of the Gorda slab from analyses of a 155-mile- (250-km-) long, north-south seismic refraction-reflection profile across a region in northwestern California presumed to have been modified by the passage of the Mendocino triple junction. We conclude that the data of Beaudoin et al. (1996; 1998) provide the highest resolution imaging available for the location and geometry of the southern boundary of the Gorda plate. To determine the source-to-site distance we located the point defined by the intersection between the down-dip limit of the transition zone derived by Fluck et al. (1997) and the southern edge of the Gorda plate as determined by Beaudoin et al. (1998) (Figure 3-61). From trigonometric relations, the depth to this point 12.4 miles (20 km) and the horizontal distance between this point and the two dam sites provide source-to-site distances of approximately 100 miles (160 km) (for Golden Gate and Sites) (Figure 3-63a).

### 3.6.2 Intraplate Sources

The Mendocino triple junction region is one of the most seismically active areas in the western United States. A large percentage of the seismic activity in the Mendocino region occurs in the subducting Gorda slab, which is shortening in a north-south direction in response to compression imposed by buttressing of the Pacific plate along the Mendocino fault (Figure 3-59). Evidence of S-curved magnetic anomalies and densely distributed seismicity in the Mendocino region led Silver (1971) and Wilson (1989) to argue that internal deformation of the southern edge of the Gorda plate is accommodated by

northeast-southwest oriented left-lateral shearing subparallel to the spreading fabric. This hypothesis is consistent with the distribution of aftershocks and first motion studies following the 1980 $M_s$ 7.2 Eureka earthquake that ruptured a 75-mile (120-km-) long left-lateral fault in the Gorda plate (Smith et al., 1993).

The largest instrumentally recorded intraplate earthquake in the Gorda plate is the 1980 Eureka earthquake. Surface-wave magnitude for this event was estimated at $M_s$ 7.2 (Smith et al. 1993), and estimates of the maximum moment magnitude are $M_w$ 7.3 to 7.4 (Dengler et al., 1992; Velasco et al., 1994). Two other large earthquakes, the July 13, 1991 $M_w$ 6.8 and the August 17, 1991 $M_w$ 7.1 events, also ruptured conjugate strike-slip faults accommodating north-south shortening in the internally deforming Gorda plate (Velasco et al., 1994). Following Dengler et al. (1992), we conservatively conclude that intraplate earthquakes in the subducting Gorda plate may be as large as $M_w$ 7.5. Although the largest earthquakes appear to have strike-slip mechanisms and occur north and northwest of the Mendocino triple junction (Smith et al., 1993; Wang and Rogers, 1994), we cannot preclude $M_w$ 7+ earthquakes in the Gorda slab at depths greater than 19 miles (>30 km), and as much as 93 miles (150 km) east of the subduction zone (Beaudoin et al., 1996). For example, Weaver and Shedlock (1996) estimated a 28-37 (45-60 km) source depth for Gorda slab events. We believe that large intraplate earthquakes at depths greater than 19 miles (30 km) are plausible in light of the February 28, 2001 $M_w$ 6.8 Nisqually earthquake that occurred 32 miles (52 km) beneath Olympia, Washington within the subducting Juan de Fuca plate.

We calculate the closest distance between the DWR dam sites and seismic events in the slab from trigonometric relations between the horizontal distance to the southeastern corner of the Gorda plate, and depth to the slab. Based on seismic imaging by Beaudoin et al. (1996, 1998), the closest horizontal distance from the dam sites and southeasternmost edge of the subducted Gorda slab is approximately 40 miles (65 km) (Figure 3-60). The minimum estimated depth to the top of the slab, determined from data in Weaver and Shedlock (1996) and the results of new work performed for this study (Chapter 4), is 28 miles (45 km). The closest straight-line distance through the crust

between the dam sites and the southern edge of the subducted Gorda slab is thus 50 miles (80 km).

# 4.0 SEISMICITY

## 4.1 INTRODUCTION

We evaluated earthquake activity in northwestern California to identify potential seismic sources capable of generating significant ground motion at the proposed DWR dam sites, and to further characterize the seismotectonic setting of the study region. The boundaries of the seismicity study region were selected to include potential seismic sources within 62 miles (100 km) of the dam sites, and to provide sufficient data to evaluate the seismic activity of geologic structures identified as potentially significant in earlier phases of this study. The study region extends from latitude 38 to 41 degrees north and from longitude 124.5 to 120.5 degrees west. A catalog of earthquake locations and magnitudes was compiled for the Sacramento Valley region covering the area shown on Figure 4-1.

For the purpose of this study, the earthquake record can be divided into two time periods, herein referred to as the historical period (1850 through 1969), and the instrumental period (1970 through 2000). The historical period covers the time prior to the installation of short-period seismic networks, which generally occurred in the 1970's for much of the western United States (Engdahl and Rinehart, 1991). In California, modern networks have been operating since 1967 (Oppenheimer et al., 1992). By 1970, network coverage in northern California was sufficient for earthquakes to be recorded on three or more stations, a necessary requirement for computationally rigorous hypocentral determinations (Klein et al., 1988). Earthquake activity in the study region currently is monitored by the Northern California Seismic Network (NCSN) and by seismograph stations operated by the University of California, Berkeley (UCB).

Sources for the instrumental catalog are NCSN and UCB. The instrumental seismicity catalog includes data on earthquake origin time, location, magnitude, number of observations, location error statistics, and an overall hypocentral location quality assessment. Merging the NCSN and UCB catalogs produced an integrated seismicity

Figure 4-1

catalog. Because the areas covered by these networks overlap, duplicate recordings of earthquakes exist. These redundancies were identified and eliminated by giving preference to the NCSN locations. This issue is more fully discussed in Sections 4.2 and 4.3, below.

## 4.2 HISTORICAL SEISMICITY

### 4.2.1 Compilation of the Historical Catalog

Primary data sources used for the historical seismicity catalog include the University of California, Berkeley (UCB), the National Earthquake Information Center (NEIC), Real et al. (1978), Toppozada et al. (1981), and Townley and Allen (1939). These sources contain information on event location, intensity, magnitude (when available) and extended comments on the cultural and geologic effects of the earthquakes.

The UCB historical catalog combines data from the Townley-Allen catalog of Pacific coast earthquakes (Townley and Allen, 1939) from 1769 to May 2, 1910, and the UCB catalog from May 6, 1910 through 1970. The UCB historical catalog was supplemented with data from Toppozada et al. (1981) for pre-1900 earthquakes in California.

There is a wide range of accuracy in the epicentral locations of historical earthquakes. Factors influencing accuracy include the date of the earthquake, proximity to population centers, and earthquake magnitude. Location errors for non-instrumental events in the study area range from about 9 to 62 miles (15 to 100 km) (Toppozada et al., 1981). Estimated magnitudes of the events also vary. Many of the events recorded prior the 1920's were assigned intensity values based on felt reports, whereas events that occurred after 1920 were assigned instrumentally based Richter magnitudes ($M_L$). The Townley-Allen catalog does not contain intensity-based magnitude data. Because of the disparity in use of magnitude scales between various institutions and the uncertainties associated with magnitudes estimated from felt reports, the magnitudes for the historic earthquakes should be regarded with caution. Even the estimates of Richter magnitudes for post-1920

events should be treated cautiously because accurate magnitude calculations depend on an average of well-distributed station estimates and the validity of applying Richter's southern California attenuation relationship to events in other regions. These and other problems related to consistent estimates of earthquake magnitude between the various reporting agencies were not resolved in this study.

### 4.2.2 Completeness of the Historical Record

Completeness of the historical catalog varies in direct proportion to felt intensity reports and population density. Before the gold rush in central California in 1849, information on earthquakes was obtained from written records of the Franciscan missions located on the California coast from San Diego in the south to Sonoma in the north (Toppozada et al., 1981). Events rarely were recorded unless they caused significant damage; thus, only earthquakes of M 7 or greater that occurred within 62 miles (100 km) of the coast appear in the catalogs prior to 1850.

The discovery of gold in 1848 along the South Fork of the American River 30 miles (49 km) east of Sacramento triggered the California Gold Rush of 1849. Population density increased significantly as gold prospectors moved into the region, arriving by sea through San Francisco and via overland emigration routes, and headed east to the Sierra Nevada. Communities were established in the Sacramento Valley and throughout the Sierra to support the mining industry. The city of Sacramento was founded in 1849. Discovery of gold in the Feather River led to the establishment of Marysville in 1851. Gold discoveries in the Trinity River followed shortly thereafter, drawing population to the north. Chico was established in 1872 and Red Bluff in 1876. As these communities developed, numerous newspapers were founded to serve the citizens of the region. These newspapers are a crucial source of information about post-1850 earthquakes in northern California.

Newspaper accounts generally provide a good estimate of the time of earthquake occurrence and intensity, but the location precision depends on the number of people

observing the event and the accuracy of their observations. By the 1850's, the magnitude detection threshold was lowered to M 6.0 for the gold country (in the Sierra Nevada range from Quincy south to Mariposa), and to M 6.5 for the rest of the region (Toppozada et al., 1981). It was not until the 1870's, when the population had increased in the northern Sacramento Valley, that newspaper coverage was complete and the detection magnitude threshold decreased to M 6 for the majority of the study area (Toppozada et al., 1981). By the late 1880's, seismographs had been installed at Mt. Hamilton and Berkeley, although the first published catalogs did not appear until 1910. In the 1920's, a program was started in California to use a standardized seismograph (i.e., the Wood-Anderson torsion seismograph) to facilitate earthquake research. In 1939, a Wood-Anderson instrument was installed at Mineral, about 62 miles (100 km) northeast of the Sites Project. A high-sensitivity Benioff seismograph was installed at Mineral in 1949, enabling routine detection and location of M 3 events in this region (Urhammer, 1991). By 1950, the detection threshold decreased to M 3 for most of the study area (Engdahl and Rinehart, 1991).

### 4.2.3 Significant Regional Historical Earthquakes

This section reviews significant historical earthquakes in the regional seismicity study area, exclusive of the Sacramento Valley. These earthquakes illustrate and help characterize the seismic potential of source zones in areas adjacent to the Sacramento Valley that may affect the project area. Potential regional seismic sources include: the Bartlett Springs fault zone in the northern Coast Ranges to the west of the Sacramento Valley; the Cascadia subduction zone to the northwest; and the Sierran Nevada range to the east.

Moderate to strong earthquakes have been reported in northern California since the mid 1800's. Historical seismicity in the study region is summarized on Figure 4-2. The red pentagon symbols on the map represent the location of 19$^{th}$ century earthquakes taken from Toppozada et al. (1981). The location and magnitude of these earthquakes are based on reports of intensities of ground shaking. The green squares (magnitudes reported) and

Figure 4-2

triangles (no magnitude reported) represent earthquake epicenters from the UCB catalog for the period 1910 to 1950. These event locations were determined using data from the seismographs in the region. The blue squares (magnitudes reported) and triangles (no magnitudes reported) represent earthquake epicenters from 1950 through 1969. The installation of a higher-gain seismograph at Mineral in 1949 considerably improved the location of earthquakes in this period (Uhrhammer, 1991). Significant historical earthquakes that occurred in relatively close proximity to the DWR dam sites are discussed below.

#### *4.2.3.1 Northern Coast Ranges*

Earthquake activity in the northern Coast Ranges is directly related to interactions between the major lithospheric plates (Hill et al., 1991; Castillo and Ellsworth, 1993). As described in Chapter 2, transpressional motion between the Pacific Plate and the Sierra Nevada microplate is accommodated across a 62 mile (100 km) -wide northwest-trending zone of distributed shear that extends from San Francisco Bay to the vicinity of the Mendocino Triple Junction near Cape Mendocino. The major strike-slip faults of this zone are the San Andreas fault, which ruptured along the coast in 1906; the Maacama, Healdsburg, and Rodgers Creek fault zones to the east of the San Andreas fault; and further east, the Bartlett Springs and Green Valley fault zones (Castillo and Ellsworth, 1993; Section 3.5). Crustal shortening is accommodated by structures in the Coast Range-Sierran Block boundary zone (e.g., segments of the blind Great Valley thrust fault). Relative convergent motion between the Gorda plate, a structural element of the larger Juan de Fuca plate, and the Sierra Nevada microplate is accommodated along the Cascadia subduction zone, which extends from the Mendocino Fracture Zone north to British Columbia. At the latitude of the Mendocino transform the Gorda plate is undergoing internal deformation as it is subducting into the mantle (McPherson, 1989; Hill et al., 1990). Much of the seismicity in the vicinity of Cape Mendocino is related to shallow deformation in the overlying Sierran microplate (McPherson, 1989; Hill et al., 1990; Section 3.6).

*4.2.3.1.1 March 31, 1898, Sonoma County, $M_L$ 6.2*

This earthquake was located north of San Pablo Bay in Sonoma County (Toppozada et al., 1981; Figure 4-2). Maximum Modified Mercalli intensity (MMI) of IX was observed at Schellville (just south of Sonoma) and at the Mare Island Naval Yard. Extensive ground cracking was reported at Schellville and Mare Island. Houses were shaken from their foundations at these locations and along the Petaluma River (Toppozada et al., 1981). The area of MMI VIII+ ground motion was about 205 $mi^2$ (530 $km^2$) (Toppozada et al., 1981). The earthquake was felt in Williams and Colusa at an intensity of V and IV, respectively (Toppozada et al., 1981). The area of maximum intensity encompasses the Rodgers Creek fault zone to the west. However, the uncertainty of epicentral location based on felt intensity does not permit an association with a specific fault (Wong, 1991). Estimates of the magnitude for this event range from $M_L$ 6.2 to $M_L$ 6.7 (Ellsworth, 1990; Toppozada, 1992).

*4.2.3.1.2 April 15, 1898, Mendocino County, M 6.5*

This earthquake was located along the coast near Mendocino (Figure 4-2). It caused intensity IX damage at Greenwood 15 miles (24 km) south of Mendocino and at Noyo 9 miles (14 km) north of Mendocino; Toppozada et al., 1981). Intensity V effects were observed at Willows (Toppozada et al., 1981). The San Andreas fault is located approximately 6 miles (10 km) offshore and could reasonably be assumed to be the causative fault. Ellsworth (1990) has calculated a magnitude of M 6.5 for this earthquake.

*4.2.3.1.3 December 21, 1954, Arcata, M 6.6*

This earthquake was located onshore in Humboldt County about 12 miles (20 km) northeast of Arcata (Figure 4-2). The earthquake caused an estimated $2.1 million in damage and resulted in one death. This event is significant because it is probably related to slip along a thrust fault accommodating strain in the upper plate of the Cascadia subduction zone (Tobin and Sykes, 1968; Smith and Knapp, 1980). In contrast, the majority of earthquakes in the region are intraplate (i.e., Gorda slab) events.

#### *4.2.3.2 Western Sierra Nevada*

The western foothills of the Sierra Nevada are an area of low to moderate seismic activity (Figures 4-1 and 4-2). The largest historical earthquake in this region was a $M_L$ 5.7 event located near Chico in 1940. The foothills region between Willows and Chico was active in the historical period as it is currently. On July 24, 1903 a $M_L$ 4.5 (MMI VII) earthquake occurred near Willows (Real et al., 1978). On May 24, 1966 a $M_L$ 4.6 earthquake occurred just east of Chico, and on April 29, 1968 a M 4.7 event occurred 9 miles (15 km) east of Willows (Figure 4-2). Details of some of the historic earthquakes are provided below.

##### *4.2.3.2.1 January 7, 1881, M 5.0*

An earthquake on January 7, 1881 occurred in the vicinity of Red Bluff (Figure 4-2). Toppozada et al. (1981) reported intensity V-VI effects in Red Bluff and Lovelock. They also noted a possible foreshock, felt in Red Bluff and Chico, on January 2. The location estimated by Toppozada et al. (1981) is west of the Chico monocline, about halfway between Red Bluff and Chico.

##### *4.2.3.2.2 June 6, 1884, M 4.2*

Toppozada et al. (1981) located this event north-northwest of the town of Red Bluff (Figure 4-2) and assigned it a MMI V. It apparently was not a widely felt earthquake (Toppozada et al., 1981).

##### *4.2.3.2.3 February 8, 1940, Chico, $M_L$ 5.7*

This is the largest historical earthquake in the western Sierra Nevada (Figure 4-2). Bolt and Miller (1975) reported a $M_L$ 5.7 and Richter (1958) reported a M6 for the event. The Bolt and Miller (1975) location is about 22 miles (35 km) northeast of Chico. Richter (1958) reported damage at Chico and Grass Valley to the southwest and southeast, respectively. Richter (1958) also reported that the earthquake was difficult to locate and that there was evidence that it might have occurred as deep as 22 miles (35 km). This event and the November 18, 1942 earthquakes near Sterling City (see below) occurred in the vicinity of the Quaternary Cohasset Ridge or Beaver Creek faults.

*4.2.3.2.4 November 18, 1942, Sterling City, M 4.8*

Two events of M 4.8 (Ake, 1991) occurred 15 seconds apart on November 18, 1942, a few km southeast of Sterling City (Bolt and Miller, 1975). The location of these events is about 9 miles (15 km) southeast of the 1940 event and about 19 miles (30 km) northeast of Chico. Two MMI Vl reports from Sterling City (Bolt and Miller, 1975) for each event may be an additive result of two earthquakes occurring so close together in time. The maximum intensities and resulting magnitudes of these earthquakes, therefore, may be less than MMI VI and M 4.8, respectively.

### *4.2.3.3 Coast Ranges – Sierran Block Boundary Zone*

The DWR dam sites lie along the western edge of the Sacramento Valley in a tectonic zone referred to as the Coast Ranges-Sierran Block (CRSB) boundary zone (Wong and Ely, 1983). The CRSB boundary zone is part of the broad transpressional boundary between the Pacific Plate and Sierra Nevada microplate (Chapter 2). The CRSB boundary zone is an active fold and thrust belt between the high-angle, northwest-striking dextral faults of the Coast Ranges and the Sierran Block. It is underlain by the Great Valley fault, a system of blind, segmented thrust faults (see detailed discussion in Chapters 2 and 3). Evidence for seismic activity of blind thrust faults in the southern CRSB boundary zone includes the occurrence of the 1982 $M_L$ 5.4 New Idria, the 1983 $M_L$ 6.7 Coalinga, and the 1985 $M_L$ 5.5 North Kettleman Hills earthquakes in the western San Joaquin Valley (Eaton, 1985). The historic 1889 $M_L$ 6 Antioch earthquake and the 1892 $M_L$ 6+ Winters-Vacaville sequence (O'Connell et al., 2001) provide evidence of the seismogenic potential of the northern CRSB boundary zone in the southwestern Sacramento Valley. These and other significant earthquakes in the CRSB boundary along the Sacramento Valley are discussed below.

*4.2.3.3.1 May 19, 1889, Antioch, M 6*

This earthquake (Figure 4-2) demolished many chimneys in the town of Antioch (MMI VII) and caused some ground cracking on Main Street (Toppozada et al., 1981). Intensity VIII effects were observed in Collinsville, about 6 miles (10 km) to the north.

On September 10, 1965, a $M_L$ 4.9 earthquake also occurred in this region. A prominent north-trending zone of microseismicity traverses the area, with the majority of earthquake focal depths in the range of 10 to 14 miles (16 to 23 km). This evidence clearly indicates continued activity in the region of the 1889 earthquake.

*4.2.3.3.2 April 19 – 30, 1892, Winters-Vacaville, $M_L$ 5.5 – 6.4*

The first earthquake in this sequence of three significant events occurred on April 19, 1892 (Figure 4-2). The highest intensities (MMI IX) were observed at Allendale, located between Winters and Vacaville, where structures collapsed, were shifted from their foundations, or wrenched apart (Toppozada et al., 1981). Fissures extending about a mile were observed near Allendale, which suggests the possibility of surface rupture (Toppozada et al., 1981) although secondary rupturing or ground failure from strong shaking may be a more likely explanation (Bennett, 1987; WLA, 1997). Extensive damage (MMI VIII) was reported at Winters and Vacaville and intensity VII effects were reported at Williams (Toppozada et al., 1981). Toppozada et al. (1981) have estimated the magnitude of this event at $M_L$ 6.4.

The second earthquake occurred on April 21, 1892, causing considerable damage to structures already weakened by the April 19 event. This event appears to be closer to Winters (Figure 4-2) as that town suffered more damage on April 21 than on April 19 (Ellsworth, 1990). MMI VI effects were reported at Williams and Willows (Toppozada et al., 1981). Toppozada et al. (1981) have estimated the magnitude of the April 21 event at $M_L$ 6.2.

The third earthquake occurred on April 30, 1892. This event was smaller than the previous earthquakes and is considered an aftershock of the April 19 event. The maximum reported intensities (MMI VI) were at Davis and Sacramento, east of the April 19 and 21 events (Figure 4-2), and the magnitude is estimated at $M_L$ 5.5 (Toppozada et al., 1981).

Two significant earthquakes occurred after the 1892 sequence in 1902 and 1904 (Toppozada et al., 1981). The first occurred on May 18, 1902, about 5 miles (8 km) east of Vacaville at Elmira. Maximum reported intensity was MMI VII-VIII. Real et al. (1978) have estimated the magnitude at $M_L$ 5.5. The second occurred on July 30, 1904, at Winters, with MMI VI effects reported. Real et al. (1978) have estimated the magnitude for this event at $M_L$ 4.5. These earthquakes are located in the meizoseismal areas of the 1892 events and are probably aftershocks.

O'Connell et al. (2001) conclude that the likely sources of the 1892 Winters-Vacaville earthquake sequence were blind, west-dipping segments of the Great Valley fault. A possible modern analog for the 1892 Allendale sequence is the May 2, 1983, Coalinga earthquake ($M_L$ 6.7), which occurred within a reach of the CRSB boundary zone in the San Joaquin Valley. This 1983 earthquake has been located at a depth of 6 miles (10 km) beneath the Coalinga anticline (Rymer and Ellsworth, 1990, and papers therein). Seismological studies document a thrusting mechanism on a plane dipping approximately 30 degrees to the southwest (Eberhardt-Phillips, 1989). There was no surface rupturing associated with the mainshock, although surface rupture was observed following a $M_L$ 5.2 aftershock on the nearby Nunez fault, an east-dipping high-angle reverse fault located about 9 miles (14 km) west of the mainshock in the hanging wall of the seismogenic thrust fault (Eberhardt-Phillips, 1989).

*4.2.3.3.3 October – December, 1943, Maxwell Swarm*

A swarm of small earthquakes occurred in the region between Maxwell and Williams from October to December 1943. The UCB network recorded five earthquakes, ranging from $M_L$ 3.6 to $M_L$ 4.0. The UCB catalog at this time probably was complete down to M 3.5 so the many smaller earthquakes typically present in swarms probably were not detected. In the UCB catalog the sequence starts on October 14, 1943 with two earthquakes, a $M_L$ 3.6 event 5.5 miles (9 km) southwest of Sites and a $M_L$ 3.7 event 2.5 miles (4 km) southeast of Sites. On November 15 a $M_L$ 4.0 event occurred 9 miles (14 km) southeast of Sites (between Maxwell and Williams) followed the next day by a $M_L$ 3.8 event 10 miles (16 km) southeast of Sites. The final event recorded in the catalog was

a $M_L$ 4.0 earthquake located about 12 miles (19 km) southeast of Sites (5 km northwest of Williams) on December 4, 1943. The epicentral resolution of the UCB seismic network at this time was poor and information on focal depths is not in the catalog. This swarm occurred in the vicinity of the well-recorded Maxwell swarms in 1980 and 1982 (Wong et al., 1988; Section 4.3.3). These swarms extend north-south between Williams and Maxwell.

## 4.3 INSTRUMENTAL SEISMICITY

The instrumental seismicity data used in this study consist of earthquake location parameters, phase data, and focal mechanism solutions from the Northern California Earthquake Data Center (NCEDC), a joint project of the U.S. Geological Survey and the University of California Berkeley Seismological Laboratory. The NCEDC is a long-term archive and distribution center of seismologic and geodetic data from northern and central California. The primary earthquake data acquisition system for the NCEDC is the Northern California Seismic Network (NCSN) operated by the USGS in Menlo Park. The NCSN is a dense telemetered array of short-period seismometers deployed throughout northern and central California to provide data on phase arrival times, first motions of phase arrivals, and wave amplitudes. As of 1998 there were 376 stations in this network operated by the USGS. An additional 92 stations operated by UCB, the California Institute of Technology, and University of Nevada, Reno, and the Department of Water Resources (DWR) are also recorded. Figures 4-3 and 4-4 show the distribution of seismograph stations in the region for the periods of 1900 to 1979 (Figure 4-3) and 1980 to 2000 (Figure 4-4).

### 4.3.1 Compilation of the Instrumental Catalog

The catalog of earthquakes used in this study contains events recorded by the NCSN from 1970 through 2000, covering the region from latitude 38 to 41 degrees north and longitude 120.5 to 124.5 degrees west. There are 131,741 earthquakes in this dataset ranging in magnitude from M 0.0 to M 6.1. Explosion events from quarries or other

Figure 4-3

Figure 4-4

sources were deleted from the NCSN catalog if they were identified as such (the catalog entry is annotated with a "Q" by USGS analysts). Figure 4-1 shows a refined subset of this catalog that contains those earthquakes that have higher quality hypocentral locations. Earthquake locations shown on this map are derived from hypocentral solutions that have root-mean-square (RMS) errors ≤ 0.25 seconds, epicentral location errors (ERH) ≤ 2.5 km and focal depth errors (ERZ) ≤ 5.0 km. The symbols for earthquakes on Figure 4-1 are scaled in size by magnitude and are colorized by focal depth. The final instrumental catalog for the seismicity study area contains 100,034 earthquakes.

### 4.3.2 Completeness of the Instrumental Catalog

**The magnitude level at which earthquake detection is complete depends on the spacing of seismograph stations. In the densest areas of the network (e.g., the central Coast Ranges), event detection is complete down to M 1.4 (Oppenheimer et al., 1993). In regions of greater spacing between seismograph locations (e.g., the Klamath Mountains), detection may only be complete to M 2.6 (Oppenheimer et al., 1993). In the CRSB boundary zone seismographic station coverage is sparse except in the Red Banks region, which is monitored by the five stations of DWR's Red Banks Microseismic Network. Data from this network is routinely incorporated into the NCSN.**

### 4.3.3 Regional Seismicity, 1970 – 2000

Figure 4-1 shows the distribution of earthquakes in the region from 1970-2000. Events that do not satisfy the quality restrictions described above are not shown. The distribution of epicenters from 1970 to 2000 is similar to that of the historical earthquakes (Figure 4-2). The most prominent zones of seismic activity are in the northern Coast Ranges, and are associated with faults of the San Andreas fault system and active subduction of the Gorda plate beneath the North American plate (Hill et al., 1991; Castillo and Ellsworth, 1993). East of the Sacramento Valley, there is a low to moderately active zone of seismicity that coincides with the Walker Lane Belt as it extends northwest from the Lake Tahoe region to Lassen Peak; this seismogenic zone has been referred to in the literature as the Sierra Nevada – Great Basin boundary zone (Van Wormer and Ryall, 1980). In the Sacramento Valley, seismic activity occurs at a relatively low level and tends to be

associated in clusters (Wong et al., 1988). Some of these clusters are isolated such as in the vicinity of Lake Oroville (related to the 1975 $M_L$ 5.7 Oroville earthquake; Hill et al., 1991), in the vicinity of Williams (the Maxwell and Colusa swarms; Wong et al., 1988) and near the town of Madison (site of a M 4.2 event in 1978; Wong, 1992). Other clusters are more diffusely distributed such as the activity in the Willows area and the zone of seismicity extending from Red Bluff to Redding. As can be seen in Figure 4-1, the earthquakes in the Sacramento Valley are located significantly deeper than events in the northern Coast Ranges to the west and the Sierra Nevada to the east.

#### *4.3.3.1 Northern Coast Ranges*

##### *4.3.3.1.1 Maacama Fault*

The Maacama fault extends approximately 84 miles (135 km) northwest from Healdsburg to Laytonville (Section 3.5.2). A prominent zone of seismicity is associated with this fault (Hill et al., 1991). Epicenters generally lie east of the trace, which is consistent with observed eastern dip of the seismogenic fault plane (see Section 2.2; Castillo and Ellsworth, 1993). Figure 4-1 shows that seismicity along the Maacama fault is generally restricted to the upper 9 miles (15 km) of the crust. Seismicity is deepest along the northern three-quarters of the fault and shallows considerably along the segment near Clear Lake, in the vicinity of the Geysers geothermal area. Epicenters along the Maacama fault form lineaments that are subparallel to the fault (Castillo and Ellsworth, 1993). At the northern termination of the fault seismicity becomes more diffuse, and north of Laytonville seismic activity ceases.

##### *4.3.3.1.2. Bartlett Springs Fault Zone*

The Bartlett Springs fault zone is a 70-mile (113-km) long system of faults that extends from the vicinity of the Indian Valley Reservoir northwest to Round Valley (Castillo and Ellsworth, 1993; Section 3.5.3). Seismicity along the Bartlett Springs fault zone (Figure 4-1) is discontinuous along strike compared to the activity along the Maacama fault. Earthquakes occur in dense clusters primarily along the Twin Valley, McLeod Ridge, and Coyote Ridge segment (Hill et al., 1991; Plate 1). There are very few earthquakes along

the fault south of the Twin Valley segment to the intersection with the Hunting Creek Fault. North of the Coyote Ridge segment, the sparse clusters of earthquakes seem to have a more northerly trend, especially in Round Valley where earthquakes appear to extend in a northerly direction between the northwest-striking Bartlett Springs and Etsel Ridge faults (Castillo and Ellsworth, 1993; Plate l). As shown in Figure 4-1, earthquakes are nucleating at depths between 3 and 9 miles (5 and 15 km), generally east of the main trace of the fault.

*4.3.3.1.3 Green Valley Fault System*

The Green Valley fault system is a discontinuous zone of north- to northwest-striking late Quaternary and Holocene faults that extends from Suisun Bay northwest to near Clear Lake (Figure 1-3). Discontinuous clusters of seismicity trending north and northwest are associated with the structural elements of this fault system (Wong, 1990). The closest active segment of this system to the DWR dam sites (located 28 miles [45 km] to the north) is the north-striking Hunting Creek fault (Plate 1), which has been shown to have Holocene activity (see summary of literature in WLA, 1997). Interestingly, recent seismicity is not associated with the Hunting Creek fault but occurs in a northwest alignment approximately 10 km to the west (Wong, 1990). Figure 4-1 shows that the seismicity related to these structures is located at shallower depths than along the Bartlett Springs fault.

*4.3.3.1.4 Gorda Plate*

Although the Cascadian subduction zone is capable of generating large magnitude earthquakes, as evidenced by the 1992 $M_w$ 7.2 Cape Mendocino earthquake, the distance between the proposed damsites and the probable locus of a large interplate event is such that ground motions from smaller but closer seismogenic source zones will control the design of the dams (this issue is addressed quantitatively in Chapter 7). For this study we are concerned with the potential for a large intraplate earthquake to occur within the Gorda slab as it descends beneath the northern Coast Ranges and the Sacramento Valley. Large downdip intraplate earthquakes that precede large interplate subduction zone events have been observed along the Middle America trench (McNally et al., 1986;

McNally and Gonzalez-Ruiz, 1986) and the Peru-Chile trench (Dewey and Spence, 1979; Beck and Ruff, 1984; Astiz and Kanamori, 1986).

Earthquake activity in the Gorda plate is shown in Figure 4-1 as the 'warmer' colored symbols (green to red) north of latitude 40.25 degrees. These events are located from 9 to 15 miles (15 to 25 km) depth near the coast and deepen gradually to the east. This trend in seismicity represents a dipping Benioff-Wadati zone, which is commonly associated with active subduction zones around the world (Smith and Knapp, 1980). Because the seismic interface between the plates is restricted in down-dip extent by the rheological properties of the crust the large interplate events are restricted to the region near the coast (Byrne et al., 1988; see Section 3.6). The deeper seismicity in the Benioff-Wadati zone represents brittle failure within the Gorda plate during its descent into the mantle (Walter, 1986). No large-magnitude earthquakes from this deeper zone have been recorded, perhaps because the Gorda plate is very fragmented at its southern end (McPherson, 1989; Hill et al., 1990).

#### *4.3.3.2 Western Sierran Microplate*

In the central Sacramento Valley and the foothills of the Sierra Nevada, seismicity occurs at a low rate relative to the northern Coast Ranges (Hill et al., 1991). The largest event in this region is the $M_L$ 5.7 Lake Oroville earthquake in August, 1975 (Langston and Butler, 1976). In contrast to the linear alignments of epicenters along active faults to the west, seismicity generally occurs in clusters scattered throughout the region (Wong et al., 1988). This clustering is similar to patterns of seismicity in the central Sierra Nevada to the south and the Basin and Range to the east. Figure 4-1 shows that seismicity in the northern Sierra Nevada is generally shallow, deepening to the west in the Sacramento Valley. The seismically active regions include: the area west of Lake Almanor; an area in the northern part of the Sacramento Valley northeast of Red Bluff; the Lake Oroville region; and the area between Willows and Chico in the central part of the valley (Hill et al., 1991). Some of the significant seismicity patterns are discussed below.

*4.3.3.2.1 August 1, 1975, Oroville, $M_L$ 5.7*

On August 1, 1975 a $M_L$ 5.7 earthquake occurred in the Sierran foothills 7 miles (11 km) southwest of Lake Oroville (Sherbourne and Hauge, 1975; Lahr, et al., 1976; Morrison et al., 1978). This event was strongly felt throughout the Sacramento Valley and caused some damage in the town of Oroville. The mainshock was located using teleseismic phases at a relatively shallow depth of 3.4 miles (5.5 km) on a normal fault oriented north-south, dipping approximately 65 degrees to the west, and a rake of –70 degrees (Langston and Butler, 1976). The distribution of aftershocks also is consistent with a north-striking, west-dipping fault, a pattern that is readily visible in Figure 4-5 with the shallower (black) epicenters to the east of the deeper (blue) epicenters to the west (Lester et al., 1975). Surface fractures mapped by Clark et al. (1976) were formed above the up-dip projection of the fault zone delineated by the aftershocks. The sense of motion (west-side-down) and orientation of the fractures (north-south) also are consistent with focal mechanisms that indicated primarily normal dip-slip motion (Clark et al., 1976). Because of the proximity of the earthquake to Lake Oroville, it has been suggested that the event was triggered by the impoundment of water for the reservoir (see Section 4.6.1)

*4.3.3.2.2 Red Bluff Region*

Seismic activity in this region is located northeast of the city of Red Bluff and generally south of the Battle Creek fault. Seismicity has been occurring at a low, consistent rate since 1981 (Wong et al., 1988). Earthquakes commonly nucleate at depths ranging from 3 to 15 miles (5 to 25 km), with several events located at depths between 25 and 43 miles (40 and 70 km). These deeper events may have come from the subducted Gorda plate (Walter, 1986). Although seismograph coverage is adequate in this region relative to other Central Valley locations, no coherent pattern of epicenters is apparent on Figure 4-1.

Figure 4-5

*4.3.3.2.3 Willows Region*

Seismic activity in the Willows region is diffusely distributed with a tendency for spatial clustering along the axis of the Sacramento Valley, east of the Corning and Willows faults (Section 3.5.12; Figure 4-5). Figure 4-1 shows that the earthquakes in this area have focal depths significantly deeper than those occurring along the active strike-slip faults to the west (Hill et al., 1991). Two main clusters are visible in Figure 4-5: one at the latitude of Willows along the Sacramento River, and one further to the north at the latitude of Orland. Wong et al. (1988) have suggested that the Willows and Corning faults are the sources of this activity. Seismicity is more broadly distributed to the northeast across the valley with an apparent northwest alignment of epicenters near Chico. West of the Willows clusters seismicity is also diffuse, with the area south of the town of Willows tending to have more activity.

Seismic activity in the Willows region has occurred throughout the twentieth century (Marks and Lindh, 1978; Figure 4-2). In 1903 a $M_L$ 4.5 earthquake occurred near Willows (Real e tal., 1978). In 1966 a $M_L$ 4.6 earthquake occurred just east of Chico and in 1968 a $M_L$ 4.7 earthquake occurred in the southern Willows cluster. In 1971 a $M_L$ 4.1 earthquake occurred between Willows and Maxwell (Figure 4-5) but the NCSN location is poor due to lack of coverage. Magnitudes of earthquakes recorded since 1971 have all been less than M 4.

### 4.3.4 Seismicity in the Northern Coast Ranges – Sierran Block Boundary Zone, 1970 – 2000

Seismicity along the CRSB boundary zone in the Sacramento Valley is diffusely distributed compared to the concentration of earthquakes along the Maacama and Bartlett Springs faults in the adjoining northern Coast Ranges to the west (Figure 4-1). In some areas seismicity is concentrated in clusters (e.g., near the towns of Maxwell and Williams; Figure 4-5). In other areas the seismicity is more diffuse.

Seismic activity in the northern CRSB boundary zone is low and diffusely distributed in

the area west of the Corning and Willows faults between Sites and Red Bluff (Figure 4-5). The largest event to have been recorded in this area was a $M_L$ 4.2 on September 3, 1982, which occurred north of the Stony Gorge Reservoir.

Seismicity in the CRSB boundary zone between the town of Sites and city of Fairfield tends to occur in small clusters (Figure 4-1). Activity in the Maxwell region, southeast of the dam sites, is shown on Figure 4-5. The hypocenters extend to greater depths than earthquakes along the Bartlett Springs fault to the west or in the Lake Oroville region on the eastern side of the valley. Focal depths of the Willows earthquakes to the north are even deeper. Two clusters of seismicity have occurred in this region during the past several decades: one just west of Maxwell and Williams, with epicenters trending north-south; and one between Williams and Colusa, with epicenters trending northwest (Figure 4-5). The first, referred to here as the Maxwell swarm, consists of two groups of events spaced closely together in space and time. The first sequence began in 1980, with a $M_L$ 4.3 event occurring on November 11 in the northern part of the swarm, near Maxwell. This sequence lasted until mid-December and included five events with magnitude between three and four. The second Maxwell sequence was located to the south, northwest of the town of Williams. This sequence started on December 2, 1982 and lasted until December 5, 1982. Fourteen earthquakes were reliably located by NCSN, ranging in magnitude between 1.5 and 3.3. The second cluster, referred to as the Colusa swarm, occurred during a five month period, from April to September, 1985. These earthquakes are aligned in a northwest direction and range in magnitude from 0.1 to 3.8. During 1989 another, smaller, swarm of microseismicity occurred in the Maxwell area. This pattern of spatial and temporal clustering is similar to the 1943 activity in the Maxwell area discussed in Section 4.2.3.3.3.

Seismicity in the CRSB boundary zone south of the Maxwell and Colusa swarms occurs at a relatively low level and tends to appear in clusters such as in the Dunnigan Hills and near the town of Madison. The earthquakes in the Dunnigan Hills have a northwest trend that may parallel the axis of the Dunnigan Hills anticline (Figure 4-1; Wong et al., 1988).

Madison, which is south of the Dunnigan Hills, was the site of a $M_L$ 4.2 earthquake on Spetember 8, 1978. This event caused minor damage in Winters (Wong et al., 1988).

## 4.4 FOCAL DEPTHS IN THE STUDY REGION

We analyzed focal depths in the study region to estimate the thickness of the seismogenic crust (Hill et al., 1991). To visualize the maximum depth of seismicity in the study area, the circles representing epicenters on Figure 4-1 are colorized according to their focal depths. The vertical error associated with the NCSN-computed earthquake focal depths shown on the map is ± 3 miles (± 5 km). Three cross-sections (Figure 4-6) through the study area (Figure 4-7 [Section A-A' through 40°N], Figure 4-8 [Section B-B' through 39.75°N], and Figure 4-9 [Section C-C' through Sites and Golden Gate dam sites]) allow comparison of focal depths within the Sierran microplate. The locations of these cross sections are identical to those of the three crustal-scale cross sections presented in Chapter 2 (i.e., Figures 2-3, 2-4 and 2-5). Locations of the geologic sections are shown in Figure 1-3.

### 4.4.1 Northern Coast Ranges

Focal depths for earthquakes in the northern Coast Ranges south of Cape Mendocino generally range in depth up to 9 miles (15 km; Hill et al., 1991). The focal depths tend to become shallower going from the north to the south, especially along the Healdsburg and Rodgers Creek faults (Figure 4-1). In general, heat flow in the Coast Ranges is high and reaches a maximum in the Clear Lake region about 124 miles (200 km) south of Cape Mendocino (Lachenbruch and Sass, 1980). It has been postulated that as the Mendocino triple junction and the Gorda plate have migrated north along the coast of California, a sub-crustal 'window' or "slab gap" has developed that allows upwelling asthenospheric mantle to come in direct contact with the lithosphere of the Sierra Nevada microplate (Dickinson and Snyder, 1979; Lachenbruch and Sass, 1980). The Geysers steam field southwest of Clear Lake is evidence of the high heat flow in this region. The intense

Figure 4-6

Figure 4-7

Figure 4-8

Figure 4-9

clustering of shallow events (3 miles [5 km] or less; shown as black circles on Figure 4-1) in this area most likely is related to the high heat flow, which has locally elevated the brittle-ductile transition zone and base of seismicity (Eberhart-Phillips and Oppenheimer, 1984; Castillo and Ellsworth, 1993).

The elevated heat flow anomaly in the northern Coast Ranges also decreases from west to east (Lachenbruch and Sass, 1980). Figure 4-1 shows that seismicity deepens from the Maacama fault to the Bartlett Springs fault and significantly deepens to the east in the Sacramento Valley. This trend is seen most clearly in Section B-B' (Figure 4-8). Figure 4-10 shows histograms of focal depths for this region derived from the refined NCSN dataset described in Section 4.3.1. The mean focal depth for earthquakes associated with the Maacama fault is 4 ± 0.6 miles (6.4 ± 0.1 km) and 95 percent of the events are located at depths ≤ 6.8 miles (11 km). The mean focal depth for earthquakes associated with the Bartlett Springs fault is 5.3 ± 0.6 miles (8.5 ± 0.1 km) and 95 percent of the events are located at depths ≤ 8.7 miles (14 km). This eastward deepening of the seismogenic zone is consistent with the decline in the heat flow and a similar pattern is associated with the Hayward and Green Valley fault zones in the San Francisco area (Lachenbruch and Sass, 1980; Hill et al., 1990).

#### *4.4.1.1 Focal Depths in the High Coast Ranges*

The distribution of focal depths in the high Coast Ranges in the western part of Tehama County appears to be transitional between the shallow seismicity associated with the transform boundary to the west and the significantly deeper earthquakes to the east in the Sacramento Valley (Section B-B', Figure 4-8). The shallow earthquakes are restricted to an area bounded by the Middle Fork of the Eel River on the west and the western margin of the Sacramento Valley on the east. In this region the Coast Ranges reach their maximum elevation at South Yolla Bolly (8088 feet [2466 m]).

The association of elevated topography and shallow seismicity may be causal. Benz et al. (1992) conducted a study of teleseismic P-wave velocity variations in northern California, and concluded that a region of low upper mantle P-wave velocity exists in the

Figure 4-10

approximate area of the western Tehama County seismicity. They note a correlation between the elevated topography of the Coast Ranges and the presence of an aseismic lower crust/upper mantle. They interpret this as evidence of a "slab window" in the wake of the migrating Gorda plate that allows the underlying asthenosphere to be in direct contact with the base of the North American lithosphere. The presence of warm, thermally bouyant asthenospheric mantle directly beneath the crust may support the elevated topography. Focal mechanisms from the earthquakes in the high Coast Ranges (see following section) suggest that the upper crust is in tension, possibly as a result of associated gravitational buoyancy forces acting on the elevated topography (see discussion in Chapter 5).

### 4.4.2 Sierran Microplate

Focal depths along an east-west traverse across the Sierran microplate vary from shallow along the boundary with the Basin and Range to the east (see, for example, the Lake Almanor region on Figure 4-1) to very deep in the Sacramento Valley (Section A-A', Figure 4-7). There is no discernable north-south variation in the average depth of seismicity in the Sierran microplate as there is in the Coast Ranges. Seismicity generally is confined to the boundary zones with adjacent regions. Heat flow declines westward from highs at the Sierra Nevada-Great Basin boundary to a low beneath the Sacramento Valley (Henyey and Lee, 1976). Figure 4-11 shows the distribution of focal depths in the Lake Oroville region, at the eastern margin of the Sacramento Valley. The mean focal depth for the Oroville earthquakes is 3.4 ± 0.1 miles (5.4 ± 0.1 km) and 95 percent of the events are located at depths ≤ 6 miles (10 km). In the Red Bluff region, in the northern part of the Sacramento Valley, the mean focal depth (Figure 4-11) is 10 ± 0.6 miles (16.0 ± 0.9 km) and 95 percent of the events are located at depths ≤ 16 miles (26 km). The Red Bluff region seems to be transitional with respect to focal depths as the regions directly to the east are characterized by relatively shallow seismicity and the regions to the north and south are characterized by predominantly deeper seismicity (Figure 4-1). Seismicity in the Willows region, including the area around Chico, is located at a mean depth of 11.8 ±

Figure 4-11

0.3 miles (19.0 ± 0.4 km) and 95 percent of the events are located at depths ≤ 16 miles (26 km; Figure 4-11).

### 4.4.3 Coast Ranges – Sierran Block Boundary Zone

Focal depths for regions in the CRSB boundary zone are transitional from the Coast Ranges to the Sierran microplate, and thus, may vary considerably (Figures 4-8 and 4-9). In the north, earthquakes in the western part of Tehama County have focal depths that range from less than 3 miles (5 km) in the west to 25 miles (40 km) in the east over a distance of 37 miles (60 km). The mean focal depth for these events is 5.2 ± 0.4 miles (8.4 ± 0.7 km) and 95 percent of the events are located at depths ≤ 12.5 miles (20 km; Figure 4-12). Earthquakes in the vicinity of Maxwell have focal depths that range from near surface to 19 miles (30 km). The mean focal depth for these events is 9.3 ± 0.7 miles (14.9 ± 1.1 km) and 95 percent of the events are located at depths 14 miles (≤ 23 km; Figure 4-12). In the area west of Sacramento, focal depths are variable ranging from near surface to 20 miles (33 km) with a mean focal depth of 6.5 ± 0.6 miles (10.4 ± 1.0 km) and 95 percent of the events are located at depths 12.5 miles (≤ 20 km; Figure 4-12).

To the south, earthquakes occurring in the Antioch region are clustered at significantly deeper focal depths. The mean focal depth for these events is 11.7 ± 0.2 miles (18.8 ± 0.3 km) and 95 percent of the events are located at depths ≤ 14 miles (23 km; Figure 4-12).

## 4.5 REGIONAL STRESS PATTERNS

### 4.5.1 Characterization of Tectonic Stresses From Focal Mechanisms

Focal mechanisms from well-located earthquakes in the study region were used to investigate the state of stress. The mechanisms were determined using event phase data archived at NCEDC. The program FPFIT (Reasenberg and Oppenheimer, 1985) was used to calculate the solutions. This program finds the best-fit double couple fault plane solution for a given set of observed first motion polarities for an earthquake. The

Figure 4-12

observed polarities are inverted using a two-stage grid search procedure that finds a source model (focal mechanism) that minimizes a normalized weighted sum of first motion discrepancies. The program relies on the hypocentral location and ray take-off angles provided in the NCSN data. The accuracy of the resulting focal mechanism is critically dependent on the event locations calculated by NCSN. Because the hypocentral locations are dependent on such variables as station coverage and the velocity model used in the inversion, the accuracy may vary widely over this region. For this phase of the study only high-quality solutions from earthquakes with well-constrained hypocentral locations were selected. The following criteria were applied:

- Only events greater than or equal to magnitude 1 were accepted.
- Focal depths must be greater than 0.6 miles (1.0 km).
- Hypocentral locations must have a root-mean-squared travel time residual less than 0.50 sec.
- At least 10 valid first motion readings must be available for each event.
- Events that did not converge to a solution within a specified number of iterations were rejected.
- Solutions with misfit values greater than 0.20 were rejected.
- Solutions with uncertainties in strike and/or dip greater than 20 degrees were rejected. The rake is the least stable parameter and uncertainties greater than 20 degrees were accepted.

In some cases, the program found more than one fault plane solution that would fit the data. This often happens in areas where the station coverage is less than optimal (such as in the Sacramento Valley) or the velocity structure of the region is poorly constrained. In these situations the following additional constraints were applied, providing the event met the above criteria:

- Station distribution ratio must be less than 0.40. This eliminates mechanisms with a large number of stations that lie near nodal planes.
- If two or more solutions for the same earthquake had similar uncertainties, then the solution with the fewest discrepant observations was chosen. If two or more solutions had similar number of discrepant observations, the solution with the fewest discrepant impulsive arrivals was chosen.

Solutions that failed to converge to a minimum were rejected.

The focal mechanisms calculated in this study are used to estimate the orientation of the principal stresses in the seismogenic crust (Figure 4-13). The local orientation of the maximum and minimum principal stresses are assumed to be parallel to the seismic P- and T-axes, respectively, derived from the focal mechanisms. This permits a comparison of tectonic styles in the region and also provides a framework for assessing the potential for seismogenic reactivation of pre-existing structures. There may be considerable variability in the estimated orientations of the principal stresses for individual focal mechanisms. In order to estimate the stresses acting on the source zones, a best-fit solution for groups of P-and T-axes was calculated using the program PTPLOT (Reasenberg and Oppenheimer, 1985). This program summarizes the distribution of the axes for events in a source zone and calculates a best-fit stress model for all the individual focal mechanisms. A solution is generated for the maximum and minimum principal stress axes independently and 95 percent confidence regions about the axes are calculated.

### 4.5.2 Stress Patterns in Northern California

#### *4.5.2.1 Northern Coast Ranges*

Northwest-directed dextral shear along the Pacific-Sierran plate boundary at the latitude of the dam sites is distributed across the San Andreas, Maacama, and Bartlett Springs faults (Castillo and Ellsworth, 1993). Figures 4-13, 4-14 and 4-15 show the orientation of

Figure 4-13

Figure 4-14

Figure 4-15

P and T axes for the Maacama and Bartlett Springs faults. The segment of the San Andreas fault in the northern Coast Ranges has been relatively aseismic since the 1906 rupture.

The Maacama fault is characterized by predominantly strike-slip faulting with the maximum compressive stress generally oriented north-northeast (N16°E) and the least compressive stress oriented west-northwest (N68°W, Figure 4-14), consistent with deformation driven by northwest-directed right-lateral shear along the plate margin (Castillo and Ellsworth, 1993).

The Bartlett Springs fault is characterized by a horizontal least compressive stress orientation of west-northwest (N63°W; Figure 4-15). The girdling of P axes (Figure 4-15) indicates that significant normal and normal-oblique faulting is occurring in addition to strike-slip faulting, suggesting that seismogenic faulting may be occurring on more northerly striking planes than the geologic evidence indicates. In general, the trend of the girdling axes is consistent with the north-northeast orientation of principal compressive stress observed throughout the region. The T axes also are consistent with the general west-northwest orientation of active dextral strike-slip faults in the region.

The Green Valley fault system, which includes the Hunting Creek fault (WLA, 1997; Plate 1), is characterized by shallowly plunging P axes oriented north-northeast (N30°E; Figure 4-16), similar to the orientation along the Bartlett Springs fault and rotated slightly clockwise relative to the Maacama fault. The T axis fit to the data is oriented about S54°E (Figure 4-16). The T axes tend to girdle across the focal sphere suggesting that there is significant reverse to reverse-oblique deformation occurring, as previously observed by Wong (1990).

#### *4.5.2.2 Gorda Plate*

Seismic P- and T- axes orientations for earthquakes within the subducted Gorda plate are shown in Figure 4-17. The dip of the Gorda plate has been estimated at 10 to 14 degrees to the east (Jachens and Griscom, 1983; Smith et al., 1993) and is thought to extend down

Figure 4-16

Figure 4-17

to 50 – 56 miles (80 – 90 km) beneath the Cascade Range near Lassen Peak (Walter, 1986; Smith and Knapp, 1980).

Four hundred events with focal depths greater than or equal to 9.3 miles (15 km) are included in Figure 4-17. The stress model resolved for these earthquakes suggests a maximum horizontal compressive stress oriented north-south and a minimum horizontal compressive stress oriented east-west. This model suggests that the main mode of deformation in this part of the subducting Gorda plate is strike-slip faulting, with right-lateral slip on northwest-trending planes and/or left-lateral slip on northeast-trending planes. The north-south compression of the Gorda plate as it is obliquely subducted to the northeast beneath the North American plate is in response to a component of convergence between the larger, older Juan de Fuca plate to the north and the Pacific plate to the south (Jachens and Griscom, 1983; Wilson, 1986). Within the offshore Gorda basin, the Gorda plate has been shown to be responding to the north-south directed compression by brittle failure along vertical, left-lateral strike-slip faults oriented to the northeast, as evidenced by the 1980 M 7.2 Eureka earthquake (Smith et al., 1993; Hill et al., 1990). This mode of deformation continues to some extent as the plate is subducted beneath northern California.

The distribution of the P axes in Figure 4-17 shows that there is another subgroup of earthquakes within the subducting Gorda slab. These events, which comprise approximately 25 percent of the events analyzed, are represented by the cluster of P axes around the nearly vertical intermediate stress axis in Figure 4-17. The T axes for these earthquakes are subhorizontal and oriented east-west, and the stress model suggests normal slip on predominantly north-south trending nodal planes. The orientation of T axes for these earthquakes range from northeast to southeast and generally plunge less than 30 degrees. It is likely that these events represent the release of stress from internal deformation of the brittle Gorda plate as it is pulled into the mantle (Smith et al., 1993).

#### *4.5.2.3 Western Sierran Microplate*

Seismic P and T axes from the Red Bluff region at the extreme northern end of the western Sierran microplate are shown in Figure 4-13 and 4-18. The stress model fit to the data indicate that the horizontal principal stress is compressive and oriented northwest-southeast (N34°W; Figure 4-18). Both the P and T axes girdle the focal sphere suggesting a complex pattern of faulting. For this study only earthquakes located at depths shallower than 22 miles (35 km) were analyzed as we are interested in deformation in the upper brittle crust. As Figure 4-1 shows there are a few events with significantly deeper focal depths in the Red Bluff region. Cockerham (1984) and Walter (1986) have studied intermediate focus earthquakes in this region of northern California and provided convincing arguments that they represent a Wadati-Benioff zone arising from subduction of the Gorda plate. These events, which include two small earthquakes ($M < 3$) southeast of Red Bluff located at depths of 50 and 54 miles (80 and 87 km), one of which exhibited a thrust faulting mechanism (Walter, 1986), most likely related to internal deformation of the slab.

The 1975 Lake Oroville earthquake sequence provides an unambiguous characterization of the stresses in the western foothills of the Sierra Nevada at the latitude of the DWR dam sites. Figure 4-19 shows that the horizontal principal stress, as suggested by T-axes orientations, is the least compressive stress and is oriented west-northwest (N83°W; Figure 4-19). The P axes are strongly clustered around the vertical axis (Figure 4-19). The stress model suggests the predominant mode of faulting is by normal slip along north-south trending nodal planes as observed by Bufe et al. (1976). The inferred stress regime is consistent with the surface normal faulting observed after the August 1, 1975 mainshock, which showed west-side down motion on north-striking fault planes (Section 4.3.3.2.1; Clark et al., 1976).

The stress model derived from P and T axes in the Willows region, west of Lake Oroville, shows a similar orientation of the least compressive stress axis, although there

Figure 4-18

Figure 4-19

is considerable scatter in the data, as evidenced by the large confidence intervals about the stress axes (Figure 4-20). Part of the scatter is due to the lack of precision in the event locations because seismograph coverage in the Sacramento Valley is not as favorably spaced as it is in some regions of the Coast Ranges (Figure 4-3 and 4-4). An additional source of scatter arises from the grouping of both the north and south Willows clusters in the stress model. In the stress model fit to these data the T axis is subhorizontal and trends west-northwest (N84°W; Figure 4-20) similar to Oroville sequence (Figure 4-19) and to the events in the high Coast Ranges (Section 4.5.2.4). The P axis for this model is subhorizontal to moderately plunging (Figure 4-20), which suggests that strike-slip faulting predominates. The diffuse girdling pattern of both the P and T axes indicate that there are also significant numbers of normal- and reverse-slip earthquakes occurring in the region. Figure 4-5 shows the stress axes derived from modeling the Willows clusters separately. The north Willows cluster contains more strike-slip events while the south cluster is dominated by normal faulting events. In both clusters there are some reverse-slip events but the predominant horizontal principal stress for both is the east-west oriented minimum compressive stress. Individual focal mechanisms for some of the earthquakes in the Willows region are shown in Figure 4-21.

Wong et al. (1988) relocated one event from the Willows region and determined that the earthquake was due to reverse slip on north or northwest-striking nodal planes located 14 miles (23 km) deep. In this study we have determined a similar solution but the orientation of the subhorizontal P axis (S53°W) and the near vertical T axis (N85°E) indicates that this event may not be representative of the general population of earthquakes in the Willows region (see Figure 4-20). In addition, the epicentral location reported by Wong et al. (1988), if projected to the focal depth of 14 miles (23 km), lies too far to the west of the steeply east-dipping Willows fault to be indicative of motion on that structure. We do, however, agree with their suggestion that the Willows fault may be seismogenic and may extend into the lower crust.

Figure 4-20

Figure 4-21

#### *4.5.2.4 High Coast Ranges*

Seismic T axes for earthquakes in the high Coast Ranges in the western part of Tehama County trend east-west (N84°W; Figure 4-22), and the majority of P axes are steeply inclined, indicating that normal faulting is the dominant style of deformation in this region. Figure 4-23 shows individual focal mechanisms for some of the events in this area. Some of the deeper events shown in this figure actually may be occurring in the Gorda plate (e.g., the normal faulting event on January 14, 1998 located at a depth of 29 miles [46 km]). As discussed previously, the presence of shallow asthenospheric mantle near the base of the crust may account for the elevated topography in this section of the Coast Ranges (Benz et al., 1992). An associated increase in heat flow also would cause the base of the seismogenic zone (equivalent to the thermally controlled brittle-ductile transition zone) to be elevated. This is consistent with the observed predominance of normal faulting earthquakes with relatively shallow focal depths (less than 9.3 miles [15 km]).

#### *4.5.2.5 Maxwell*

Focal mechanisms for earthquakes near Maxwell (Figure 4-24) show that the P axes generally are oriented east-west (N88°W; Figure 4-24), which is roughly perpendicular to the axis of the folds in the CRSB boundary zone near Sites (e.g., the Sites anticline on Figure 4-5). The T axes girdle the focal sphere suggesting the occurrence of reverse-oblique slip as well as strike-slip mechanisms. The focal mechanism in Figure 4-25 for the largest earthquake ($M_L$ 4.3) in the Maxwell area on November 24, 1980; located at a depth of 12 miles (19 km), shows reverse slip on either a shallow west-dipping or a steep east-dipping plane that strikes northwest. Although there are few earthquakes in the region of the active folding and thrusting to the west, and no well-constrained focal mechanisms available, the geologic evidence points towards an east-west horizontal compressive stress direction (WLA, 1997).

#### *4.5.2.6 Colusa Region*

Focal mechanisms from events in the Colusa swarm (Figure 4-26 and 4-27) are fit to a stress model in which the horizontal compressive stress is oriented northeast-southwest

Figure 4-22

Figure 4-23

Figure 4-24

Figure 4-25

Figure 4-26

Figure 4-27

(N65E°W; Figure 4-26). The best-fit T axis is subhorizontal and oriented north-northwest (N18°W; Figure 4-26) suggesting that the predominant mode of deformation is strike-slip (Figure 4-5). The scatter in the T-axes distribution indicates there are some earthquakes exhibiting reverse and/or reverse-oblique slip. The three largest events in the 1985 swarm (April 18, May 21, and May 31; Figure 4-27) indicate that reverse slip is occurring on northwest-striking, southwest-dipping planes, or northeast-striking, southeast-dipping planes. The diffuse northwest trend of the epicenters in Figure 4-5 would seem to support failure on northwest-striking planes. Slip on northwest-striking, southwest-dipping fault planes is also consistent with Quaternary crustal shortening documented in this region (Chapter 3). The significance of the rotation of the horizontal compressive stress relative to the Maxwell earthquakes is not clear. Figure 4-27 shows that some of the focal mechanisms are not well constrained due poor station coverage.

## 4.6 RELOCATION OF EARTHQUAKES IN THE CENTRAL SACRAMENTO VALLEY

A preliminary analysis to relocate earthquakes in the central Sacramento Valley between latitude 39 degrees and 40 degrees north was conducted for this study. The purpose of the analysis was to confirm the focal depths of events in the vicinity of the DWR damsites. Sibson (1982) has suggested that the transition from seismic activity to seismic quiescence in the shallow crust marks the depth of the change in crustal deformation from brittle to ductile. As has been mentioned previously earthquakes in the central Sacramento Valley nucleate at significantly deeper depths than those in the Coast Ranges to the west and the Sierra Nevada to the east (Figure 4-1; Figure 4-5; Figure 4-10; Figure 4-11). Although there are some earthquakes in the Coast Ranges that locate at depths greater than 9 miles (15 km), the vast majority of events are restricted to depths above 7 to 9 miles (12 to 15 km; Hill et al., 1991). The seismicity cross-sections in Figures 4-8 and 4-9 show the pronounced thickening of the seismogenic crust from the San Andreas fault to the Sierran Foothills.

Accurate location of earthquakes in the central Sacramento Valley is made difficult by the lack of seismographs in the central part of the valley. Generally, a station distribution

similar to the depth of the earthquakes being studied is desirable in order to constrain the inversion. As can be seen in Figures 4-3 and 4-4 there are few stations in the valley itself. In this initial assessment we try to counter the poor station distribution by using other geophysical data to constrain the velocity structure of the crust. For example, Godfrey et al. (1999) developed a velocity model for the central Sacramento Valley at this latitude based on an 125-mile (200-km) long east-west reflection-refraction profile collected in 1993 during the Mendocino triple junction seismic experiment (Godfrey et al., 1995; Trehu, 1995; Beaudoin et al., 1996). We use their interpretation of the velocity structure in seismic line 1 that extends from Fort Bragg to Lake Oroville, and which is further constrained by using density and magnetic models (Godfrey et al., 1997), to specify the velocity structure in this region.

We first used a joint hypocentral determination algorithm to develop an ad hoc one-dimensional model of velocity and related station corrections for the region. We used the computer program VELEST (Roecker, 1981; Kraadolfer, 1989) to develop the initial reference model (Kissling et al., 1994). Between 200 and 300 earthquakes of magnitude greater than 1.5 in the central part of the valley were used to develop the reference model. These events were selected based on the error statistics of their location in the NCSN dataset. Events were excluded from this phase of the analysis if they had less than 10 observations, a gap in coverage exceeding 180 degrees, an RMS error exceeding 0.25 sec, a focal depth less than 3 miles (5 km), and epicentral errors less than 9 miles (15 km). Our starting model consisted of layers with velocities that progressively increased with depth. Once the hypocentral locations stabilized the inversion was re-run, this time allowing low velocity layers to develop. The use of low velocity layers is justified in this case because the model derived by Godfrey et al. (1997) from line 1 clearly indicates the presence of low velocity material (Sierran affinity material) structurally underlying the Great Valley ophiolite (See Figure 4-8). The resulting velocity model does not correspond to the model derived by Godfrey et al. (1997) because of the diverse crustal structure the raypaths traverse to the surrounding stations, which may be up to 125 miles (200 km) away.

Having developed an initial reference model consisting of the revised velocity model and a suite of stations corrections (i. e., time delays), we then optimized the relative location of the events. For this phase we relocated the earthquakes using the double-differencing approach of Waldhauser and Ellsworth (2000). The double-differencing technique takes advantage of the fact that if the hypocentral separation between two earthquakes is small compared to the event-station distance and the scale of crustal heterogeneities, then the ray paths between the source region and a common station are similar along most of the ray path (Waldhauser and Ellsworth, 2000). The difference in travel times for two closely spaced events observed at a common station can be attributed to the difference in spatial locations of the events. This approach optimizes the location of the earthquakes relative to each other and, in well-conditioned cases, allows the illumination of structural details such as fault planes in the crust (Waldhauser and Ellsworth, 2000).

Figures 4-28 and 4-29 show the result of this preliminary analysis of the earthquakes in the central Sacramento Valley. The hypocenters in these figures have been relocated using the double-differencing algorithm combined with the VELEST-derived reference model. Focal mechanisms have been determined for many of the relocated events using the techniques described earlier (Section 4.5.1). Figure 4-28 is a seismicity cross-section traversing northeast through the Maxwell and Colusa swarms, the Willows clusters, and terminating in the foothills near the Chico Monocline. The N70°E orientation of the cross section was selected to highlight the spatial association of the Willows seismicity with the Corning and Willows faults. The inferred orientation of the Corning fault is shown on Figure 4-28 as a dashed pink line that dips 70 degrees to the east (Harwood and Helley, 1987). The events of the Willows clusters can be seen to be spatially associated with the Corning and Willows faults over a depth range of 6 to 17 miles (10 to 27 km) with the most intense clustering located between 11 and 14 miles (18 and 23 km). This compares favorably with the pattern shown in the seismicity section in Figure 4-9, which was constructed along a similar trend. The section line in Figure 4-9 intersects the Corning

Figure 4-28

Figure 4-29

fault at a different location than in Figure 4-28 so there is a difference in the apparent dip of the fault. The cross-section in Figure 4-28 is not favorably oriented to highlight any association with seismicity on the Chico monocline fault. The inferred dip is shown as vertical.

Figure 4-29 is a seismicity cross-section that trends north-south through the central Sacramento Valley. The south Willows cluster is located directly beneath the town of Willows, and the north Willows cluster lies beneath Orland. There appears to be a trend towards shallowing of the base of the seismogenic crust going from Willows north to Corning. The small cluster of very shallow events north of Corning are located in the Sierran foothills southeast of Red Bluff. This view of seismicity again shows that the seismogenic crust extends to greater depths in the central part of the valley. Note also the concentration of seismicity at mid to lower crustal depths in the Willows region compared to the Maxwell and Colusa swarms to the south. The cause for this may be that deformation is occurring in the weaker Sierran affinity material (Godfrey et al., 1997) that has been overthrust by the more rigid Great Valley ophiolite (Godfrey and Dilek, 2000; see Figure 4-8 and 4-9).

The recalculated focal mechanisms for this dataset are shown in Figures 4-28 and 4-29 as circles colored according the rake angle of the event. Red circles correspond to reverse-slip, blue circles correspond to normal-slip and green circles correspond to strike-slip events. Preliminary stress models fit to these data are very similar to those presented in Section 4.5 except for the Maxwell swarm, which appears to be more dominated by strike-slip events than reverse-slip events.

### 4.6.1 Reservoir-Induced Seismicity

Reservoir-induced seismicity (RIS), which is the triggering of earthquakes by the physical processes that accompany the impoundment of reservoirs, is recognized as a potential hazard to many large dams. Worldwide, at least five earthquakes of magnitude 6 and greater have been associated with reservoir impoundment (Gupta, 1992; Seeber et al.,

1995). The largest known reservoir-induced earthquake was a $M_w$ 6.3 at the Koyna dam in western India (Gupta and Rastogi, 1976). This earthquake (December 10, 1967) resulted in 200 deaths, over 1500 injuries, and caused considerable damage to the engineered structures in the vicinity of the dam (Gupta and Rastogi, 1976).

Because of the potential to seriously damage impoundment structures and cause catastrophic flooding, RIS has been intensively studied (Gupta and Rastogi, 1976; Simpson, 1986; O'Reilly and Rastogi, 1986). It is not clear, however, what physical mechanism predominates in the triggering of earthquakes by impoundment and under what circumstances the hazard is increased. A correlation is observed between dam height and increased seismicity, which suggests that the potential for inducing earthquakes should be considered in dam design (Packer et al., 1979). Two mechanisms are thought to be acting in the triggering of faults, acting either independently or in concert (Simpson et al., 1988; Scholz, 1990):

(1) A change in elastic stress in the underlying crust as the reservoir is filled or goes through fill and release cycles; and
(2) An increase in fluid pore pressure at depths at which earthquakes nucleate thereby reducing the effective normal stress acting on the fault plane.

The combined effects of change in elastic stress and pore fluid diffusion may explain the occurrence of earthquakes at reservoirs a number of years after initial impoundment during periods when the lake level fluctuates. For example, the Koyna earthquake occurred five and a half years after impoundment, and the M 5.3 Aswan dam earthquake (Egypt; November 14, 1981) occurred seventeen years after impoundment (Simpson et al., 1988).

Several possible cases of reservoir–induced seismicity in northern California have been evaluated (Allen, 1982). The best known is the $M_L$ 5.7 earthquake at Oroville, approximate 31 miles (50 km) east of the DWR dam sites in the Sierran foothills, on August 1, 1975 (Toppozada and Morrison, 1982). Anderson et al. (1982) has suggested

that an increase in seismicity in the CRSB boundary zone during a period of rapid filling of the San Luis Reservoir may be a possible case of RIS. Based on an apparent increase in seismicity during a rapid filling in the late 1950's, DWR (1978) suggested that Lake Berryessa may represent a case of RIS. In the San Francisco Bay area, Wong and Strandberg (1996) investigated possible cases of RIS at Briones and Del Valle reservoirs. In the northern Sacramento Valley, some investigators also proposed that an increase in microseismicity at Lake Shasta during filling was an induced event (Packer et al., 1979; Baecher and Keeney, 1982). These examples are discussed in greater detail in the following two sections.

### 4.6.2 Lake Oroville, Butte County

Lake Oroville is a 4400 million-cubic-meter-capacity reservoir with maximum depth of 722 feet (220 m), located in Butte County approximately 31 miles (50 km) east of the DWR damsites (Figure 4-1). The 771-foot-high (235-m) earth-fill dam was constructed in 1967. No change in seismicity was observed during the initial filling or during the following seven years of normal operation (Toppozada and Morrison, 1986). The 1975 ) Oroville earthquake sequence began in late June during the summer drawdown. Following a reduction in reservoir level during the previous winter to repair the intakes to the power plant, the lake was filled rapidly by the spring runoff. The $M_L$ 5.7 mainshock, which occurred on August 1, was preceded by two M 4+ foreshocks and followed by two M 4+ aftershocks on August 2. The aftershock sequence decayed over several months. The events occurred on the Cleveland Hills fault about 7 miles (11 km) southwest of the dam (Section 4.3.3.2.1; Lahr et al., 1976; Savage et al., 1976). The focal depth for the mainshock was probably around 5 km and most of the aftershocks were between 3 and 6 miles (5 and 10 km) deep (Langston and Butler, 1976). Fracturing at the surface was consistent with the projected plane of the aftershocks and with the sense of motion from focal mechanisms. Trenching indicated that there had been prior rupturing of this fault (Clarke, 1976). The aftershock sequence was monitored by seismographs deployed after the mainshock; consequently, the rupture plane was well identified. Focal mechanisms determined from the aftershock monitoring study exhibit predominantly normal slip on west-dipping planes (Bufe et al., 1976).

Numerous investigations have been conducted with the intention of demonstrating the link between the reservoir and the Oroville sequence. Gupta (1992) presented a summary of these studies. One mechanism proposed by Toppozada and Morrison (1982) suggested that the increase in vertical load from the impoundment acted to increase the normal stress acting on the west-dipping fault plane. During the nearly eight years of normal operation fluid from the reservoir was forced down towards the fault plane, gradually increasing the pore fluid pressure. As the pressure increased the effective normal stress restraining the fault was reduced. Rupture occurred during the summer drawdown when the load from the reservoir was reduced, releasing the strain energy stored on the fault. Toppozada and Morrison (1982) have observed that the seismicity continued during each subsequent seasonal fluctuation, at least between 1975 and 1982, but at a decreasing rate. This suggests that the strain has been relieved in the 1975 rupture zone, although not necessarily in the surrounding region.

The distance of the hypocenter from the reservoir and the length of time elapsed between impoundment and seismic strain release suggest that, if this is a case of induced seismicity, then the mechanism may have been related to a change in pore fluid pressure as well as a change in elastic stress due to loading.

### 4.6.3 Lake Berryessa

Lake Berryessa, impounded by Monticello Dam in 1957, is located in the CRSB boundary zone approximately 56 miles (90 km) south of Sites. The 234 million-cubic-meter reservoir has a maximum water depth of 279 feet (85 m) and began to fill at a rapid rate in 1958 (DWR, 1978). In 1958, 11 earthquakes occurred in the vicinity of the lake compared to an average of 1.2 events per year from 1944 to 1956 (DWR, 1978). In the following year, 1959, 4 earthquakes occurred. Subsequently, an average of 1 event per year occurred from 1960 to 1971 (DWR, 1978). Based on this pattern, DWR (1978) suggested that the increase in seismicity beginning in 1958 was a case of RIS, and that it might recur if the reservoir were significantly expanded in size. Wong and Strandberg

(1996) reviewed the DWR report and, while noting the uncertainty of the earthquakes recorded before the 1970's, concluded that it is a possible case of RIS.

### 4.6.4 San Luis Reservoir

San Luis Reservoir is located in the southern CRSB boundary zone on the west side of the San Joaquin Valley near Los Banos. The 260-million-cubic-meter impoundment has a maximum water depth of 341 feet (104 m; Anderson et al., 1982). Based on records from a seismograph station installed prior to filling in 1967, the average rate of earthquake occurrence from 1966 to 1979 within 12 miles (20 km) of the reservoir was approximately 10 event per year (Anderson et al., 1982). During a period of rapid inflow in January and February 1969, 41 earthquakes were recorded in the vicinity, followed by an additional 38 events during the remainder of the year. Subsequent to this, seismicity returned to the background level (Anderson et al., 1982). Anderson et al. (1982) consider the 1969 activity to be an instance of RIS. Wong and Stranberg (1996) reviewed this work and classified the San Luis activity as a questionable case of RIS, noting that in 1974 a swarm of 11 earthquakes occurred at the southern end of the reservoir during a period when there were no significant changes in water level.

### 4.6.5 Lake Shasta

Shasta Dam was completed in 1945 to impound the 4,552,00 acre-foot Shasta Reservoir. The depth of the water column at the dam is approximately 525 feet (160 m). The lake began filling in December 1943. A short period seismograph (station SHS) was installed near Shasta Dam to monitor the reservoir. During 1944 a number of small earthquakes were recorded at SHS, leading some observers to add Shasta Lake to the list of possible RIS cases (Packer et al., 1979). Station SHS was operated for ten years by the U.S. Coast and Geodetic Survey and in 1952 was turned over to UCB to be included in their network. The original records for this period, which covered the intial filling of the reservoir, are apparently lost (LaForge and Hawkins, 1986). Urhammer and Wright (1985) examined the relation between the seismicity recorded at SHS in 1944 compared to the rate of seismicity during the period 1952 – 1963. They concluded that there was no

statistical difference between the 1944 seismicity and the background rate. They did not observe a correlation between the rate of seismicity and intial impoundment or subsequent lake level fluctuations during this period. In 1983 additional stations were added to the region around Shasta Lake to provide increased the coverage of microseismic activity. LaForge and Hawkins (1986) reviewed these results and concluded that there was no indication of reservoir-induced seismicity at Lake Shasta.

### 4.6.6 Potential for Induced Seismicity in the Vicinity of the Dam Sites

The probability of the occurrence of earthquakes in and around a reservoir may be increased by impoundment through the two mechanisms cited above. The effect of increase in elastic stress due to the load depends on the tectonic environment. An increase in elastic stress will increase the chances of failure on normal faults and decrease the probability of failure on thrust faults (Scholz, 1990). For vertical strike-slip faults an increase in vertical load would have no addition effect outside of increasing the pore fluid pressure. The zone of influence around a reservoir in which elastic stress changes occur may be between 6 and 9 miles (10 and 15 km; Scholz, 1990). The effect of increased pore fluid pressure may be due to diffusion through fractures driven by the load applied by the water column or a decrease in pore volume by an increase in volumetric strain from the change in elastic stress (Simpson et al., 1988). An investigation of these effects at a number of RIS sites has led Simpson et al. (1988) to suggest that they are manifested as two general types of reservoir-induced seismicity patterns: rapid response, in which activity increases almost immediately on the first filling of the reservoir, and delayed response, in which increased activity does not occur until several seasonal filling cycles have occurred.

There are many cases of reservoir-induced seismicity in which the response to impoundment is rapid and the increase in activity is almost immediate. The response of the crust to the filling of Lake Mead is a good example. The 466-foot-high (142-m) Hoover Dam impounds Lake Mead, which began filling in 1935. Earthquake activity started in 1936. In 1937, as the 35,000 million-cubic-meter reservoir neared its normal operating level, over 100 earthquakes were felt locally (Gupta, 1992). Seismicity

continued sporadically culminating in a M 5 earthquake in May 1939. In other cases, such as Koyna and Oroville, the onset of seismic activity is delayed for a number of years after the reservoir has been filled and is operating normally. In general, it has been observed that cases of rapid response tends to produce swarms of small shallow earthquakes located in the immediate vicinity of the reservoir and cases of delayed response tend to produce larger deeper earthquakes located at some distance (approximately 6 miles [10 km] in the cases of Koyna and Oroville) from the reservoir (Scholz, 1990).

Induced earthquakes appear to be triggered by very small stress changes, sometimes a fraction of a bar (Scholz, 1990). This suggests that the faults are in a state of pre-critical stress, requiring only minor reductions in effective normal stress to relieve strain. In regions where the principal tectonic stress is extensional these conditions for failure may be easier to meet. Most examples of induced seismicity occur in regions of low tectonic loading dominated by normal faulting or strike-slip faulting (Scholz, 1990). The DWR damsites are located in the actively folding and thrusting section of the CRSB boundary zone where the maximum principal stress is expected to be horizontal. Despite its proximity to Lake Oroville, the tectonic environment at Sites is distinctly different. The Sites anticline is inferred to overlie an east-dipping reverse fault that represents a backthrust to the underlying west-dipping blind detachment fault at approximately five km below the surface (Figure 4-7). Fracture permeability might reasonably be expected to be less in this compressional environment relative to the extensional environment across the valley. Fluid from the proposed reservoir could still diffuse down to seismogenic depths (3 miles [5 km]) if the pressure is high enough (i.e., a deep water column behind the dam). But the increase in elastic stress from the reservoir would tend to reinforce the normal stress across the detachment fault, moving it away from failure conditions. Although much remains to be learned about the causitive mechanisms for reservoir-induced seismicity, based on previous cases it would seem that conditions at Sites and Golden Gate do not favor the triggering of earthquakes by construction or operation of a reservoir.

# 5.0 SEISMOTECTONICS

## 5.1 INTRODUCTION

In this chapter we characterize the kinematics of deformation in contemporary seismic source zones in the northern Sacramento Valley and northeastern Coast Ranges near the DWR dam sites. As understood for this study, "contemporary seismic source zones" are discrete, well-defined clusters of small earthquakes. Although most of the clusters of events discussed in this chapter are not associated with known faults, some of the earthquakes are spatially clustered in the north-central Sacramento Valley around the Corning fault, and some occur near the Bartlett Springs fault (Figure 5-1). We assume that these earthquakes provide an instantaneous, local snapshot of active deformation of the crust. The purpose of analyzing these earthquakes is to better understand the current tectonic setting of the dam sites, and to assess whether evaluations of fault activity based on geologic data (Chapter 3) are consistent with local and regional patterns of seismicity.

Our approach is to analyze groups of focal mechanisms from earthquakes within the seismic source zones to evaluate the average three-dimensional strain of the crustal volume containing the earthquakes. The patterns of strain obtained from this analysis are used to determine if the earthquakes are accommodating shearing of the crust (i.e., strike-slip deformation), or whether the crust is being thickened, (thrust deformation) or thinned (extension).

## 5.2 DESCRIPTION OF CONTEMPORARY SEISMIC SOURCE DOMAINS

Based on spatial clustering of earthquake epicenters, we identify six discrete seismic source zones within about 30 miles (50 km) of the Sites and Golden Gate dam sites. These seismogenic zones are here referred to as "domains", and are described in detail in the following sections.

Figure 5-1

### 5.2.1 Colusa Domain

The Colusa domain is located about 9 miles (15 km) west of the Sutter Buttes, and about 12.5 miles (20 km) east-southeast of the dam sites (Figure 5-1). The majority of events in this domain occur in the upper 15 to 16 miles (25 km) of the crust (Chapter 4). Cross-sections of hypocenters indicate that the earthquakes may lie along a subvertical, northwest-striking plane (Figure 4-28). A total of 25 focal mechanisms with acceptable quality parameters were selected from events in the Colusa domain for additional analysis. The focal mechanisms generally indicate that this domain is characterized by strike-slip and reverse-oblique faulting (Chapter 4).

### 5.2.2 Maxwell Domain

A discrete cluster of earthquakes is located just east of the town of Maxwell, approximately 5 miles (8 km) east of the dam sites. The majority of events occur in the 3 to 14 mile (5 to 22 km) depth range. Cross-sections of hypocenters indicate that the Maxwell domain earthquakes may lie along a subvertical to steeply northeast-dipping plane (Figure 4-28). A total of 24 focal mechanisms with acceptable quality parameters were selected from events in the Maxwell domain for further detailed analysis. The focal mechanisms indicate predominantly strike-slip faulting with subordinate reverse faulting.

### 5.2.3 Willows Area

The north-central Sacramento Valley in the vicinity of Willows and between Williams and Red Bluff is a persistent source region for small earthquakes (i.e., $M \leq 4$). Earthquakes in this area are spatially associated with the late Cenozoic Greenwood anticline and Corning fault (Harwood and Helley, 1987). We identify two domains in the Willows area (i.e., Willows North and Willows South) based on the presence of two discrete, spatially segregated clusters of events. Both of these clusters lie directly east of the Greenwood anticline (Chapter 4).

#### 5.2.3.1 Willows North Domain

Earthquakes in the Willows North domain are located in the central Sacramento Valley due west of Chico, about 25 miles (40 km) northeast of the dam sites (Figure 5-1). Events in the Willows North cluster form a northwest-striking, subvertical to steeply northeast-dipping planar alignment of hypocenters (Figure 4-28). The majority of these events occur in the 9 to 15 mile depth range (15 to 24 km). A total of 36 focal mechanisms with acceptable quality parameters were selected from the Willows North domain for kinematic analysis. The mechanisms primarily indicate strike-slip and thrust faulting.

#### 5.2.3.2 Willows South Domain

Earthquakes in the Willows South domain are located west-northwest of the town of Oroville (Figure 5-1). The Willows South cluster is located about 20 miles (32 km) northeast of the dam sites. Hypocenters of these events form a northwest-striking, northeast-dipping planar alignment (Figure 4-28), similar to the Willows North domain events. The majority of the Willows South earthquakes generally occur between 9 to 22 miles depth (15 to 35 km). Thirty-five focal mechanisms with acceptable quality parameters were selected from the Willows South domain for additional analysis. The mechanisms primarily indicate strike-slip and normal faulting.

### 5.2.4 High Coast Ranges Domain

Distributed seismicity occurs in the high northern Coast Ranges west of the foothills region and northeast of the Bartlett Springs fault, about 31 miles (50 km) northwest of the DWR dam sites (Figure 5-1). Summit elevations in this region generally are about 3300 ft (1 km) higher than areas of the Coast Ranges to the south and west. For convenience, we refer to this area as the "High Coast Ranges" domain. Most of the earthquakes in this domain occur in the 3 to 11 mile (5 to 18 km) depth range. The earthquakes appear to distributed throughout this region, and are not concentrated in clusters or organized into planar alignments. No Quaternary faults have been mapped or recognized in this region. A total of 217 focal mechanisms with acceptable quality parameters were selected from

the High Coast Ranges domain for detailed analysis. The mechanisms indicate that seismogenic deformation in this region primarily is characterized by normal faulting with subordinate strike-slip faulting.

### 5.2.5 Bartlett Springs Fault

The southern Bartlett Springs fault is a persistent source of small earthquakes (Castillo and Ellsworth, 1993). The closest approach of seismicity along and adjacent to the Bartlett Springs fault to the DWR dam sites is about 22 miles (35 km) (Figure 5-1). We obtained 17 focal mechanisms from earthquakes along or adjacent to the southern end of the fault zone for detailed analysis. The mechanisms are characterized by a mix of strike-slip and normal faulting.

## 5.3 CHARACTERIZATION OF SEISMOGENIC DEFORMATION

### 5.3.1 Analytical Approach

We used the method of Twiss et al. (1993) to evaluate incremental strain accommodated by earthquakes within the domains described in Section 5.2. The analysis consists of inverting seismic P and T axes from groups of focal mechanisms for a best-fit incremental strain tensor that characterizes the average deformation of the volume of crust in which the earthquakes are located. The theoretical basis for the inversion is discussed in detail by Twiss et al. (1991), Twiss et al. (1993), and Twiss and Unruh (1998). Examples of how this approach is used to evaluate regional seismogenic deformation include Unruh et al. (1996) and Unruh and Lettis (1998). We used an automated grid-searching algorithm (FLTSLP; R. Twiss and L. Guenther, UC Davis) to perform the inversion. The parameters of the best-fit strain tensor obtained from the inversion include:

1) Three independent parameters that uniquely define the orientations of the three principal axes of the incremental strain tensor (d1, maximum lengthening; d3, maximum shortening; d2, intermediate principal axis);

2) A scalar parameter $D$ (the deformation rate parameter), which is defined by a ratio of the differences in the principal incremental strains that characterize the shape of the incremental strain ellipsoid,

$$D \equiv \frac{d_2 - d_3}{d_1 - d_3} \quad ; \qquad (1)$$

For a constant volume deformation, the values of $D$ define how the deformation departs from a plane strain.

3) A scalar parameter $W$ that characterizes the relative vorticity (i.e., relative incremental rotation), of rigid, fault-bounded blocks about an axis parallel to $d_2$ (Twiss et al., 1993):

$$W \equiv \frac{(\omega_{13} - w_{13})}{0.5(d_1 - d_3)} \qquad (2)$$

where $w_{13}$ is a component of the antisymmetric part of the large scale velocity gradient tensor that describes the average large scale rotation rate about $d_2$ (i.e., the macrovorticity), and $\omega_{13}$ is an independent component describing the local block rotation rate about $d_2$, and $w_{13}$ and $\omega_{13}$ are components in the principal coordinates of $\boldsymbol{d}$. Zero values of $W$ imply that fault-bounded blocks are rotating at the same rate as the macrovorticity; if the axis of macrovorticity is parallel to the positive $d_2$ coordinate axis, positive and negative values of $W$ imply local block rotation rates greater than and less than the macrovorticity, respectively. As a first approximation, we ignore components of the relative vorticity about the other principal axes. Twiss et al. (1993) discuss systematic relations between $W$ and fault-block geometry for various kinematic block rotation models.

For this analysis, we focus on the geometry of the incremental strain tensors obtained from the inversions. We ignore the value of the net vorticity parameter $W$ because it only characterizes the relative rotation rate of fault-bounded blocks; the net vorticity does not contribute to the average strain (i.e., change of shape) of the crustal volume containing

the earthquakes. The orientations of $d_1$ and $d_3$ and the value of the shape parameter $D$ describe the orientation and shape of the incremental strain ellipsoid.

An additional parameter (V) derived from the incremental strain tensor characterizes the net vertical component of the seismogenic deformation (Unruh et al., in press). This parameter permits direct assessment of whether the bulk strain accommodates net thinning or thickening of the crust. If the parameter V is zero, then the deformation is characterized by horizontal shearing and does not include significant thinning or thickening of the crust. Positive values of V indicate net crustal thickening, and negative values indicate net crustal thinning. In general, we interpret non-zero values of V as follows: $1 \geq V \geq 0.8$, primarily crustal thickening; $0.8 \geq V \geq 0.2$, oblique crustal thickening (i.e., "transpression"); $0.2 \geq V \geq -0.2$, horizontal shearing; $-0.2 \geq V \geq -0.8$; oblique crustal thinning (i.e., "transtension"); and $-0.8 \geq V \geq -1$, primarily crustal thinning. These ranges of values provide a simple (if arbitrary) means of distinguishing "transpressional" and "transtensional" deformations from transcurrent shearing.

The seismogenic deformation also is characterized in terms of the direction of maximum dextral shear associated with the incremental strain tensors obtained from the inversions. For a given strain tensor, there exists a plane on which the right-lateral shear strain is a maximum. This plane is parallel to the $d_2$ axis and bisects the orthogonal $d_1$ and $d_3$ axes in quadrants appropriate for resolved right-lateral shear (there is a complementary, orthogonal plane on which left-lateral shear is a maximum). The maximum dextral shear vector lies in this plane and is orthogonal to the $d_2$ axis. This representation is useful, because the study area lies within the influence of distributed right-lateral plate motion between the Pacific plate and stable North America. The northern Coast Ranges and Walker Lane belt, which border the western and eastern margins, respectively, of the Sierra Nevada microplate (Chapter 2), are tectonically active regions dominated by northwest-directed dextral shear. We anticipate that crustal shearing in north-central California, if present, likely will be associated with these plate boundaries and characterized by northwest dextral shear; thus, deriving the shear plane and slip vector for

maximum dextral shear allows direct comparison of the seismogenic strain in the study area to distributed plate-boundary deformation.

### 5.3.2 Results

The results of the inversions (i.e., values of the parameters described in Section 5.3.1, above) are presented in Table 5-1. The direction of maximum right-lateral shear strain also is determined for domains characterized by "transpressional" and "transtensional" values of the parameter V (Table 5-1). Seismogenic deformation in individual domains is described in greater detail as follows.

**Table 5-1** Results of Kinematic Inversions of Focal Mechanisms

| **Domain Name** | **d1 (trend, plunge)** | **d3 (trend, plunge)** | **D** | **W** | **V** | **Cos-1 (Mean Cos Error)** | **Number of data** | **Maximum dextral shear rate (strike/dip/rake); rake indicates direction footwall moves (positive rake values are below the horizontal)** |
|---|---|---|---|---|---|---|---|---|
| Colusa | 146, -59 | 240, -2 | 0.3 | -0.2 | 0.7 | 8.2096 | 24 | N2°W/55°E/52°N |
| Maxwell | 329, 60 | 242, -2 | 0.3 | 0.2 | 0.7 | 8.3528 | 24 | N1°W/55°E/52°N |
| Willows North | 123, -37 | 54, 26 | 0.6 | 0.4 | 0.2 | 8.2602 | 36 | N5°W/82°E/56°N |
| Willows South | 100, -0.2 | 191, 11 | 0.5 | 0.4 | -0.1 | 11.5044 | 35 | N34°W/82°NE/-9°NW |
| High Coast Ranges | 115, 7 | 64, -79 | 0.5 | 0.2 | -1 | 8.8715 | 217 | Normal slip on NNE-striking faults |
| Bartlett Springs Fault | 289, -18 | 144, -68 | 0.6 | -0.2 | -0.8 | 4.0252 | 17 | Right-normal oblique slip |

#### 5.3.2.1 Colusa Domain

Seismicity in the Colusa domain primarily is characterized by transpressional shearing of the crust. The strain geometry obtained from the focal mechanism inversions generally is characterized by NW-SE shortening. The maximum extensional principal strain ($d_1$) plunges more steeply than the maximum shortening strain ($d_3$), generating a component of net vertical extension and crustal thickening. We refer to this style of deformation as

"oblique crustal thickening" because it includes a significant component of horizontal shear.

Maximum dextral shear strain associated with the seismogenic deformation is characterized by right-reverse oblique slip on a NNW-striking, east-dipping plane (Table 5-1). The orientation of the maximum dextral shear plane is similar to the NNW-striking, steeply east-dipping planar alignment of Colusa domain hypocenters (Figure 4-28). Based on these results, we interpret that the Colusa domain events represent right-reverse oblique slip on a blind, NNW-striking fault.

#### 5.3.2.2 Maxwell Domain

Seismogenic deformation in the Maxwell domain is characterized by "transpression", and is very similar to that of the Colusa domain (Table 5-1). The strain geometry is characterized by NE-SW shortening and oblique crustal thickening. Maximum dextral shear strain in this domain is characterized by right-reverse oblique slip on a NNW-striking, east-dipping plane (Table 5-1). The orientation of the maximum dextral shear plane is similar to the planar organization of hypocenters in the Maxwell domain. We interpret that the Maxwell events are generated by right-reverse oblique slip on a blind, NNW-striking fault.

#### 5.3.2.3 Willows North and Willows South Domains

Inversion results from Willows North and South indicate that seismogenic deformation in these domains is characterized by east-west to west-northwest-east-southeast extension, and north-northeast-south-southwest shortening (Table 5-1). This strain geometry suggests that crustal shearing is the dominant style of deformation with minor vertical deformation. The best-fit model for the Willows North domain includes a small component of net thickening (i.e., V = 0.2; Table 5-1), which is depicted by showing a pair of "shortening" arrows on Figure 5-1. The best-fit value of the parameter V for the Willows South domain is slightly negative (V = -0.1; Table 5-1). This value of V is probably not statistically distinguishable, and so the deformation geometry for Willows

South is depicted on Figure 5-1 as predominantly strike-slip with pairs of both extensional and shortening arrows.

Based on the best-fit inversion parameters, maximum dextral shear strain in the two Willows domains is resolved on north to northwest-striking, very steeply east-dipping planes (Figure 5-1). For comparison, the clusters of seismicity in these two domains form north- to northwest-striking, east-dipping planes. We thus interpret that earthquakes in the Willows domains are generated by dextral slip on two blind, northwest-striking faults.

#### 5.3.2.4 High Coast Ranges Domain

The High Coast Ranges domain primarily is characterized by WNW-ESE extension and crustal thinning (Table 5-1). Maximum shear strain in this domain is accommodated by nearly pure dip-slip motion on moderately dipping, NE-SW-striking normal faults.

#### 5.3.2.5 Bartlett Springs Fault

Seismicity in the vicinity of the southern Bartlett Springs fault is characterized by transtensional crustal shearing (Table 5-1). The maximum extensional principal strain is subhorizontal and oriented west-northwest-east-southeast, and the maximum shortening principal strain plunges steeply southeast.

## 5.4 DISCUSSION

Seismogenic deformation in the Sacramento Valley domains east of the DWR dam sites (Colusa, Maxwell, Willows North, Willows South) is characterized by crustal shearing with varying components of vertical deformation. The seismicity is associated with right-oblique slip on blind, north- to northwest-striking faults. Dextral strike-slip faulting in these regions is consistent with accommodation of distributed right-lateral shear east of the Pacific Plate.

Deformation in the Colusa, Maxwell and Willows North domains is characterized by "transpression" with varying components of net crustal thickening. These results indicate that seismogenic deformation accommodates a component of NE-directed shortening, which is consistent with geologic evidence for late Cenozoic activity of segments of the blind Great Valley thrust fault in the west-central and northwestern Sacramento Valley. The direction of maximum shortening in these domains is at a high angle to the north-south and NW-SE trends of folds and thrust faults in the Coast Range foothills region directly to the west.

In contrast to shearing and transpression in the Sacramento Valley, seismogenic deformation in the Coast Ranges west of the dam sites (i.e., the Bartlett Springs and High Coast Ranges domains) is characterized by crustal extension and transtensional shearing. Transtension along the Bartlett Springs fault is consistent with a northwest-striking dextral fault and the presence of pull-apart basins such as Lake Pillsbury (Plate 1).

The strike-slip and "transpressional" strain geometries obtained from this analysis are consistent with the neotectonic setting of northwestern California, which is traversed by the transpressional boundary between the Pacific plate and the Sierra Nevada microplate (discussed in Chapter 2). The extensional and "transtensional" strains in the High Coast Ranges and Bartlett Springs domains, however, are anomalous in the regional transpressional setting. We infer that secondary forces, affecting the state of stress and style of faulting in the upper crust, may arise from gravity acting on variations in the thickness and density of the mantle lithsophere beneath northwestern California. These postulated secondary forces are superimposed on regional forces associated with large-scale plate motion, and thus may create domains like the High Coast Ranges with distinctly different styles of deformation from surrounding regions.

This hypothesis can be evaluated in a general way by comparing variations in styles of seismogenic deformation with variations in the thickness and density of the mantle lithosphere. For example, the transition from transpression and crustal thickening in the Sacramento Valley to transtension and crustal thinning in the Coast Ranges is correlated

with upper mantle P-wave velocity anomalies imaged by teleseismic tomographic methods (Benz et al., 1992, Benz and Zandt, 1993). Specifically, Benz and Zandt (1993) identify an area of anomalous high P-wave velocity in the 19 to 44 mile depth range (30-70 km) beneath the northern Sacramento Valley called the "Sutter Buttes Anomaly". This feature is spatially associated with the Colusa, Williams and Willows seismogenic domains. The anomalous high velocities obtained from the teleseismic analysis imply that the mantle in this region is relatively cold and dense. Benz and Zandt (1993) also identify an area of anomalous low P-wave velocities (i.e., the "Clear Lake Anomaly") in the 19 to 44 mile depth range (30-70 km) beneath the High Coast Ranges domain. Here, the low velocities imply that the mantle is relatively warm and less dense. The north-trending boundary between the areas of high and low velocity in the upper mantle is at about longitude 122° 15' W, approximately between the Maxwell and Bartlett Springs domains.

We attribute components of net crustal thickening and thinning above these velocity perturbations to buoyancy forces associated with east-west variations in upper mantle density. It has long been recognized that gravitational body forces acting on variations in lithospheric density can give rise to horizontal forces that tend to thicken or thin the lithosphere (e.g., Fleitout and Froidevaux, 1982; Molnar and Lyon-Caen, 1988; see Jones et al., 1996 for additional discussion). In general, thin or thermally buoyant mantle (with relatively low P-wave velocities) is capable of supporting locally high surface elevations, and may be associated with tensile buoyancy forces and crustal extension. In contrast, unusually thick, cold, and negatively bouyant lithospheric mantle (associated with relatively high P-wave velocities) will predictably give rise to compressional horizontal buoyancy forces that can drive crustal thickening. The Basin and Range province is an example of a region where active extension is associated with a warm, thin and buoyant mantle lithosphere, and large tensile buoyancy forces (Jones et al., 1996). The western Transverse Ranges is underlain by thick and cold (high P-wave velocities) mantle lithosphere, and associated compressional buoyancy forces may be affecting the state of stress in this region (Sonder, 1990).

We interpret low P-wave velocities in the upper mantle beneath the High Coast Ranges and Bartlett Springs domains as evidence for the presence of a "slab window" or "slab gap" in the wake of the migrating Gorda plate that exposes the base of the lithosphere to upwelling asthenospheric mantle (Chapter 2). The buoyant mantle probably supports the local high elevation of this region (i.e., Furlong, 1984), which in turn could give rise to tensile buoyancy forces to drive the observed seismogenic crustal extension. These tensile forces also may be influencing the behavior and geometry of the Bartlett Springs fault. Seismogenic faulting along the southern end of the fault is strongly transtensional, consistent with the left-stepping, en echelon pattern of faults in the Coyote Rocks and Elk Creek segments (Plate 1), as well as the presence of fault-bounded basins like the one that hosts Lake Pillsbury reservoir.

Similarly, we interpret the high P-wave velocities in the upper mantle beneath the Sacramento Valley as evidence for the presence of anomalous thick and cold mantle lithosphere, which in turn could give rise to compressive buoyancy forces. We interpret that the locally derived buoyancy forces combine with the more regional plate-derived shearing stresses to drive transpressional seismogenic deformation in the central Sacramento Valley.

The seismogenic Willows faults underlie the Greenwood anticline, which shows geomorphic evidence for late Quaternary activity (Chapter 3). Growth of the anticline can be reconciled with strike-slip faulting at depth if there is a component of reverse slip on the blind faults in the Willows domain. To test this hypothesis, we used forward modeling techniques to evaluate the direction of maximum resolved shear on the Willows faults for the strain tensors obtained from the focal mechanism inversions. This approach provides a means of assessing the slip direction on a fault of a given orientation that most directly accommodates the seismogenic deformation as characterized by the incremental seismic strain tensor. The direction of maximum resolved incremental shear is obtained by calculating the tensor product of the incremental strain tensor and a unit vector normal to the shear plane of interest. The result is a vector that in general is not perpendicular to the shear plane. The normalized component of this vector resolved in the plane gives the

direction of maximum resolved shear associated with the incremental strain tensor (for a detailed description of this analytical approach and examples of how it is applied, see Unruh et al. 1997).

From cross-sections of the Willows North and Willows South hypocenters, we assume that the blind, seismogenic faults in these domains strike north-south to N20°W, and range in dip from 80°E to vertical. Forward modeling results for the Willows North domain indicate that the expected direction of slip on faults with this range of orientations is right-reverse oblique. Modeling results for the Willows South domain indicate primarily right-lateral strike slip with a small normal component.

The forward modeling results for the Willows North domain are consistent with observed late Cenozoic growth of the Greenwood anticline (Chapter 3). Specifically, the field evidence for late Cenozoic activity of the fold described in Section 3.5.12 was obtained from a site about one-half mile (1 km) south of the town of Orland. The Willows North cluster of events is approximately centered on the town of Orland, so the active section of the anticline is associated with these earthquakes. The small normal slip component predicted for the blind Willows South fault is not in conflict with available field relations; however, no positive evidence for late Quaternary surface deformation of any kind has been reported to date in the vicinity of the earthquakes. We note that the misfit value for the best-fit Willows South incremental strain tensor is relatively high (Table 5-1). This implies that the small negative value of V for this domain is poorly resolved by the data. Because the small component of predicted normal slip is strongly dependent on the strain geometry (i.e., the value V), we conclude that it, too, is poorly resolved by the data.

## 5.5 SUMMARY

Patterns of seismogenic deformation in large areas of the study region are systematically correlated with velocity anomalies in the lower lithosphere, and thus may reflect the influence of local gravitational buoyancy forces. In particular, we interpret that crustal extension in the High Coast Ranges domain is associated with the presence of buoyant asthenospheric mantle in the "slab window", which has formed in the wake of the

migrating Gorda slab. Tensile buoyancy forces in the High Coast Ranges also may be influencing the behavior of the Bartlett Springs fault, which skirts the southwestern edge of the domain. Extensional deformation appears to be confined to the areas of the high Coast Ranges located 25 miles (40 km) or more to the west of the dam sites. Based on analysis of seismicity data from the Maxwell domain, we interpret that deformation in the vicinity of the dam sites is characterized northeast-southwest crustal shortening, consistent with geologic evidence for Quaternary activity of folds and thrust faults in the foothills region.

Northwest dextral shear associated with distributed plate motion is a significant component of the seismogenic deformation in the central Sacramento Valley. Field evidence for late Quaternary activity of the northern Greenwood anticline is consistent with seismotectonic analyses indicating that earthquakes in the Willows North domain are generated by right-reverse oblique slip on a blind northwest striking fault beneath the fold.

# 6.0 EARTHQUAKE HAZARDS

## 6.1 MAXIMUM EARTHQUAKE MAGNITUDES

Based on review of published and unpublished data, as well as detailed investigations performed for this study, we recognize the following geologic structures as active sources of moderate- to large-magnitude earthquakes within a 31-mile (50-km) radius of the Sites and Golden Gate dam sites (Plate 1):

- The Funks and Bear Valley segments of the Great Valley blind thrust fault system beneath the western Sacramento Valley
- Northeast-striking dextral faults that pass through or near the dam sites (i.e., the GG-2, GG-3 and S-2 faults)
- The Bartlett Springs fault
- The Corning Fault

Additionally, we recognize the Cascadia subduction zone as an active source of large intraplate earthquakes and great megathrust earthquakes that may contribute significantly to long-period ground shaking hazards at the Sites and Golden Gate dam sites. Maximum magnitudes and site-source distances for these faults and seismic sources are summarized in Table 6-1.

Consistent with current state-of-practice, we use empirical relations among rupture parameters (i.e., fault rupture length, rupture area, and maximum coseismic displacement) and magnitude to estimate maximum earthquake magnitudes. Because detailed paleoseismic data on coseismic displacement are not available for most faults in the study region, and specifically are not available for blind thrust faults, we rely on estimates of rupture length and rupture area to derive maximum earthquake magnitudes.

**Table 6-1 Earthquake Sources, Sites and Golden Gate Dam Sites**

| Fault Name | Sense Of Displacement | Maximum Magnitude | Closest Approach, Sites Dam Site | Closest Approach, Golden Gate Dam Site |
|---|---|---|---|---|
| Funks segment, Great Valley fault | thrust/reverse | $M_W$ 6.6 | 4 miles (6.5 km) | 3.6 miles (5.8 km) |
| Bear Valley segment, Great Valley fault | thrust/reverse | $M_W$ 6.8 | 4.8 miles (7.7 km) | 4.4 miles (7.0 km) |
| GG-2, GG-3 and S-2 faults | Right-lateral strike slip | $M_W$ 5.4 | 0 miles (0 km) | 0 miles (0 km) |
| Bartlett Springs fault | Right-lateral strike slip | $M_W$ 6.6 | 20 miles (32 km) | 22 miles (35 km) |
| Corning fault | thrust/reverse | $M_W$ 6.7 | 20 miles (32 km) | 18 miles (29 km) |
| Cascadia Subduction Zone | thrust/reverse | $M_W$ 9 | 100 miles (160 km) | 100 miles (160 km) |
| Intraplate Events (Gorda Plate source) | Strike slip; normal | $M_W$ 7.5 | 53 miles (85 km) | 53 miles (85 km) |

The empirical relationships used in the maximum magnitude calculations are those developed by Wells and Coppersmith (1994). Analysis of subsets of the data base of earthquake source parameters used in the regressions reveals that statistical descriptors of fit (e.g., correlation coefficients, standard deviations) are not significantly improved by the subdivision of the data by sense of fault slip or tectonic environment. In general, the correlation coefficients for the regressions indicate very strong correlations (r = 0.8-0.9) and the standard deviations are approximately 0.25 magnitude unit (Wells and Coppersmith, 1994).

## 6.2 FUNKS SEGMENT, GREAT VALLEY FAULT SYSTEM

### 6.2.1 Rupture Length

Based on analysis of seismic reflection data from the northwest Sacramento Valley, we interpret that the Great Valley fault system is divided into a series of discrete fault segments (see Chapter 3 and Appendix A for a complete discussion). For convenience, we refer to the segment directly adjacent to and underlying the dam sites as the Funks segment (Appendix A; Figure 6-1). The next closest segment to the dam sites is the Bear Valley segment, which is directly south of the Funks segment (Figure 6-1).

The Funks segment of the Great Valley fault is imaged on seismic line 798 as a reflector in the 5.0-6.5 km depth range that juxtaposes both east and west-dipping strata above against a package of bright, high amplitude, subhorizontal reflectors below (Appendix A; Figure 3-2). We interpret that the dip of the thrust fault increases west of the Fruto syncline axis, forming a west-dipping thrust ramp. We further interpret that the south end of the fault is imaged on seismic line SV-12 (Figure 3-3), which trends east-west and passes between the Sites and Golden Gate dam sites. Specifically, we associate the Funks segment with a west-dipping reflector in the 3.8 to 4.4 mile (6-7 km) depth range at the west end of line SV-12 that juxtaposes east-dipping layered reflectors above against west-dipping reflectors below. Based on our analysis of the subsurface structure in these two seismic lines, we interpret that the strike of the Funks segment ramp is about

Figure 6-1

N28°W, similar to the general northwest strike of bedding in the western limb of the Fruto syncline estimated from geologic mapping by Brown and Rich (1961).

Our estimate of the ramp strike is based on the trend of the structure contours (Figure 6-1), which in turn is dependent on our interpretation of the Funks segment fault plane in seismic line SV-12. There is some uncertainty in determining the depth of the fault in line SV-12 owing to the inherent difficulty in imaging complex structures, loss of the fold near the western end of the line, and dependence of reflector geometry on the velocity model used to perform a pre-stack depth migration of the model (Dan O'Connell, U.S. Bureau of Reclamation, personal communication, 2002). We acknowledge that the dip discordance we associate with the Funks segment may be about 0.5 km closer to the earth's surface than in our preferred interpretation (Figure 3-3). If this "shallower" interpretation is correct, then the intersection points of the Funks segment structure contours with line SV-12 would shift to the west, and the apparent strike of the ramp would be more to the north than as shown in Figure 6-1. Interestingly, patterns of fluvial incision indicated by the residual topographic map (Figure 3-55) suggest a generally north-trending region of relatively high incision over the Funks segment, rather than a northwest-trending region parallel to the structure contours on the fault. If the region of high incision is directly related to the patterns of uplift produced by slip on the fault, then we would expect both incision patterns and the fault to have the same general orientation. The topographic residual map may support a "shallow reflector" interpretation of SV-12. Given our uncertainty in the precise location of the fault, we adopt our preferred interpretation of line SV-12 for characterizing the Funks segment as a seismic source because it conservatively places the top of the ramp closer to the dam sites (Figures 6-2 and 6-3) and thus implies a shorter site-source distance.

Based on analysis of seismic reflection data, we interpret that the northern termination of the Funks segment lies between Hunters and Logan Creeks (Appendix A; Figure 6-1). As discussed in Section 3.4.3.1, we interpret that the southern termination of the Funks segment coincides with the S-2 fault. Total length of the Funks segment measured between its northern and southern terminations is 11 miles (17 km) (Section 3.4.3.1).

### 6.2.2 Rupture Width

Based on our structure contour interpretation of the Great Valley system, the Funks segment thrust ramp dips about 27° to the southwest (Figures 6-2 and 6-3). If it is assumed that the thrust ramp maintains a constant dip, then it would be about 9 miles (15 km) deep in the vicinity of the Bartlett Springs fault, where the brittle-ductile transition occurs at a depth of 9 miles (15 km) (Section 4.4.3). We therefore adopt 9 miles (15 km) as the maximum depth of brittle rupture on the Funks segment.

We assume that coseismic rupture of the Funks segment extends from the base of the brittle crust at least as far updip as the top of the ramp (i.e., Point A on Figures 6-2 and 6-3). The width of the ramp measured from the brittle-ductile transition to point A is about 12.5 miles (20 km). To assess the likely updip extent of rupture, either to or beyond point A, we reviewed data on the dimensions of thrust faults that have ruptured during moderate to large magnitude earthquakes, and selected a conservative rupture width for the Funks segment that is consistent with empirical observations.

Analysis of earthquake source dimensions reveals that rupture surfaces commonly have elliptical shapes, with the strike dimension typically greater than the dip dimension (Nicol et al., 1996). Rupture geometry is characterized by its aspect ratio, which is defined as the rupture length divided by rupture width. Nicol et al. (1996) surveyed the literature on earthquake rupture dimensions, and found that the aspect ratio for the majority of faults of all types (strike-slip, normal and reverse) falls between 1 and 3, indicating that rupture length typically ranges from one to three times the rupture width.

Using data on rupture dimensions from the catalog of earthquakes reported in Wells and Coppersmith (1994), we calculated and plotted the rupture aspect ratio for 30 thrust/reverse earthquakes as a function of magnitude (Figure 6-4). Aspect ratio was calculated using subsurface rupture length and rupture width in Wells and Coppersmith (1994), and plotted vs. moment magnitude. The data show that the minimum documented aspect ratio for moderate to large thrust/reverse earthquakes is

Figure 6-2

Figure 6-3

Figure 6-4

about 0.8. There is a general trend in the data toward higher aspect ratios with increasing magnitude, which implies that that the rupture length of a large earthquake (M > 6.5) is typically greater than the rupture width.

We assume that earthquakes on the Funks segment will be similar in character to the well-documented thrust/reverse fault earthquakes in the Wells and Coppersmith (1994) database. Based on the data in Figure 6-4, we assume that the rupture aspect ratio for the Funks segment will not be less than about 0.8. For an 11-mile (17-km) rupture length, we conservatively adopt a rupture width of about 14 miles (22 km), which represents an aspect ratio of 0.77. This model implies that rupture will propagate about 1 mile (2 km) east of the top of the ramp (point A in Figures 6-2 and 6-3), to an average depth of about 3.4 miles (5.5 km; i.e., to point B in Figure 6-2). In addition to being consistent with empirical data on thrust/reverse rupture aspect ratios, a 22-km rupture width is conservative because it brings the rupture to within the closest approach of both dam sites (Figures 6-2 and 6-3).

### 6.2.3 Maximum Earthquake Magnitude, Funks Segment

For a maximum rupture length of 10.6 miles (17 km) and maximum rupture width of 13.75 miles (22 km), we calculate the potential rupture area of the Funks segment to be 146 square miles (374 $km^2$). Based on empirical relations between rupture area and magnitude for all earthquakes (Wells and Coppersmith, 1994), the associated earthquake magnitude is $M_w$ 6.6. The same result is obtained by using the Wells and Coppersmith (1994) regression for magnitude vs. reverse/thrust earthquakes only. We therefore adopt $M_w$ 6.6 as the maximum magnitude for earthquakes on the Funks segment of the Great Valley fault (Table 6-1).

### 6.2.4 Aseismic Hanging Wall Deformation East of the Ramp-Flat Transition, Funks Segment

Although our rupture model assumes that slip on the Funks segment terminates about 2 km east of the ramp-flat transition, our kinematic model for growth of the Sites anticline and slip on the Salt Lake fault infers that slip along the flat extends well east of this point

(see discussion in Section 3.3). It is possible to reconcile the rupture model with the kinematic model if slip propagates east of the rupture termination through an aseismic mechanism. In this section, we test this hypothesis with numerical models based on elastic dislocation theory.

#### 6.2.4.1 Modeling Approach

Our modeling approach is premised on the assumption that coseismic displacement on the Funks segment imposes an elastic strain on the surrounding crust, which in turn is manifest as patterns of surface uplift and folding. The modeling algorithm uses linear elasticity theory to calculate stresses, strains and surface displacements associated with slip on the thrust fault at depth.

Elastic dislocation models have been used in a variety of cases to examine fault interaction, surface and subsurface displacements, and stress triggering of earthquake rupture. For example, Roering et al. (1996) used elastic dislocation models to interpret fault geometry and seismic hazard of a blind thrust in the peninsula region of the San Francisco Bay Area, California. They used structural geologic techniques to define the geometry of a folded stratigraphic horizon above the fault, and inverse numerical modeling to fit fault geometries and slip distributions to the observed deformation. In a similar but more comprehensive study, Taboada et al. (1993) examined complex deformation associated with several faults in the Betic Cordillera of Spain. Their study used elastic dislocation models to interpret the subsurface geometry of, and long term displacements on, the faults. Calculated displacements in the region around the faults were compared to a deformed stratigraphic horizon that had been identified on the basis of field mapping and borehole data. The best-fit models were used to estimate long-term slip rates on the faults.

Elastic modeling methods also have been used to evaluate the distribution and magnitude of rupture on the blind Northridge thrust fault associated with patterns of coseismic surface displacements determined from geodetic studies following the 1994 Northridge earthquake (Hudnut et al., 1996).

### 6.2.4.2 Methodology

We idealized the Funks segment fault geometry as two rectangular faults representing the ramp and flat reaches of the fault (Figure 6-5). The ramp dips at 27° and extends for 20 km in the down-dip direction, from a depth of about 4 miles (6 km) to the brittle-ductile transition at about 9 miles (15 km). The flat extends 6 miles (10 km) east of the top of the ramp and is inclined at a 13° angle. Both the ramp and flat reaches are 11 miles (17 km) long in the strike direction.

We included traction-free surfaces representing the Salt Lake fault and the blind Sites thrust fault beneath the Sites anticline. Both of these structures are confined to the hanging wall of the Funks segment. The Salt Lake fault was modeled as a planar surface dipping 65 degrees to the east and extending from the surface to intersect the flat portion of the blind thrust. The Sites blind thrust fault was modeled as a planar surface dipping 65 degrees to the east, and separate models were run in which the width of the blind thrust fault was fixed at about 1 miles and 2.5 miles (i.e., 2 and 4 km, respectively). Model cases were run with: (1) about 3.3 feet (1 m) of slip on the blind thrust ramp only; (2) about 3.3 feet (1 m) of slip on the ramp and 1.25 miles (2 km) of the flat; and (3) about 3.3 feet (1 m) of slip on the ramp and 2.5 miles (4 km) of the flat.

Modeling was performed with Poly3D (Thomas, 1993), a three dimensional, displacement discontinuity computer program that uses the boundary element method (Crouch and Starfield, 1983) to calculate stress, strain, and displacement fields in an isotropic, homogeneous, linear elastic medium with prescribed faults and/or other discontinuities. Values of stress, strain and displacement are calculated at user-defined observation points using the solutions for angular dislocations in a homogeneous linear elastic half space given by Comninou and Dundurs (1975) and Jeyakumaran et al. (1992). The earth is idealized as a homogeneous, isotropic, linear elastic medium with material properties appropriate for near surface, upper-crustal rocks (shear modulus is chosen to be 30 GPa, and Poisson's ratio is taken to be 0.25).

Figure 6-5

We modeled coseismic rupture of the ramp-flat pair by imposing a constant displacement of 3.3 feet (1 m) on the ramp segment, and varying the updip extent of displacement on the flat fault segment.

#### 6.2.4.3 Model Results

Figure 6-6 shows plan views of modeled surface displacements for the case of 3.3 feet (1 m) of slip on the ramp and about 1.25 miles (2 km) of the flat of the blind thrust. Horizontal displacements radiate outward from the center of the flat in a general eastward direction, with a maximum of about 9.5 inches (24 cm) of horizontal displacement. The effect of the having the Salt Lake fault as a traction-free surface in the model is to disrupt the smooth contours of horizontal displacement, reducing the displacements slightly when compared with model cases without the fault present. Vertical displacements show a pattern with two maxima; vertical displacements reach about 11 inches (28 cm) in the region just east of the surface trace of the Salt Lake fault, and a second maxima of about 10 inches (26 cm) is centered on the ramp-flat transition.

Figure 6-7 shows vertical surface displacements along a line running normal to the strike of the faults through the fault centers. The model results include a broad anticlinal uplift above the ramp west of the Salt Lake fault, as well as abrupt uplift east of the fault. A maximum of about 14 inches (34 cm) of vertical displacement, corresponding to about 4 inches (10 cm) of vertical separation on the Salt Lake fault, occurs with 3.3 feet (1 m) of slip on the ramp extending (2.5 miles) 4 km of the flat. The models with this slip distribution also show a slight double peak in displacements west of the Salt Lake fault, with the smaller peak equivalent to antiformal uplift. Including a blind thrust fault in the model to approximate the Sites blind thrust does not have a dramatic effect on the surface displacement profile. Based on these models, therefore, the Salt Lake fault has the more significant effect on surface displacement distribution during seismic events on the Funks segment.

If the Salt Lake fault dips 65° to the east, then about 4.5 inches (11 cm) of net slip on the fault are required to produce the vertical separation observed in the models. The 4.5

Figure 6-6

Figure 6-7

inches (11 cm) of modeled slip is a result of an assumed 3.3 ft (1 m) displacement on the Funks segment at depth. Because elastic behavior is governed by linear constitutive relationships, the predicted displacement on the Salt Lake fault will be proportionally greater if the initial coseismic slip on the Funks segment is greater than 3.3 feet (1 m). For comparison with our model parameters, estimates of average coseismic slip on the blind Northridge thrust fault during the M6.7 1994 Northridge earthquake range from about 3.3 feet to 4.4 feet (1.0 to 1.3 m) (Wald et al., 1996). We conclude that the model displacement of 3.3 feet (1 m) is appropriate for evaluating triggered slip on the Salt Lake fault from a $M_w$ 6.6 earthquake on the Funks segment.

#### 6.2.4.4 Conclusions

The model results indicate that triggered slip on the Salt Lake fault may occur to relax elastic strains in the upper crust imposed by coseismic slip on the Funks segment, provided that the Salt Lake fault is a "weak" structure that cannot support significant shear stresses. The models uniformly predict about 4 inches (10 cm) of vertical separation across the Salt Lake fault for a variety of rupture scenarios, including those where rupture on the Funks segment terminates well to the west of the fault. We thus conclude that the observed Quaternary displacements on the Salt Lake fault may have occurred as a result of aseismic slip or triggered slip in response to ruptures on the Funks segment of the Great Valley thrust fault that extend only about 1.5 miles (2 km) east of the top of the ramp.

## 6.3 BEAR VALLEY SEGMENT, GREAT VALLEY FAULT

The Bear Valley segment of the Great Valley blind thrust fault is imaged by seismic lines SV-12 and 807 (Appendix A). The fault is imaged in line SV-12 as a west-dipping reflector south of the S-2 fault that juxtaposes east-dipping strata of the Great Valley Group above against a package of bright, west-dipping reflectors below. The Bear Valley segment flattens abruptly eastward beneath the western Sacramento Valley. On line 807, the Bear Valley segment is imaged as a west-dipping feature that similarly juxtaposes oppositely dipping reflectors. From preparation of a structure contour map of

the Great Valley fault system in the northwestern Sacramento Valley (Figure 6-1), we interpret that the strike of the Bear Valley segment is about due north-south.

Based on analysis of seismic line SV-12, we interpret that the northern boundary of the Bear Valley segment is the S-2 fault. The southern segment boundary is not imaged directly by reflection data available for this study. From inspection of Shell line 806 (in Constenius et al., 2000), which crosses the southern end of the Wilbur Springs anticline south of line 807, and from analysis of geomorphic and structural geologic features in this region, we interpret that the southern segment boundary is located at about latitude N 39° 07' (Chapter 3). We adopt a length of 14.4 miles (23 km) for the Bear Valley segment.

Based on analysis of seismic lines SV-12 and 804, we interpret that the dip of the Bear Valley segment is about 20° to the west. We infer that coseismic rupture on the fault will extend from the base of the brittle crust at a depth of 9.4 miles (15 km) to a depth of about 4.4 miles (7 km). The vertical projection of the 4.4 mile (7 km) depth contour lies along the western margin of the Sacramento Valley, and also is coincident with the eastern limit of significant late Cenozoic incision (Figure 3-55). We interpret lack of late Cenozoic surface uplift east of this contour as evidence for no significant uplift of the hanging wall of the Bear Valley thrust fault, which in turn implies that coseismic slip terminates at or west of the projection of the 4.4 mile (7 km) depth contour. Total fault width measured between 9.4 miles and 4.4 miles depth (15 to 7 km depth) is 14.4 miles (23 km). We note that this rupture width implies a rupture aspect ratio of 1 for a 14.4-mile- (23-km-) long fault.

For a fault width and length of 14.4 miles (23 km), the potential rupture area is 207 square miles (529 $km^2$). Regressions on magnitude vs. rupture area for all earthquakes predicts a $M_w$ 6.7 earthquake on the Bear Valley segment, and similar regressions using data from thrust/reverse earthquakes only predicts a $M_w$ 6.8 earthquake (Wells and Coppersmith, 1994). We conservatively adopt $M_w$ 6.8 as the maximum earthquake for the Bear Valley segment. Closest straight-line distance of the Bear Valley segment to the

Sites dam site is 4.8 miles (7.7 km) (Figure 6-8); the closest approach of the fault to the Golden Gate dam site is 4.4 miles (7.0 km).

## 6.4 NORTHEAST-STRIKING DEXTRAL FAULTS

The kinematic model adopted for this study relates slip on northeast-striking faults (GG-1, GG-2, GG-3 and S-2; Figure 3-1) that pass through or near the dam sites to slip on the Funks segment of the Great Valley thrust fault system (Section 3.3). Our preferred interpretation is that these structures move sympathetically during moderate to large earthquakes on the Funks thrust ramp. The faults behave like tear faults in the hanging wall of the Great Valley fault, and are interpreted to terminate or sole out at depth against the Great Valley fault. These tear faults also may be a source of aftershocks. Based on our analysis of seismic reflection data, we conclude that the northeast-striking faults are confined to the hanging wall block of the blind thrust fault and that their maximum rupture depth is 5 km. The exception is fault GG-1, which has such a short surface trace (Figure 3-1) that we interpret it to terminate in the upper 1.2-1.9 miles (2-3 km). Given its limited rupture dimensions, we conclude that fault GG-1 is not a seismic source.

From measurements of the length of the surface traces, faults GG-2, GG-3 and S-2 have potential rupture areas of about 7.8 to 10 square miles (20 to 25 $km^2$). From regression relations in Wells and Coppersmith (1994), we calculate an associated range of magnitudes from $M_w$ 5.3 to $M_w$ 5.4. We adopt $M_w$ 5.4 as the maximum earthquake for faults GG-2, GG-3, and S-2 (Table 6-1).

## 6.5 BARTLETT SPRINGS FAULT

The Bartlett Springs fault is a northwest-striking, 70-mile- (113-km-) long zone of discontinuous faults and shears that extends from east of Clear Lake to Round Valley (Plate 1). The fault is a broad, 0.6- to 1.9-mile- (1- to 3-km-) wide zone of shearing that locally exhibits evidence of late Quaternary activity (Section 3.5.3). The Bartlett Springs fault appears to be an immature fault system that has not integrated into a through-going fault. Detailed studies suggest that it can be divided into six structural segments

Figure 6-8

(Geomatrix Consultants, 1986). Evidence for Holocene displacement was observed on the 11-mile- (18-km-) long Coyote Rocks segment northeast of Clear Lake (Geomatrix, 1986) (Plate 1). The Coyote Rocks segment traverses the Lake Pillsbury basin, a probable tectonic pull-apart structure, and paleoseismic evidence shows that multiple Holocene surface-rupture events have occurred on the Coyote Rocks segment. The closest approach of the Bartlett Springs fault zone to the Sites and Golden Gate dam sites is 20 and 22 miles (32 and 35 km), respectively (Table 6-1).

Based on the discontinuous nature of the Bartlett Springs fault zone, and evidence for structural segmentation of the fault zone cited by Geomatrix (1986), we conclude that it is unlikely that the entire 70-mile- (113-km-) long fault ruptures in a single event. Multiple-segment rupture appears unlikely on the Bartlett Springs fault because segment boundaries are well-defined, and because the segments adjacent to the Coyote Rocks segment do not display evidence of a similar history of repeated late Pleistocene and Holocene events (Geomatrix Consultants, 1986).

We adopt a rupture length of 11 miles (18 km) for the Coyote Rocks segment, which is the segment of the Bartlett Springs fault that is closest to the Sites and Golden Gate dam sites. Regressions on magnitude vs. surface-rupture length in Wells and Coppersmith (1994) indicate that an 11-mile-long (18 km) rupture is associated with a $M_w$ 6.6 earthquake. If the Coyote Rocks segment dips 60° to the northeast (Chapter 2), and if the depth to the brittle-ductile transition in this region is about 9.4 miles (15 km; Chapter 4), then the potential rupture width of the Coyote Rocks segment is about 10.6 miles (17 km). The corresponding rupture area is 117 square miles (306 $km^2$). Regressions on magnitude vs. rupture area in Wells and Coppersmith (1994) indicate a $M_w$ 6.5 earthquake. We conservatively adopt $M_w$ 6.6 as the magnitude for a maximum earthquake on the most proximal segment (i.e., Coyote Rocks) of the Bartlett Springs fault to the DWR dam sites (Table 6-1).

## 6.6 CORNING FAULT

The Corning fault is a north-striking, subvertical to steeply east-dipping structure that underlies the north-central Sacramento Valley (Harwood and Helley, 1987). WLA (1997) divided the Corning fault into several geometric segments, each of which is associated with an anticline:

- A northern segment associated with an unnamed, south-plunging fold that extends approximately 9 miles (15 km) south of the town of Red Bluff;
- A central reach associated with the North and South Corning Domes that extends for a combined north-south distance of approximately 12.4 to 15.5 miles (20-25 km); and
- A southern reach associated with the doubly-plunging Greenwood anticline, which is developed along the southern 15.5 to 18.7 mile (25-30 km) reach of the Corning fault.

Total length of the Corning fault is approximately 43 miles (70 km) (Plate 1).

WLA (1997) inferred late Quaternary movement on the central and southern segments of the Corning fault based on folding of Quaternary strata at the Corning Domes and uplift above the Greenwood anticline, respectively. The closest approach of the Corning fault (southern segment) to Sites and Golden Gate dam sites is 20 miles and 18 miles (32 km and 29 km), respectively (Table 6-1).

We evaluated the earthquake potential of the southern reach of the Corning fault because of its proximal location relative to the DWR dam sites. Detailed analysis of relocated earthquakes in the northern Sacramento Valley indicates that there are two discrete linear alignments of epicenters associated with the southern reach of the fault (Chapter 4). We interpret that these two linear clusters of earthquakes represent two discrete faults at depth. The largest and closest cluster is about 13 miles (21 km) long. We therefore adopt 13 miles (21 km) as the maximum rupture length for a fault associated with the

southern reach of the Corning fault. From regressions on rupture length vs. magnitude in Wells and Coppersmith (1994), we calculate an associated $M_W$ 6.6 earthquake.

Detailed analysis of seismicity (Chapter 4) further documents that small earthquakes in the vicinity of the southern reach of the Corning fault occur in the 3 to 16 mile (5 to 26 km) depth range. We interpret the vertical distribution of background earthquakes to indicate that the likely vertical extent of rupture in this region is 13 miles (21 km). If it is assumed that the fault dips 70° to the east, then the maximum rupture width is about 14 miles (22 km). The corresponding maximum rupture area for a 13-mile- (21-km-) long rupture is thus 182 square miles (462 $km^2$). The associated magnitude from regressions on magnitude vs. rupture area in Wells and Coppersmith (1994) is $M_W$ 6.7. We conservatively adopt $M_W$ 6.7 as the maximum magnitude for the proximal southern segment of the Corning fault (Table 6-1).

## 6.7 THE CASCADIA SUBDUCTION ZONE

Geological and geophysical evidence provide the basis for the current scientific consensus that the Cascadia subduction zone is capable of generating great earthquakes with rupture lengths greater than 560 miles (>900 km) (Atwater et al., 1995; Hyndman and Wang, 1995; Fluck et al., 1997; Nelson et al., 1995; Satake et al., 1996). A rupture of this size would involve the northern California portion of the Cascadia margin. Below, we summarize estimates for the potential rupture length and width that dictate the maximum magnitude of earthquakes on the Cascadia plate interface.

### 6.7.1 Rupture Length

The maximum potential rupture length for the CSZ is based on geological evidence for concurrent coseismic subsidence in estuaries from northern California to Vancouver Island (Nelson et al., 1995). Statistically equivalent radiocarbon ages on fossil trees and marsh herbs killed by coseismic subsidence of the youngest buried soil archived at numerous Pacific Northwest estuaries support the interpretation that an earthquake on the Cascadia megathrust that occurred about 300 years ago ruptured at least 560 miles (900

km) of the plate interface (Nelson et al., 1995). Uncertainties in radiocarbon dating techniques also permit the interpretation that a series of shorter segments of the plate boundary ruptured independently. If the latter scenario is correct, then this series of lesser earthquakes would have occurred in less than 20 years based on dated earthquake-killed trees at sites 422 miles (680 km) apart (Nelson et al., 1995). We believe that a single, great earthquake rupturing the entire Cascadia subduction zone is a simpler, more plausible interpretation of the data.

Satake et al. (1996) found several Japanese tsunami records from AD 1700 that could not be explained by local seismicity or by historical earthquake records and paleoseismic evidence in South America, Alaska or Kamchatka. According to Satake et al. (1996), the most likely source of this tsunami is the Cascadia subduction zone. On the basis of tsunami wave heights, Satake et al. (1996) estimated that the earthquake ruptured the entire length of the Cascadia margin. This evidence, in addition to geological evidence from estuaries in the Pacific Northwest cited above, is incorporated in geophysical studies that assess the seismic potential of the subduction zone (Fluck et al., 1997; Hyndman and Wang, 1995). We adopt the estimate of 620 miles (1,000 km) (Hyndman and Wang, 1995), the approximate distance between the Mendocino triple junction and Vancouver Island, for the maximum rupture length of the Cascadia margin.

### 6.7.2 Rupture Width

Recent studies suggest that the coseismic rupture width of a subduction zone can be estimated from the combined downdip extent of the interseismic locked and transition zones, as determined by elastic dislocation modeling (Fluck et al., 1997). The width of the potential Cascadia rupture surface has been estimated by elastic dislocation and numerical thermal modeling of the locked and transition zones (Fluck et al., 1997; Hyndman and Wang, 1995). Hyndman and Wang (1995) showed that variations in the locked zone estimated from geodetic data correlated with thermal variations along the fault at depth. The maximum downdip temperature for the locked zone corresponds to 350°C and the maximum downdip temperature for the transition zone corresponds to 450°C (Hyndman and Wang, 1995).

Fluck et al. (1997) developed a three-dimensional dislocation model of the entire length of the CSZ that has an average locked zone width of 37 miles (60 km) and a transition zone width of 37 miles (60 km). The widths of these zones in the model are greater in offshore Washington where the plate dip is shallow, and narrower in offshore Oregon and Vancouver Island. Therefore, we conclude that the best estimate for the maximum rupture area for the entire length of the CSZ is 74.5 miles (120 km) based on the average combined widths of the locked and transition zones modeled offshore Oregon, Washington, and Vancouver Island (Fluck et al., 1997).

### 6.7.3 Maximum Earthquake

The magnitude of the maximum earthquake can be estimated by empirical relations between moment magnitude and rupture area (Wells and Coppersmith, 1994; Wyss, 1979) and by calculating the magnitude from the seismic moment (Hanks and Kanamori, 1979). Taking the maximum rupture parameters (e.g., a fault length of 620 miles (1000 km) equal to the entire length of the Cascadia margin and an average downdip width of 74.5 miles (20 km) based on the combined widths of the locked and transition zones) we calculate a maximum rupture area of 46,310 square miles (120,000 $km^2$), which corresponds to a $M_w$ 8.9 to $M_w$ 9.0 earthquake based on empirical relations documented by Wells and Coppersmith (1994). The empirical relation proposed by Wyss (1979) predicts a maximum magnitude of $M_w$ 9.2. Calculating the magnitude from the seismic moment ($M_o$) according to the equation of Hanks and Kanamori (1979),

$$M_w = {}^{2}/_{3} \log M_o - 10.7$$

predicts a maximum moment magnitude of $M_w$ 9.2. For this calculation, we compute the seismic moment from the equation:

$$M_o = d\mu A$$

where the displacement ($d$ = 75.5 feet (23 m)) equals the product of the plate convergence rate (42 mm/yr) and the average earthquake recurrence interval (550 years); the shear modulus ($\mu$) equals 3 x $10^{11}$ dyn/cm$^2$.

Based on analysis of geological evidence along the western North America coast from British Columbia to northern California, Nelson et al. (1995) concluded that the maximum size of Cascadia subduction earthquakes is approximately $M_w$ 9. This estimate is supported by analysis of Japanese tsunami records that provide evidence for the time and size of the most recent giant Cascadia earthquake in 1700 A.D. Numerical modeling of tsunami heights from Japan indicate that the entire length of the subduction zone ruptured during the 1700 A.D. earthquake in a $M_w$ 9 event (Satake et al., 1996). Based on these calculations, and the current consensus regarding seismic potential of the Cascadia subduction zone (Nelson et al., 1995), we adopt the estimate of $M_w$ 9 for the maximum earthquake on the Cascadia plate interface (Table 6-1).

Given the geometry of the southern edge of the subducting Gorda Plate and the downdip extent of rupture on the subduction zone discussed in Section 3.6.1, the closest approach of a Cascadia earthquake to the DWR dam sites is 100 miles (160 km) (Table 6-1).

## 6.8 INTRAPLATE EARTHQUAKES IN THE GORDA PLATE

Over 80% of well-located microearthquakes recorded by the Humboldt Bay seismic network between 1974 and 1984 occurred in the Gorda plate (McPherson, 1989; Smith et al., 1993). Several recent intraplate earthquakes within the Gorda plate have reached or exceeded $M_w$ 6.5, including two large strike-slip events that occurred on July 13, 1991 ($M_w$ 6.8) and August 17, 1991 ($M_w$ 7.1), and two large strike-slip aftershocks following the 1992 Cape Mendocino earthquake that occurred on April 26, 1992 ($M_w$ 6.5, 6.6) (Velasco et al., 1994). The largest historical earthquake documented in northern California (January 1922; $M_s$ 7.6) occurred in the Gorda plate (Smith and Knapp, 1980). Fault rupture during these earthquakes accommodated north-south shortening along northeast- and northwest-striking, conjugate strike-slip faults that deform the Gorda plate

due to north-directed compression across the Gorda-Pacific plate boundary (Smith et al., 1993; Velasco et al., 1994; Wilson, 1989).

We conservatively adopt the maximum magnitude estimated by Dengler et al. (1992), $M_w$ 7.5, for intraplate earthquakes in the Gorda plate (Table 6-1). Although several studies have noted a distinct change in the focal mechanisms of Gorda plate events as the subducting slab passes the Mendocino triple junction to the east (Dengler et al., 1992; Smith et al., 1993; Wang and Rogers, 1994), we cannot preclude the possibility that a large-magnitude ($M_w$ 7+) intraplate event could occur in the subducting slab at greater than 19 miles (>30 km) depth. This caveat is supported by the probable source regions for intraplate earthquakes delineated by Weaver and Shedlock (1996) who predict that large-magnitude ($M_w$ >7) earthquakes within the Gorda slab likely will occur between 28 to 37 miles (45 to 60 km) below the western Sacramento Valley. The closest approach of the Gorda slab to the DWR dam sites is 53 miles (85 km) (Table 1; see discussion in Section 3.6.2).

## 6.9 SURFACE RUPTURE HAZARDS

### 6.9.1 Salt Lake Fault

Based on evidence for late Quaternary surface-rupturing events from paleoseismic trenching studies summarized in Section 3.4.2, we conclude that surface rupture has occurred on the Salt Lake fault during or following arthquakes on the Funks segment of the Great Valley thrust fault system. Our preferred interpretation of the trench data is that the approximately 5 foot (1.5 m) reverse offset of the Quaternary strath bedrock surface documented in the trenches is the result of cumulative displacement from several events, rather than a single event. Based on restoration of a faulted contact in the Quaternary deposits overlying the bedrock surface (Figure 3-44; see Section 3.4.2 for discussion), we interpret that a maximum of about 16 inches (40 cm) of reverse displacement may occur during an individual surface rupture on the Salt Lake fault.

Subsurface relationships in the trenches alternatively can be interpreted as evidence that up to 47 inches (120 cm) of displacement occurred during a single event (Section 3.4.2). The trench data therefore suggest that the extreme range in displacement during surface-rupturing events is 16 to 47 inches (40 to 120 cm). We strongly favor the lower end of this range because progressive restoration of offset strata in the trench log is best accomplished with several smaller events of about 16 inches (40 cm) rather than fewer larger events (Section 3.4.2).

The results of elastic dislocation modeling presented in Section 6.2.4.3 also indicate that displacements on the Salt Lake fault are likely to be closer to 16 inches (40 cm) than 47 inches (120 cm). The models predict displacements of about 4.5 inches (11 cm) for earthquakes that accommodate an average of 3.3 feet (1 m) of coseismic slip during a $M_w$ 6.6 earthquake on the Funks segment of the Great Valley fault. As discussed in Section 6.2.4.3, comparison with the 1994 Northridge earthquake suggests that an average coseismic displacement of about 3.3 feet (1.0 m) is probably appropriate for a $M_w$ 6.6 earthquake. Given the linear scaling of elastic constitutive relationships, coseismic slip of about 33 feet (10 m) would be required to produce about 47 inches (120 cm) of triggered slip on the Salt Lake fault. The associated earthquake magnitude would be higher by at least an order of magnitude, which is unreasonable given the maximum potential rupture dimensions of the Funks segment. We therefore conclude that triggered surface displacements on the Salt Lake fault during a moderate to large earthquake on the Funks segment of the Great Valley fault are likely to range from 4.5 inches to 16 inches (11 cm to 40 cm).

### 6.9.2 Northeast-Striking Dextral Faults

Paleoseismic trench investigations for this study document no Holocene surface displacement on the GG-1, GG-2, GG-3 and S-2 faults (Chapter 3). Our preferred kinematic model for the structural evolution of the area directly around the dam sites, however, posits that movement on these faults may be related to movement at depth on the blind Funks segment of the Great Valley fault (Section 3.3). Given this structural model, our conclusion that the Funks segment is an active seismic source is in apparent

contradiction with evidence for no activity of the northeast-striking dextral faults. This apparent contradiction arises in part from poor age constraints on the timing of late Quaternary events on the Funks segment and the northeast-striking faults. Paleoseismic data presented in Chapter 3 provide indirect evidence for a minimum of three earthquakes on the Funks segment during the past 30,000 to 70,000 years. It is possible that the last Funks segment earthquake occurred in latest Pleistocene time (i.e., about 10,000 years ago), just prior to deposition of undeformed early Holocene sediments overlying the GG-1, GG-2, GG-3 and S-2 faults, which were exposed in trenches and documented during this investigation. Thus, the oldest deposits available for evaluating activity of the GG-1, GG-2, GG-3 and S-2 faults may post-date the last surface-faulting event on these structures. Alternatively, it is possible that the GG-1, GG-2, GG-3 and S-2 faults are not kinematically related to the Great Valley fault or, if they are that they are not reactivated during every earthquake on the Funks segment.

Given these uncertainties, we conservatively assume that the GG-1, GG-2, GG-3 and S-2 faults may accommodate minor displacement during a moderate to large earthquake on a proximal segment of the Great Valley fault (i.e., the Funks and Bear Valley segments). In the following sections, we employ several different analytical approaches to estimate potential coseismic surface displacements on the northeast-striking dextral faults.

#### 6.9.2.1 Surface Displacement as a Fraction of Coseismic Slip on the Funks Segment

This approach assumes that the displacement of Cretaceous stratigraphic units by the northeast-striking dextral faults has accumulated incrementally and proportionally during individual earthquakes on the Funks segment of the Great Valley thrust fault. We further assume that the ratio of incremental slip on the dextral faults to slip on the Funks segment of the Great Valley thrust system during an earthquake is the same as the ratio of total, cumulative slip on these structures.

Based on offset reflectors in seismic lines, we infer that total reverse slip on the Great Valley thrust fault is about 5 miles (8 km) (Appendix A). Total slip on the dextral faults

measured from offset Upper Cretaceous stratigraphic contacts is shown on Figure 3-1, and summarized as follows:

Fault GG-1: 246 ft ± 82 ft (75 m ± 25 m)
Fault GG-2: 1312 ft, +197 ft/ -98.5 ft (400 m, + 60 m/ -25 m)
Fault GG-3: 1575 ft ± 66 ft (480 m ± 20 m)
Fault S-2: 558 ft, +164 ft/ -180.5 ft (170 m, +50m/ -55 m)

These values can be expressed as a percentage of the total 5 miles (8 km) of slip on the Great Valley fault:

Fault GG-1: 1% (±0.3 %)
Fault GG-2: 5% (approximately ±0.5 %)
Fault GG-3: 6% (±0.3 %)
Fault S-2: 2% (±0.6 %)

If slip on the GG and S faults exhibits these proportional relationships to coseismic slip on the Funks segment at depth, and if 1 m of slip occurs on the Funks segment during a $M_w$ 6.6 earthquake (Section 6.2.4.3), then the predicted surface displacements are:

Fault GG-1: 0.4 inches ± 0.12 inches (1 cm ± 3 mm)
Fault GG-2: 2 inches ± 0.2 inches (5 cm ± 5 mm)
Fault GG-3: 2.4 inches ± 0.12 inches 6 cm (± 3 mm)
Fault S-2: 0.8 inches ± 0.24 inches (2 cm ± 6 mm)

A conservative assumption is that the total dextral slip over all of the GG and S faults may be concentrated on a single northeast-striking fault during a given earthquake, rather than distributed among the four faults as shown above. The summed dextral displacement on the GG and S faults for 3.3 feet (1.0 m) of coseismic slip on the Funks segment in the previous example is 5.5 inches (14 cm), with a combined uncertainty of about 1 inch (± 2 cm). We attach low a low likelihood to this scenario.

To summarize, our preferred model predicts a range of displacements on the GG and S faults between about 0.5 and 2.5 inches (1 to 6 cm), depending on the individual faults. Maximum surface displacement of about 5.5 inches (14 cm) is predicted if all of the sympathetic dextral slip occurs on a single fault.

#### 6.9.2.2 Magnitude of Dextral Slip Necessary to Accommodate Tectonic Wedging

In this model, we assume that dextral slip on the northeast-striking dextral faults accommodates propagation of the tectonic wedge structure created by the intersection of the Salt Lake fault with the blind Funks segment of the Great Valley fault. The tectonic wedge structure is illustrated by Figure 3-2, and the kinematics of wedge propagation are discussed in Section 3.3. We assume that coseismic slip on the Salt Lake fault is a result of rupture on the Funks segment of the Great Valley thrust fault and eastward propagation of the wedge tip beneath the Sacramento Valley (Figure 3-2). We further assume that no propagation of the wedge structure occurs south of the GG-1, GG-2, GG-3 and S-2 faults, such that dextral offset on these structures accommodates the full differential movement of the wedge structure to the north. This is a conservative assumption because it implies that slip on the Salt Lake fault constrains the maximum propagation of the wedge, and consequently the maximum resolved dextral slip across the dextral faults.

We assume that the component of reverse slip on the east-dipping Salt Lake fault resolved in the horizontal plane represents the magnitude of wedge propagation that occurs during earthquakes on the Funks segment of the Great Valley thrust fault. Based on the analysis and discussion in Section 6.2.4.3, we assume that the range of likely displacement is about 4 to 16 inches (11 to 40 cm). We also assume that the fault dips parallel to bedding; mapping by Brown and Rich (1961) indicates that Upper Cretaceous strata adjacent to the Salt Lake fault dip about 60° to 80° in the vicinity of Hunters Creek. The horizontal component of motion accommodated by 4 to 16 inches (11 to 40 cm) of slip on a fault dipping 60° to 80° ranges from about 1 to 8 inches (2 to 20 cm). This displacement could be fully accommodated by slip on a single northeast-striking fault (i.e., 8 inches (20 cm)), or it could be distributed across faults GG-1, GG-2, GG-3 and S-

2. In a simple model, we assume that the horizontal motion of the wedge is distributed equally across the four dextral faults. With this assumption, coseismic slip on each of the four faults could range from about 0.25 inches to 2 inches (0.5 to 5 cm). Alternatively, the slip could be distributed among the four faults in the same proportions as the total dextral slip is distributed, similar to the model discussed in the previous section. For this model, 1 to 8 inches (2 to 20 cm) of total dextral shear is distributed among the faults as follows:

Fault GG-1: about 0.1 inches to 0.6 inches (0.2 to 1.4 cm)
Fault GG-2: about 0.7 inch to 3 inches (0.7 cm to 7 cm)
Fault GG-3: about 0.4 inches to 3.4 inches (0.9 cm to 8.6 cm)
Fault S-2: about 0.2 inches to 1.2 inches (0.3 cm to 3 cm)

The extreme range of surface displacement on the northeast-striking dextral faults thus predicted by this model is about 0.1 inches to 8 inches (0.2 to 20 cm). The high end of this range is based on the assumption that all of the differential east-directed displacement of the tectonic wedge is accommodated by dextral slip on a single northeast-striking fault. We favor distribution of the total wedge displacement across the GG-1, GG-2, GG-3 and S-2 faults, and thus our preferred range of coseismic displacement on an individual fault for this model is about 0.25 inches to 3.4 inches (0.5 to 9 cm).

#### 6.9.2.3 Slip Predicted by Elastic Dislocation Models

In this approach we assume that dextral slip on the GG-1, GG-2, GG-3 and S-2 faults releases elastic strain of the hanging wall block produced by slip on the blind Funks and Bear Valley segments of the Great Valley thrust fault, similar to the mechanical assumptions used to model triggered slip on the Salt Lake fault (Section 6.2.4). We used elastic models to evaluate potential surface displacements on these structures associated with coseismic rupture of the Funks segment at depth. We assume that the GG-2, GG-3, and S-2 faults behave as vertical friction-free surfaces that relax some of the elastic strain in the upper crust associated with an earthquake on the Funks or Bear Valley segment.

We further assume that these faults terminate down-dip against the flat portion of the Funks segment. The displacement gradient across these faults predicted by the models is taken to approximate the potential surface displacement on these structures. The modeling parameters used in this approach are discussed in Section 6.2.4.2. All models were scaled to duplicate the depth of faults and their relative distances as inferred from analysis of geologic maps (Brown and Rich, 1961) and seismic reflection data (Appendix A).

We investigated two general models of surface displacement on the northeast-striking GG-2, GG-3 and S-2 faults triggered by coseismic rupture of the underlying Great Valley fault. In the first model, we assumed that the southern extent of coseismic rupture on the Funks segment of the Great Valley fault directly underlies the northeast-striking faults. In the second model, we investigated potential surface displacement on the faults triggered by rupture of the Bear Valley segment to the south. Fault lengths and locations were as shown in Figure 6-1. Results from each of the models are discussed in the following sections.

*6.9.2.3.1 Funks Segment Model Results*

In this model, we imposed a constant displacement of 3.3 feet (1 m) on the Funks segment, including both the ramp portion and 2 km of the flat portion, consistent with the rupture width adopted for the maximum earthquake on this fault. The Funks segment is assumed to terminate to the south directly below the S-2 fault. The model results indicate that total differential displacement across the three faults is about 2.5 inches (6 cm) of right-lateral slip (Figure 6-9). If the deformation is distributed uniformly, slip on individual faults is less than an inch (i.e., about 2 cm). Surface displacement vectors (Figure 6-9b) diverge across the tear faults, indicating that a small component of horizontal extension and opening may be resolved across the structures in addition to dextral shear.

We ran a similar model with the southern boundary of the Funks segment located beneath the GG-2 fault (i.e., beneath the northernmost of the four northeast-striking tear faults).

The results, not shown here, indicate a similar pattern of surface displacements with a maximum differential of about 2 inches (4 to 5 cm) across the three faults. We conclude that our preferred model and interpretation of the Funks segment terminating southward beneath the S-2 fault also is conservative because it produces the largest surface displacements on the northeast-striking tear faults. The maximum slip on these structures predicted by this model is on the order of about 2.5 inches (6 cm), distributed across the three faults.

*6.9.2.3.2 Bear Valley Segment Model Results*

For the Bear Valley segment model, we imposed a constant displacement of 1m on the Bear Valley segment, which lies directly south of the Funks segment. The fault is about 0.5 to 1 mile (1-2 km) deeper than the Funks segment, and based on analysis of seismic reflection data is modeled to be a north-striking plane with a constant dip of 21 degrees toward the west. We assumed that coseismic slip on the Bear Valley segment is parallel to the dip of the Funks segment, so the resulting slip is slightly right-oblique. In this model, coseismic slip extends from the brittle-ductile transition at 9.4 miles (15 km) depth to a depth of 4.7 miles (7.5 km). The results from this model (Figure 6-10) give a maximum differential of about 1.5 inches (4 cm) of left-lateral displacement across the three tear faults.

*6.9.2.3.3 Discussion*

Because the individual and cumulative horizontal separations on the GG and S faults are right-lateral, the left-lateral displacements predicted by the Bear Valley rupture model appear to be in direct contradiction to the field data. This may indicate that the fault geometry and slip direction used in the model do not accurately depict the process of fault rupture on the Bear Valley segment. Alternatively, it is possible that seismic events alternate on the Bear Valley and Funks segments, with right-lateral displacements triggered by the Funks segment events being partially recovered by induced left-lateral displacements caused by Bear Valley segment events.

Figure 6-9

Figure 6-10

The right-lateral displacements on the GG and S faults predicted by the model for coseismic rupture on the Funks segment are greater than the left-lateral displacements predicted by rupture on the Bear Valley segment. This model result is consistent with the kinematic interpretation of the tear faults discussed in Section 3.3, which attributes relative right-lateral slip on these structures to the more shallow dip of the flat part of the Funks segment relative to the Bear Valley segment. If the models accurately reproduce patterns of triggered slip, then we anticipate that with equal numbers of earthquakes on both segments the cumulative net displacement over time will be dextral, as observed. Regardless of the kinematics of cumulative displacement across the northeast-striking faults, the elastic dislocation models show that the maximum displacements triggered by events on segments of the Great Valley fault will be on the order of about 2 inches (6 cm).

#### 6.9.2.4 Conclusions

The two models that explicitly relate the magnitude of slip on the blind thrust fault to slip on the northeast-striking faults in the hanging wall block both predict up to about 3.4 inches (1 to 9 cm) of surface displacement on the GG and S faults. The first model predicts maximum displacements up to about 5.5 inches (14 cm) if all of the deformation is accommodated by slip on a single fault rather than distributed across several faults. Maximum surface displacements of about 8 inches (20 cm) are predicted by the tectonic wedge model (Section 5.2.2.2), using the most conservative assumptions about coseismic slip on the Salt Lake fault and distribution of deformation across the GG and S faults. We prefer lower values of about 0.25 inches to 3.4 inches (0.5 to 9 cm) predicted by this model with less conservative assumptions; these lower values are more consistent with the results of the first model and the elastic dislocation models. Based on results obtained from all three modeling approaches, we conclude that maximum surface displacements on the GG and S faults probably will not exceed about 8 inches (20 cm), and are likely to be lower (on the order of about 2.4 to 4 inches (i.e., 6 to 10 cm).

# 7.0 GROUND MOTION ANALYSIS

## 7.1 INTRODUCTION

This chapter provides an evaluation of the estimated strong ground shaking at the Sites and Golden Gate dam sites during maximum earthquakes from active seismic sources in the study region. The vibratory ground motion produced by an earthquake can be quantitatively described in a variety of ways. Release of stored elastic strain during an earthquake causes the ground surface at a point to oscillate in a range of frequencies, each of which is persistent for a certain length of time as the earthquake waves pass by. The horizontal and vertical acceleration of a point on the ground due to shaking varies as a function of earthquake magnitude and type, regional and local geology, site-source distance, and frequency of vibration. Given a record of the ground acceleration versus time, the horizontal and vertical accelerations can be integrated to obtain horizontal and vertical velocities and displacements of the ground surface. It is common engineering practice to characterize earthquake ground motion by plotting the maximum magnitude of the response of a simple one-degree-of-freedom oscillator as a function of vibration period and damping ratio of the oscillator. This type of plot is known as a *response spectrum* (Chopra, 1981). Response quantities that are computed include absolute acceleration, relative velocity, relative displacement, and basal shear.

For this study, calculated earthquake ground motions are presented in a series of response spectra that plot spectral absolute acceleration (in units of g, the acceleration due to gravity) as a function of vibration period (in seconds) for a damping ratio of 5% of critical. Section 7.2 describes published empirical attenuation relations used to derive spectral acceleration as a function of earthquake magnitude and site-source distance. Section 7.3 describes the selection of the controlling source, which is the seismic source that produces the maximum levels of strong ground shaking at the Sites and Golden Gate dam sites. Section 7.4 presents the maximum earthquake response spectra calculated for the controlling seismic source.

The response spectra presented in this report do not describe displacements or strains that may be experienced by engineered structures at the Sites and Golden Gate dam sites. These quantities cannot be computed without accounting for the duration of shaking at a given period, and without a priori knowledge or modeled estimate of the vibration response of the structure itself. Using published empirical attenuation relations, it is common to obtain relatively high spectral accelerations (i.e., > 1g) at periods in the range of about 0.1 sec to 1 sec for moderate magnitude earthquakes that occur within 10 to 20 km of a site. In terms of evaluating the stability of a structure, these high values at shorter periods may be less significant than lower accelerations at longer periods, depending on the actual size, geometry and design of the structure.

## 7.2 COMPUTATIONAL APPROACH

Using maximum earthquake magnitudes and site-to-source geometry derived in Chapter 6, we computed response spectra for major dams using the following two-step approach:

1) Calculate the 84th-percentile, 5%-damped response spectra from the Abrahamson and Silva (1997) and Sadigh et al. (1997) attenuation equations, and average the results. We also computed 50th-percentile, 5%-damped average response spectra using the same attenuation relations for comparison with the 84th-percentile spectra; and

2) Modify the resulting response spectrum for fault-rupture directivity effects using the procedure in Somerville et al. (1997).

The Abrahamson and Silva (1997) and Sadigh et al. (1997) attenuation equations are briefly described in the following subsections.

### 7.2.1 Abrahamson and Silva (1997)

The basic form of the attenuation equations derived by Abrahamson and Silva (1997) is:

$$ln\ Y = f_1(M,r) + Ff_3(M) + HWf_4(M,r) + Sf_5(\overline{pga}_{rock})$$

where: $Y$ = 5% damped spectral acceleration in g

$M$ = moment magnitude

$r$ = closest distance from site to fault rupture in km

$F$ = fault type (1 for reverse, 0.5 for reverse/oblique, and 0 otherwise)

$HW$ = dummy variable for hanging wall sites (1 for sites over wall, and 0 otherwise)

$S$ = dummy variable for site class (0 for rock or shallow soil, 1 for deep soil)

$\overline{pga}_{\text{rock}}$ = expected value of peak ground acceleration on rock

$f_i$ = functions given in Abrahamson and Silva (1997)

Abrahamson and Silva (1997) derived one set of equations for horizontal components and another set for vertical components. For the ground-motion calculation, the rock-site form of the equations was selected by setting S = 0. For both maximum events at both dam sites, $F = 1$ and $HW = 1$ were selected, because the faults were thrust and the sites were on the hanging walls.

### 7.2.2 Sadigh et al. (1997)

The basic form of the Sadigh et al. (1997) equations for rock sites is

$$ln(Y) = C_1 + C_2M + C_3 (8.5 - M)^{2.5} + C_4 ln(r + exp(C_5 + C_6M)) + C_7 ln(r + 2) + F ln (1.2)$$

where: $Y$ = 5% damped spectral acceleration in g

$M$ = moment magnitude

$r$ = closest distance from site to fault rupture in km

$F$ = fault type (1 for reverse and 0 otherwise)

$C_i$ = functions given in Sadigh et al. (1997)

The above equation pertains only to horizontal components, as Sadigh et al. (1997) did not derive a similar set of equations for vertical components. For the ground-motion calculation of both maximum events at both dam sites, F = 1 was selected.

## 7.3 SELECTION OF CONTROLLING SEISMIC SOURCE

Based on a comparison of response spectra for maximum earthquakes described in Chapter 6, earthquakes on the Funks and Bear Valley segments of the Great Valley fault were selected as the controlling maximum earthquakes from the standpoint of the seismic design. In addition to these fault segments, potentially significant crustal faults and associated maximum moment magnitudes ($M_w$) of interest include: (1) the GG-2, GG-3, and S-2 faults ($M_w$ 5.4) adjacent to the sites, (2) Bartlett Springs fault ($M_w$ 6.6), and (3) Corning fault ($M_w$ 6.7) (Table 6-1). The comparison also included a great earthquake ($M_w$ 9.0) on the interplate portion of the Cascadia subduction zone, and a large intraplate earthquake ($M_w$ 7.5) from the Gorda plate (Wadati-Benioff zone) (Table 6-1).

The 84th percentile response spectra for the crustal faults were computed using Abrahamson and Silva (1997) and Sadigh et al. (1997) equations by following the two-

step procedure described in Section 7.2. The spectral comparisons are shown in Figures 7-1 and 7-2 for the Golden Gate and Sites dam sites, respectively. Note that at periods, T > 0.1 sec, which is the band of engineering interest, the spectra for the maximum earthquake on the Funks and Bear Valley segments are virtually identical and are significantly greater than the spectra from the other three events. Only the zero period ordinate (which represents the peak ground acceleration - PGA) for the GG-2, GG-3, and S-2 faults is greater than the PGA for the Funks and Bear Valley segments by approximately 20%. This difference is not important; dams properly designed to maximum earthquakes on the Funks and Bear Valley segments should not be adversely affected by a small ($M_w$ 5.4) earthquake on any of the local faults.

Spectral comparisons similar to those for the crustal faults are presented for the Cascadia subduction zone events in Figures 7-3 and 7-4 for the Golden Gate and Sites dam sites, respectively. At all periods, the spectra for maximum earthquakes on the Funks and Bear Valley segments are greater than the spectra for the subduction events by factors of approximately 3 to 5. This difference is so great that the longer durations from the subduction events should not adversely affect the performance of the dams designed to the much larger amplitude (but shorter duration) motions generated by the maximum earthquakes on the Funks and Bear Valley segments.

## 7.4 MAXIMUM EARTHQUAKE RESPONSE SPECTRA

As discussed in Chapter 6, maximum earthquake magnitudes were estimated for each of the Funks and Bear Valley segments. For the purposes of the ground-motion calculation, the relevant parameters for each maximum earthquake (ME) are listed in Table 7-1.

Figure 7-1

Figure 7-2

Figure 7-3

Figure 7-4

**Table 7-1** ME Parameters for Ground-Motion Calculation

| Dam | Controlling Fault | Maximum Moment Magnitude (M) | Closest Distance, r (km) | Attenuation Parameters | | | | | |
|---|---|---|---|---|---|---|---|---|---|
| | | | | Abrahamson & Silva | | | Sadigh et al. | Somerville et al. | |
| | | | | S | F | HW | F | Y | Φ |
| Golden Gate | Funks Segment | 6.6 | 5.8 | 0 | 1 | 1 | 1 | 1 | 13° |
| | Bear Valley Segment | 6.8 | 7.0 | 0 | 1 | 1 | 1 | 1 | 18° |
| Sites | Funks Segment | 6.6 | 6.5 | 0 | 1 | 1 | 1 | 1 | 16° |
| | Bear Valley Segment | 6.8 | 7.7 | 0 | 1 | 1 | 1 | 1 | 18° |
| Note: Because of uncertainty in measurement, a value of Φ = 0° was used for directivity correction in all cases. | | | | | | | | | |

The fault-related parameters listed in this table were based on the fault geometries discussed in Chapter 6 and shown in Figures 6-2, 6-3 and 6-8. The angle Φ is uncertain, but was judged to be small for all cases, as shown in these figures. For conservatism it was taken as 0° for the ground-motion calculation.

### 7.4.1 Average Response Spectra

The 84th percentile level of 5% damped spectral accelerations from both ME events were computed for each site by:

1) Substituting the parameters from Table 7-1 into the Abrahamson and Silva and the Sadigh et al. attenuation equations;

2) Adding to the resulting *ln (Y)* values the standard deviations published with these equations; and

3) Taking the antilogs.

The resulting spectra are shown in Figure 7-5 for the Golden Gate dam site and Figure 7-6 for the Sites dam site. The pairs of response spectra from the Abrahamson and Silva and the Sadigh et al. equations were averaged to produce the 84th percentile spectra in Figure 7-7 (Golden Gate) and Figure 7-8 (Sites); the corresponding 50th percentile (median) spectra are also shown in these two figures for reference. These 84 percentile spectra represent the completion of Step (1) in Section 7.2, above.

### 7.4.2 Directivity Correction

The Somerville et al. (1997) equations for dip-slip faults were used for the directivity correction. These equations are of the form

$$y = C_1 + C_2 \, Y \cos \Phi ,$$

where: $y$ is the correction factor for fault-rupture directivity effects; $Y$ is a dimensionless length as defined in Figure 5 of Somerville et al.; $\Phi$ is an angle also defined in the same Figure 5; and, $C_1$ and $C_2$ are regression coefficients in Table 4b of the same reference.

For a given maximum earthquake scenario, the period-dependent $y$ values were first computed using values of $Y = 1$ and $\Phi = 0$, as stated in Table 7-1. The exponentials of these values, $e^y$, were then multiplied by the corresponding average 84th percentile response spectra to obtain the directivity-corrected spectra. Comparisons of the average 84th percentile response spectra with and without this correction are shown in Figure 7-9 (Golden Gate) and Figure 7-10 (Sites). Note that the directivity correction affects periods greater than 0.5 sec and its effect increases with increasing period. Except at 0.75 sec, the directivity scaling increases the average 84th percentile response spectra.

## 7.5 SUMMARY

Based on a comparison of response spectra for maximum earthquakes on active seismic sources evaluated for this study (Table 6-1), earthquakes on the Funks and Bear Valley segments of the Great Valley fault were selected as the controlling maximum earthquakes

(Table 7-1). At periods that lie within the band of engineering interest (i.e., T > 0.1 sec), the spectra for maximum earthquakes on the Funks and Bear Valley segments are virtually identical.

At all periods the spectra for these controlling events are greater than the spectra for much larger, but more distant, Cascadia subduction zone earthquakes by factors of approximately 3 to 5. This difference suggests that subduction events should not adversely affect the performance of dams designed to the much larger amplitude but shorter duration motions generated by maximum earthquakes on the Funks and Bear Valley segments. The PGA for a postulated maximum aftershock on the GG-2, GG-3, and S-2 faults at zero distance from the dam sites is greater than the PGA for the Funks and Bear Valley segments by approximately 20%. The damped spectral acceleration for the controlling events, however, is greater than that for the maximum aftershock at periods T > 0.1 sec. We conclude that dams properly designed to maximum earthquakes on the Funks and Bear Valley segments should not be adversely affected by an aftershock or small ($M_w$ 5.4) earthquake on any of the local faults.

Figure 7-5

Figure 7-6

Figure 7-7

Figure 7-8

Figure 7-9

Figure 7-10

# 8.0 REFERENCES


Abrahamson, N., and Silva, W., 1997, Empirical Response Spectral Attenuation Relations for Shallow Crustal Earthquakes: Seismological Research Letters, v. 68, no.1, Seismological Society of America, p. 94-127.

Ake, J., 1991, Seismicity in the Sierra Foothills of California, Preliminary Investigations: U.S. Bureau of Reclamation Seismotectonic Report 91-1, Denver, Colorado, 34 p.

Allen, C.R., 1982, Reservoir-induced seismicity earthquakes and engineering policy: California Geology, November 1982, p. 248-250.

Anderson, L.W., LaForge, R., and Anders, M.H., 1982, Seismotectonic study of the San Luis area eastern Diablo Range, California: U.S. Bureau of Reclamation Seismotectonic Report 82-2, 7 p.

Argus, D.F., and Gordon, R.G., 1991, Current Sierra Nevada-North American motion from Very Long Baseline Interferometry: implications for the kinematics of the western United States: Geology, v. 19, p. 1085 -1088.

Argus, D.F., and Gordon, R.G., 2001, Present tectonic motion across the Coast Ranges and San Andreas fault system in central California: Geological Society of America Bulletin, v. 113, p. 1580-1592.

Astiz, L., and Kanamori, H., 1986, Interplate coupling and temporal variations of mechanisms of intermediate-depth earthquakes in Chile: Bulletin of the Seismological Society of America, v. 76, p.1614-1622.

Atwater, B.F., and 15 others, 1995, Summary of coastal geologic evidence for past great earthquakes at the Cascadia subduction zone: Earthquake Spectra, v. 11, p. 1-18.

Atwater, B.F., and Hemphill-Haley, E., 1997, Recurrence intervals for great earthquakes of the past 3500 years at northeastern Willapa Bay: Washington, United States Geological Survey Professional Paper 1576, 108 p.

Atwater, T., 1970, Implications of plate tectonics for the Cenozoic tectonic evolution of western North America: Geological Society of America Bulletin, v. 81, p. 3513-3536.

Atwater, T., and Stock, J., 1998, Pacific-North American plate tectonics of the Neogene southwestern United States: an update: International Geological Review, v. 40, p. 375-402.

Baecher, G.B., and Kenney, R.L., 1982, Statistical examination of reservoir-induced seismicity: Bulletin of the Seismological Society of America, v. 72, p. 553-569.

Bailey, E.H., Blake, M.C., Jr., and Jones, D.L., 1970, On-land Mesozoic oceanic crust in California Coast Ranges: United States Geological Survey Professional Paper 700-C, p. 70-81.

Beaudoin, B.C., and 10 others, 1996, Transition from slab to slabless: Results from the 1993 Mendocino triple junction seismic experiment: Geology, v. 24, p. 195-199.

Beaudoin, B.C., Hole, J.A., Klemperer, S.L., and Tréhu, A.M., 1998, Location of the southern edge of the Gorda slab and evidence for an adjacent asthenospheric window: results from seismic profiling and gravity: Journal of Geophysical Research, v. 103, p. 30,101-30,115.

Beck, S., and Ruff, L., 1984, Seismicity and subduction along the Peru trench (abstract): EOS, Transactions of the American Geophysical Union, v. 65, p. 998.

Bennett, J.H., 1987, Winters-Vacaville earthquakes, 1892: California Geology, v. 40, p. 75-83.

Benz, H.M., Zandt, G., and Oppenheimer, D.H., 1992, Lithospheric structure of northern California from teleseismic images of the upper mantle: Journal of Geophysical Research, v. 97, p. 4791-4807.

Benz, H.M., and Zandt, G., 1993, Teleseismic tomography: lithospheric structure of the San Andreas fault system in northern and central California, in Iyer, H.M., and Hirahara, K., "Seismic Tomography: Theory and Practice": Chapman and Hall, London, p. 440-465.

Blake, M.C. Jr., Helley, E.J., Jayko, A.S., Jones, D.L., and Ohlin, H.N., 1992, Geologic map of the Willows 1:100,000 quadrangle, California: United States Geological Survey Open File Report 92-271, 38 p. plus map.

Bolt, B.A., and Miller, R.D., 1975, Catalog of earthquakes in northern California and adjoining area 1 January 1910 – 31 December 1972, Seismographic Stations, University of California, Berkeley, 567 p.

Brankman, C.M., and Aydin, A., 2000, Uplift and contractional deformation along a segmented strike-slip fault system: the Gargano Promontory, southern Italy: in review, Journal of Structural Geology.

Brown, R.D. Jr., 1964, Geologic map of the Stonyford quadrangle, Glenn, Colusa and Lake counties, California: United States Geological Survey Mineral Investigations Fields Studies Map MF-279.

Brown, R.D. Jr., and Rich, E.I., 1961, Geologic map of the Lodoga quadrangle, Glenn and Colusa counties, California: United States Geological Survey Oil and Gas Investigations Map OM-210, scale 1:48,000.

Bufe, C.G., Lester, F.W., Lahr, K.M., Lahr, J.C., Seekins, L.C., and Hanks, T.C., 1976, Oroville earthquakes: normal faulting in the Sierra Nevada foothills: Science, v. 192, p. 72-74.

Bull, William B., 1991, Geomorphic responses to climatic change: Oxford University Press, New York, NY, United States, 326 p.

Bullard, T.F., and Lettis, W.R., 1993, Quaternary fold deformation associated with blind thrust faulting, Los Angeles Basin, California: Journal of Geophysical Research, v. 98, no. B5, p. 8349-8369.

Burnett, A.W., and Schumm, S.A., 1983, Active tectonics and river response in Louisiana and Mississippi: Science, v. 222, p. 49-50.

Byrne, D.E., Davis, D.M., and Sykes, L.R., 1988, Loci and maximum size of thrust earthquakes and the mechanics of the shallow region of subduction zones: Tectonics, v. 7, p. 833-857.

California Department of Water Resources, 1978, West Sacramento Valley fault and seismicity, Glen Complex, Colusa Reservoir, Berryessa Enlargement: unpublished report, Division of Design and Construction, Project Geology Branch, 43 p.

California Department of Water Resources, 1978, West Sacramento Valley fault and seismicity study: unpublished preliminary report, 48 p.

California Department of Water Resources, 1999, Integrated Storage Investigations: North of Delta Offstream Storage Investigation, Phase One Fault and Seismic Hazards Investigation: unpublished report, Northern District Office, 68 p.

Carver, G.A., Jayko, A.S., Valentine, D.W., and Li, W.H., 1994, Coastal uplift associated with the 1992 Cape Mendocino earthquake, northern California: Geology, v. 22, p. 195-198.

Castillo, D.A., and Ellsworth, W.L., 1993, Seismotectonics of the San Andreas fault system between Point Arena and Cape Mendocino in Northern California: Implications for the development and evolution of a young transform: Journal of Geophysical Research, v. 98, p. 6543-6560.

Chuber, S., 1961, Late Mesozoic stratigraphy of the Elk Creek-Fruto area, Glenn County, California: Ph.D. dissertation, Stanford University, 115 p. plus maps.

Clark, M.M., Sharp, R.V., Castle, R.O., and Harsh, P.W., 1976, Surface faulting near Lake Oroville in August 1975: Bulletin of the Seismological Society of America, v. 66, p. 1101-1110.

Clarke, S.H., and McLaughlin, R.J., 1992, Neotectonic framework of the southern Cascadia subduction zone-Mendocino triple junction region: in Burke, R.M. and Carver, G.A., eds., Guidebook for the Field trip to Northern Coastal California, Friends of the Pleistocene, June 1992.

Cockerham, R.S., 1984, Evidence for a 180-km-long subducted slab beneath northern California: Bulletin of the Seismological Society of America, v. 74, p. 569-576.

Comninou, M.A., and Dundurs, J., 1975, The angular dislocation in a half-space: Journal of Elasticity, v. 5, p. 203-216.

Constenius, K.N., Johnson, R.A., Dickinson, W.R., and Williams, T.A., 2000, Tectonic evolution of the Jurassic-Cretaceous Great Valley forearc, California: implications for the Franciscan thrust-wedge hypothesis: Geological Society of American Bulletin, v. 112, p. 1703-1723.

Corps of Engineers, 1986, Geologic and seismologic investigation, Black Butte Lake, Stony Creek, California: USACE Sacramento District, 87 p. plus appendices.

Crouch, S.L., and Starfield, A.M., 1983, Boundary Element Methods in Solid Mechanics: Unwin Hyman, London.

Dehlinger, P., and Bolt, B., 1984, Seismic parameters along the Bartlett Springs fault zone in the Coast Ranges of northern California: Bulletin of the Seismological Society of America, v. 74, p. 1785-1798.

Dehlinger, P., and Bolt, B., 1985, Jointly determined focal parameters along a fault in California's northern Coast Range: Tectonophysics, v. 118, p. 293-299.

Dengler, L, Carver, G., and McPherson, R., 1992, Sources of North Coast Seismicity: California Geology, v. 45, p. 40-53.

dePolo, C.M., and Ohlin, H.N., 1984, The Bartlett Springs fault zone: an eastern member of the California plate boundary system: Geological Society of America Abstracts with Programs, Annual Meeting, v. 16, no. 6, p. 486.

Dewey, J.W., and Spence, W., 1979, Seismic gaps and source zones of recent large earthquakes in coastal Peru: Pure and Applied Geophysics, v. 117, p. 1148-1171.

Dickinson, W.R., and Rich, E.I., 1972, Petrologic intervals and petrofacies in the Great Valley sequence, Sacramento Valley, California: Geological Society of America Bulletin, v. 83, p. 3007-3024.

Dickinson, W.R., and Seely, D.R., 1979, Structure and stratigraphy of forearc regions: American Association of Petroleum Geologists Bulletin, v. 63, p. 2-31.

Dickinson, W.R., and Snyder, W.S., 1979, Geometry of subducted slabs related to the San Andreas transform: Journal of Geology, v. 87, p. 609-627.

Division of Safety of Dams, 1995, DSOD fault activity guidelines for use in deterministic fault activity assessments: unpublished memo by William Fraser, 1 p.

Earth Science Associates, 1980, Seismic and fault activity study, proposed Glenn Reservoir complex: prepared for the California Department of Water Resources, Sacramento, California.

Eaton, J.P., 1985, The May 2, 1983 Coalinga earthquake and its aftershocks: a detailed study of the hypocenter distribution and of the focal mechanisms of the larger aftershocks, in Rymer, J. and Ellsworth, W.L., eds., Mechanics of the May 2, 1983 Coalinga earthquake: United States Geological Survey Open File Report 85-44, p. 132-201.

Eberhart-Phillips, D., 1989, Active faulting and deformation of the Coalinga anticline as interpreted from three-dimensional velocity structure and seismicity: Journal of Geophysical Research, v. 94, p. 15,565-15,586.

Eberhart-Phillips, D., and Oppenheimer, D. H., 1984, Induced seismicity in the Geysers geothermal area, California: Journal of Geophysical Research, v. 89, p. 1191-1207.

Ellsworth, W.L., 1990, Earthquake history, 1769-989, in Wallace, R.E., ed., The San Andreas Fault System, California: United States Geological Survey Professional Paper 1515, p. 152-181.

Ellsworth, W.L., 1991, Earthquake History, 1769-1989: in Wallace, R.E., The San Andreas Fault System, California, United States Geological Survey Professional Paper 1515, p. 153-187.

Engdahl, E.R., and Rinehart, W.A., 1991, Seismicity map of North America project: in Slemmons, D.B., Engdahl, E.R., Zoback, M.D., and Blackwell, D.D., eds., Neotectonics of North America: Geological Society of America Decade Map Volume 1, Boulder, Colorado, p. 21-27

Fleitout, L., and Froidevaux, C., 1982, Tectonics and topography for a lithosphere containing density heterogeneities: Tectonics, v. 1, p. 21-56.

Fluck, P., Hyndman, R.D., and Wang, K., 1997, Three-dimensional dislocation model for great earthquakes of the Cascadia subduction zone: Journal of Geophysical Research, v. 102, p. 20,539-20,550.

Fraser, W.A., 1997, Seismic source characterization for dam site analysis in California: ASDSO Western Region Technical Seminar, Earthquake Engineering for Dams, Sacramento, California, p. 3-17.

Freymueller, J.T., Murray, M.H., Segall, P., and Castillo, D., 1999, Kinematics of Pacific-North America plate boundary zone, northern California: Journal of Geophysical Research, v. 104, p. 7419-7441.

Furlong, K.P., 1984, Lithospheric behavior with triple junction migration; an example based on the Mendocino triple junction: Physics of the Earth and Planetary Interiors, v. 36, p. 213-223.

Geomatrix Consultants, 1986, Final report: geological assessment of the seismic potential of the Bartlett Springs shear zone for Scott Dam, Lake County, California: prepared for Pacific Gas & Electric Company, San Francisco, California, 51 p. plus figures.

Godfrey, N.J., Beaudoin, B.C., Lendl, C., Meltzer, A., and Luetgert, J., 1995, Data report for the 1993 Mendocino Triple Junction Seismic Experiment, Northern California: United States Geological Survey Open File Report 95-275, 83 p.

Godfrey, N.J., Beaudoin, B.C., Klemperer, S.L., and the Mendocino Working Group, 1997, Ophiolitic basement to the Great Valley forearc basin, California, from seismic and gravity data: implications for crustal growth at the North American continental margin: Geological Society of America Bulletin, v. 108, p. 1536-1562.

Godfrey, N. J. and Dilek, Y., 2000, Mesozoic assimilation of oceanic crust and island arc into the North American continental margin in California and Nevada: Insights from geophysical data, in Dilek, Y., Moores, E., Elthon, D., and Nicolas, A., Ophiolites and Oceanic Crust: New Insights from Field Studies and the Ocean Drilling Program: Geological Society of America Special Paper 349, p. 365-382.

Goldfinger, C., Nelson, C.H., and Johnson, J.E., 2001, Holocene seismicity of Cascadia subduction zone based on the turbidite event record: Seismological Research Letters, v. 72, p. 254.

Gupta, H.K., 1992, Reservoir-Induced Earthquakes: Elsevier, New York, 364 p.

Gupta, H.K., and Rastogi, B.K., 1976, Dams and Earthquakes, Developments in Geotechnical Engineering, v. 11: Elsevier Scientific Publishing Co., Amsterdam, 229 p.

Hack, J.T., 1973, Stream-profile analysis and stream-gradient index: United States Geological Survey Journal of Research, v. 1, p. 421-429.

Harbert, W., and Cox, A., 1989, Late Neogene motion of the Pacific plate: Journal of Geophysical Research, v. 94, p. 3052-3064.

Harlan-Miller-Tait Associates, 1983, Report of fault evaluation of the Cottonwood Creek Project: prepared for the U.S. Army Corps of Engineers, Sacramento District, contract DACWO5-82-C-0074, 98 p.

Harlan-Miller-Tait Associates, 1984, Supplemental fault evaluation of the Cottonwood Creek Project: prepared for the U.S. Army Corps of Engineers, Sacramento District, contracts DACW05-84-D-1635 and DACWO5-84-P-2499, 32 p. plus appendices.

Hart, E.W., and McJunkin, R.D., 1983, Surface faulting northwest of Coalinga, California, June and July 1983, in Bennett, J.H., and Sherburne, R.W., eds., The 1983 Coalinga, California earthquakes: California Division of Mines and Geology Special Publication 66, p. 201-220.

Harwood, D.S., and Helley, E.J., 1987, Late Cenozoic tectonism of the Sacramento Valley, California: United States Geological Survey Professional Paper 1359, 46 p.

Hauksson, E., Jones, L.M., and Hutton, K., 1995, The 1994 Northridge earthquake sequence in California: seismological and tectonic aspects: Journal of Geophysical Research, v. 100, p. 12,335-12,355.

Helley, E.J., and Harwood, D.S., 1985, Geologic map of the Late Cenozoic deposits of the Sacramento Valley and Northern Sierran Foothills, California: United States Geological Survey Miscellaneous Field Studies Map MF-179, 5 plates.

Helley, E.J., and Jaworowski, C., 1985, The Red Bluff pediment: a datum plane for locating Quaternary structures in the Sacramento Valley, California: United States Geological Survey Bulletin 1628, 13 p.

Henstock, T.J., and Levander, A., 2000, Lithospheric evolution in the wake of the Mendocino triple junction: structure of the San Andreas Fault system at 2 Ma: Geophysical Journal International, v. 140, p. 233-247.

Henyey, T.L., and Lee, T.C., 1976, Heat flow in the Lake Tahoe, California-Nevada, and the Sierra Nevada-Basin and Range transition: Geological Society of America Bulletin, v. 87, p. 1179-1187

Hill, D.P., Eaton, J.P., Ellsworth, W.L., Cockerham, R.S., and Lester, F.W., 1991, The seismotectonic fabric of central California: in Slemmons, D.B., Engdahl, E.R., Zoback, M.D., and Blackwell, D.D., eds., Neotectonics of North America, Geological Society of America Decade Map Volume 1, Boulder, Colorado, p. 107-132

Hill, D.P., Eaton, J.P., and Jones, L.M., 1990, Seismicity, 1980-1986, in Wallace, R.E., ed., The San Andreas Fault System, California: United States Geological Survey Professional Paper 1515, p. 115-151.

Hilley, G.E., and Arrowsmith, J.R., 2000, Thrust fault slip rates deduced from coupled geomorphic and tectonic models of active faults and folds in the San Francisco Bay Area: Collaborative Research with Arizona State University, and University of California, Davis: USGS award number 1434-H-97-GR-03113, National Earthquake Hazards Reduction Program Final Technical Report, 9 plates, 82 p.

Hitchcock, C.S., and Kelson, K.I., 1999, Growth of late Quaternary folds in southwest Santa Clara Valley, San Francisco Bay area, California: implications of triggered slip for seismic hazard and earthquake occurrence: Geology, v. 27, p. 391-394.

Hudnut, K., Shen, Z., Murray, M., McClusky, S., King, R., Herring, T., Hager, B., Feng, Y., Fang, P., Donnellan, A., and Bock, Y., 1996, Co-seismic displacements of the 1994 Northridge, California, earthquake: Seismological Society of America Bulletin, v. 86, p. S19-S36.

Hyndman, R.D., and Wang, K., 1995, The rupture zone of Cascadia great earthquakes from current deformation and the thermal regime: Journal of Geophysical Research, v. 100, p. 22,133-22,154

Ingersoll, R.V., 1978, Paleogeography and paleotectonics of the late Mesozoic forearc basin of northern and central California, in Howell, D.G., and McDougall, K.A., eds., Mesozoic Paleogeography of the Western United States: Pacific Coast Paleography Symposium 2, Pacific Section, Society of Economic Paleontologists and Mineralogists, p. 471-482.

Ingersoll, R.V., and Dickinson, W.R., 1990, Great Valley Group (Sequence), Sacramento Valley, California, in Ingersoll, R.V., and Nilsen, T.H., eds., Sacramento Valley Symposium and Guidebook: Pacific Section, Society of Economic Paleontologists and Mineralogists, v. 65, p. 183-215.

Jachens, R.C., and Griscom, A., 1983, Three-dimensional geometry of the Gorda plate beneath northern California: Journal of Geophysical Research, v. 88, p. 9375-9392.

Jachens, R.C., Griscom, A., and Roberts, C.W., 1995, Regional extent of Great Valley basement west of the Great Valley, California: Implications for extensive tectonic wedging in the California Coast Ranges: Journal of Geophysical Research, v. 100, p. 12,769-12,790.

Jacoby, G., Carver, G., and Wagner, W., 1995, Trees and herbs killed by an earthquake ~300 yr ago at Humboldt Bay: California Geology, v. 23, p. 77-80.

Jayko, A.S., Blake, M.C. Jr., and Harms, T., 1987, Attenuation of the Coast Range ophiolite by extensional faulting, and nature of the Coast Range "thrust": Tectonics, v. 6, p. 475-488.

Jennings, C.W., 1994, Fault activity map of California and adjacent areas, with locations and ages of recent volcanic eruptions: California Department of Conservation, Division of Mines and Geology, Geologic Data Map No. 6, scale 1:750,000.

Jennings, C.W., and Strand, R.G., compilers, 1960, Ukiah sheet *of* Geologic map of California: California Division of Mines, scale 1:250,000.

Jeyakumaran, M., Rudnicki, J.W., and Keer, L.M., et al., 1992, Modeling slip zones with triangular dislocation elements: Bulletin of the Seismological Society of America, v. 82, p. 2153-2169.

Jones, C.H., Unruh, J.R., and Sonder, L.J., 1996, The role of gravitational potential energy in active deformation in the southwestern United States: Nature, v. 381, p. 37-41

Jones, D.L., Bailey, E.H., and Imlay, R.W., 1968, Stratigraphy and structural significance of Buchia zones, northwestern Sacramento Valley, California [Abs.]: Geological Society of America Special Paper 101, p. 104.

Jones, D.L., Bailey, E.H., and Imlay, R.W., 1969, Structural and stratigraphic significance of Buchia zones in the Colyear Springs-Paskenta area, California: United States Geological Survey Professional Paper 647-A, 24 p.

Keller, E.A., and Pinter, N., 1996, Active tectonics, earthquakes, uplift, and landscape: Prentice-Hall, Inc.

Kirby, J.M., 1943, Rumsey Hills area: California Division of Mines and Geology Bulletin 118, p. 601-605.

Kissling, E., Ellsworth, W.L., Eberhart-Phillips, D., and Kradolfer, U., 1994, Initial reference models in local earthquake tomography: Journal of Geophysical Research, v. 99, p.19,635-19,646.

Kradolfer, U., 1989, Seismische tomographie in der Schweiz mittels lockaler erdeben, Doktor der Naturwissenschften, Edge. Tech. Hochsch, Zurich, 109 p.

Klein, F.W., Eaton, J.P., and Lester, F.W., 1988, Seismic station data for northern California and surrounding area, United States Geological Survey Open File Report 88-448.

Lachenbruch, A.H., and Sass, J.H., 1980, Heat flow and energetics of the San Andreas fault zone: Journal of Geophysical Research, v. 85, p. 6185-6222.

LaForge, R.C., and Hawkins, F.F., 1986, Seismotectonic study of northernmost California for the Shasta, Keswick, Spring Creek debris, Trinity, Lewiston and Whiskeytown Dams, Central Valley Project: U.S. Bureau of Reclamation, Seismotectonic Report 86-1, 130 p.

Lahr, K.M., Lahr, J.C., Lindh, A.G., Bufe, C.G., and Lester, F.W., 1976, The August 1975 Oroville earthquakes: Bulletin of the Seismological Society of America, v. 66, p. 1085-1100.

Langston, C.A., and Butler, R., 1976, Focal mechanism of the August 1, 1975 Oroville earthquake: Bulletin of the Seismological Society of America, v. 66, p. 1111-1120.

Lawton, J.E., 1956, Geology of the north half of the Morgan Valley Quadrangle and the south half of the Wilbur Springs Quadrangle: Ph.D. dissertation, Stanford University, California, 223 p. plus maps.

Lettis, W.R., 1982, Late Cenozoic stratigraphy and structure of the western margin of the central San Joaquin Valley, California: United States Geological Survey Open File Report 82-526, 315 p.

Lettis, W.R., Bachhuber, J.L., Witter, R.C., Brankman, C.M., Randolph, C.E., Barka, A., Page, W.D., and Kaya, A., 2001, Influence of releasing stopovers on surface fault rupture and fault segmentation: examples from the August 17, 1999 Kocaeli earthquake on the North Anatolian Fault, Turkey, Bulletin of the Seismological Society of America, v. 92, p. 19-42.

Lester, F.W., Bufe, C.G., Lahr, K.M., and Stewart, S.W., 1975, Aftershocks of the Oroville earthquake of 1 August 1975 in Sherbourne, R.W., and Hauge, C.J., eds., Oroville, California, earthquake, 1 August 1975: California Division of Mines and Geology Special Report 124, p. 131-138.

Loewen, B.A., 1992, Deformation of lower Cretaceous through Tertiary strata in the Rumsey Hills-Capay Valley area: implications for late Cenozoic motion of an east-tapering underthrust wedge: M.S. thesis, University of California, Davis, 84 p.

Maerten, L., Willemse, E.J.M., Pollard, D.D., and Rawnsley, K.D., 1999, Slip distributions on intersecting normal faults: Journal of Structural Geology, v. 21, no. 3, p. 259-271.

Marks, S.M., and Lindh, A.G., 1978, Regional seismicity of the Sierran foothills in the vicinity of Oroville, California: Bulletin of the Seismological Society of America, v. 68, p. 1103-1115.

Marple, R.T., and Talwani, P., 1993, Evidence of possible tectonic upwarping along the South Carolina coastal plain from an examination of river morphology and elevation data: Geology, v. 21, p. 651-654.

McLaughlin, R.J., and Nilsen, T.H., 1982, Neogene non-marine sedimentation in small pull-apart basins of the San Andreas fault system, Sonoma County, California: Sedimentology, v. 29, p. 865-876.

McLaughlin, R.J., Ohlin, H.N., Thormahlen, D.J., Jones, D.L., Miller, J.W., and Blome, C.D., 1989, Geologic map and structure sections of the Indian Valley-Wilbur Springs geothermal area, northern Coast Ranges, California: United States Geological Survey Miscellaneous Investigations Series Map I-1706.

McNally, K., and Gonzalez-Ruiz, J.R., 1986, Predictability of the whole earthquake cycle and source mechanics for large earthquakes ($7.0 < Mw < 8.1$) along the Middle America Trench offshore Mexico (abstract): Earthquake Notes, v. 57 no. 1, p. 22.

McNally, K., Gonzalez-Ruiz, J.R., and Stolte, C., 1986, Seismogenesis of the great 1985 ($Mw = 8.1$) Michoacan, Mexico earthquake: Geophysical Research Letters, v. 13, p. 585-588.

McPherson, R.C., 1989, Seismicity and focal mechanisms near Cape Mendocino, northern California, unpublished Masters thesis: Humboldt State University, Arcata, California, 75 p.

Meltzer, A.S., 1988, Crustal structure and tectonic evolution: central California: Ph.D. dissertation, Rice University, Houston, Texas, 284 p. plus plates.

Merritts, D., and Vincent, K.R., 1989, Geomorphic response of coastal streams to low, intermediate, and high rates of uplift, Mendocino triple junction region, northern California: Geological Society of America Bulletin, v. 12, p. 1373-1388

Merritts, D.J., 1996, The Mendocino triple junction: Active faults, episodic coastal emergence, and rapid uplift: Journal of Geophysical Research, v. 101, p. 6051-6070.

Molnar, P., and Lyon-Caen, H., 1988, Some simple physical aspects of the support, structure, and evolution of mountain belts, in Clark, S. P., Jr., Burchfiel, B. C., and Suppe, J., ed., Processes in Continental Lithospheric Deformation: Geological Society of America Special Paper 218, p. 179-207.

Mount, V.S., and Suppe, J., 1987, State of stress near the San Andreas fault: Implications for wrench tectonics: Geology, v. 15, p. 1143-1146.

Morrison, P.W., Stump, B.W., Uhrhammer, R, 1978, The Oroville earthquake sequence of August 1975: Bulletin of the Seismological Society of America, v. 66, p. 1065-1084.

Moxon, I.W., 1988, Sequence stratigraphy of the Great Valley basin in the context of convergent margin tectonics, in Graham, S.A., ed., Studies of the Geology of the San Joaquin Basin: Pacific Section, Society of Economic Paleontologists and Mineralogists, v. 60, p. 3-28.

Moxon, I.W., 1990, Stratigraphic and Structural Architecture of the San Joaquin-Sacramento Basin: Ph.D. dissertation, Stanford University, 371 p. plus plates.

Moxon, I.W., and Graham, S.A., 1987, History and controls of subsidence in the Late Cretaceous-Tertiary great Valley forearc basin, California: Geology, v. 15, p. 626-629.

Munk, L.P., 1992, Stratigraphy, geomorphology, soils and neotectonic interpretation of the Dunnigan Hills, California: Ph.D. dissertation, University of California, Davis, 124 p.

Murray, M.H., Marshall, G.A., Lisowski, M., and Stein, R.S., 1996, The 1992 M=7 Cape Mendocino, California, earthquake: Coseismic deformation at the south end of the Cascadia megathrust, Journal of Geophysical Research, 101, 17,707-17,725

Nelson, A., and 11 others, 1995, Radiocarbon evidence for extensive plate-boundary rupture about 300 years ago at the Cascadia subduction zone: Nature, v. 378, p. 371-374.

Niemi, T.M., and Hall, N.T., 1992, Late Holocene slip rate and recurrence of great earthquakes on the San Andreas fault in northern California: Geology, v. 20, p. 195-198.

O'Connell, D.R.H., and Unruh, J.R., 2000, Updated Evaluation of Faults Within 10 km of Monticello Dam, Solano Project: U.S. Bureau of Reclamation, Report 99-5.

O'Connell, D.R.H., Unruh, J.R., and Block, L.V., 2001, Source Characterization and Ground Motion Modeling of the 1892 Vacaville-Winters Earthquake Sequence, California: Bulletin of the Seismological Society of America, v. 91, p. 1471-1497.

Oppenheimer, D., and 19 others, 1993, The Cape Mendocino, California, earthquakes of April 1992: Subduction at the triple junction: Science, v. 261, p. 433-438.

Oppenheimer, D., Klein, F., Eaton, J., and Lester, F., 1993, The Northern California Seismic Network Bulletin, January – December 1992: United States Geological Survey Open File Report 93-578, 45 p.

O'Reilly, W., and Rastogi, B.K., (eds.), 1986, Induced Seismicity: Physics of the Earth and Planetary Interiors, v. 44, p. 73-199.

Packer, D.R., Cluff, L.S., Kneupfer, P.L., and Withers, R.J., 1979, A study of reservoir-induced seismicity: U.S. Geological Survey Open File Report 80-1092, 279 p.

Page, B.M., 1982, Migration of the Salinian composite block, California, and disappearance of fragments: American Journal of Science, v. 282, p. 1694-1734.

Page, B.M., and Engebretson, D.C., 1985, Correlation between the geologic record and computed plate motions for central California: Tectonics, v. 3, p. 133-155.

Platt, J.P., 1986, Dynamics of orogenic wedges and uplift of high-pressure metamorphic rocks: Geological Society of America Bulletin, v. 97, p. 1037-1053.

Ramirez, V.R., 1992, Geology and deep structure of the Rumsey Hills area, Sacramento Valley, California, in Erskine, M., Unruh, J., Lettis, W., and Bartow, A., eds., Field Guide to the tectonics of the boundary between the Coast Ranges and Great Valley of California: Guidebook 70, Pacific Section, American Association of Petroleum Geologists, p. 85-94.

Real, C.R., Toppozada, T.R., and Parke, D.L., 1978, Earthquake catalog of California, January 1, 1900 - December 31, 1974: California Division of Mines and Geology Special Publication 52, 15 p.

Reasenberg, P.A. and Oppenheimer, D.H., 1985, FPFIT, FPPLOT, and FPPAGE: Fortran computer programs for calculating and displaying earthquake fault-plane solutions: United States Geological Survey Open File Report 85-739, 109 p.

Rich, E.I., 1971, Geologic map of the Wilbur Springs quadrangle, Colusa and Lake Counties, California: United States Geological Survey Miscellaneous Field investigations Map I-538, 1:48,000 scale.

Rich, E.I., unpublished manuscript, Late Mesozoic stratigraphy along west-central margin Sacramento Valley, California, 98 p. plus compilation map.

Richter, C.F., 1958, Elementary Seismology: W.H. Freeman and Company, Inc., San Francisco and London, 534 p.

Roecker, S.W., 1981, Seismicity and tectonics of the Pamir-Hindu Kush region of Central Asia: Ph.D. thesis, Massachusetts Institute of Technology, Cambridge, 297 p.

Russell, R.D., 1931, The Tehama Formation of northern California: Ph.D. dissertation, University of California, Berkeley, 133 p.

Rymer, M.J., and Ellsworth, W.L., 1990, Introduction in Rymer, M.J., and Ellsworth, W.L., eds., The Coalinga, California, earthquake of May 2, 1983: United States Geological Survey Professional Paper 1487, p. 1-2.

Sadigh, K., and others, 1997, Attenuation relationships for shallow crustal earthquakes based on California strong motion data: Seismological Research Letters, v. 58, no. 1, p. 180-189.

Satake K., Shimazaki, K., Tsuji, Y., and Ueda, K., 1996, Time and size of a giant earthquake in Cascadia inferred from Japanese tsunami records of January 1700: Nature, v. 379, p. 246-251.

Saucedo, G.J., and Wagner, D.L., 1992, Geologic map of the Chico Quadrangle: California Division of Mines and Geology 1°x2° series, scale 1:250,000.

Savage, W.U., Tocher, D., and Birkhahn, P.C., 1976, A study of small aftershocks of the Oroville, California, sequence of August 1975: Engineering Geology, v. 10, p. 371-385.

Scholz, C.H., 1990, The Mechanics of Earthquakes and Faulting: Cambridge University Press, Cambridge, 439 p.

Schumm, S.A., 1977, The Fluvial System: John Wiley and Sons, New York, 338 p.

Seeber, L., Ekstrom, G., Jain, S.K., Murty, C.V.R., Chandak, N., and Armbruster, J.G., 1995, The 1993 Killari earthquake in central India: A new fault in Mesozoic basalt flows?: Journal of Geophysical Research, v. 101, p. 8543-8560.

Sherbourne, S.W., and Knapp, J.S., and McPherson, R.C., 1993, Seismicity of the Gorda plate, structure of the continental margin, and eastward jump of the Mendocino Triple Junction: Journal of Geophysical Research, v. 98, p. 8153-8171.

Sibson, R.H., 1982, Fault zone models, heat flow, and the depth distribution of earthquakes in the continental crust of the United States: Bulletin of the Seismological Society of America, v. 72, p. 151-163.

Silver, E.A., 1971, Tectonics of the Mendocino triple junction: Geological Society America Bulletin, v. 82, p. 2965-2978.

Simpson, D.W., 1976, Seismicity changes associated with reservoir loading: Engineering Geology, v. 10, p. 123-150.

Simpson, D.W., Leith, W.S., and Scholz, C.H., 1988, Two types of reservoir-induced seismicity: Bulletin of the Seismological Society of America, v. 78, p. 2025-2040.

Smith, S.W. and Knapp, J.S., 1980, The northern termination of the San Andreas fault in R. Streitz and R. Sherburne (eds), Studies of the San Andreas Fault Zone in Northern California: California Division of Mines and Geology Special Report 140, p. 153-164.

Smith, S.W., Knapp, J.S., and McPherson, R.C., 1993, Seismicity of the Gorda plate, structure of the continental margin, and an eastward jump of the Mendocino triple junction: Journal of Geophysical Research, v. 98, p. 8153-8171.

Somerville, P.G., and others, 1997, Modification of Empirical Strong Ground Motion Attenuation Relations to Include the Amplitude and Duration Effects of Rupture Directivity: Seismological Research Letters, v. 68, no. 1, p. 199-222.

Sonder, L., 1990, Effects of density contrasts on the orientation of stresses in the lithosphere: relation to principal stress directions in the Transverse Ranges, California: Tectonics, v. 9, p. 761-771.

Stearns, Richard G., 1967, Warping of the western highland rim peneplain in Tennessee by ground-water sapping: Geological Society of America Bulletin v. 78; no. 9, p. 1111-1124.

Steele, W.C., 1980, Quaternary stream terraces in the northwestern Sacramento Valley, Glenn, Tehama, and Shasta Counties, California: United States Geological Survey Open File Report 80-512.

Strahler, A.N., 1952, Dynamic basis of geomorphology: Geological Society of America Bulletin, v. 63, p. 923-938.

Stuiver, M., and P.J., Reimer, 1993, Radiocarbon calibration program "Calib 3.0.3": Radiocarbon, v. 35, p. 215-230.

Suppe, J., 1983, Geometry and kinematics of fault-bend folding: American Journal of Science, v. 283, p. 684-721.

Taboada, A., Bousquet, J.C., and Philip, H., 1993, Coseismic elastic models of folds above blind thrusts in the Betic Cordilleras (Spain) and evaluation of seismic hazard: Tectonophysics, v. 220, p. 223-241.

Taylor, G.C., and others, 1980, Surface rupture associated with the Mammoth Lakes earthquakes of 25 and 27 May, 1980: California Division of Mines and Geology Special Report 150, p. 49-67.

Thomas, A.L., 1993, Poly3D: A three-dimensional, polygonal element, displacement discontinuity boundary element computer program with applications to fractures, faults, and cavities in the Earth's crust: MS thesis, Stanford University.

Tobin, D.G., and Sykes, L.R., 1968, Seismicity and tectonics of the northeast Pacific Ocean: Journal of Geophysical Research, v. 73, p. 3821-3845.

Toppozada, T.R., Real, C.R., and Parke, D.L., 1981, Preparation of isoseismal maps and summaries of reported effects for pre-1900 California earthquakes: California Division of Mines and Geology Open File Report 81-11 SAC, 182 p.

Toppozada, T.R., and Morrison, P.W., 1982, Earthquakes and lake levels at Oroville, California: California Geology, v. 35, p. 115-118.

Townley, S.D., and Allen, M.W., 1939, Descriptive catalog of earthquakes of the Pacific Coast of the United States 1869 to 1928: Seismological Society of America Bulletin, v. 29, p. 1-297.

Trehu, A., 1995, Pulling the rug out from under California: Seismic images of the Mendocino triple junction region: EOS (Transaction, American Geophysical Union), v. 76, p. 369.

Twiss, R.J., Protzman, G.M., and Hurst, S.D., 1991, Theory of slickenline patterns based on the velocity gradient tensor and microrotation: Tectonophysics, v. 186, p. 215-239.

Twiss, R.J., Souter, B.J., and Unruh, J.R., 1993, The effect of block rotations on the global seismic moment tensor and patterns of seismic P and T axes: Journal of Geophysical Research, v. 98, p. 645-674.

Twiss, R.J., and J.R. Unruh, 1998, Analysis of fault-slip inversions: do they constrain stress or strain rate?: Journal of Geophysical Research, v. 103, p. 12,205-12,222.

Unruh, J.R., and Moores, E.M., 1992, Quaternary blind thrusting in the southwestern Sacramento Valley, California: Tectonics, v. 11, p. 192-203.

Unruh, J.R., Loewen, B.A., and Moores, E.M., 1995, Progressive arcward contraction of a Mesozoic-Tertiary fore-arc basin, southwestern Sacramento Valley, California: Geological Society of America Bulletin, v. 107, p. 38-53.

Unruh, J.R., Munk, L.P., Loewen, B.A., Moores, E.M., and Southard, R.J., 1993, Quaternary blind thrusting in the southwestern Sacramento Valley, California: Final Technical Report for National Earthquake Hazards Reduction Program contract 14-08-0001-G2059, Department of the Interior, United States Geological Survey.

Unruh, J.R., Simpson, G.D., Fowler, W., and Lettis, W.R., 1994, Results of Phase 1, seismic hazard investigation, proposed Cortina Rancheria landfill site: unpublished report prepared for Wyse, Inc., and Earthworks Industries, Inc., 9 p.

Unruh, J.R., Twiss, R.J., and Hauksson, E., 1996, Seismogenic deformation field in the Mojave block and implications for the tectonics of the eastern California shear zone: Journal of Geophysical Research, v. 101(B4), p. 8335-8362.

Unruh, J.R., and Lettis, W.R., 1998, Kinematics of transpressional deformation in the eastern San Francisco Bay region California: Geology, v. 26, p. 19-22.

Unruh, J.R. and Sonder, L.J., 1999, Buoyancy forces, plate stresses, and tectonic thickening of the Los Angeles Basin: implications for the strength of the western Transverse Ranges lithosphere, southern California: EOS (Transactions, American Geophysical Union), v. 80, no. 46, p. F1002.

Upp, R.R., 1982, Holocene activity on the Maacama fault, Mendocino County, California: Ph.D. dissertation, Stanford University, California, 112 p. plus plates.

Urhammer, R.A., 1991, Northern California seismicity, in Slemmons, D.B., Engdahl, E.R., Zoback, M.D., and Blackwell, D.D., eds., Neotectonics of North America: Geological Society of America Decade Map Volume 1, Boulder, Colorado, p. 99-106

Urhammer, R.A. and Wright D.H., 1985, Pattern analysis of small explosions and earthquakes recorded near Lake Shasta, California (1952-1963): unpublished report to the U.S. Bureau of Reclamation.

Van Wormer, J.D., and Ryall, A.S., 1980, Sierra Nevada – Great Basin boundary zone: Earthquake hazard related to structure, active tectonic processes, and anomalous patterns of earthquake occurrence: Bulletin of the Seismological Society of America, v. 70, p. 1557-1572.

Velasco, A.A., Ammon, C.J., and Lay, T., 1994, Recent large earthquakes near Cape Mendocino and in the Gorda plate: Broadband source time functions, fault orientations, and rupture complexities: Journal of Geophysical Research, v. 99, p. 711-728.

Verdonck, D. and G. Zandt, 1994, Three-dimensional crustal structure of the Mendocino triple junction region from local earthquake travel times, Journal of Geophysical Research, v. 99, p. 22,843-22,858.

Wagner, D.L., and Bortugno, E.J., 1982, Geologic map of the Santa Rosa quadrangle: California Division of Mines and Geology 1°x2° series, scale 1:250,000.

Wakabayashi, J., and Moores, E.M., 1988, Evidence for collision of the Salinian block with the Franciscan subduction zone: California: Journal of Geology, v. 96, p. 245-253.

Wakabayashi, J., and Smith, D.L., 1994, Evaluation of recurrence intervals, characteristic earthquakes, and slip rates associated with thrusting along the Coast Range-Central Valley geomorphic boundary, California: Bulletin of the Seismological Society of America, v. 84, p. 1960-1970.

Wakabayashi, J., and Unruh, J.R., 1995, Tectonic wedging, blueschist metamorphism, and exposure of blueschists: are they compatible?: Geology, v. 23, p. 85-88.

Wald, D.J., Heaton, T.H., and Hudnut, K.W., 1996, The slip history of the 1994 Northridge, California, earthquake determined from strong motion, teleseismic, GPS and leveling data: Bulletin of the Seismological Society of America, v. 86(1b), p. S49-S70.

Waldhauser, F., and Ellsworth, W.L., 2000, A double-difference earthquake location algorithm: Method and application to the northern Hayward fault: Bulletin of the Seismological Society of America, v. 90, p. 1353-1368.

Walter, S.R., 1986, Intermediate focus earthquakes associated with Gorda plate subduction in northern California: Bulletin of the Seismological Society of America, v. 76, p. 583-588.

Wang, K., and Rogers, G.C., 1994, An explanation for the double seismic layers north of the Mendocino triple junction: Geophysical Research Letters, v. 21, p. 121-124.

Weaver, C.S., and Shedlock, K.M., 1996, Estimates of seismic source regions from the earthquake distribution and regional tectonics in the Pacific Northwest, in A.M. Rogers, T.J. Walsh, W.J. Kockelman and G.R. Priest (eds), Assessing Earthquake Hazards and Reducing Risk in the Pacific Northwest, Vol. 1: United States Geological Survey Professional Paper 1560, p. 285-306.

Wells, D.L., and Coppersmith, K.J., 1994, New empirical relationships among magnitude, rupture length, rupture width, rupture area, and surface displacement: Bulletin of the Seismological Society of America, v. 84, p. 974-1002.

Wentworth, C.M., Blake, M.C. Jr., Jones, D.L., Walter, A.W., and Zoback, M.D., 1984, Tectonic wedging associated with emplacement of the Franciscan assemblage, California Coast Ranges, in Blake, M.C. Jr., ed., Franciscan Geology of Northern California: Pacific Section, Society of Economic Paleontologists and Mineralogists, v. 43, p. 163-173.

Wentworth, C.M., and Zoback, M.D., 1989, The style of late Cenozoic deformation at the eastern front of the California Coast Ranges: Tectonics, v. 8, p. 237-246.

Wentworth, C. and Zoback, M., 1990, Structure of the Coalinga region and thrust origin of the earthquake, in Rymer, M.J., and Ellsworth, W.L., eds, the Coalinga, California, Earthquake of May 2, 1983: United States Geological Survey Professional Paper 1487, p. 41-68.

Willemse, E.J.M., Pollard, D.D., and Aydin, A., 1996, Three-dimensional analyses of slip distributions on normal fault arrays with consequences for fault scaling: Journal of Structural Geology, v. 18, p. 295-309.

William Lettis & Associates, 1997, Seismotectonic evaluation: Stony Gorge and East Park Dams, Orland Project; Monticello Dam, Solano Project: Final Report prepared for the Bureau of Reclamation, U.S. Department of Interior, Denver, Colorado, 146 p. plus appendices and plates.

Williams, T.A., 1997, Basin-Fill Architecture and Forearc Tectonics, Cretaceous Great Valley Group, Sacramento Basin, Northern California: Ph.D. dissertation, Stanford University, 412 p. plus plates.

Wilson, D.S., 1986, A kinematic model for the Gorda deformation zone as a diffuse southern boundary of the Juan de Fuca plate: Journal of Geophysical Research, v. 91, p. 10,259-10,269.

Wilson, D.S., 1989, Deformation of the so-called Gorda plate: Journal of Geophysical Research, v. 94, p. 3065-3075.

Wong, I.G., and Ely, R.W., 1983, Historical seismicity and tectonics of the Coast Ranges-Sierra block boundary: implications to the 1983 Coalinga earthquakes, in Bennet, J., and Sherburne, R., eds., The 1983 Coalinga, California Earthquakes: California Division of Mines and Geology Special Publication 66, p. 89-104.

Wong, I.G., Ely, R.W., and Kollman, A.C., 1988, Contemporary seismicity and block tectonics of the northern California and central Coast Ranges-Sierran block boundary zone, California: Journal of Geophysical Research, v. 93, p. 7813-7833.

Wong, I.G., 1990, Seismotectonics of the Coast Ranges in the vicinity of Lake Berryessa, northern California: Bulletin of the Seismological Society of America, v. 80, p. 935-950.

Wong, I.G., 1991, Contemporary seismicity, active faulting and seismic hazards of the Coast Ranges between San Francisco bay and Healdsburg, California: Journal of Geophysical Research, v. 96, p. 19,891-19,904.

Wong, I.G., 1992, Earthquake activity in the Sacramento Valley, California and its implications to active geologic structures and contemporary tectonic stresses, in Chevren, V.B., and Edmundson, W.F., eds., Structural geology of the Sacramento Basin: American Association of Petroleum Geologists, Pacific Section, p. 5-14.

Wong, I.G., and Strandberg, J., 1996, Assessing the potential for triggered seismicity at the Los Vaqueros Reservoir, California: U.S. Committee on Large Dams, Annual Meeting and Lectures, Los Angeles, California, 15 p.

Woodward-Clyde Consultants, 1989, Seismotectonic study for Monticello Dam: prepared for Solano County Water Policy Advisory Committee, 66 p. plus bibliography and appendix.

Working Group on California Earthquake Probabilities, 1996, Database of potential sources for earthquakes larger than magnitude 6 in northern California: United States Geological Survey Open File Report 96-705, 40 p. plus figures.

Wright, L.A., 1976, Late Cenozoic fault patterns and stress fields in the western Great Basin and westward displacement of the Sierra Nevada block: Geology, v. 4, p. 489-494.

Yamaguchi, D.K., Atwater, B.F., Bunker, D.E., Benson, B.E., and Reid, M.S., 1997, Tree-ring dating the 1700 Cascadia earthquake: Nature, v. 389, p. 922-923.

Zoback, M.D., and 13 others, 1987, New evidence on the state of stress of the San Andreas fault system: Science, v. 238, p. 1105-1111.

Zoback, M.D., and Zoback, M.L., 1989, Tectonic stress field of the continental United States: in Pakiser, L.C. and Mooney, W.D., eds., Geophysical framework of the Continental United States: Geological Society of America Memoir 172, p. 523-540.

# APPENDIX A
# ANALYSIS AND INTERPRETATION OF SEISMIC REFLECTION PROFILES

## A.1 ANALYTICAL APPROACH

We analyzed seismic reflection profiles to evaluate the subsurface structure of the northwestern Sacramento Valley, with emphasis on determining the location and geometry of blind thrust faults. The reflection data comprise an array of eight east-west lines and two north-south lines, altogether which total about 270 line-km of data (Figure A-1). The seismic data were jointly licensed to the California Department of Water Resources and the U.S. Bureau of Reclamation to support seismic hazard investigations in northwestern California. Dr. Dan O'Connell (U.S. Bureau of Reclamation) reprocessed the reflection data to produce pre-stack, migrated depth sections (Figures A-2 through A-11).

Surface faults and major stratigraphic contacts on geologic maps (Brown and Rich, 1961; Chuber, 1961) were plotted on the east-west-trending sections, which are "dip sections" oriented at a high angle to north-south structural trends in the study area. Selected stratigraphic contacts and faults were projected to depth on the dip sections and correlated with reflectors on the crossing north-south (i.e., "strike") sections. Stratigraphic and structural features then were traced north and south along the strike sections as a check of internal consistency in the interpretation of the dip sections. The interpreted locations of blind thrust faults on individual lines were used to prepare a structure contour map delineating segments of the blind thrust system beneath the Sacramento Valley-Coast Ranges boundary (Figure A-1; see also Sections 2.3 and 3.4.3).

## A.2 STRATIGRAPHY

Much of the geology within the seismic reflection array (Figure A-1) was mapped by Brown and Rich (1961) and Chuber (1961). Both groups of workers developed different stratigraphic subdivisions of the Great Valley Group (Figure A-12). The easiest unit to identify and correlate across the boundary between the two maps is the Turonian (Upper

Cretaceous) Venado sandstone, which is mapped as Venado Formation by Chuber (1961), and "Unit 8" by Brown and Rich (1961) (Figure A-12). The Venado sandstone underlies a prominent strike ridge (i.e., "Logan Ridge") that can be traced continuously across the boundary between the two maps.

Subsequent to the work of Brown and Rich (1961) and Chuber (1961), Dickinson and Rich (1972) proposed a simplified and unified stratigraphy for the Great Valley Group (GVG) based primarily on the lithology of major sandstone units (Figure A-12). They combined the Upper Jurassic and Lower Cretaceous GVG strata into two units (i.e., the Stony Creek and Lodoga "petrofacies"). The basal (Cenomanian) Upper Cretaceous unit was named by Boxer petrofacies. The Venado sandstone directly overlies the Boxer Formation and represents the basal unit of the Turonian-Coniacian Cortina petrofacies. The uppermost unit of the GVG in the Dickinson and Rich subdivision is the Campanian-Maastrichtian Rumsey petrofacies (Figure A-12). Rich (unpublished manuscript) subsequently formalized the descriptions of the petrofacies as "formations" (for additional discussion and overview, see Ingersoll and Dickinson, 1990). We adopt the stratigraphy of Dickinson and Rich (1972) and Rich (unpublished manuscript) for the purpose of interpreting the reflection data.

Based on analysis of high altitude imagery and aerial photography, the contact between the Stony Creek and Lodoga Formations was formally associated by Constenius et al. (2000) with a locally angular "discontinuity" between sandstone strike ridges in the lower Great Valley Group section. The "discontinuity" of Constenius et al. (2000) specifically is associated with the erosional base of a conglomeratic sandstone within the Wintun Formation mapped by Chuber (1961), and is near the base of "Unit 4" mapped by Brown and Rich (1961) (Figure A-12).

When projected to depth and correlated among seismic reflection lines, the "discontinuity" separating the Stony Creek and Lodoga Formations (blue-colored marker in Figures A-13 through A-22) is associated with a regionally distinct change in the reflective character of the lower GVG section. The Stony Creek Formation is

characterized by sequences of high-amplitude reflectors ranging from hundreds of meters to over a kilometer in thickness. These reflector sequences project updip to prominent strike ridges in the outcrop belt that are underlain by erosionally resistant conglomeratic units (e.g., "Gravelly Ridge", Clark Ridge", etc.; see Moxon, 1990 for additional description of these conglomerate units). In contrast, the Lodoga Formation above the discontinuity is significantly less reflective. The differences in reflector character and amplitude between the Stony Creek and Lodoga Formations probably are related to textural variations in the sedimentary rocks. Specifically, the congomerates in the Stony Creek Formation are interbedded with mudstone. Differences in acoustic velocities between the conglomerates and mudstones could give rise to large impedence contrasts within the Stony Creek Formation, thus accounting for the bright appearance of the reflectors on the reflection lines (D. O'Connell, U.S. Bureau of Reclamation, personal communication, 2001).

The bright reflector packages associated with conglomerates in the Stony Creek Formation (seismic markers colored purple, Figures A-13 to A-22) can be traced downdip on the east-west lines parallel to bedding beneath the Fruto syncline. The Stony Creek conglomerate reflectors on the dip lines can be tied to similar packages of reflectors on the strike lines, and traced north and south as a discontinuous zone of high-amplitude reflectors in the 5 km to 7 km depth range below the Stony Creek-Lodoga contact (e.g., purple reflector packages below blue marker in Figure A-22). In the strike lines, the Lodoga and Boxer Formations above the basal Lodoga unconformity are characterized by laterally continuous, closely spaced reflectors that exhibit less variation in amplitude than those in the underlying Stony Creek Formation.

The other principal stratigraphic contact plotted on the reflection lines (green marker) is the basal Venado sandstone member of the Cortina Formation (Figure A-10), which is crossed by dip lines 798, 782 and 001, and can be correlated and traced northward on strike line 783. Although Upper Cretaceous units in the northern part of the seismic array are covered by the Pliocene-Pleistocene Tehama Formation, the approximate location of the Venado sandstone on dip line 805 can be determined from open-hole logs. The

Humble "Michael" exploration well drilled about 3.1 km south of line 805 (Figure A-1) encountered the top of the Venado sandstone at about 1825 m (6000 ft) depth (Williams, 1997). The interpreted location of the Venado sandstone on line 805 was determined by projecting the "Michael" data along a north-northwest azimuth parallel to regional structural strike (Figure A-19), which is assumed to be parallel to the trend of the north-northwest-striking Orland Buttes hogback ridge. The interpreted Venado contact is tied to strike line 783 where it crosses dip line 805.

The "Michael" well encountered a major unconformity or normal fault at a depth of about 3800 m (12,500 ft; Figure A-19). Rocks above the contact are Cenomanian-age strata of the Boxer Formation; rocks below the contact contain Valangian fossils, indicating that they are part of the Stony Creek Formation (Williams, 1997). The Lodoga Formation is missing across the contact. When projected onto line 805 and tied to strike line 783, the contact can be traced parallel to bedding southward and correlated with the discontinuity above the Stony Creek Formation. This interpretation implies that the Lodoga Formation is cut out stratigraphically or structurally between the outcrop belt and the subsurface of the western Sacramento Valley where the "Michael" well is located.

Detailed analysis of seismic reflection data by Williams (1997) strongly suggests that the stratigraphic discontinuity in the "Michael" well is an angular unconformity between the Upper Cretaceous Great Valley Group strata and the Stony Creek Formation. When seismic sections are flattened along reflectors associated with Upper Cretaceous strata, a pronounced dip discordance is present at the equivalent depth of the discontinuity in the stratigraphic section encountered by the "Michael" well (Figure 16 in Williams, 1997). The underlying reflectors, which are associated with Stony Creek Formation strata, dip westward beneath the horizontal Upper Cretaceous strata. These relationships suggest that the Upper Jurassic and Lower Cretaceous Great Valley Group strata were tilted westward and eroded prior to eastward onlap of the Upper Cretaceous section. This relationship previously was inferred by Chuber (1961) when he recognized that it was not possible to tie the full thickness of the lower Great Valley Group in the outcrop belt to the section in the "Michael" well.

## A.3 STRUCTURE

From west to east, major map-scale structures crossed by the east-west seismic lines include the Stony Creek fault, Fruto syncline, Sites anticline and the Salt Lake fault. Not all of these structures are crossed by all of the dip lines. We use dip line 001 (Figure A-1), which is the longest of the east-west lines and extends westward to outcrops of the Coast Range ophiolite (CRO), to illustrate structural interpretations that are less completely documented by some of the other dip lines.

The Stony Creek fault is the structural contact between the CRO and the Great Valley Group (GVG), and is crossed by the western end of seismic line 001 (Figure A-17). The surface fault trace is associated with the base of an east-dipping section of laterally continuous, coherent, layered reflectors that project updip to outcrops of east-dipping lower GVG strata. There is a downward tapering body of high amplitude reflections beneath the layered GVG strata that projects updip to the surface exposures of the CRO.

We interpret that the Coast Range fault is at the base of the layered GVG section and extends downdip parallel to bedding in the western limb of the Fruto syncline (Figure A-17). The GVG reflectors correspond to strata of the Stony Creek, Lodoga and Boxer Formations, and they also can be traced downdip beneath the axis of the Fruto syncline. The downward-tapering reflective body beneath the Stony Creek fault is interpreted to be a fragment of the CRO. The less reflective rocks structurally below the CRO project updip to exposures of the Franciscan complex that crop out west of the end of seismic line 001. The tapering geometry of the reflecting body suggests that the ophiolite thins downward and that, at depth, the Franciscan complex rocks come in close proximity to the basal GVG strata. The interpreted downdip thinning of the CRO on line 001 is similar to changes in outcrop thickness of the ophiolite along strike in the eastern Coast Ranges (Ukiah 2° geologic map, CDMG 1960), and suggests that the CRO remnants form a body of irregular shape and thickness in 3-D.

The Sites anticline and Fruto syncline are well expressed as antiformal and synformal folds, respectively, in layered reflectors in the upper 5-10 km of line 001 (Figure A-13)

and the other dip profiles. The folds are separated from a package of bright layered reflectors with different structure below by a poorly imaged, west-dipping interface. We interpret the west-dipping interface to be a blind thrust fault that dips beneath the eastern Coast Ranges (red marker, Figure A-17), and thus part of the Great Valley fault system (Section 2.3). The thrust fault underlies the Fruto syncline and Sites anticline, and separates these structures from a broad synform in the footwall in the depth range of about 5-12 km. The Sites anticline is a fault-propagation fold formed above the tip of the blind, west-dipping thrust fault. We interpret that the Stony Creek fault extends downdip beneath the east-dipping package of lower GVG and is truncated against the blind, west-dipping thrust fault (Figure A-17).

The synformally folded reflectors in the footwall of the blind thrust fault are well imaged in dip lines 798, 782, 001, 781, 805 and 808. They can be traced laterally on strike lines 011 and 783 as packages of bright reflectors in the 8-10 km depth range, and thus represent a regionally extensive body of rocks with consistent reflector characteristics. The structural position of these rocks in the footwall of the west-dipping thrust fault suggests that they are either lower Great Valley Group strata (Unruh et al., 1995) or upper parts of the ophiolitic basement of the Sacramento Valley (Constenius et al., 2000). Given the stratigraphic and structural evidence described in Section A.2 for mid-Cretaceous westward tilting of the lower Great Valley Group section beneath the western Sacramento Valley, we prefer the interpretation that the west-dipping reflectors in the footwall of the thrust are Stony Creek-equivalent rocks.

This interpretation is consistent with results of recent studies of the subsurface structure of the northwestern Sacramento Valley. Constenius et al. (2000) presented time- and depth-migrated versions of several Texaco seismic lines north of seismic line 808, which is the northernmost seismic line in our array (Figure A-1). In particular, Texaco line 5 (Figure 8 in Constenius et al. 2000) is parallel to and located just a few kilometers north of line 808. The reflector geometries in Texaco line 5 are very similar to those in line 808. Both lines image a package of northeast-dipping reflectors in the upper 3-5 kilometers of the eastern part of the line that correspond to Upper Cretaceous Great

Valley Group strata. The two seismic sections also image a series of subhorizontal high-amplitude reflectors at 2-5 km depth in the western parts of the lines (i.e., the purple reflectors in line 808; Figure A-20) that correspond to the bright conglomeratic reflectors in the Stony Creek Formation (see discussion in Section A.2). Significantly, Constenius et al. (2000) interpret a westward-thickening package of layered reflectors imaged in the 5-10 km depth range on Texaco line 5 as "Jurassic-Cretaceous Stony Creek" rocks. These rocks are equivalent to the package of synformally folded reflectors below the thrust in line 808 (Figure A-20), and are consistently imaged the footwall of the west-dipping thrust fault throughout the seismic array (Figure A-1).

The relationship between the basement of the Sacramento Valley and the highly attenuated Coast Range ophiolite exposed in the Coast Ranges to the west was a subject of an extensive investigation by Godfrey et al. (1997). Based on analysis and modeling of geophysical data, Godfrey et al. (1997) inferred that a 5- to 10-km-thick body of magnetic rocks directly underlies the Great Valley Group strata beneath the western Sacramento Valley and the eastern Coast Range foothills. These rocks have P-wave velocities of about 5-6 km/s and are have moderate magnetic intensities (about 2.75-3.75 A/m). The rocks have higher velocities and magnetizations than the overlying GVG strata, but lower velocities and magnetizations than ophiolitic basement rocks beneath the central and eastern Sacramento Valley (Godfrey et al., 1997). As modeled, the magnetic body dips homoclinally east beneath the outcrop belt and flattens beneath the Sacramento Valley, similar to the large-scale structure of the Great Valley Group section. Godfrey et al. (1997) interpreted that the magnetic body is a "melange" of fragmented mafic rocks and serpentinized ultramafic rocks, both of which are relatively magnetic, plus Franciscan Complex rocks that are relatively non-magnetic. Godfrey et al. (1997) inferred that the magnetic ophiolitic rocks were derived from the ophiolitic basement beneath the Sacramento Valley, and that they had been tectonically mixed and interleaved with the Franciscan complex by a tectonic wedging process.

The east-west magnetic model of Godfrey et al. (1997) is located at about the same latitude as seismic line 781. Unfortunately, line 781 is relatively short and the geometries

of deep reflector bodies are difficult to discern, making it a less than optimal seismic line for comparison with the geophysical model. Because deep reflector geometries are better imaged by line 001, we project the boundaries of magnetic bodies modeled by Godfrey et al. (1997) about 10 km south onto line 001 (Figure A-23) for comparison with the reflection data. The top of the magnetic bodies generally corresponds to the lower extent of the Great Valley Group reflectors. The magnetic crust (2.5 A/m) and mantle (4.25 A/m) of the Sacramento Valley ophiolitic basement modeled by Godfrey et al. underlie the eastern part of seismic line 001 (Figure A-23). In particular, the upper part of the ophiolite is associated with a package of bright, west-dipping reflectors that flatten westward beneath the Sites anticline at about 8-10 km depth. To the west, Godfrey et al. 1997) modeled a body of magnetic "melange" (3.75 A/m) at about 9 to 16 km depth beneath the Fruto syncline (Figure A-23). This body appears to correspond to a package of bright, east-dipping reflectors in the 10 to 15 km depth range. The western limit of this body, as modeled by Godfrey et al. (1997), corresponds to the location of the blind, west-dipping thrust fault (Figure A-17). Godfrey et al. (1997) model east-dipping magnetic bodies with lower magnetizations (2.5 and 0.7 A/m) beneath east-dipping Stony Creek strata. These magnetic boundaries project updip to outcrops of the Coast Range ophiolite structurally beneath the Stony Creek strata, and to blueschist-grade rocks of the Franciscan Complex.

Based on the comparison of the magnetic model of Godfrey et al. (1997) with seismic line 001, we interpret the deep reflective bodies beneath the Great Valley Group strata in the eastern Coast Ranges to be fragments of ophiolitic crust that have been tectonically incorporated into the Franciscan complex. It is unlikely, however, that the ophiolitic fragments were incorporated by tectonic wedging only, because thrust-related deformation thickens the crust, whereas both map and subsurface relationships indicate that blueschist-grade rocks of the Franciscan complex are in structural contact with relatively shallow upper crustal rocks, indicating net crustal attenuation. We favor an alternative hypothesis that the magnetic bodies underlying the western outcrops of Great Valley Group strata are fragments of ophiolitic crust and mantle that were mixed with the Franciscan rocks by attenuational processes, not thrust wedging (e.g., Platt, 1987; Unruh

and Wakabayashi, 1995). In this model, the magnetic bodies comprise a 4- to 10-km-wide zone of attenuated crust beneath the Great Valley Group, the upper contact of which is the Coast Range fault as defined by Platt (1987) and Jayko et al. (1987). The attenuation of the ophiolite and exhumation of the blueschist rocks below the Coast Range fault occurred prior to movement on the blind thrust fault that folded the structurally overlying Great Valley Group and formed the east-dipping homoclinal flank of the Coast Ranges.

## A.4 INTERPRETATION OF INDIVIDUAL REFLECTION LINES

Based on analysis of all of the dip lines, we interpret that a blind, west-dipping thrust fault or faults is present beneath the western Sacramento Valley and eastern Coast Range foothills along the entire north-south length of the seismic reflection array. These faults are equivalent to the "Great Valley" fault as defined by the US Geological Survey (1996) and the Department of Water Resources (1999). The geometries of the blind thrust-fault segments, as well as the Sites anticline and Fruto syncline, vary along strike. In the following sections, we describe the structure of individual seismic lines in detail.

### A.4.1 Line 807

Seismic line 807 is the southernmost line in the array (Figure A-1). It trends ENE-WSW and is about 10 km long. Reflectors in the upper 4 km of line 807 generally dip eastward, consistent with geologic mapping by Rich (1971) that indicates this region is underlain by east-dipping strata of the Great Valley Group. The reflection data image an apparent antiformal fold in the upper 6 to 8 km of the western part of the line (Figure A-13). This antiform is persistent through various steps in the data processing flow, and probably is an image of a real anticline (D. O'Connell, U.S. Bureau of Reclamation, personal communication, 2002). If this is correct, then the axis of the anticline lies beneath Antelope Valley.

The east-dipping reflectors in the upper 6-8 km of the line are juxtaposed at depth against a package of bright, west-dipping reflectors in the 8-10 km depth range. We interpret that the east-dipping reflectors overlie a blind, west-dipping thrust fault (Figure A-13).

Patterns of cross-reflectors above the thrust may be artifacts of the depth migration; however, if the dip discordances represent real structure, then they may be produced by interpenetrating thrust faults that accommodate buckling and thickening of the hangingwall of the thrust fault, and thus responsible for development of the apparent anticline beneath Antelope Valley.

### A.4.2 Line SV-12

Line SV-12 trends east-west and passes between the Sites and Golden Gate dam sites (Figure A-1). From west to east, the seismic line crosses the axis of Sites anticline, Fault GG-2, Fault S-3 and Fault S-2. The central and eastern parts of the line are located in the Sacramento Valley, east of the foothills region. Total length of the line is about 29 km (Figure A-14).

The upper 4 to 6 km of the western half of SV-12 images east-dipping layered reflectors associated with east-dipping Upper Cretaceous Great Valley Group strata. The Venado sandstone (green marker; Figure A-14) is present within this section. The east-dipping strata flatten eastward beneath the Sacramento Valley. Below about 6 km depth, the east-dipping and subhorizontal layered reflectors are underlain by a series of bright, west-dipping reflector packages. In the central part of line SV-12, the east-dipping reflectors are juxtaposed against west-dipping reflectors below by a west-dipping interface. We interpret this west-dipping interface to be a blind, west-dipping thrust fault that flattens at a depth of about 5 km beneath the eastern half of the seismic line. The thrust fault can be traced westward to a point beneath the surface trace of Fault S-2 (Figure A-14); west of this point, the discordance between east- and west-dipping reflectors is not clearly discernable. If projected westward, downdip, the fault would intersect the western edge of line SV-12 at about 9 km depth (see dashed red line, Figure A-14).

The western part of line SV-12 images another discordance between east and west-dipping reflectors in the 6 to 7.5 km depth range, directly above the projected down-dip continuation of the thrust fault discussed above (Figure A-14). Note that the shallower dip discordance does not extend much east of the surface trace of fault S-2. We interpret

this shallower dip discordance to be associated with a southern end of the next segment of the Great Valley thrust fault to the north. In this interpretation, line SV-12 crosses the structural boundary between the Bear Valley segment, which is imaged by line 807 and the eastern part of SV-12, and the Funks segment, which is imaged by line 798 and the western part of SV-12 (Figure A-1). The thrust fault segments are separated 1.5 km vertically at the boundary, which appears to be coincident with the S-2 fault.

There is no obvious offset of shallow reflectors associated with fault S-2 in line SV-12. It is possible that a few hundred meters of vertical separation created by right-lateral offset of east-dipping Great Valley Group reflectors is not resolvable at this scale, or by these particular seismic data. There is some discontinuity in reflectors beneath the surface trace of Fault GG-3 (Figure A-14) that may be related to movement on the fault; however, the structural complexity and loss of fold near the west end of the line makes interpretation problematic. If the reflector discontinuity is related to movement on GG-3, then the fault does not appear to cut or extend below the Funks segment of the Great Valley fault.

Line SV-12 also crosses fault S-3 (Figure A-14). There is no obvious vertical displacement of reflectors in the vicinity of the fault, consistent with the interpretation that it is a flexural slip, bedding-parallel fault that has accommodated reverse shearing within the upper Great Valley Group section during uplift and eastward tilting.

### A.4.3 Line 798

Line 798 is located between Hunters Creek and the Sites and Golden Gate dam sites (Figure A-1). Total length of Line 798 is about 29 km. From west to east, map-scale geologic structures crossed by this line include the Fruto syncline, Sites anticline and Salt Lake thrust fault (Brown and Rich, 1961).

Line 798 images a subhorizontal to west-dipping reflecting horizon in the 5.0-7.5 km depth range along most of the length of the seismic section (i.e., red marker in Figure A-15). The reflecting horizon separates strata in the upper 5-6 km, that are folded about the

axes of the Fruto syncline and Sites anticline, from generally subhorizontal to west-dipping reflectors below. Significantly, the axes of the Fruto syncline and Sites anticline cannot be traced below the 5.0-6.5 km reflecting horizon. The horizon and associated dip discordance can be confidently traced as far west as shotpoint 615. West of this point, the horizon and associated dip discordance cannot be clearly distinguished in the reflection data, possibly due to a loss in fold with proximity to the west end of the seismic line. The reflecting horizon can be traced east of shotpoint 1000 as a lower-amplitude feature that clearly separates east-dipping reflectors beneath the western Sacramento Valley margin from west-dipping reflectors below.

We interpret the reflecting horizon to be a west-dipping thrust fault beneath the Fruto syncline and Sites anticline (red marker in Figure A-15). The fault dips shallowly and effectively forms a detachment beneath these folds, separating them from the subhorizontal to west-dipping reflectors below. The Sites anticline is interpreted to be a west-vergent fault-propagation fold developed above a blind, east-dipping thrust fault that splays upward from the detachment (Figure A-15). The surface trace of the Salt Lake fault is projected to depth parallel to the dip of the reflectors associated with bedding in the Upper Cretaceous Great Valley Group rocks (Boxer Formation). This geometry suggests that the Salt Lake fault is a backthrust fault accommodating east-directed underthrusting and tectonic wedging, similar to the model proposed by Wentworth et al. (1984) and Namson and Davis (1987) for the Coalinga anticline and related structures in the western San Joaquin Valley.

We interpret that the dip of the detachment horizon increases west of the Sites anticline axis and forms a west-dipping thrust ramp, consistent with the appearance of the fault on seismic lines north of line 798 (see following discussion). Line 798 (Figure A-15) also images the major stratigraphic and structural features discussed in Sections 2.0 and 3.0. The bright, high-amplitude reflectors in the Stony Creek Formation (highlighted in purple) project to surface exposures of conglomeratic units in the lower Great Valley Group section. The “discontinuity” (blue marker) between the Stony Creek and Lodoga Formations of Constenius et al. (2000) is associated with a distinct change in reflective

character within the Great Valley Group section in the Fruto syncline. The downdip projection of the Venado sandstone member of the Cortina Fomration is shown by the green marker (Figure A-15). Synformally folded reflectors (yellow) in the footwall of the thrust fault are interpreted to be deformed lower Great Valley Group strata (see discussion in Section A.3).

### A.4.2 Line 782

Seismic Line 782 trends east-west and passes just north of Logan Creek (Figure A-1). The western half of this line is very crooked, with segments up to several kilometers long that alternately trend normal and parallel to structural strike. Consequently, the appearance of bedding and structures is distorted in the western part of the line. Total length of the line is 24 km. From west to east, Line 782 crosses the Fruto syncline and Sites anticline (Chuber, 1961).

Based on patterns of folded reflectors in Line 782, the Fruto syncline and Sites anticline are confined to the upper 5-8 km of the crust, and are separated from broad, synformally folded reflectors below by a poorly imaged, west-dipping planar discordance in reflector geometry (i.e., red marker, Figure A-16). We interpret this feature to be a west-dipping thrust fault. We trace the thrust fault up-dip to the east and interpret that it terminates at about 5 km depth below the eastern limb of the Sites anticline. In contrast to Line 798, Sites anticline on Line 782 appears to be an east-vergent fault-propagation fold developed above the tip of the west-dipping thrust fault. Complex patterns of crossing reflectors suggest that shortening in the core of the anticline is accommodated by backthrusting.

Chuber (1961) did not recognize or map a continuation of the Salt Lake fault north of Logan Creek, in the vicinity of line 782. Upper Cretaceous GVG strata generally are covered with Pliocene-Pleistocene deposits of the Tehama Formation in the vicinity of Line 782, and thus it is possible that the Salt Lake fault is covered or otherwise not visible or well expressed. It is also possible, however, that the Salt Lake fault dies out between Line 798 and Line 782 because the geometry of the thrust fault and Sites anticline change dramatically. If the displacement on the underlying blind thrust fault

goes to zero below the eastern limb of the Sites anticline at the latitude of Line 782, and if all of the displacement at the thrust tip is consumed by shortening in the core of the fold, then a backthrust fault like the Salt Lake fault is not required to terminate east-directed displacement at the western edge of Sacramento Valley. We favor this latter interpretation, and thus do not show the Salt Lake fault on the interpretation of line 782 (Figure A-16)

Line 782 (Figure A-16) images other major stratigraphic and structural features discussed in Sections 2.0 and 3.0, including:

High-amplitude reflectors in the Stony Creek Formation (purple markers) that project to surface exposures of conglomerates in the lower Great Valley Group;
A distinct change in reflective character within the Great Valley Group section associated with the "discontinuity" (blue marker) between the Stony Creek and Lodoga Formations (Constenius et al., 2000); and
Synformally folded reflector packages in the footwall of the west-dipping thrust fault (Figure A-12).

### A.4.3 Line 001

Seismic Line 001 extends east-west across the entire Coast Ranges-Sacramento Valley boundary at the latitude of the town of Willows (Figure A-1). Total length of the line is about 34 km. The west end of the line is located in outcrops of the Coast Range ophiolite, and from west to east the line crosses the Stony Creek fault, Fruto syncline, and Sites anticline.

This line is described in detail in section A.3, and will only be briefly summarized here. There is a distinct west-dipping interface (red marker, Figure A-17) imaged by Line 001 that separates layered reflectors in the upper 7-8 km that are folded about the axes of the Fruto syncline and Sites anticline, from underlying reflectors that are folded into a broad synform. We interpret this interface to be a blind, west-dipping thrust fault beneath the Sites anticline. The tip of the thrust fault is located at about 4-5 km depth beneath the

synformal hinge at the base of the east limb of the anticline. Sites anticline is interpreted to be a fault-propagation fold, similar to its appearance on Line 782 directly to south (Section 2.2). The thrust fault has an apparent dip of about 14° in the plane of the seismic section, and it intersects the western edge of the seismic line at a depth of about 12 km (Figure A-17).

There is a discordance in reflector dip in the footwall of the blind thrust fault, at about 10.5 km depth below the western limb of the Fruto syncline. The discordance separates a package of east dipping, high-amplitude reflectors below from a package of synformally folded reflectors above. This dip discordance may be the structural contact between the Great Valley Group and underlying attenuated ophiolite (i.e., the Stony Creek fault). If this interpretation is correct, then movement on the west-dipping thrust fault may have displaced this contact about 7 km (Figure A-17).

### A.4.4 Line 781

Line 781 is 20 km long, trends east-west, and is located just east of the town of Elk Grove. The line runs approximately parallel to California Highway 281 (Figure A-1). From west to east, Line 781 crosses the Fruto syncline axis and partially crosses the western limb of the Sites anticline.

Line 781 images a west-dipping discordance in reflector dip (i.e., red marker, Figure A-18) at about 8-9 km depth beneath the eastern end of the line. The dip discordance juxtaposes shallow, west-dipping reflectors associated with the western limb of the Sites anticline, against deeper subhorizontal reflectors (Figure A-18). We interpret this dip discordance to mark the position of a blind, west-dipping thrust fault. To the west, we project the thrust fault between steeply east-dipping reflectors above 10-12 km, and subhorizontal reflectors below. The dip of the fault may increase slightly east of the Fruto syncline axis. We interpret that the thrust fault intersects the western edge of the line at about 13 km depth.

### A.4.5 Line 805

Line 805 is 18 km long, trends NE-SW to east-west, and is located at the latitude of the town of Orland in the northwestern Sacramento Valley (Figure A-1). The seismic line passes along the southern margin of Black Butte reservoir. The surface geology along much of Line 805 is characterized by deposits of the Pliocene-Pleistocene Tehama formation; there are few outcrops of the underlying Great Valley Group strata. Stratigraphic contacts shown on the interpreted version of Line 805 (Figure A-19) are projected into the plane of the seismic line from outcrops to the west, and have been mapped into the plane of Line 805 by correlating units from the south along strike lines 783 and 011, both of which intersect and cross Line 805. The seismic line crosses an antiformal pattern of bedding dips mapped as the "Paskenta Nose anticline" (Corps of Engineers, 1986).

The data clearly image a synformal hinge in reflectors associated with upper Great Valley Group strata above about 5 km at the eastern end of the seismic line. The hinge can be confidently traced downward to about 5 km depth, below which the dips of the reflectors diverge from the synformal geometry. We interpret the synformal hinge to be the base of the forelimb of an east-vergent fault-propagation fold developed above a blind, west-dipping thrust fault (red marker, Figure A-19). The "Paskenta Noes" anticline is analogous to, and may be the northern continuation of, the Sites anticline mapped south of line 805. We interpret the eastern tip of the thrust to be at about 5 km depth. Unlike the dip lines to the south (i.e., 798, 782, 001 and 781), the inferred thrust fault in line 805 is not associated with a distinct, planar, west-dipping dip discordance. We interpret that the thrust fault dips west and divides the seismic line such that subhorizontal to east-dipping reflectors in the upper 5-10 km of the western half of the seismic line are structurally separated from the package of bright, west-dipping to subhorizontal reflectors in the lower 5-10 km in the east part of the line (Figure A-19).

We acknowledge that the thrust fault in line 805 is not associated with a well-defined dip discordance as in line 001, and that there is significant uncertainty in our interpretation of the location and dip of the fault. We note, however, that the antiformally folded

reflectors in the upper 5 km associated "Paskenta Nose"anticline are distinct from the synformally folded reflectors below about 5 km depth. We believe that the simplest explanation for the vertical variations in reflector dip is folding of the upper crust above a blind, west-dipping thrust fault, and that this interpretation is consistent with the regional structure imaged by other seismic lines in the array south of line 805. We estimate that the vertical uncertainty in our interpretion of depth to the thrust fault shown on Figure A-19 is $\pm$ 1.5 km.

### A.4.6 Line 808

Line 808 is 18 km long, trends northeast-southwest, and passes just north of Black Butte reservoir (Figure A-1). The surface geology and subsurface structural features crossed by this line are similar to those crossed by Line 805 to the south. The major synformal hinge above the tip of a west-dipping thrust fault beneath the valley margin is located at the eastern end of the line. We interpret that the thrust fault (red marker, Figure A-20) separates subhorizontal to east-dipping reflectors in the upper 5-10 km of the western half of the seismic line from bright, west-dipping to subhorizontal layered reflectors in the lower 5-10 km in the east part of the line in the vicinity of shotpoint 850 (Figure A-20).

As discussed above for line 805, we acknowledge significant uncertainty in our interpretation of the location and dip of the thrust fault in line 808. Given regional structural trends, we maintain that blind thrust faulting and fault-propagation folding are the simplest, most parsimonious explanations for the vertical variations in reflector dip imaged in line 808. We estimate that the vertical uncertainty in our interpretion of depth to the thrust fault shown on Figure A-20 is $\pm$ 1.5 km.

### A.4.7 Strike Lines 011 and 783

The two north-south-trending strike lines (011 and 783; Figure A-1) are subparallel to bedding strike, and consequently do not cross many stratigraphic contacts along their length. Major stratigraphic units and structures shown at depth on the interpreted strike lines (Figures A-21 and A-22) are derived from correlation with crossing dip lines. The location of the Venado sandstone at the northern end of strike line 783 (orange marker,

Figure A-22) is inferred by first projecting the depth to the top of the Venado from the Humble Michael well northward to line 805, then correlating the Venado reflector on 805 with line 783 at the point where the two seismic lines intersect.

The strike lines provide a basis for evaluating existing mapping of the Paskenta fault, the surface trace of which projects southeast toward Black Bute reservoir (Plate 1). The Paskenta fault is interpreted by Moxon (1988) and Constenius et al. (2000) to have formed as a north-dipping normal fault in late Jurassic-early Cretaceous time. The fault trace in outcrop has been rotated to a northwest strike by uplift and eastward tilting along the western margin of the Sacramento Valley (see discussion in Section 3.5.6). The fault is covered by deposits of the Pliocene-Pleistocene Tehama Formation in the vicinity of Black Butte reservoir, and thus the continuation of the fault into the area spanned by the seismic array is uncertain (Plate 1).

If the Paskenta fault is present at the latitude of the Orland Buttes, then it should be expressed as a north-down displacement of the lower Great Valley Group section on the north ends of strike lines 783 and 011. Specifically, the fault should displace the top of the Stony Creek Formation down to the north. As discussed in Section A.2, the upper contact of the Stony Creek Formation as observed in outcrop at the latitude of seismic line 001 is a "discontinuity" or unconformity with the overlying Lodoga Formation. The discontinuity can be projected into the subsurface on line 001 and correlated with reflectors in lines 783 and 011 where the lines cross; in turn, the unconformity at the top of the Stony Creek Formation can be traced northward on strike line 783 to dip line 805 at the northern end of the array (i.e., blue marker on Figure A-22). The upper contact of the Stony Creek Formation in the "Michael" near line 805 also is an unconformity. The unconformity encountered by the well can be projected onto seismic line 805, and in turn traced updip parallel to bedding on that line to the intersection with line 783. The unconformity can be correlated with seismic markers on line 783 and traced southward. As shown in Figure A-22, the unconformity at the top of the Stony Creek Formation (blue marker) on line 783 can be reasonably correlated from the intersection with line 001 to the intersection with line 805 across the projection of the Paskenta fault with no

significant north-down offset. The Venado sandstone member of the Cortina Formation (green marker, Figure A-22) similarly can be traced along line 783 from the intersection with line 001 to the intersection with line 805. Based on these relationships, we conclude that the Paskenta fault does not project as far south as the Orland Buttes, and thus is not directly imaged by the seismic lines at the northern end of the array.

## A.5 STRUCTURE CONTOUR MAP

Based on our interpretation of individual reflection lines acquired for this study, as well as analysis of a seismic line through the northern Rumsey Hills published by Constenius et al. (2000), we prepared a structure contour map of the Great Valley thrust fault system to assess the geometry of individual fault segments. The map was derived by plotting the depth to the thrust faults along individual seismic lines, then drawing contours of equal depth (contour interval = 1 kilometer) consistent with the interpreted reflection data. Where the trend of the contours was poorly constrained by reflection profiles, we assumed that fault strike at depth is similar to the bedding strike at the surface. The resulting map is shown in Figure A-1.

In our interpretation, the system of blind thrust faults imaged by the reflection data consists of at least five discrete segments. From south to north, the segments are informally designated as follows (Figure A-1):

- Bear Valley Segment (length, 22 km)
- Funks Segment (length, 17 km)
- Willows Segment (length, 12 km)
- Elk Creek Segment (length, 12 km)
- Orland Segment (minimum length, 16 km)

The Funks segment exhibits a tectonic wedge geometry; that is, there is a ramp-flat transition at the west end of seismic line 798 that has produced some fault-bend folding of the hanging wall block, and backthrusting has occurred along the Salt Lake fault to accommodate underthrusting of the hanging wall block beneath the western Sacramento

Valley margin. In contrast, the Bear Valley, Willows, Elk Creek and Orland segments are characterized by fault-propagation folding; i.e., displacement on the thrust fault is consumed by folding of the hanging wall block, with no obvious backthrusting or wedging at the thrust tip. The Willows, Elk Creek and Orland segments progressively steepen northward, and the eastern limit of deformation steps abruptly eastward moving north of the boundary between the Elk Creek and Orland segments (Figure A-1).

The majority of segment boundaries are shown on the structure contour map as discrete zones across which there are abrupt elevation differences between individual thrust sheets. We do not interpret the segment boundaries to be vertical tear faults. Rather, we favor the interpretation that the magnitude of slip on the faults diminishes with proximity to the edges of the faults. The exception is the segment boundary between the Bear Valley and Funks segments, which is associated with the northeast-striking dextral GG-1, GG-2, GG-3 and S-2 faults (Figure A-1). In this case, we infer that the dextral faults are tear faults that extend at least to the top of the more shallow Funks segment.

# APPENDIX B
# PALEOSEISMIC TRENCHES

## B.1 INTRODUCTION

We excavated thirty-one paleoseismic trenches and test pits at fourteen locations, to assess the activity of four major northeast-striking faults (GG-1, GG-2, GG-3, and S-2; Figure B-1), the north-striking Salt Lake fault in the vicinity of the Golden Gate and Sites damsites (Figure B-2), and the north-striking S-3 fault. Trench locations were selected from areas where the Department of Water Resources previously had secured permission from landowners to conduct geologic investigations. In conjunction with the trench investigations, we conducted detailed geomorphic mapping at these sites to precisely determine the fault locations and stratigraphy of late Quaternary deposits.

At each trench locality, we cleaned and examined one or both walls of each trench. Stratigraphic contacts and boundaries were flagged, surveyed electronically and logged at scales of approximately 1:20 to 1:40. Where suitable charcoal samples were found, the ages of the deposits containing the charcoal were evaluated by direct radiocarbon analysis. The degree of soil development at each site was evaluated via detailed soil profile descriptions to reconstruct the depositional history at each site, provide additional age constraints on deposits, and correlate stratigraphic units among trench sites.

In this appendix, we describe: (1) the trench logs for each paleoseismic trench and test pit; (2) the stratigraphic units exposed within each trench; and (3) summarize the soils profiled in trenches (full soil descriptions are presented in Appendix C).

## B.2 FAULT GG-1

### B.2.1 Trenching Investigations Across The GG-1 Fault

Remnants of five fluvial terraces are preserved on the north side of Funks Creek, and they overlie the projected trace of the GG-1 fault. We excavated three trenches across the

projected trace of the GG-1 fault at this location (Figure B-1). We first excavated Trench FT-4a within the hillslope north of Funks Creek to locate and characterize the GG-1 fault in bedrock (Figure B-1 and 3-10). We then sited fault trench FT-4b (Figure 3-11) on the highest, and presumably oldest, remnant surface north of Funks Creek to determine if the deposits overlying the projection of the fault are offset. Instability of the trench and the presence of poorly stratified colluvial deposits led us to site an additional trench (Trench FT-4c; Figures B-3 and B-4) on a lower, and younger, alluvial terrace downslope of trenches FT-4a and FT-4b.

### B.2.2 Trench Stratigraphy

#### B.2.2.1 Trench FT-4a, Northeast Wall

Trench FT-4a, was a 22-foot-long (7 m), 12 ft (4 m) deep vertical cut in the hillside approximately 100 feet (30 m) downslope of bedrock truncated by the GG-1 fault (Figure B-1). The vertical cut exposed a two-foot-wide (0.6 m) zone of faulting in bedrock, overlain by 3 feet (1 m) of unfaulted colluvial slope deposits (Figure 3-10). After an initial assessment, we extended the excavation both east and west for a total length of 56 feet (17 m), and deepened the excavation, to confirm that the entire fault zone was present in the exposure.

#### B.2.2.2 Trench FT-4b, Northeast Wall

We sited fault trench FT-4b on the highest remnant geomorphic surface north of Funks Creek, and across the projection of the mapped trace of fault GG-1 (Figure B-1). We interpret that this surface is correlative to the broad Qt1 terrace present south of the creek. However, the 79-foot-long (24 m), 13-foot-deep (4 m) trench exposed massive colluvial deposits, not stream terrace deposits as expected. Due to the instability of the trench walls, we prepared a coarse log of the exposure without entering the excavation (Figure 3-11). Two distinct colluvial units, and the sub-horizontal contact between the units, crossed the projection of the GG-1 fault and exhibited no fault offset or disruption.

### B.2.2.3 Trench FT-4c, Northeast and Southeast Walls

We sited Trench FT-4c on the Qt2 terrace surface approximately 40 feet south of Trench FT-4a, across the projection of the mapped trace of fault GG-1 (Figure B-1). Trench FT-4c extended 75 feet (23 m) along a N46°W trend sub-parallel to Funks Creek, and exposed 16 feet (5 m) of fluvial deposits within the stream terrace mapped as Qt2. We identified eight distinct alluvial units based on variations in color, texture, and grain size distribution (Figure B-3). Of these eight units, the upper four (Units 5 through 8) probably are latest Holocene or younger deposits. Specifically, the unconsolidated nature of the bedded sands and silts exposed in these units, the presence of a buried shotgun shell in the upper portion of unit 6, and minimal soil development in underlying units 4 and 5 suggest that these deposits are historic overbank or flood deposits. These units are too young to evaluate activity of the GG-1 fault per DSOD criteria, and therefore are not discussed in detail here. Full descriptions are provided on the trench log (Figure B-3).

The basal alluvial unit (Unit 1; Figure B-3) exposed in trench FT-4c consists of sandy gravel with minor clay. The upper contact of this unit is unfaulted and apparently undeformed. This unit is overlain by clay with gray and reddish-brown mottles (Unit 2), and sandy gravel (Unit 3). Interbeds of clay, sand, and gravel within unit 3 pinch out laterally. Charcoal samples from the interbeds provided a radiocarbon date of 1170 to 1290 AD (Table 3-3; Section 3). Unit 4, which overlies the interbeds in unit 3, consists of poorly bedded sand, silt, and clay containing sub-horizontal lenses of coarse, sandy gravel. Radiocarbon analysis of charcoal collected from unit 4 provide a calibrated age of 1520 to 1940 AD (Table 3-3), which is slightly younger and thus stratigraphically consistent with the dates from the underlying unit. The lower contact of unit 4 is clear, planar, and undeformed.

At the eastern end of the trench (Figure B-3), several of the interbeds in unit 3 appear to roll over in an antiformal structure. Because bedding within fluvial units and stratigraphic contacts directly above and below the dipping interbeds in unit 3 are undeformed, we conclude that the antiformal geometry of the interbeds in unit 3 is not tectonic in origin. To confirm this, we deepened and cleaned the eastern end of the

trench and southeast wall. The log of these exposures is shown in Figure B-4. The inclined bedding may be the product of deposition over an existing streamside feature. These finely laminated sediments originally may have covered, and taken the form of, a fluvial point bar or sloped channel margin. Alternatively, the beds may have been folded after deposition by tree throw. Excavation of the opposite trench wall revealed abundant horizontal tubular voids and roots, consistent with the presence of vegetation and roots in unit 3 subsequent to deposition.

### B.2.3 Summary of Trench Exposures, GG-1 Fault

Three trenches across the GG-1 fault document that the structure is a discrete, well-defined, narrow zone of shearing less than 2 feet (0.6 m) wide. Based on the presence of unfaulted colluvial deposits in trench FT-4b on the highest, and oldest, remnant surface north of Funks Creek, it is likely that there has been no surface rupture during the Holocene. This interpretation is based on correlation of the surface to the broad Holocene Qt1 terrace present south of Funks Creek and downstream. Late Pleistocene deposits were not encountered in trenches across the GG-1 fault, and thus there are no observations that permit assessment of late Pleistocene or older Quaternary activity.

## B.3 FAULT GG-2

### B.3.1 Trenching Investigations Across the GG-2 Fault

The GG-2 fault was trenched at two separate locations near the Golden Gate damsite where stream terrace and alluvial fan deposits overlie the mapped trace of the fault (Figure B-1). Extensive modification from a quarrying operation downstream of the Golden Gate dam site has obscured geomorphic expression of stream terraces at the site of Trenches FT-3a and FT-3b. Despite cultural modifications of the landforms and deposits, the site for trench FT-3a was selected because our mapping indicated that no other, older terrace deposits are present across the fault to evaluate and document fault activity. In addition, the Bureau of Reclamation previously opened a trench across the GG-2 fault at this location (C. Howard, USBR, personal communication, 1999), and the

FT-3a trench was sited in an attempt to re-excavate the original Bureau of Reclamation trench.

Trench FT-5 extended 72 feet (22 m) along a N35°W trend, and was excavated in the surface of an alluvial fan (Qf1) deposited adjacent to a south-draining tributary of Funks Creek (Figure B-1). An exposure of the GG-2 fault in sandstone beds of the Great Valley Group is present in a streamcut exposure approximately 30 feet (10 m) southwest of the trench site. Truncated sandstone beds on the hillside northeast of the trench site also constrained the location of the GG-2 fault. Trench FT-5 was excavated to the maximum operating depth of the excavating equipment (approximately 15 feet (4.5 m)). Although bedrock is exposed in the adjacent ephemeral stream channel, no bedrock was exposed at the base of the trench during excavation (Figure 3-17), indicating that several meters of relief must be present on the bedrock surface between the trench and stream-cut exposure. We interpret that this relief was generated during a prior episode of incision of the tributary stream, followed by aggradation and accumulation of at least 4.5 m of deposits above the base of the channel in bedrock.

### B.3.2 Trench Stratigraphy

#### B.3.2.1 FT-3a, North Wall

Trench FT-3a, sited across the projected trace of the GG-2 fault (Figure 3-13), extended 39 feet (12 m) sub-parallel to the base of the adjacent hillslope, and was oriented east-west (N35°W; Figure 3-14). We identified three distinct types of bedrock juxtaposed by the main fault trace and a secondary splay: (1) bedded sandstone (bedding dips 35°E); (2) massive sandstone; and (3) laminated mudstone (bedding dips 57°E). The main fault plane strikes N46°E and dips 88° to the southeast (Figures 3-14 and 3-15). Slickensides on the fault plane record predominately horizontal (i.e., strike-slip) motion, with a minimal dip-slip component. The fault zone is well defined and the main fault is less than one to two feet wide (0.3 to 0.6 m).

Faulted bedrock exposed in Trench FT-3a is overlain by unfaulted colluvial deposits (Units 1 through 3; Figures 3-14 and 3-15). The colluvial deposits directly overlying

bedrock (Unit 1) consist of brownish yellow poorly-sorted gravel that contains boulders up to 2.5 feet (0.9 m) diameter. These coarse deposits, probably derived locally from the underlying bedrock, are overlain by finer-grained yellowish brown silty colluvium (Unit 2) containing angular to subangular gravel. Radiocarbon analysis of charcoal collected from Unit 2 provide a calibrated age of 379-170 BC (Table 3-3). Unit 2 is overlain by similar dark yellowish brown silt containing angular clasts and well-developed prismatic soil structure (i.e., unit 3; Figure 3-13). We interpret unit 3 to represent pedogenic alteration and soil profile development on unit 2; thus, unit 2 is the parent material (or C horizon) of the modern soil.

#### B.3.2.2 Trench FT-3b, North Wall

Trench FT-3b was sited across the projection of the GG-2 fault, on an apparent terrace located downslope of, and southwest of, the FT-3a trench (Figures B-1, 3-13). This test pit exposed man-made fill and unfaulted terrace deposits covering a bedrock exposure of the GG-2 fault (Figure 3-16). No charcoal was recovered from deposits exposed in test pit FT-3b. Based on the relative topographic position and lack of soil development, we infer that these terrace deposits probably are late Holocene to Historic. If this is correct, the unfaulted deposits exposed in trench FT-3b provide no data on late Pleistocene and older activity of the GG-2 fault.

#### B.3.2.3 Trench FT-5, South Wall

Trench FT-5 exposed layered, sub-horizontal colluvial deposits with locally inset stream channel deposits. We interpret this to reflect both alluvial and colluvial depositional processes on the fan surface. Six distinct units are identified in trench FT-5 (Figure 3-17). The lower four units are colluvial deposits distinguished on the basis of color, texture, clast composition and stratigraphic position. These colluvial deposits appear to have been reworked by stream processes and contain inset stream channel deposits. The upper two units logged in the trench are not distinct deposits, but rather are interpreted to be horizons of the modern soil profile developed on the upper colluvial deposits.

The basal unit exposed in trench FT-5 (Unit 1) consists of dark yellowish-brown colluvial clay with minor (<3%) sand lenses. The overlying unit (Unit 2) is a dark yellowish-

brown sandy clay colluvium containing 5-10% sand and minor (less than 5%) weathered clasts. Unit 2 also contains a laterally extensive lens of clast-supported, poorly-sorted sandy fluvial gravel within a matrix of medium-dense, moist, clayey sand (Unit 2a; Figure 3-17).

Unit 3 is a dark yellowish-brown to dark brown colluvial sandy clay. The unit is 2.5 feet (0.75 m) thick, moist, very stiff, massive and contains angular fragments of sandstone and mudstone. It has abundant fine pores and clasts with thin clay films, and contains a lens-shaped sandy gravel channel deposit. Dark brown clay films are present in pervasive, sub-vertical fractures. The lower contact of the unit is gradual. Based on the accumulation of illuvial clay, this unit probably represents a weakly developed soil that was buried by the overlying units following a brief period of landscape stability and pedogenesis.

Unit 4 is a yellowish-brown sandy clay colluvium exposed for the entire length of the trench. Unit 4 ranges in thickness from 2.5 to 1.5 feet (0.75-0.5 m), is moist, very stiff, and massive with well-developed clay films. The clay films coat pervasive fractures. The unit contains 20-30% medium to coarse weathered sand and lithic fragments of sandstone and mudstone. The lower contact is gradual.

### B.3.3 Summary of Trench Exposures, GG-2 Fault

Three trenches across the GG-2 fault show that the fault is a narrow sub-vertical shear zone, less than one to two feet wide (0.3 to 0.6 m), that juxtaposes contrasting bedrock units. Kinematic indicators from the FT-3a exposure indicate predominantly horizontal (i.e., strike-slip) displacement. Based on the presence of unfaulted alluvial and colluvial deposits in trench FT-5 on a fan surface that is graded to early Holocene Qt1 terrace, we interpret that there has been no surface rupture on the GG-2 fault during the Holocene. Late Pleistocene deposits were not encountered in trenches across the GG-2 fault, and thus there are no observations that permit assessment of late Pleistocene or older Quaternary activity.

## B.4 FAULT GG-3

### B.4.1 Trenching Investigations Across the GG-3 Fault

The GG-3 fault was trenched at two separate sites (south of Funks Creek within fault trenches FT-2a and 2b, and north of Funks Creek within FT-7; Figure B-1) and exposed in three bedrock test pits (TPE-1, TPE-2, and TPE-3). Fault trench FT-2a was 72 feet (22 m) long, and oriented east-west within a broad alluvial plain that extends across the inferred projection of the GG-3 fault (Figure 3-20). The GG-3 fault location was constrained by four hollow-stem rotary auger boreholes drilled by DWR along an east-west transect across the fault in July, 1999. These boreholes documented a pronounced down-to-the-east step in the elevation of the buried bedrock surface across the projection of the GG-3 fault (Figure 3-19). The bedrock step is buried by alluvial valley fill likely correlative with Qt1 terrace deposits, based on our mapping along Funks Creek and soil descriptions performed for this study.

Trench FT-2a (Figure 3-21) could not be safely excavated deep enough to expose the GG-3 fault in bedrock because of shallow groundwater conditions. To confirm that trench FT-2a extended across the projection of the fault, we extended the trench to the west by excavating trench FT-2b (Figure 3-22). In addition, we excavated three test pits (TPE-1, TPE-2, and TPE-3) across the fault trace on the linear ridge to the northeast to confirm the location of the main fault trace (Figure B-1). Test pit TPE-1 (Figure B-1; Figure 3-22) exposed a west-dipping fault (N30°E/36°W) in bedrock (Figure 3-24). Test pit TPE-2 (Figure 3-25), located 400 feet (122 m) southwest of TPE-1 (Figure B-1), extended 62 feet (19 m) east-west, parallel to two truncations of sandstone bedding. Test-pit TPE-2 exposed a sub-vertical shear zone in bedrock obscured by krotovina (a large animal burrow).

We excavated a third test pit (TPE-3), adjacent to test pit TPE-2 (Figure B-1), in order to provide an additional exposure of the GG-3 fault, and confirm the presence or absence of another fault at the base of the ridge. Test pit TPE-3 was oriented N45°W and extended east approximately 125 feet (38 m) from the midpoint of the slope across the base of the

hillslope (Figure B-1). Test pit TPE-3 exposed east-dipping, interbedded sandstone and mudstone of the Great Valley Group overlain by a thin (1 to 2 feet thick (0.5 m)) veneer of colluvial deposits (Figure 3-26). Faulted and overturned bedrock near the upper part of the trench, on projection of the fault exposed in the adjacent TPE-2 testpit, likely represents the GG-3 fault trace.

We postulated that a secondary fault trace may be coincident with the slope break along the base of the linear ridge. At the base of the slope, however, test pit TPE-3 exposed unfaulted mudstone bedrock overlain by up 13 feet (4 m) of massive, unfaulted alluvium (Figure 3-26). The absence of a fault bounding the base of the hill, as well as exposures of the GG-3 fault in the three test pits on the side of the ridge, confirmed that the GG-3 fault is expressed as a single linear fault trace that extends along the hillslope as mapped.

Based on the three test-pit fault exposures, and the DWR borehole transect, we conclude that fault GG-3 is a well-defined, single fault trace and that fault trench FT-2a crosses the GG-3 fault. In the interest of due diligence, we decided to extend trench FT-2a 56 feet (17 m) to the west by excavating FT-2b (Figure B-1; Figure 3-22). The goal of this additional excavation was to expose and characterize bedrock west of the main step in bedrock revealed by the DWR borehole transect, and confirm that trench FT-2a crossed the entire GG-3 fault zone. FT-2b exposed shallow bedrock west of the projection of the GG-3 fault, confirmed the presence of the step in bedrock inferred from the boreholes, and exposed sub-vertical shears within bedrock that likely represent the western margin of the GG-3 fault zone, and which coincide with the mapped location of the GG-3 fault.

The FT-7 trench site is located on the margin of a laterally extensive fluvial terrace mapped as Qt1 north of Funks Creek (Figure B-1). The GG-3 fault is expressed as a well-defined tonal and vegetation lineament on the hillside northeast of the trench site, and the fault clearly truncates sandstone beds that crop out along the upper slope above the terrace tread. The trench was 92 feet (28 m) long, oriented N22°W, and crossed the projection of the GG-3 fault (Figures B-5 and B-6).

### B.4.2 Trench Stratigraphy

#### B.4.2.1 Trenches FT-2a and FT-2b

We identified five distinct alluvial units (Units 1 through 5) within fault trenches FT-2a and FT-2b that extend along the entire length of the trench; the upper two units (Units 4 and 5) probably represent soil horizons developed on the uppermost alluvial unit (Unit 3; Figures 3-21 and 3-22). A radiocarbon age of 9,250 + 40 yr from unit 2 (Table 3-3) indicates that the alluvial deposits in the trenches are early Holocene or younger. The contacts between units logged in the trenches are undeformed, and internal unit stratigraphy and soils are not disturbed, providing evidence for no Holocene surface faulting on the GG-3 fault.

The basal unit exposed in trenches FT-2a and FT-2b (Unit 1) consists of brown silt with minor (<1%) pebbles to 3 inches (7 cm) diameter (Figures 3-21 and 3-22). Unit 1 is overlain by texturally and lithologically similar deposits of Units 2 and 3, which are characterized by minor variations in the abundance of pebbles. Stratigraphic contacts between units 1, 2, and 3 are defined by vertical variations in grain size and texture. We interpret units 1 through 3 to be overbank flood deposits based on rounding of the scattered pebbles, and the fine-grained, well-sorted, character of the sediments.

Unit 4 is lithologically and texturally identical to the underlying Unit 3, but has a well-developed prismatic structure with clay coatings on soil fracture faces. We interpret unit 4 to be the B horizon of the modern soil developed on the package of overbank deposits represented by units 1 through 3. Unit 5 has coarse blocky soil structure, and is interpreted to be the A horizon of the modern soil.

The modern soil profile (Profiles SP-1 and SP-2; Appendix C) exposed by the FT-2a and FT-2b trenches is 250-290 cm thick with a dark gray A-horizon (Unit 5). Accumulation of translocated clay has formed a thick Bt horizon (Unit 4) with blocky to prismatic soil structure and distinct to prominent clay films. Vertical fractures, or shrinkage cracks, extend from the ground surface into or through the Bt horizon. Sand grains are

weathered to silt and clay. Gravel clasts are moderately weathered (can be broken with the hands) to extremely weathered (can be cut with a knife).

Of all the soils examined in detail in the vicinity of the Golden Gate and Sites damsites, the soil profile in trench FT-2a (Profile SP-1; Appendix C) is the only profile with horizons confidently interpreted as belonging to a buried soil. Two buried soil horizons are located within Unit 2 at a depth of about 7 feet (2.1 m). These horizons are directly beneath a sandy bed in Unit 3 that can be traced laterally along the entire length of the trench. The upper buried horizon (216-242 cm on Soil Profile SP-1; Appendix C) consists of a silty clay loam with strong prismatic structure and abundant clay films. The lower buried horizon (242-264 cm) has a similar texture and structure and contains Stage I carbonate. These horizons were designated a buried soil because clay films and pedogenic structure are better developed than in the overlying soil. The presence of Stage I carbonate also is unique to this profile. We infer that this buried soil probably represents a brief soil-forming interval in the latest Pleistocene-early Holocene history of the study region. Due to the lateral variability in soil properties and depositional processes, this soil probably is only developed and preserved locally.

#### B.4.2.2 Trench FT-7, North Wall

The FT-7 trench exposed thinly-bedded mudstone, siltstone, and sandstone of the Great Valley Group overlain by Quaternary sand, silt, and clay, with scattered subrounded cobbles (Figure B-5). We interpret the Quaternary deposits to consist of an mixture of alluvium from Funks Creek and colluvium from the adjacent hillslope. We identified two distinct packages of Quaternary deposits overlying Cretaceous bedrock: a colluvial unit (Unit 1) overlain by an alluvial unit (Unit 2). Three distinct soil horizons (Units 3, 4 and 5) represent the modern soil profile developed on the upper alluvial deposits of Unit 2.

Bedrock exposed at the base of trench FT-7 is light gray to tan, massive, fine to coarse sandstone and layers of thinly laminated muddy siltstone (Figures B-5 and B-6). The sandstone generally is very hard, but contains softer interbeds of fine-grained sandy

siltstone. Many of the siltstone beds are completely disaggregated by pervasive fracturing.

Bedrock in trench FT-7 is overlain by colluvium (Unit 1) containing subangular to subrounded sandstone clasts that range in size from 0.5-50 cm (Figures B-5 and B-6). The clasts range in color from buff brown to grey brown to rusty brown. The colluvium consists of plastic to slightly plastic silty clay loam (30-35% clay) with weak angular blocky structure and fine to medium (5-20 mm) soil peds. There are no clay films present on ped faces near the top of the unit; however, clay films do coat peds and fractures in the underlying bedrock.

Unit 2 is alluvial silty clay to silty clay loam (35-40% clay) with less than 5% subangular to subrounded gravel. Unit 2 overlies both colluvial deposits of Unit 1 and bedrock, and varies in thickness from less than one foot (25 cm) on the north side of the trench to 4 feet (1.5 m) thick on the south side of the trench. Unit 2 contains few (<2%) sandstone clasts that are up to 20 cm in diameter. It has moderate angular blocky structure and is extremely hard. There are clay films on ped faces and some carbonate filaments along roots and pores.

Units 3, 4, and 5 comprise the modern soil profile, exposed for the entire length of the trench. Unit 3 has strong blocky structure (blocks 1.5-10 cm wide), prominent to distinct clay films, pressure faces, reddish brown color, and vertical shrinkage cracks. There are very few clasts in the unit. Pressure faces are shiny, planar, and undulating with or without striations. Soil peds break into phoroidal (seed-like) shapes. Single ped faces are up to 10 cm across. The lower contact of the unit is gradual to diffuse and irregular. There is a prominent carbonate horizon exposed between 21.5 and 27 m at the base of colluvial unit 4 that is 50 cm thick. The carbonate horizon has abundant white filaments with greyish coatings on ped faces.

Unit 5 is a grey-brown silty sand that is exposed for the entire length of the trench. The unit is 1.5 to 2.5 feet (0.5-0.75 m) thick and has prominent horizontal partings, many

roots, and vesicular pores. The unit has fewer vertical shrinkage cracks than the unit below it and the lower contact is gradual. There are no clay films or pressure faces. The structure is massive and breaks to granular when disturbed. This unit represents the A-horizon of the modern soil.

Weathered sandstone bedrock exposed at the base of Trench FT-7 contains v-shaped cracks or fissures containing soil material that is distinct from the C soil horizon material directly above (Figures B-5 and B-6). The in-filling material is a fine sandy clay loam with distinct reddish clay films, similar to those found coating bedding planes and joints in the adjacent bedrock. Angular fragments of bedrock are supported by the fine soil matrix. We do not believe that these cracks are of tectonic origin, but rather interpret the fill to be derived from older soil material that once formed a thick layer over the bedrock. We infer that this material was erosionally stripped from the bedrock, leaving only small, protected remnants that had infiltrated bedrock cracks and fissures (Figure 3-28). Based on our detailed profile of the modern soil on the north wall of the trench (Figure B-5; Profile SP-6; Appendix C), we infer that, subsequent to the erosion of the older soil, approximately three meters of alluvium and colluvium were deposited over the bedrock. The present soil profile is developed in this younger material, and is substantially younger than the weathered relict soil preserved in the bedrock cracks and slots. No shear fabric or other evidence of youthful faulting was observed in the older soil material that fills the cracks in bedrock. We therefore conclude that the older soil material post-dates the last surface-faulting event in the GG-3 fault.

### B.4.3 Summary of Trench Exposures, GG-3 Fault

Three trenches and three soil pits document that the GG-3 fault is a narrow (less than 2-ft wide), sub-vertical to west-dipping, bedrock shear zone. A radiocarbon age of 9,250 + 40 yr from the lower part of Trench FT-2 and soil profile development indicate that unfaulted basal alluvial deposits in the trench are early Holocene or younger (Table 3-1). These unfaulted and undeformed sediments extend across the fault and provide direct evidence for no Holocene surface faulting.

## B.5 FAULT S-2

### B.5.1 Trenching Investigations Across the S-2 Fault

In the vicinity of the Sites damsite, the S-2 fault is covered by Holocene to historic deposits along Stone Corral Creek. The very young age of these deposits renders them unsuitable for evaluating activity of the fault per DSOD criteria. In addition, the instability of the terrace remnants adjacent to the creek, extensive cultural modifications (including road fill), and environmental restrictions made trenching the S-2 fault along Stone Corral Creek logistically impractical. We thus elected to excavate alluvial deposits that extend across the S-2 fault at two locations near Funks Reservoir, approximately 1.5 miles (2.4 km) northeast of the Sites damsite (Figure B-1). Although somewhat distant from the Sites damsite, these locations provide better opportunities to characterize the activity of the S-2 fault than sites along the creek.

Trench FT-6 extended 95 feet (29 m) north-south across the projection of truncated sandstone bedding exposed near the top of a small, flat hill (Figure B-1). Trench FT-8, located approximately 100 feet (30 m) to the east, extended 45 feet (14 m), north-south (N5°E), across the S-2 fault. Trench FT-9 extended 80 feet (24.5 m) north-south (330°) across the projection of fault S-2 within a broad, flat alluvial surface adjacent to Funks Reservoir (mapped as Qt1), on the Bureau of Reclamation property.

### B.5.2 Trench Stratigraphy

#### B.5.2.1 Trench FT-6, East Wall

Trench FT-6 exposed Great Valley Group sandstone overlain by up to three feet (1 m) of Quaternary alluvial deposits (Figure 3-30). Yellowish-brown sandstone bedrock exposed in the trench varies from massive, with no discernable sedimentary structure, to thinly bedded with minor cross beds. Near the center of the trench, a coherent 3-foot-wide (1-m-wide) sandstone block is bounded on both sides by faults. These faults coincide with the northeast-striking projection truncated sandstone beds exposed 20 feet northwest of the FT-6 trench; we interpret them to comprise the S-2 fault zone.

The southeast side of the sandstone block is heavily fractured, and clay gouge and pulverized bedrock is present between discrete shear planes. Wedge-shaped infillings of soil material are present in cracks, crevices and fissures in the bedrock adjacent to and within the fault zone. Close inspection of the fill material revealed that the fillings are comprised of a mixture of pulverized bedrock and alluvium. Based primarily on the lack of shear fabric in this material and the absence of shearing in the overlying deposits, we interpret that the alluvium worked its way down into the fractured bedrock by non-tectonic, soil-forming processes (see discussion in Section B-4.2.2; Figure 3-28).

The contact between the bedrock and overlying Quaternary alluvium is a relatively flat, sub-horizontal surface with minor irregularities (Figure 3-30). The bedrock surface likely was cut by stream erosion and thus is a buried fluvial 'strath' (stream-cut) surface. We identify three distinct alluvial units in the alluvium overlying the bedrock surface (Units 1, 2, and 3). These units probably are not different deposits (i.e., distinct stratigraphic units), but rather represent a single alluvial deposit with vertical horizonation associated with the modern soil profile.

The basal alluvial unit (Unit 1) consists of 6 to 10 inches (15-25 cm) of tan-brown sand. The sand contains minor vertical soil cracks and may represent the C horizon of the modern soil. Carbonate flecks are disseminated throughout the unit and appear to have been translocated downward into fractures in the bedrock. Clasts of rusty brown sandstone, and a distinct 2 to 4 inch (5-10 cm) thick layer of carbonate is present near the base of the unit. The sandstone clasts are similar to concretions present in the underlying sandstone bedrock and probably were erosionally plucked the bedrock, possibly during formation of the bedrock strath surface. Krotovinas (i.e., animal burrows) are common throughout the unit.

Unit 1 is overlain by 1.5 to 2 feet (0.5-0.75 m) of dark brown sand with angular blocky structure (Unit 2; Figure 3-30). The lower contact of Unit 2 is gradational. There are a few rusty brown sandstone clasts at the base of Unit 2, and krotovinas are common. Unit 2 represents the B horizon of the modern soil developed in unit 1, which represents the

unweathered parent material of the soil. Unit 3 is 11 inches (25 cm) thick and consists of grey-brown sand characterized by blocky soil structure, prominent horizontal partings, and a gradational lower contact. Unit 3 is interpreted to be the A horizon of the modern soil.

The soil profile represented by units 1, 2 and 3 consists of a 30-cm-thick A horizon over a 60- to 90-cm-thick Bt horizon, both consisting of silty clay loam devoid of gravel clasts (Soil Profile SP-5; Appendix C). The A horizon is slightly grayer than the underlying Bt horizon and exhibits massive to granular structure with prominent horizontal partings. The Bt horizon is also a silty clay loam. The Bt horizon is broken into 3 sub-horizons: Bt1, Bt2, and Bt3. Bt1 and Bt2 have prominent angular blocky structure. Blocks are cubical in shape, 2 to 3 cm across, and line up along vertical fractures. Distinct clay films coat the ped faces.

The Bt3 horizon is distinct from the Bt1 and Bt2 horizons in that its structural blocks are irregular in shape. Stage I pedogenic carbonate is present. The top of this horizon (at 99 cm depth) is coplanar with the bedrock surface. The base of the horizon is abrupt and irregular.

The IIC horizon fills a wedge-shaped crack or fracture in the bedrock, and is similar to the overlying Bt horizon in texture except that it contain 10-25% subangular gravel clasts. The presence of angular gravel clasts of varying sizes scattered randomly in a fine matrix is consistent with the interpretation that the fill is of colluvial origin. Clay content, estimated by shaking samples in a jar of water, is about 30% in this horizon. The percentage of clay in the overlying horizon is about 20%, although this difference may not be significant within the uncertainty of the measuring technique. The IIC horizon differs from the overlying Bt horizon in two ways: (1) it exhibits massive with weak fine angular blocky structure, in contrast to the angular blocky structure of the Bt horizon; and (2) the IIC horizon generally is redder (7.5YR 5/4, 4/4) or darker brown (10YR 4/4, 4/3). Clay films do not cover planar ped faces, rather they coat grains, line pores such as root

holes, and coat irregular bumpy ped faces. The reddish colors match those that coat fractures and bedding planes in the bedrock.

We interpret that the IIC horizon formed in an older deposit that predates the overlying material (i.e., the soil profile with the A and B horizons), and thus was present in the bedrock fractures when the fluvial units were deposited. The IIC material has been weathered, compacted, penetrated by roots, and has been subject to accumulation of secondary pedogenic materials. Shear fabric or textures diagnostic of fault gouge were not observed in the IIC material within the fissure. We conclude that the most recent surfac-faulting event on the S-2 fault predates the deposition and weathering of the IIc material. The characteristics of the overlying soil are consistent with an age of Early Holocene; thus, the IIC material is somewhat older than Early Holocene.

#### B.5.2.2 Trench FT-8, East Wall

Trench FT-8 exposed massive, fractured sandstone in fault contact (N60°E/70°SE) with interbedded sandstone, mudstone, and siltstone of the Great Valley Group (Figure 3-31). The bedrock units are pervasively sheared and fractured. Mudstone beds typically are sheared to the point that bedding is obliterated. Several of the sandstone beds are discontinuous and highly fractured. A block of sandstone adjacent to the main fault has been altered to a blue color with a rusty orange weathering rind. At the upward termination of the main fault in bedrock, there is a v-shaped opening filled with material similar to that in the overlying sand of Unit 1. Based on the lack of shear fabric or other features characteristic of faulting in this material, we interpret that this material was deposited within a pre-existing surface crack or fracture

Bedrock in trench FT-8 is overlain by 6 to 13 feet (2 to 4 m) of late Quaternary fluvial deposits. The basal alluvial deposit (Unit 1) is a 2.5-foot-thick (0.75 m), fine- to medium-grained loose sand with minimal soil structure. Sandy, pebbly lenses are present within unit 1, including a layer of coarse sand at the base of the deposit that is approximately 10 cm thick. The unit is intensely bioturbated, with abundant krotovinas,

and distinguished by the presence of 5 to 25 cm diameter rusty brown sandstone clasts at the base.

Unit 2 is a 2.8-foot-thick (0.85 m), tan-brown sand that is exposed along the entire length of the trench. The lower contact of this unit is sharp and distinct. In the southern part of the trench, unit 2 overlies bedrock with no intervening unit 1 deposits. Unit 2 has many vertical cracks, which have enabled transport of carbonate downward from the overlying deposits. Carbonate is concentrated in isolated zones along the top of the unit. There are a few rusty brown sandstone clasts near the base, and krotovinas are present throughout.

Near the center of the trench, the contact between bedrock and alluvial unit 1 is near vertical and exhibits about 0.45 m of local relief (Figure 3-31). The origin of the steep contact does not appear to be tectonic based on the lack of shear fabric or gouge along the contact, and the fact that there are no fractures in the overlying fluvial deposits of Units 1 and 2. Based on the presence of fluvial deposits on the bedrock surface, and the close proximity of the trench to the modern stream channel, we interpret that the vertical face is the edge of a buried strath-cut surface on the bedrock.

Unit 3 is a 1.6 foot (0.5 m) thick, dark brown soil with blocky structure. The lower contact is gradational over 2 inches (5 cm). A 4 to 6 inch (10-15 cm) thick layer of carbonate present at the bottom of the unit extends across the entire length of the trench. Based on structure and clay content, this unit probably is the B-horizon of the modern soil. Unit 4 is a 1.6 foot (0.5 m) thick, gray brown soil unit with prominent horizontal partings and block soil structure. The lower contact is gradational with unit 5 over 4 to 6 inch (10-15 cm). This unit represents the A-horizon of the modern soil (Figure 3-31).

#### B.5.2.3 Trench FT-9

Trench FT-9 exposed interbedded sandstone, siltstone, and mudstone of the Great Valley Formation overlain by 12 feet (3.75 m) of bedded fluvial deposits (Figures 3-32 and 3-33). Fluvial deposits within trench FT-9 exhibit stratification and distinct bedding, and overlie a subhorizontal erosional or ‘strat’ surface on the bedrock. The northern 20 feet

(6 meters) of the trench were not logged in detail due to unsafe conditions; major units were logged by dropping a tape from the surface and sighting across to the estimated contacts.

The logged portion of the east wall of trench FT-9 (herein referred to as FT-9a) was 69 feet (21m) long and exposed sandstone, siltstone, and laminated mudstone of the Great Valley Group. Bedrock is overlain by 12 feet (3.75 m) of Quaternary fluvial deposits (Figure 3-32). During excavation, the northern end of the trench collapsed. Consequently, the upper stratigraphic units are missing in the northern section of the log of the eastern wall (Figure 3-32).

The western side of the collapsed trench (herein referred to as FT-9b) was excavated into three benches for trench stability (Figure 3-32). The logged portion of the west side of trench FT-9 extended 43 feet (13 m) long and exposed 12 feet (3.75 m) of Quaternary fluvial deposits (Figure 3-33). Approximately 2.5 feet (0.75 m) of thinly bedded mudstone, siltstone, and sandstone bedrock was exposed at the north end of the trench. Because the bedrock exposures were in the unsafe part of the trench, the bedrock and overlying deposits are not described in detail.

Units 1, 3, 5, 6 and 7 from the log of the east wall of trench FT-9a can be correlated to the same stratigraphic positions on the west wall. A fluvial channel deposit containing a distinctive water-lain tephra is inset into Unit 3 on the west wall, and herein is labeled Unit 4. Unit 4 also was observed on the east trench wall in the part of the trench that collapsed. Field observations indicate that Unit 4 stratigraphically overlies Units 1 and 2b at the bottom of the east wall (i.e., above a depth of 3 m in the collapsed part of trench FT-9a; Figure 3-32), which were uncovered when the trench was deepened to remove fill material from the collapse. These relations thus indicate that Units 1 and 2b overlying bedrock on the east trench wall are older than Unit 4, despite the fact that Unit 4 does not appear on the log of the east trench wall. Units 1 and 2b directly overlie the main traces of the S-2 fault zone (Figure 3-32), and are not faulted.

Bedrock exposed at the base of the trench includes: yellowish-brown bedded sandstone with numerous subvertical fractures; massive fractured sandstone; and thinly bedded mudstone, siltstone, and sandstone. Individual beds range in thickness from less than 1 inch to 6 inches (1-15 cm). White calcium carbonate stringers with a clayey texture are present along bedding planes and fractures. The sandstone is soft and breaks apart easily with a hammer. Thicker sandstone beds are slightly harder. Sand grains are subrounded and medium to coarse. The composition of the sand grains is approximately 90% quartz and 10% dark lithics. Many of the thin interbeds have been extremely altered and some have been replaced by white calcium carbonate (clay). In several places the alteration is so complete that bedrock structure is completely absent.

The bedrock surface underlying Quaternary deposits in trench FT-9a is a subplanar platform with minor erosional irregularities (Figure 3-32). Between horizontal distance 1 and 3 m (see horizontal scale), the flat platform has been channeled, producing approximately 0.8 feet (0.25 m) of local erosional relief. Rusty-brown colored sandstone clasts ranging in size from 5-25 cm are present on the bedrock surface. Based on their lithology, we infer that these clasts are derived from a local bedrock source.

Bedrock is overlain by approximately 4 m of fluvial deposits (units 1-7). Unit 1 is a 5 to 6 foot (1.5-1.75 m) thick, massive fluvial sand deposit that is in depositional contact with bedrock. The unit contains stringers of gravel and CaCO3, nodules of iron oxide, and black particles of mudstone. Additionally, flecks of carbonate are present throughout the deposit. The soil structure developed in this unit is weak to moderate. Unit 1 locally is incised by fluvial channels that comprise Unit 2 (e.g., Figure 3-32).

Unit 2 is a bedded fluvial sand deposit that is approximately 5 feet (1.5 m) thick. This unit is divided into units 2a and 2b because they are both inset channel deposits at the same approximate stratigraphic level. Although it is unlikely that the two channels were active at the same time, they both represent a period of incision and downcutting through an older fluvial deposit (unit 1), followed by channel deposition and aggradation.

Units 3 through 6 comprise a package of fluvial deposits that can be traced along the entire length of the trench. Unit 3 is a sandy fluvial deposit with a high concentration of $CaCO_3$. The unit has an abrupt upper contact and a lower gradational contact. Based on the presence of the carbonate, this unit may represent a buried soil that was stripped prior to the deposition of overlying deposits. Alternatively, it may be a distinct stratigraphic unit that was deposited as part of the fluvial package. In this interpretation, textural differences between units 3 and 5 may have preferentially localized the carbonate accumulation along the contact.

Unit 4 is channel deposit containing a distinctive water-lain tephra. Unit 4 appears to be inset into Unit 3 on the west wall of the trench, and it unconformably overlies Unit1. As discussed above, this deposit was observed stratigraphically above units 1 and 2b on the east wall in the vicinity of the trench collapse. We estimated that the orientation of thalweg of the channel containing the ash is 12°NE/N20°E by sighting across the trench. The general trend of the tephra deposit is N15°E to N25°E.

Unit 5 is a sandy fluvial deposit characterized by the presence of flecks of carbonate and, as exposed in the west trench wall, pervasive krotovinas (animal burrows). This unit varies in thickness from 25-65 cm and has an abrupt sharp lower contact. A lens of carbonate at the top of the unit is interpreted to be the textural B-horizon of the modern soil.

Units 6 and 7 are horizons of the modern soil profile developed in the uppermost sandy fluvial deposits, of which unit 5 represents the C-horizon or parent material. Unit 6 is exposed from 10 m to the south end of the trench, exhibits a well-developed blocky structure, and has a gradational lower contact. It represents the B-horizon of the modern soil. Unit 7 is exposed from 10 m to the south end of the trench, is gray-brown and characterized by prominent horizontal partings. The lower contact of this unit is gradational over 4 to 6 inches (10-15 cm). This unit represents the A-horizon of the modern soil. These soil horizons (Units 6 and 7) are described in more detail below.

The soil profile within trench FT-9 (SP-7 in Appendix C) is characterized by a grayish upper A-horizon (0-17 cm) with a massive to granular structure. The A-horizon grades to an underlying, transitional A/B horizon similar in color to the A-horizon, but with a blocky structure found in the underlying B horizon. The Bt horizon (50-137 cm) is thick and is characterized by a prominent blocky structure. Ped faces within the Bt horizon are planar, and at right angles, giving the peds a cube-like shape. This structure is similar to the structure of Bt horizons described in soil profiles SP-1, 4, 5, and 6.

The contact between the Bt and Btk horizons locally is abrupt and may be marked by a thin (<2 mm) layer of laminar carbonate. The abruptness of the boundary and continuity of this horizon is attributed to the presence of a stratigraphic bed that has localized deposition of the carbonate. Carbonate within the Btk horizon (132-196 cm) is disseminated as fine tubular pore fillings, and it coats fracture faces.

The C-horizon (196-358 cm) varies from sandy loam to clay loam and exhibits stratification and channeling typical of fluvial deposits. Some gravel stringers are present. Carbonate is common, again as fine tubular pore fillings and fracture coats.

Soil profile 7 is very similar to other profiles estimated to be of early Holocene age. This profile does have a greater amount of carbonate than other profiles, but this feature may be attributed to factors other than age. Allowing for a small amount of additional time to develop this carbonate, we estimate an age of latest Pleistocene to mid Holocene for this soil.

### B.5.3 Summary of Trenching Results, S-2 Fault

The S-2 fault is a narrow (less than 2-ft wide) sub-vertical bedrock shear zone. The fault zone is overlain by unfaulted Early Holocene colluvial and alluvial deposits. Small packages of colluvial deposits appear to have developed along zones of sheared rock associated with the fault, similar to soil-filled cracks documented in Trench FT-6 across the GG-3 fault. Based on the absence of similar age soil material in the overlying

deposits, lack of shearing, and the presence of similar soil-filled cracks outside of the inferred fault zones, we interpret these deposits to have a non-tectonic origin.

## B.6 SALT LAKE FAULT

### B.6.1 Trenching Investigations Across the Salt Lake fault at Hunters Creek

As part of our evaluation of the Salt Lake fault, we trenched Quaternary deposits adjacent to Hunters Creek that cover the mapped surface trace of the fault. Based on our photogeologic mapping and field observations, we interpret that terrace deposits along Funks Creek that cover the projection of the Salt Lake fault upstream of the Golden Gate damsite are Holocene or younger and the youngest terraces may even be historic. Radiocarbon dates from our paleoseismic trenches across the GG-1 fault near the Golden Gate site within similar, correlative terraces confirm the very young age of these deposits (Table 3-3). In addition, lack of fault exposures and the absence of geomorphic expression provide poor constraints on the likely location of the Salt Lake beneath terraces along Funks Creek. Given that the overlying deposits that are too young for evaluation of inactivity of the fault, per DSOD criteria, as well as the broad uncertainty in the location of the fault, we examined Quaternary deposits along other streams that cross the Salt Lake fault north of Funks Creek as potential targets for paleoseismic trenching.

We decided to trench Pleistocene terrace deposits along Hunters Creek that cross the fault approximately 6.4 miles (10.3 km) northeast of the Golden Gate damsite. Based on our geomorphic mapping, we identified stream terraces that cover the projection of the Salt Lake fault. Folded and faulted bedrock exposed in the north bank of Hunters helped us constrain the location of the Salt Lake fault. Although distant from the Golden Gate and Sites damsites, older terrace deposits adjacent to Hunters Creek provide a stratigraphic record sufficient for characterization of the activity, per DSOD criteria, of the Salt Lake fault.

We initially excavated a shallow, 4 ft (1.3 m) deep trench (FT-HC1) across the trace of the Salt Lake fault approximately 100 feet (30 m) north of Hunters Creek (Figures B-2

and 3-35). Based on identification of a westward-down step in bedrock during trenching, we locally deepened the trench near the center of the excavation. At this location, the fault is expressed by a 3 ft (1 m) down-to-the-west step in bedrock and corresponding warp in overlying stream gravels (fault trench FT-HC1; Figures 3-37 and 3-38). Although apparently deformed across the fault, deflection of bedded stream gravels across the step in bedrock at the fault could also be explained by depositional processes, including fluvial draping over a pre-existing bedrock scarp. We therefore decided to excavate an additional trench within thicker gravel deposits approximately 30 feet (10 m) to the north. At this location, we excavated a 12-foot-deep (3.5 m deep) trench that exposed faulted alluvial gravels (fault trench FT-HC2; Figures 3-40, 3-41, and 3-42). Based on ambiguous stratigraphic relations within the younger deposits exposed in fault trenches FT-HC1 and FT-HC2, we decided to trench south of Hunters Creek in order to evaluate whether Holocene deposits were faulted. Fault trench FT-HC3 (Figure B-7) provided limited information on the activity of the Salt Lake fault due to the presence of a strong vertisol that obscured shallow stratigraphic relations, and deep deposits that prevented exposure of the Salt Lake fault in bedrock.

Based on our field mapping, we excavated a trench (Trench SL-T1) across the southern Salt Lake fault north of Stone Corral Creek. The purpose of the trench was to confirm the location of the main trace of the Salt Lake fault and, in combination with our geologic mapping and trenching of the topographic saddle to the east, document that the Salt Lake fault, or a related fault strand, does not extend beneath the proposed Sites dam site. Trench SL-T1 was located approximately 0.4 miles (0.6 km) northeast of the town of Sites, north of the main Sites-Maxwell Road across the eastern margin of the fault. In addition, in order to preclude the presence of a strand of the Salt Lake fault beneath the Sites dam site, we trenched across a broad valley and topographic saddle located 0.5 miles (0.8 km) northeast of Sites (Figure B-1 and 3-34). Across the north-south valley north of the sites, we opened three trenches (Trenches S-T1, S-T2 and S-T3; Figures B-8, B-9 and B-10). At the topographic saddle we excavated three east-west trenches (Trenches S-T4a, S-T4b and S-T5; Figures B-12, B-13, B-14, B-15 and B-16). Stratigraphic relations exposed in the Hunters Creek fault trenches (FT-HC1, FT-HC2,

and FT-HC3), southern Salt Lake fault trench (T-SL1), and the topographic saddle (S-T4a and b, are described in detail below.

### B.6.2 Trench Stratigraphy

#### B.6.2.1 Trench FT-HC1

Bedrock exposed in trench FT-HC1 consists of vertical to sub-vertical sandstone and mudstone beds in fault contact (N60°E/70°SE) with sheared mudstone and siltstone (Figures 3-37 and 3-38). The bedrock units are pervasively sheared and fractured. Within the fault zone, mudstone beds are sheared to the point that bedding is destroyed.

Within the north wall of trench FT-HC1 a large, subangular bedrock boulder is bounded by faults (Figure 3-37). Within the south wall of trench FT-HC1, the bedrock boulder is not present and a large cast of the southern margin of the boulder is preserved within the trench wall (Figure 3-38). The boulder within the north wall is sitting on a flat erosional surface cut on sandstone and mudstone and is bounded on the east by a remnant of well-developed soil containing rounded pebbles (Unit 1). Soil development is consistent with an older (Pleistocene?) buried soil (Soil profile SP-9; Appendix C). The soil is faulted and the boulder appears to have been rotated within the fault zone, suggesting fault displacement subsequent to emplacement of the boulder and development of the soil.

One possible origin for the boulder is that it is locally derived from degradation of a fault scarp developed in bedrock, i.e. collapse of the scarp. However, it is also possible that the boulder was deposited within the same pebbly silt stream deposit as that in which the relict soil, located between the boulder and bedrock to the east, is developed.

Bedrock, the boulder, and the relict soil have been eroded resulting in a sub-horizontal upper strath surface. This surface is down-dropped to the west approximately 3 feet (1 m). The entire package (bedrock, boulder, and soil) is thrust over coarse, bedded stream gravel (Unit 2). The inferred fault scarp is overlain by a two-foot (0.7 m) thick package of coarse, sandy gravel (Unit 3) that is significantly thicker west of the fault and appears warped across the fault zone. A small colluvial deposit (Unit 4), most likely derived

from the underlying Unit 3 gravels, is preserved west of the warp in Unit 3. Sandy gravel of Unit 5 is not found in the footwall of the fault. In the hanging wall, Unit 5 is overlain by sandy silt of Unit 7, possibly correlative to similar silty sand of Unit 6 in the western portion of the trench. A young stream channel deposit (Unit 8), with minimal soil development, is incised into Units 5 and 7.

Faulted soils and offset stream gravels exposed in Trench FT-HC1 clearly document Quaternary activity on the Salt Lake fault. However, no datable material was obtained from Trench FT-HC1. Soil profile SP-9 (Appendix C) of the faulted buried soil exhibits a well-developed stage III Bt horizon, suggestive of a late Pleistocene age. More than one surface-rupturing event likely is preserved in the trench stratigraphy based on the presence of the large boulder adjacent to a possible buried fault scarp, inferred rotation of the boulder subsequent to deposition, and the presence of overlying warped stream gravels.

#### B.6.2.2 Trench FT-HC2

Bedrock exposed in trench FT-HC2 consists of sub-vertical, interbedded sandstone and mudstone in fault contact (076°/88°SE to 020°/58°E) with sheared mudstone and siltstone (Figures 3-40, 3-41, and 3-42). Bedrock is down-dropped approximately 4.5 ft (1.5 m) forming a buried west-facing scarp. Bedding changes across the fault from interbedded sandstone and mudstone oriented 005°/88°E to predominately mudstone oriented 355°/72°W. Bedrock west of the fault is pervasively sheared and fractured.

The Salt Lake fault consists of an east-dipping zone of sheared bedrock approximately 1.5 to 3 feet (0.5 to 1 m) wide. Within the fault zone, the main fault strand generally dips approximately 60° to 70° to the east. Secondary shears within the fault zone dip 60° to 88° and bound faulted bedrock blocks. The main fault strand is best expressed within the south wall of Trench FT-HC2 as a well-defined main fault trace with up to 3 inches (5 cm) of fault gouge. Small (1-2 cm diameter) rounded stream pebbles from terrace gravels overlying bedrock are incorporated in the fault gouge.

The 4.5 ft (1.5 m) step in bedrock across the Salt Lake fault is overlain by 4.5 to 9 feet (1.5 to 3 m) of late Quaternary fluvial deposits. The basal alluvial deposit, Unit 1, consists of carbonate-cemented, clast-supported stream gravels preserved only within the foot wall west of the fault. Unit 1 is in conformable contact with similar, uncemented clayey gravels of Unit 2. On the south wall of Trench FT-HC2 (Figure 3-42), similar gravels correlated to Unit 2 are preserved within the hanging wall east of the fault. On the north wall of Trench FT-HC2 (Figure 3-39), it is unclear whether gravels of unit 2 are preserved within the hanging wall. Unit 1 contains and probably is correlative to Unit 2. The carbonate matrix of Unit 1 may be the result of localized precipitation of carbonate from groundwater ponded atop bedrock against the Salt Lake fault.

Units 1 and 2 are overlain by 1.5 feet (0.5 m) of well-bedded, well-sorted clayey gravel consisting of well-rounded pebbles (Unit 3). Gravel beds within Unit 3 in the hanging wall appear backtilted, coincident with overall eastward tilting of the underlying bedrock strath surface. Gravel beds within Unit 3 in the foot wall are sub-horizontal but increasingly vertical adjacent to the fault zone (Figures 3-40 and 3-42). In the south wall of the trench (Figure 3-40), beds within Unit 3 are rotated to subvertical between two strands of the faults.

The locations of calcium carbonate ($CaCO_3$) coatings on the bottoms of pebbles within fluvial gravels of Unit 3 provide additional evidence that the gravels have been progressively deformed by the Salt Lake fault. In the relatively undeformed beds located about 3 feet (1 m) west of the fault, 22 of 25 clasts (88%) had bottom coatings at a depth of 93 to 111 inches (237-282 cm) below the ground surface (Table B-1). The high percentage of bottom coatings is consistent with the preferential precipitation of carbonate, either as part of soil development or groundwater processes, at the bottoms of the pebbles. In the vertically deformed section, adjacent to and within the fault zone, 9 of 25 clasts had left side coatings, 7 had left and bottom coatings, 4 had bottom coatings, 3 had bottom and right side coatings, 1 had a right side coating, and 1 had a coating that covered the top, left side, and the bottom (Table B-1). The high percentage of carbonate coatings found on the tops and sides of the pebbles in the vertical section near the fault

suggest that gravel beds of Unit 3 have been deformed by the fault and that this deformation took place after deposition of the carbonate coatings. The variation in the location of the coating in the deformed section suggests some rotation of individual pebbles, in addition to overall folding of the gravel beds, may have occurred during deformation and/or reflect progressive rotation during several deformation events. Coatings located on the top or side on the pebbles appeared to be somewhat degraded, possibly reflecting post-deformation dissolution of the carbonate.

**TABLE B-1** Position of Carbonate Rinds on Pebbles

Rinds on the sides of the pebbles are assumed to have been rotated from an original bottom-of-pebble position.

| **Position of rind on pebble *** | **Number of pebbles** | |
|---|---|---|
| | **Deformed section of bed** | **Undeformed section of bed** |
| Bottom | 4 | 22 |
| Left side | 9 | 0 |
| Bottom and left side | 7 | 0 |
| Top, bottom, and left side | 1 | 0 |
| Right side | 1 | 0 |
| Bottom and right side | 3 | 2 |
| All sides | 0 | 1 |
| **TOTAL SAMPLED** | **25** | **25** |

* As seen in the southwest wall of Trench FT-HC2, downthrown side of the Salt Lake fault. Vertical section (deformed section) of gravel bed is located adjacent to the fault plane at 220 to 240 cm depth. Horizontal section of gravel bed is located 1 to 2 meters away from the fault plane at 237 to 282 cm depth.

Unit 4 consists of approximately 2 feet (0.75 m) of poorly sorted, moderately bedded fluvial gravel. Unit 4, although not as well-bedded as the underlying gravels in Unit 3, is

clearly faulted and is thicker in the foot wall of the fault than in the hanging wall. Approximately 9 feet (3 m) east of the fault, within the hanging wall, Unit 4 is only about 1.5 feet (0.5 m) and appears to have been eroded prior to deposition of the overlying fluvial flood deposits of Units 6 and 7.

Unit 5 consists of approximately 1 to 2 feet (0.3 to 0.7 m) of poorly sorted, unbedded clayey gravel similar to that of underlying gravel within Unit 4. Unit 5 is thickest directly west of the projection of the main fault strand (Figures 3-40 and 3-41). Based on the similarity of Unit 4 to the underlying gravels of Unit 3, location adjacent to the fault scarp, and thinning of Unit 4 within the hanging wall east of the fault and foot wall west of the fault, we believe that Unit 4 is a colluvial deposit derived from erosion of the underlying faulted gravels of Unit 4. In the south and north walls of Trench FT-HC2 (Figures 3-40 and 3-41), sheared mudstone and sandstone is thrust over bedded gravel of Units 1, 2, 3, and 4.

Units 6 and 7 are fine-grained overbank deposits consisting of yellowish-brown silt with minor gravel. These units are horizons of the modern soil profile. Unit 6 is exposed from 10 m to the south end of the trench, exhibits a well-developed blocky structure, and has a gradational lower contact. It represents the B-horizon of the modern soil. Unit 7 is exposed from 10 m to the south end of the trench, is gray-brown and characterized by prominent horizontal partings. The lower contact of this unit is gradational over 4 to 6 inches (10-15 cm). This unit represents the A-horizon of the modern soil.

The soil profile within trench FT-HC2 (SP-11 in Appendix C) is characterized by a upper A-horizon with a massive to granular structure. The Bt horizon (50-137 cm) is thick and is characterized by a prominent blocky structure. Ped faces within the Bt horizon are planar, and at right angles, giving the peds a cube-like shape. This structure is similar to the structure of Bt horizons described in soil profiles in the Funks Creek area.

The upper modern soil horizons are formed in young deposits, possibly 8-15 ka, based on similarity to early Holocene soils dated in the Funks Creek area. It is possible that fault

offset of Unit 5 predates the development of the early Holocene soil profile within Units 5 through 7. However, a drop in the abundance of clay films across the projection of the main fault strand through Unit 5 suggests that offset of the deposit could post-date the soil. An alternative explanation of the drop in clay films is that differences in the abundance of clay films reflects changes in the parent gravels juxtaposed across the fault. However, colluvial gravels of Unit 5 are very similar to, and appear to have been derived from, underlying fluvial gravels of Unit 4.

The lower portion of the soil profile within Units 3 and 4, all IIB horizons, are significantly older based on the presence of hard, dense CaCO3 coatings and the presence of distinct to prominent reddish clay films that coat the CaCO3 (Soil Profile 11; Appendix C). Based on soil development, the estimated age of the older gravels range from 30 ka to 150 ka. These late Pleistocene gravels are clearly deformed and faulted by the Salt Lake fault.

#### B.6.2.3 Trench FT-HC3

Trench FT-HC3 extended east-west across the projection of the Salt Lake fault within a late Holocene terrace located south of Hunters Creek. Although excavated to the maximum working depth of the equipment, the trench was not deep enough to expose bedrock and thus the Salt Lake fault was not exposed (Figure B-7). However, based on projection of exposures of the fault within trenches FT-HC1 and FT-HC2 and within bedrock exposed along Hunters Creek, we believe that trench FT-HC3 crossed the trace of the Salt Lake fault.

Trench FT-HC3 exposed 9 feet (3 m) of late Holocene fluvial and colluvial deposits. The basal colluvial deposit (Unit 1) is a 2.5-foot-thick (0.75 m), hard, very dark brown to dark yellowish brown pebbly clay. The unit contains abundant rounded pebbles, suggesting that the deposits may have a fluvial origin. The basal unit (Unit 1) is overlain by a series of interlapping stream deposits consisting of silt to sandy gravel lenses (Figure B-7).

The original stratigraphy of Unit 1 is obscured by pedogenic churning associated with development of a vertisol within the deposits (see Soil Profile SP-12; Appendix C). Due to the development of deep, vertical soil peds, any original stratigraphic and structural features have been obliterated and thus the presence or absence of fault-related deformation can not be documented within Unit 1. In addition, the degree of soil development within the deposits is suggestive of early to mid-Holocene age (J. Sowers, pers. comm, 2000; Soil Profile SP-12; Appendix C). The combination of deposits that are too young for evaluation of inactivity of the fault, per DSOD criteria, presence of a vertisol that obscures stratigraphy, and the broad uncertainty on the location of the Salt Lake fault limits the utility of assessing late Quaternary fault activity within Trench FT-HC3.

### B.6.2.4 Trench Exposure SL-T1

Trench SL-T1 extended 217 feet (66 m) east-west across the eastern margin of the Salt Lake fault (Figure 3-34). The trench exposed mudstone of the Cretaceous Great Valley Group (Figures 3-39 and 3-43). We documented 59 ft (18 m) of intensely sheared and disrupted mudstone at the western end of the trench juxtaposed against over 155 feet (48 m) of relatively intact, north-south trending, east-dipping bedded mudstone exposed in the eastern portion of the trench. Within the shear zone exposed in the western end of the trench, fractures cut bedding, and typically are coated with calcium carbonate. Mudstone bedding, where preserved, generally trends north-south and dips east but locally is intensely sheared with vein-infilling evidence for repeated displacement. Unsheared mudstone bedrock west of the fault zone contains minor, bedding-parallel fractures. Based on the well-developed shear zone within bedrock, coincident with geomorphic surface features and projection of the exposure of the fault along Stone Corral Creek to the south, we conclude that the shear zone exposed in trench SL-T1 is the Salt Lake fault shear zone.

With the exception of a thin colluvial soil layer, the trench did not expose late Quaternary stratigraphy. The colluvial deposits extend across the Salt Lake fault zone and are not

deformed, faulted, or sheared. However, the colluvial soil is poorly developed and thus the colluvial deposits likely are late Holocene or younger.

#### B.6.2.5 Trenches S-T1, S-T2, S-T3, S-T4a and –T4b, and S-T5 east of the Salt Lake Fault

Trenching of a broad valley and topographic saddle north of the Sites dam site, northeast of the town of Sites, documented the absence of a through-going major shear zone. We excavated three trenches (Trenches S-T1, S-T2, and S-T3; Figure B-8, B-9, and B-10) across subtle topographic features coincident with minor carbonate float within the north-south trending valley to document whether the observed features were related to a strand of the southern Salt Lake fault. These trench locations are shown on figures B-1 and 3-34. We excavated three trenches (Trenches S-4a, -b, and ST-5; Figures B-13 and B-14) across a prominent topographic saddle north of the proposed Sites dam site (shown on Figures B-1, B-13, and B-14) to document the presence or absence of faulting.

With the exception of the minor bedrock fault exposed in trenches within the topographic saddle (Trenches S-T4a, b, and ST-5; Figures B-13 and B-14), no major shear zones were observed in the trenches. The trenches, in conjunction with our mapping and exposure of the Salt Lake fault (trench SL-T1) northwest of Sites, showed that the Salt Lake fault, or a related fault strand, does not extend beneath the proposed Sites dam site.

### B.6.3 Summary of Trenching Results, Salt Lake Fault

In summary, three trenches across the Salt Lake fault at Hunters Creek provide information on the location, morphology, and activity of the fault. Results of our paleoseismic trenching show that the fault is expressed as a narrow 1-2 ft (0.25 to 0.5 m) wide, east-dipping (60° to 80°), fault plane. The presence of well-developed clay gouge, rotated pebbles and boulders within the fault zone, stratigraphic correlation of progressively faulted units, and the presence of multiple colluvial wedges provide evidence of repeated incremental displacement on the Salt Lake fault within the late Quaternary. Pleistocene gravels with soil development estimated to be between 30,000 to

100,000 years old are offset and warped. Based on DSOD criteria, we conclude that the Salt Lake fault should be classified as a latest Pleistocene-active fault.

Trenching of the topographic saddle north of the Sites dam site, northeast of the town of Sites, documented the absence of a major shear zone. With the exception of one minor bedrock fault, no major shear zones were observed in the trenches. The trenches showed that the Salt Lake fault, or a related fault strand, does not extend beneath the proposed Sites dam site. Based on exposure of a well-developed shear zone in trench SL-T1 approximately 0.4 miles (0.7 km) west of the saddle, coincident with mapped geomorphic surface features and projection of the exposure of the Salt Lake fault along Stone Corral Creek, we conclude that the main Salt Lake fault is located west of the Site dam site.

With the exception of a thin colluvial soil layer, the SL-T1 trench across the southern Salt Lake fault near Sites did not expose late Quaternary stratigraphy. The colluvial deposits extend across the Salt Lake fault zone and are not deformed, faulted, or sheared. However, the colluvial soil is poorly developed and thus the colluvial deposits likely are late Holocene or younger. During our earlier geomorphic mapping of stream terraces along Stone Corral Creek, we did not identify Quaternary deposits of sufficient age for evaluation of fault activity (i.e. DSOD criteria). Based on our mapping and previous paleoseismic investigations along Hunters Creek to the north that document offset of late Quaternary deposits, we conservatively assume that the southern Salt Lake fault is active.

## B.7 TRENCHING INVESTIGATIONS ACROSS SADDLE DAMS 1 AND 2

We conducted trenching of proposed Saddle Dams 1 and 2 to document depth to bedrock and bedrock type. We trenched along the western portion of Saddle Dam 1 within a topographic low to a fence on the east end of the trench. Mudstone bedrock was exposed at the westernmost end of the trench but we did not expose bedrock elsewhere along the axis (Figure B-18). We obtained a minimum thickness of colluvial deposits of 16.5 feet near the center of the trench.

Bedrock was exposed within the trench along the axis of the main Saddle Dam 2 (B-19, -20, -21). The Salt Lake fault zone was exposed in a separate trench across the westernmost portion of Saddle Dam 1 (Figure B-22).

## B.8 S-3 FAULT

### B.8.1 Trenching Investigations Across the S-3 Fault

We excavated three trenches (FT-T1-S3, FT-T2-S3, and FT-T5-S3; Figure B-1) across S-3 fault, north of the GG-3 fault. The purpose of these trenches was to confirm the location of the fault and characterize the width of the fault zone across the proposed reservoir outlet structure. These trenches were excavated within bedrock across the inferred trace of the fault. Trench locations were chosen based on our previous air photo interpretation and field mapping, the presence of a prominent east-facing scarp, and the presence of carbonate float.

In addition, we excavated three adjacent paleoseismic trenches (T3-S3, T4-S3, and T6-S3; Figure B-1) within the oldest mapped stream terrace south of Funks Creek. These trenches were excavated to confirm the location of the S-3 fault near the Golden Gate dam site and to evaluate the activity of the S-3 fault, specifically to document the presence or absence of vertical and/or horizontal offset of late Quaternary deposits. The trenches exposed the S-3 fault in bedrock, the unfaulted back edge of the stream terrace, and overlying unfaulted early Holocene terrace deposits.

### B.8.2 Trench Stratigraphy

#### B.8.2.1 Trench Exposure T1-S3

Trench FT-T1-S3 was 65 feet (20 m) long, 5 feet (1.5 m) deep, and oriented east-west across the S-3 fault (Figures 3-9). We excavated trench FT-T1-S3 across an east-facing scarp located based on our field mapping (Figure 3-48). The scarp coincides with a resistant east-dipping sandstone bed exposed in the center of the trench (Figure 3-49*)*. The trench exposed the S-3 fault in bedrock, overlain by a thin mantle of unfaulted colluvial deposits. The S-3 fault is expressed as a well-defined zone of bedding-parallel

faulting approximately 6 feet (2 m) wide. The fault zone is within east-dipping bedded mudstone bounded by unfaulted, intact interbedded sandstone and mudstone (Figure 3-49). Steeply east-dipping to sub-vertical faults within the S-3 fault zone truncate bedding.

#### B.8.2.2 Trench Exposure T2-S3

The FT-T3-S3 trench was 30 feet (10 m) long and oriented east-west across the S-3 fault approximately 0.6 miles (1 km) south of Funks Creek (Figures 3-9 and 3-47). We excavated trench FT-T2-S3 across an east-facing scarp coincident with the mapped trace of the S-3 fault. As in trench FT-T1-S3, the scarp coincides with a resistant east-dipping sandstone bed exposed as a dip slope at the west end of the trench (Figure 3-50). In order to obtain a better exposure of the fault in bedrock, we benched the trench at approximately 6-foot-depth (2-m-depth) and deepened the trench for a total depth of 9 feet (3 m).

Trench FT-T2-S3 exposed the S-3 fault in bedrock (Figure 3-50). The S-3 fault is expressed as a well-defined zone of bedding-parallel faulting approximately 9 feet (3 m) wide within east-dipping bedded mudstone. Within the S-3 fault zone, locally intense shearing obscures relict mudstone bedding and steeply east-dipping to sub-vertical fault shears truncate beds. Along major shears, well-developed clay fault gouge with abundant calcium carbonate is common. East of the fault zone, mudstone bedrock is relatively intact with minor bedding parallel fractures (Figure 3-50). The intact sandstone bed west of the fault has formed a scarp along much of the mapped trace of the S-3 fault, providing evidence that the S-3 fault is preferentially located within the same stratigraphic horizon along strike.

Within trench FT-T2-S3, the S-3 fault is overlain by unfaulted colluvial deposits. The colluvium is up to 3 feet (1 m) thick and is thickest across the S-3 shear zone where hillslope erosion has preferentially removed less-resistant material present within the shear zone. The colluvium consists of brown silty clay with minor subangular sandstone clasts and has poorly developed soil structure. Above the S-3 shear zone, erosion

apparently has undercut mudstone beds, causing these beds to tilt uphill. Alternatively, internal deformation within the fault zone tilted the beds to subhorizontal bedding. These beds have then been exposed by erosional exhumation of the fault zone.

### B.8.2.3 Trench Exposures FT-T3-S3, FT-T4-S3, FT-T5-S3, and FT-T6-S3

Three trenches (FT-T3-S3, FT-T4-S3, and FT-T6-S3) were excavated across the southern margin of the Qt1 stream terrace south of Funks Creek (Figures 3-9 and 3-47). At this location the back edge of the terrace, cut into bedrock of the Great Valley Group, obliquely crosses the S-3 fault (Figures 3-47 and 3-51). We excavated trenches across the terrace margin in order to document the presence or absence of: (1) vertical offset of terrace deposits that overlie the S-3 fault zone, and (2) horizontal offset of the terrace back edge across the fault.

Trench FT-T3-S3 was 36 feet (11 m) long, up to 5 feet (1.5 m) deep, and oriented east-west across the S-3 fault (Figure 3-9). We excavated trench FT-T3-S3 across an east-facing scarp coincident with the edge of stream terrace Qt1 based on our field mapping (Figure 3-51). The scarp coincides with a resistant east-dipping sandstone bed exposed in western end of the trench (Figure 3-52).

The trench exposed the S-3 fault in bedrock overlain by unfaulted stream terrace deposits, which in turn are covered by slope-derived colluvial deposits (Figure 3-52). The S-3 fault is expressed in trench FT-T1-S3 as a well-defined zone of bedding-parallel faulting approximately 4 feet (1.5 m) wide. The fault zone is within east-dipping bedded mudstone bounded by unfaulted, intact interbedded mudstone on the east and resistant sandstone on the west (Figure 3-52). Within the S-3 fault zone, steeply east-dipping shears primarily are bedding parallel although several truncate bedding. The S-3 shear zone and adjacent intact bedrock have been eroded by Funks Creek, forming a horizontal bedrock strath surface covered by stream terrace deposits. At this location, the stepped back edge of the terrace is coincident with the western margin of the S-3 shear zone, although bedded gravels at the base of the terrace are undeformed.

Based on the coincidence of the S-3 fault zone with the back edge of stream terrace Qt1, we decided to excavate trench FT-T4-S3 6 feet (2 m) to the north. Trench FT-T4-S3 (Figure 3-53) was 23 feet (7 m) long, up to 5 feet (1.5 m) deep, and oriented east-west across the S-3 fault. We excavated trench FT-T4-S3 across the edge of stream terrace Qt1 (Figure 3-51). As in trench FT-T3-S3, the trench exposes a resistant east-dipping sandstone bed in western end of the trench and inset terrace deposits of Qt1 (Figure 3-53). In trench FT-T4-S3, the stepped back edge of the terrace is located west of the S-3 shear zone. The stream-cut surface at the base of the terrace crosses the S-3 shear zone, and intact mudstone bedrock west of the fault, with no apparent vertical offset. In addition, bedded gravels at the base of the terrace that cross the fault zone clearly are undeformed.

We excavated a trench north of trench FT-T6-S3 across the S-3 fault zone and inferred Qt1 terrace margin. At this location, the back edge of the Qt1 terrace is located east of the S-3 fault. Our intention was to confirm that the terrace back edge was not laterally offset by the S-3 fault. Trench FT-T6-S3 was 49 feet (15 m) long, up to 5 feet (2 m) deep, and oriented east-west across the S-3 fault (Figure 3-9). At this location, however, a topographic swale and associated stream channel deposits, intersects terrace Qt1 within the western portion of the trench. As a result, the stratigraphy within trench FT-T6-S3 is not as clear as in the adjacent trenches (Figure B-24). In particular, we were unable to definitely identify the terrace back edge, although we believe that it is located near the center of the trench. If our interpretation is correct, there is no observable lateral offset of the early Holocene Qt1 terrace across the S-3 fault. Alternatively, if the inferred channel associated with the topographic swale is actually the western margin of terrace Qt1, the terrace margin may parallel the fault and we can not definitely preclude lateral offset across the S-3 fault. Our preferred interpretation, supported by our geomorphic mapping of the Qt1 terrace surface, is that there is no offset of the Qt1 terrace across the S-3 fault.

The FT-T5-S3 trench was 26 feet (9 m) long and oriented east-west across the S-3 fault south of Funks Creek (Figure B-1). We excavated trench FT-T5-S3 across an east-facing scarp coincident with the mapped trace of the S-3 fault, several tens of meters north of

the GG-3 fault. As in the other trenches across the S-3 fault, the scarp coincides with a resistant east-dipping sandstone bed exposed as a dip slope at the west end of the trench. FT-T5-S3 exposed the S-3 fault in bedrock as a well-defined zone of bedding-parallel faulting approximately 6 feet (2 m) wide within east-dipping bedded mudstone. Within the S-3 fault zone, locally intense shearing obscures relict mudstone bedding and steeply east-dipping to sub-vertical fault shears truncate beds. An intact sandstone unit within the fault appears to be either a sandstone bed or dike caught up in the fault zone and bounded by bedding parallel shears.

### B.8.3 Summary of Trenching Results, S-3 Fault

Six trenches at across the S-3 fault reveal that the structure is a narrow zone of bedding-parallel shearing. Based on our mapping, and confirmed by trenching, the S-3 fault is preferentially located within a distinct stratigraphic contact between a resistant sandstone bed and thick mudstone unit along strike within Great Valley Group bedrock. The presence of an intact sandstone bed bounding bedding-parallel shears within more ductile mudstone suggest that the S-3 fault has accommodated layer-parallel shearing.

The trenches across the S-3 fault confirm the mapped offset of the S-3 fault by the S-2, GG-3, and GG-2 faults, strongly suggesting that the S-3 fault is an older, probably inactive structure. Based on trenches within early Holocene terrace deposits across the S-3 that document the absence of horizontal and vertical fault displacement, the S-3 fault has not experienced surface displacement events in the Holocene. The cumulative offset of the S-3 fault by the GG faults, and localized drag folding of the S-3 fault across the S-2 fault, suggest repeated and incremental offset of the S-3 fault over time.

# APPENDIX C
## Soil Profile Descriptions

---

## C.1 INTRODUCTION

Soil descriptions presented in Appendix C are based on procedures established by SCS Soil Survey Staff (1975; 1992). Seven soil profiles (SP-1 through SP-7) in five fault trenches (FT-2, FT-5, FT-6, FT-7, and FT-9) in the vicinity of the Golden Gate and Sites damsites, five (SP-8 through SP-12) in three fault trenches (HC-FT-1, HC-FT-2, and HC-FT-3) and one test pit in the vicinity of Hunters Creek were described. Soil profile locations are shown on trench logs (Chapter 3 and Appendix B).

## C.2 SUMMARY

All profiles exhibit a similar pattern of soil development characterized by:

- Accumulation of organic matter, typically forming a dark gray A-horizon 60-90 cm thick.
- Accumulation of translocated clay forming a thick Bt-horizon (base @ 250-290 cm) having blocky to prismatic soil structure and distinct to prominent clay films.
- Vertical fractures, or shrinkage cracks, that extend from the ground surface into, or through, the Bt-horizon.
- In-place weathering of primary grains. Sand grains are weathered to silt and clay. They appear as sand grains in an undisturbed sample but disintegrate when the moist soil is worked with the fingers. Gravel clasts are moderately weathered (can be broken with the hands) to extremely weathered (can be cut with a knife).
- Local, discontinuous accumulation of stage I CaCO3 in the lower Bt-horizon.
    - A single soil-profile formed on the present surface. Buried soils are weak to non-existent.

- Parent material for the soils is alluvium and colluvium derived from Great Valley Group sandstones, siltstones, and shales.

Soil 1 in FT-2 (described in SP-1 and SP-2; Appendix A) developed in fine-grained alluvium in the valley bottom of Funk Creek. Gravel percentages are very low, generally below 5%. Silt, clay, and fine sand dominate. This trench is located in a backwater part of the valley, and thus the depositional surface probably received distal facies overbank deposits. Profiles 3 and 4, in FT-5, are formed in poorly sorted alluvium and colluvium on a gently sloping flat associated with a tributary and a side hollow. The landscape surface is continuous from the tributary flat to the valley bottom, thus it is reasonable to expect these soils might be the same age. Soil Profile 6 is a deep profile developed in a uniform mixture of alluvial material from Funk Creek and colluvial material from the adjacent hillslope.

Soil-profile development in all the described exposures is consistent with an age of early Holocene to latest Pleistocene (i.e., 8 to15 ka). No reddening suggestive of an earlier age was observed; colors are 10YR hues (based on the Munsell soil color chart). Although clay content is high and clay films present, much of the clay is primary. The primary clay has been redistributed to form the observed clay films and structure, but there does not seem to be a significant accumulation in the Bt horizon over that present in the C-horizon, nor is there significantly less clay in the A-horizon where it might have been lost through illuviation.

An age of latest Pleistocene to early Holocene is consistent with the radiocarbon analyses of samples collected from the fault trenches (Table 3-3). This age estimate is also consistent with the general climatic model for late Quaternary weathering, erosion, and sedimentation in the Coast Ranges (Bull, 1991; Lettis, 1982). During a full glacial period during the Pleistocene-Holocene transition, increased effective moisture and more dense vegetation likely would result in the accumulation of a thick weathered mantle on the hillslopes. A change in climate to drier conditions and less vegetation, such as is thought

to have occurred during the Holocene-Pleistocene transition, likely would precipitate erosion of the weathered mantle and accumulation of that weathered debris as alluvium in valley bottoms.

Atwater, T., and Stock, J., 1998, Pacific-North American plate tectonics of the Neogen southwestern United States: an update: International Geological Review, v. 40, p. 375-402.

Benz, H.M., Zandt, G., and Oppenheimer, D.H., 1992, Lithospheric structure of northern California from teleseismic images of the upper mantle: Journal of Geophysical Research, v. 97, p. 4791-4807.

Brankman, C.M., and Aydin, A., 2000, Uplift and contractional deformation along a segmented strike-slip fault system: the Gargano Promontory, southern Italy, in review, Journal of Structural Geology.

Comninou, M.A., and Dundurs, J., 1975, The angular dislocation in a half-space, Journal of Elasticity, 5, 203-216.

Crider, J.G., and Pollard, D.D., 1998, Fault linkage; three-dimensional mechanical interaction between echelon normal faults, Journal of Geophysical Research, B, 103; 10, p. 24,373-24,391.

Crouch, S.L., and Starfield, A.M., 1983, Boundary Element Methods in Solid Mechanics, Unwin Hyman, London.

Dixon, T.H., Miller, M., Farina, F., Wang, H., Johnson, D., 2000, Present-day motion of the Sierra Nevada block and some tectonic implications for the Basin and Range province, North American Cordillera: Tectonics, v. 19, p. 1-24.

Hudnut, K., Shen, Z., Murray, M., McClusky, S. , King, R. , Herring, T., Hager, B., Feng, Y., Fang, P., Donnellan, A., and Bock, Y. , 1996, Co-seismic displacements of the 1994 Northridge, California, earthquake: Seismological Society of America Bulletin, v. 86, p. S19-S36.

Jeyakumaran, M., Rudnicki, J.W., and Keer, L.M., et al., 1992, Modeling slip zones with triangular dislocation elements, Bulletin of the Seismological Society of America, 82, 2153-2169.

Kattenhorn, S.A., Aydin, A., and Pollard, D.D., 2000, Joints at high angles to normal fault strike: an explanation using 3-D numerical models of fault-perturbed stress fields, Journal of Structural Geology, 22, p. 1-23.

Lettis, W.R., Bachhuber, J.L., Witter, R.C., Brankman, C.M., Randolph, C.E., Barka, A., Page, W.D., and Kaya, A., 2001, Influence of releasing stopovers on surface fault rupture and fault segmentation: examples from the August 17, 1999 Kocaeli earthquake on the North Anatolian Fault, Turkey, submitted to Bulletin of the Seismological Society of America.

Maerten, L., Willemse, E.J.M., Pollard, D.D., and Rawnsley, K.D., 1999, Slip distributions on intersecting normal faults, Journal of Structural Geology, 21, 3, p. 259-271.

Meltzer, A.S., 1988, Crustal structure and tectonic evolution: central California: Ph.D. dissertation, Rice University, Houston, Texas, 284 p. plus plates.

Moxon, I.W., and Graham, S.A., 1987, History and controls of subsidence in the Late Cretaceous-Tertiary great Valley forearc basin, California: Geology, v. 15, p. 626-629.

O'Connell, D.R.H., and Unruh, J.R., 2000, Updated Evaluation of Faults Within 10 km of Monticello Dam, Solano Project: U.S. Bureau of Reclamation, Report 99-5, .

Roering, J.J., Arrowsmith, J.-R., and Pollard, D.D., 1996, Characterizing the deformation and seismic hazard of a blind thrust fault near Stanford, California; coeseismic elastic modeling, Open File Report OF 96-0267, U. S. Geological Survey, p. 41-44.

Taboada, A., Bousquet, J.C., and Philip, H., 1993, Coseismic elastic models of folds above blind thrusts in the Betic Cordilleras (Spain) and evaluation of seismic hazard, Tectonophysics, 220, 1-4, p. 223-241.

Thomas, A.L., 1993, Poly3D: A three-dimensional, polygonal element, displacement discontinuity boundary element computer program with applications to fractures, faults, and cavities in the Earth's crust, MS thesis, Stanford University.

Willemse, E.J.M., Pollard, D.D., and Aydin, A., 1996, Three-dimensional analyses of slip distributions on normal fault arrays with consequences for fault scaling, Journal of Structural Geology, 18, p. 295-309.

Dickinson, W.R., and Snyder, W.S., 1979, Geometry of subducted slabs related to the San Andreas transform: Journal of Geology, v. 87, p. 609-627.

Jennings, C.W., 1994, Fault activity map of California and adjacent areas, with locations and ages of recent volcanic eruptions: California Department of Conservation, Division of Mines and Geology, Geologic Data Map No. 6, scale 1:750,000.

Wakabayashi, J., and Moores, E.M., 1988, Evidence for collision of the Salinian block with the Franciscan subduction zone, California: Journal of Geology, v. 96, p. 245-253.

Page, B.M., 1982, Migration of the Salinian composite block, California, and disappearance of fragments: American Journal of Science, v. 282, p. 1694-1734.

Platt, J.P., 1986, Dynamics of orogenic wedges and uplift of high-pressure metamorphic rocks: Geological Society of America Bulletin, v. 97, p. 1037-1053.

William Lettis & Associates, 1997, Seismotectonic evaluation: Stony Gorge and East Park Dams, Orland Project; Monticello Dam, Solano Project: Final Report prepared for the Bureau of Reclamation, U.S. Department of Interior, Denver, Colorado, 146 p. plus appendices and plates.

Bull, William B., 1991,Geomorphic responses to climatic change: Oxford Univ. Press. New York, NY, United States, p. 326.

Schumm, S. A., 1977, The Fluvial System: John Wiley and Sons, New York, 338 p.

Stearns, Richard G., 1967, Warping of the Western Highland Rim peneplain in Tennessee by ground-water sapping: Geological Society of America Bulletin.78; 9, Pages 1111-1124.

Strahler, Arthur N., 1952, Dynamic basis of geomorphology: Geological Society of America Bulletin.63; 9, Pages 923-938. 1952.

Chapter 4 References

Ake, J., 1991 Seismicity in the Sierra Foothills of California, Preliminary Investigations: U.S. Bureau of Reclamation Seismotectonic Report 91-1, Denver, Colorado, 34 pp.

Allen, C. R., 1982, Reservoir-induced seismicity earthquakes and engineering policy, California Geology, November 1982, p. 248-250.

Argus, D. F. and Gordon, R. G., 1991, Current Sierra Nevada-North American motion from Verly Long Baseline Interferometry: implications for the kinematics of the western United States: Geology, v. 19, p. 1085 -1088.

Benz, H. M., Zandt, G. and Oppenheimer, D. H., 1992, Lithospheric structure of northern California from teleseismic images of the upper mantle, v. 97, p. 4791- 4807.

Bolt, B. A. and Miller, R. D., 1975, Catalog of earthquakes in northern California and adjoining area 1 January 1910-31December 1972, Seismographic Stations, University of California, Berkeley, 567 pp.

Castillo, D. A., and Ellsworth, W. L., 1993, Seismotectonics of the San Aandreas fault system between Point Arena and Cape Mendocino in Northern California: Implications for the development and evolution of a young transform, Journal of Geophysical Research, v. 98, p. 6543-6560.

Clark, M. M., Sharp, R. V., Castle, R. O., and Harsh, P. W., 1976, Surface faulting near Lake Oroville in August 1975, Bulletin of the Seismological Society of America, v. 66, p. 1101-1110.

Clarke, S. H. and McLaughlin, R. J., 1992, Neotectonic framework of the southern Cascadia subduction zone-Mendocino triple junction region: in Burke, R. M. and Carver, G. A., eds., Friends of the Pleistocene Guidebook for the Field trip to Northern Coastal California, June 1992.

Dickinson, W. R., and Snyder, W. S., 1979, Geometry of subducted slabs related to the San Andreas transform, Journal of Geology, v. 87, p. 609-627.

Eberhart-Phillips, D. and Oppenheimer, D. H., 1984, Induced seismicity in the Geysers geothermal area, California, Journal of Geophysical Research, v. 89, p. 1191-1207.

Ellsworth, W. L., 1991, Earthquake History, 1769-1989: in Wallace, R. E., The San Andreas Fault System, California, U.S. Geological Survey Professional Paper 1515, p. 153-187.

Engdahl, E. R. and Rinehart, W. A., 1991, Seismicity map of North America project: in Slemmons, D. B., Engdahl, E. R., Zoback, M. D., and Blackwell, D. D., eds., Neotectonics of North America, p. 21-27, Geological Society of America Decade Map Volume 1, Boulder, Colorado.

Godfrey, N. J., Beaudoin, B. C., and Klemperer, S. L., 1997, Ophiolitic basement to the Great Valley forearc basin, California, from seismic and gravity data: Implications for crustal growth at the North American continental margin, Geological Society of America, v. 108, p. 1536-1562.

Godfrey, N. J. and Dilek, Y., 2000, Mesozoic assimilation of oceanic crust and island arc into the North American continental margin in California and Nevada: Insights from geophysical data, XXXXXXXXXXXXXXX

Gupta, H. K., 1992, Reservoir-induced earthquakes, Elsevier, New York, 364 pp.

Harwood, D. S., and Helley, E. J., 1987, Late Cenozoic tectonism of the Sacramento Valley, California, U.S. Geological Survey Professional Paper 1359, 46 pp.

Hill, D. P., Eaton, J. P., Ellsworth, W., L., Cockerham, R. S., and Lester, F. W., 1991, The seismotectonic fabric of central California: in Slemmons, D. B., Engdahl, E. R., Zoback, M. D., and Blackwell, D. D., eds., Neotectonics of North America, p. 107-132, Geological Society of America Decade Map Volume 1, Boulder, Colorado.

Jachens, R. C. and Griscom, A., 1983, Three-dimensional geometry of the Gorda plate beneath northern California, Journal of Geophysical Research, v. 88, p.9375-9392.

Jachens, R. C., Griscom, A., and Roberts, C. W., 1995, Regional extent of Great Valley basement west of the Great Valley, California: Implications for extensive tectonic wedging in the California Coast Ranges, Journal of Geophysical Research, v. 100, p.12769-12790.

Jennings, C., 1994, Fault activity map of California and adjacent areas, California Division of Mines and Geology, California Geologic Data Map Series, Map No. 6.

Klein, F. W., Eaton, J. P., and Lester, F. W., 1988, Seismic station data for northern California and surrounding area, U.S. Geological Survey Open File Report 88-448.

Lachenbruch, A. H. and Sass, J. H., 1980, Heat flow and energetics of the San Andreas fault zone, Journal of Geophysical Research, v. 85, p.6185-6222.

LaForge, R. C. and Hawkins, F. F., 1986, Seismotectonic study of northernmost California for the Shasta, Keswick, Spring Creek debris, Trinity, Lewiston and Whiskeytown Dams, Central Valley Project, U. S. Bureau of Reclamation, Seismotectonic Report 86-1, 130 pp.

Langston, C. A. and Butler, R., 1976, Focal mechanism of the August 1, 1975 Oroville earthquake, Bulletin of the Seismological Society of America, v. 66, p. 1111-1120.

McPherson, R. C., 1989, Seismicity and focal mechanisms near Cape Mendocino, northern California: 1974-1984, masters thesis, Humboldt State University, Arcata, California, 75 pp.

Mount, V. S. and Suppe, J., 1987, State of stress near the San Andreas fault: Implications for wrench tectonics, Geology, v. 15, p. 1143-1146.

Oppenheimer, D., Klein, F., Eaton, J., and Lester, F., 1993, The Northern California Seismic Network Bulletin, January – December 1992, U.S. Geological Survey Open File Report 93-578, 45 pp.

Packer, D. R., Cluff, L. S., Kneupfer, P. L., and Withers, R. J., 1979, A study of reservoir-induced seismicity, Woodward-Clyde Consultants, U.S.A.

Real, C. R., Toppozada, T. R., and Parke, D. L., 1978, Earthquake catalog of California, January 1, 1900-December 31, 1974, California Division of Mines and Geology Special Publication 52, 15 pp.

Reasenberg, P. A. and Oppenheimer, D. H., 1985, FPFIT, FPPLOT, and FPPAGE: Fortran computer programs for calculating and displaying earthquake fault-plane solutions, U. S. Geological Survey Open File Report 85-739, 109 pp.

Richter, C. F., 1958, Elementary Seismology: W. H. Freeman and Company, Inc., San Francisco and London, 534 pp.

Scholz, C. H., 1990, The mechanics of earthquakes and faulting, Cambridge University Press, Cambridge, 439 pp.

Smith, S. W. and Knapp, J. S., 1980, The northern termination of the San Andreas fault: in Streitz, R. and Sherburne, R. S., eds., Studies of the San Andreas Fault Zone in Northern California, California Division of Mines and Geology Special report 140, p. 153-164.

Tobin, D. G. and Sykes, L. R., 1968, Seismicity and tectonics of the northeast Pacific Ocean, Journal of Geophysical Research, v. 73, p. 3821-3845.

Toppozada, T. R., Real, C. R., and Parke, D. L., 1981, Preparation of isoseismal maps and summaries of reported effects for pre-1900 California earthquakes, California Division of Mines and Geology Open File Report 81-11 SAC, 182 pp.

Toppozada, T. R. and Morrison, P. W., 1982, Earthquakes and lake levels at Oroville, California, California Geology, v. 35, p. 115-118.

Townley, S. D. and Allen, M. W., 1939, Descriptive catalog of earthquakes of the Pacific Coast of the United States 1869 to 1928, Seismological Society of America Bulletin, v. 29, p. 1-297.

Urhammer, R. A., 1991, Northern California seismcity: in Slemmons, D. B., Engdahl, E. R., Zoback, M. D., and Blackwell, D. D., eds., Neotectonics of North America, p. 99-106, Geological Society of America Decade Map Volume 1, Boulder, Colorado.

Urhammer, R. A. and Wright D. H., 1985, Pattern analysis of small explosions and earthquakes recorded near Lake Shasta, California (1952-1963), Bulletin of the Seismological Society of America.

Walter, S. R., 1986, Intermediate focus earthquakes associated with Gorda plate subduction in northern California, Bulletin of the Seismological Society of America, v. 76, p. 583-588.

WLA (Wm. Lettis & Associates), 1997, Seismotectonic evaluation, Stony Gorge and East Park Dams (Orland Project) and the Monticello Dam (Solano Project), Northern Coast Ranges, California, prepared for U.S Bureau of Reclamation, Denver, Colorado, 145 pp.

Wong, I. G., 1991, Contemporary seismicity, active faulting and seismic hazards of the Coast Ranges between San Francisco bay and Healdsburg, California, Journal of Geophysical Research, v. 96, p. 19891-19904.

Wong, I. G. and Ely, R. W., 1983, Historical seismicity and tectonics of the Coast Ranges-Sierran Block boundary: Implications to the 1983 Coalinga, California earthquakes: in Bennett, J. H. and Sherburne, R. W., eds., The 1983 Coalinga, California Earthquake, California Division of Mines and Geology Special Report 66, p. 89-104.

Wright, L. A., Late Cenozoic fault patterns and stress fields in the western Great Basin and westward displacement of the Sierra Nevada block, Geology, v. 4, p. 489-494.

Zoback, M. D. and Zoback, M. L., 1989, Tectonic stress field of the continental United States: in Pakiser, L. C. and Mooney, W. D., eds., Geophysical framework of the continental United States, Geological Society of America Memoir 172, p. 523-540.

3.4.2.3 Activity Assessment, Salt Lake Fault

Based on evidence for a minimum of three surface-faulting events that have deformed a gravel deposit estimated to be 100 ka in age, we conservatively conclude that the Salt Lake fault likely has been active during the past 35,000 years. The fault should thus be considered active per DSOD (1995) criteria.

Although the Salt Lake fault exhibits evidence for multiple late Quaternary surface ruptures, we do not believe that the fault is likely to be an independent source of moderate to large earthquakes. Seismic reflection data analyzed for this study (Appendix A) show that the Salt Lake fault dips east, parallel to bedding in adjacent strata of the Great Valley group, and terminates downdip against the Funks segment of the Great Valley fault at a maximum depth of 5 km (Figure 3-2). These relations indicate that the Salt Lake fault is confined to the shallow upper crust where little seismic moment is released during earthquakes; the fault does not extend to deeper, higher-strength regions of the crust where significant elastic strain energy accumulates and moderate to large magnitude earthquakes nucleate (Sibson, 1982). We therefore conclude that the Salt Lake fault probably is not capable of storing and releasing significant elastic strain energy.

Our preferred explanation for Quaternary surface rupture is that triggered or sympathetic movement occurs on the Salt Lake fault moves during moderate to large magnitude earthquakes on the underlying Funks segment of the Great Valley fault. Triggered slip on faults from nearby earthquakes is a relatively well-documented phenomenon. For example, triggered aseismic slip was observed on thrust faults in the southwestern Santa Clara Valley following the 1989 Loma Prieta earthquake, which occurred on a blind reverse-oblique fault beneath the Santa Cruz mountains to the southwest (Hitchcock and Kelson, date). Triggered, aseismic slip also was documented on the Hilton Creek fault, an active segment of the Sierra Nevada frontal fault system, during a sequence of moderate earthquakes in Long Valley caldera to the north in 1980 (ref, date).

A more relevant example, and a potential analogue for the Salt Lake fault, is the Nunez fault, which is located along the western margin of the San Joaquin Valley in the Coast Ranges-Sierran Block boundary zone (CRSBZ) and is associated with the Coalinga anticline. The Nunez fault produced localized surface rupture, and possibly several small (M 5) aftershocks in the upper 5 km of the crust, following the 1983 M 6.3 Coalinga

earthquake on a segment of the Great Valley fault at 10-13 km depth (Hart and McJunkin, 1983). Like the Salt Lake fault, the Nunez fault dips east and is antithetic to the west-dipping thrust fault that was the source of the mainshock. The example of the Nunez fault suggests that relatively shallow reverse faults in the CRSBZ may produce localized surface rupture during moderate to large magnitude earthquakes on blind thrust faults, rather than acting as independent seismic sources.

Using the Nunez fault as an analogue, we infer that the relatively shallow Salt Lake fault may rupture at the surface sympathetically during or following a larger event on the Funks segment of the Great Valley fault at depth. It is possible that the Salt Lake fault may produce some aftershocks following an earthquake on the Funks segment, but given its shallow depth it is not likely to be a significant, independent seismic source for moderate to large magnitude earthquakes.

S-3 Fault text (insert at end of section 3.4.3)

Our preferred interpretation of the S-3 fault is that it has accommodated layer-parallel shearing of bedding during uplift and eastward tilting of the Great Valley group strata along the western margin of the Sacramento Valley. The majority of shearing on the S-3 fault may have occurred in the early stages of uplift and tectonic wedging, as discussed in Section 3.3 (see also Figure 3-3a, b). Based on map relations, we interpret that the original trace of the S-3 fault has been offset by the S-2, GG-3 and GG-2 faults, which we infer to have occurred during growth of the Sites anticline (Figure 3-3c). If this interpretation is correct, and if the S-3 fault remains parallel to bedding downdip, then it is likely that the fault dies out in the upper 3-4 km depth range as the Great Valley strata flatten eastward beneath the Sacramento Valley (Figure 3-2). Like the Salt Lake fault, the S-3 fault lacks significant rupture area and does not extend deep enough to be an independent source of earthquakes (see discussion, section 3.4.2.3). In the current tectonic setting, we infer that the S-3 fault may produce minor, aseismic surface displacement during incremental uplift of the Great Valley associated with a moderate to large earthquake on the underlying Great Valley fault, but it is very unlikely that the S-3 fault is and independent seismic source.

1.3.13 Seismicity Analysis

Historical and instrumentally recorded seismicity in northwestern California was evaluated to identify potential seismic sources capable of generating significant ground motion at the DWR dam sites. The boundaries of the seismicity study region were selected to include potential seismic sources within 100 km of the dam sites and to provide sufficient data to evaluate the seismic activity of potentially significant geologic structures. The study region extends from 38 to 41 degrees north and from 124 to 121 degrees west. Analyses consisted of: compilation of a catalog of earthquake locations and magnitudes; assessment of significant historical earthquakes; evaluation of focal depths; calculation of focal mechanisms; and inversion of seismic P and T axes from focal mechanisms to interpret the orientations and relative magnitudes of the principal stresses.

### 1.3.14 Analysis of Ground Motions

A deterministic analysis was performed to develop ground motion response spectra for preliminary dam design studies. The deterministic analysis uses one or more attenuation relationships to provide an estimate of ground motion at the site based on the largest earthquake that may occur on a fault at the fault's closest approach to the site. The deterministic approach does not consider the rate or probability of earthquake occurrence.

The method to compute the response spectra was dictated by information received in phone conversations in the spring of 2001 with S.Verigin and J.Howard of the California Division of Safety of Dams (DSOD). Based on recommendations from its advisory committee, DSOD prefers a two-step approach for computing maximum earthquake response spectra:

(1) Calculate the 84th-percentile, 5%-damped response spectra from the Abrahamson and Silva (1997) and Sadigh et al. (1997) attenuation equations, and average the results; and
(2) Modify the resulting response spectrum for fault-rupture directivity effects using the procedure in Somerville et al. (1997).

According to DSOD, its advisory committee felt that the Abrahamson and Silva (1997) and Sadigh et al. (1997) equations, published in the January/February 1997 issue of Seismological Research Letters, were better suited for computing ground motions from

shallow crustal California earthquakes than other recent equations, such as those also published in the same SRL issue.

Additional text for the end of Section 5.1.1.1.

The simplest earthquake scenario is a rupture that is limited to the west-dipping ramp, west of point A on Figures 5-2 and 5-3. The 1994 Northridge earthquake in southern California is an example of a thrust-fault earthquake that ruptured a moderately dipping thrust fault in the depth interval between about 20 km and 7 km. Extensive aftershock activity occurred in the upper 7 km of the crust above the mainshock rupture plane (Hauksson et al., 1995), but release of significant seismic energy was confined to the 10-20 km depth interval (Hudnut et al., 1996; Wald et al., 1996). If the Northridge earthquake is an analog for rupture of the Funks segment, then we would anticipate the mainshock rupture to occur on the ramp west of point A (Figures 5-2 and 5-3) and diffuse aftershock activity to occur in the hanging wall block east of point A.

An alternative and more conservative scenario assumes that rupture propagates beyond the abrupt change in fault dip at point A and extends eastward along the flat. There are no documented analogs of California thrust-fault earthquakes where rupture propagated from a ramp to a flat across an abrupt change in fault dip. The 1983 Coalinga earthquake may have propagated upward from a less steeply-dipping fault segment to a more steeply dipping fault segment (Wentworth and Zoback, 1990); however, this is the opposite of the upward-shallowing geometry we infer for the Funks segment (Figures 5-2 and 5-3).

To assess whether coseismic displacement is likely to extend east of the ramp, we used numerical modeling methods to evaluate surface deformation associated with various rupture scenarios for the Funks segment. The modeling methods, results and conclusions are presented in the following sections.

Additional References for Section 7:

Hauksson, E., Jones, L.M. and Hutton, K. , 1995, The 1994 Northridge earthquake sequence in California: seismological and tectonic aspects: Journal of Geophysical Research, v. 100, p. 12,335-12,355.

Hudnut, K.W., Z. Shen, M. Murray, S. McClusky, R. King, T Herring, B. Hager, Y. Feng, P. Fang, A. Donnellan and Y. Bock, 1996, Co-seismic displacements of the 1994 Northridge, California, earthquake: Bulletin of the Seismological Society of America, v.86(1b), p. S19-S36.

Wald, D.J., T.H. Heaton and K.W. Hudnut, The slip history of the 1994 Northridge, California, earthquake determined from strong motion, teleseismic, GPS and leveling data: Bulletin of the Seismological Society of America, v. 86(1b), p. S49-S70.

Wentworth, C. and Zoback, M., 1990, Structure of the Coalinga region and thrust origin of the earthquake, in Rymer, M.J., and Ellsworth, W.L., eds, the Coalinga, California, Earthquake of May 2, 1983: United States Geological Survey Professional Paper 1487, p. 41-68.

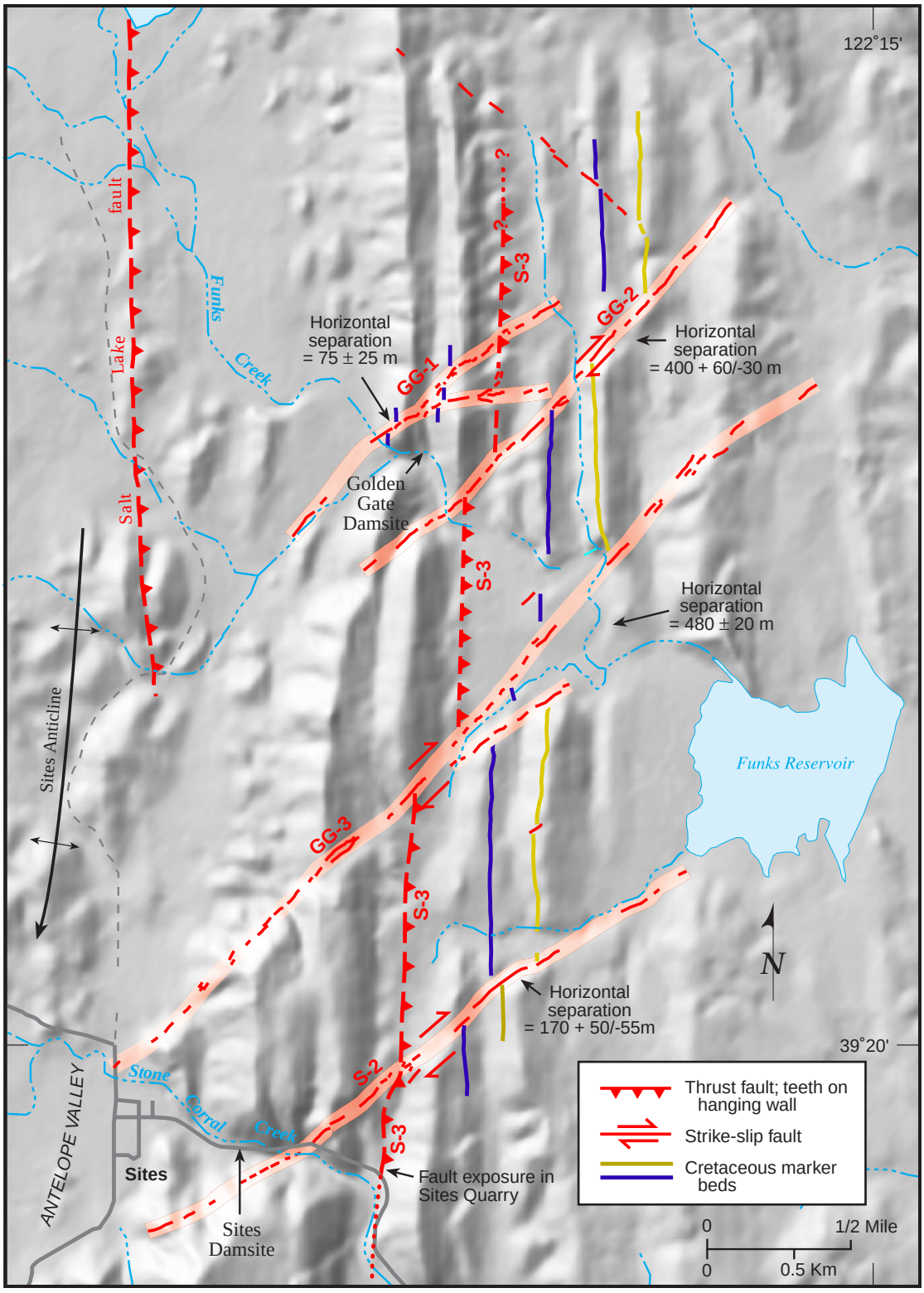


PHASE 2 FAULT AND SEISMIC HAZARDS INVESTIGATION
NORTH OF DELTA OFFSTREAM STORAGE
DWR-INTEGRATED STORAGE INVESTIGATION

**Shaded Relief Map Showing Faults in the Vicinity of the Sites and Golden Gate Damsites**

WLA William Lettis & Associates, Inc. | Figure E-1

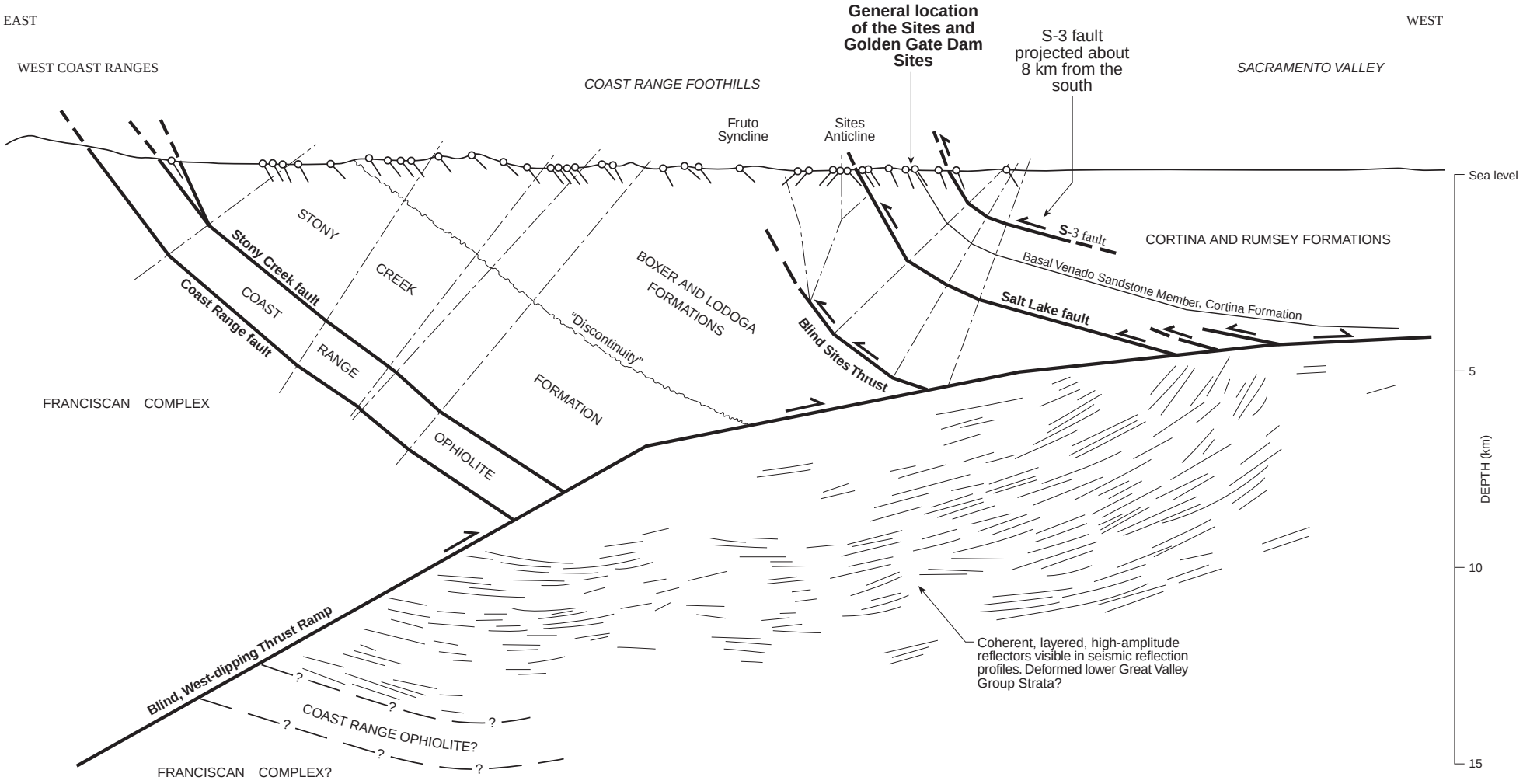


Surface geology modified from Brown and Rich (1961) and Brown (1964)

PHASE 2 FAULT AND SEISMIC HAZARDS INVESTIGATION
NORTH OF DELTA OFFSTREAM STORAGE
DWR-INTEGRATED STORAGE INVESTIGATION

**Cross Section Showing Major Map-scale Structures in the Study Area, and their Relationship to Structures Imaged by Seismic Reflection Profiles**

WLA William Lettis & Associates, Inc. | Figure E-2

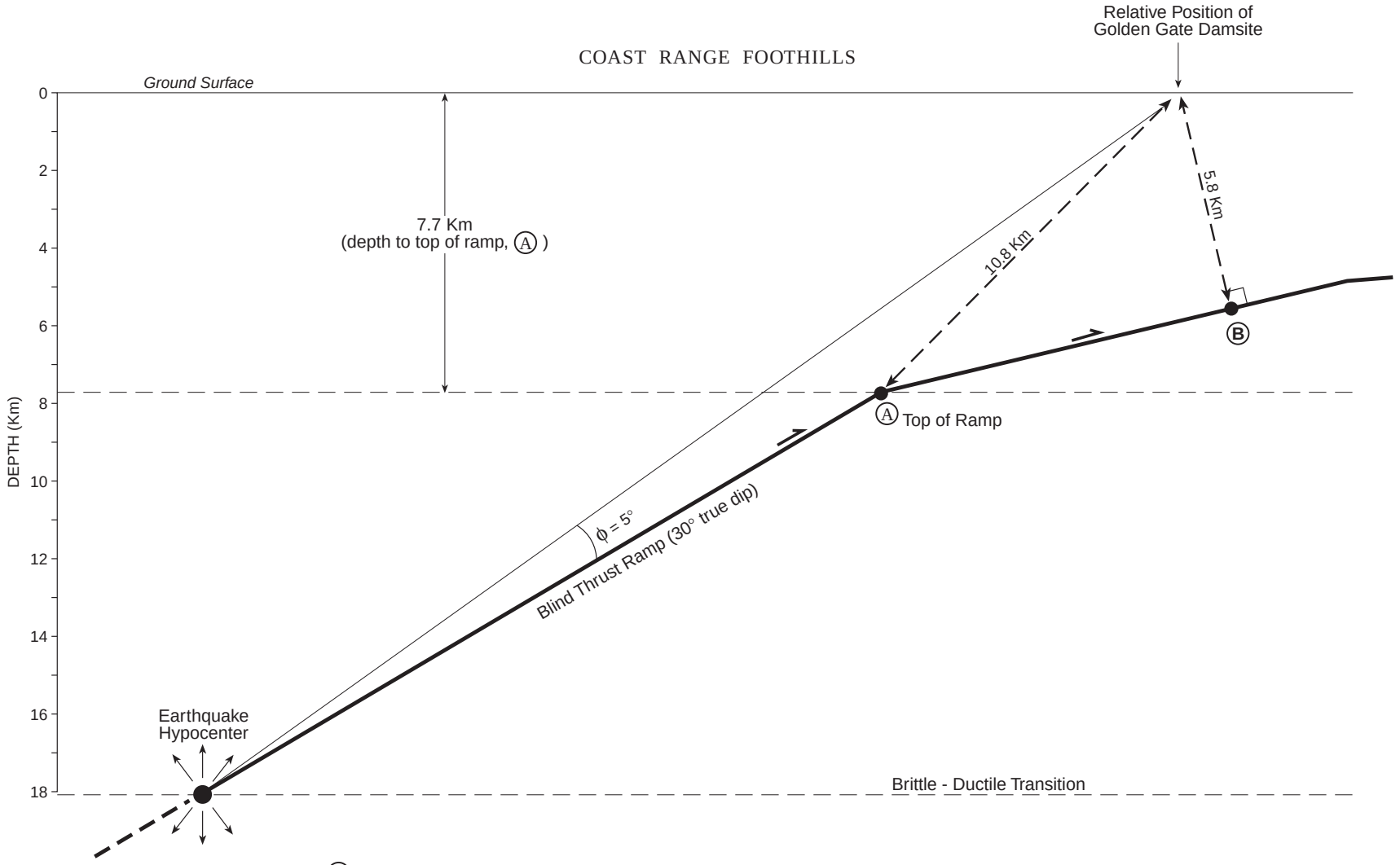


Ⓐ Top of 30°-dipping thrust ramp

Ⓑ Closest approach of thrust fault to dam site

PHASE 2 FAULT AND SEISMIC HAZARDS INVESTIGATION
NORTH OF DELTA OFFSTREAM STORAGE
DWR-INTEGRATED STORAGE INVESTIGATION

**Site-Source Geometry, Golden Gate Damsite**

WLA William Lettis & Associates, Inc.

Figure E-3

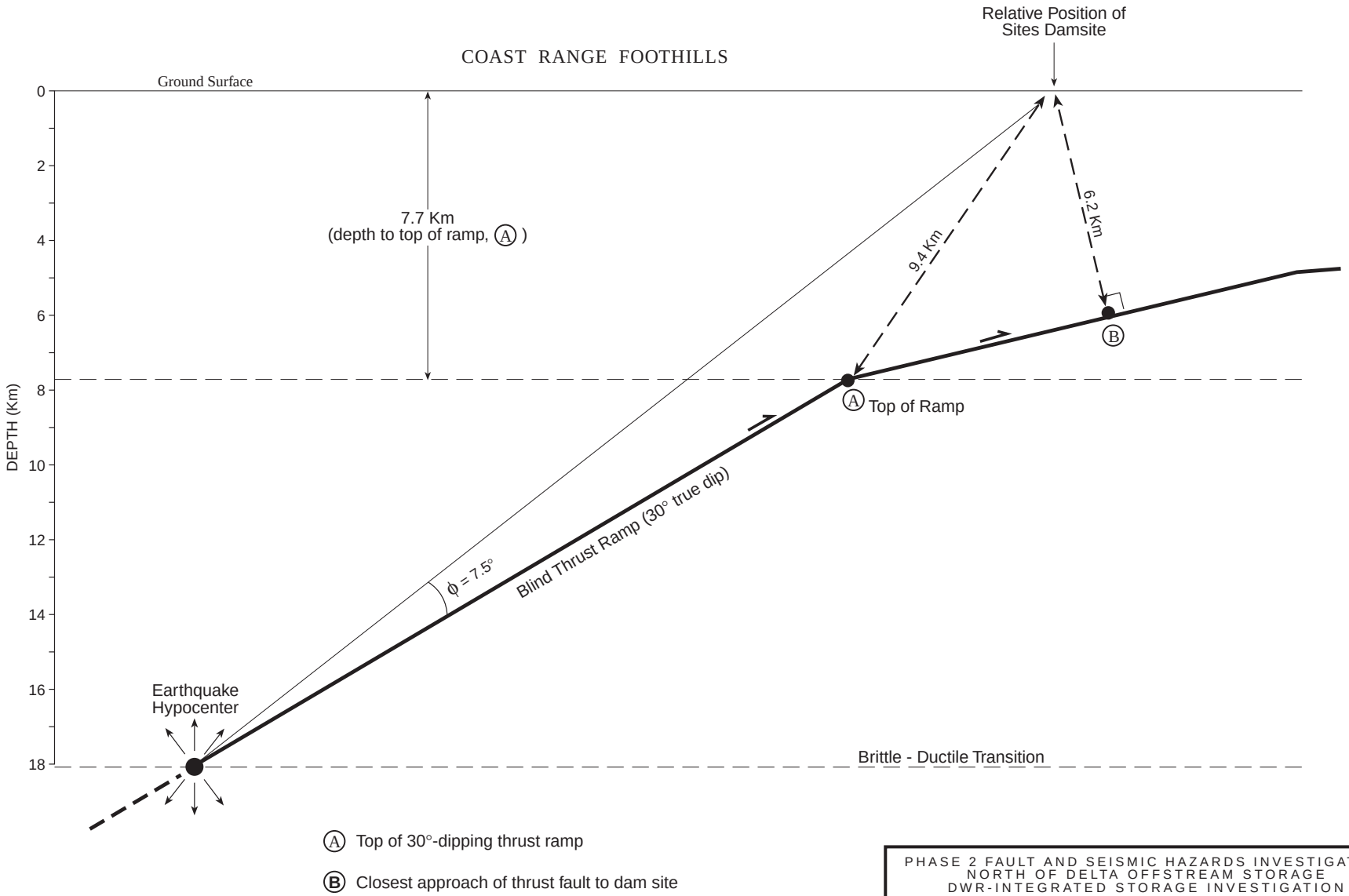


Ⓐ Top of 30°-dipping thrust ramp

Ⓑ Closest approach of thrust fault to dam site

PHASE 2 FAULT AND SEISMIC HAZARDS INVESTIGATION
NORTH OF DELTA OFFSTREAM STORAGE
DWR-INTEGRATED STORAGE INVESTIGATION

**Site-Source Geometry, Sites Damsite**

WLA William Lettis & Associates, Inc.

Figure E-4

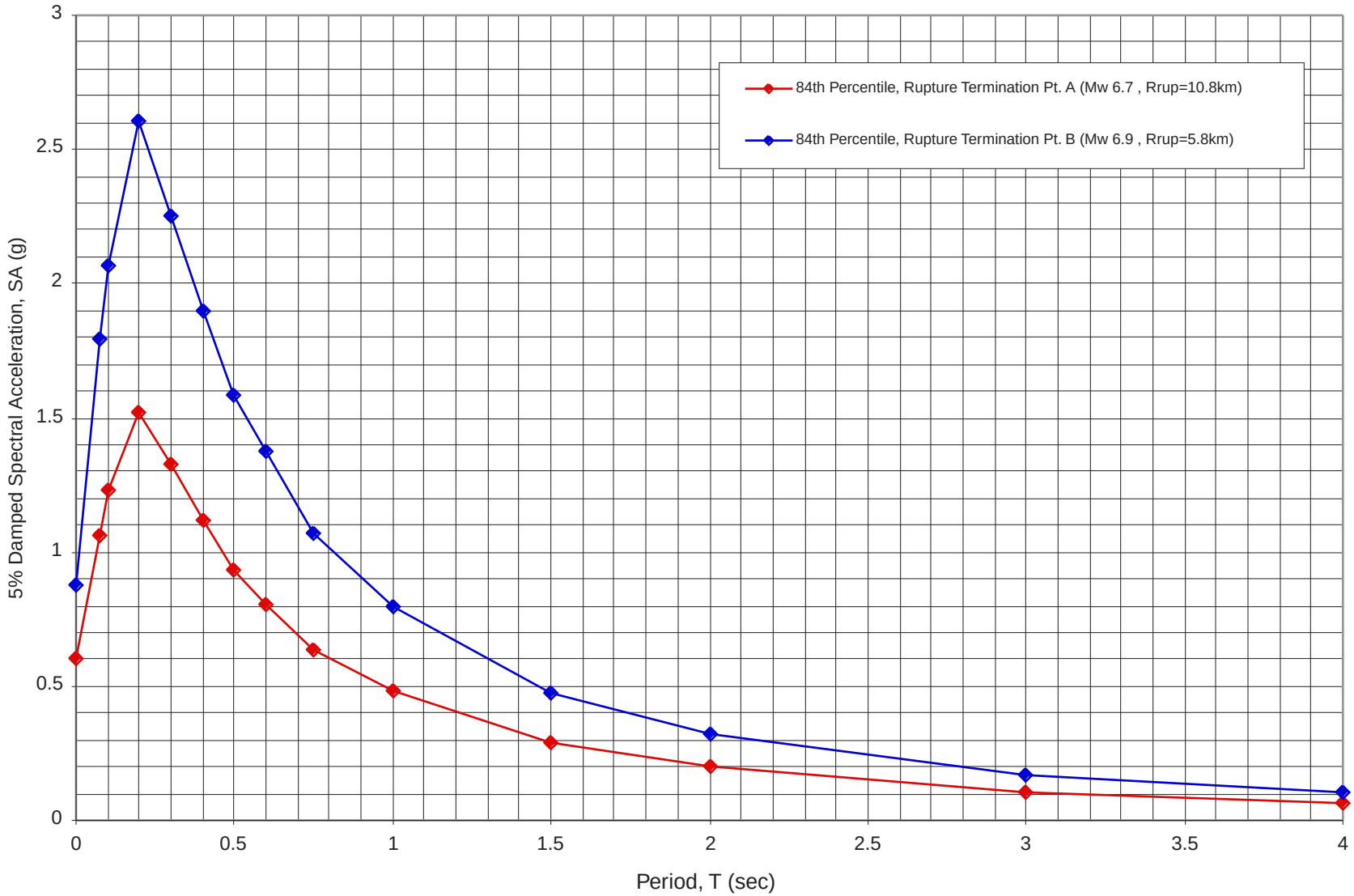


See Figure E-3 for locations of Point A and B relative to the dam site.

PHASE 2 FAULT AND SEISMIC HAZARDS INVESTIGATION
NORTH OF DELTA OFFSTREAM STORAGE
DWR-INTEGRATED STORAGE INVESTIGATION

**Golden Gate Dam Site, California--Average of 84th Percentile Deterministic Response Spectra (Without Directivity)**

WLA William Lettis & Associates, Inc. URS

Figure E-5

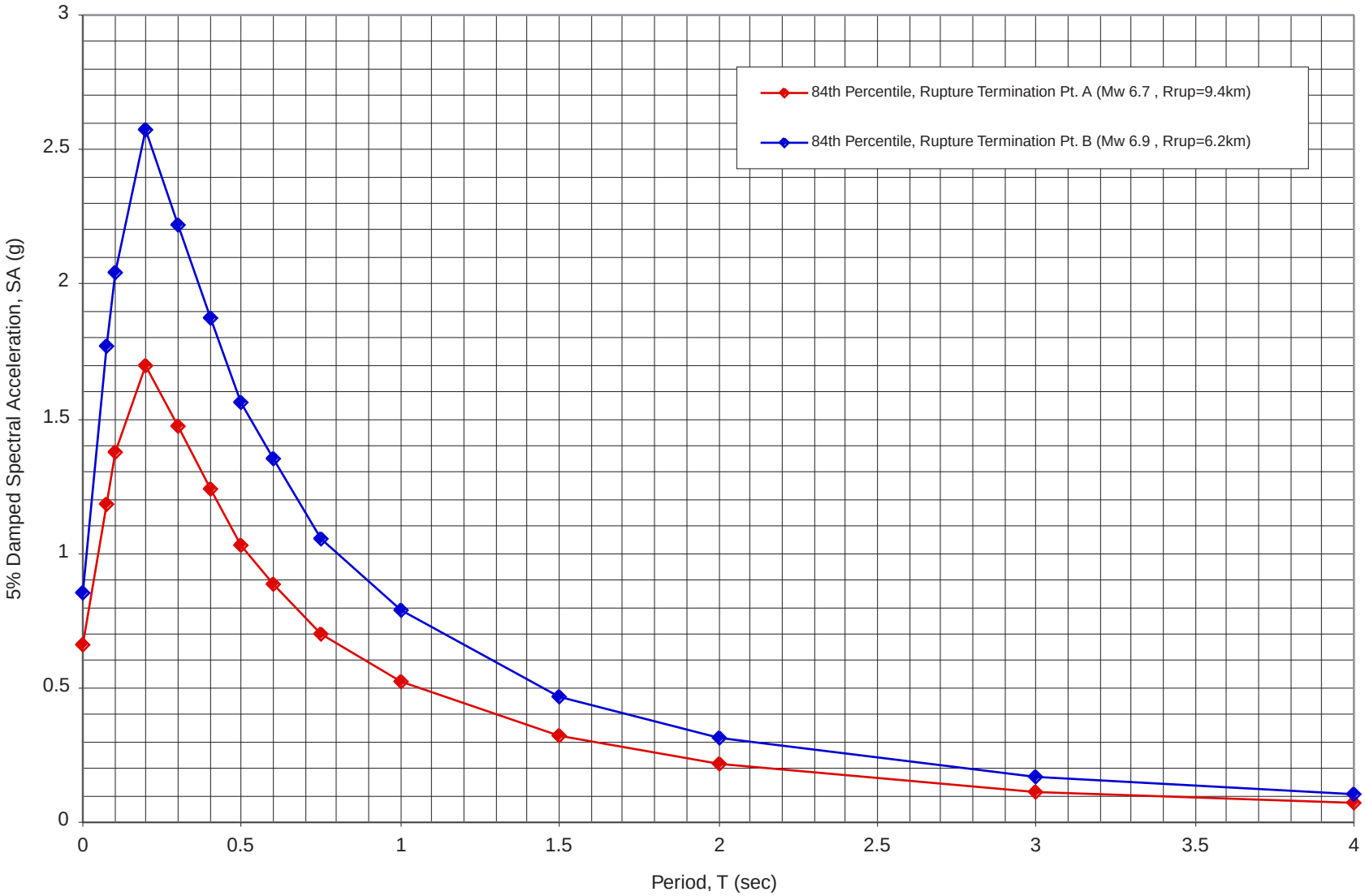


See Figure E-3 for locations of Point A and B relative to the dam site.

PHASE 2 FAULT AND SEISMIC HAZARDS INVESTIGATION
NORTH OF DELTA OFFSTREAM STORAGE
DWR-INTEGRATED STORAGE INVESTIGATION

**Sites Dam Site, California--Average of 84th Percentile Deterministic Response Spectra (Without Directivity)**

WLA William Lettis & Associates, Inc. URS

Figure E-6

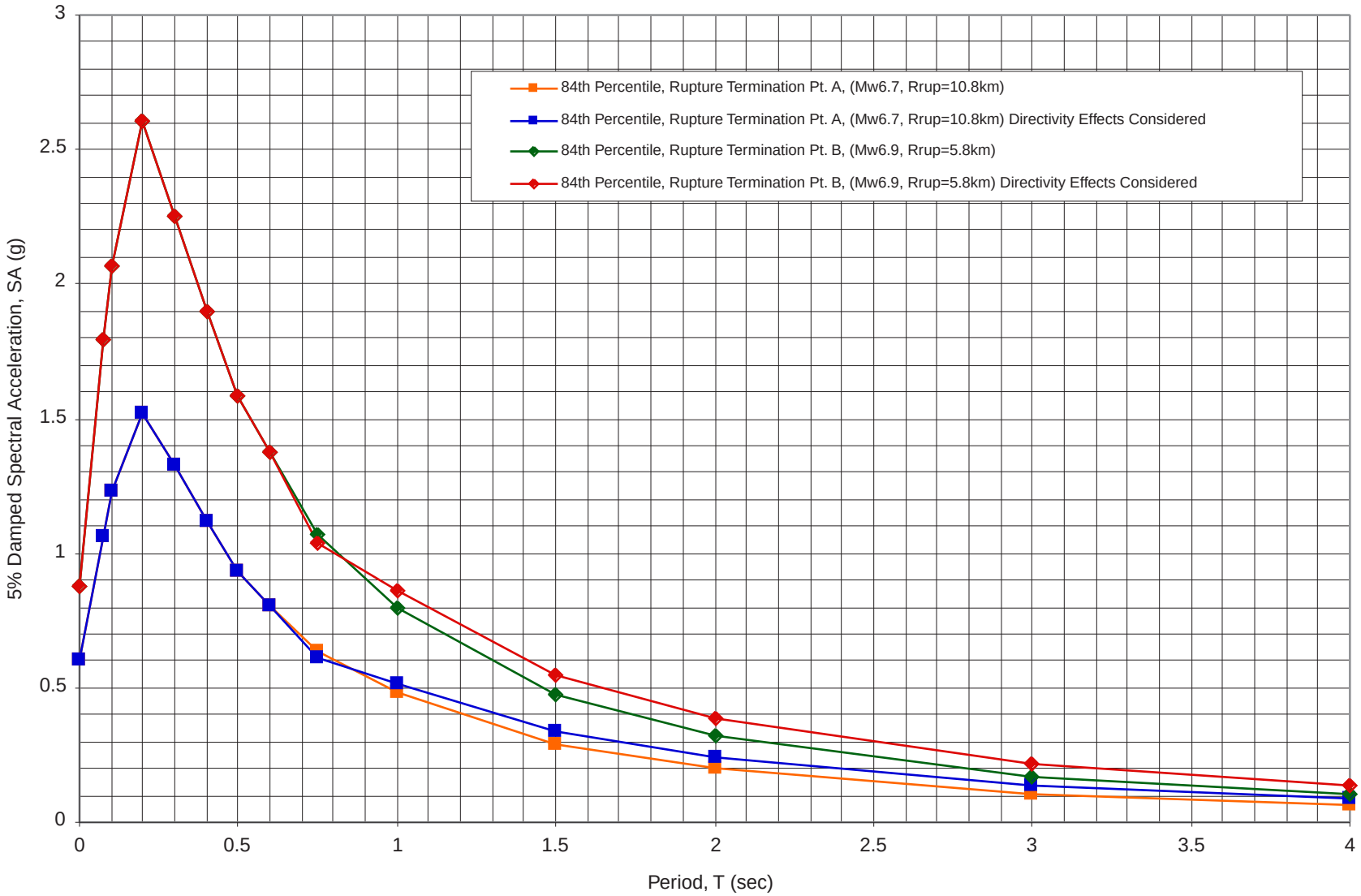


PHASE 2 FAULT AND SEISMIC HAZARDS INVESTIGATION
NORTH OF DELTA OFFSTREAM STORAGE
DWR-INTEGRATED STORAGE INVESTIGATION

**Golden Gate Dam Site, California--84th Percentile Deterministic Response Spectra (With and Without Directivity)**

WLA William Lettis & Associates, Inc. URS Figure E-7

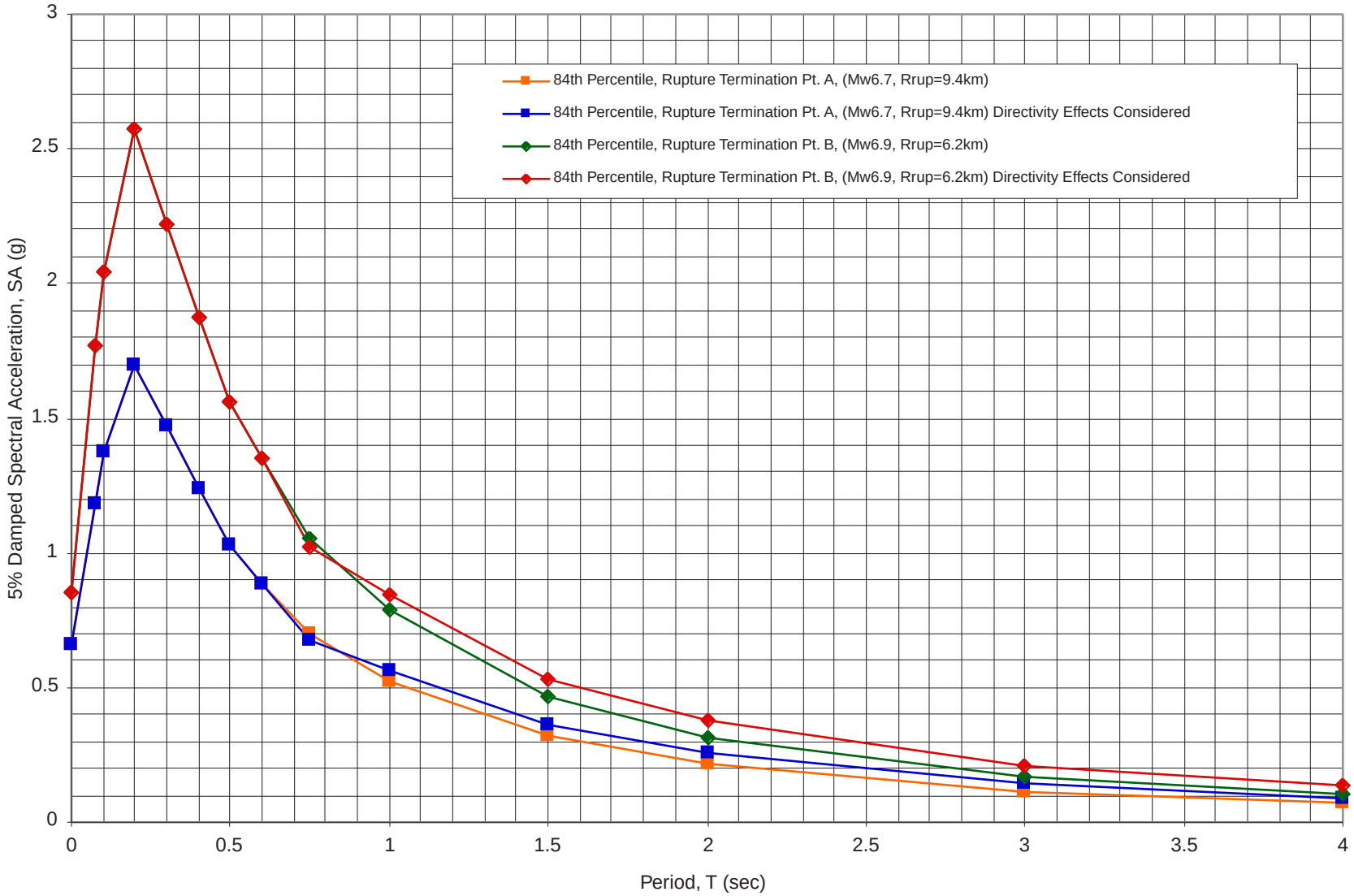


PHASE 2 FAULT AND SEISMIC HAZARDS INVESTIGATION
NORTH OF DELTA OFFSTREAM STORAGE
DWR-INTEGRATED STORAGE INVESTIGATION

**Sites Dam Site, California--84th Percentile Deterministic Response Spectra (With and Without Directivity)**

WLA William Lettis & Associates, Inc. URS

Figure E-8

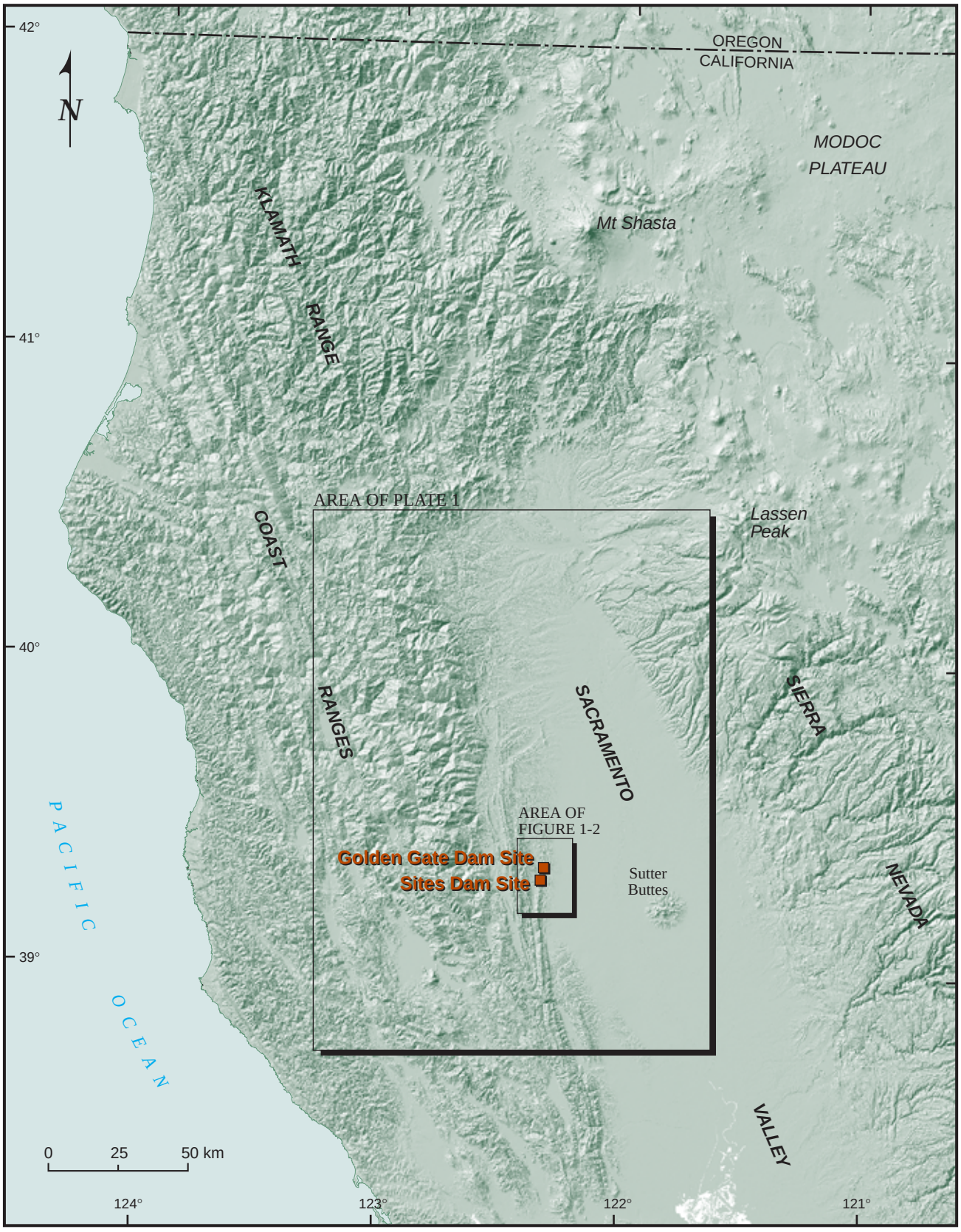


PHASE 2 FAULT AND SEISMIC HAZARDS INVESTIGATION
NORTH OF DELTA OFFSTREAM STORAGE
DWR-INTEGRATED STORAGE INVESTIGATION

**Location of the Sites and Golden Gate dam sites, Northwestern California**

WLA William Lettis & Associates, Inc. | Figure 1-1




0 1 2 km

PHASE 2 FAULT AND SEISMIC HAZARDS INVESTIGATION
NORTH OF DELTA OFFSTREAM STORAGE
DWR-INTEGRATED STORAGE INVESTIGATION

**Location of Sites and Golden Gate Dam Sites, Northwestern Sacramento Valley**

WLA William Lettis & Associates, Inc. | Figure 1-2

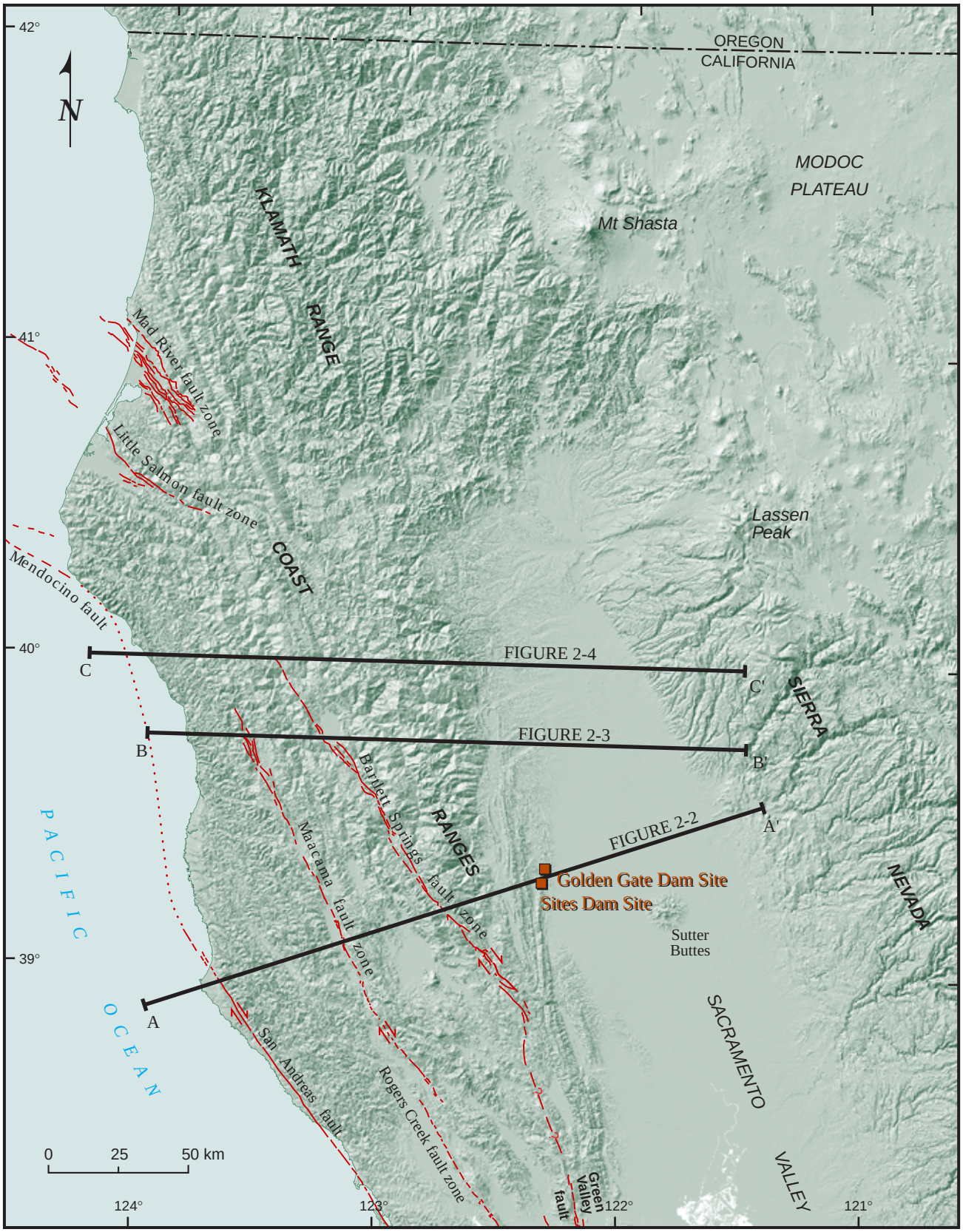


PHASE 2 FAULT AND SEISMIC HAZARDS INVESTIGATION
NORTH OF DELTA OFFSTREAM STORAGE
DWR-INTEGRATED STORAGE INVESTIGATION

**Major Faults of the San Andreas System (south of latitude 40°), and Faults in the Cascadia Forearc Region (north of latitude 40°)**

WLA William Lettis & Associates, Inc. | Figure 1-3

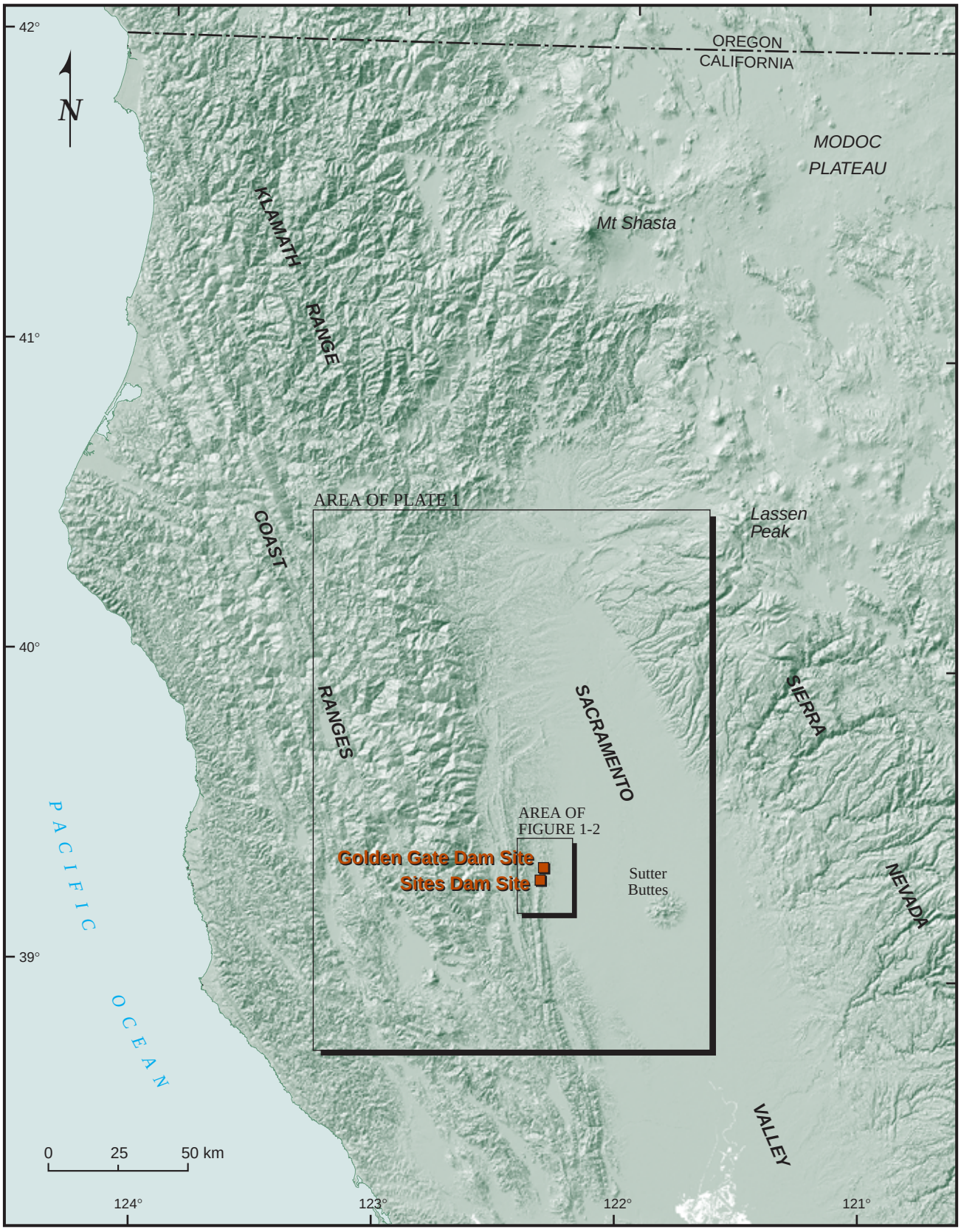


PHASE 2 FAULT AND SEISMIC HAZARDS INVESTIGATION
NORTH OF DELTA OFFSTREAM STORAGE
DWR-INTEGRATED STORAGE INVESTIGATION

**Location of the Sites and Golden Gate dam sites, Northwestern California**

WLA William Lettis & Associates, Inc. | Figure 1-1




0 1 2 km

PHASE 2 FAULT AND SEISMIC HAZARDS INVESTIGATION
NORTH OF DELTA OFFSTREAM STORAGE
DWR-INTEGRATED STORAGE INVESTIGATION

**Location of Sites and Golden Gate Dam Sites, Northwestern Sacramento Valley**

WLA William Lettis & Associates, Inc. | Figure 1-2

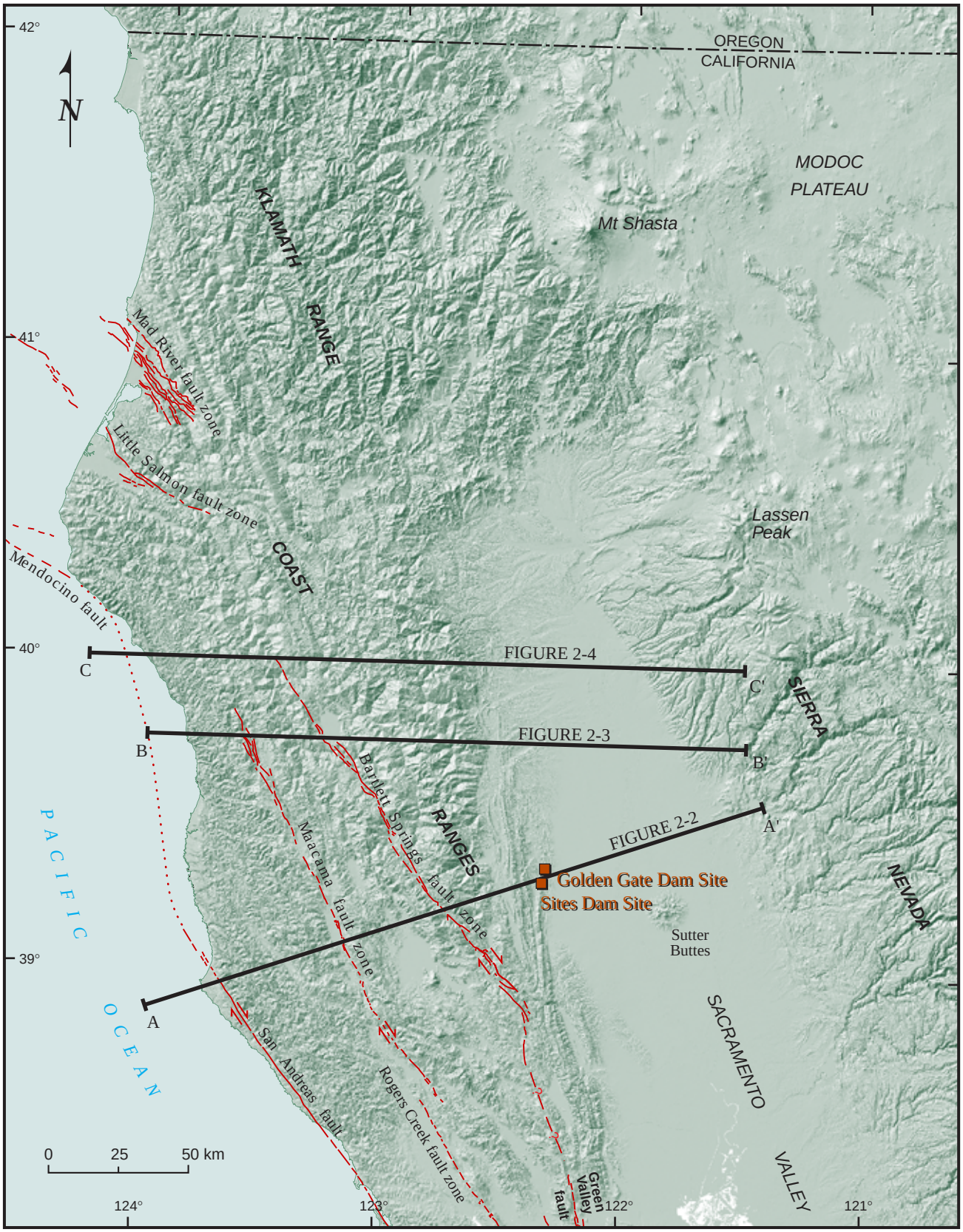


PHASE 2 FAULT AND SEISMIC HAZARDS INVESTIGATION
NORTH OF DELTA OFFSTREAM STORAGE
DWR-INTEGRATED STORAGE INVESTIGATION

**Major Faults of the San Andreas System (south of latitude 40°), and Faults in the Cascadia Forearc Region (north of latitude 40°)**

WLA William Lettis & Associates, Inc. | Figure 1-3

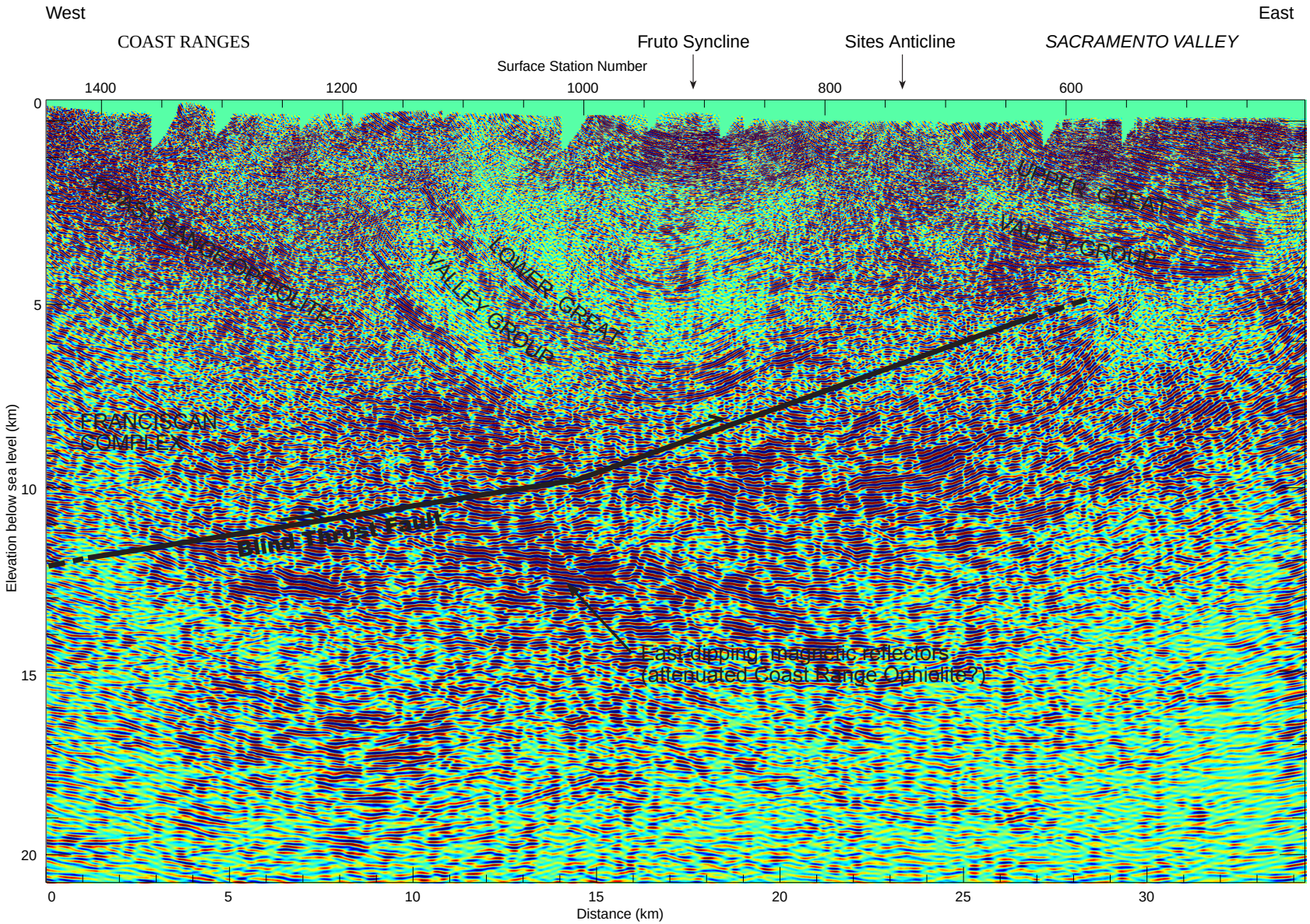


PHASE 2 FAULT AND SEISMIC HAZARDS INVESTIGATION
NORTH OF DELTA OFFSTREAM STORAGE
DWR-INTEGRATED STORAGE INVESTIGATION

**Seismic Reflection Profile Showing Thrust Fault Beneath Folds, Western Sacramento Valley**

WLA William Lettis & Associates, Inc.

Figure 2-1

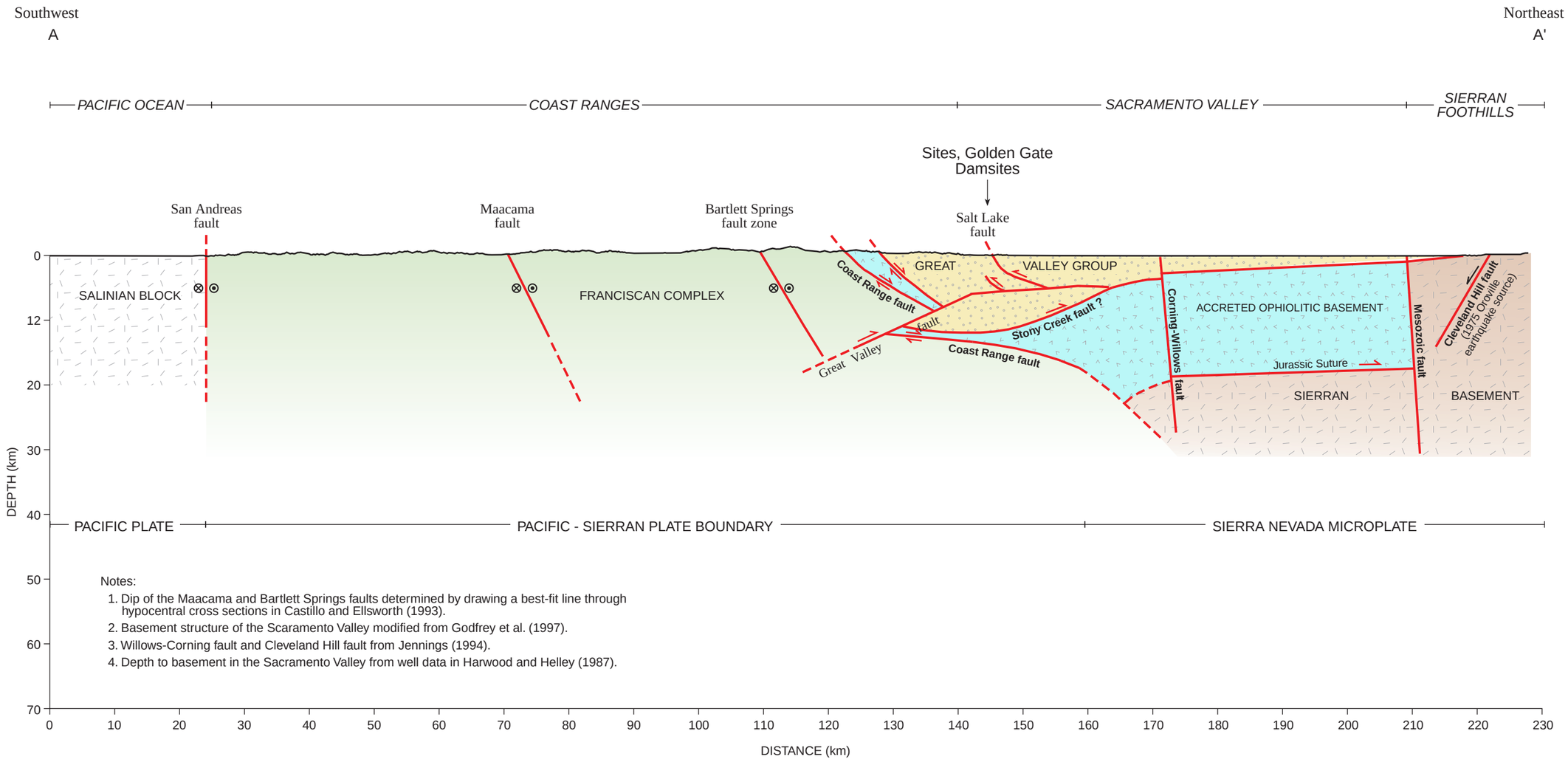


Notes:

1. Dip of the Maacama and Bartlett Springs faults determined by drawing a best-fit line through hypocentral cross sections in Castillo and Ellsworth (1993).
2. Basement structure of the Scaramento Valley modified from Godfrey et al. (1997).
3. Willows-Corning fault and Cleveland Hill fault from Jennings (1994).
4. Depth to basement in the Sacramento Valley from well data in Harwood and Helley (1987).

PHASE 2 FAULT AND SEISMIC HAZARDS INVESTIGATION
NORTH OF DELTA OFFSTREAM STORAGE
DWR-INTEGRATED STORAGE INVESTIGATION

**Regional Cross Section (A-A') through the Northern Coast Ranges, Sacramento Valley, and Western Sierra Nevada Foothills**

WLA William Lettis & Associates, Inc.

Figure 2-2

West

B

East

B'

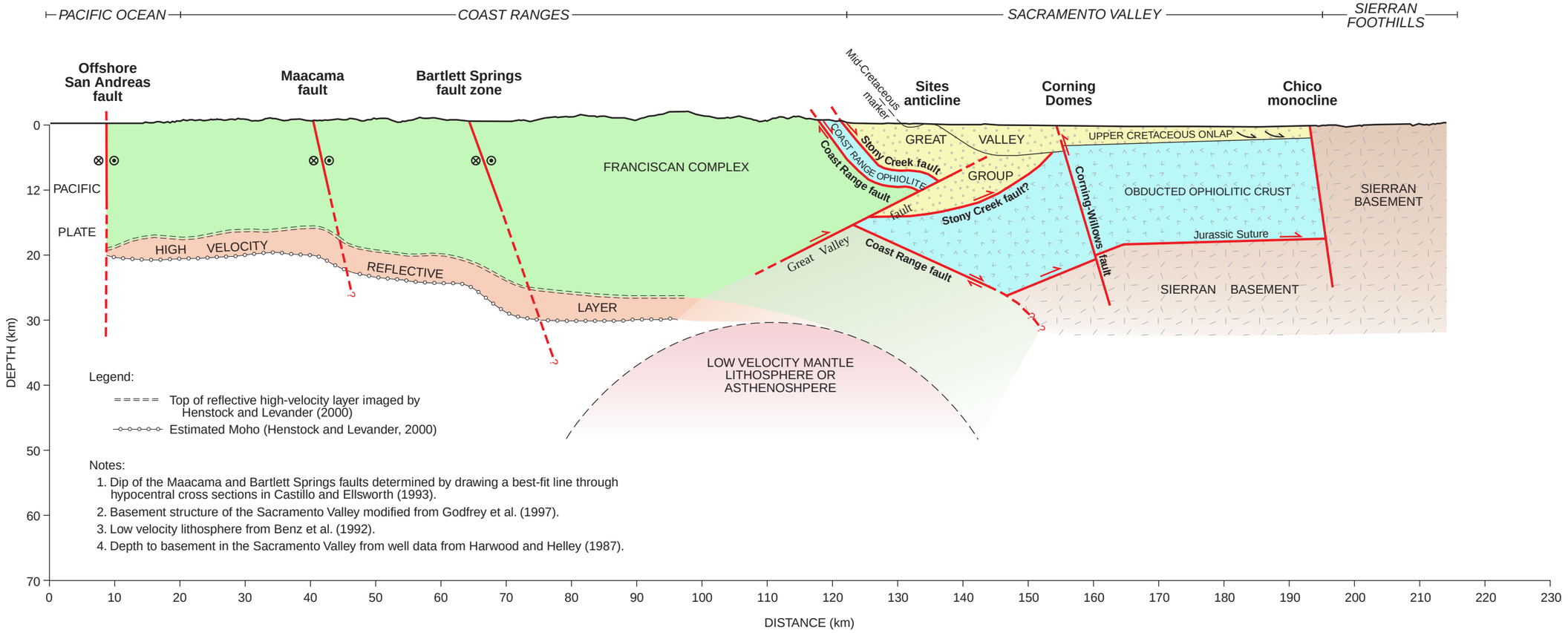


Legend:

===== Top of reflective high-velocity layer imaged by Henstock and Levander (2000)

Estimated Moho (Henstock and Levander, 2000)

Notes:

1. Dip of the Maacama and Bartlett Springs faults determined by drawing a best-fit line through hypocentral cross sections in Castillo and Ellsworth (1993).
2. Basement structure of the Sacramento Valley modified from Godfrey et al. (1997).
3. Low velocity lithosphere from Benz et al. (1992).
4. Depth to basement in the Sacramento Valley from well data from Harwood and Helley (1987).

PHASE 2 FAULT AND SEISMIC HAZARDS INVESTIGATION
NORTH OF DELTA OFFSTREAM STORAGE
DWR-INTEGRATED STORAGE INVESTIGATION

**Regional East-West Cross Section (B-B') at Latitude 39.75°N**

WLA William Lettis & Associates, Inc.

Figure 2-3

West
C

East
C'

PACIFIC OCEAN | COAST RANGES | SACRAMENTO VALLEY | SIERRA NEVADA

San Andreas fault

(Projection of Maacama fault trace from south)

Bartlett Springs fault zone

Coast Range fault

Mid-Cretaceous marker

Sacramento River

Chico Monocline

Cohasset Ridge fault

COAST RANGE OPHIOLITE

GREAT VALLEY GROUP

Stony Creek fault

Corning-Willows fault

ACCRETED OPTHIOLITE

BASEMENT

SIERRAN BASEMENT

FRANCISCAN COMPLEX

PACIFIC PLATE

Base of Crust (underplating?)

Maximum elevation of upwelling asthenosphere

("Slab Window" ?)

Great Valley fault

Coast Range fault

Southern Cascadia Subduction Zone

Southern edge of the Gorda Plate

DEPTH (km)

0
12
20
30
40
50
60
70

0 10 20 30 40 50 60 70 80 90 100 110 120 130 140 150 160 170 180 190 200 210 220 230

DISTANCE (km)

Notes:

1. Location and geometry of the southern edge of the Gorda plate modified from Beaudoin et al. (1998).
2. Dip of the Maacama and Bartlett Springs faults determined by drawing a best-fit line through hypocentral cross sections in Castillo and Ellsworth (1993).
3. Basement structure of the Sacramento Valley modified from Godfrey et al. (1997).
4. Depth to basement in the Sacramento Valley from well data in Harwood and Helley (1987).

PHASE 2 FAULT AND SEISMIC HAZARDS INVESTIGATION
NORTH OF DELTA OFFSTREAM STORAGE
DWR-INTEGRATED STORAGE INVESTIGATION

**Regional East-West Cross Section (C-C') at Latitude 40°N**

WLA William Lettis & Associates, Inc. | Figure 2-4

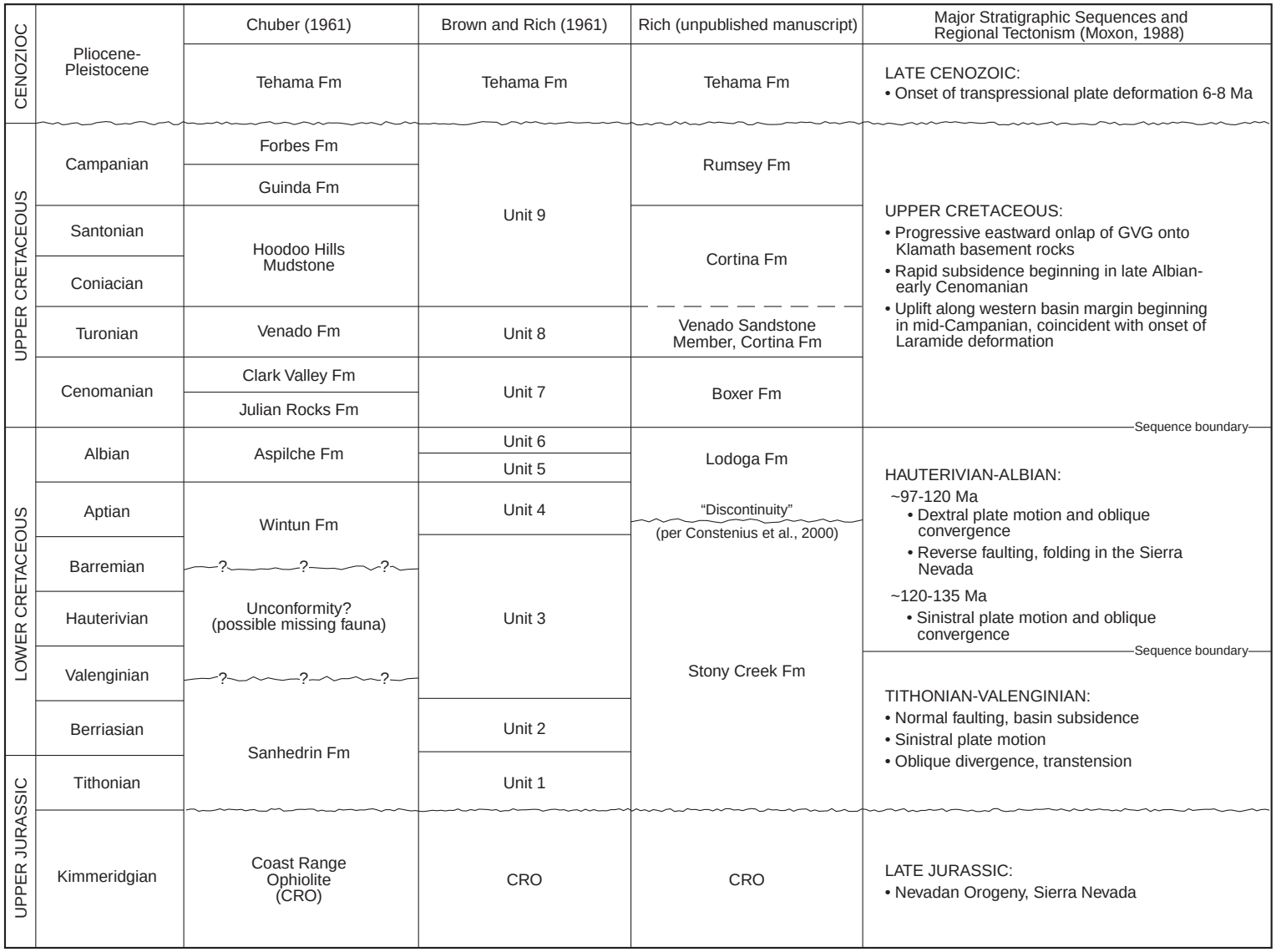


PHASE 2 FAULT AND SEISMIC HAZARDS INVESTIGATION
NORTH OF DELTA OFFSTREAM STORAGE
DWR-INTEGRATED STORAGE INVESTIGATION

**Stratigraphic Correlation Chart for the Study Region**

WLA William Lettis & Associates, Inc. | Figure 2-5

Fault GG-1

Fault GG-2

GG-2 fault exposure

FT-5

FT-4a

FT-4b

FT-4c

FT-3a

FT-3b

GOLDEN GATE
DAM SITE

FUNKS CREEK

bedrock?

fill

EXPLANATION

Fault– solid where feature mapped in field, dotted where inferred; shaded zone delineates wider fault zone based on mapped and inferred faults

FT-7 Trench and test pit location

GEOLOGIC UNITS

| | |
|---|---|
| Qhc | Modern stream channel deposits |
| Qfp | Modern floodplain deposits |
| Qt5 | Historic strath terrace on bedrock |
| Qt5<br>Qt4<br>Qt3<br>Qt2 | Historic Terrace deposits (Qt5-youngest; Qt2 oldest) |
| Qt1 | Late Holocene terrace deposits |
| Qf | Late Holocene alluvial fan deposits |
| Qc | Late Holocene colluvial deposits |
| Qls | Late Holocene landslide |
| Kugv | Undifferentiated Cretaceous Great Valley Group bedrock |

0 100 200 METERS

MATCHLINE WITH FIGURE 2-7

PHASE 2 FAULT AND SEISMIC HAZARDS INVESTIGATION
NORTH OF DELTA OFFSTREAM STORAGE
DWR-INTEGRATED STORAGE INVESTIGATION

**Map of Geomorphic Surfaces and Quaternary Geologic Deposits along Funks Creek in the Vincinity of the Golden Gate Damsite**

WLA William Lettis & Associates, Inc. | Figure 2-6

MATCHLINE WITH FIGURE 2-6

Fault GG-3

FT-7

TPE-1

TPE-2

TPE-3

FUNKS CREEK

FUNKS RESERVOIR

N

EXPLANATION

Fault– solid where feature mapped in field, dotted where inferred; shaded zone delineates wider fault zone based on mapped and inferred faults

FT-7 Trench and test pit location

GEOLOGIC UNITS

- Qhc Modern stream channel deposits
- Qfp Modern floodplain deposits
- Qt5, Qt4, Qt3, Qt2 Historic Terrace deposits (Qt5-youngest; Qt2 oldest)
- Qt1 Late Holocene terrace deposits
- Qf Late Holocene alluvial fan deposits
- Qc Late Holocene colluvial deposits
- Qls Late Holocene landslide
- Kugv Undifferentiated Cretaceous Great Valley Group bedrock

0 100 200 METERS

PHASE 2 FAULT AND SEISMIC HAZARDS INVESTIGATION
NORTH OF DELTA OFFSTREAM STORAGE
DWR-INTEGRATED STORAGE INVESTIGATION

**Map of Geomorphic Surfaces and Quaternary Geologic Deposits along Funks Creek in the Vicinity of Golden Gate Dam Site**

WLA William Lettis & Associates, Inc. Figure 2-7




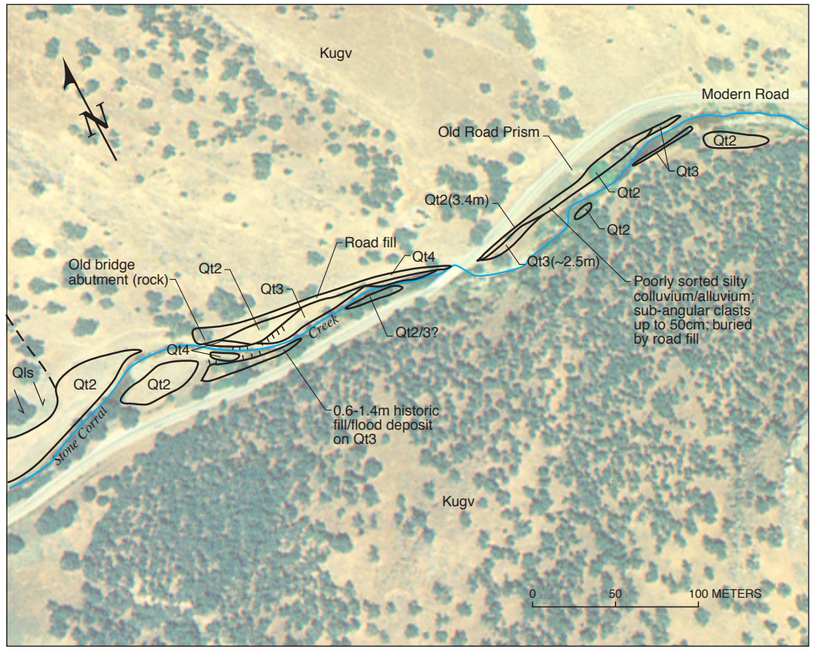


EXPLANATION

- Photo lineament (based on interpretation of aerial photograph)
- Fault– solid where feature mapped in field, dotted where inferred; shaded zone delineates wider fault zone based on mapped and inferred faults
- FT-7 — Trench and test pit location

GEOLOGIC UNITS

| | |
|---|---|
| Qhc | Modern stream channel deposits |
| Qhc | Modern floodplain deposits |
| Qt5 | Historic strath terrace on bedrock |
| Qt5, Qt4, Qt3, Qt2 | Historic Terrace deposits (Qt5-youngest; Qt2 oldest) |
| Qt1 | Late Holocene terrace deposits |
| Qf | Late Holocene alluvial fan deposits |
| Qc | Late Holocene colluvial deposits |
| Qls | Late Holocene landslide |
| Kugv | Undifferentiated Cretaceous Great Valley Group bedrock |

0 100 200 METERS

PHASE 2 FAULT AND SEISMIC HAZARDS INVESTIGATION
NORTH OF DELTA OFFSTREAM STORAGE
DWR-INTEGRATED STORAGE INVESTIGATION

**Map of Geomorphic Surfaces and Quaternary Geologic Deposits along Stone Corral Creek In the Vincinity of the Sites Damsite**

WLA William Lettis & Associates, Inc. | Figure 2-8

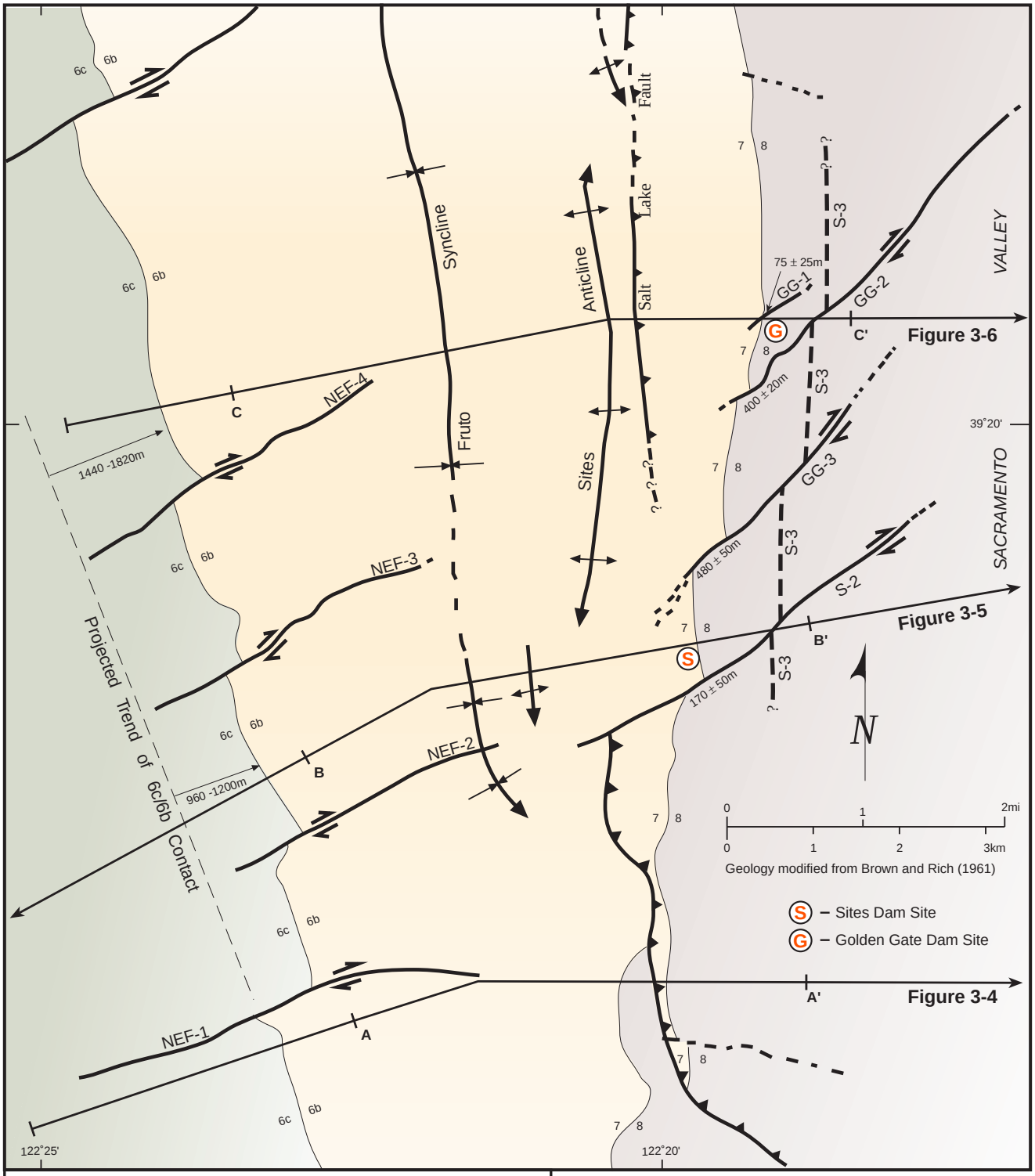


**EXPLANATION**

- Thrust fault , teeth on hanging wall (dashed where approximate; queried where uncertain
- Strike-slip fault, dashed where approximate
- Fault; dashed where approximate
- Cross section; arrows indicate where section extends beyond map boundary
- Axis of plunging syncline, dashed where approximate
- Axis of plunging anticline, dashed where approximate
- Contacts between Cretaceous Great Valley Group strata mapped by Brown and Rich (1961)

PHASE 2 FAULT AND SEISMIC HAZARDS INVESTIGATION
NORTH OF DELTA OFFSTREAM STORAGE
DWR-INTEGRATED STORAGE INVESTIGATION

**Bedrock Structures near the Sites and Golden Gate Damsites.**

William Lettis & Associates, Inc.

Figure 3-1

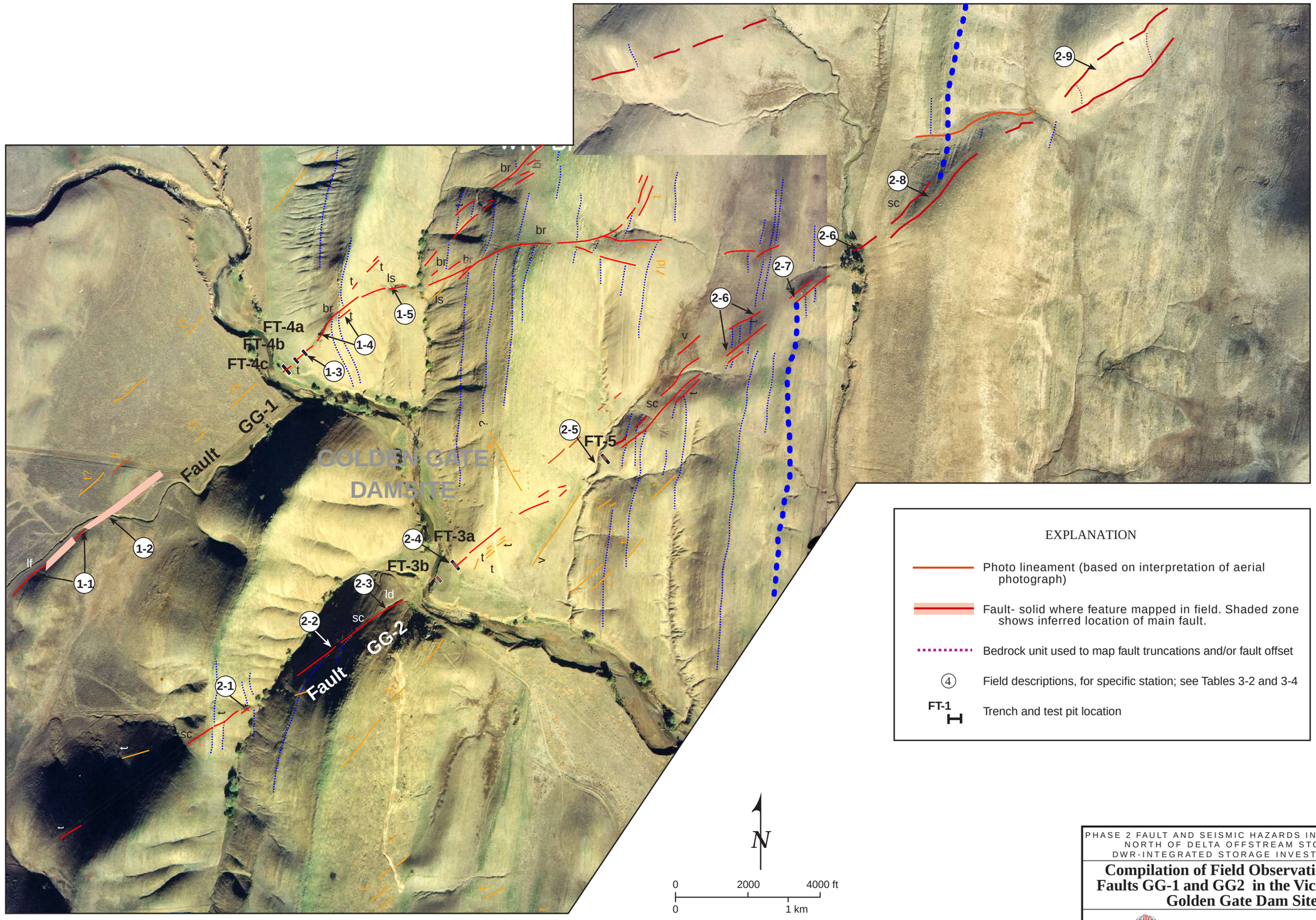


EXPLANATION

- Photo lineament (based on interpretation of aerial photograph)
- Fault- solid where feature mapped in field. Shaded zone shows inferred location of main fault.
- Bedrock unit used to map fault truncations and/or fault offset
- (4) Field descriptions, for specific station; see Tables 3-2 and 3-4
- FT-1 Trench and test pit location

PHASE 2 FAULT AND SEISMIC HAZARDS INVESTIGATION
NORTH OF DELTA OFFSTREAM STORAGE
DWR-INTEGRATED STORAGE INVESTIGATION

**Compilation of Field Observations along Faults GG-1 and GG2 in the Vicinity of the Golden Gate Dam Site**

WLA William Lettis & Associates, Inc.

Figure 3-8

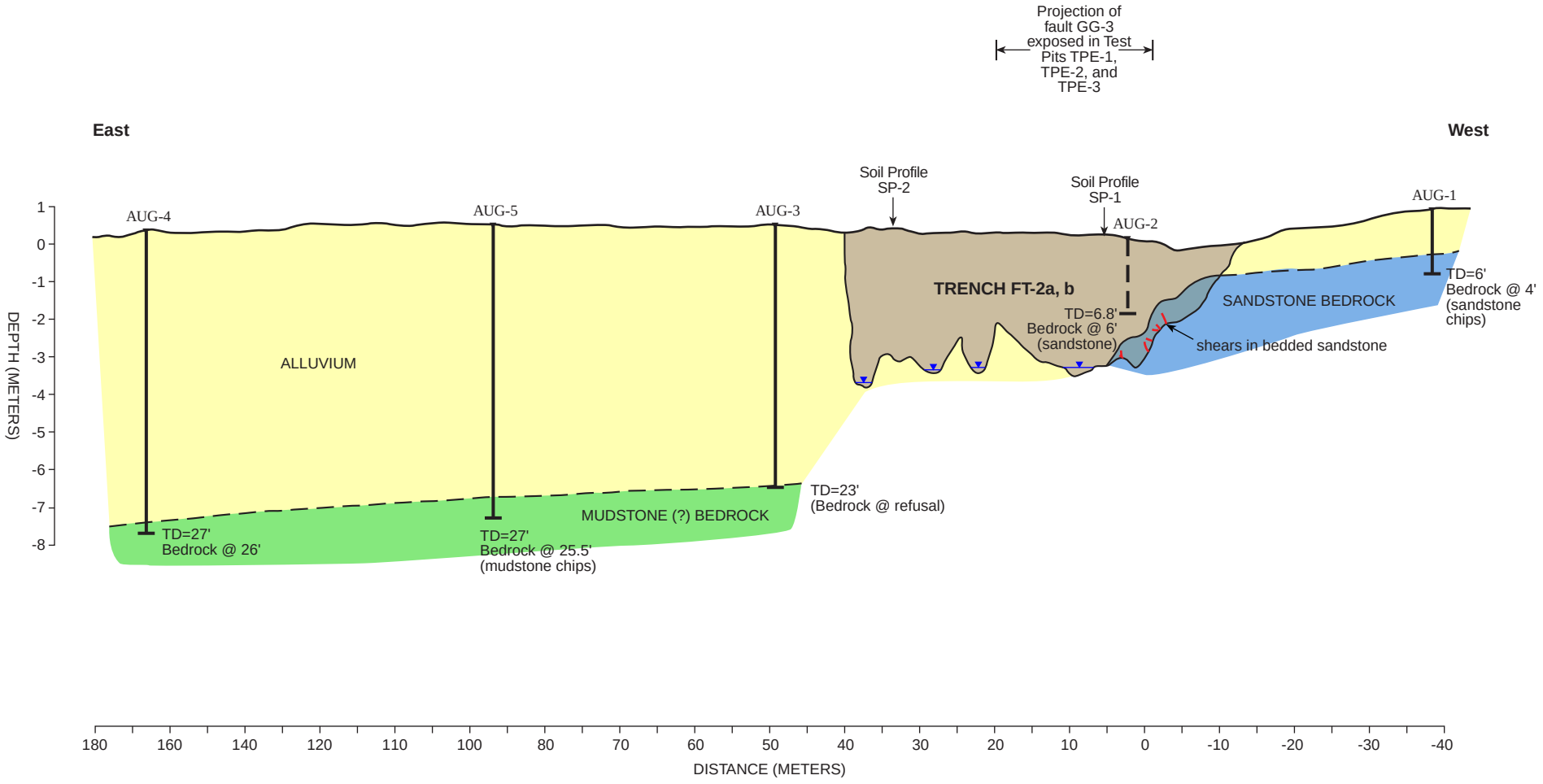


PHASE 2 FAULT AND SEISMIC HAZARDS INVESTIGATION
NORTH OF DELTA OFFSTREAM STORAGE
DWR-INTEGRATED STORAGE INVESTIGATION

**East-West Cross-Section across Fault GG-3, Golden Gate Site**

WLA William Lettis & Associates, Inc.

Figure 3-18

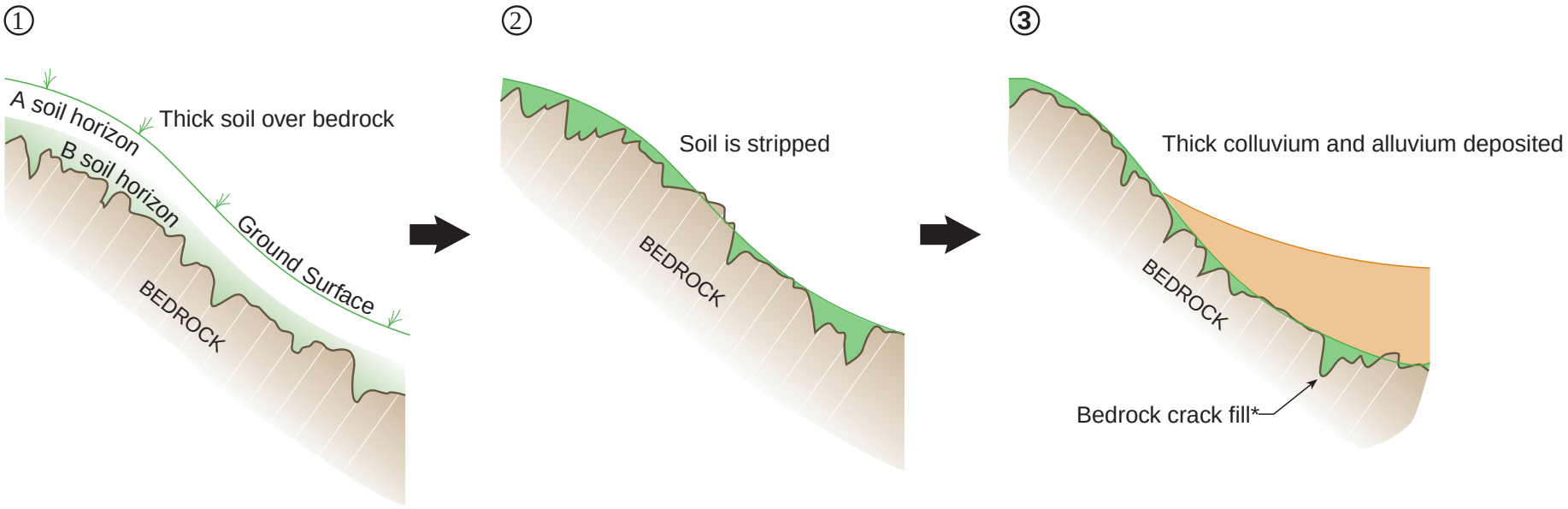


*Bedrock crack fill material has reddish clay films, roots, holes, and fragments of angular bedrock. The reddish clay films match the coatings on fracture surfaces in bedrock, but are not found in the overlying C or Bt soil horizons.

PHASE 2 FAULT AND SEISMIC HAZARDS INVESTIGATION
NORTH OF DELTA OFFSTREAM STORAGE
DWR-INTEGRATED STORAGE INVESTIGATION

**Conceptual diagram showing interpreted origin of soil-filled fissures in bedrock. Fracture fill material may be the remnant of older soil developed over bedrock, including within bedrock cracks (Step 1), subsequently stripped (Step 2), and then buried by younger alluvium and alluvium (Step 3)**

WLA William Lettis & Associates, Inc. | Figure 3-27

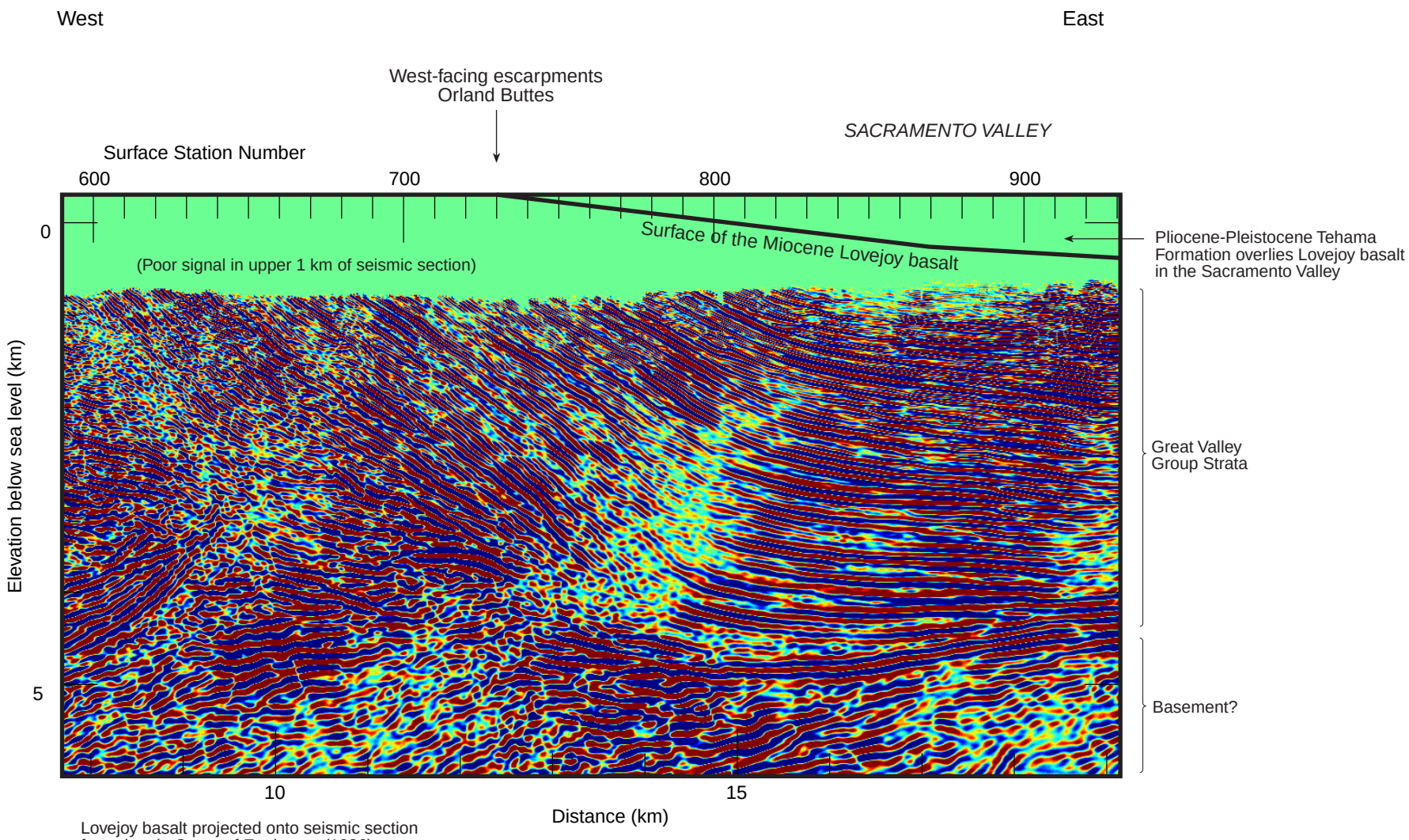


Lovejoy basalt projected onto seismic section from data in Corps of Engineers (1986)

PHASE 2 FAULT AND SEISMIC HAZARDS INVESTIGATION
NORTH OF DELTA OFFSTREAM STORAGE
DWR-INTEGRATED STORAGE INVESTIGATION

**Detail of Seismic Line 805 across the Southern End of the Orland Buttes**

WLA William Lettis & Associates, Inc. | Figure 3-47

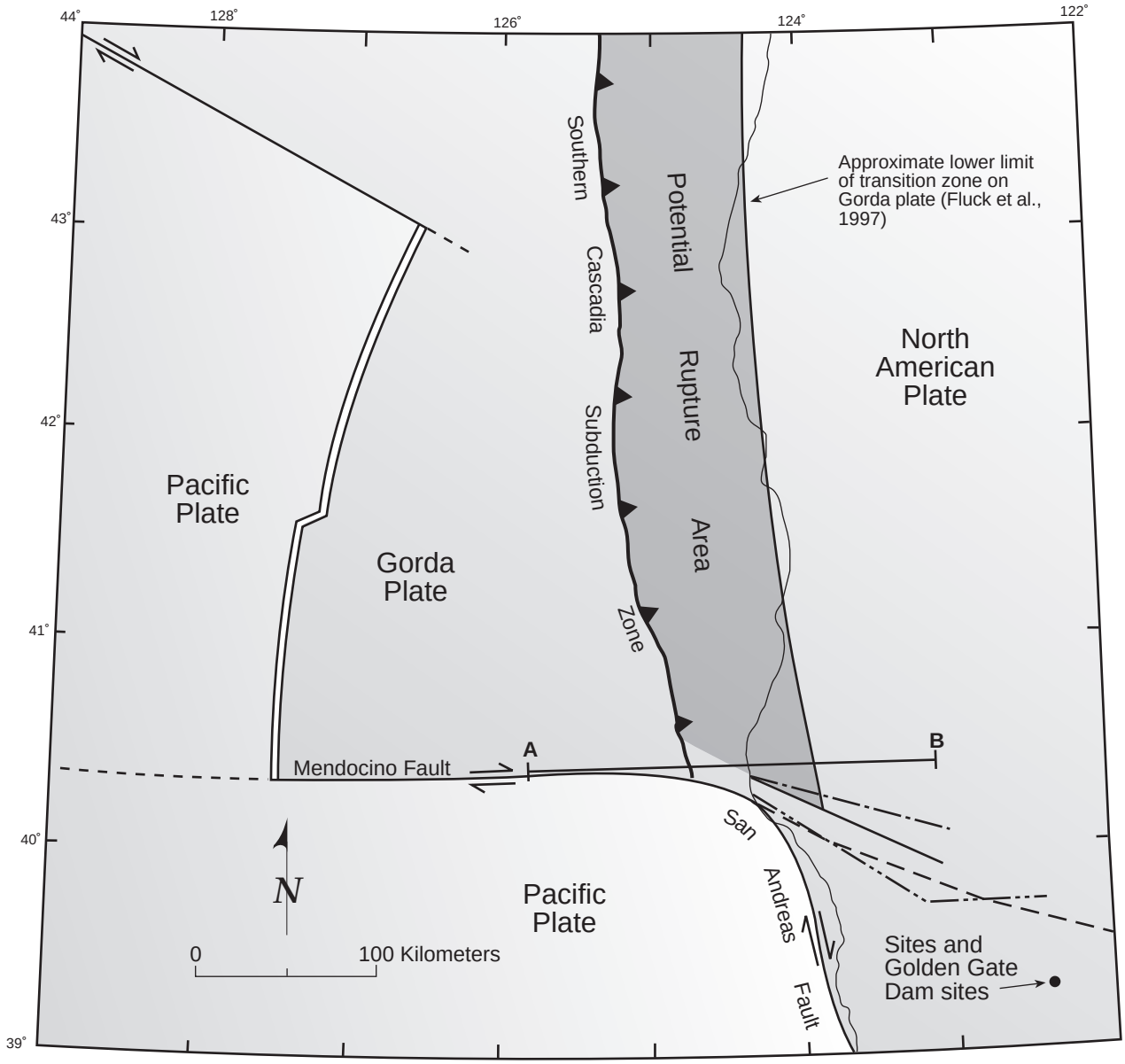


Estimated Position of Southern Edge of the Gorda Plate

- Verdonck and Zandt, 1994
- Beaudoin et al., 1998
- Wilson, 1989
- Jachens and Griscom, 1983

The intersection between the lower limit of the "transition" zone on the Gorda plate, based on modeling by Fluck et al. (1997), and the southern edge of the Gorda plate estimated by Beaudoin et al. (1998), represents the closest approach to the study site for possible rupture of the Cascadia subduction zone.

The southeastern-most point of the southern edge of the Gorda slab, as modeled by Beaudoin et al. (1998), represents the closest approach to the study site for possible earthquakes in the intraplate source zone.

PHASE 2 FAULT AND SEISMIC HAZARDS INVESTIGATION
NORTH OF DELTA OFFSTREAM STORAGE
DWR-INTEGRATED STORAGE INVESTIGATION

**Map showing the estimated position of the southern edge of the subducting Gorda plate (modified from Jachens and Griscom, 1983)**

WLA William Lettis & Associates, Inc.

Figure 3-49

EAST

WEST

*WEST COAST RANGES*

*COAST RANGE FOOTHILLS*

*SACRAMENTO VALLEY*

Relative location of the Sites and Golden Gate Dam Sites (projected about 8km from the south)

Fruto Syncline

SItes Anticline

Sea level

5

10

15

DEPTH (km)

STONY CREEK

COAST RANGE

FRANCISCAN COMPLEX

OPHIOLITE

BOXER AND LAGODA FORMATIONS

FORMATION

"Discontinuity"

CORTINA AND RUMSEY FORMATIONS

Basal Venado Sandstone Member, Cortina Formation

**Stony Creek fault**

**Coast Range fault**

**Blind Sites Thrust**

**Salt Lake fault**

**Gently dipping Thrust "Flat"**

**Blind, West-dipping Thrust "Ramp"**

? ? ? ? ? ? ? ?

COAST RANGE OPHIOLITE?

FRANCISCAN COMPLEX?

Coherent, layered, high-amplitude reflectors visible in seismic reflection profiles. Deformed lower Great Valley Group Strata?

Surface geology modified from Brown and Rich (1961) and Brown (1964)
Reflector geometry from seismic line 798 (Appendix A)

PHASE 2 FAULT AND SEISMIC HAZARDS INVESTIGATION
NORTH OF DELTA OFFSTREAM STORAGE
DWR-INTEGRATED STORAGE INVESTIGATION

**Cross Section Showing Major Map-scale Structures in the Study Area, and their Relationship to Structures Imaged by Seismic Reflection Profiles**

WLA William Lettis & Associates, Inc.

Figure 3-2

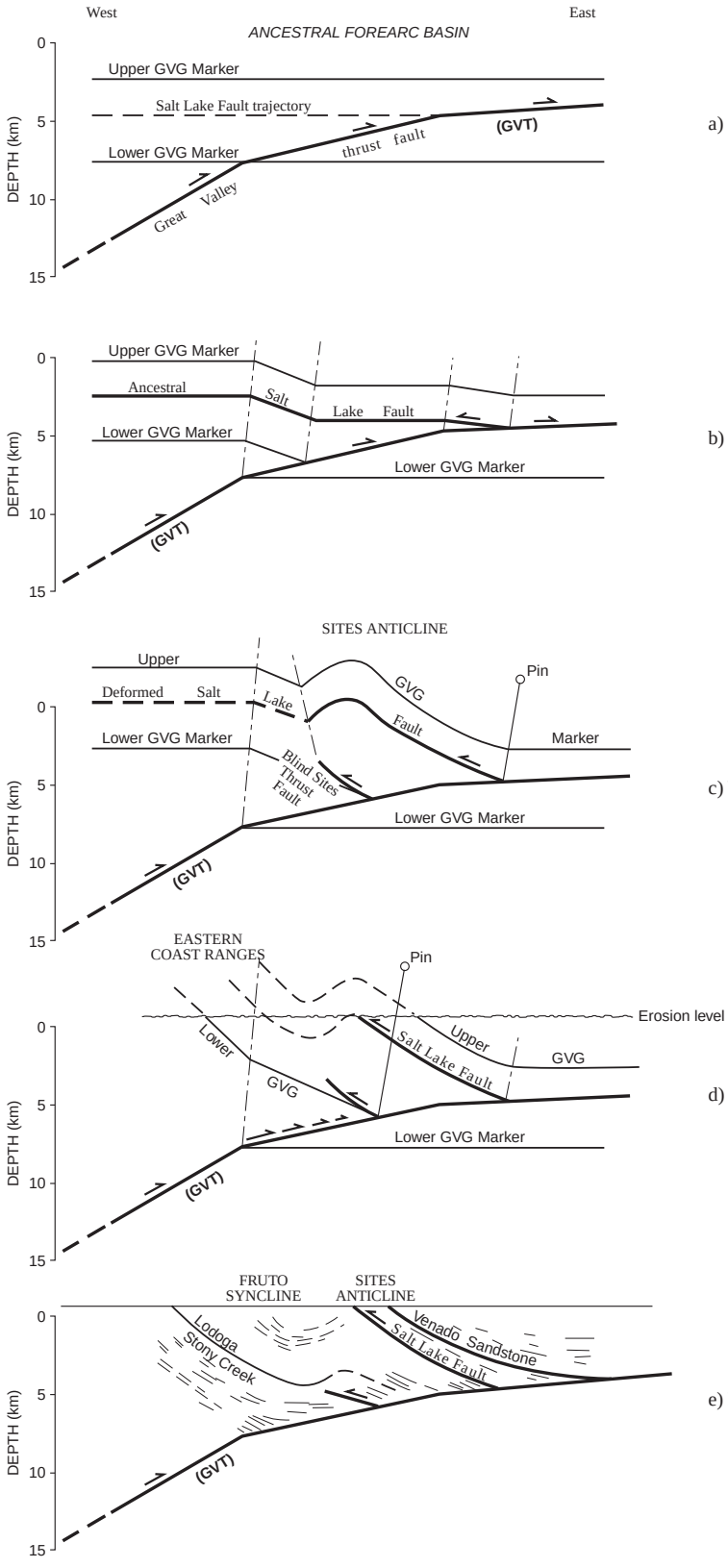


a) Initial position of Great Valley Group marker horizons; trajectory of future thrust faults

b) Initial uplift due to thrust wedging; ~4 km of wedge propagation (late Cretaceous - early Tertiary)

c) Wedge “locks” at pinned point; shortening accommodated by growth of Sites anticline (~4 km of east-directed shortening)

d) System “locks” beneath Sites anticline; shortening primarily accomodated by uplift and fault propagation of folding of the eastern Coast Ranges.Full slip occurs on GVT ramp; slip diminishes eastward on flat

e) Present structure and geometry of reflectors in seismic profile 798 (Appendix A).

PHASE 2 FAULT AND SEISMIC HAZARDS INVESTIGATION
NORTH OF DELTA OFFSTREAM STORAGE
DWR-INTEGRATED STORAGE INVESTIGATION

**Kinematic Model for Growth of the Sites Anticline**

WLA William Lettis & Associates, Inc. | Figure 3-3

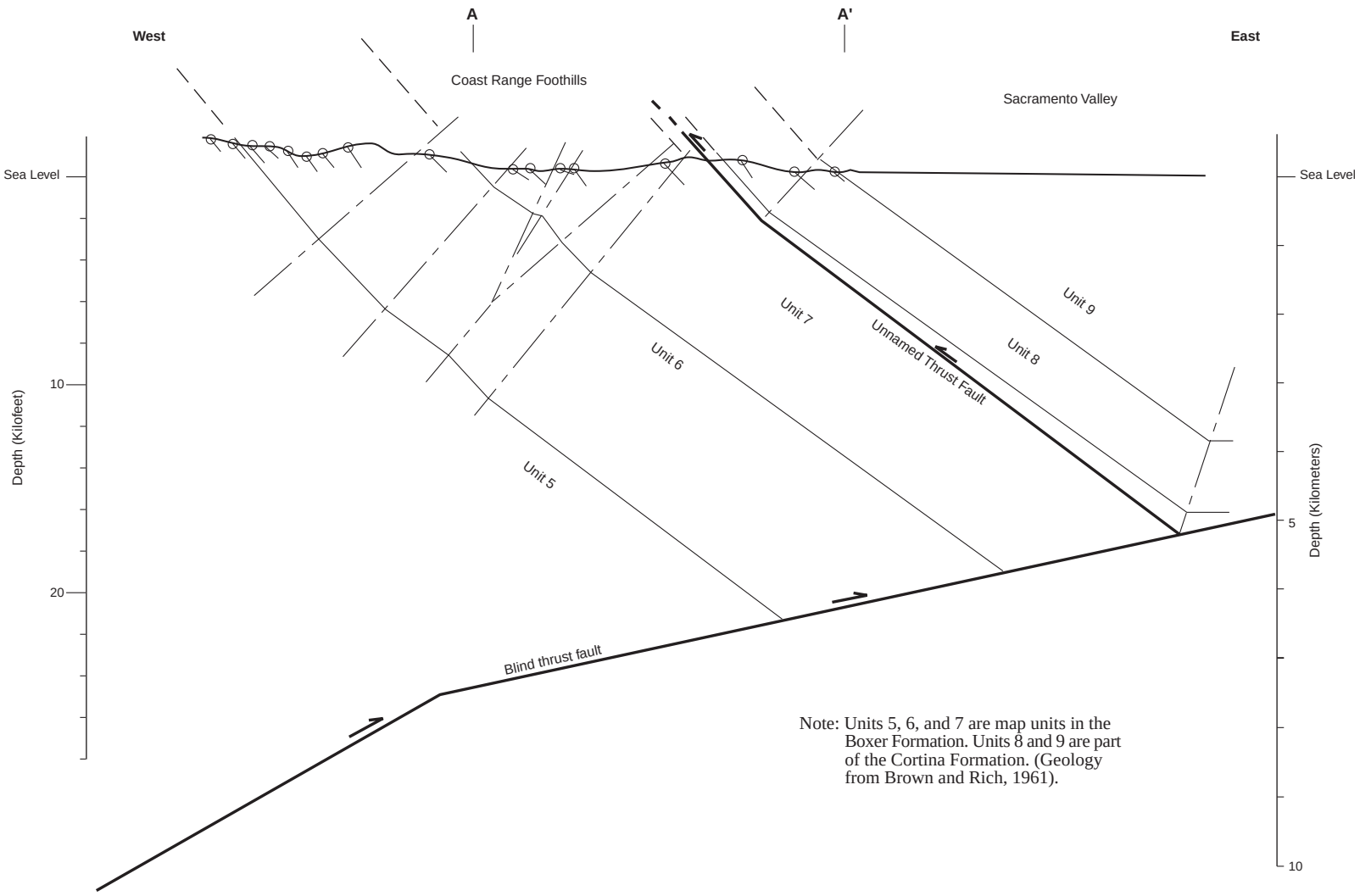


Note: Units 5, 6, and 7 are map units in the Boxer Formation. Units 8 and 9 are part of the Cortina Formation. (Geology from Brown and Rich, 1961).

PHASE 2 FAULT AND SEISMIC HAZARDS INVESTIGATION
NORTH OF DELTA OFFSTREAM STORAGE
DWR-INTEGRATED STORAGE INVESTIGATION

**Cross Section A-A'; see Figure 3-1 for Location**

WLA William Lettis & Associates, Inc.

Figure 3-4

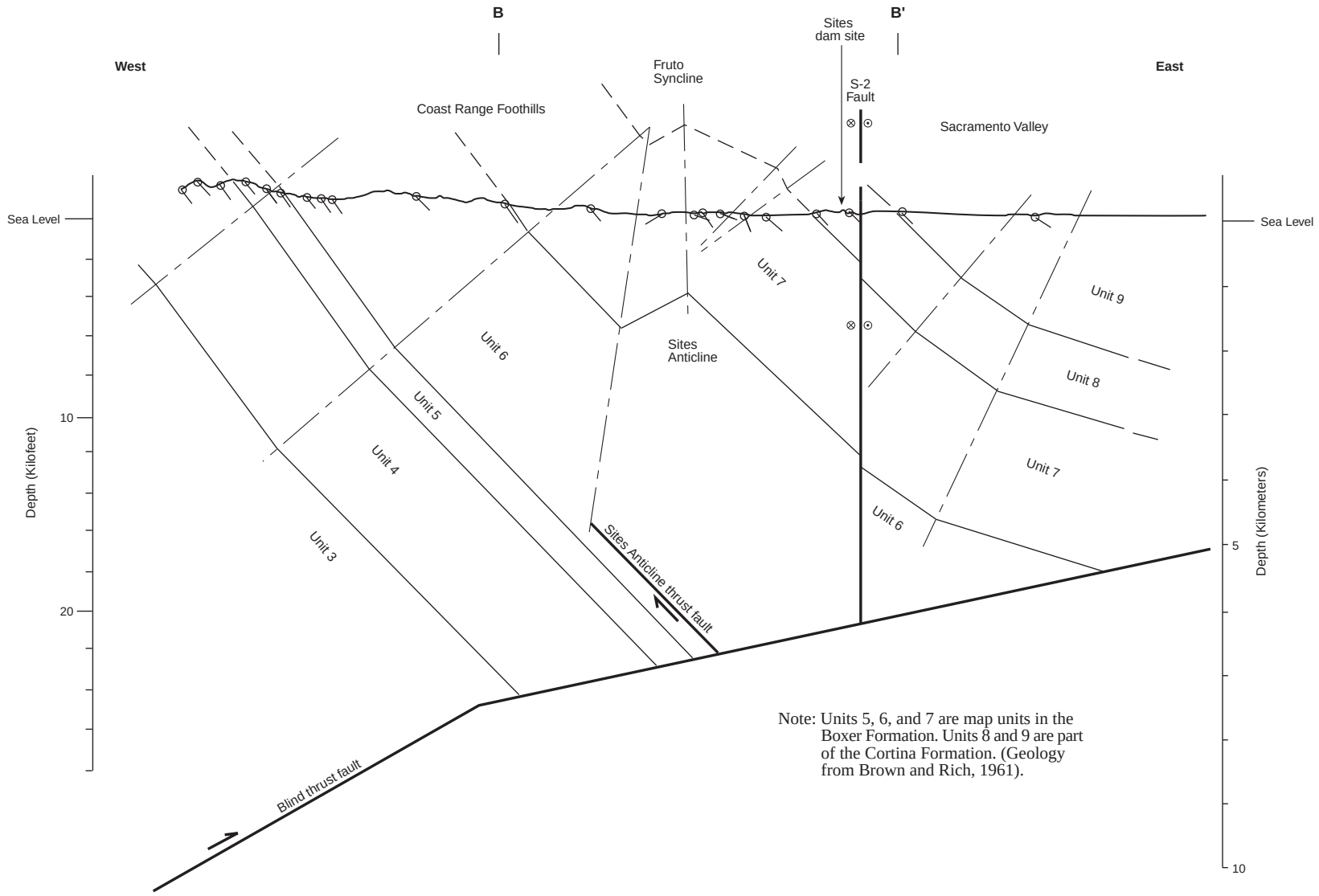


Note: Units 5, 6, and 7 are map units in the Boxer Formation. Units 8 and 9 are part of the Cortina Formation. (Geology from Brown and Rich, 1961).

PHASE 2 FAULT AND SEISMIC HAZARDS INVESTIGATION
NORTH OF DELTA OFFSTREAM STORAGE
DWR-INTEGRATED STORAGE INVESTIGATION

**Cross Section B-B'; see Figure 3-1 for Location**

WLA William Lettis & Associates, Inc.

Figure 3-5

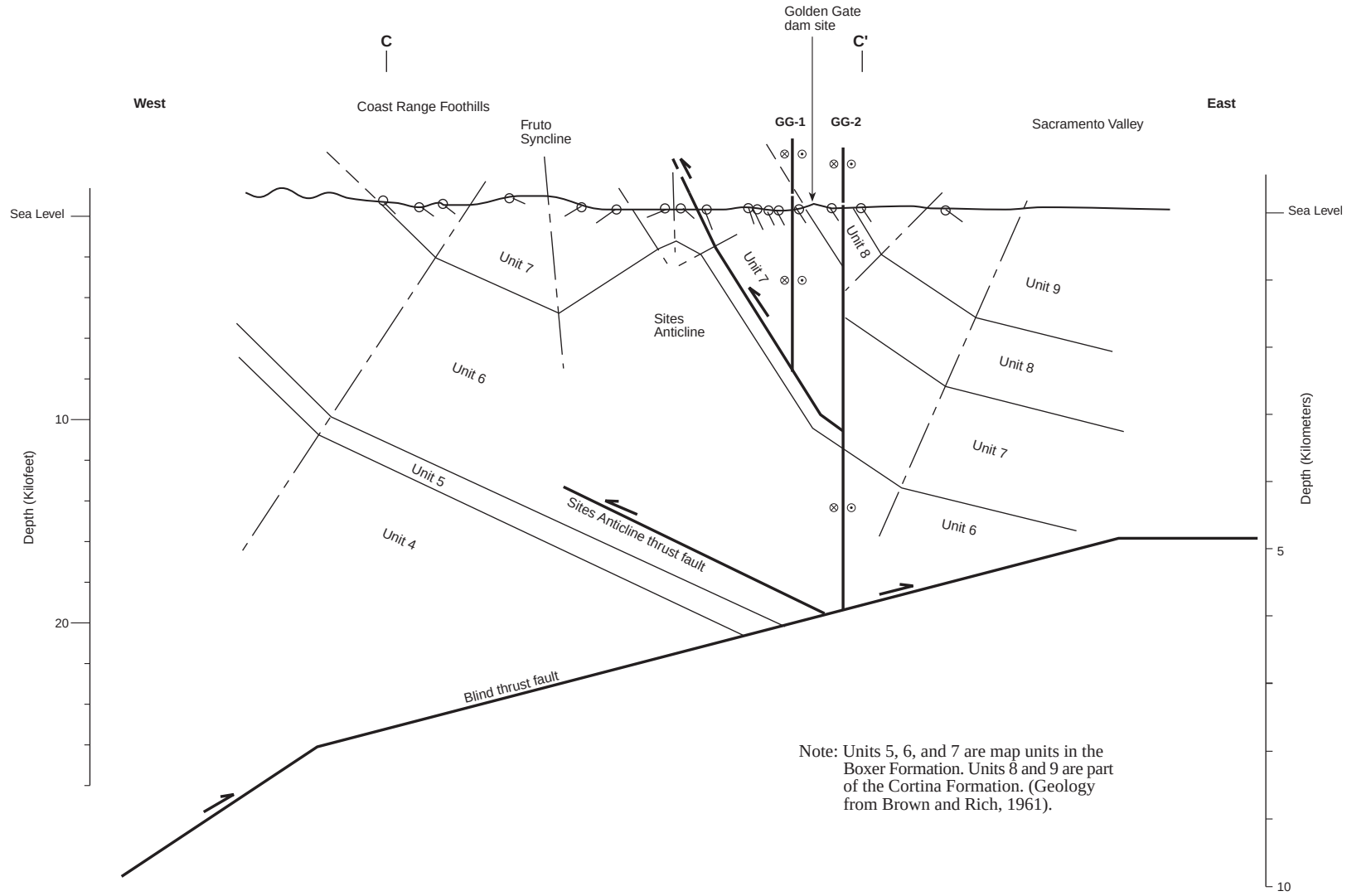


Note: Units 5, 6, and 7 are map units in the Boxer Formation. Units 8 and 9 are part of the Cortina Formation. (Geology from Brown and Rich, 1961).

PHASE 2 FAULT AND SEISMIC HAZARDS INVESTIGATION
NORTH OF DELTA OFFSTREAM STORAGE
DWR-INTEGRATED STORAGE INVESTIGATION

**Cross Section C-C'; see Figure 3-1 for Location**

WLA William Lettis & Associates, Inc.

Figure 3-6

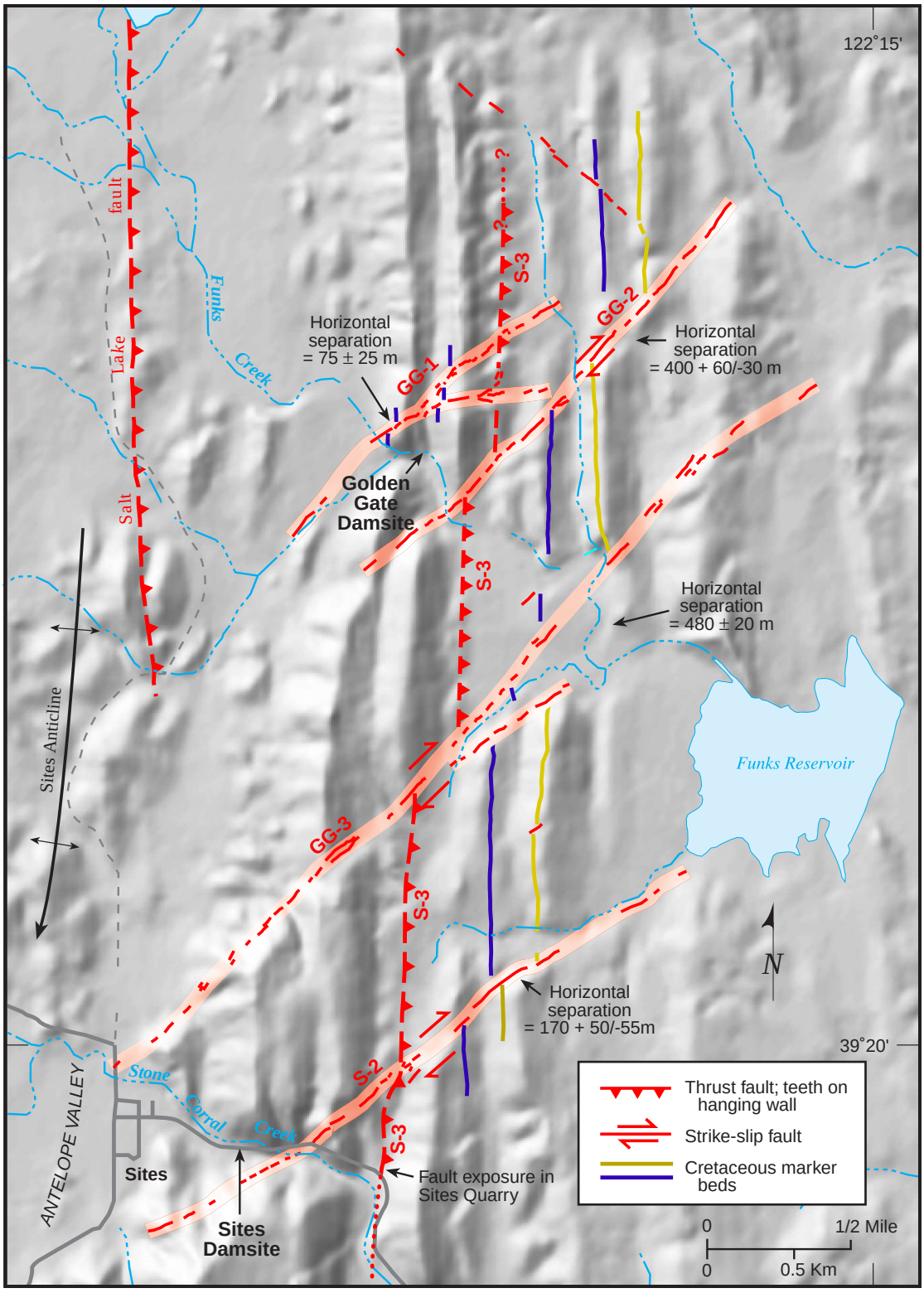


PHASE 2 FAULT AND SEISMIC HAZARDS INVESTIGATION
NORTH OF DELTA OFFSTREAM STORAGE
DWR-INTEGRATED STORAGE INVESTIGATION

**Shaded Relief Map Showing Faults in the Vicinity of the Sites and Golden Gate Damsites**

WLA William Lettis & Associates, Inc. | Figure 3-7

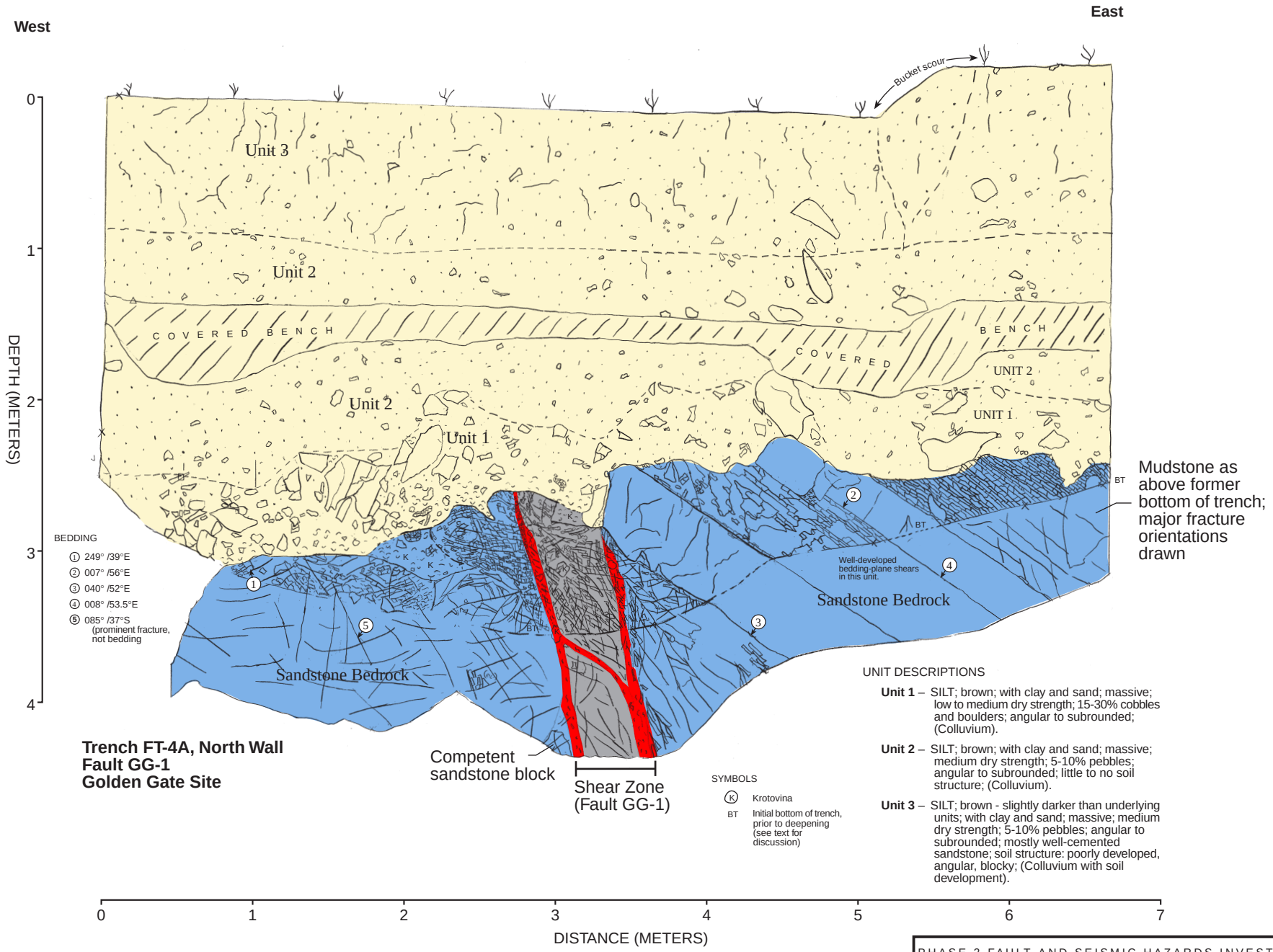


PHASE 2 FAULT AND SEISMIC HAZARDS INVESTIGATION
NORTH OF DELTA OFFSTREAM STORAGE
DWR-INTEGRATED STORAGE INVESTIGATION

**Trench FT-4a - North Wall, GG-1 Fault, Golden Gate Damsite**

WLA William Lettis & Associates, Inc.

Figure 3-9

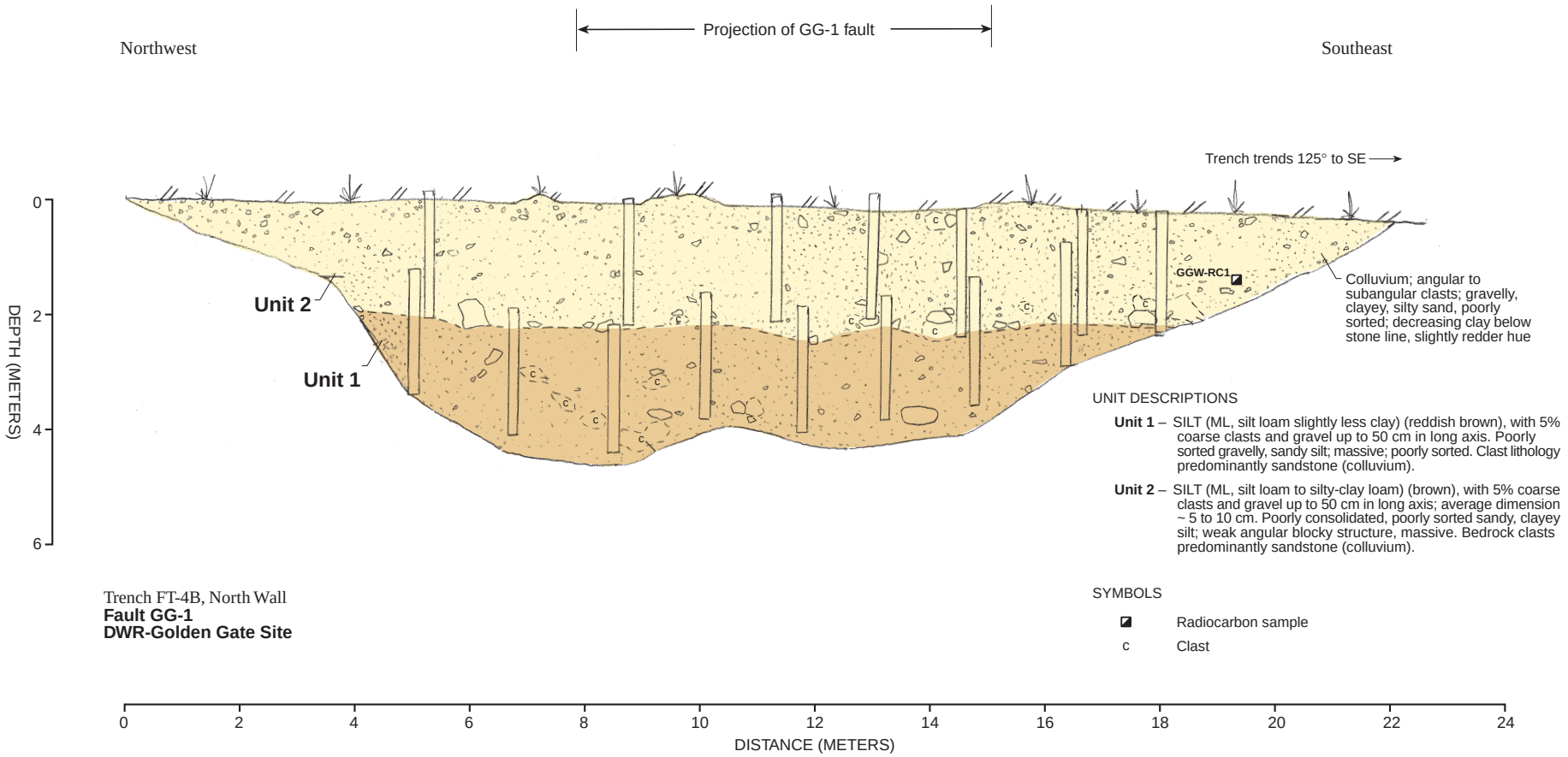


Trench FT-4B, North Wall
**Fault GG-1**
**DWR-Golden Gate Site**

PHASE 2 FAULT AND SEISMIC HAZARDS INVESTIGATION
NORTH OF DELTA OFFSTREAM STORAGE
DWR-INTEGRATED STORAGE INVESTIGATION

# Trench FT-4b - North Wall, GG-1 Fault, Golden Gate Damsite

William Lettis & Associates, Inc.

Figure 3-10

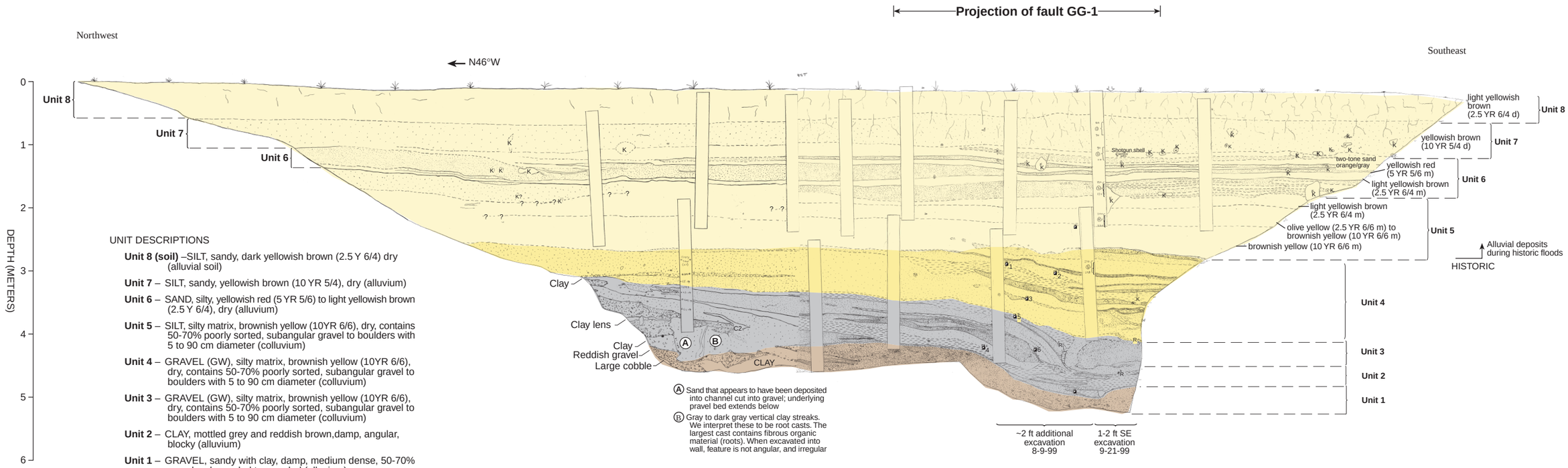


UNIT DESCRIPTIONS

**Unit 8 (soil)** –SILT, sandy, dark yellowish brown (2.5 Y 6/4) dry (alluvial soil)

**Unit 7** – SILT, sandy, yellowish brown (10 YR 5/4), dry (alluvium)

**Unit 6** – SAND, silty, yellowish red (5 YR 5/6) to light yellowish brown (2.5 Y 6/4), dry (alluvium)

**Unit 5** – SILT, silty matrix, brownish yellow (10YR 6/6), dry, contains 50-70% poorly sorted, subangular gravel to boulders with 5 to 90 cm diameter (colluvium)

**Unit 4** – GRAVEL (GW), silty matrix, brownish yellow (10YR 6/6), dry, contains 50-70% poorly sorted, subangular gravel to boulders with 5 to 90 cm diameter (colluvium)

**Unit 3** – GRAVEL (GW), silty matrix, brownish yellow (10YR 6/6), dry, contains 50-70% poorly sorted, subangular gravel to boulders with 5 to 90 cm diameter (colluvium)

**Unit 2** – CLAY, mottled grey and reddish brown,damp, angular, blocky (alluvium)

**Unit 1** – GRAVEL, sandy with clay, damp, medium dense, 50-70% gravel, subrounded to rounded (alluvium)

Ⓐ Sand that appears to have been deposited into channel cut into gravel; underlying pravel bed extends below

Ⓑ Gray to dark gray vertical clay streaks. We interpret these to be root casts. The largest cast contains fibrous organic material (roots). When excavated into wall, feature is not angular, and irregular

SYMBOLS

- Radiocarbon sample
- ss — Medium-fine lithic wacke
- sis — Fine lithic wacke, silty sandstone, massive
- ms — Mudstone, thinly bedded
- Disintegrated weathered bedrock

Trench FT-4C, North Wall
Fault GG-1
Golden Gate Site

0 1 2 3 4 5 6 7 8 9 10 11 12 13 14 15 16 17 18 19 21 21 22

DISTANCE (METERS)

PHASE 2 FAULT AND SEISMIC HAZARDS INVESTIGATION
NORTH OF DELTA OFFSTREAM STORAGE
DWR- INTEGRATED STORAGE INVESTIGATION

**Trench FT-4c - North Wall, GG-1 Fault, Golden Gate Damsite**

WLA William Lettis & Associates, Inc. | Figure 3-11




PHASE 2 FAULT AND SEISMIC HAZARDS INVESTIGATION
NORTH OF DELTA OFFSTREAM STORAGE
DWR-INTEGRATED STORAGE INVESTIGATION

**Photo, View to North, Trenches FT-3a and FT-3b, GG-2 Fault, Golden Gate Damsite**

WLA William Lettis & Associates, Inc. | Figure 3-12

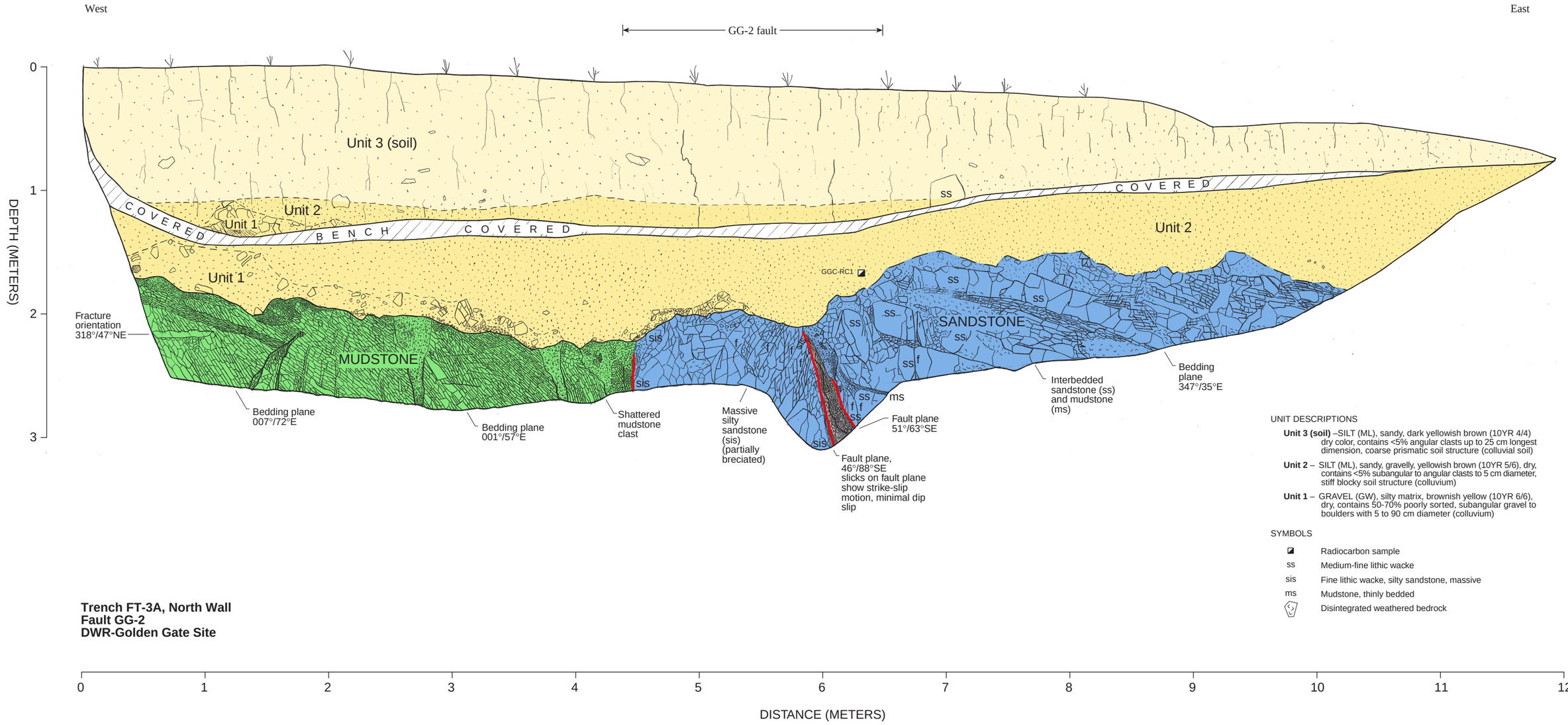


PHASE 2 FAULT AND SEISMIC HAZARDS INVESTIGATION
NORTH OF DELTA OFFSTREAM STORAGE
DWR- INTEGRATED STORAGE INVESTIGATION

**Trench FT-3a - North Wall, GG-2 Fault, Golden Gate Damsite**

WLA William Lettis & Associates, Inc.

Figure 3-13

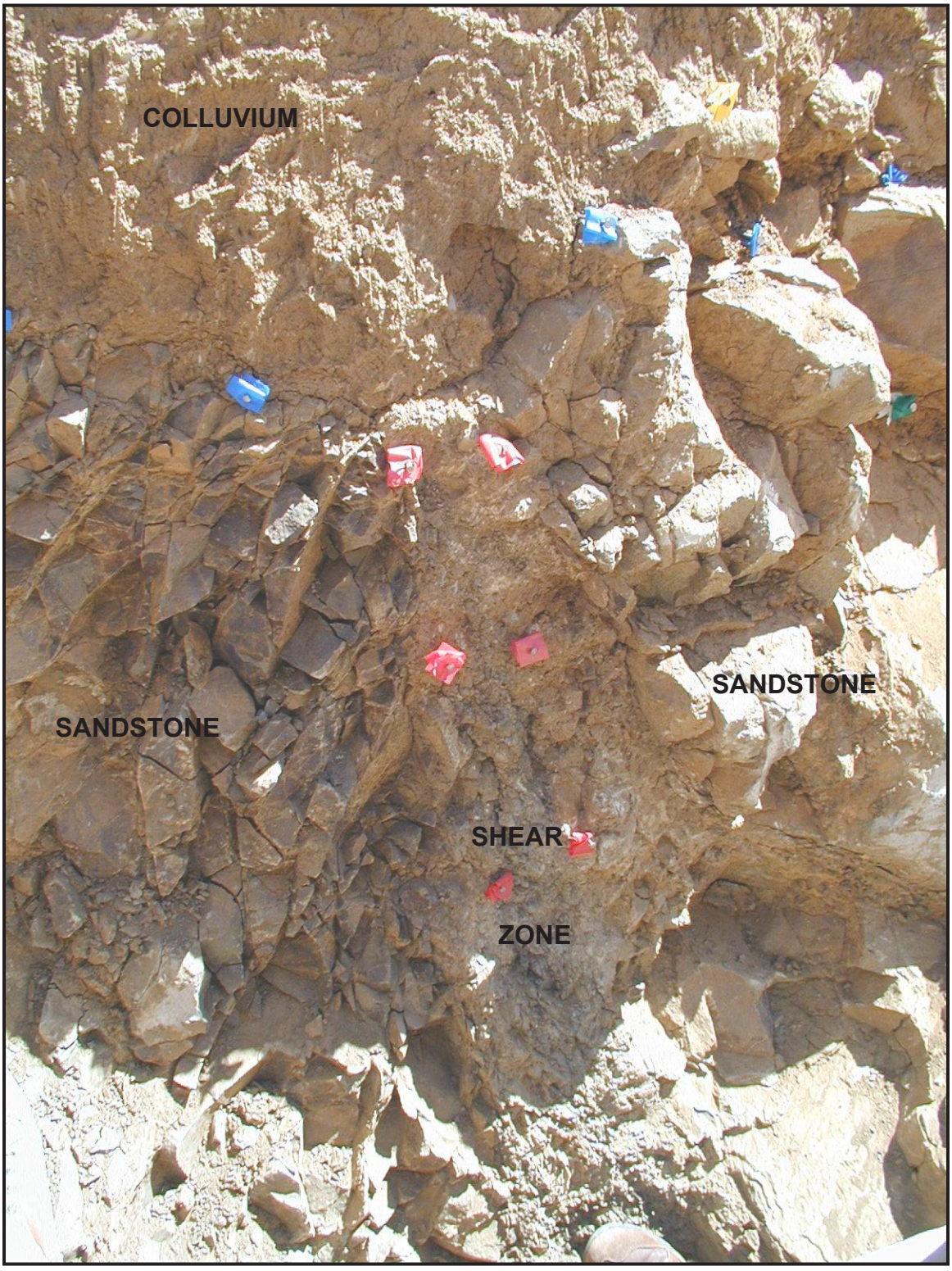


PHASE 2 FAULT AND SEISMIC HAZARDS INVESTIGATION
NORTH OF DELTA OFFSTREAM STORAGE
DWR-INTEGRATED STORAGE INVESTIGATION

**Photo, Detail of GG-2 fault, North Wall, Trench FT3a, Golden Gate Damsite**

WLA William Lettis & Associates, Inc. | Figure 3-14

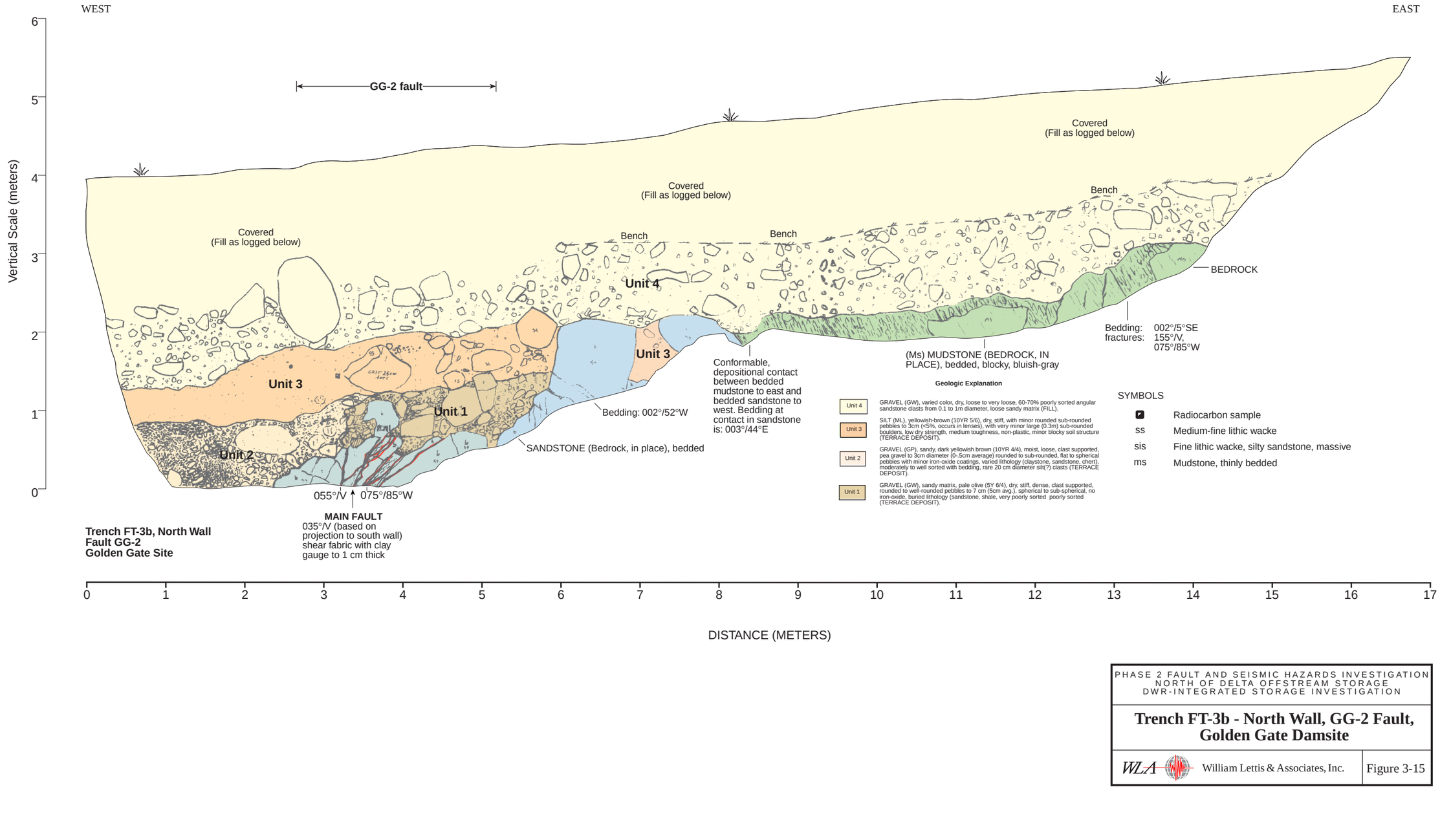


**Trench FT-3b, North Wall**
**Fault GG-2**
**Golden Gate Site**

PHASE 2 FAULT AND SEISMIC HAZARDS INVESTIGATION
NORTH OF DELTA OFFSTREAM STORAGE
DWR-INTEGRATED STORAGE INVESTIGATION

# Trench FT-3b - North Wall, GG-2 Fault, Golden Gate Damsite

William Lettis & Associates, Inc. | Figure 3-15

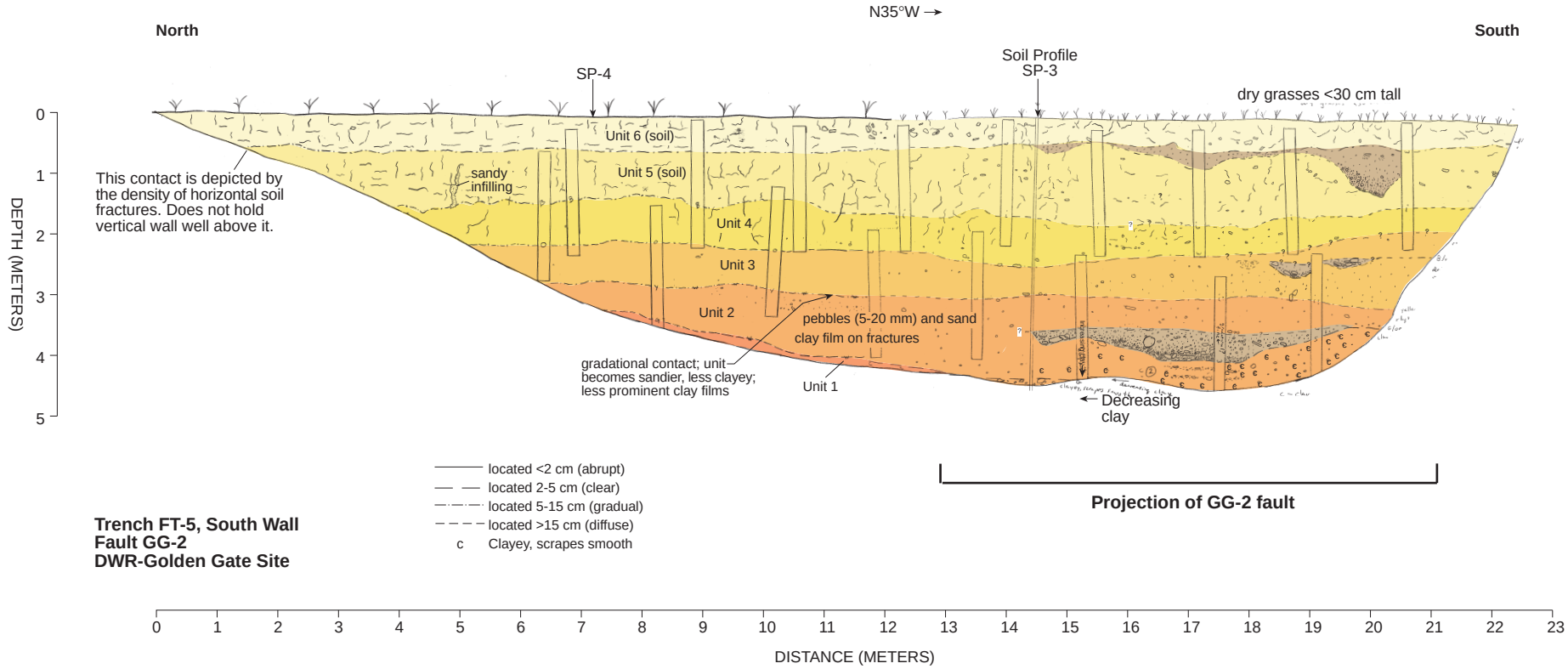


**Trench FT-5, South Wall**
**Fault GG-2**
**DWR-Golden Gate Site**

UNIT DESCRIPTIONS

Unit 6 (soil) –SILTY CLAY? WITH SAND, grayish brown 10 YR 5/2 (d), dry, very, stiff, 10-30% sand, lithic fragments up to 15 cm, pervasive partings producing subangular to subrounded peds (soil).

Unit 5 (soil) –SILTY CLAY? WITH SAND, dark brown 10 YR 3/3 (m), very stiff, moist, pervasive clay films on abundant soil partings, 10-15% medium to coarse sands, lithic fragments (sandstone, mudstone) (colluvium; B-horizon)

Unit 4– SANDY CLAY, 20-30% medium to coarse weathered sand, yellowish brown, 10 YR 5/8 (m), moist, very stiff, massive, well-developed clay films on few through-going fractures (clay from above), contains lithic fragments of sandstone and mudstone (colluvium; C horizon)

Unit 3 – CLAY, with sand, 10 YR 4/9, dark yellowish brown, moist, very stiff, massive, abundant fine posre, clasts have thin clay films; fractures have pervasive dark brown clay films, increasing brown color upwards (10YR 4/3), possibly weakly developed buried soil, contains lithic fragments of sandstone and mudstone (colluvium)

Unit 2a – GRAVEL, sandy (stream channel deposit)

Unit 2 – CLAY, with sand, dark yellowish brown, 10 YR 9/4, moist, soft, 5-10% sand, less than 5% weathered lithics, vesicles, no soil partings or clay films (colluvium)

Unit 1 – CLAY, dark yellowish brown, 10 YR 4/9 (m), moist, soft, contains clasts to 15 cm weathered lithics, few sands (<3%), more moist than above (colluvium)

PHASE 2 FAULT AND SEISMIC HAZARDS INVESTIGATION
NORTH OF DELTA OFFSTREAM STORAGE
DWR-INTEGRATED STORAGE INVESTIGATION

**Trench FT-5 - South Wall, GG-2 Fault, Golden Gate Damsite**

WLA William Lettis & Associates, Inc. | Figure 3-16

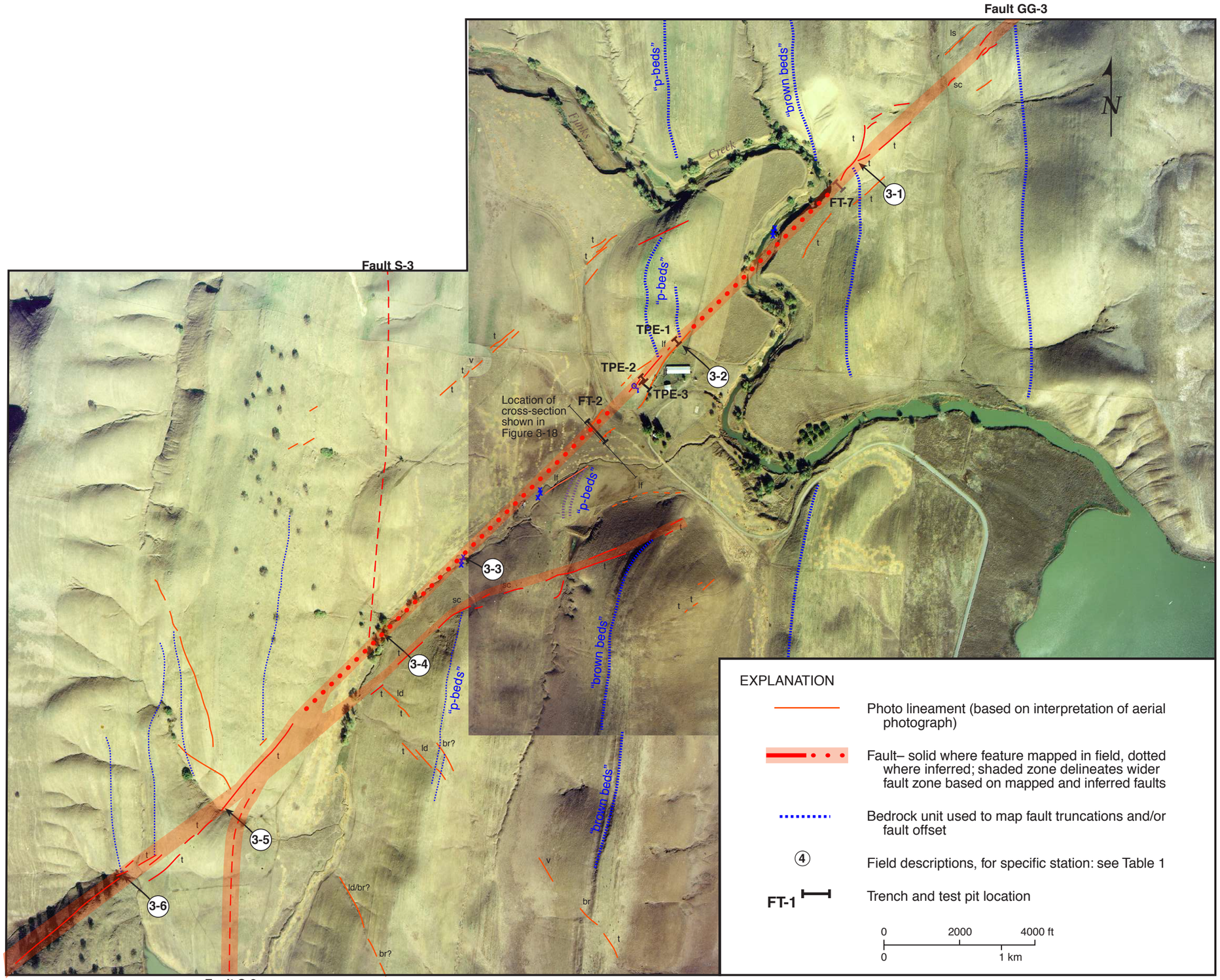


PHASE 2 FAULT AND SEISMIC HAZARDS INVESTIGATION
NORTH OF DELTA OFFSTREAM STORAGE
DWR-INTEGRATED STORAGE INVESTIGATION

**Compilation of Field Observations along Fault GG-3 in the Vicinity of the Golden Gate Dam Site**

WLA William Lettis & Associates, Inc.

Figure 3-17




PHASE 2 FAULT AND SEISMIC HAZARDS INVESTIGATION
NORTH OF DELTA OFFSTREAM STORAGE
DWR-INTEGRATED STORAGE INVESTIGATION

**Photo, View to Southwest, Trench FT-2a, GG-3 Fault, Golden Gate Damsite**

WLA William Lettis & Associates, Inc. | Figure 3-19

Southeast

Northwest

Projection of GG-3 fault

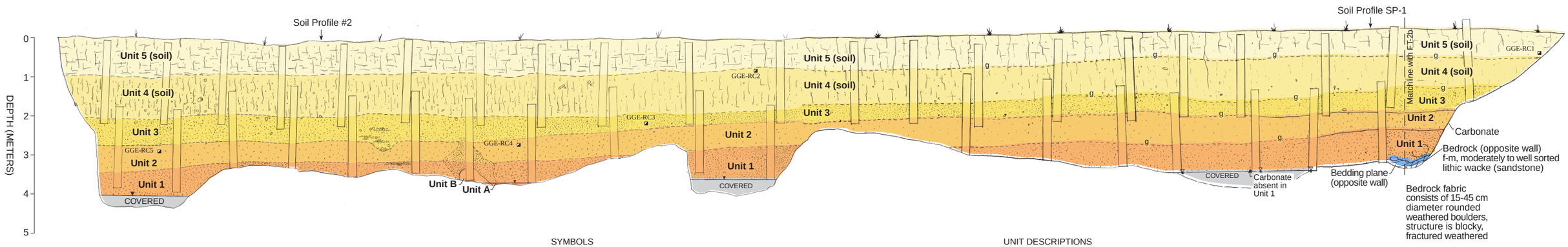


SYMBOLS

- Radiocarbon sample
- K Krotovina
- g gradational contact
- Water level

UNIT DESCRIPTIONS

**Unit5** (soil) – SILT (MH) Very dark grayish brown (10YR 3/2), dry; with 10 to 20% fine to very fine sand, <5% angular to subangular weathered clasts up to 7 mm longest dimension. Coarse blocky soil structure, horizontal and vertical partings. Clast lithology: sandstone and mudstone.

**Unit 4** (soil) –SILT (MH) Yellowish brown (10YR 5/4), dry; with 10 to 15% fine to very fine sand, 5 to 10% subangular weathered clasts up to 10 mm, average 4 to 5 mm longest dimension. Prismatic structure with minor clay coatings on pediment surfaces. Clast lithology: sandstone and mudstone. Slow dilatency, medium toughness, medium to high plasticity.

**Unit 3** – SILT (MH) Dark yellowish brown (10YR 4/4), dry; with 20% medium to fine sand; 5 to 15% pebbles up to 25 mm longest diameter, average diameter = 4 to 5 mm. Minor prismatic structure. Clast lithology: sandstone, mudstone, red silty sandstone.

**Unit 2** – SILT (MH) brown (7.5 YR 5/3), damp, medium dry strength, slow dilatancy, high toughness, very minor (<<1%) pebbles to 0.5 cm diameter (Overbank deposits).

**Unit 1** – SILT (ML) brown (7.5 YR 4/4), wet, medium dry strength, slow dilatancy, low to medium toughness, minor (<1%) lenses of gravel with well-rounded, moderately well-sorted pebbles to 7 cm (1 cm average) (Terrace/overbank deposits).

**Unit A** – CLAY (CL) Mottled brown and dark yellow brown (10YR 4/3, 10YR 4/4), with 15% fine sand and silt, <5% clasts up to 10 mm longest diameter. Dry strength = medium to high. No dilatency. Medium toughness. Low to medium plasticity. Massive to weak subangular blocky structure. (Weathered bedrock clast).

**Unit B** – CLAY (CL) Dark green gray (5BG 4/1), wet; with 10 to 15% silt to medium sand. No dilatency. Low to medium toughness. Low to medium plasticity. Massive.

Trench FT-2a, South Wall
Fault GG-3
DWR-Golden Gate site

0 1 2 3 4 5 6 7 8 9 10 11 12 13 14 15 16 17 18 19 20 21 22 23 24 25 26 27 28 29 30 31 32 33 34 35 36 37 38

DISTANCE (METERS)

PHASE 2 FAULT AND SEISMIC HAZARDS INVESTIGATION
NORTH OF DELTA OFFSTREAM STORAGE
DWR-INTEGRATED STORAGE INVESTIGATION

**Trench FT-2a, South Wall, GG-3 Fault, Golden Gate Damsite**

WLA William Lettis & Associates, Inc. | Figure 3-20

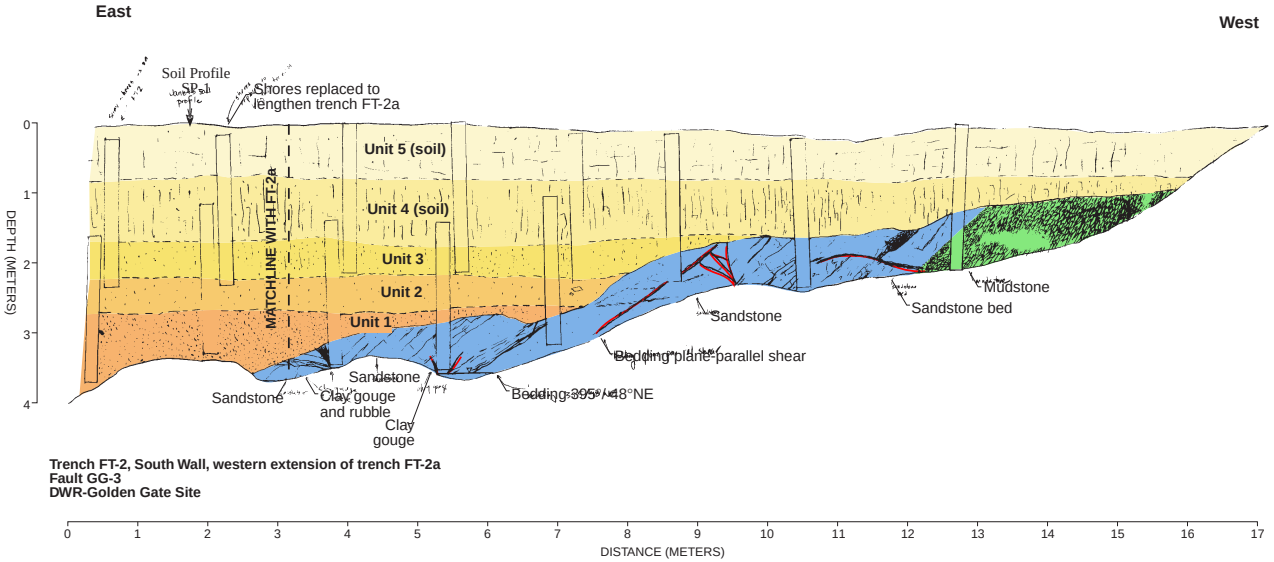


**Trench FT-2, South Wall, western extension of trench FT-2a**
**Fault GG-3**
**DWR-Golden Gate Site**

PHASE 2 FAULT AND SEISMIC HAZARDS INVESTIGATION
NORTH OF DELTA OFFSTREAM STORAGE
DWR-INTEGRATED STORAGE INVESTIGATION

# Trench FT-2b - South Wall, GG-3 Fault, Golden Gate Damsite

WLA William Lettis & Associates, Inc. | Figure 3-21

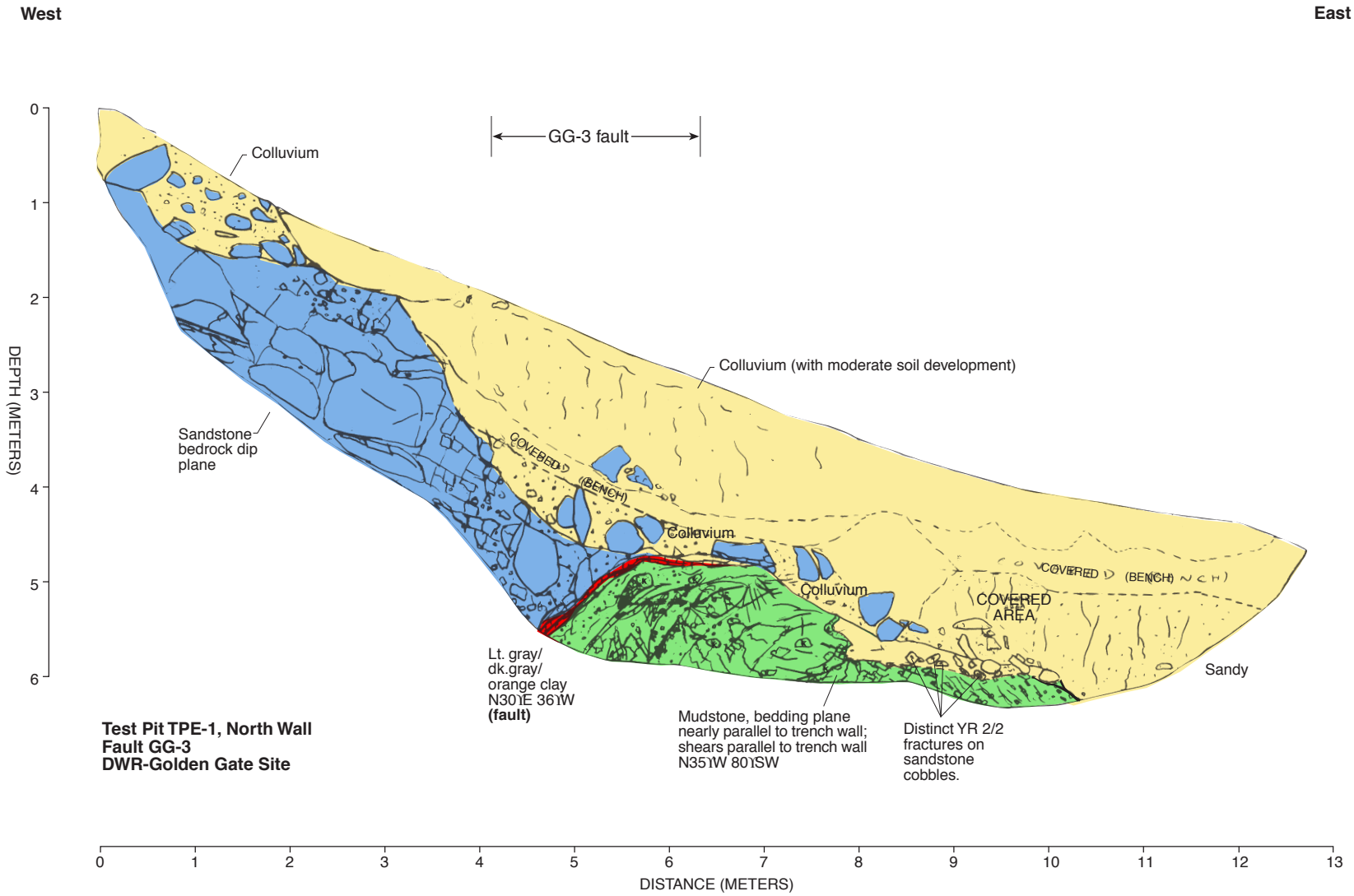


PHASE 2 FAULT AND SEISMIC HAZARDS INVESTIGATION
NORTH OF DELTA OFFSTREAM STORAGE
DWR-INTEGRATED STORAGE INVESTIGATION

**Testpit TPE-1 - North Wall, GG-3 Fault, Golden Gate Damsite**

WLA William Lettis & Associates, Inc.

Figure 3-22

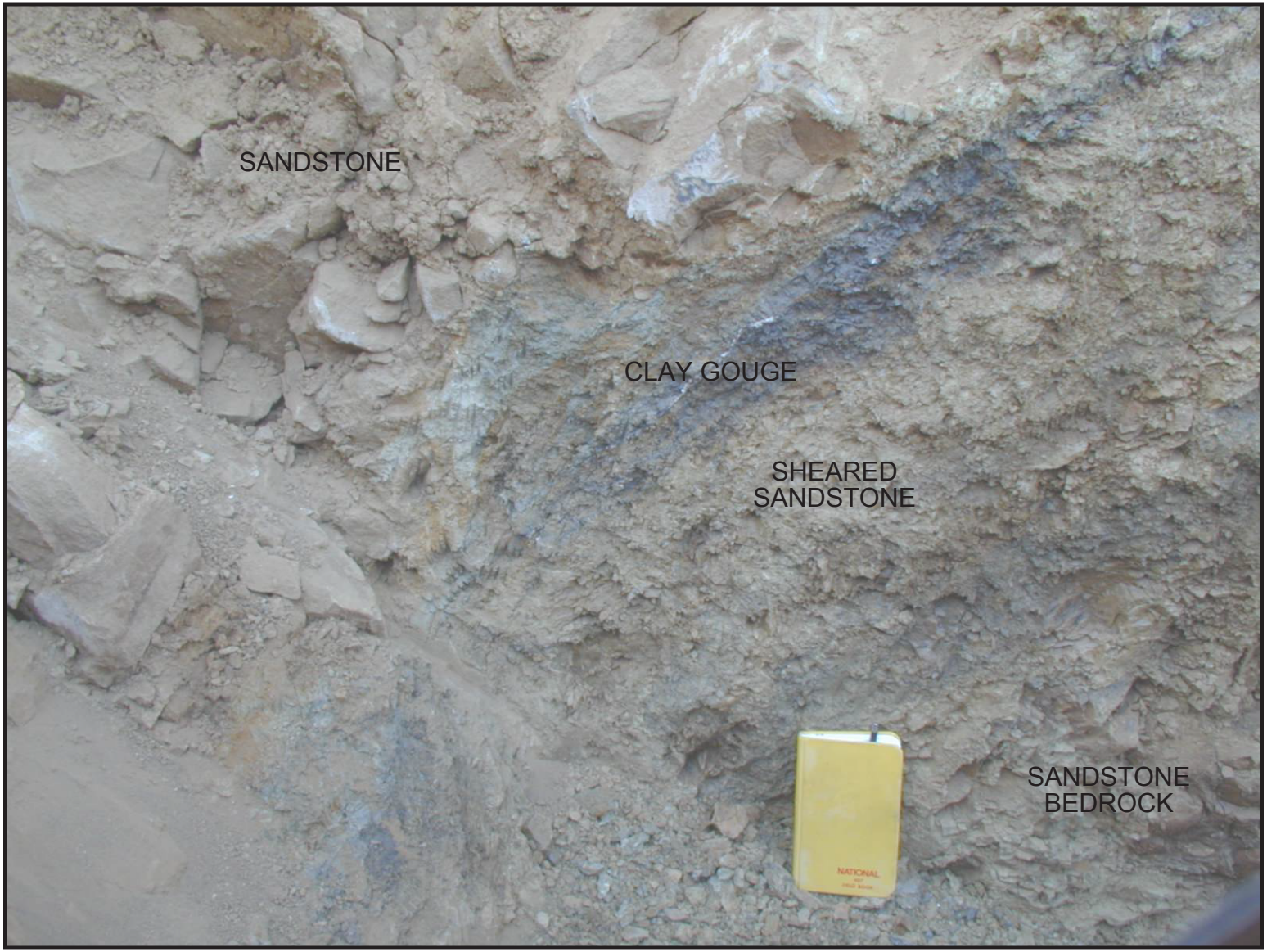


PHASE 2 FAULT AND SEISMIC HAZARDS INVESTIGATION
NORTH OF DELTA OFFSTREAM STORAGE
DWR-INTEGRATED STORAGE INVESTIGATION

**Photo, North Wall, Trench TPE-1, GG-3 Fault, Golden Gate Damsite**

WLA William Lettis & Associates, Inc. | Figure 3-23

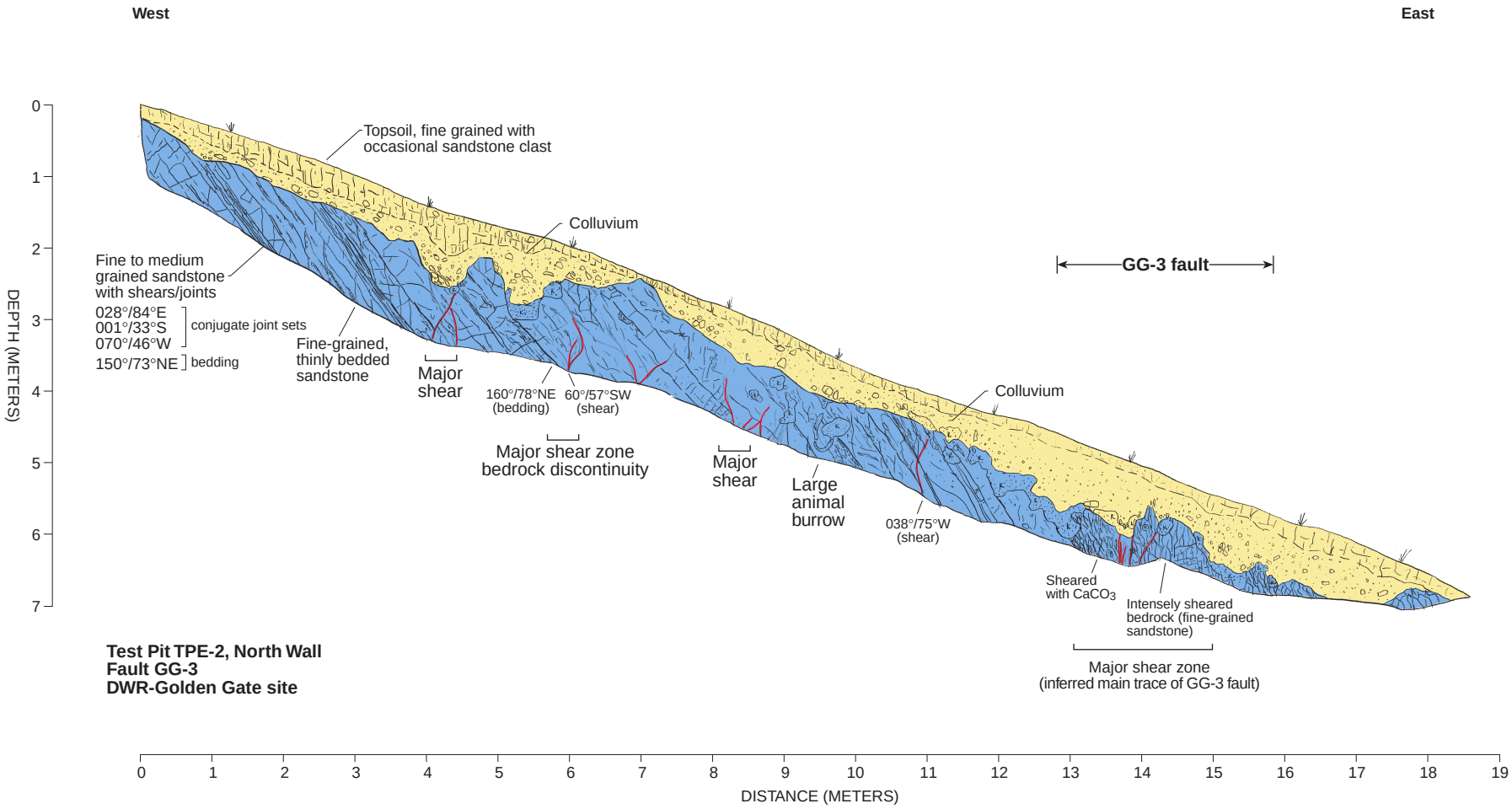


PHASE 2 FAULT AND SEISMIC HAZARDS INVESTIGATION
NORTH OF DELTA OFFSTREAM STORAGE
DWR- INTEGRATED STORAGE INVESTIGATION

**Testpit TPE-2 - North Wall, GG-3 Fault, Golden Gate Damsite**

WLA William Lettis & Associates, Inc.

Figure 3-24

**Northwest** **Southeast**

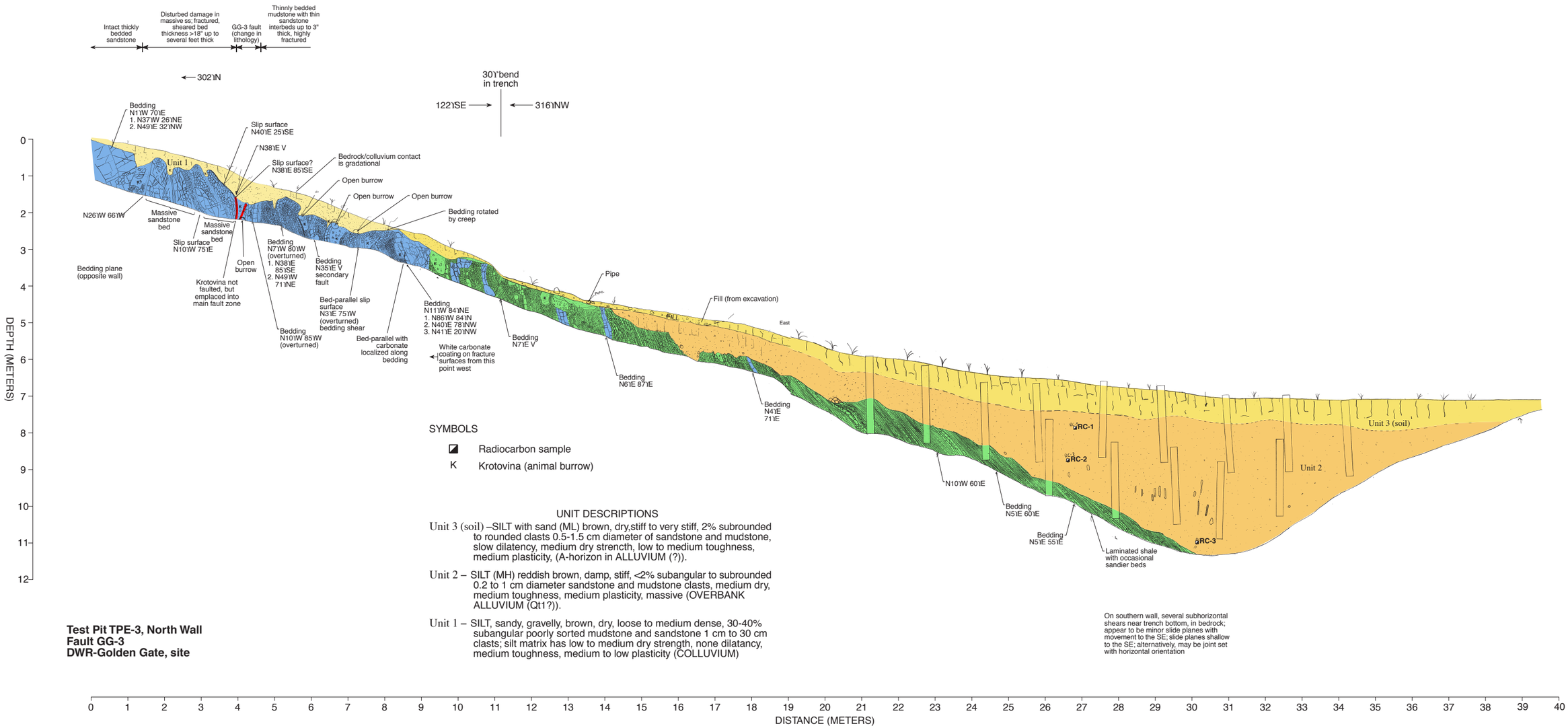


SYMBOLS

◪ Radiocarbon sample

K Krotovina (animal burrow)

UNIT DESCRIPTIONS

Unit 3 (soil) –SILT with sand (ML) brown, dry,stiff to very stiff, 2% subrounded to rounded clasts 0.5-1.5 cm diameter of sandstone and mudstone, slow dilatency, medium dry strength, low to medium toughness, medium plasticity, (A-horizon in ALLUVIUM (?)).

Unit 2 – SILT (MH) reddish brown, damp, stiff, <2% subangular to subrounded 0.2 to 1 cm diameter sandstone and mudstone clasts, medium dry, medium toughness, medium plasticity, massive (OVERBANK ALLUVIUM (Qt1?)).

Unit 1 – SILT, sandy, gravelly, brown, dry, loose to medium dense, 30-40% subangular poorly sorted mudstone and sandstone 1 cm to 30 cm clasts; silt matrix has low to medium dry strength, none dilatancy, medium toughness, medium to low plasticity (COLLUVIUM)

On southern wall, several subhorizontal shears near trench bottom, in bedrock; appear to be minor slide planes with movement to the SE; slide planes shallow to the SE; alternatively, may be joint set with horizontal orientation

**Test Pit TPE-3, North Wall**
**Fault GG-3**
**DWR-Golden Gate, site**

PHASE 2 FAULT AND SEISMIC HAZARDS INVESTIGATION
NORTH OF DELTA OFFSTREAM STORAGE
DWR-INTEGRATED STORAGE INVESTIGATION

# Testpit TPE-3 - North Wall, GG-3 Fault, Golden Gate Damsite

William Lettis & Associates, Inc.

Figure 3-25

Fault S-2

Fault S-3

Funks Reservoir

"brown beds"

"p-beds"

FT-6

FT-8

FT-9

2-1

2-2

2-3

2-4

2-5

2-6

2-7

TOWN OF SITES

Approximate position of Sites Dam footprint

Sites Quarry Fault Exposure

N

EXPLANATION

Photo lineament (based on interpretation of aerial photograph)

Fault– solid where feature mapped in field, dotted where inferred; shaded zone delineates wider fault zone based on mapped and inferred faults

Bedrock unit used to map fault truncations and/or fault offset

2-7 Field descriptions, for specific station: see Table 1

FT-7 Trench and test pit location

0 2000 4000 ft

0 1 km

PHASE 2 FAULT AND SEISMIC HAZARDS INVESTIGATION
NORTH OF DELTA OFFSTREAM STORAGE
DWR- INTEGRATED STORAGE INVESTIGATION

**Compilation of Field Observations along Fault S-2 in the Vicinity of the Sites Dam Site**

William Lettis & Associates, Inc.

Figure 3-28

**Trench FT-6, East Wall**
**Fault S-2**
**DWR-Sites**

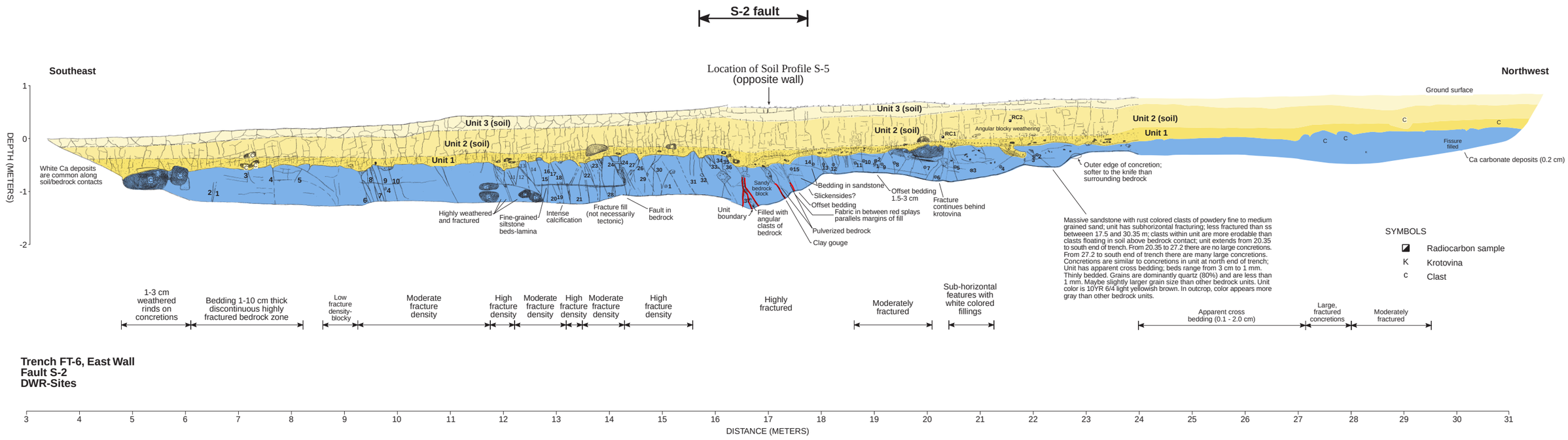





PHASE 2 FAULT AND SEISMIC HAZARDS INVESTIGATION
NORTH OF DELTA OFFSTREAM STORAGE
DWR-INTEGRATED STORAGE INVESTIGATION

**Trench FT-6 - East Wall, S-2 Fault, Golden Gate Damsite**

William Lettis & Associates, Inc.

Figure 3-29

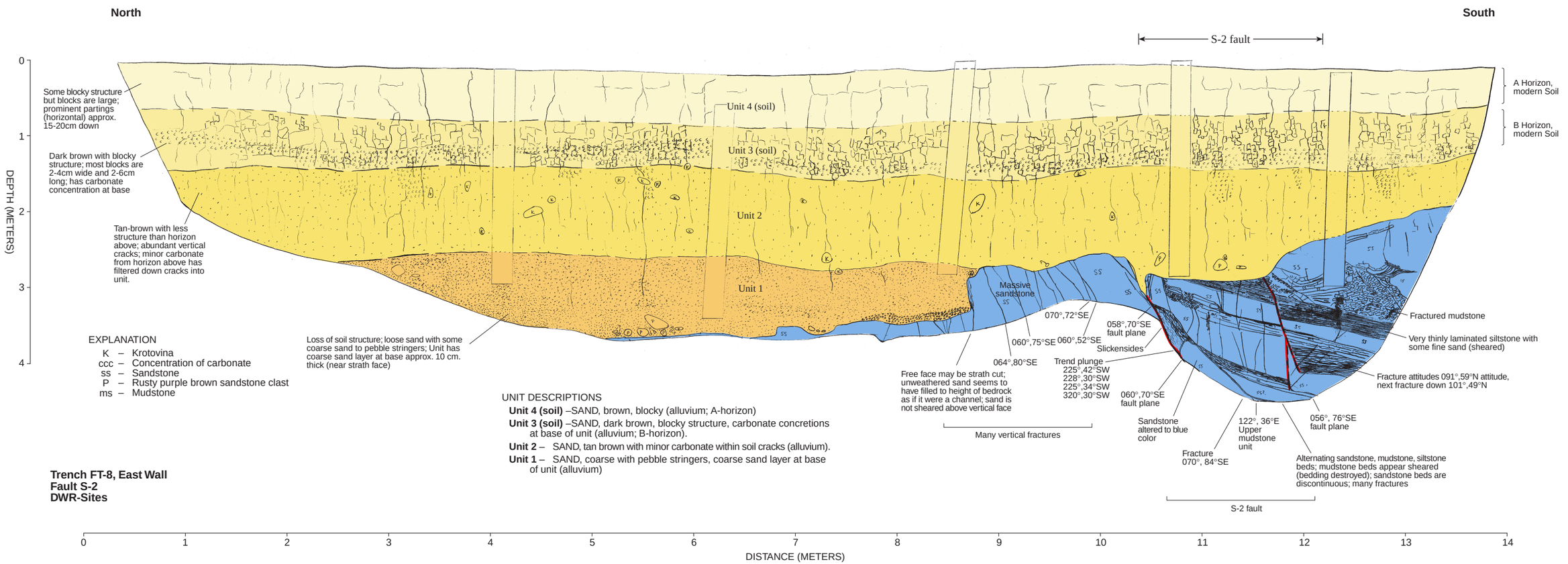


**Trench FT-8, East Wall**
**Fault S-2**
**DWR-Sites**

PHASE 2 FAULT AND SEISMIC HAZARDS INVESTIGATION
NORTH OF DELTA OFFSTREAM STORAGE
DWR-INTEGRATED STORAGE INVESTIGATION

# Trench FT-8 - East Wall, S-2 Fault, Sites

WLA William Lettis & Associates, Inc.

Figure 3-30

North

South

Inferred S-2 fault location

Soil Profile SP7

Gray brown horizontal partings

Dark brown blocky structure; blocks oriented vertical and horizontal

Absence of soil structure; massive sand with gravel stringers and iron oxidized nodules; $CaCO_3$ infilling old roots; black flecks of mudstone throughout

Structure change

Higher concentration of $CaCO_3$

Unit 7 (soil)

Unit 6 (soil)

Unit 5 (soil)

Unit 3

Unit 2a

Unit 1

Unit 2b

Unit 1

No $CaCO_3$

Prominant horizontal partings

Blocky structure oriented horizontal and vertical

Fluvial stratigraphy with coarse sand lenses with gravel stringers and a few carbonate stringers

TRENCH COLLAPSE (covered by spoils)

Project base of yellow/orange on opposite wall

Fine sand in inset channel deposit

Clayey, sandy, olive green with abundant carbonate nodules

channel sand, mod. well sorted

SPOIL

Bedding replaced with white carbonate

Bedding replaced by carbonate

Zone of no carbonate

Fracture filled with white carbonate

Thinly bedded mudstone; some beds have been replaced by carbonate

Bedded sandstone; beds range in thickness from 1 to 5 cm.

Thinly bedded mudstone; white carbonate throughout along bedding planes and fractures

Bedded sandstone with abundant fractures; beds range from 2 to 15 cm thick; sandstone is soft and breaks apart with hammer; sandstone composition is approximately 90% quartz, 10% dark lithics; grains are subrounded and medium to coarse grained; carbonate has been deposited along bedding planes.

Altered bedrock, sandy to clayey

Siltstone with sandstone stringers (fine-grained)

Gray clay, altered sandstone

White carbonate material

Shear N72°E 85°SE

Rising groundwater

N69°E 80°SE

N71°E 85°NW

Attitude of channel margin across trench to south wall: S15W N15E (approx.)

This section of trench exposed by re-excavation following collapse
Opposite trench wall of this section logged as FT-9b

**Trench FT-9A, East Wall**
**Fault S-2**
**DWR-Sites**

DEPTH (METERS)

0 1 2 3 4 5

DISTANCE (METERS)

0 1 2 3 4 5 6 7 8 9 10 11 12 13 14 15 16 17 18 19 20 21 22

PHASE 2 FAULT AND SEISMIC HAZARDS INVESTIGATION
NORTH OF DELTA OFFSTREAM STORAGE
DWR-INTEGRATED STORAGE INVESTIGATION

**Trench FT-9a - East Wall, S-2 Fault**

WLA William Lettis & Associates, Inc.

Figure 3-31

South

North

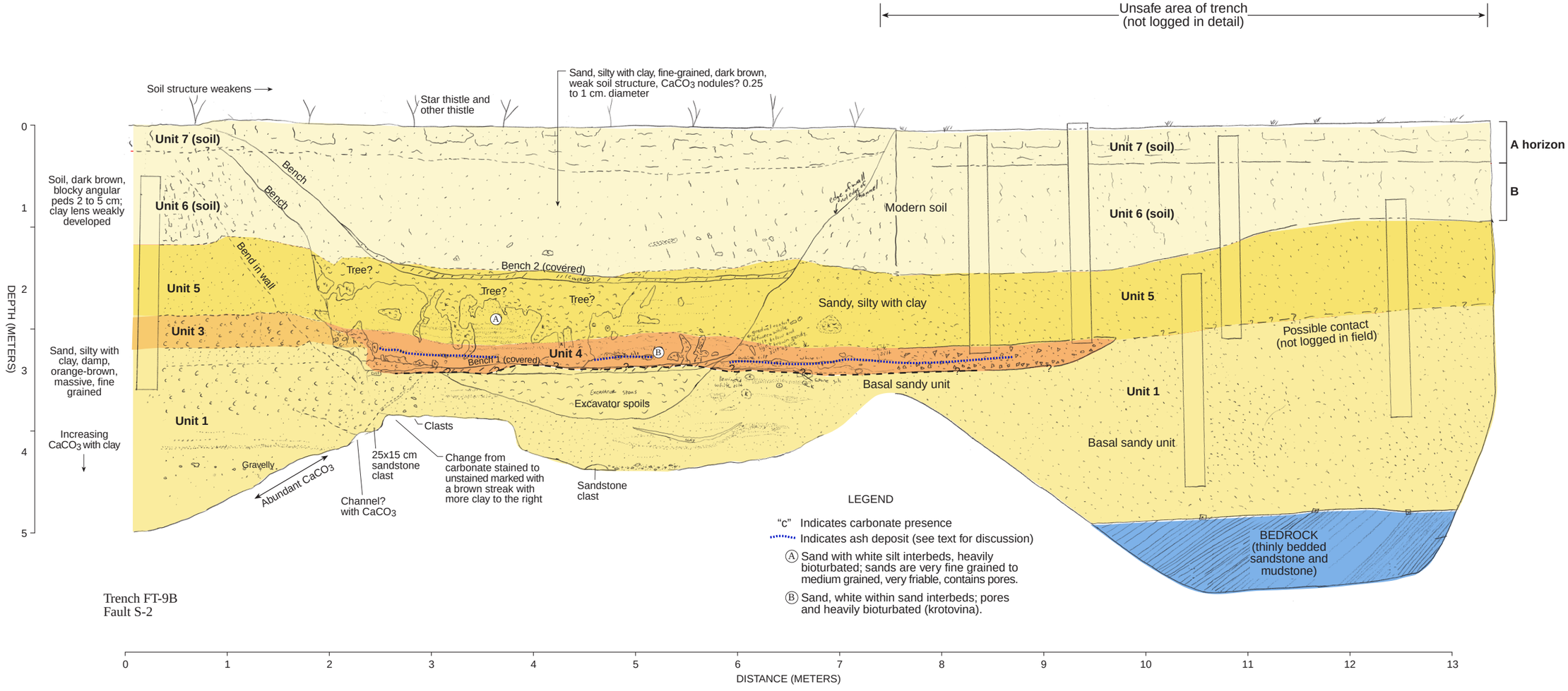


Trench FT-9B
Fault S-2

PHASE 2 FAULT AND SEISMIC HAZARDS INVESTIGATION
NORTH OF DELTA OFFSTREAM STORAGE
DWR-INTEGRATED STORAGE INVESTIGATION

**Trench FT-9b - East Wall, S-2 Fault**

WLA William Lettis & Associates, Inc.

Figure 3-32

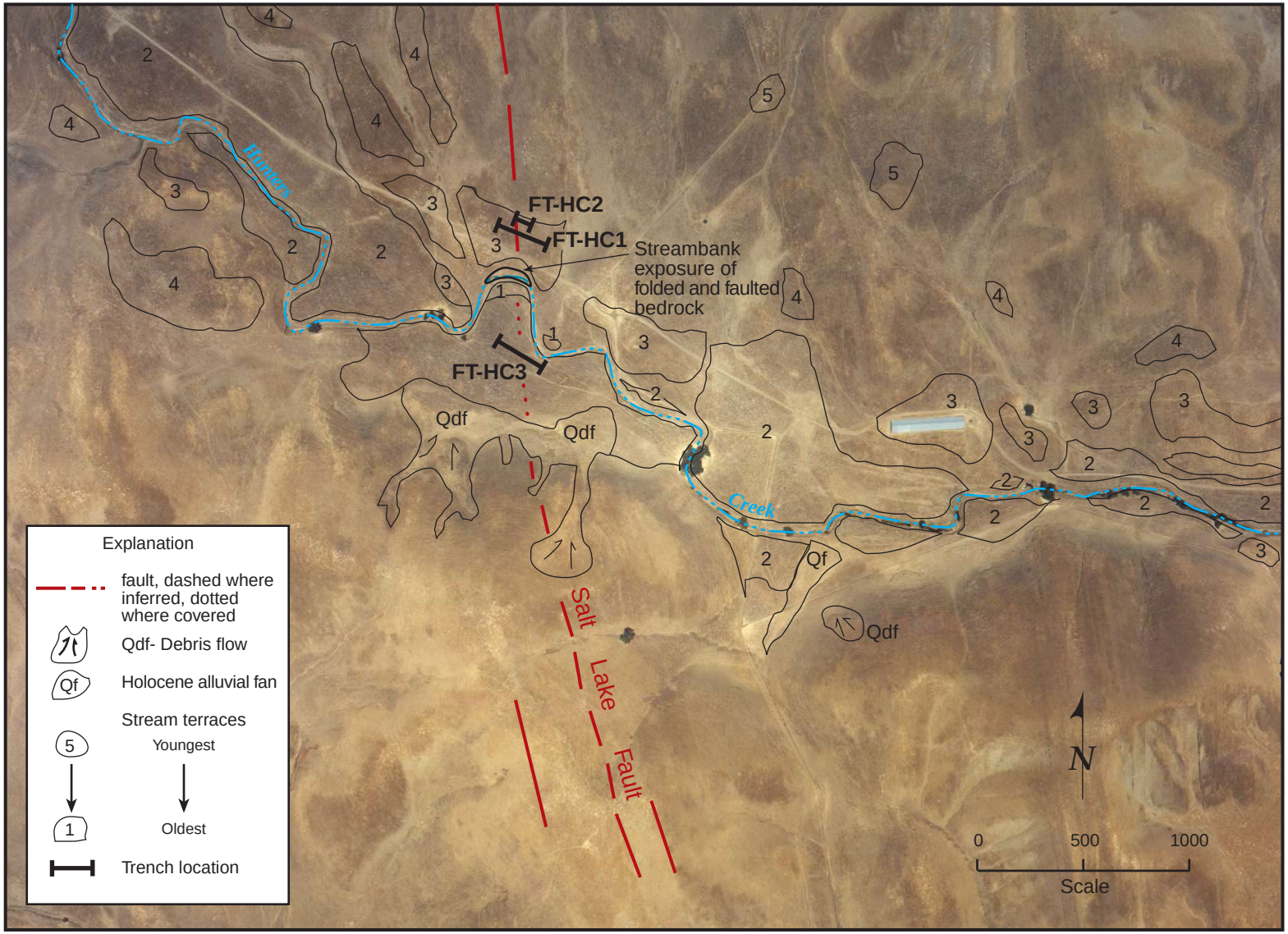


PHASE 2 FAULT AND SEISMIC HAZARDS INVESTIGATION
NORTH OF DELTA OFFSTREAM STORAGE
DWR-INTEGRATED STORAGE INVESTIGATION

**Map of geologic deposits, stream terraces, and Salt Lake fault at the Hunters Creek Trench site shown on color aerial photograph taken in June, 1999**

WLA William Lettis & Associates, Inc. | Figure 3-33




PHASE 2 FAULT AND SEISMIC HAZARDS INVESTIGATION
NORTH OF DELTA OFFSTREAM STORAGE
DWR-INTEGRATED STORAGE INVESTIGATION

**Photo, View to North, Trench FT-HC1, Salt Lake Fault, Hunters Creek**

WLA William Lettis & Associates, Inc. | Figure 3-34

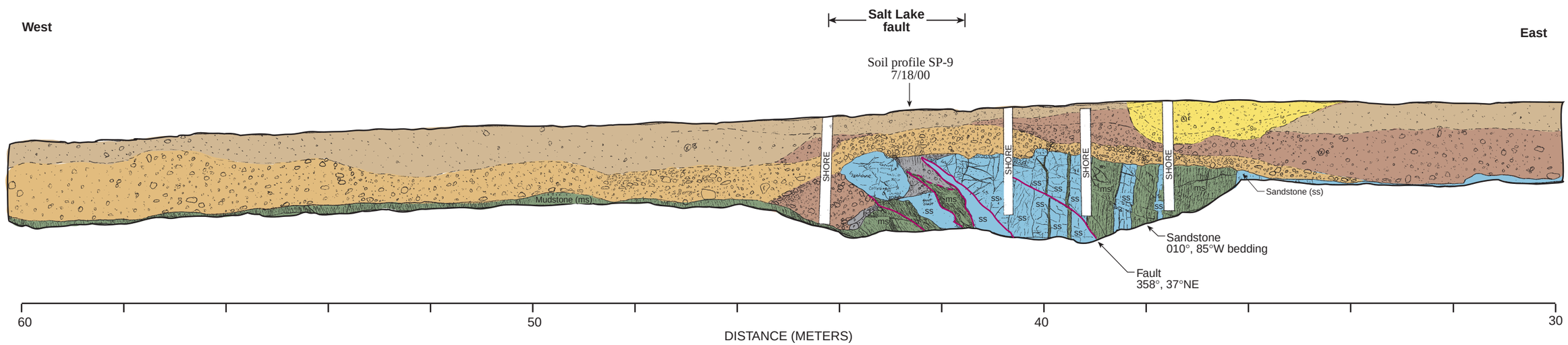


PHASE 2 FAULT AND SEISMIC HAZARDS INVESTIGATION
NORTH OF DELTA OFFSTREAM STORAGE
DWR-INTEGRATED STORAGE INVESTIGATION

**Trench FT-HC1, North Wall,
Salt Lake Fault, Hunters Creek**

WLA William Lettis & Associates, Inc.

Figure 3-35

East

West

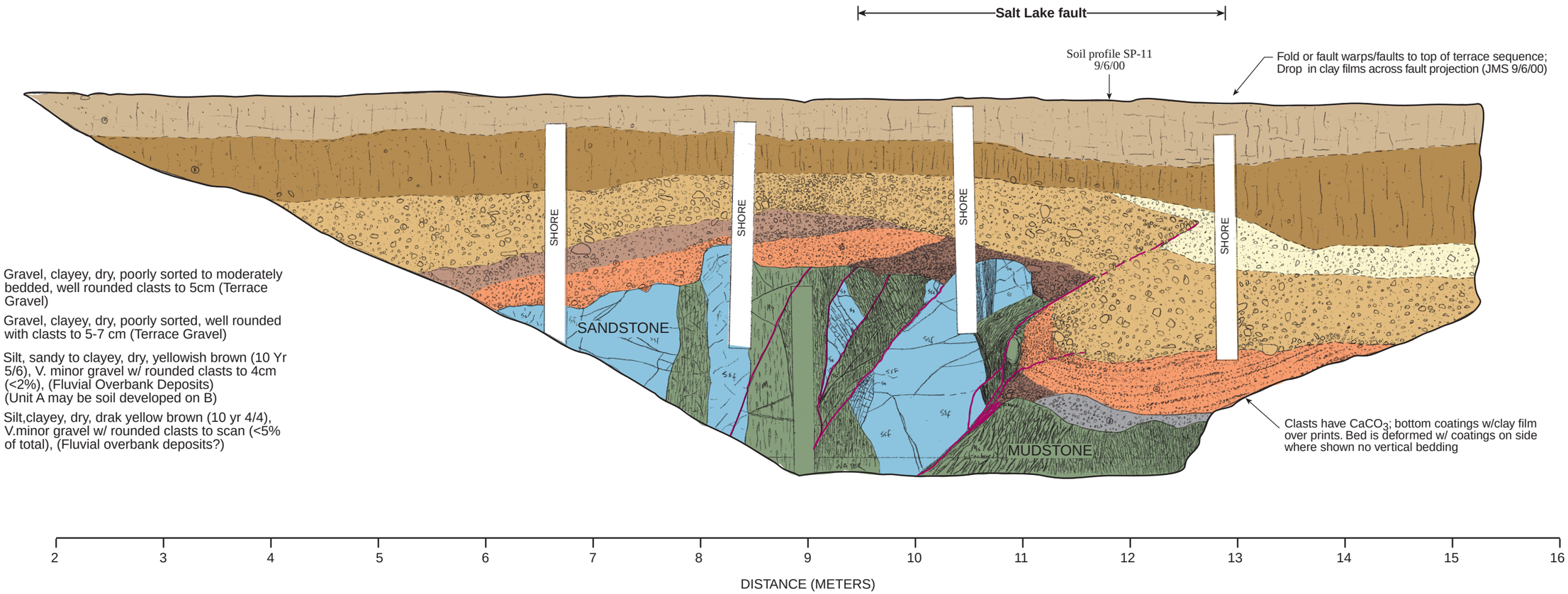


Unit 5 Gravel, clayey, dry, poorly sorted to moderately bedded, well rounded clasts to 5cm (Terrace Gravel)

Unit 6 Gravel, clayey, dry, poorly sorted, well rounded with clasts to 5-7 cm (Terrace Gravel)

Unit 7 Silt, sandy to clayey, dry, yellowish brown (10 Yr 5/6), V. minor gravel w/ rounded clasts to 4cm (<2%), (Fluvial Overbank Deposits) (Unit A may be soil developed on B)

Unit 8 Silt,clayey, dry, drak yellow brown (10 yr 4/4), V.minor gravel w/ rounded clasts to scan (<5% of total), (Fluvial overbank deposits?)

PHASE 2 FAULT AND SEISMIC HAZARDS INVESTIGATION
NORTH OF DELTA OFFSTREAM STORAGE
DWR-INTEGRATED STORAGE INVESTIGATION

**Trench FT-HC2, South Wall, Salt Lake Fault, Hunters Creek**

WLA William Lettis & Associates, Inc.

Figure 3-37

West

East

113°

Salt Lake fault

Apparent fold or fault offset of coarse gravel

SHORE

SHORE

SHORE

SHORE

SHORE

Mudstone bedrock
348°/80°E (bedding)

Water table (7/31/00)

Mudstone bedrock
355°/72°W (bedding)

Fault
076°, 88°SE
3-5 cm wavelength
mullions with 0.5-1 cm
amplitude

Fault
020°, 59°E

Mudstone bedrock
005°/80°E (bedding)

20 19 18 17 16 15 14 13 12 11 10 9 8 7 6 5 4

DISTANCE (METERS)

PHASE 2 FAULT AND SEISMIC HAZARDS INVESTIGATION
NORTH OF DELTA OFFSTREAM STORAGE
DWR-INTEGRATED STORAGE INVESTIGATION

**Trench FT-HC2, North Wall,
Salt Lake Fault, Hunters Creek**

WLA William Lettis & Associates, Inc.

Figure 3-39

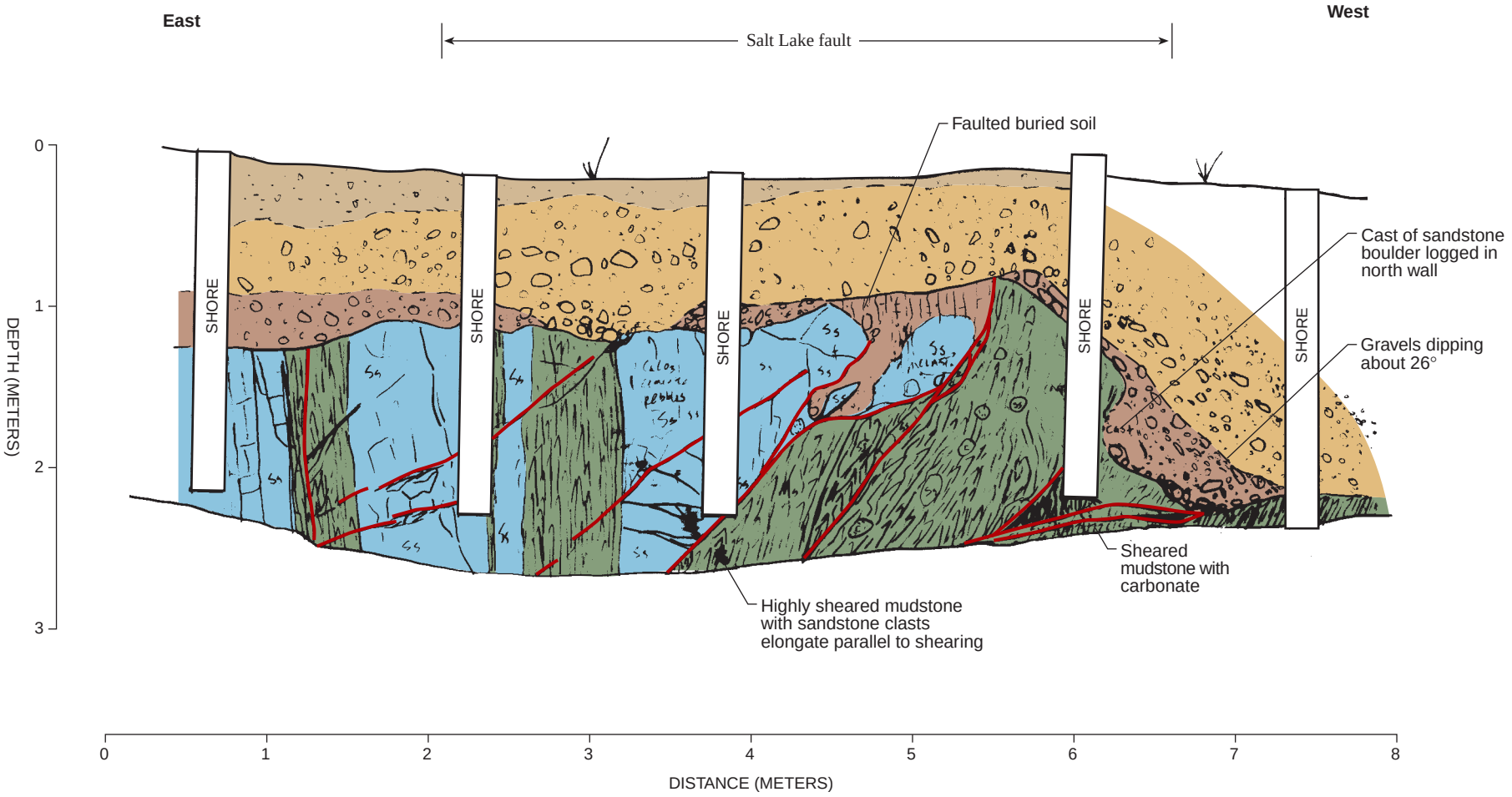


PHASE 2 FAULT AND SEISMIC HAZARDS INVESTIGATION
NORTH OF DELTA OFFSTREAM STORAGE
DWR-INTEGRATED STORAGE INVESTIGATION

**Trench FT-HC1 - South Wall, Salt Lake Fault, Hunters Creek**

WLA William Lettis & Associates, Inc. | Figure 3-36




PHASE 2 FAULT AND SEISMIC HAZARDS INVESTIGATION
NORTH OF DELTA OFFSTREAM STORAGE
DWR-INTEGRATED STORAGE INVESTIGATION

**Photo, South Wall, Trench FT-HC2, Salt Lake Fault, Hunters Creek**

WLA William Lettis & Associates, Inc. | Figure 3-38

**A** UNRESTORED

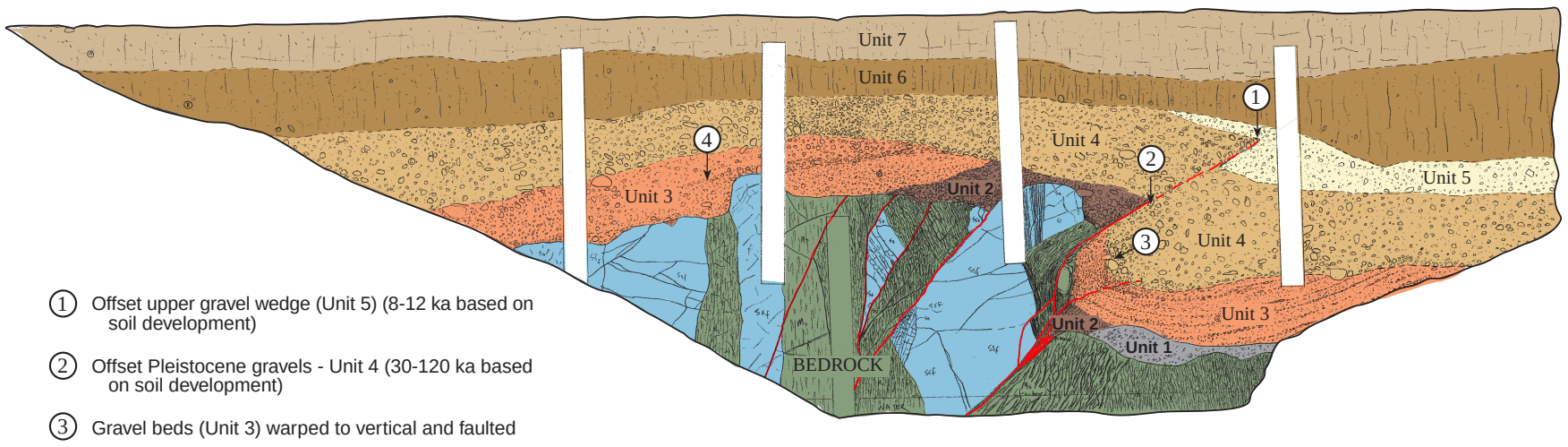


1. Offset upper gravel wedge (Unit 5) (8-12 ka based on soil development)
2. Offset Pleistocene gravels - Unit 4 (30-120 ka based on soil development)
3. Gravel beds (Unit 3) warped to vertical and faulted
4. Older Pleistocene gravels (Unit 3) back-tilted

**B** EVENT 1 RECONSTRUCTION

Fault parallel 0.4 m displacement

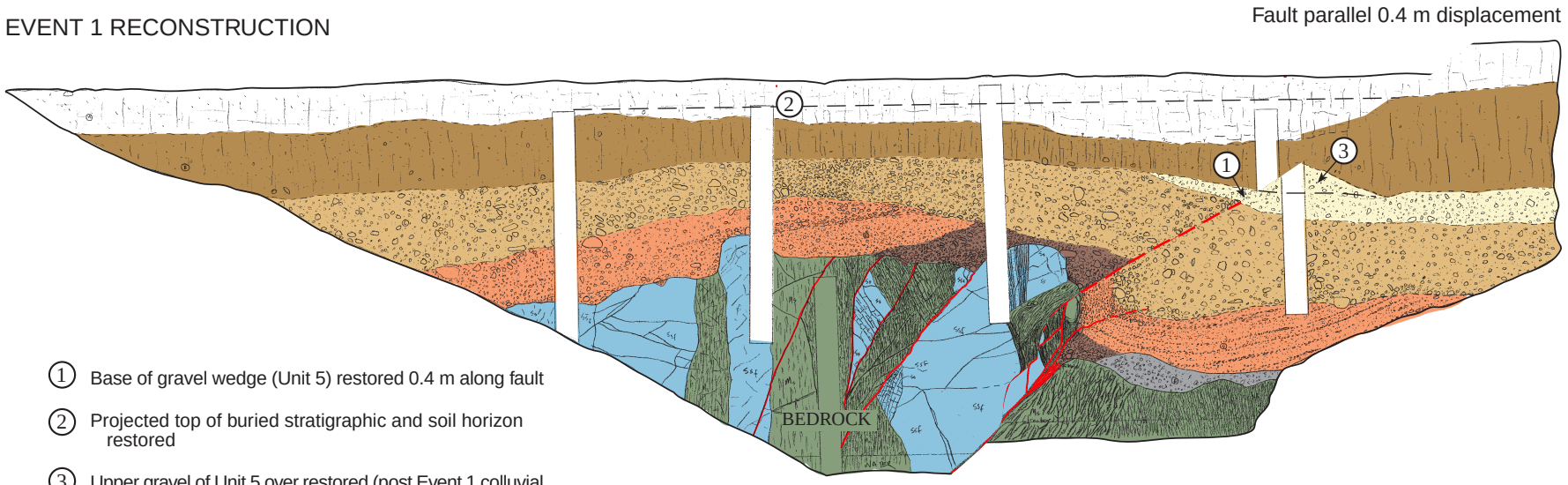


1. Base of gravel wedge (Unit 5) restored 0.4 m along fault
2. Projected top of buried stratigraphic and soil horizon restored
3. Upper gravel of Unit 5 over restored (post Event 1 colluvial wedge?)

Fault parallel 0.8 m displacement

**C** EVENT 2 RECONSTRUCTION

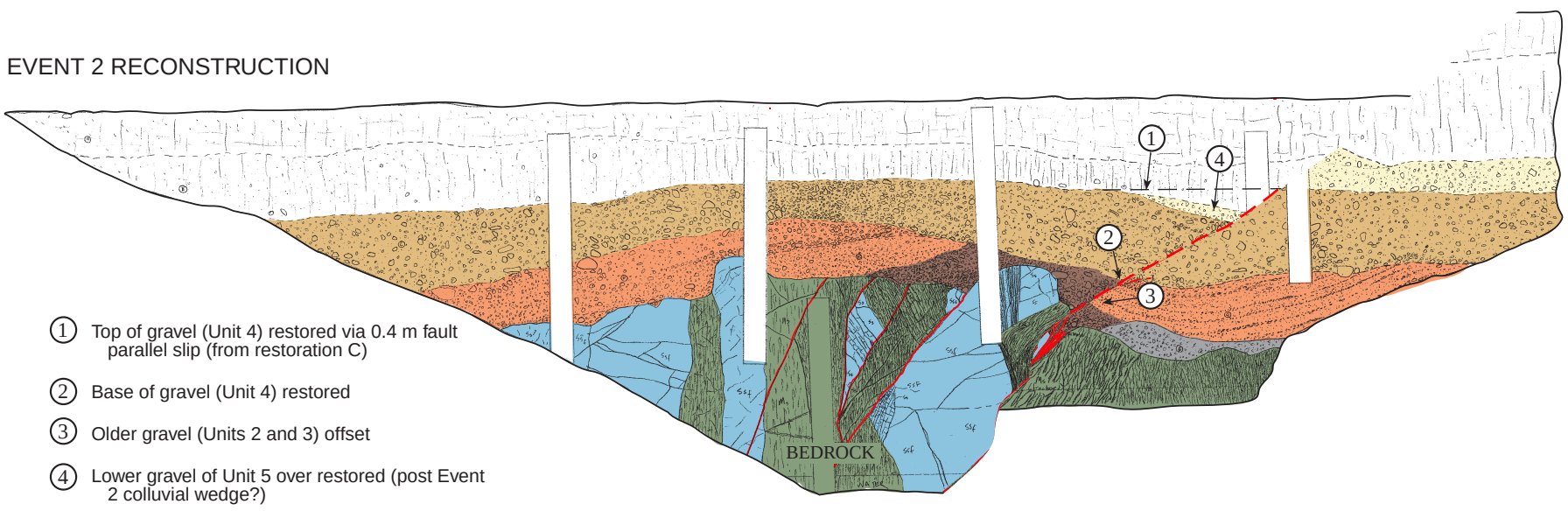


1. Top of gravel (Unit 4) restored via 0.4 m fault parallel slip (from restoration C)
2. Base of gravel (Unit 4) restored
3. Older gravel (Units 2 and 3) offset
4. Lower gravel of Unit 5 over restored (post Event 2 colluvial wedge?)

Fault parallel 1.2 m displacement

**D** EVENT 3 RECONSTRUCTION

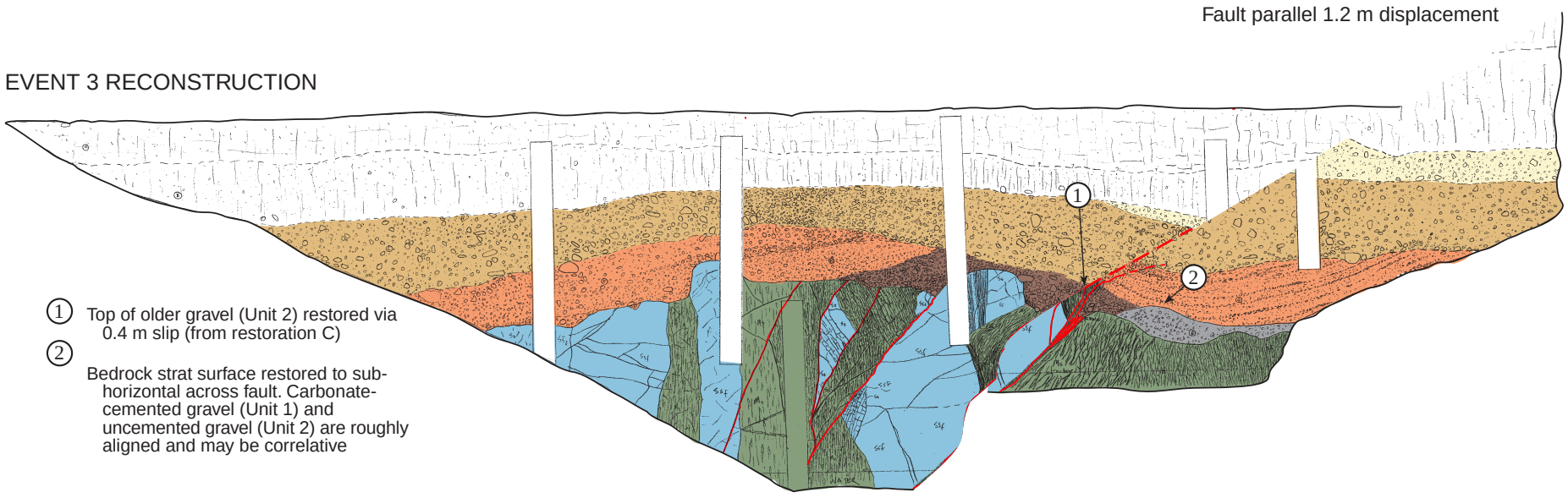


1. Top of older gravel (Unit 2) restored via 0.4 m slip (from restoration C)
2. Bedrock strat surface restored to sub-horizontal across fault. Carbonate-cemented gravel (Unit 1) and uncemented gravel (Unit 2) are roughly aligned and may be correlative

PHASE 2 FAULT AND SEISMIC HAZARDS INVESTIGATION
NORTH OF DELTA OFFSTREAM STORAGE
DWR-INTEGRATED STORAGE INVESTIGATION

**Reconstruction of Faulting - Trench FT-HC2, Salt Lake Fault**

WLA William Lettis & Associates, Inc.

Figure 3-41

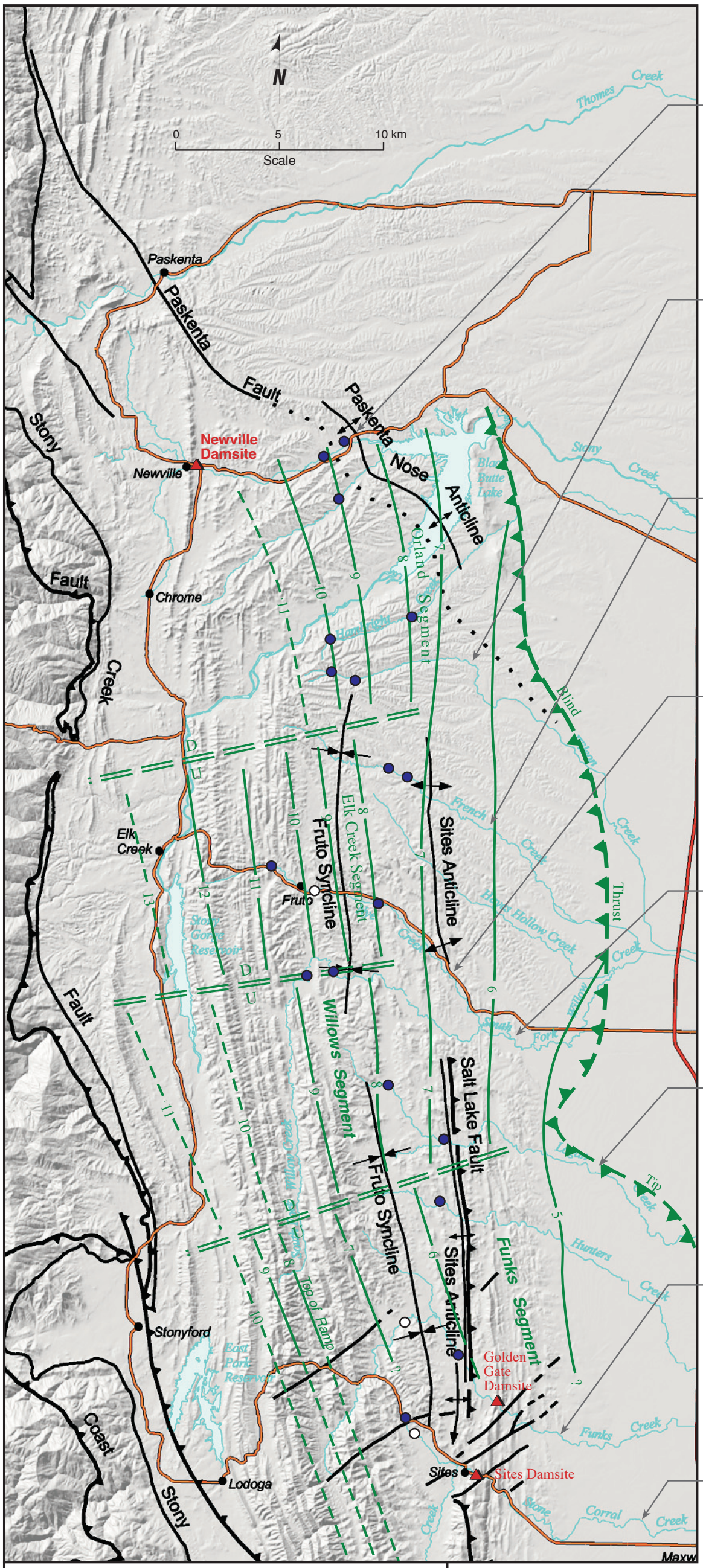


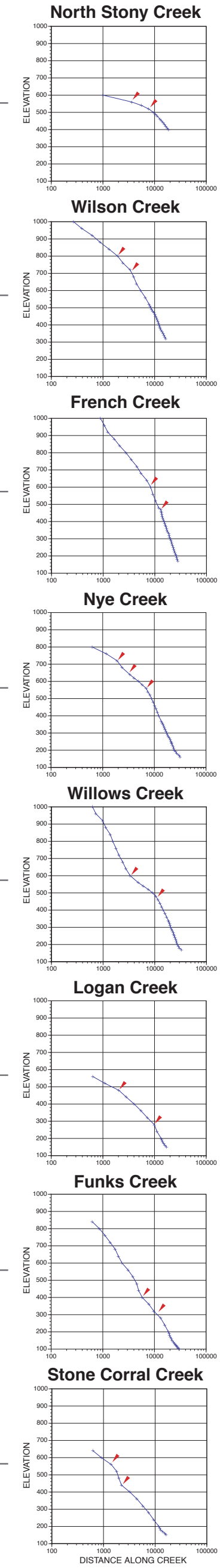


EXPLANATION

- Stream Convexity
- Stream Concavity
- 7 — Depth (in km) below sea level to top of thrust fault
- Thrust fault; teeth on hanging wall
- Fault; sense of horizontal displacement shown

PHASE 2 FAULT AND SEISMIC HAZARDS INVESTIGATION
NORTH OF DELTA OFFSTREAM STORAGE
DWR-INTEGRATED STORAGE INVESTIGATION

**Map Showing Major Streams Crossing the Study Area and Stream Channel Profiles**

WLA William Lettis & Associates, Inc. | Figure 3-44

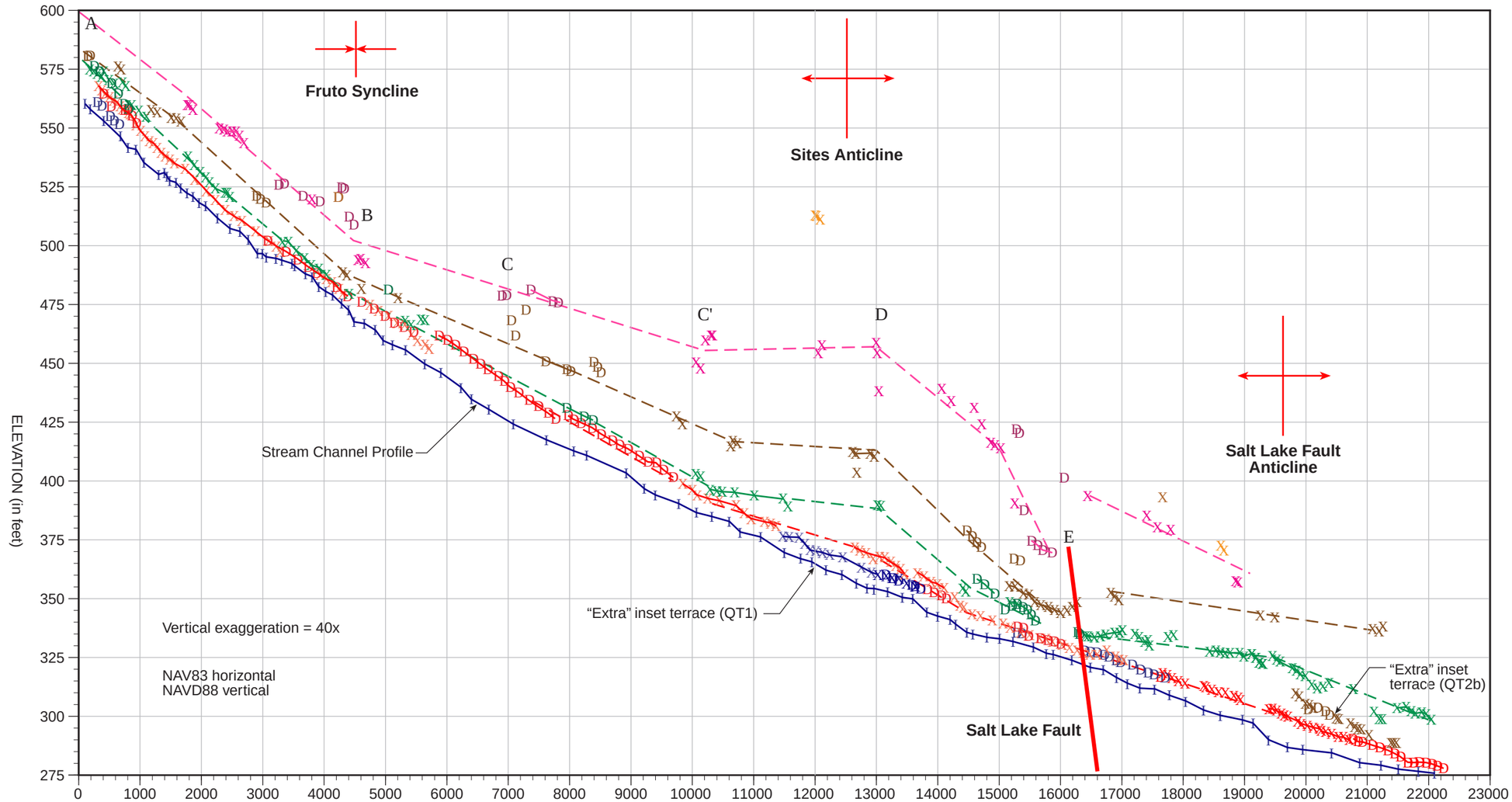


EXPLANATION

- Hunters Creek stream channel

Hunters Creek stream terrace (N=north of creek; S=south of creek)

- X QT1N
- D QT1S
- X QT2N
- D QT2S
- X QT3N
- D QT3S
- X QT4N
- D QT4S
- X QT5N
- D QT5S
- X QT6N
- Anticline
- Syncline

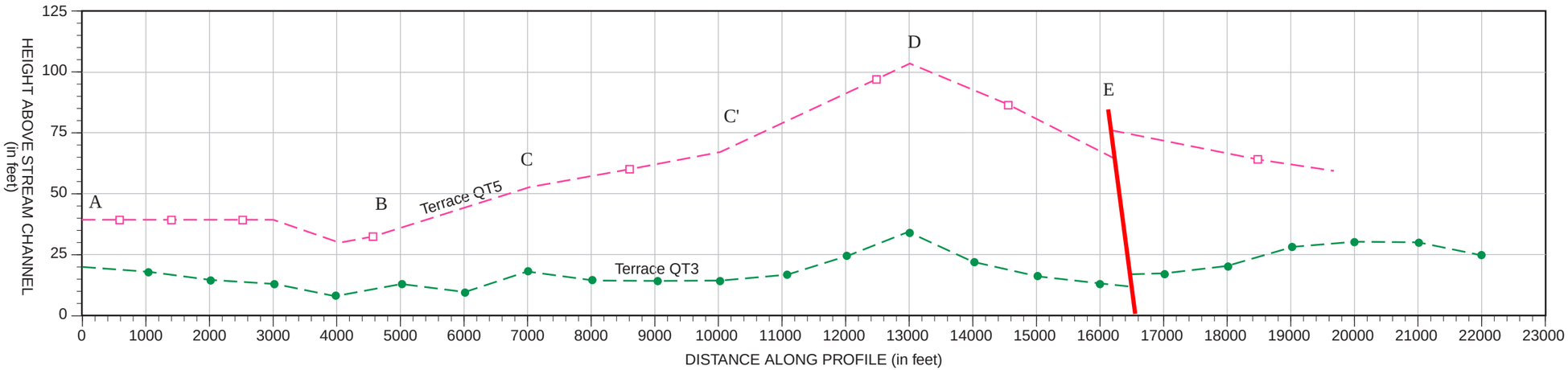


PHASE 2 FAULT AND SEISMIC HAZARDS INVESTIGATION
NORTH OF DELTA OFFSTREAM STORAGE
DWR- INTEGRATED STORAGE INVESTIGATION

**Hunters Creek Terrace Survey**
**December 4-6, 2000**

WLA William Lettis & Associates, Inc.

Figure 3-45

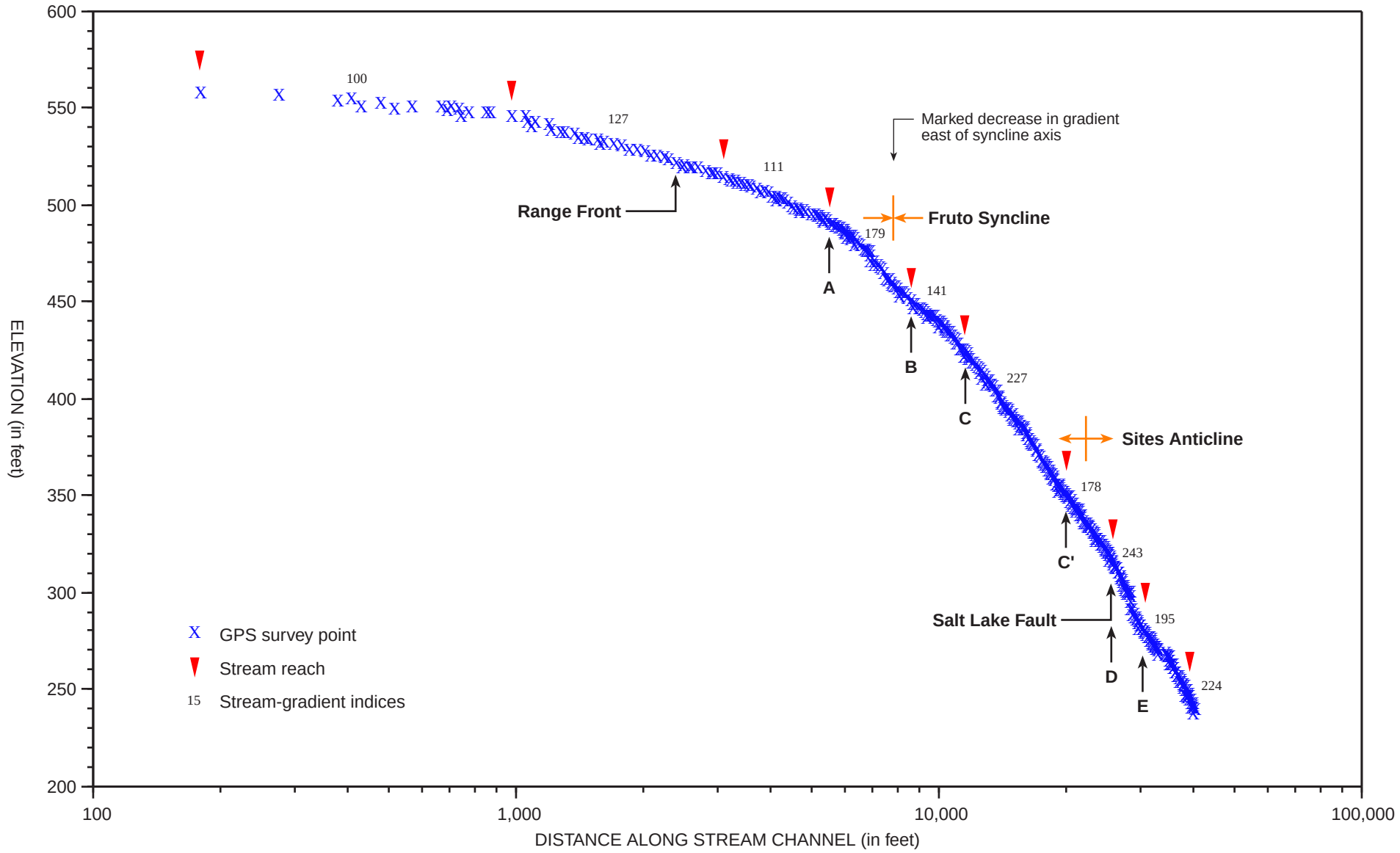


PHASE 2 FAULT AND SEISMIC HAZARDS INVESTIGATION
NORTH OF DELTA OFFSTREAM STORAGE
DWR- INTEGRATED STORAGE INVESTIGATION

**Stream Thalweg Profile of Hunters Creek**

WLA William Lettis & Associates, Inc.

Figure 3-46

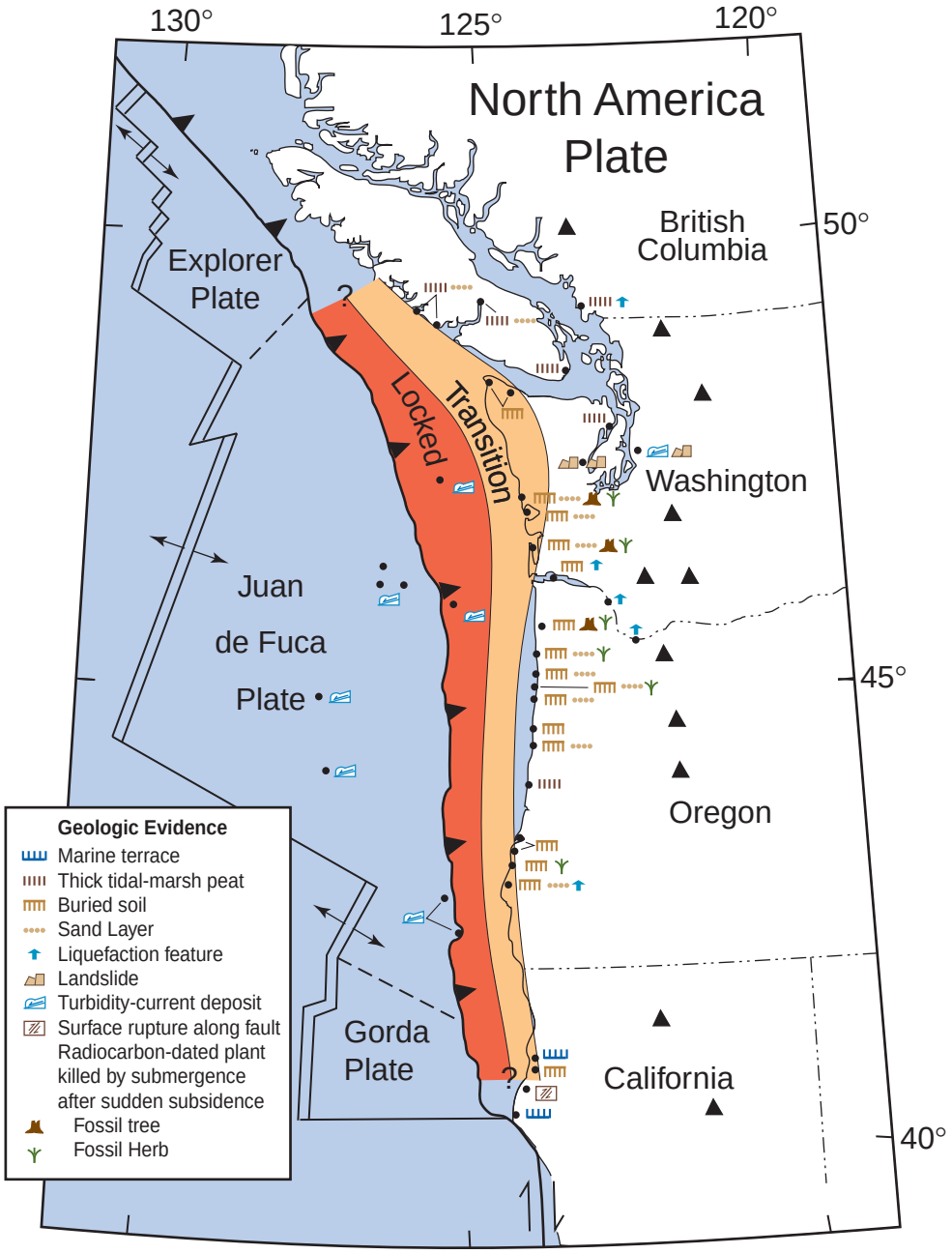


Orange and yellow shaded areas depict the locked and transition zones of the plate interface as modeled by Fluck et al. (1997) and Hyndman and Wang (1995)

PHASE 2 FAULT AND SEISMIC HAZARDS INVESTIGATION
NORTH OF DELTA OFFSTREAM STORAGE
DWR-INTEGRATED STORAGE INVESTIGATION

**Map showing the distribution of geological evidence for plate-boundary earthquakes on the Cascadia subduction zone (modified from Atwater, 1995)**

WLA William Lettis & Associates, Inc. | Figure 3-48

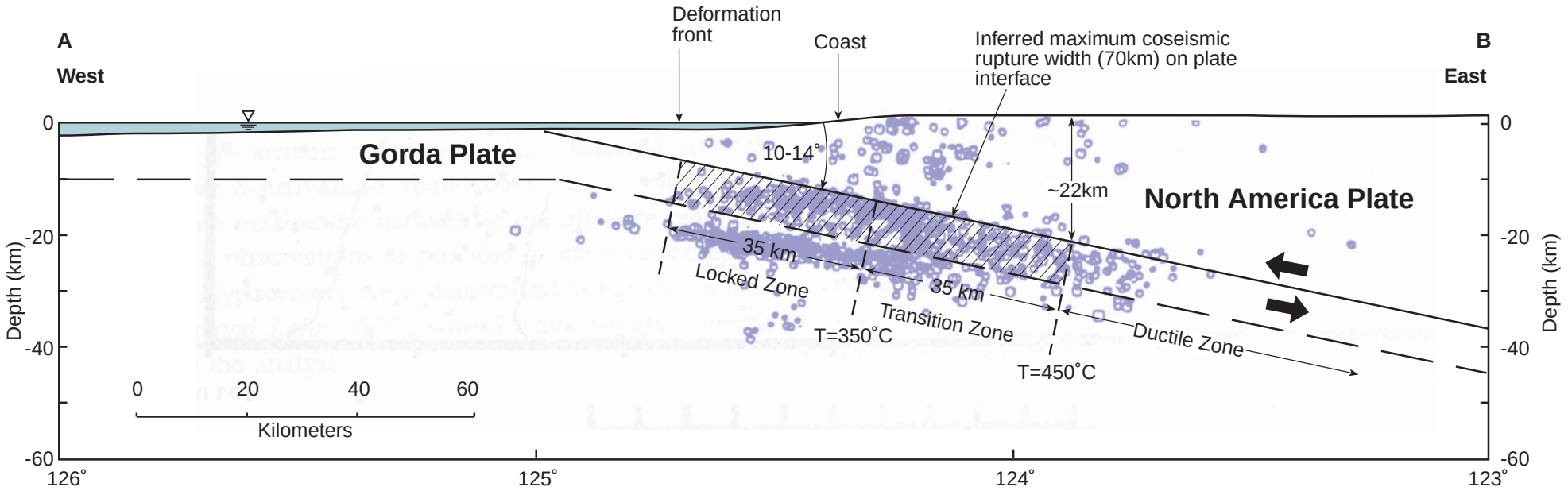


Modified from: Smith et al., 1993;
Beaudoin et al., 1996;
Fluck el al., 1997;
Hyndman and Wang, 1995.

Location of cross section A-B shown in Figure 3-49

PHASE 2 FAULT AND SEISMIC HAZARDS INVESTIGATION
NORTH OF DELTA OFFSTREAM STORAGE
DWR-INTEGRATED STORAGE INVESTIGATION

**Cross section showing the seismicity and geometry of the subducted Gorda plate beneath northwestern California**

WLA William Lettis & Associates, Inc. | Figure 3-50

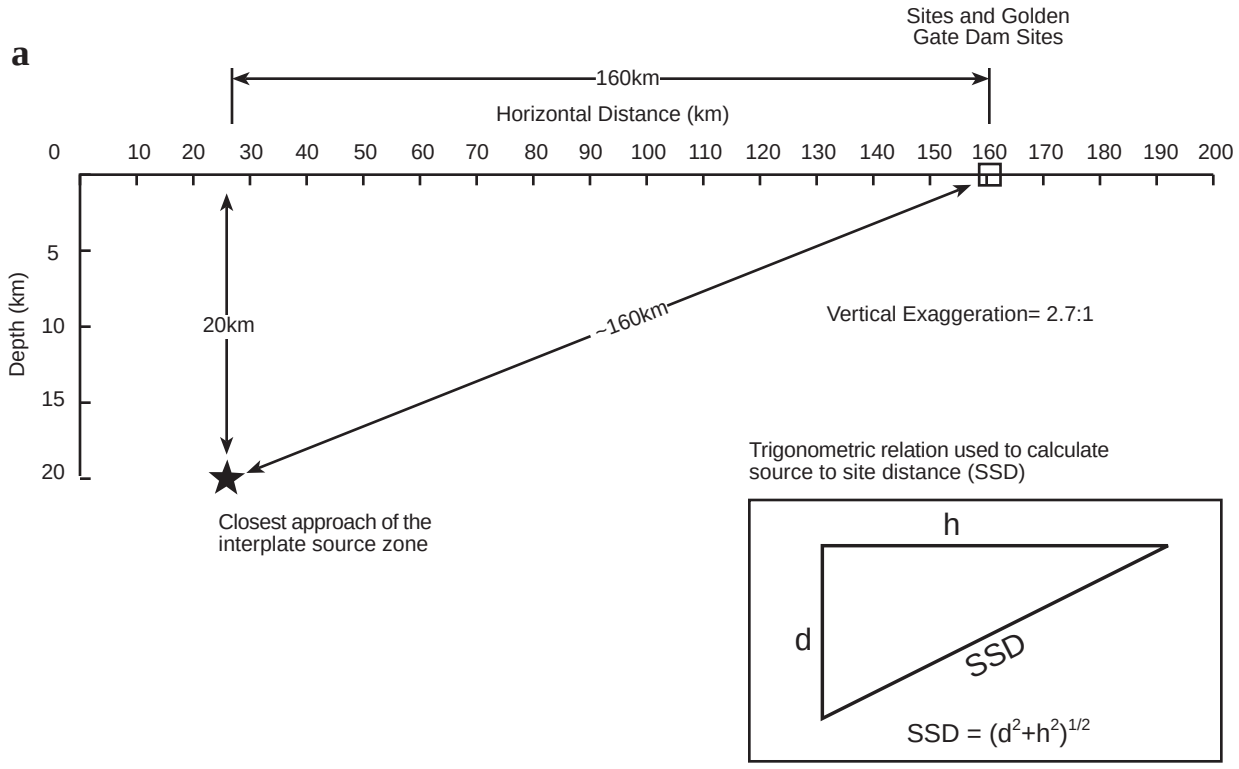


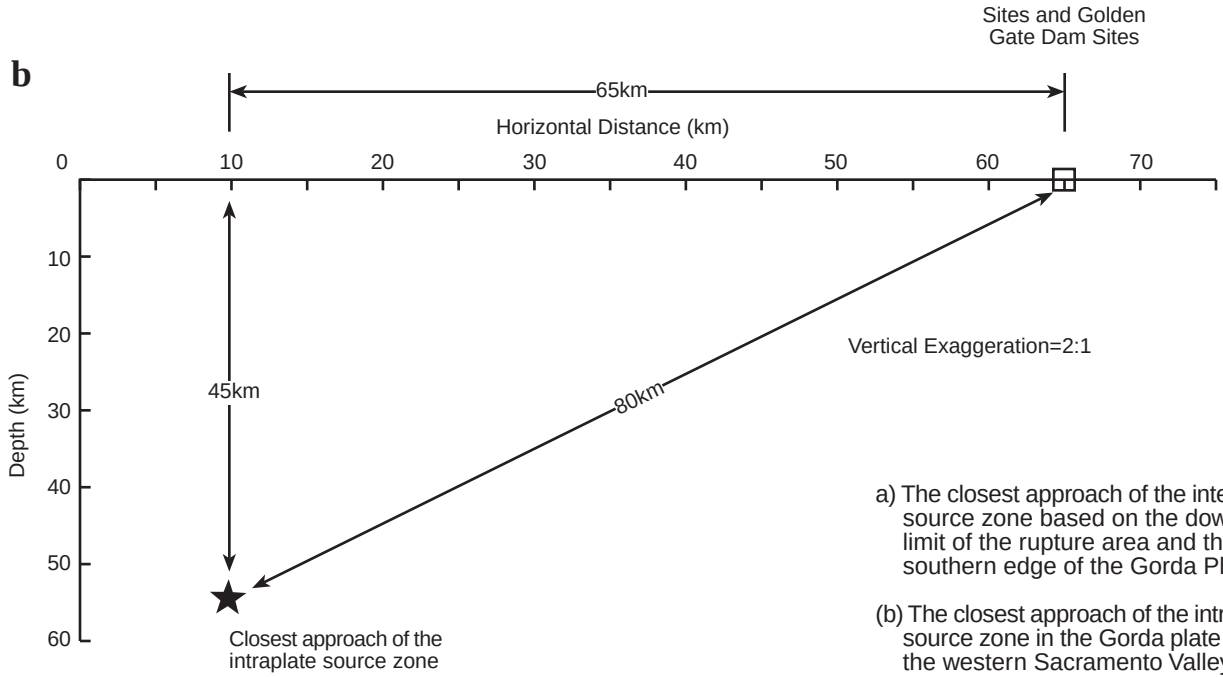


a) The closest approach of the interplate source zone based on the downdip limit of the rupture area and the southern edge of the Gorda Plate.

(b) The closest approach of the intraplate source zone in the Gorda plate below the western Sacramento Valley.

PHASE 2 FAULT AND SEISMIC HAZARDS INVESTIGATION
NORTH OF DELTA OFFSTREAM STORAGE
DWR-INTEGRATED STORAGE INVESTIGATION

**Simple schematic diagrams showing geometry and trigonometric relation used to calculate source-to-site distance (SSD) for Sites and Golden Gate dam sites**

WLA William Lettis & Associates, Inc. | Figure 3-51

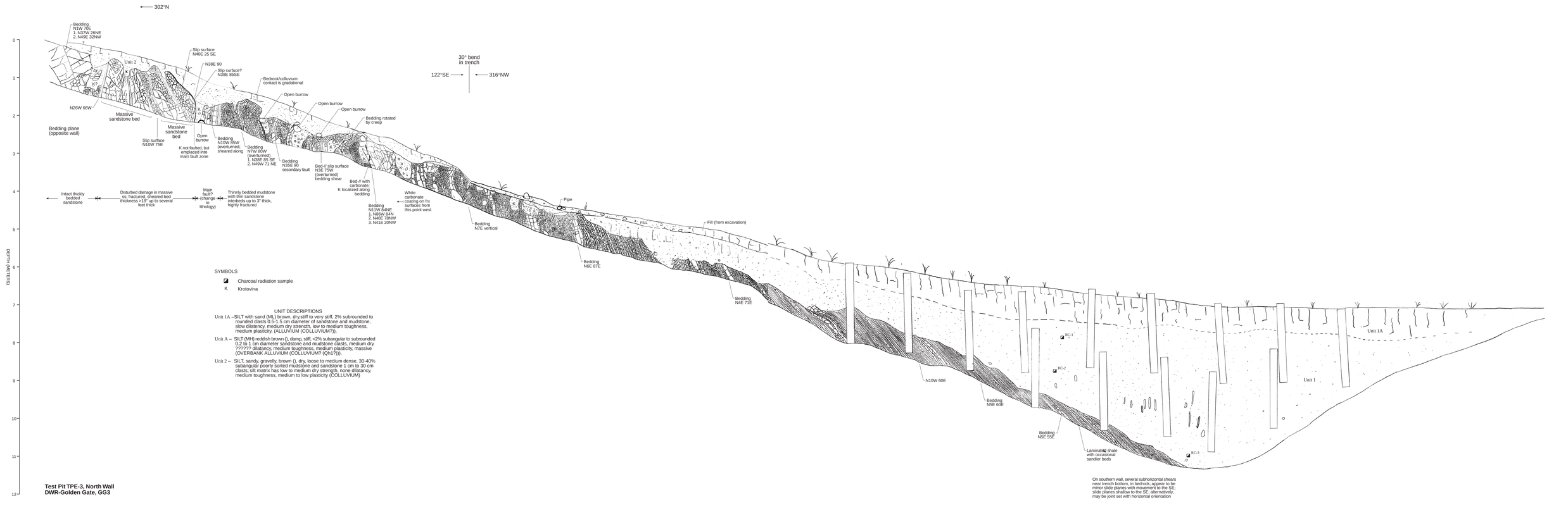


**Test Pit TPE-3, North Wall**
**DWR-Golden Gate, GG3**

West

East

Pacific Ocean | Coast Ranges | Sacramento Valley | Sierra Nevada

A

A'

San Andreas Flt

Maacama Flt

Barlett Springs Fz.

Coast Range Flt

Corning Flt.

Sacramento R.

Chico Monocline

Campbell Mound

Cohasset Ridge Flt.

North American Plate

Pacific Plate

"Slab Window "

Southern Edge Gorda Plate

Southern Cascadia Subduction Zone

YBC

YBH

KJf

lGVG

uGVG

GVO (crust)

GVO (mantle)

Stony Creek Flt

Sierran Basement

Depth (km)

0 10 20 30 40 50 60 70

0 10 20 30 40 50 60 70 80 90 100 110 120 130 140 150 160 170 180 190 200 210 220 230

Distance (km)

## Legend

Earthquake Magnitude

- 0.0 - 1.9
- 2.0 - 2.9
- 3.0 - 3.9
- 4.0 - 4.9
- 5.0 - 5.9

- uGVG - upper Great Valley Group
- lGVG - lower Great Valley Group
- GVO - Great Valley ophiolite - crust
- GVO - Great Valley ophiolite - mantle (Godfrey & Dilek, 2000)
- KJf - Jurassic-Cretaceous Franciscan Complex
- Crystalline Basement
- Dip-slip fault - arrow shows direction of motion
- Strike-slip fault - ⊗ shows motion away from viewer
- Detachment fault
- Base of Crust (Mooney & Weaver, 1989)

Notes:

Section Endpoints: 40° N, 124.25° W - 40°N, 121.5° W

Section Width: 50 km about 40° N

Earthquake Hypocenters: The 1844 earthquakes plotted have RMS location errors of ≤0.25 secretary, horizontal errors of ≤1.5 km, vertical errors ≤2.5 km, and are based on at least 10 observations. Events with magnitude ≤ 1.5 or focal depths ≤1.0 km are not included.

PHASE 2 FAULT AND SEISMIC HAZARDS INVESTIGATION
NORTH OF DELTA OFFSTREAM STORAGE
DWR-INTEGRATED STORAGE INVESTIGATION

**Seismicity Section through 40°**
**Section A-A'**

WLA William Lettis & Associates, Inc. | LAHONTAN geoscience incorporated | Figure 4-7

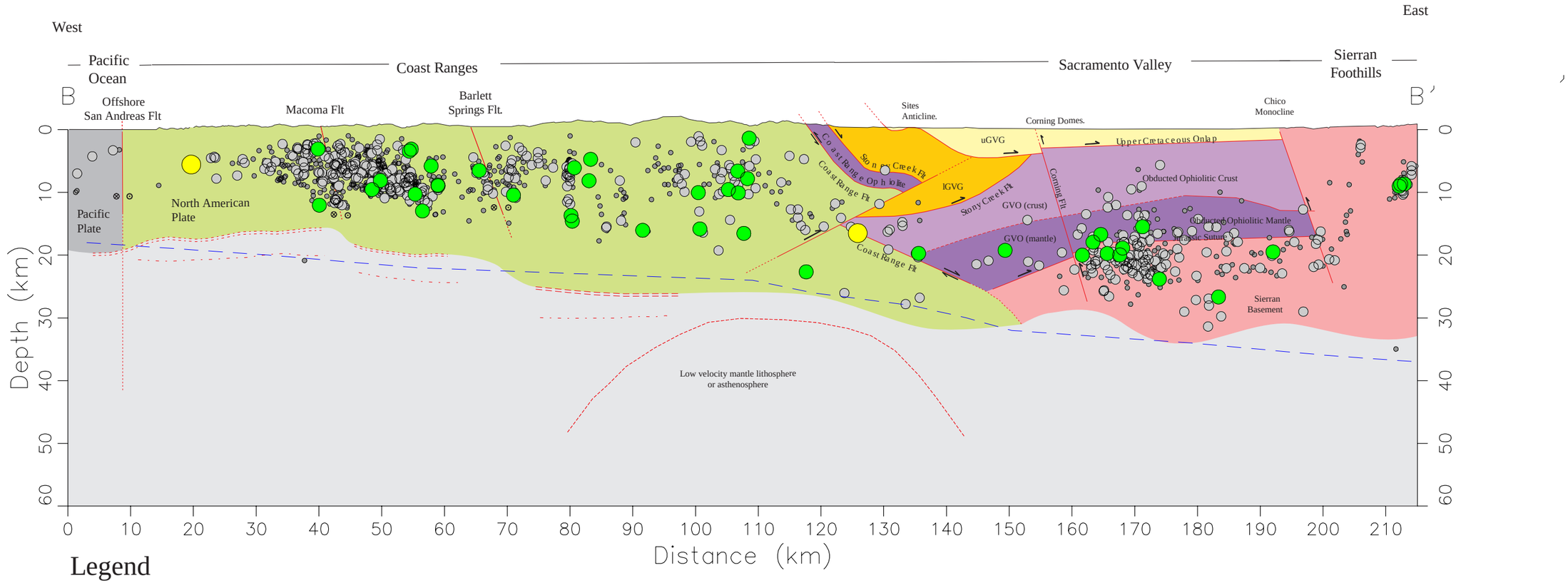


## Legend

Earthquake Magnitude

- 0.0 - 1.9
- 2.0 - 2.9
- 3.0 - 3.9
- 4.0 - 4.9
- 5.0 - 5.9

- uGVG - upper Great Valley Group
- lGVG - lower Great Valley Group
- GVO - Great Valley ophiolite - crust
- GVO - Great Valley ophiolite - mantle (Godfrey & Dilek, 2000)
- KJf - Jurassic-Cretaceous Franciscan Complex
- Crystalline Basement

- Top of reflective, high velocity layer (Henstock & Levander, 2001)
- Estimated Moho
- Dip-slip fault - arrow shows direction of motion
- Strike-slip fault - ⊗ shows motion away from viewer
- Detachment fault
- Base of Crust (Mooney & Weaver, 1989)

Notes:
Section Endpoints: 39.75° N, 124.0° W - 39.75° N, 121.5° W

Section Width: 50 km about 39.75° N

Earthquake Hypocenters: The 1350 earthquakes plotted have RMS location errors of ≤0.25 secretary, horizontal errors of ≤1.5 km, vertical errors ≤2.5 km, and are based on at least 10 observations. Events with magnitude ≤ 1.5 or focal depths ≤1.0 km are not included.

PHASE 2 FAULT AND SEISMIC HAZARDS INVESTIGATION
NORTH OF DELTA OFFSTREAM STORAGE
DWR-INTEGRATED STORAGE INVESTIGATION

**Seismicity Section Through The Proposed Newville Damsite Section B-B'**

WLA William Lettis & Associates, Inc. LAHONTAN geoscience incorporated

Figure 4-8

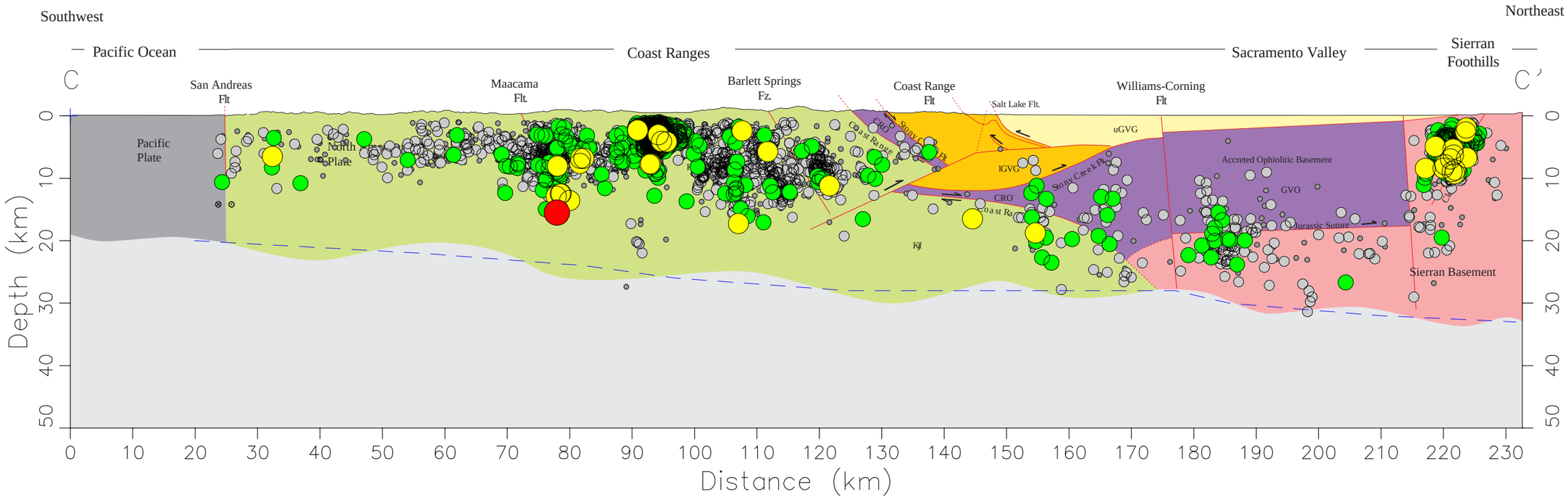


## Legend

Earthquake Magnitude

- 0.0 - 1.9
- 2.0 - 2.9
- 3.0 - 3.9
- 4.0 - 4.9
- 5.0 - 5.9

- uGVG - upper Great Valley Group
- lGVG - lower Great Valley Group
- CRO - Coast Range ophiolite
- GVO - Great Valley ophiolite - mantle (Godfrey & Dilek, 2000)
- KJf - Jurassic-Cretaceous Franciscan Complex
- Crystalline Basement
- Dip-slip fault - arrow shows direction of motion
- Strike-slip fault - ⊗ shows motion away from viewer
- Detachment fault
- Base of Crust (Mooney & Weaver, 1989)

Notes:
Section Endpoints: 38.9° N, 123.9° W - 39.6° N, 121.4° W

Section Width: 100 km

Earthquake Hypocenters: The 5651 earthquakes plotted have RMS location errors of ≤0.25 secretary, horizontal errors of ≤1.5 km, vertical errors ≤2.5 km, and are based on at least 10 observations. Events with magnitude ≤ 1.5 or focal depths ≤1.0 km are not included.

PHASE 2 FAULT AND SEISMIC HAZARDS INVESTIGATION
NORTH OF DELTA OFFSTREAM STORAGE
DWR-INTEGRATED STORAGE INVESTIGATION

**Regional Seismicity Section through Sites Project**
**Section C-C**

WLA William Lettis & Associates, Inc. LAHONTAN geoscience incorporated

Figure 4-9

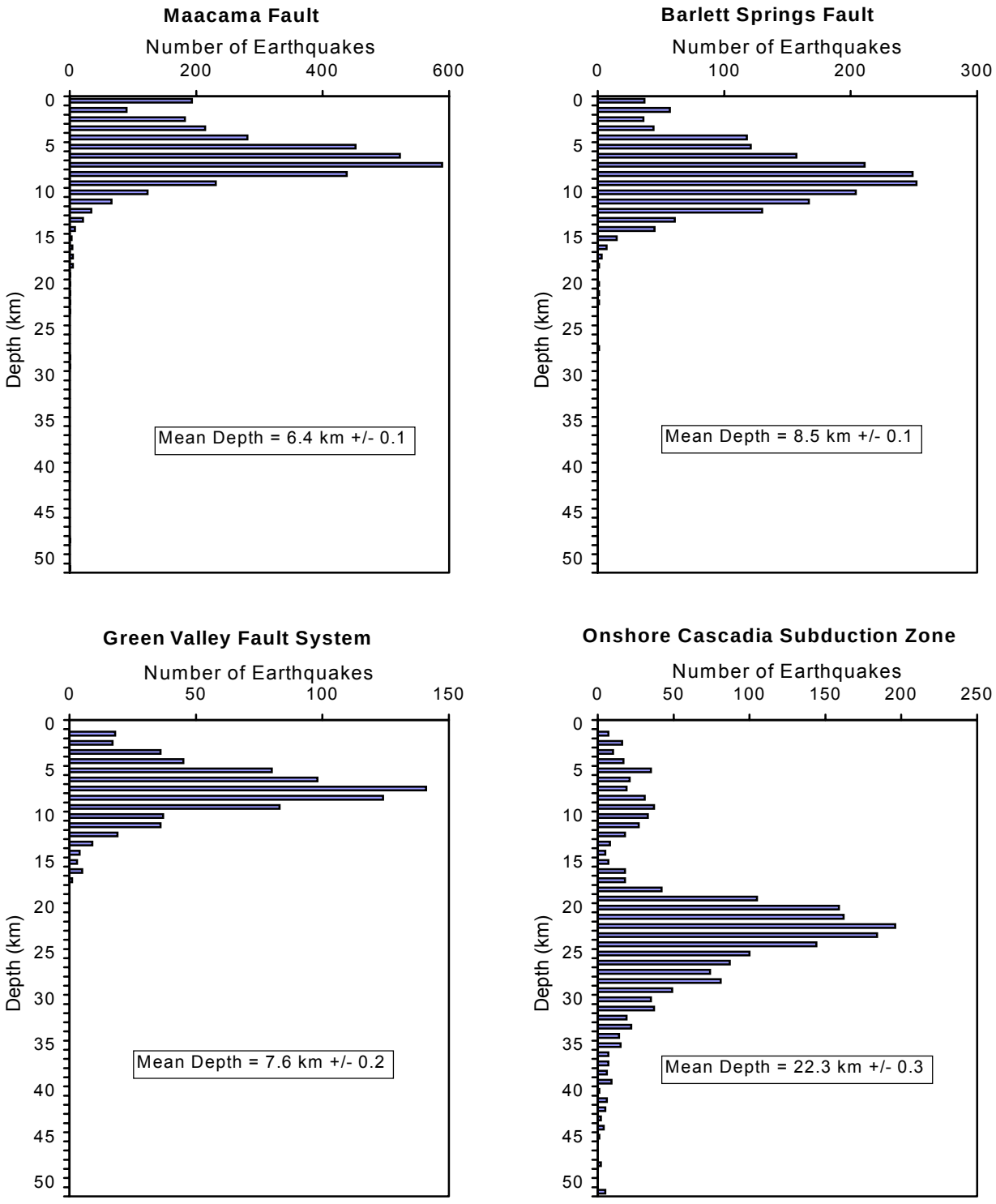


PHASE 2 FAULT AND SEISMIC HAZARDS INVESTIGATION
NORTH OF DELTA OFFSTREAM STORAGE
DWR-INTEGRATED STORAGE INVESTIGATION

**Distribution of Earthquake Focal Depths**
**Northern Coast Range Province**

WLA William Lettis & Associates, Inc. LAHONTAN geoscience Incorporated

Figure 4-10

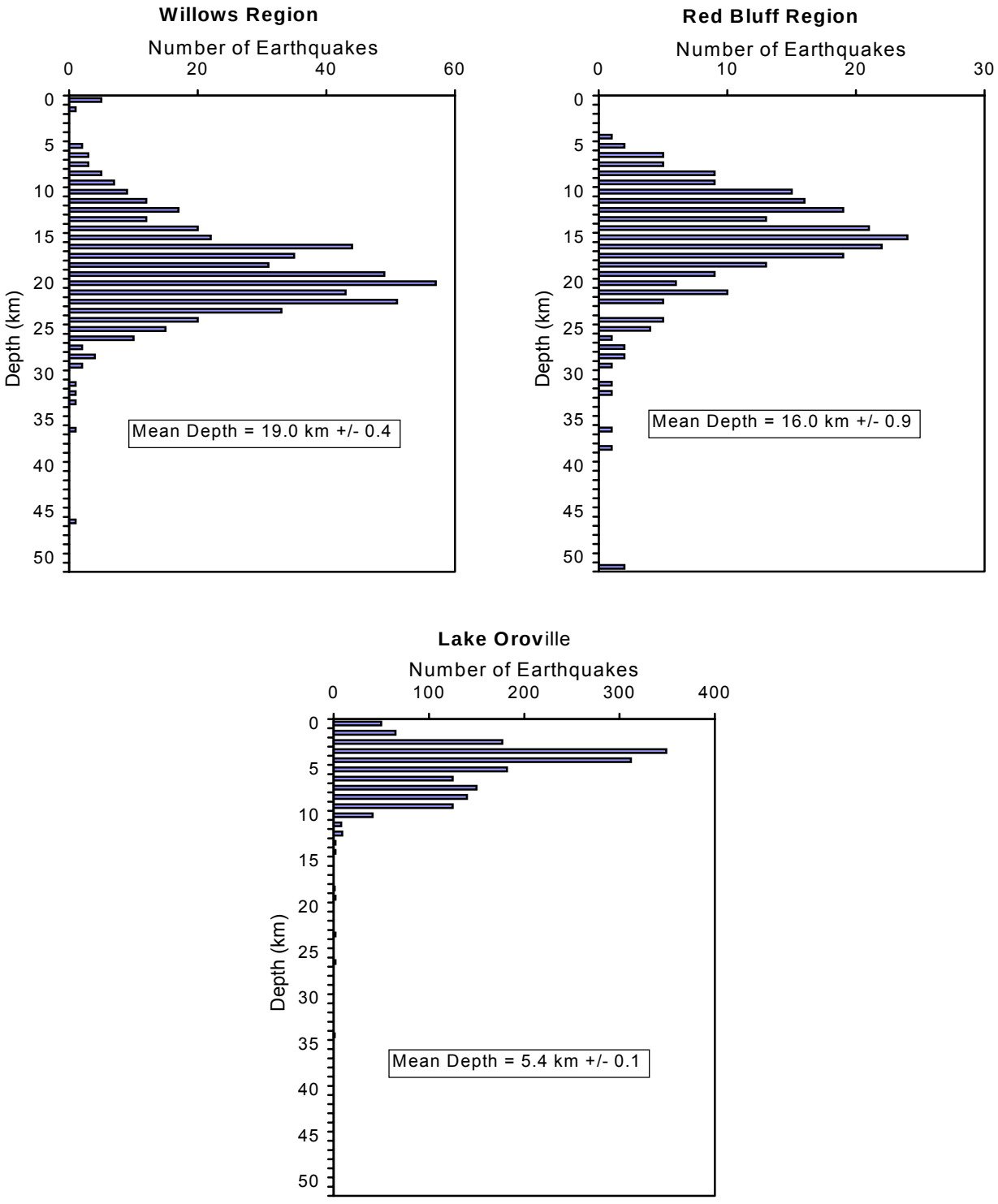


PHASE 2 FAULT AND SEISMIC HAZARDS INVESTIGATION
NORTH OF DELTA OFFSTREAM STORAGE
DWR-INTEGRATED STORAGE INVESTIGATION

**Distribution of Earthquake Focal Depths**
**Western Sierran Block Province**

WLA William Lettis & Associates, Inc. LAHONTAN geoscience incorporated

Figure 4-11

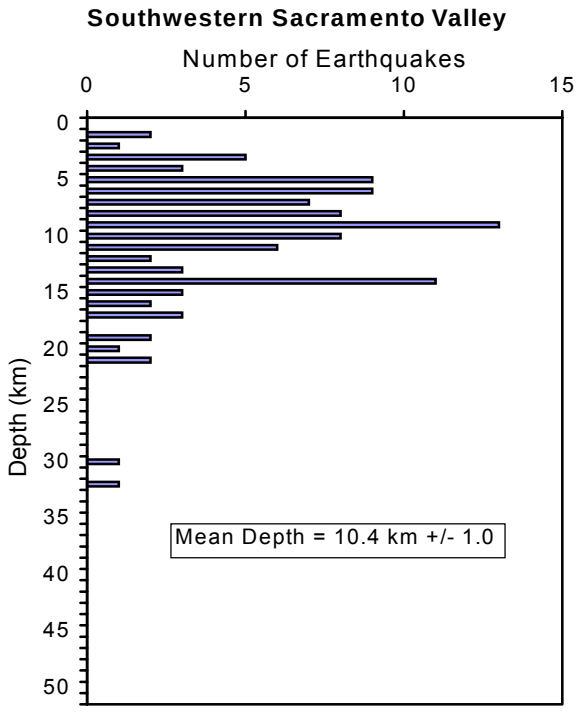


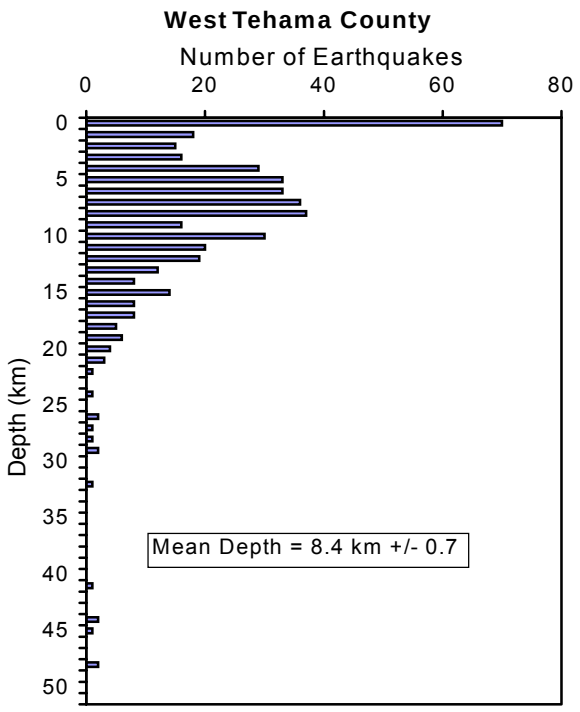


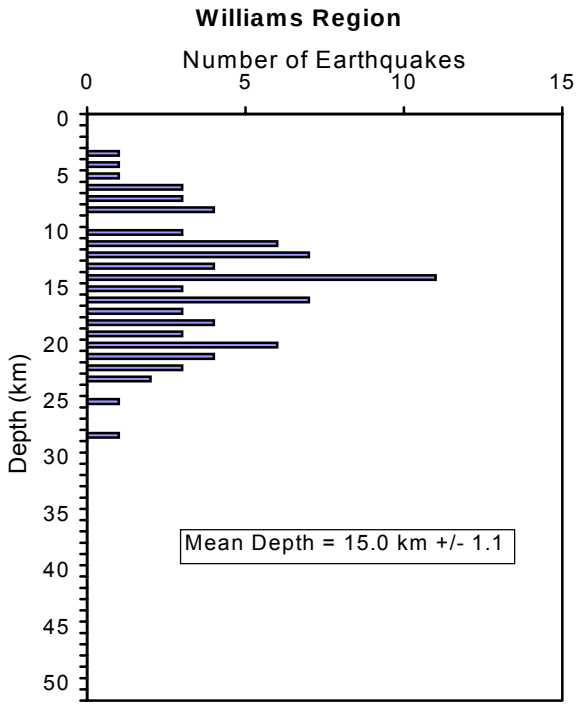


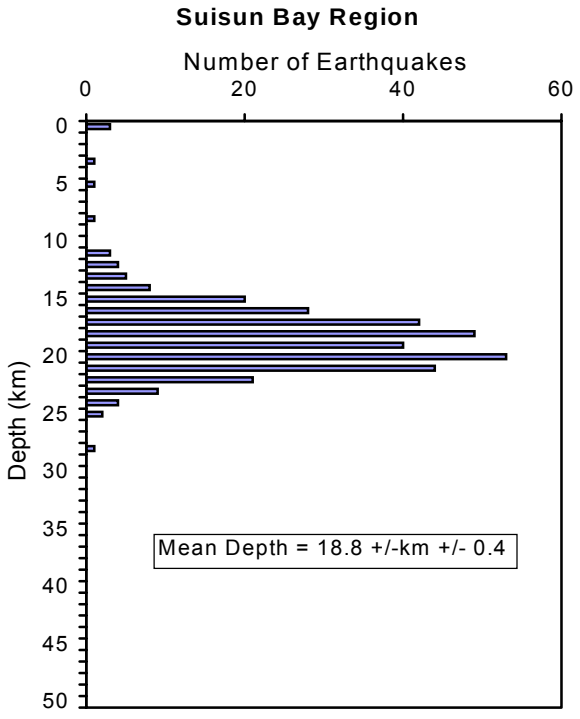


PHASE 2 FAULT AND SEISMIC HAZARDS INVESTIGATION
NORTH OF DELTA OFFSTREAM STORAGE
DWR-INTEGRATED STORAGE INVESTIGATION

**Distribution of Earthquake Focal Depths**
**CRSB Boundary Zone**

WLA William Lettis & Associates, Inc. LAHONTAN geoscience incorporated

Figure 4-12

P AXES

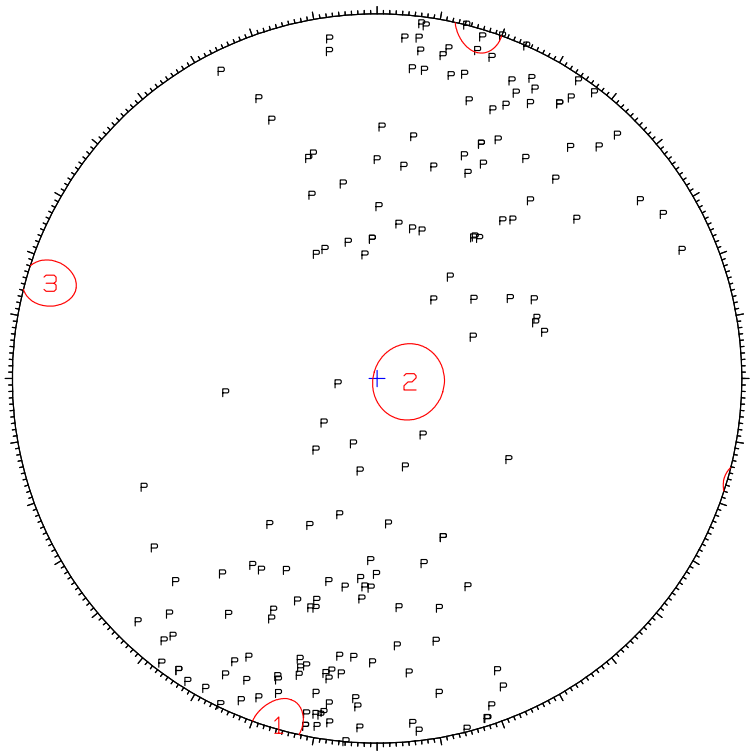


Axis 1: Declination = 196.0, Plunge = 1.2
Axis 2: Declination = 95.9, Plunge = 82.9
Axis 3: Declination = 286.2, Plunge = 6.9

T AXES

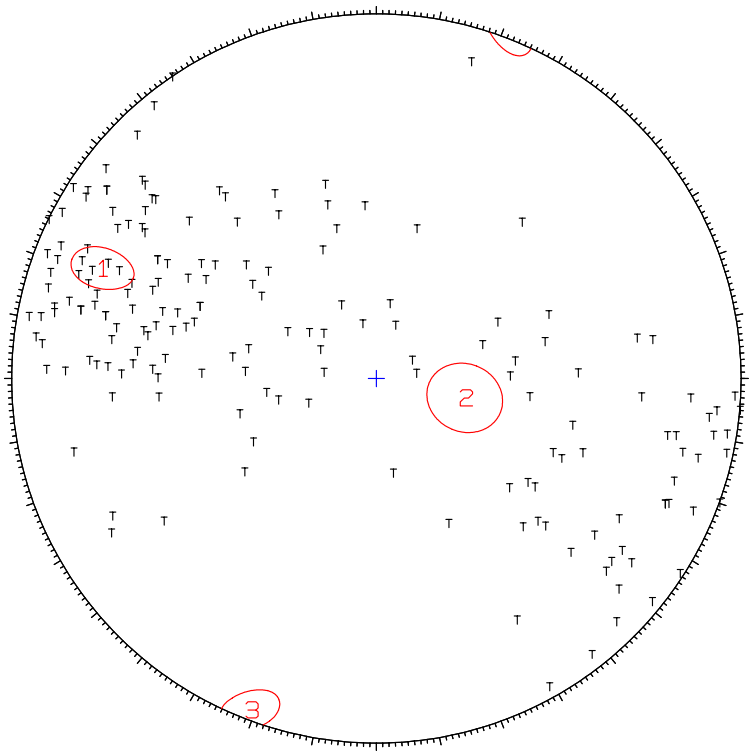


Axis 1: Declination = 291.9, Plunge = 20.0
Axis 2: Declination = 102.3, Plunge = 69.7
Axis 3: Declination = 200.8, Plunge = 3.1

PHASE 2 FAULT AND SEISMIC HAZARDS INVESTIGATION
NORTH OF DELTA OFFSTREAM STORAGE
DWR-INTEGRATED STORAGE INVESTIGATION

**Maacama Fault Zone**
**NCSN dataset 1970 - 2000**

WLA William Lettis & Associates, Inc. LAHONTAN geoscience incorporated

Figure 4-14

P AXES

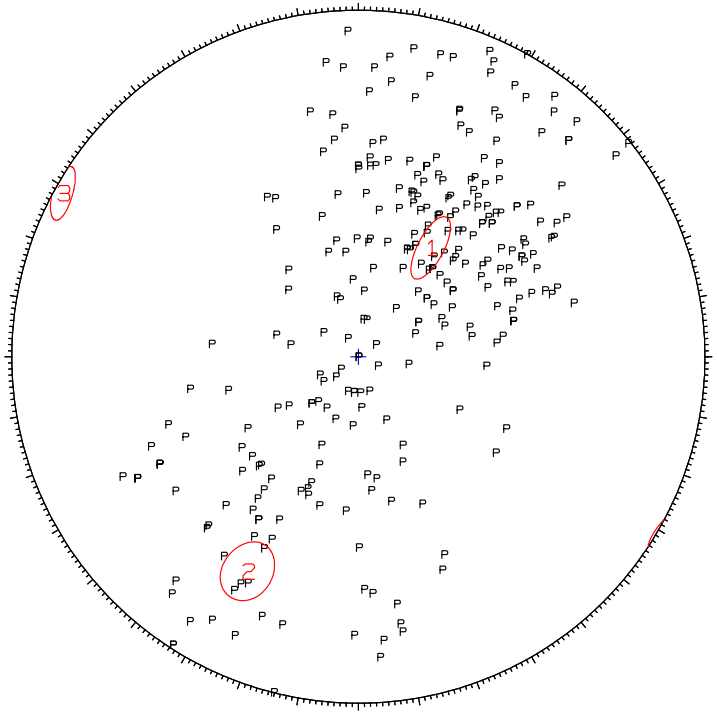


Axis 1: Declination = 33.6, Plunge = 59.0
Axis 2: Declination = 207.3, Plunge = 30.8
Axis 3: Declination = 298.9, Plunge = 2.8

T AXES

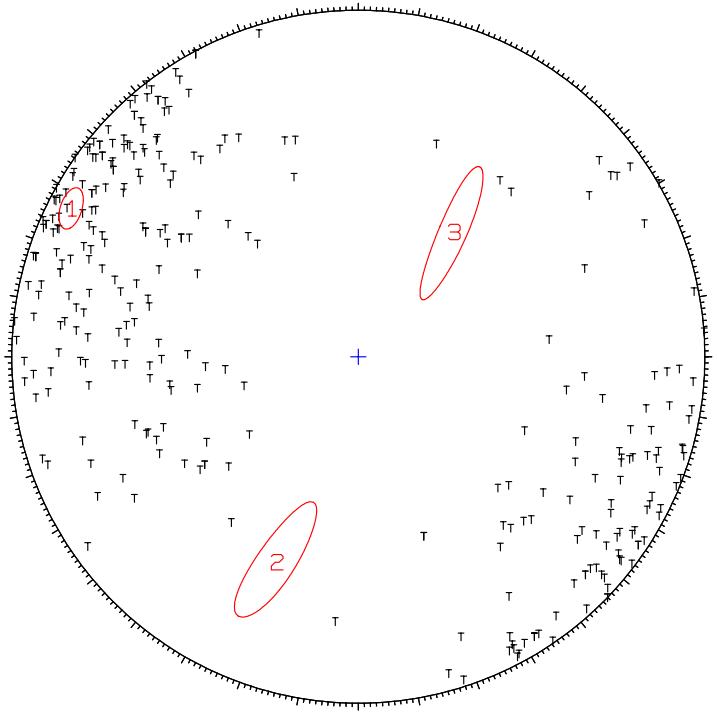


Axis 1: Declination = 297.3, Plunge = 7.4
Axis 2: Declination = 201.9, Plunge = 36.3
Axis 3: Declination = 37.2, Plunge = 52.7

PHASE 2 FAULT AND SEISMIC HAZARDS INVESTIGATION
NORTH OF DELTA OFFSTREAM STORAGE
DWR-INTEGRATED STORAGE INVESTIGATION

**Bartlett Springs Fault Zone**
**NCSN dataset 1970 - 2000**

WLA William Lettis & Associates, Inc. LAHONTAN geoscience incorporated

Figure 4-15

P AXES

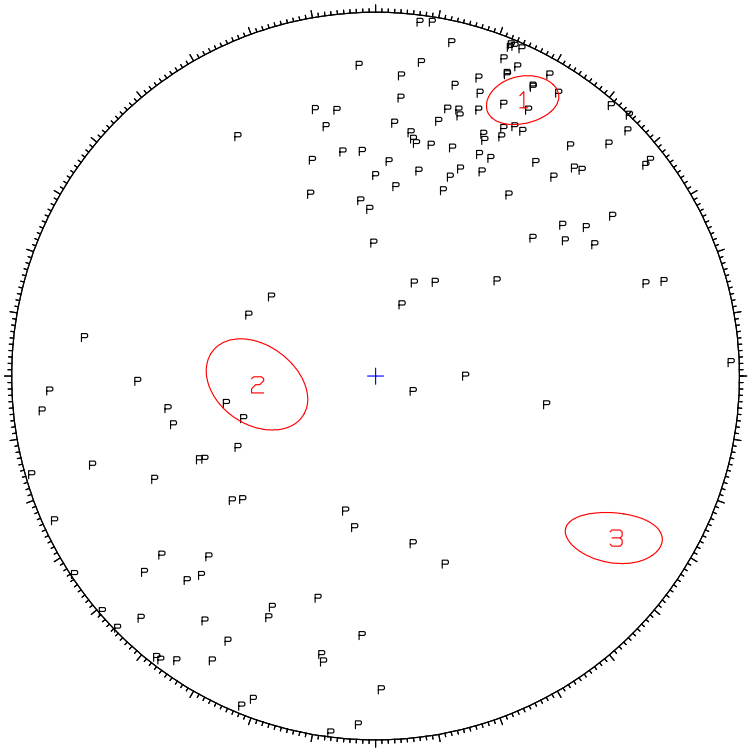


Axis 1: Declination = 28.0, Plunge = 15.1
Axis 2: Declination = 265.9, Plunge = 63.1
Axis 3: Declination = 124.1, Plunge = 21.7

T AXES

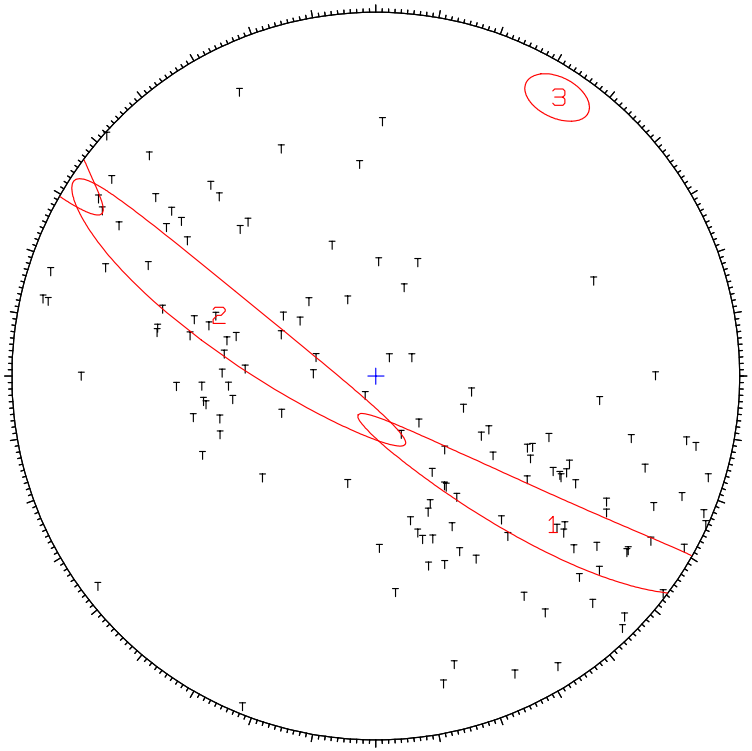


Axis 1: Declination = 130.2, Plunge = 36.9
Axis 2: Declination = 291.0, Plunge = 51.6
Axis 3: Declination = 33.0, Plunge = 9.4

PHASE 2 FAULT AND SEISMIC HAZARDS INVESTIGATION
NORTH OF DELTA OFFSTREAM STORAGE
DWR-INTEGRATED STORAGE INVESTIGATION

**Green Valley Fault System**
**NCSN dataset 1970 - 2000**

WLA William Lettis & Associates, Inc. LAHONTAN geoscience incorporated

Figure 4-16

P AXES

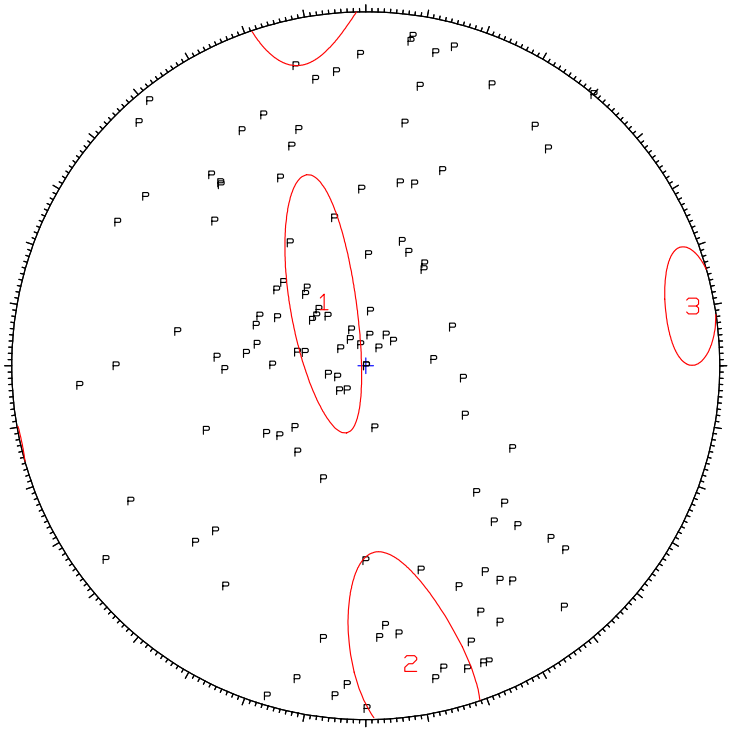


Axis 1: Declination = 326.0, Plunge = 72.3
Axis 2: Declination = 531.7, Plunge = 16.0
Axis 3: Declination = 79.6, Plunge = 7.3

T AXES

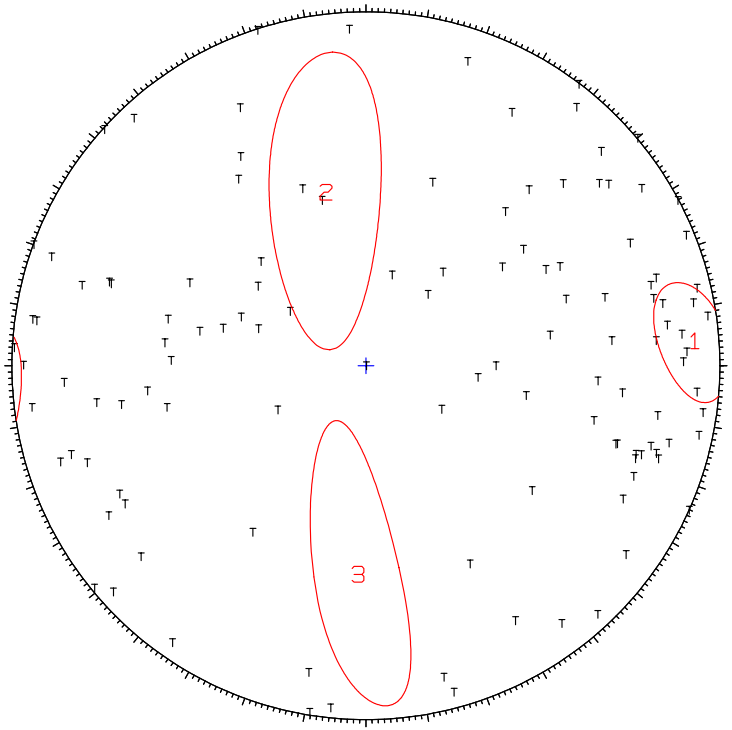


Axis 1: Declination = 85.7, Plunge = 7.9
Axis 2: Declination = 346.7, Plunge = 48.2
Axis 3: Declination = 182.5, Plunge = 40.7

PHASE 2 FAULT AND SEISMIC HAZARDS INVESTIGATION
NORTH OF DELTA OFFSTREAM STORAGE
DWR-INTEGRATED STORAGE INVESTIGATION

**Subducted Gorda Plate, Depth > 15 kilometers**
**NCSN dataset 1970 - 2000**

WLA William Lettis & Associates, Inc. LAHONTAN geoscience incorporated

Figure 4-17

P AXES

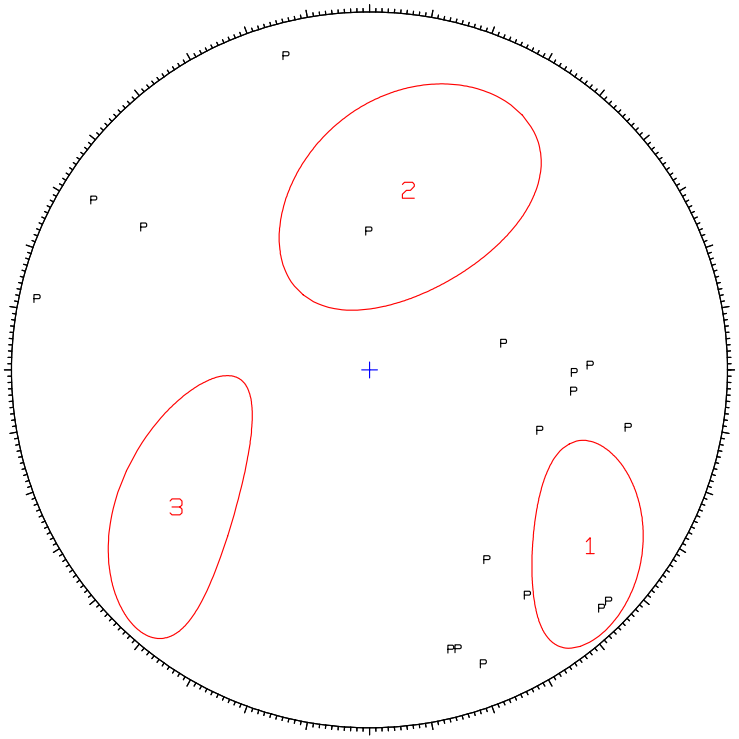


Axis 1: Declination = 128.7, Plunge = 22.5
Axis 2: Declination = 11.8, Plunge = 47.5
Axis 3: Declination = 234.9, Plunge = 33.8

T AXES

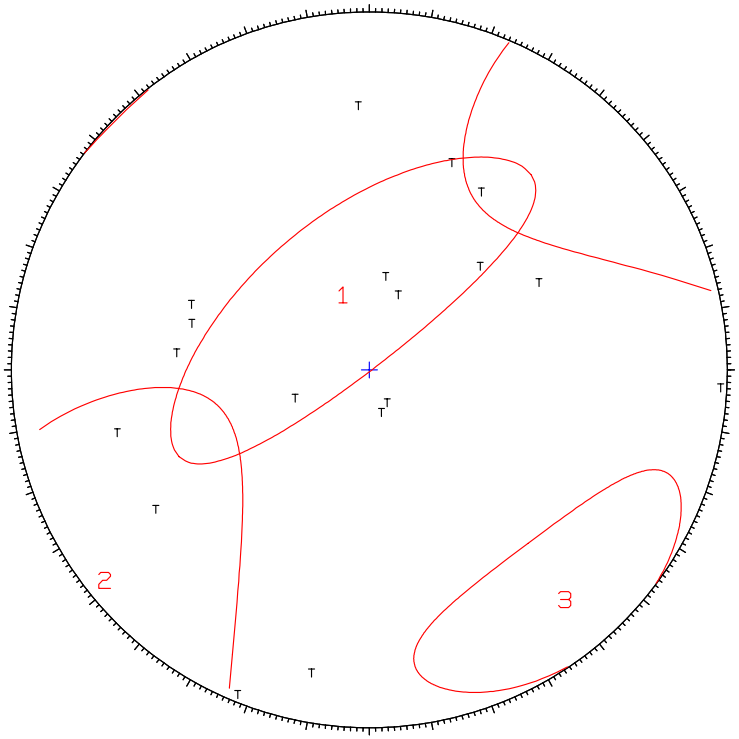


Axis 1: Declination = 339.7, Plunge = 71.8
Axis 2: Declination = 231.6, Plunge = 5.8
Axis 3: Declination = 499.8, Plunge = 17.1

PHASE 2 FAULT AND SEISMIC HAZARDS INVESTIGATION
NORTH OF DELTA OFFSTREAM STORAGE
DWR-INTEGRATED STORAGE INVESTIGATION

**Red Bluff Region**
**NCSN dataset 1970 - 2000**

WLA William Lettis & Associates, Inc. LAHONTAN geoscience incorporated

Figure 4-18

P AXES

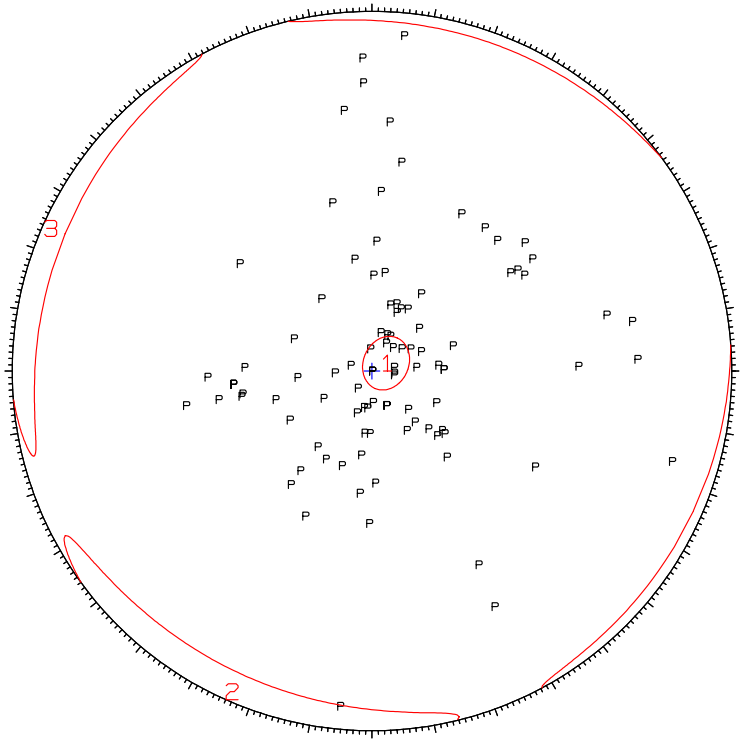


Axis 1: Declination = 60.4, Plunge = 86.3
Axis 2: Declination = 203.8, Plunge = 2.9
Axis 3: Declination = 293.9, Plunge = 2.2

T AXES

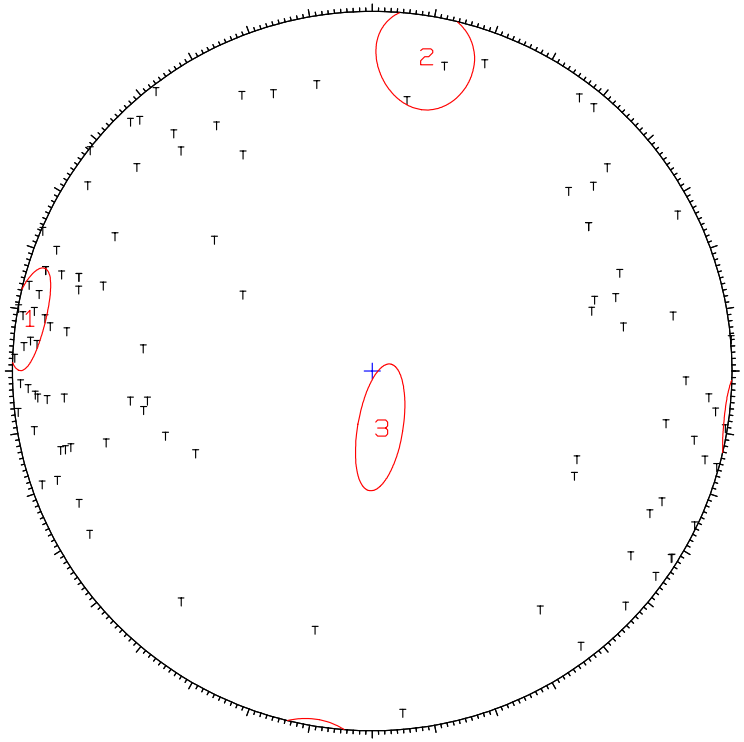


Axis 1: Declination = 278.7, Plunge = 3.8
Axis 2: Declination = 9.6, Plunge = 12.4
Axis 3: Declination = 171.9, Plunge = 77.0

PHASE 2 FAULT AND SEISMIC HAZARDS INVESTIGATION
NORTH OF DELTA OFFSTREAM STORAGE
DWR-INTEGRATED STORAGE INVESTIGATION

**Lake Oroville Region**
**NCSN dataset 1970 - 2000**

WLA William Lettis & Associates, Inc. LAHONTAN geoscience incorporated

Figure 4-19

P AXES

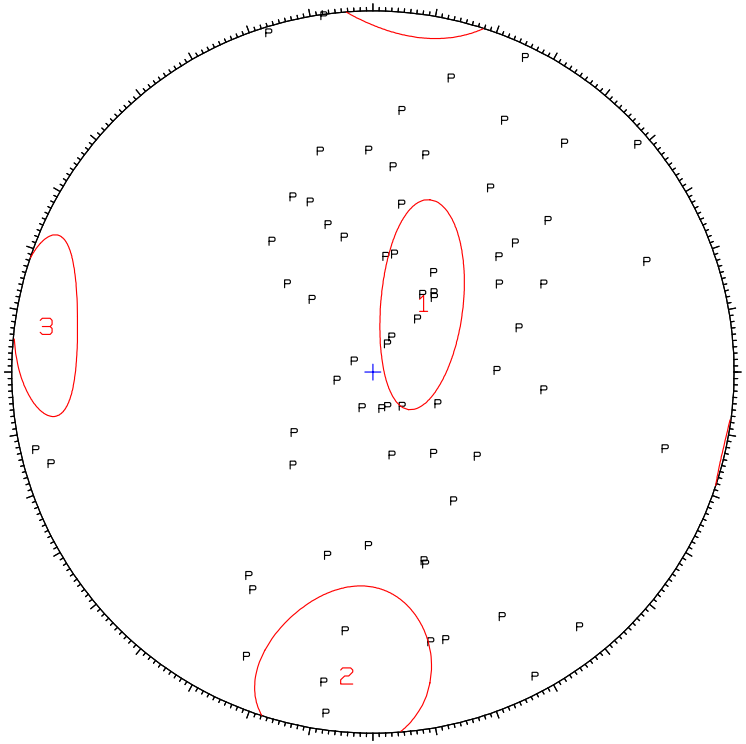


Axis 1: Declination = 35.6, Plunge = 70.9
Axis 2: Declination = 185.2, Plunge = 16.6
Axis 3: Declination = 277.9, Plunge = 9.1

T AXES

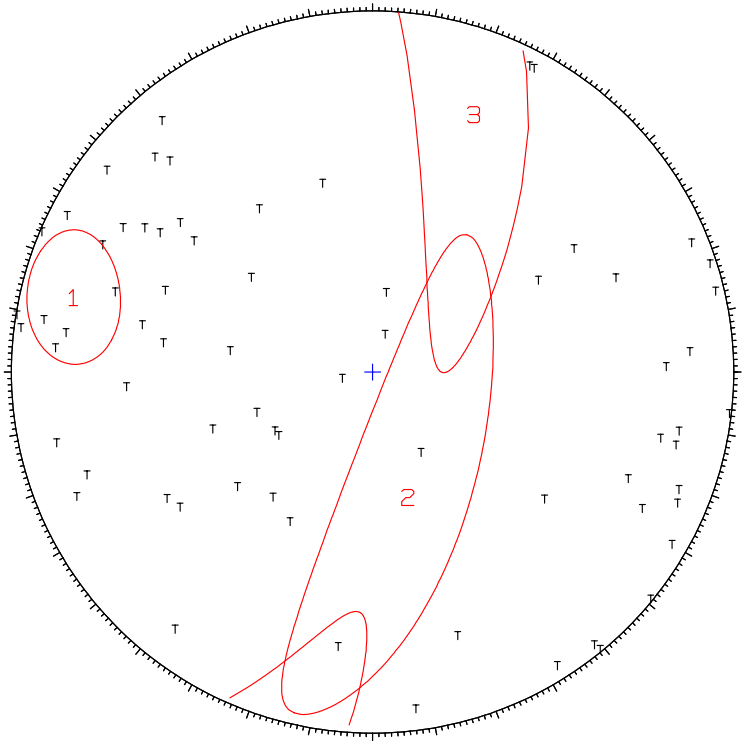


Axis 1: Declination = 283.9, Plunge = 15.3
Axis 2: Declination = 164.9, Plunge = 60.5
Axis 3: Declination = 21.1, Plunge = 24.5

PHASE 2 FAULT AND SEISMIC HAZARDS INVESTIGATION
NORTH OF DELTA OFFSTREAM STORAGE
DWR-INTEGRATED STORAGE INVESTIGATION

**Willows Region**
**P & T axes from selected earthquakes**
**NCSN dataset 1970 - 2000**

WLA William Lettis & Associates, Inc. LAHONTAN geoscience incorporated

Figure 4-20

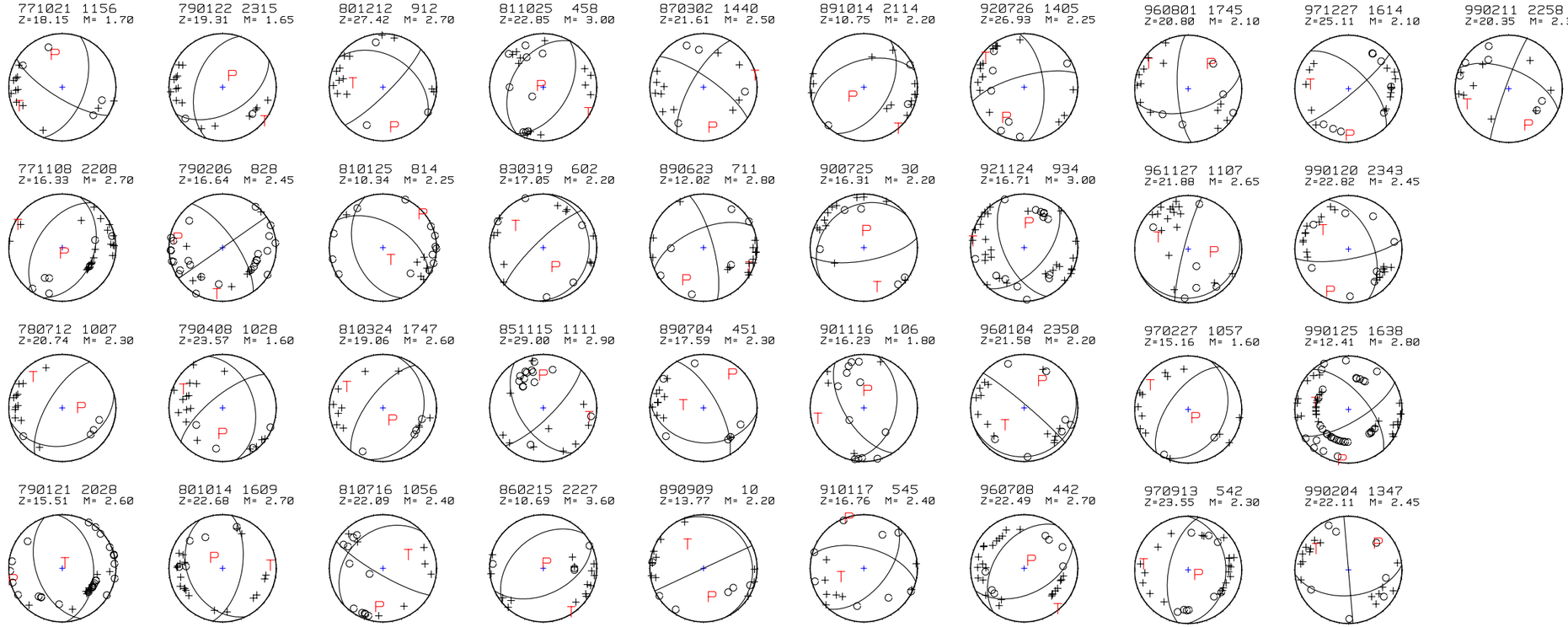


PHASE 2 FAULT AND SEISMIC HAZARDS INVESTIGATION
NORTH OF DELTA OFFSTREAM STORAGE
DWR-INTEGRATED STORAGE INVESTIGATION

**Willows Region**
**Selected Focal Mechanisms from NCSN Locations**

WLA William Lettis & Associates, Inc. LAHONTAN geoscience incorporated

Figure 4-21

P AXES

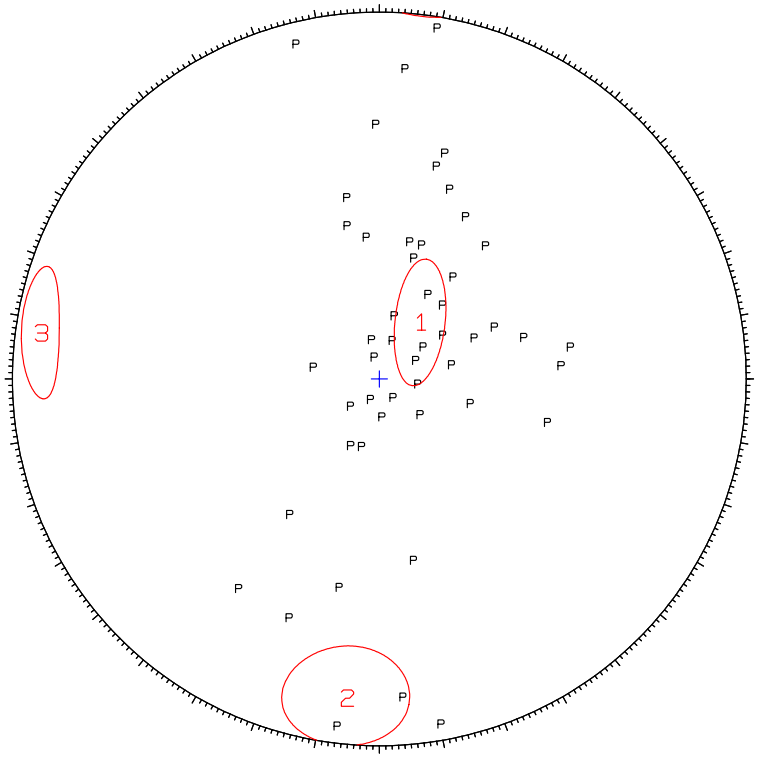


Axis 1: Declination = 35.6, Plunge = 74.5
Axis 2: Declination = 185.9, Plunge = 13.6
Axis 3: Declination = 277.7, Plunge = 7.4

T AXES

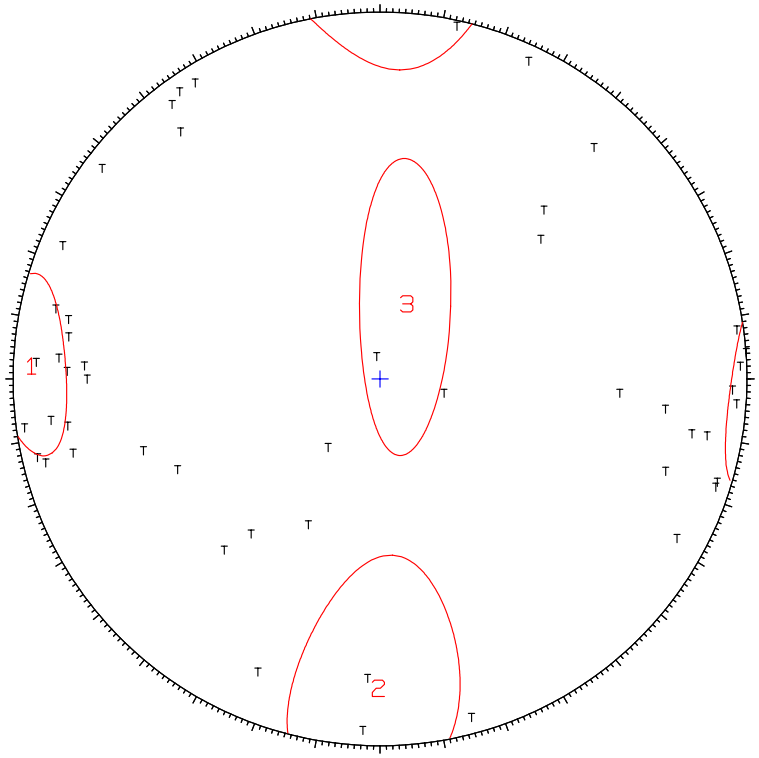


Axis 1: Declination = 272.1, Plunge = 5.1
Axis 2: Declination = 180.6, Plunge = 16.8
Axis 3: Declination = 18.6, Plunge = 72.4

PHASE 2 FAULT AND SEISMIC HAZARDS INVESTIGATION
NORTH OF DELTA OFFSTREAM STORAGE
DWR-INTEGRATED STORAGE INVESTIGATION

**West Tehama County**
**NCSN dataset 1970 - 2000**

WLA William Lettis & Associates, Inc. LAHONTAN geoscience incorporated

Figure 4-22

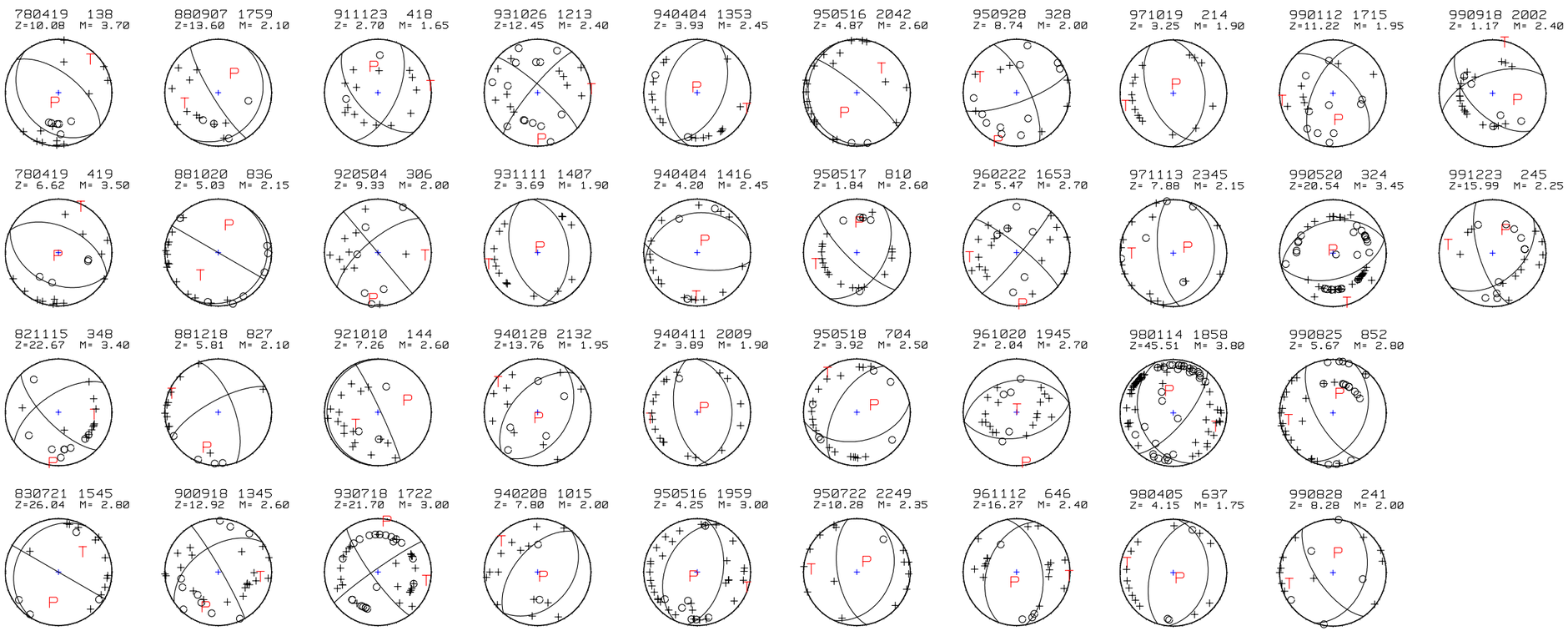


PHASE 2 FAULT AND SEISMIC HAZARDS INVESTIGATION
NORTH OF DELTA OFFSTREAM STORAGE
DWR-INTEGRATED STORAGE INVESTIGATION

**West Tehama County**
**Selected Focal Mechanisms from NCSN Locations**

WLA William Lettis & Associates, Inc. LAHONTAN geoscience incorporated

Figure 4-23

P AXES

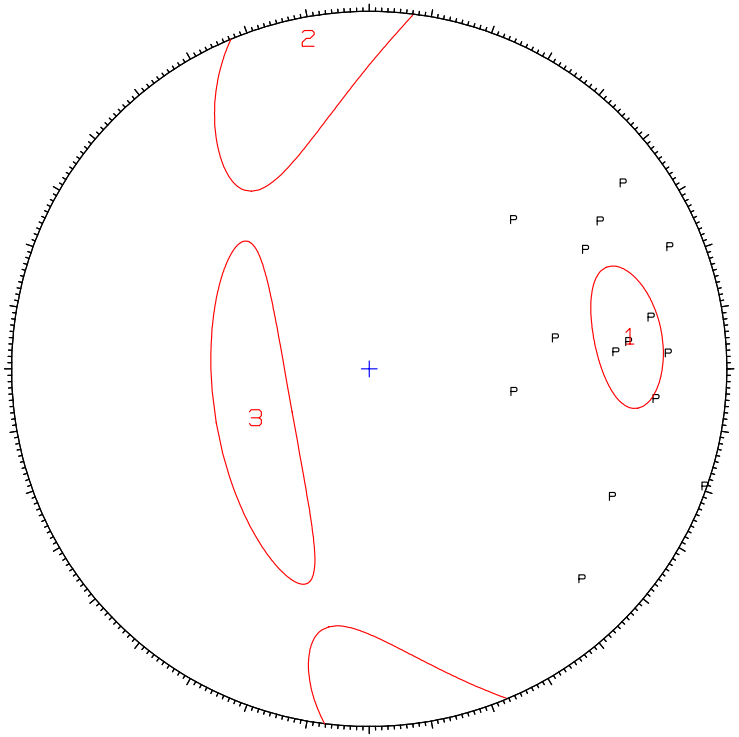


Axis 1: Declination = 82.8, Plunge = 27.8
Axis 2: Declination = 349.3, Plunge = 6.6
Axis 3: Declination = 247.1, Plunge = 61.3

T AXES

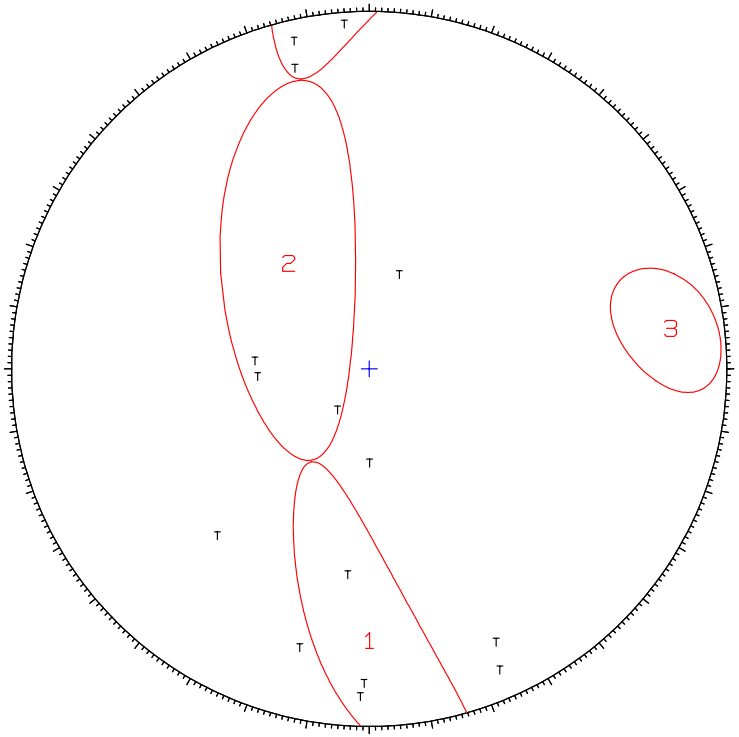


Axis 1: Declination = 180.2, Plunge = 25.0
Axis 2: Declination = 322.2, Plunge = 59.4
Axis 3: Declination = 82.3, Plunge = 16.5

PHASE 2 FAULT AND SEISMIC HAZARDS INVESTIGATION
NORTH OF DELTA OFFSTREAM STORAGE
DWR-INTEGRATED STORAGE INVESTIGATION

**Maxwell Region**
**NCSN dataset 1970 - 2000**

WLA William Lettis & Associates, Inc. LAHONTAN geoscience incorporated

Figure 4-24

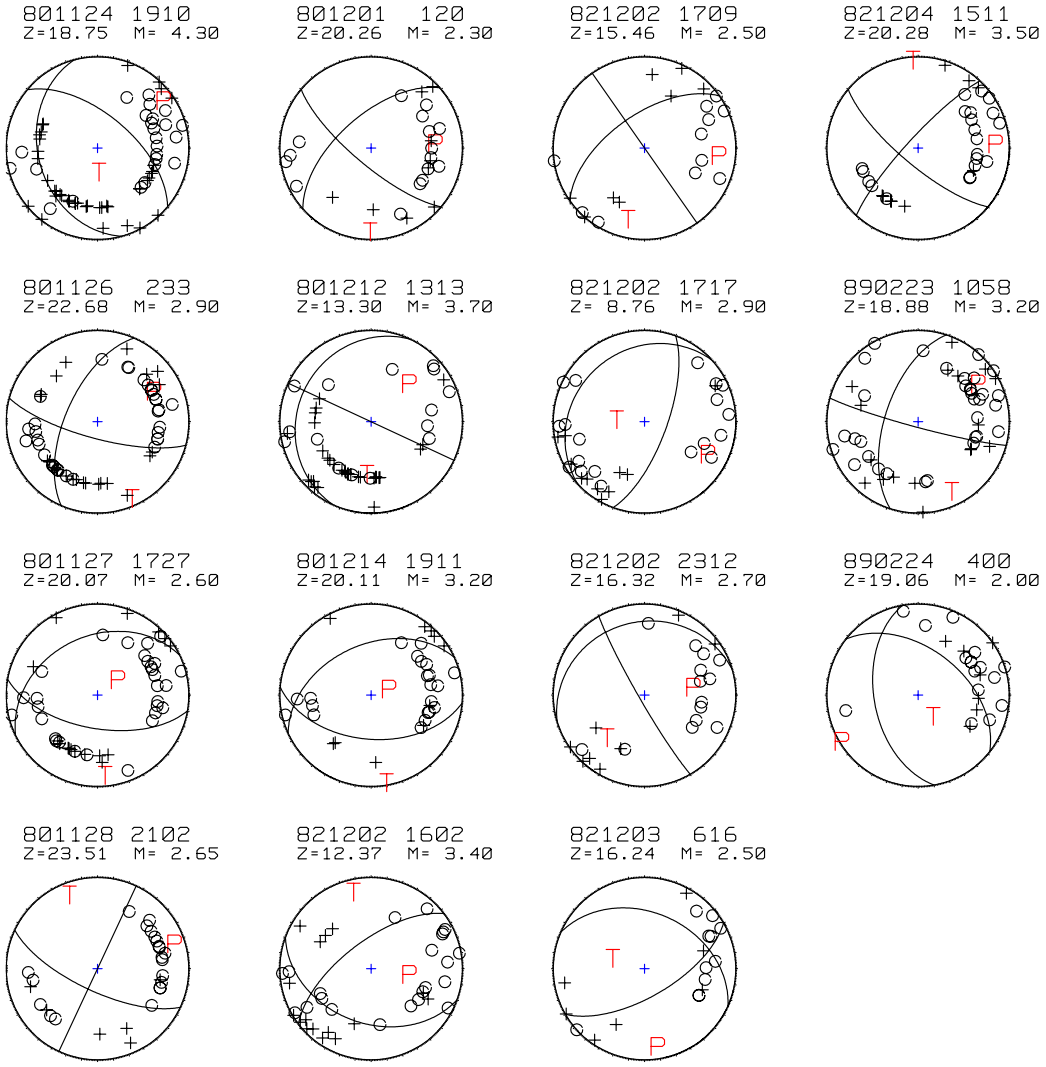


PHASE 2 FAULT AND SEISMIC HAZARDS INVESTIGATION
NORTH OF DELTA OFFSTREAM STORAGE
DWR-INTEGRATED STORAGE INVESTIGATION

**Maxwell Region**
**Selected Focal Mechanisms from NCSN Locations**

WLA William Lettis & Associates, Inc. LAHONTAN geoscience Incorporated Figure 4-25

P AXES

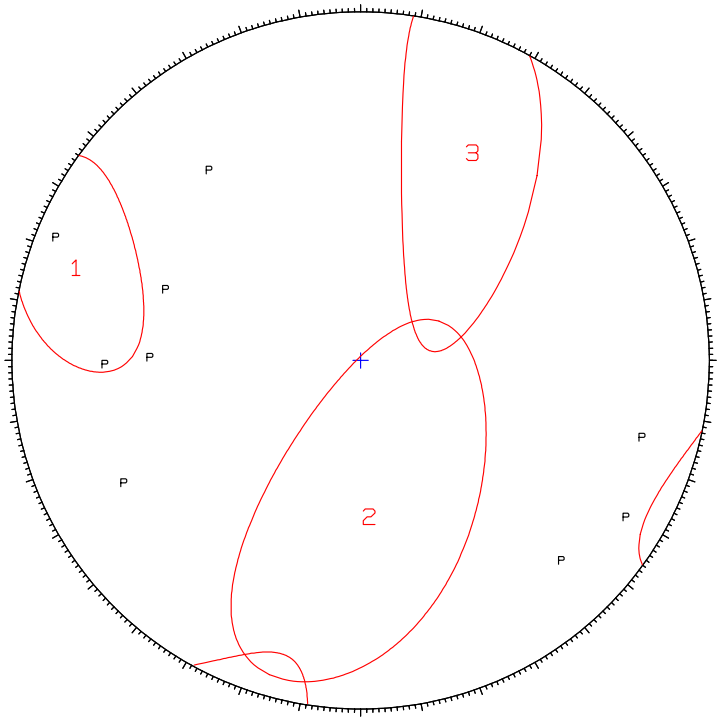


Axis 1: Declination = 288.0, Plunge = 14.9
Axis 2: Declination = 177.4, Plunge = 53.0
Axis 3: Declination = 27.9, Plunge = 33.0

T AXES

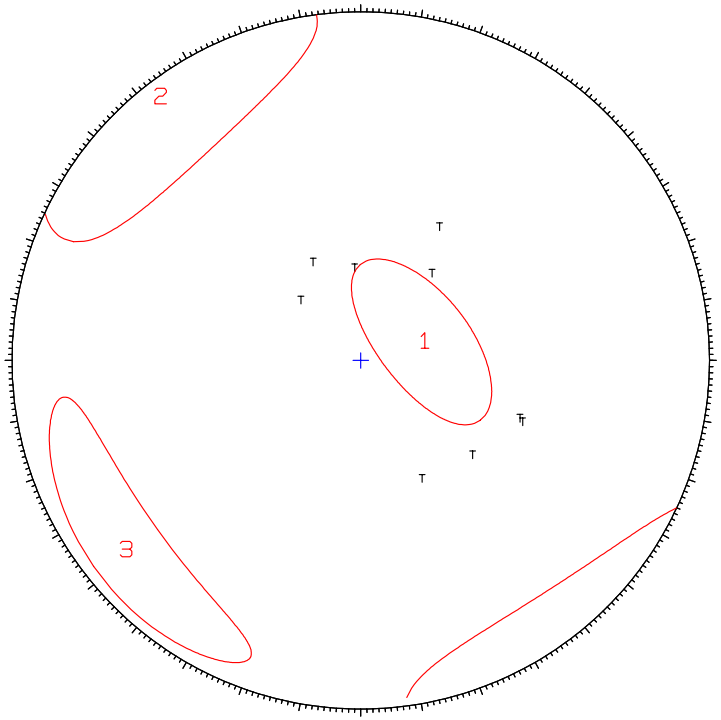


Axis 1: Declination = 72.3, Plunge = 74.6
Axis 2: Declination = 322.7, Plunge = 5.3
Axis 3: Declination = 231.3, Plunge = 14.4

PHASE 2 FAULT AND SEISMIC HAZARDS INVESTIGATION
NORTH OF DELTA OFFSTREAM STORAGE
DWR-INTEGRATED STORAGE INVESTIGATION

**Colusa Region**
**P & T axes calculated from selected earthquakes**
**NCSN dataset 1970 - 2000**

WLA William Lettis & Associates, Inc. LAHONTAN geoscience incorporated

Figure 4-26

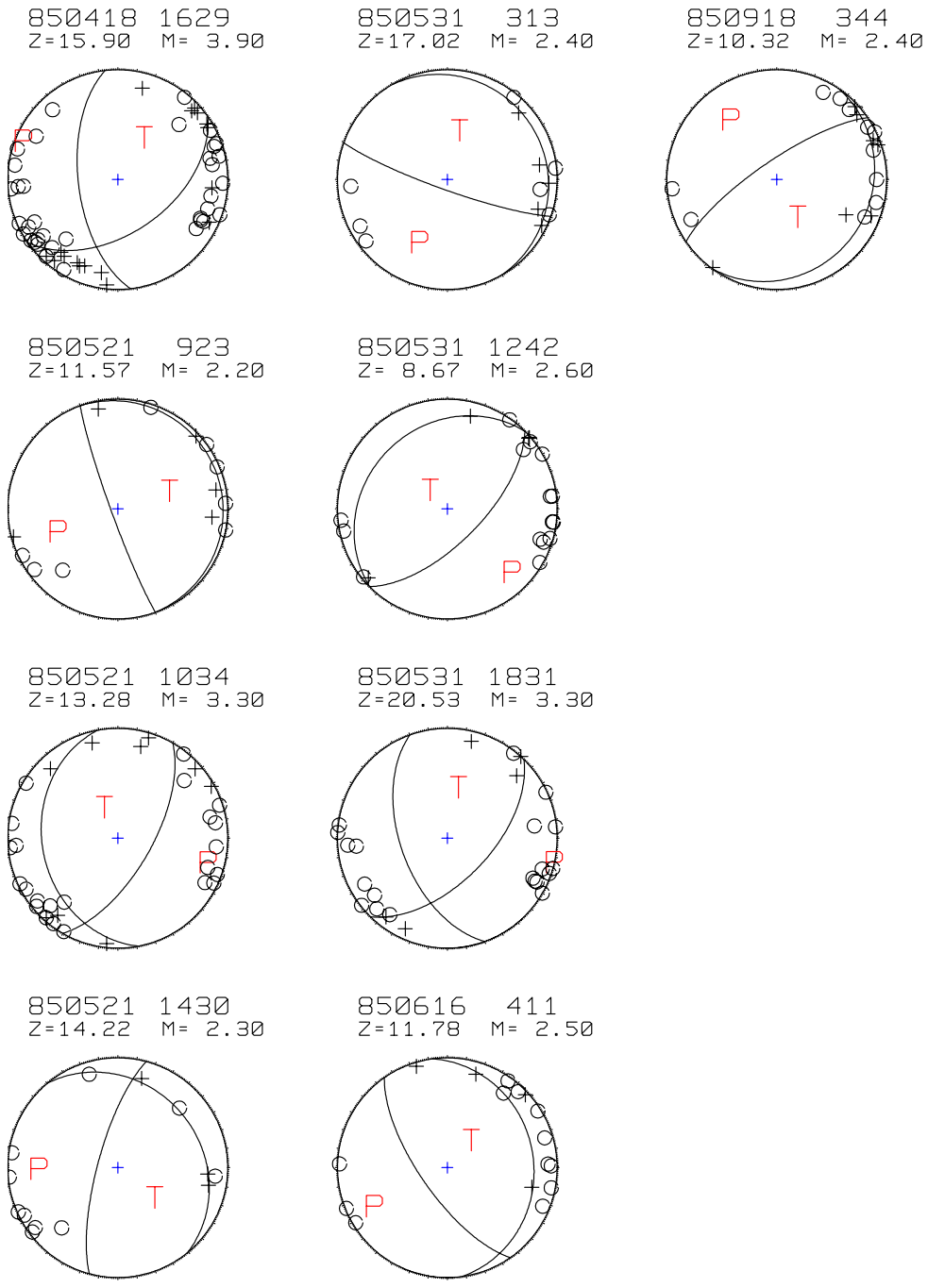


PHASE 2 FAULT AND SEISMIC HAZARDS INVESTIGATION
NORTH OF DELTA OFFSTREAM STORAGE
DWR-INTEGRATED STORAGE INVESTIGATION

**Colusa Region**
**Selected Focal Mechanisms**
**from NCSN Locations**

WLA William Lettis & Associates, Inc. LAHONTAN geoscience Incorporated

Figure 4-27

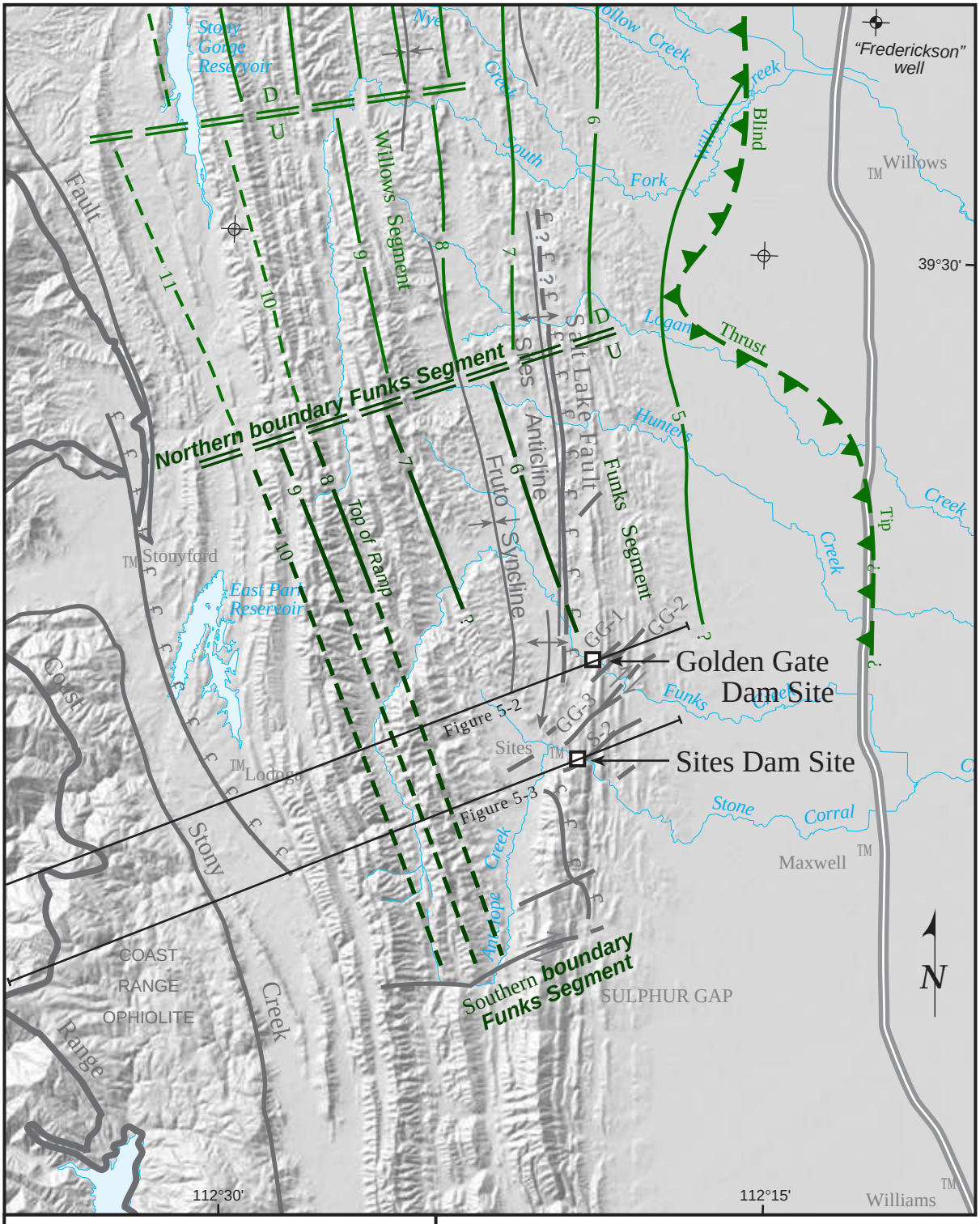


## EXPLANATION

7 — Depth (in km) below sea level to top of thrust fault

Thrust fault; teeth on hanging wall

Fault; sense of horizontal displacement shown

0 5 10 km

PHASE 2 FAULT AND SEISMIC HAZARDS INVESTIGATION
NORTH OF DELTA OFFSTREAM STORAGE
DWR-INTEGRATED STORAGE INVESTIGATION

**Interpreted Northern and Southern Boundaries of the Funks Segment, Great Valley Thrust Fault System**

WLA William Lettis & Associates, Inc.

Figure 5-1

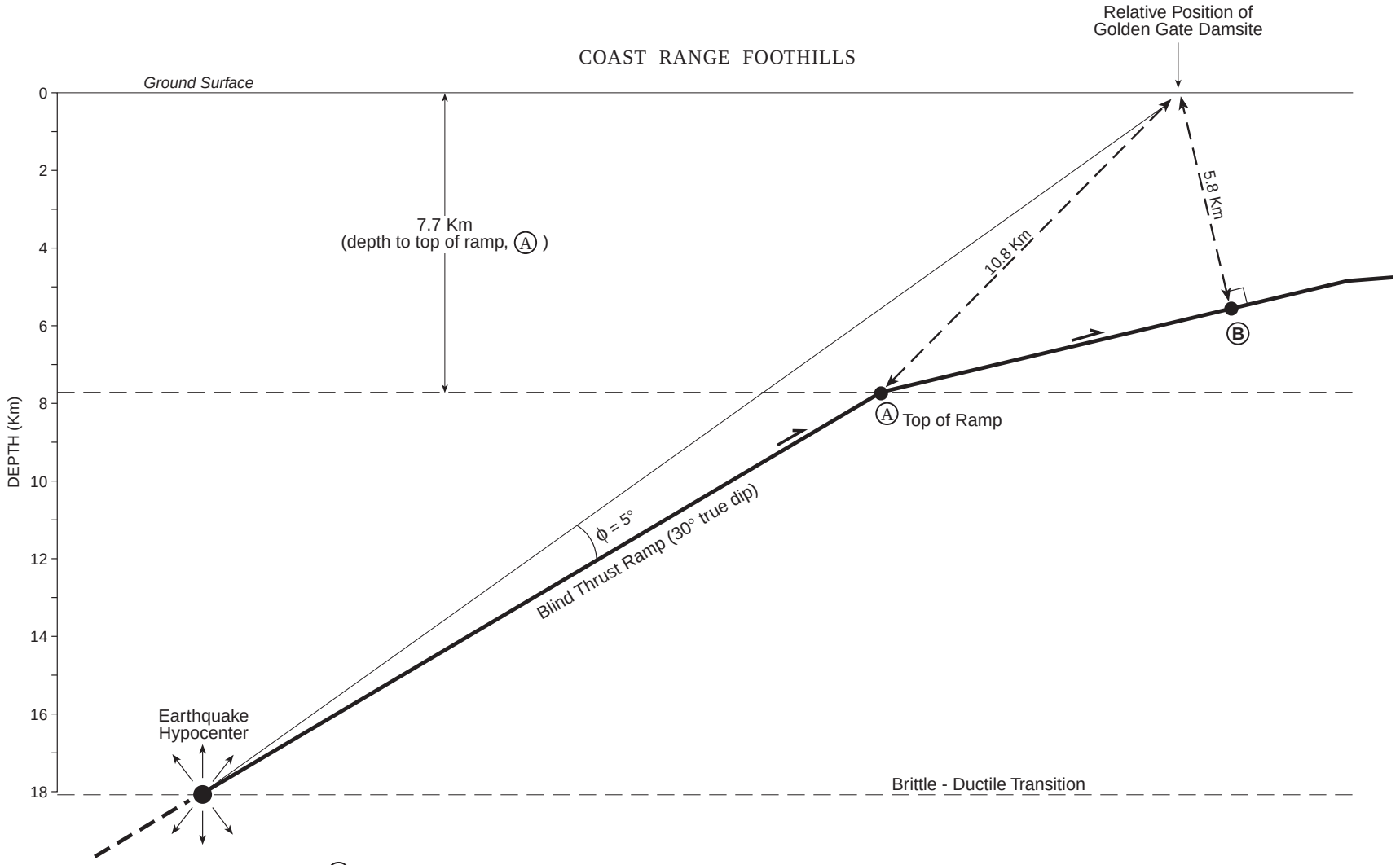


Ⓐ Top of 30°-dipping thrust ramp

Ⓑ Closest approach of thrust fault to dam site

PHASE 2 FAULT AND SEISMIC HAZARDS INVESTIGATION
NORTH OF DELTA OFFSTREAM STORAGE
DWR-INTEGRATED STORAGE INVESTIGATION

**Site-Source Geometry, Golden Gate Dam Site**

WLA William Lettis & Associates, Inc.

Figure 5-2

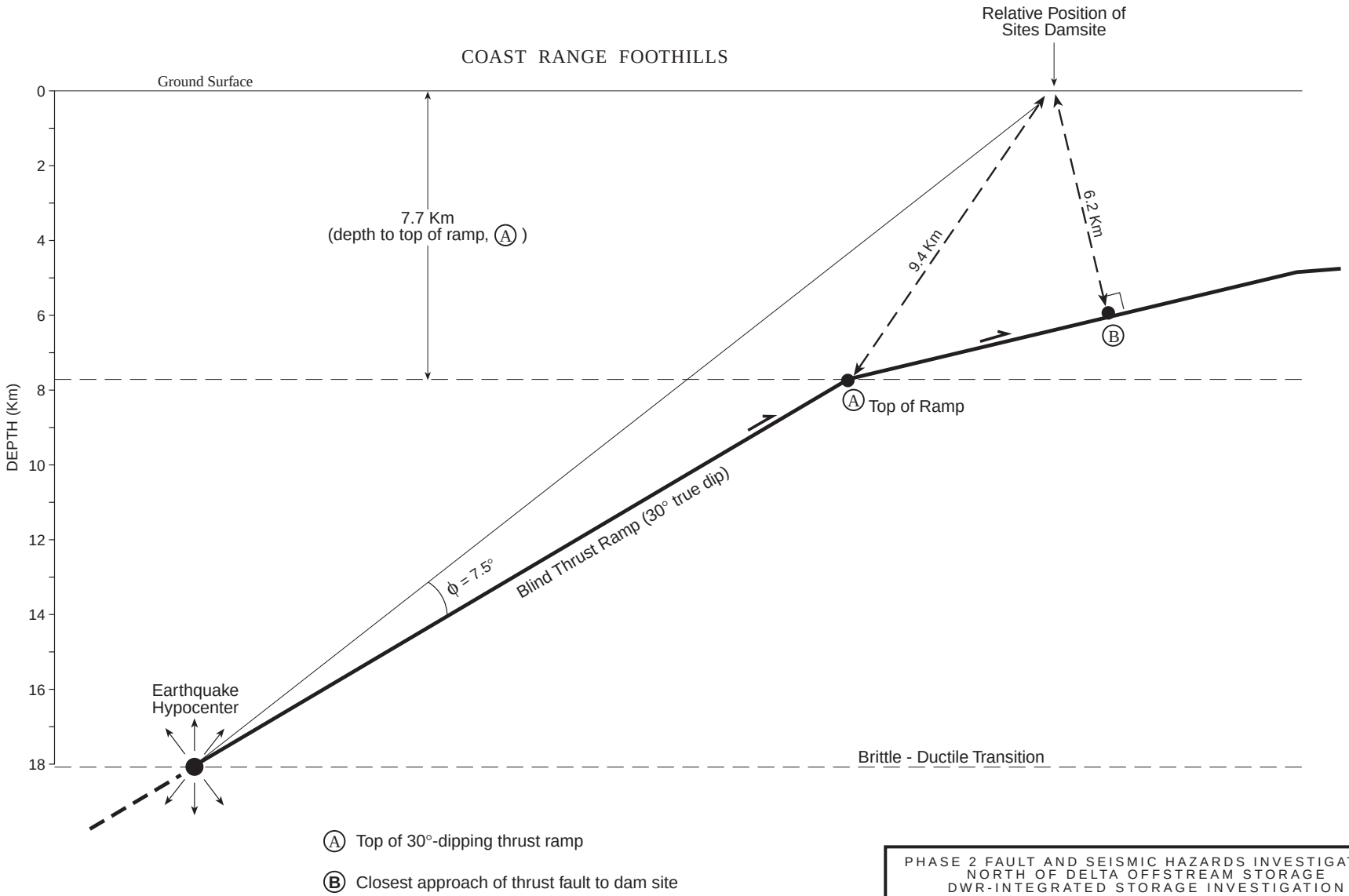


PHASE 2 FAULT AND SEISMIC HAZARDS INVESTIGATION
NORTH OF DELTA OFFSTREAM STORAGE
DWR-INTEGRATED STORAGE INVESTIGATION

**Site-Source Geometry, Sites Dam Site**

WLA William Lettis & Associates, Inc.

Figure 5-3

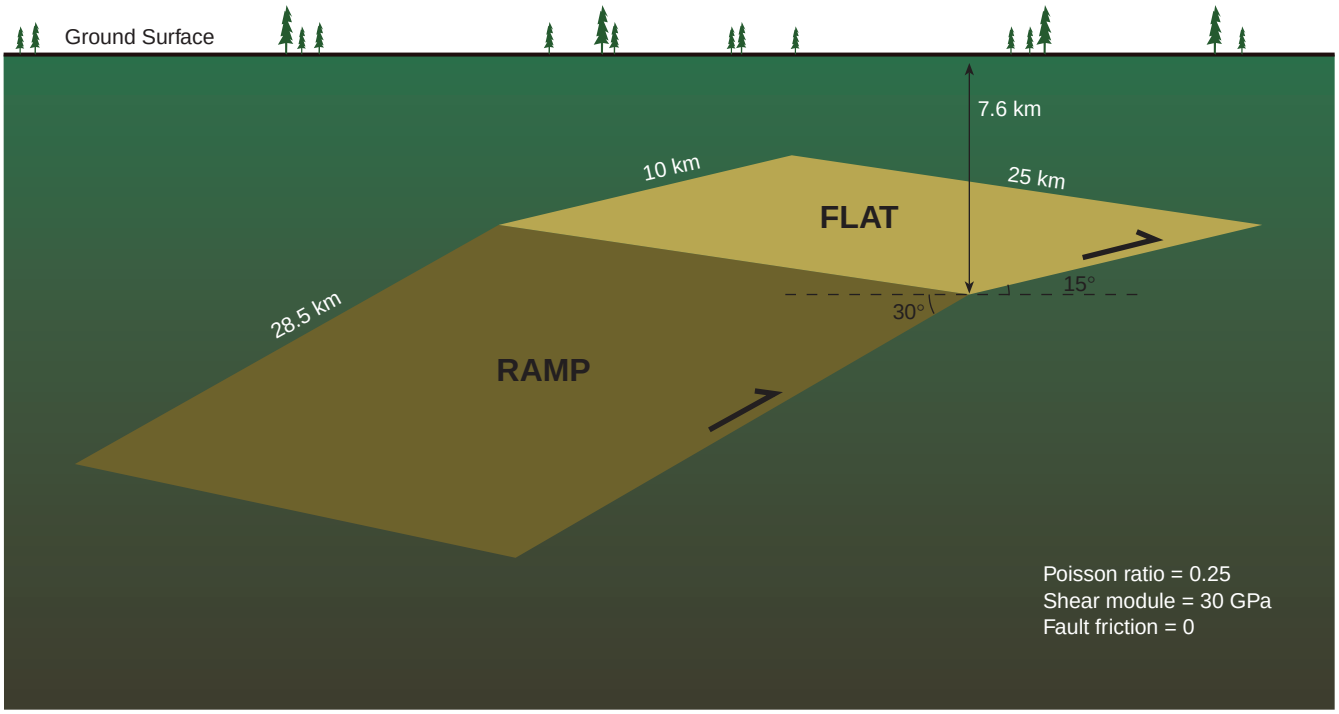


Model faults include a ramp portion and flat portion of the Funks segment. Coseismic rupture is represented by imposing 1 m of pure reverse displacement on the ramp portion, and a range of displacement from 0 to 1 m on the flat segment for various models.

PHASE 2 FAULT AND SEISMIC HAZARDS INVESTIGATION
NORTH OF DELTA OFFSTREAM STORAGE
DWR-INTEGRATED STORAGE INVESTIGATION

**Schematic Diagram Showing Poly 3-D Model Configuration**

WLA William Lettis & Associates, Inc. | Figure 5-4

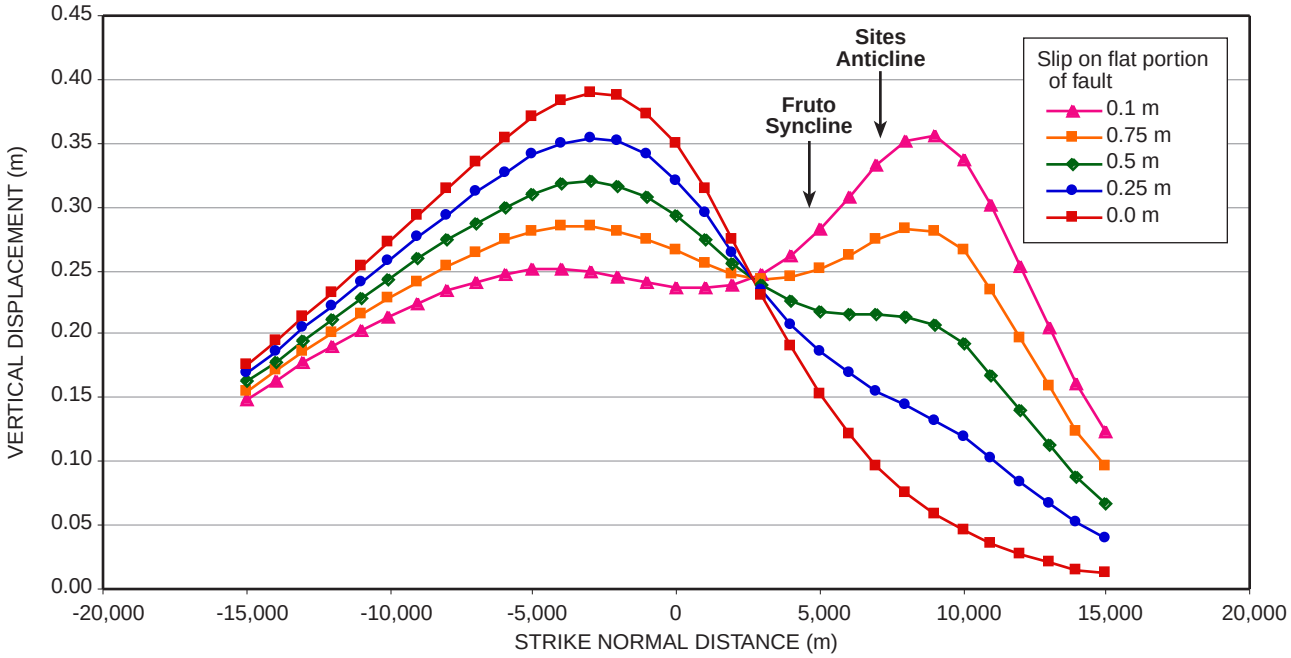


Curves represent models with different anounts of slip on flat portions of fault. Models with 0.75 m and 0.5 m of slip on flat portion of fault result in surface displacement patterns that correlate well with the location of the Sites Anticline and the Fruto Syncline. All models use 1.0 m of slip on the ramp portion of the fault. For reference, 0 marks the location of intersection between the ramp and flat portions of the fault, (i.e., Point A on Figures 5-1 and 5-2).

PHASE 2 FAULT AND SEISMIC HAZARDS INVESTIGATION
NORTH OF DELTA OFFSTREAM STORAGE
DWR-INTEGRATED STORAGE INVESTIGATION

**Profiles of a Modeled Surface Displacement from Rupture on the Ramp and 10 Km of the Flat**

WLA William Lettis & Associates, Inc. | Figure 5-5

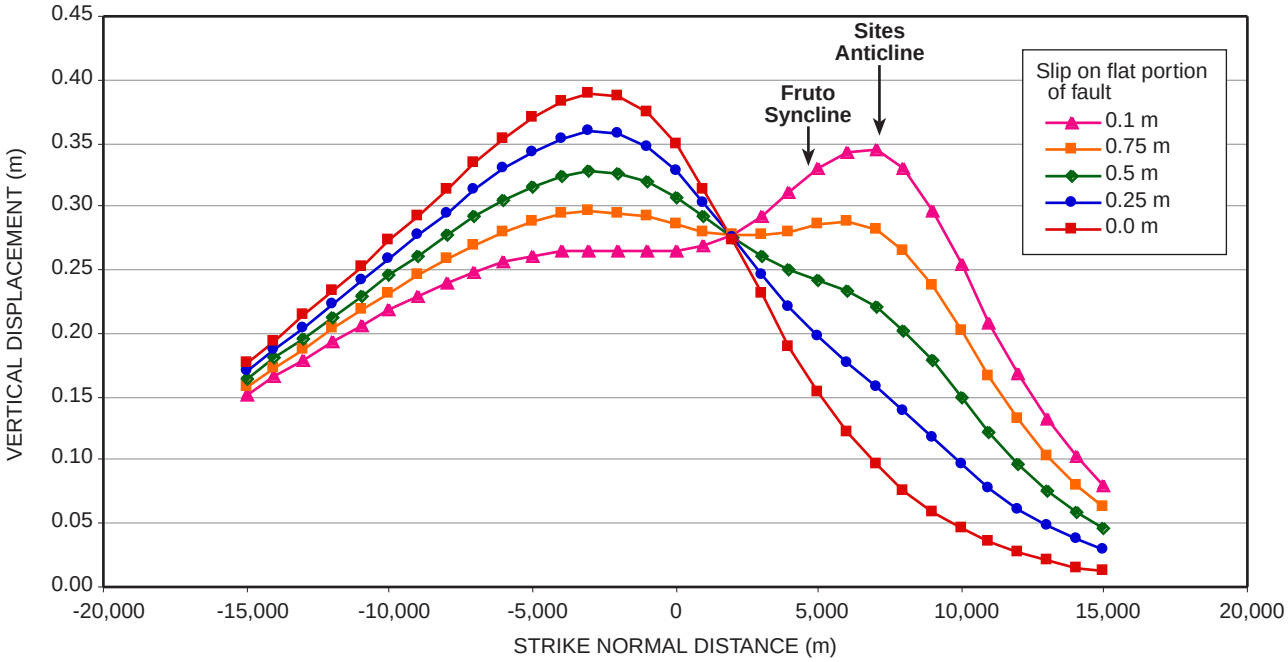


Curves represent models with different anounts of slip on flat portions of fault. Models with 1.0 m, 0.75 m and 0.5 m of slip on flat portion of fault result in surface displacement patterns that correlate well with the location of the Sites Anticline and the Fruto Syncline. All models use 1.0 m of slip on the ramp portion of the fault. For reference, 0 marks the location of intersection between the ramp and flat portions of the fault.

PHASE 2 FAULT AND SEISMIC HAZARDS INVESTIGATION
NORTH OF DELTA OFFSTREAM STORAGE
DWR-INTEGRATED STORAGE INVESTIGATION

**Profiles of a Modeled Surface Displacement from Rupture on the Ramp and 8 km of the Flat**

WLA William Lettis & Associates, Inc. | Figure 5-6

(a)

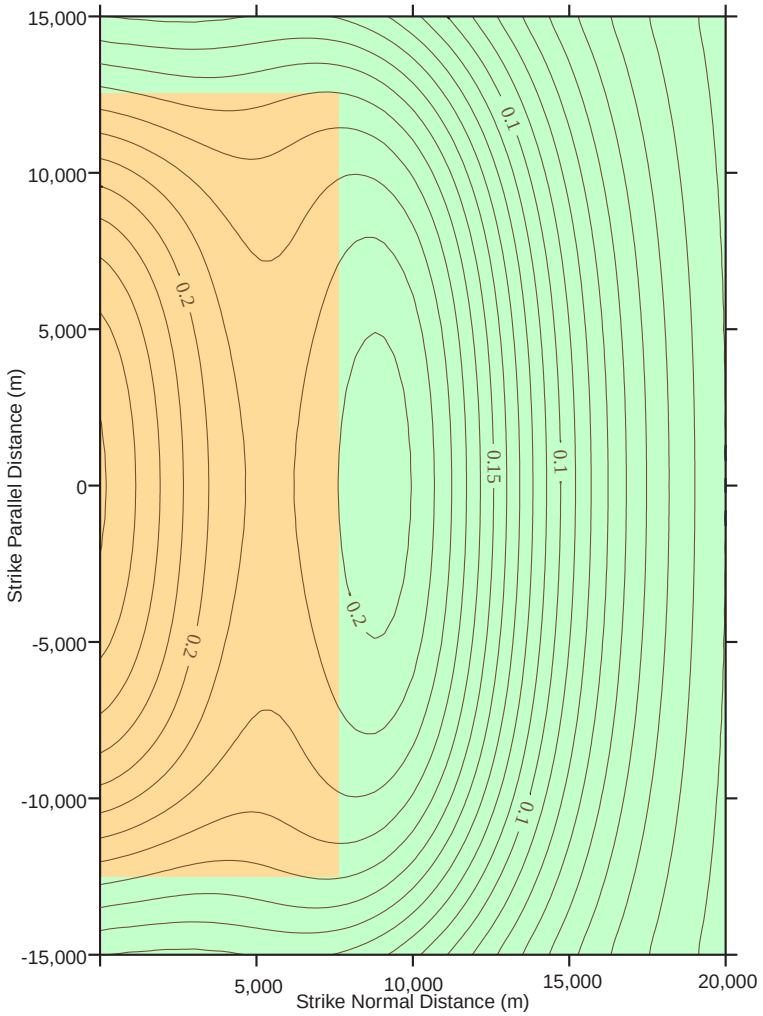


(b)

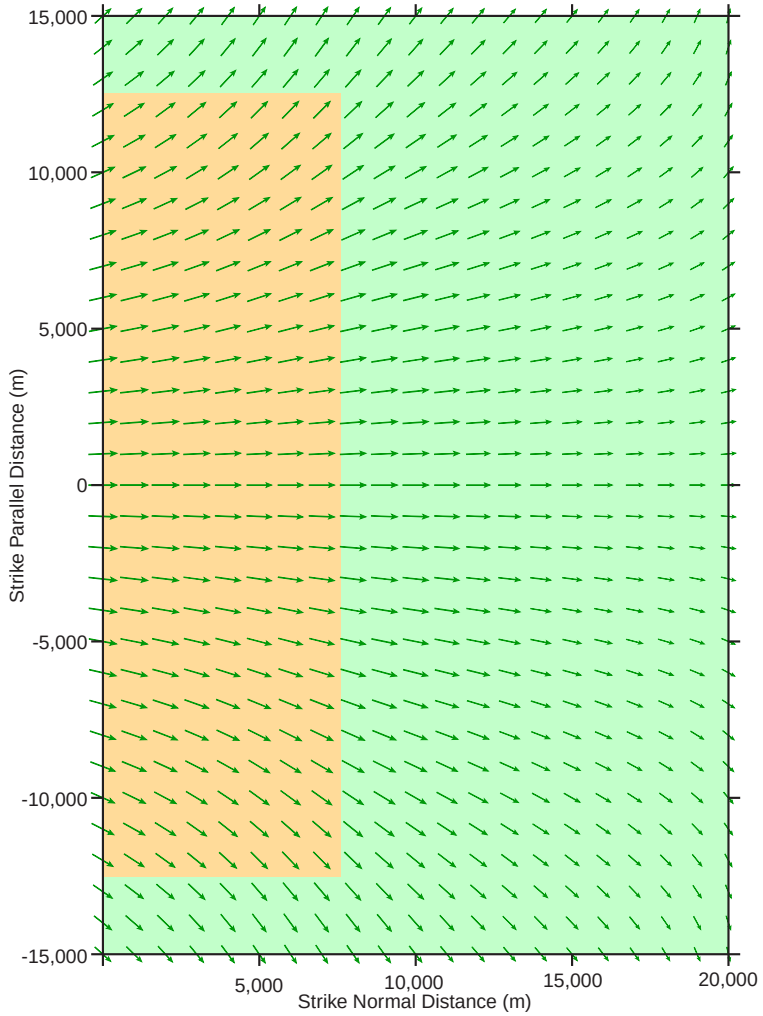


Yellow shading indicates surface projection of the flat portion of the fault.

(a) Contours of horitontal displacements at the surface. Contour interval is 0.01 m (1 cm).

(b) Vectors showing direction of horizontal displacements.

PHASE 2 FAULT AND SEISMIC HAZARDS INVESTIGATION
NORTH OF DELTA OFFSTREAM STORAGE
DWR-INTEGRATED STORAGE INVESTIGATION

**Model of Surface Displacements from Rupture on the Funks Segment of the Great Valley Fault**

WLA William Lettis & Associates, Inc.

Figure 5-7

(a)

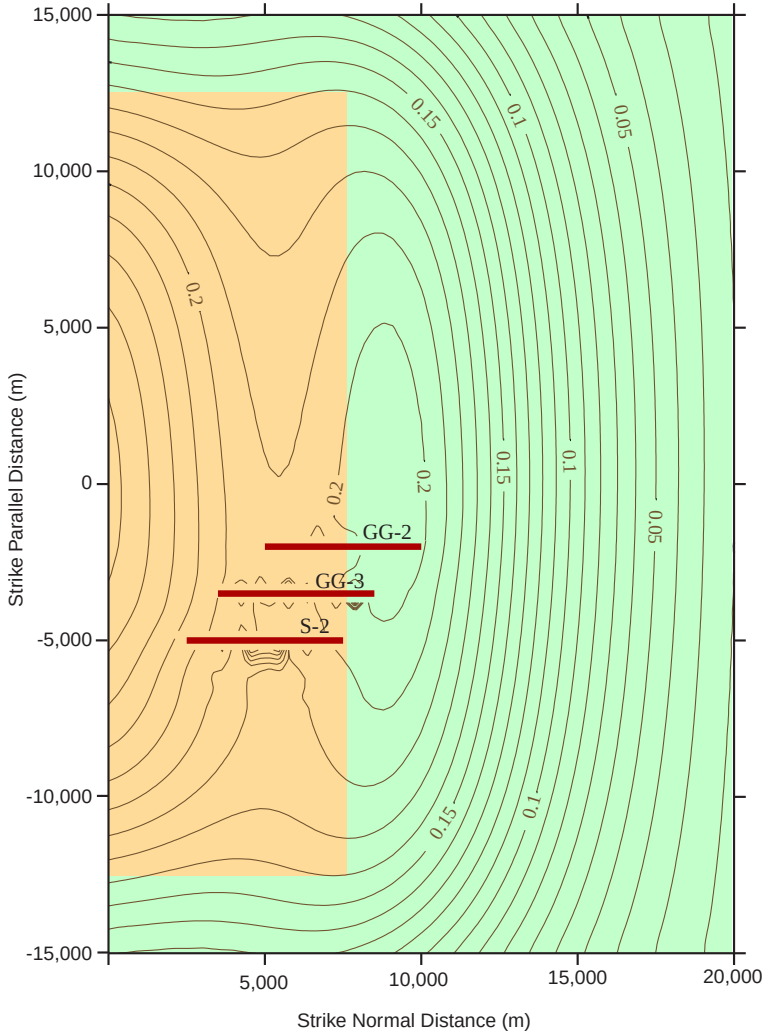


(b)

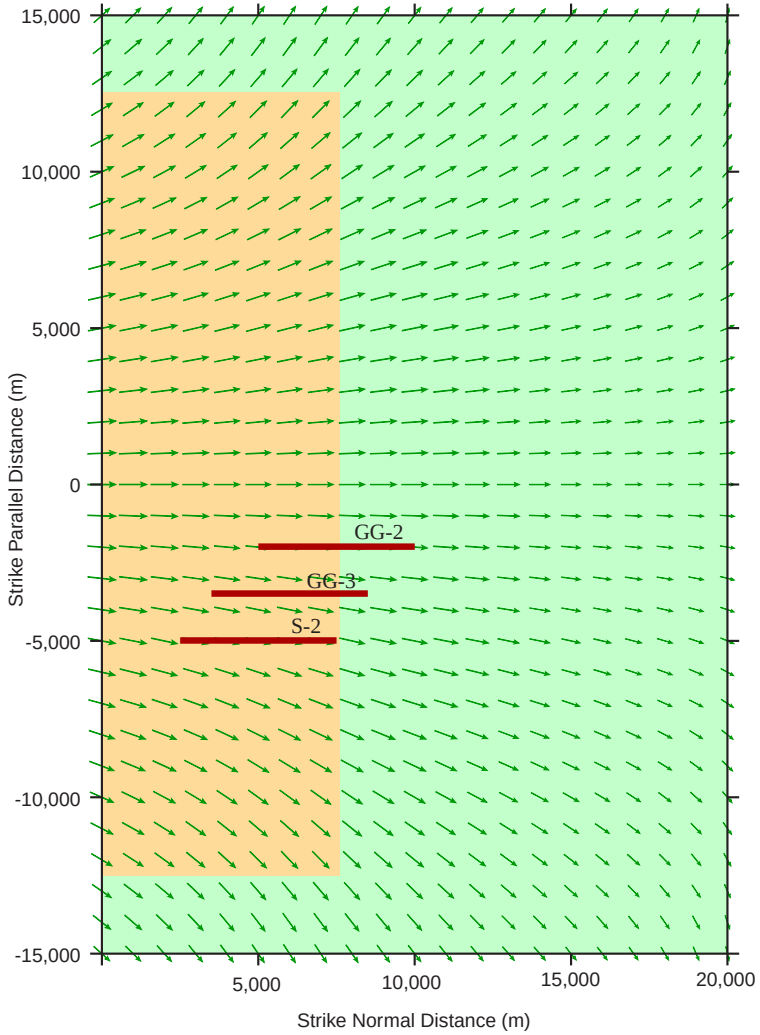


(a) Contours of horitontal displacements at the surface.
Contour interval is 0.01 m (1 cm).

(b) Vectors showing direction of horizontal displacements

PHASE 2 FAULT AND SEISMIC HAZARDS INVESTIGATION
NORTH OF DELTA OFFSTREAM STORAGE
DWR-INTEGRATED STORAGE INVESTIGATION

**Model Results Showing Effects of Tear Faults on Surface Displacements**

WLA William Lettis & Associates, Inc.

Figure 5-8

(a)

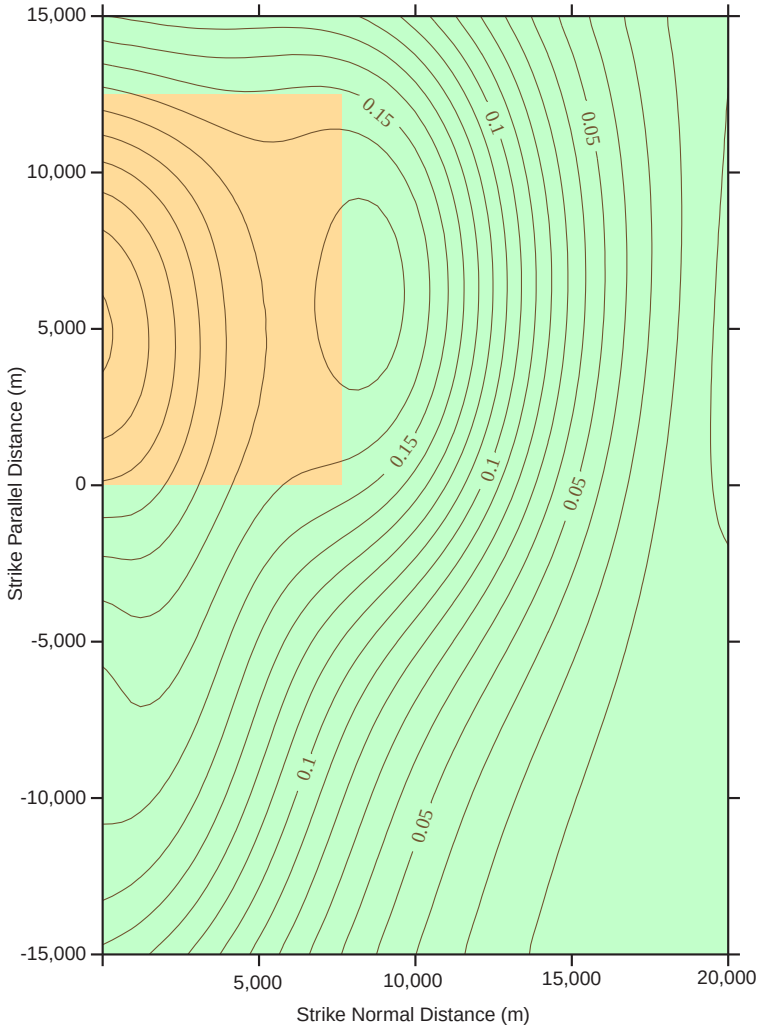


(b)

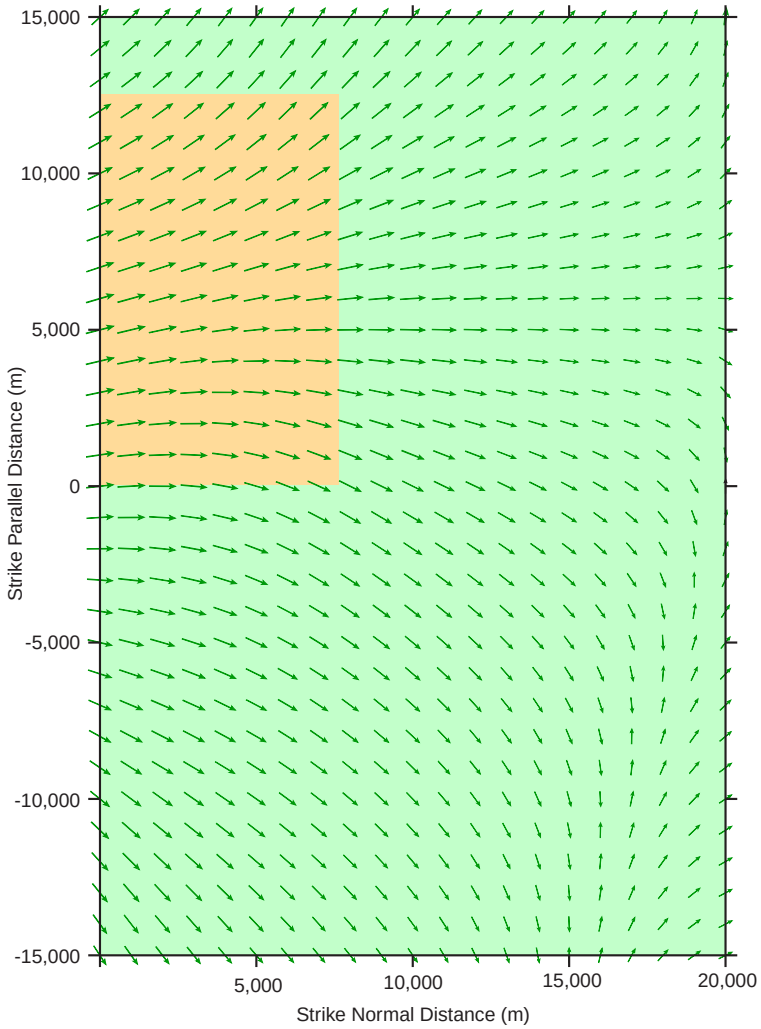


(a) Contours of horitontal displacements at the surface. Contour interval is 0.01 m (1 cm).

(b) Vectors showing direction of horizontal displacements.

PHASE 2 FAULT AND SEISMIC HAZARDS INVESTIGATION
NORTH OF DELTA OFFSTREAM STORAGE
DWR-INTEGRATED STORAGE INVESTIGATION

**Model of Surface Displacements from Rupture on the Northern Part of the Flat, Funks Segment**

WLA William Lettis & Associates, Inc.

Figure 5-9

(a)

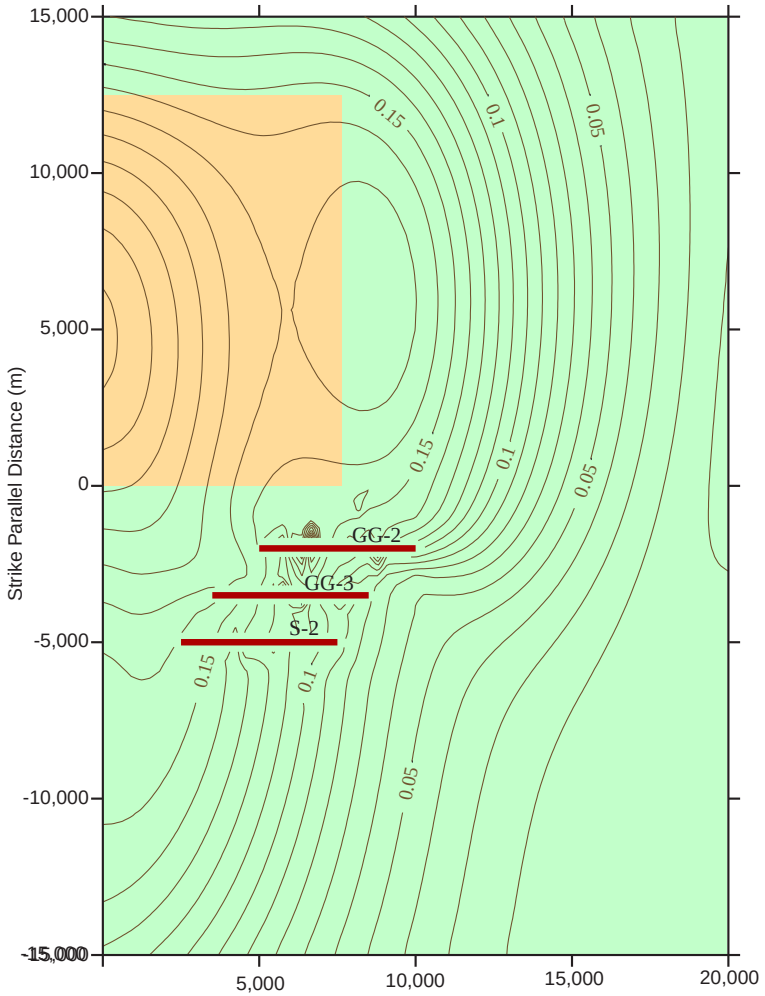


(b)

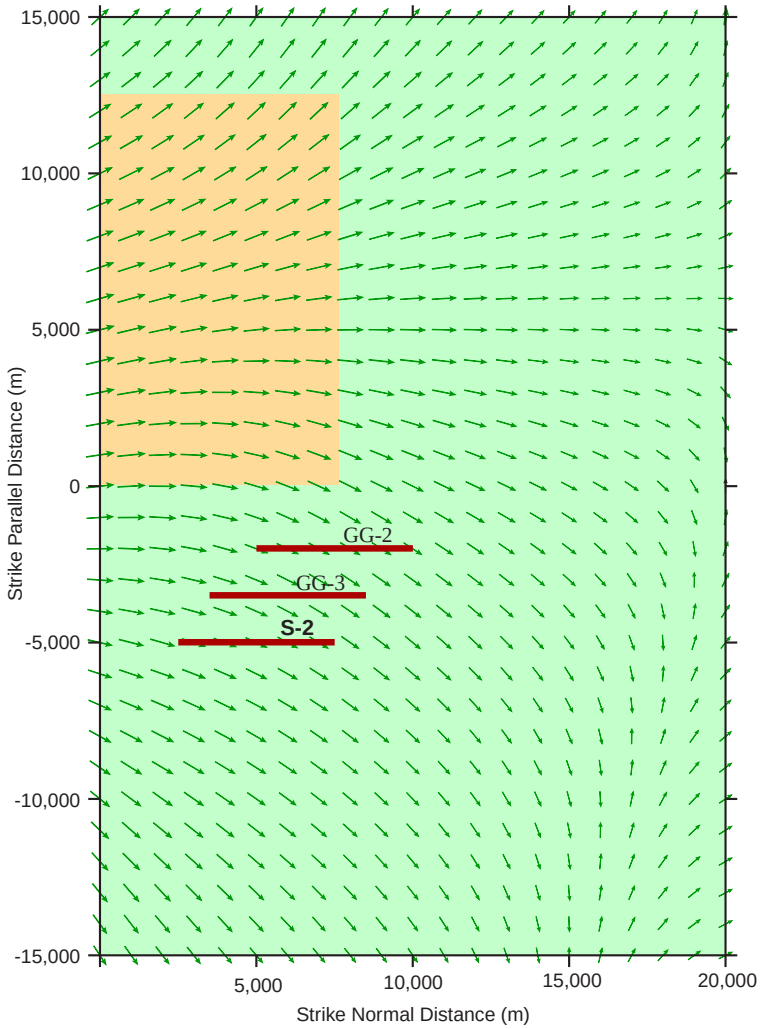


(a) Contours of horitontal displacements at the surface. Contour interval is 0.01 m (1 cm).

(b) Vectors showing direction of horizontal displacements

PHASE 2 FAULT AND SEISMIC HAZARDS INVESTIGATION
NORTH OF DELTA OFFSTREAM STORAGE
DWR-INTEGRATED STORAGE INVESTIGATION

**Model Results of Rupture on the Northern Part of the Flat with Frictionless Tear Faults**

WLA William Lettis & Associates, Inc.

Figure 5-10

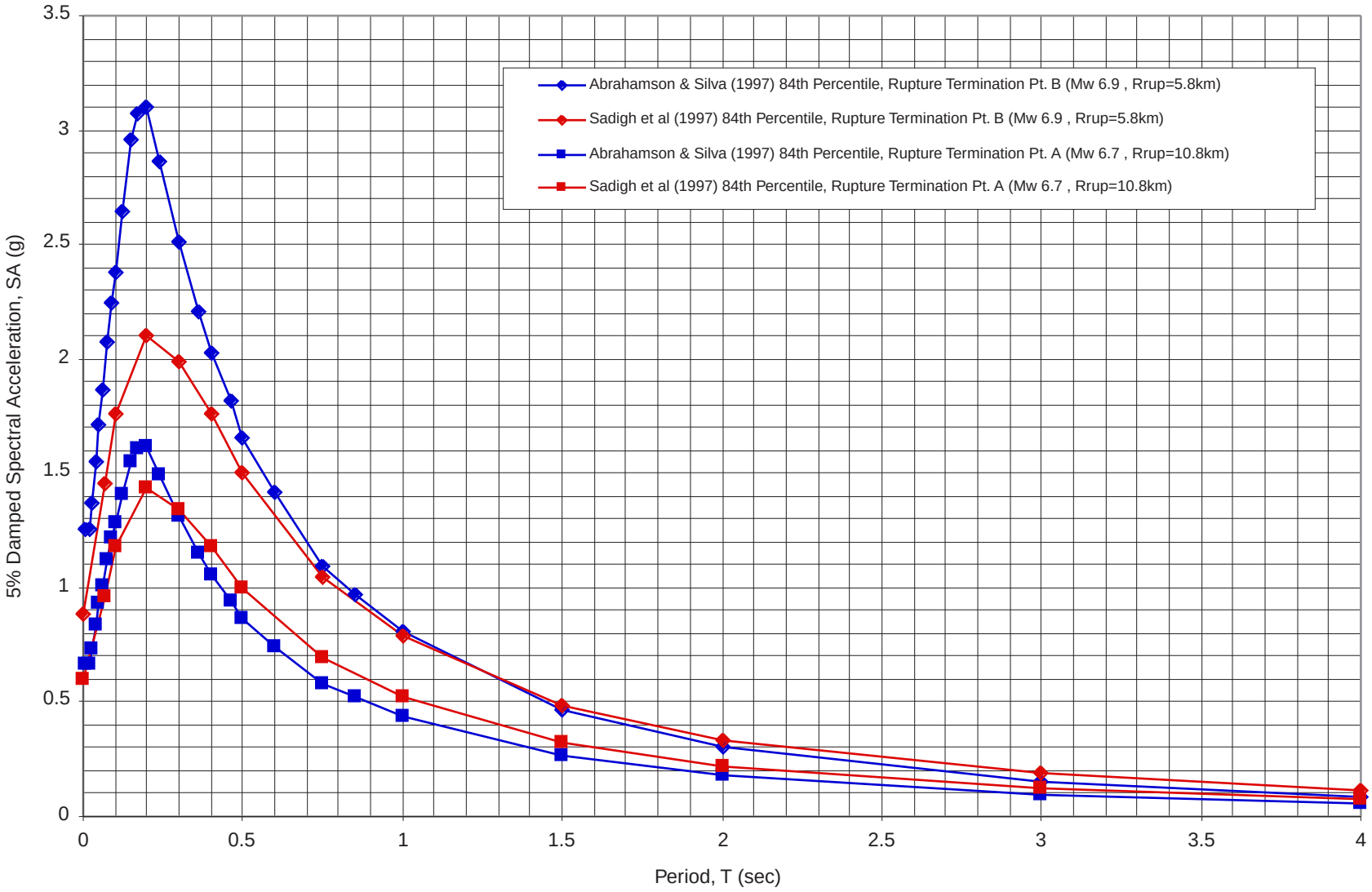


PHASE 2 FAULT AND SEISMIC HAZARDS INVESTIGATION
NORTH OF DELTA OFFSTREAM STORAGE
DWR-INTEGRATED STORAGE INVESTIGATION

**Golden Gate Dam Site, California--84th Percentile Deterministic Response Spectra (Without Directivity)**

WLA William Lettis & Associates, Inc. URS Figure 6-1

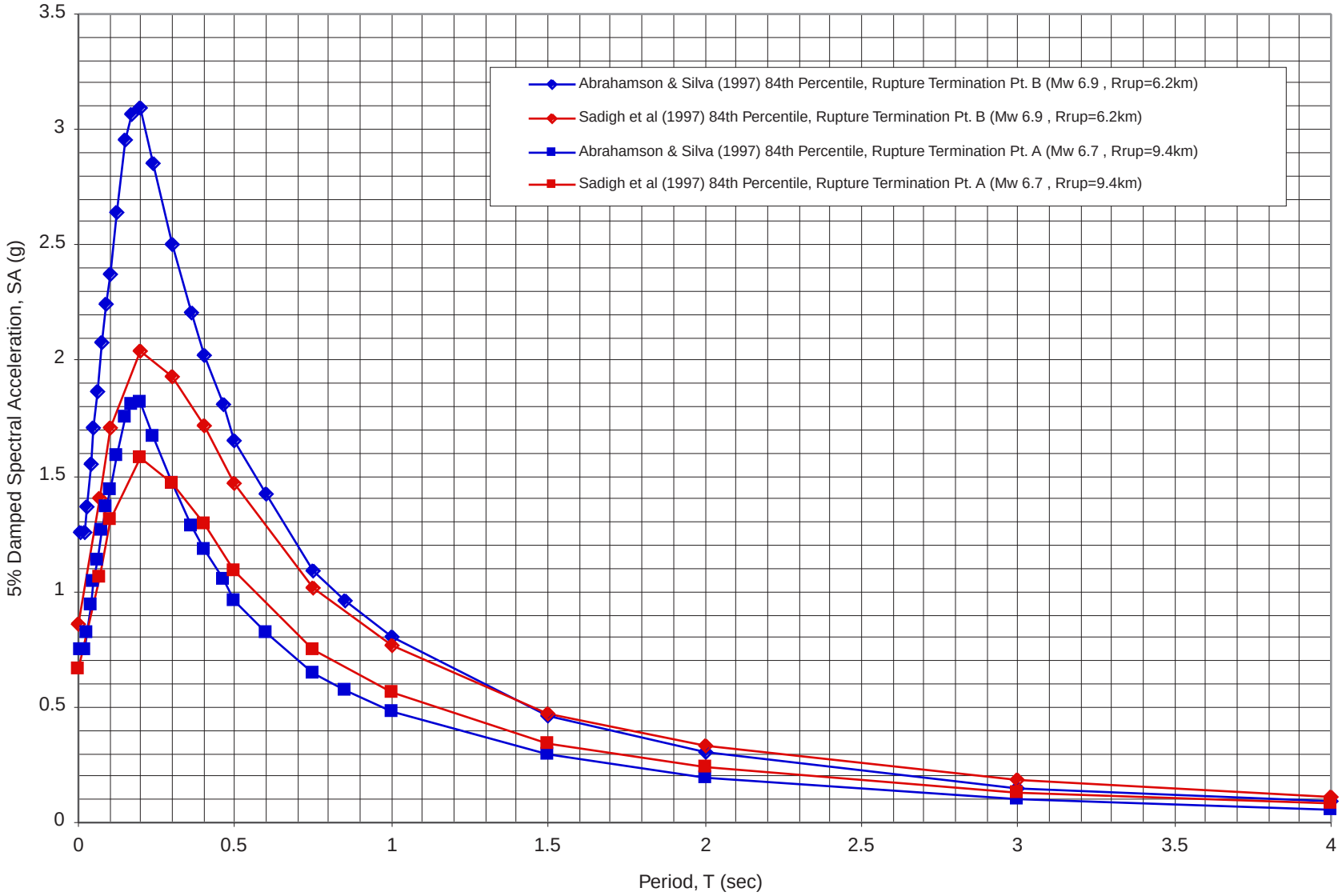


PHASE 2 FAULT AND SEISMIC HAZARDS INVESTIGATION
NORTH OF DELTA OFFSTREAM STORAGE
DWR-INTEGRATED STORAGE INVESTIGATION

**Sites Dam Site, California--84th Percentile Deterministic Response Spectra (Without Directivity)**

WLA William Lettis & Associates, Inc. URS Figure 6-2

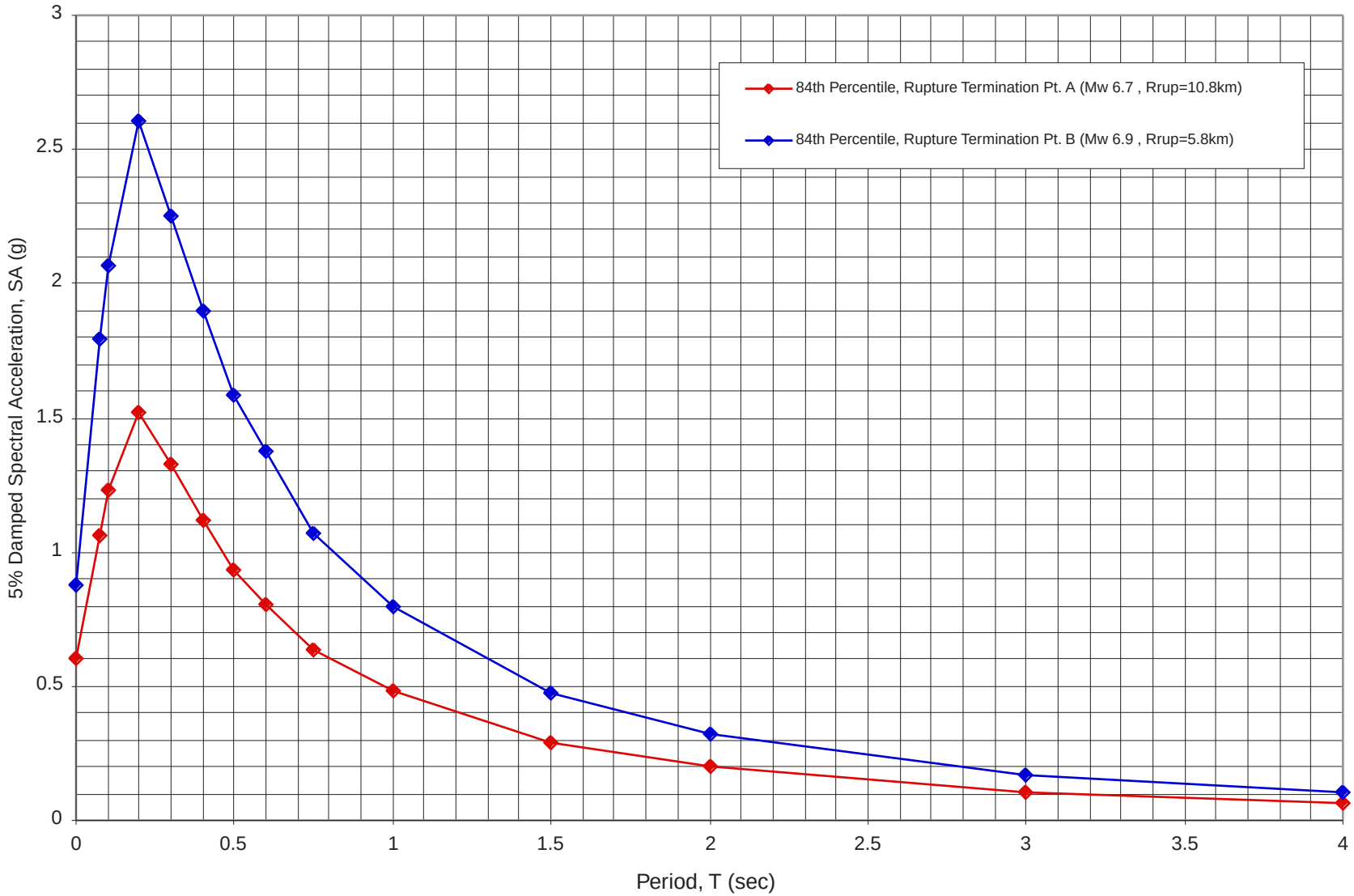


PHASE 2 FAULT AND SEISMIC HAZARDS INVESTIGATION
NORTH OF DELTA OFFSTREAM STORAGE
DWR-INTEGRATED STORAGE INVESTIGATION

**Golden Gate Dam Site, California--Average of 84th Percentile Deterministic Response Spectra (Without Directivity)**

WLA William Lettis & Associates, Inc. URS Figure 6-3

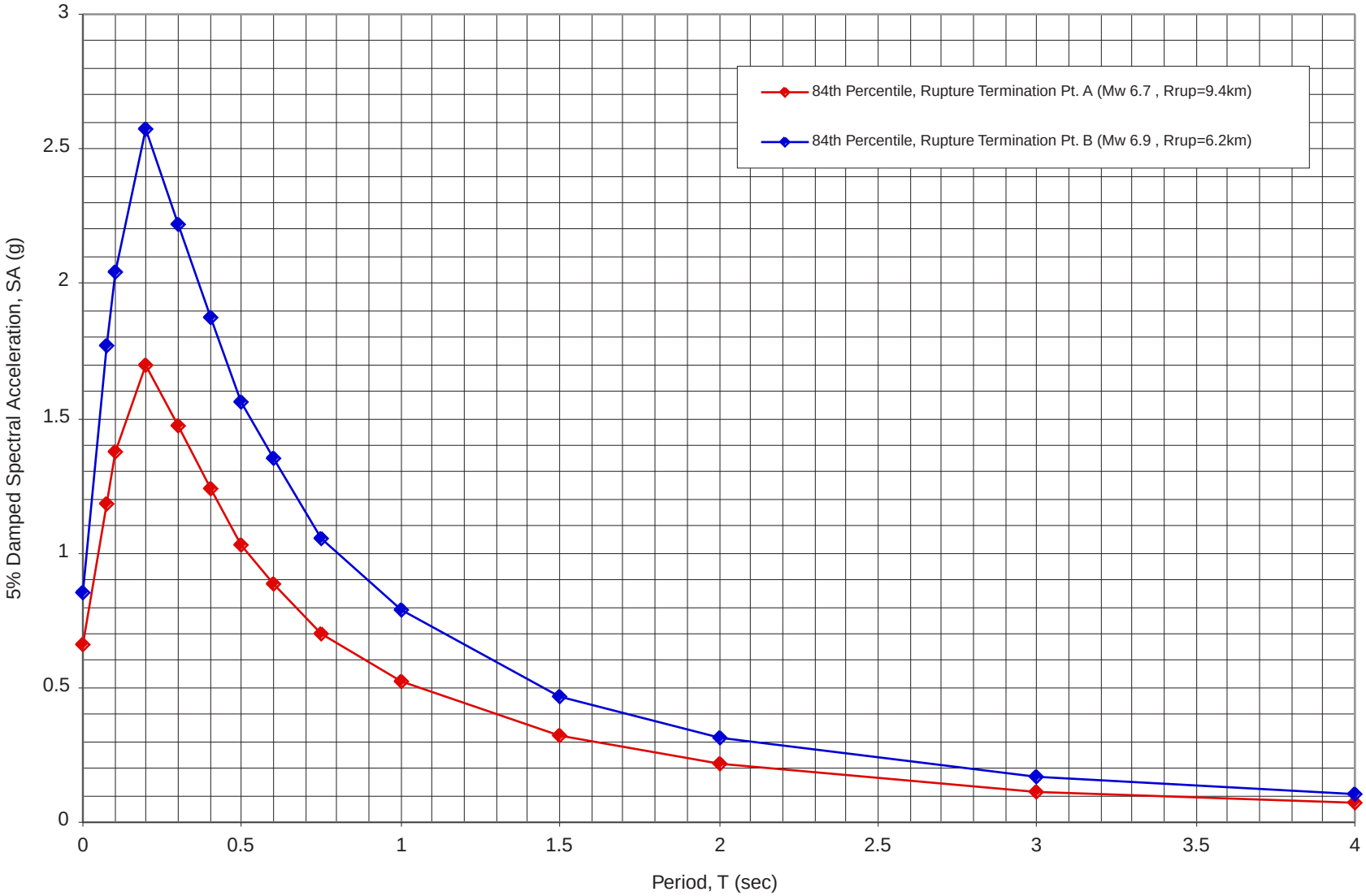


PHASE 2 FAULT AND SEISMIC HAZARDS INVESTIGATION
NORTH OF DELTA OFFSTREAM STORAGE
DWR-INTEGRATED STORAGE INVESTIGATION

**Sites Dam Site, California--Average of 84th Percentile Deterministic Response Spectra (Without Directivity)**

WLA William Lettis & Associates, Inc. URS Figure 6-4

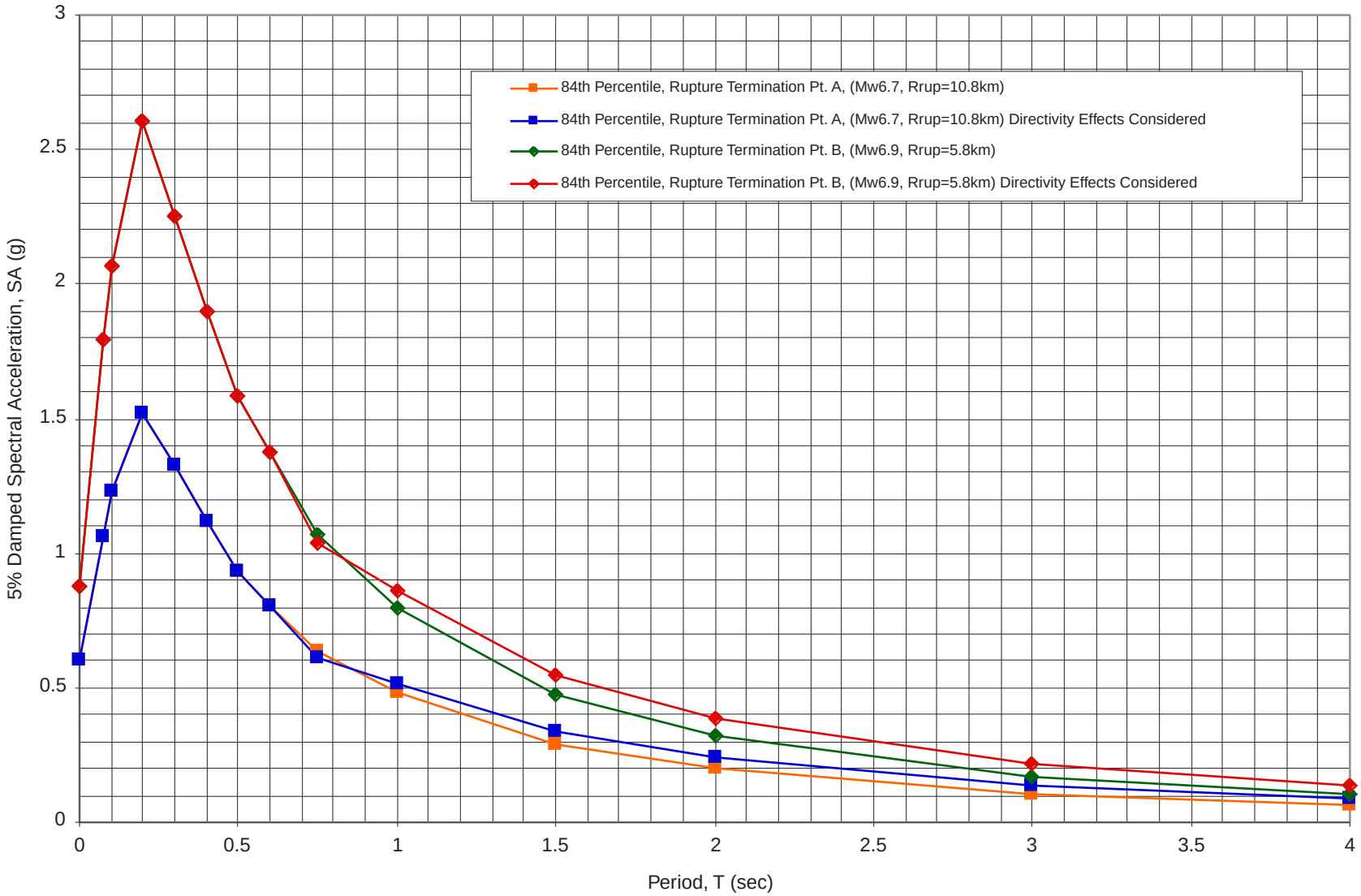


PHASE 2 FAULT AND SEISMIC HAZARDS INVESTIGATION
NORTH OF DELTA OFFSTREAM STORAGE
DWR-INTEGRATED STORAGE INVESTIGATION

**Golden Gate Dam Site, California--84th Percentile Deterministic Response Spectra (With and Without Directivity)**

WLA William Lettis & Associates, Inc. URS Figure 6-5

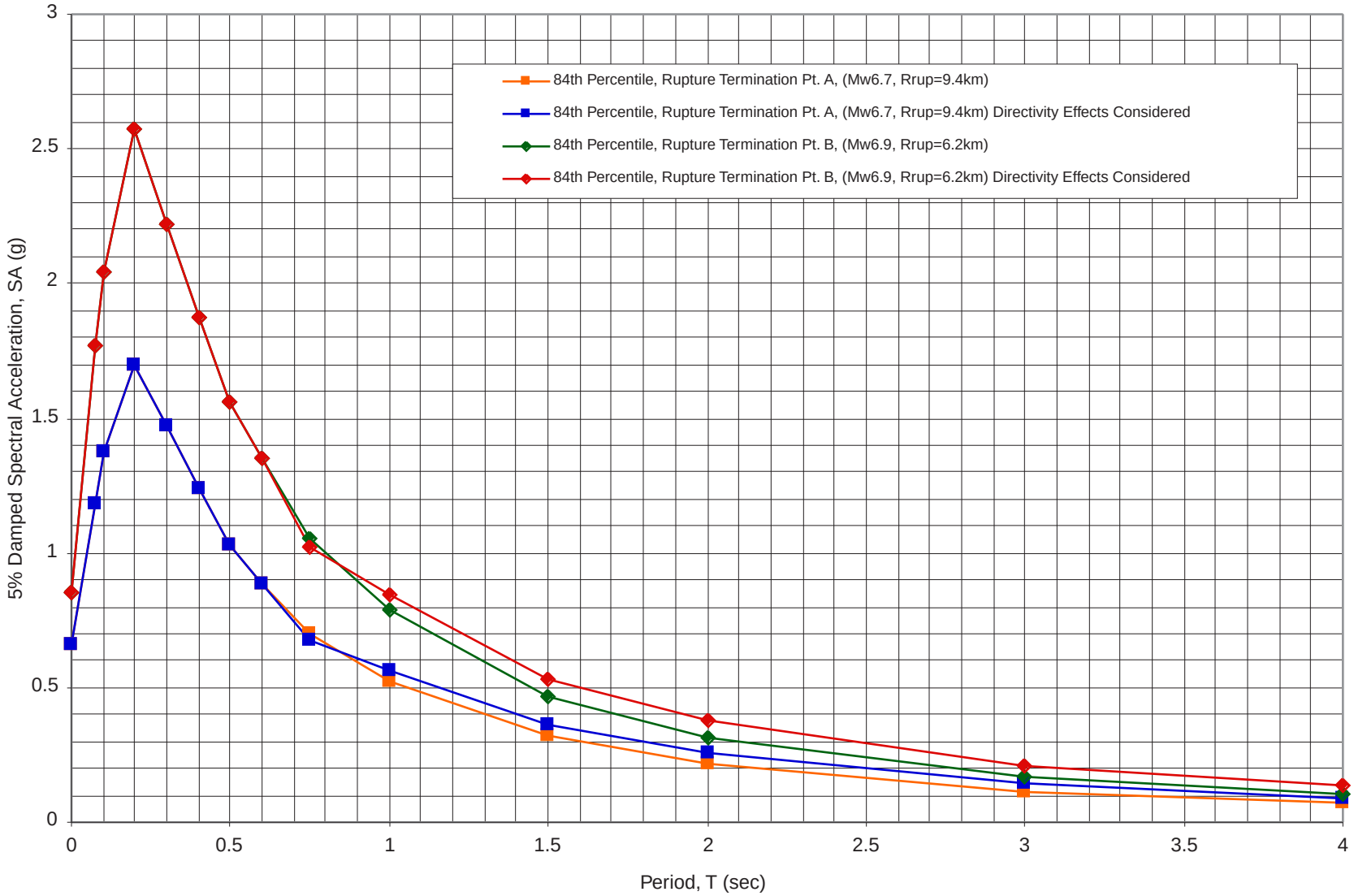


PHASE 2 FAULT AND SEISMIC HAZARDS INVESTIGATION
NORTH OF DELTA OFFSTREAM STORAGE
DWR-INTEGRATED STORAGE INVESTIGATION

**Sites Dam Site, California--84th Percentile Deterministic Response Spectra (With and Without Directivity)**

WLA William Lettis & Associates, Inc. URS Figure 6-6

123°
122°
40°
39°
N
NORTHERN
COAST
RANGES
SACRAMENTO
VALLEY
SIERRA
NEVADA
FOOTHILLS
SUTTER
BUTTES
DUNNIGAN
HILLS
RUMSEY
CRO
Coast Range Fault
Bear Creek Fault
Battle Creek U D Fault
Anderson
INKS CREEK FOLD SYSTEM
Red Bluff
Fault U D
U D Red Bluff
Chico
Monocline
Paskenta Fault
Paskenta
Thomes Creek
Newville
Stony Creek Fault
Chrome
Paskenta Nose Anticline
Black Butte Lake
Stony Creek
Hambright Creek
Corning
North Corning Dome
South Corning Dome
Sacramento River
Orland
Greenwood Fault
Elk Creek
Fruto
Fruto Syncline
Sites Anticline
Hayes Hollow Creek
Nye Creek
Stony Gorge Reservoir
Willows
Willow Creek
South Fork
Logan Creek
Hunters Creek
Salt Lake Fault
Golden Gate Dam Site
GG-1
GG-2
GG-3
Funks Creek
Sites
S-2
Sites Dam Site
Stone Corral Creek
Maxwell
Antelope Creek
SULPHUR GAP
Colusa
Williams
Arbuckle
Gridley
Sutter
Willows Fault
Sacramento River
Anticline
Elk Creek Segment
Eisel Ridge Fault
Round Valley Fault
BARTLETT SPRINGS FAULT ZONE
Coyote Rocks Segment
McLeod Ridge Segment
Twin Valley Segment
Register Rock Segment
Chalk Mountain Segment
Lake Pillsbury
Clear Lake
Lakeport
Ukiah
Hopland
Stonyford
East Park Reservoir
Lodoga
Indian Valley Reservoir
Wilbur Springs Anticline
Cherry Hill Anticline
Wilson Hunting Fault
Valley Side Fault
Sweitzer Rumsey Hills Anticline
Fault
Creek
Range
Stony
Coast
CRO
Ridge
Valley
Round
Eisel
Hunting
Wilson
Side
Sweitzer
Rumsey Hills Anticline
Wilbur Springs Anticline
Cherry Hill Anticline
Fruto Syncline
Sites Anticline
Salt Lake Fault
Paskenta Nose Anticline
Greenwood Fault
Willows Fault
Monocline
Sacramento River
Stony Creek Fault
Remnant of the Coast Range Ophiolite
Coast Range fault
Fault; dashed where approximately located, dotted where concealed, queried where uncertain. U = upthrown block, D = downthrown block
Anticline
Syncline
Plunging anticline
Plunging syncline
Thrust fault; teeth on hanging wall
Strike-slip fault
EXPLANATION
0 5 10 15 20 25 km
SCALE
Fault locations modified from Bortugno, 1982; Chuber, 1961; Division of Mines and Geology, CD-ROM 2000-006 (2000); Fox, et al. 1973; Geomatrix Consultants, 1986; Harwood, 1987; Harwood et al., 1981, Harwood and Helley, Helley, 1985; Lawton, 1956; Phipps, 1984; Saucedo, 1992; Sims et al., 1973, Taliaferro et. al (unpublished); Unruh et al., 1995; and William Lettis & Associates, Inc., 1997.
PHASE 2 FAULT AND SEISMIC HAZARDS INVESTIGATION
NORTH OF DELTA OFFSTREAM STORAGE
DWR-INTEGRATED STORAGE INVESTIGATION
# Major Structural Features in the Study Region, Northwestern California
WLA William Lettis & Associates, Inc.
Plate 1

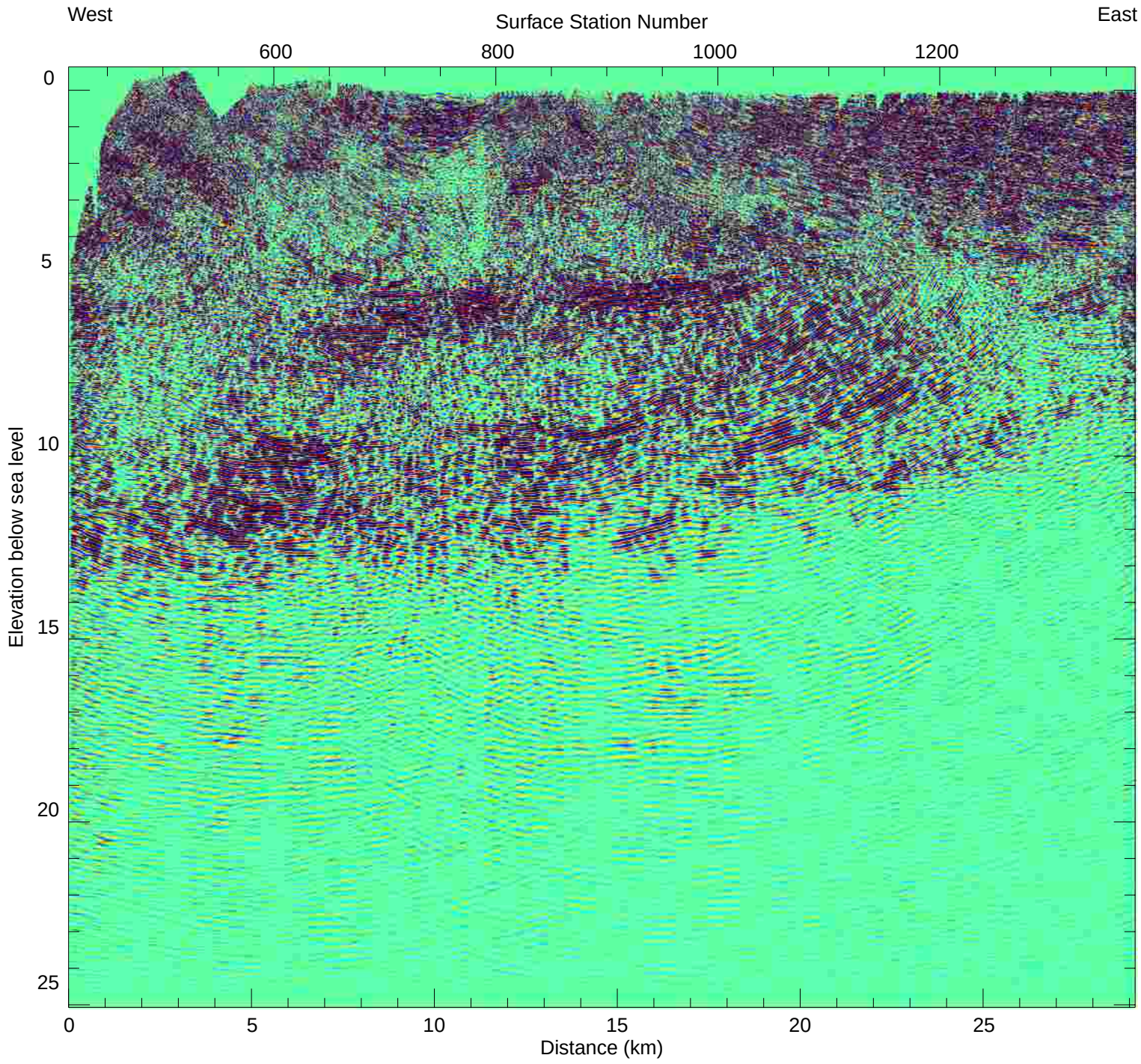


Figure A-2. Seismic line 798.

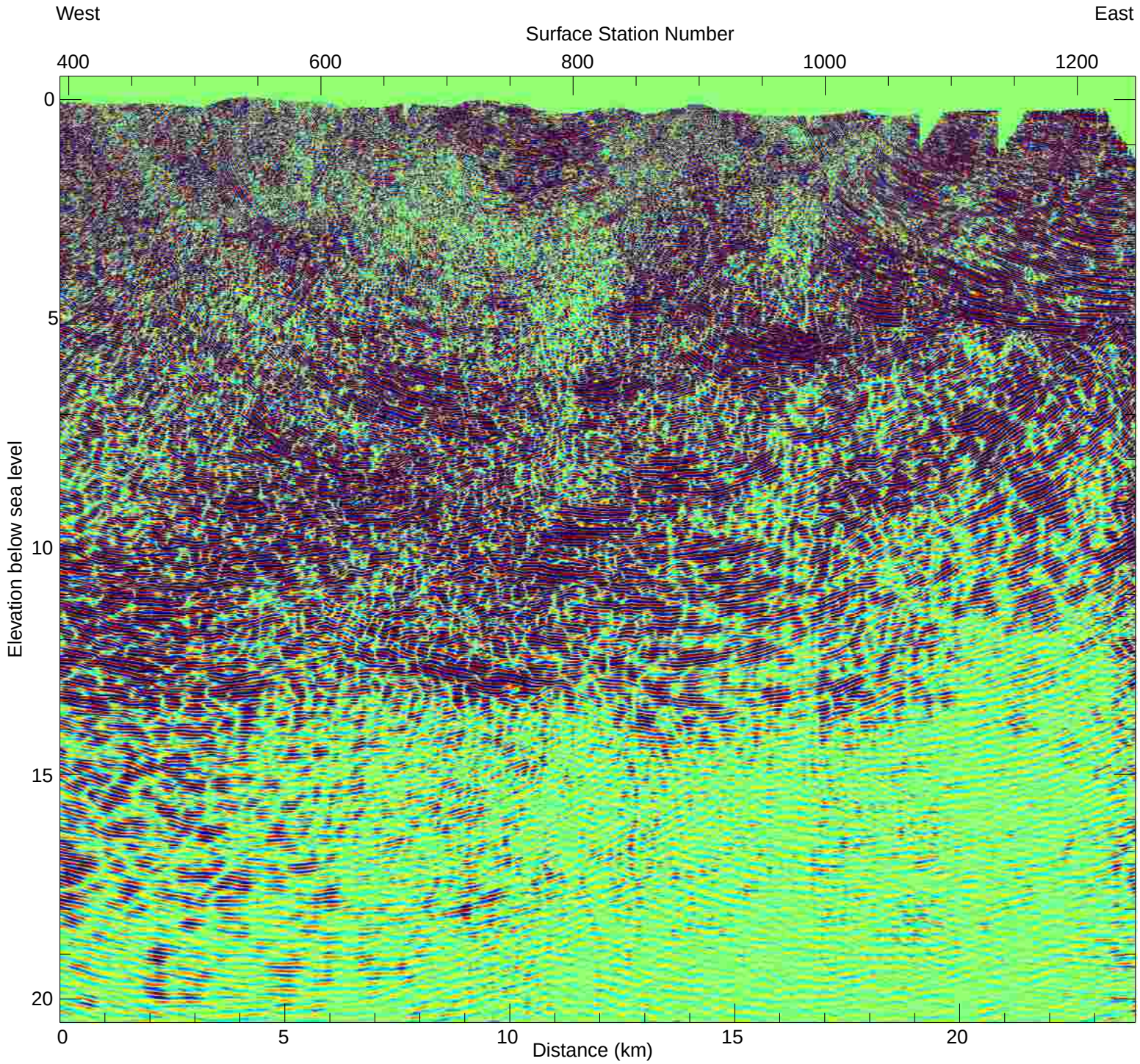


Figure A-3. Seismic line 782.

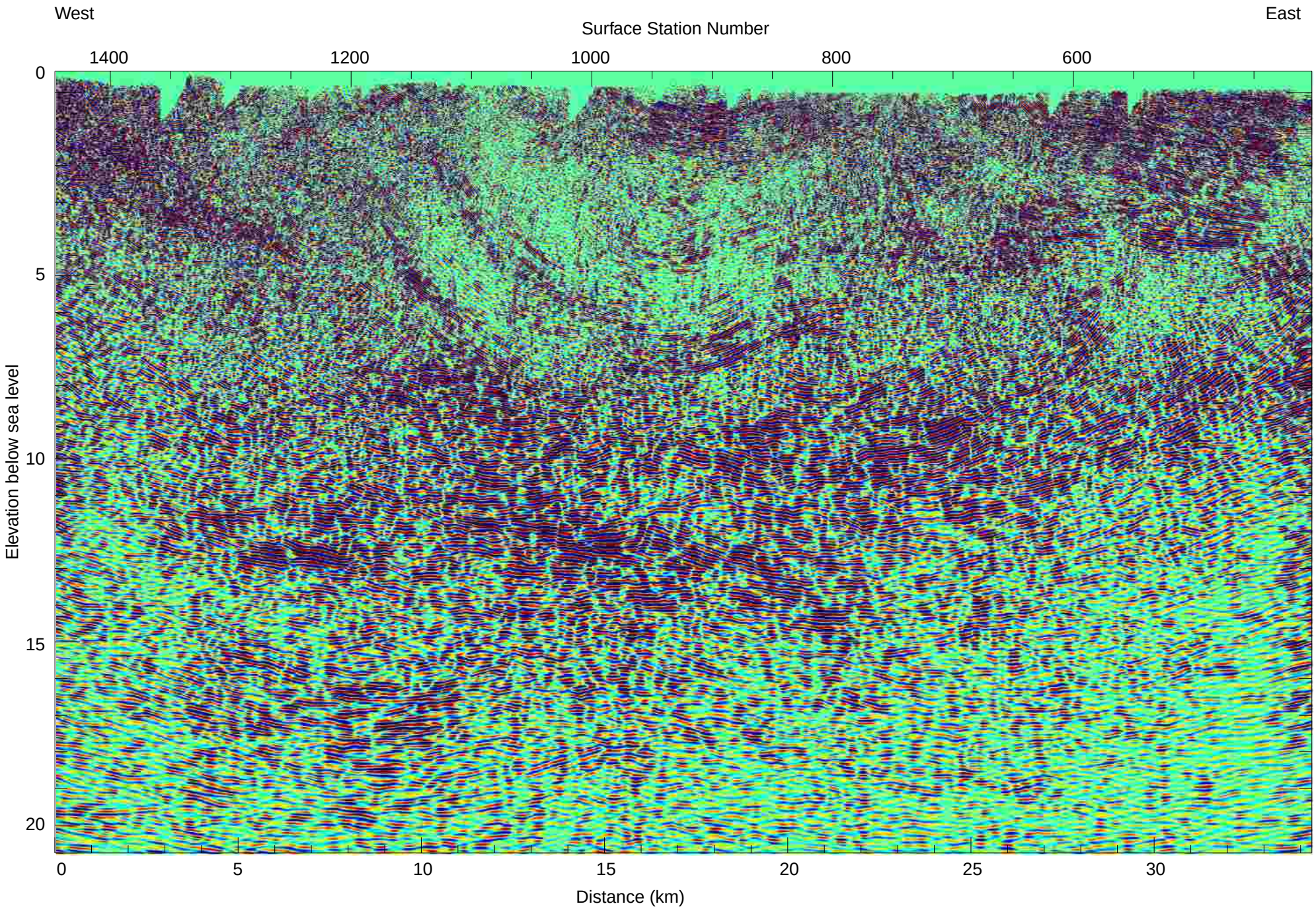


Figure A-4. Seismic line 001.

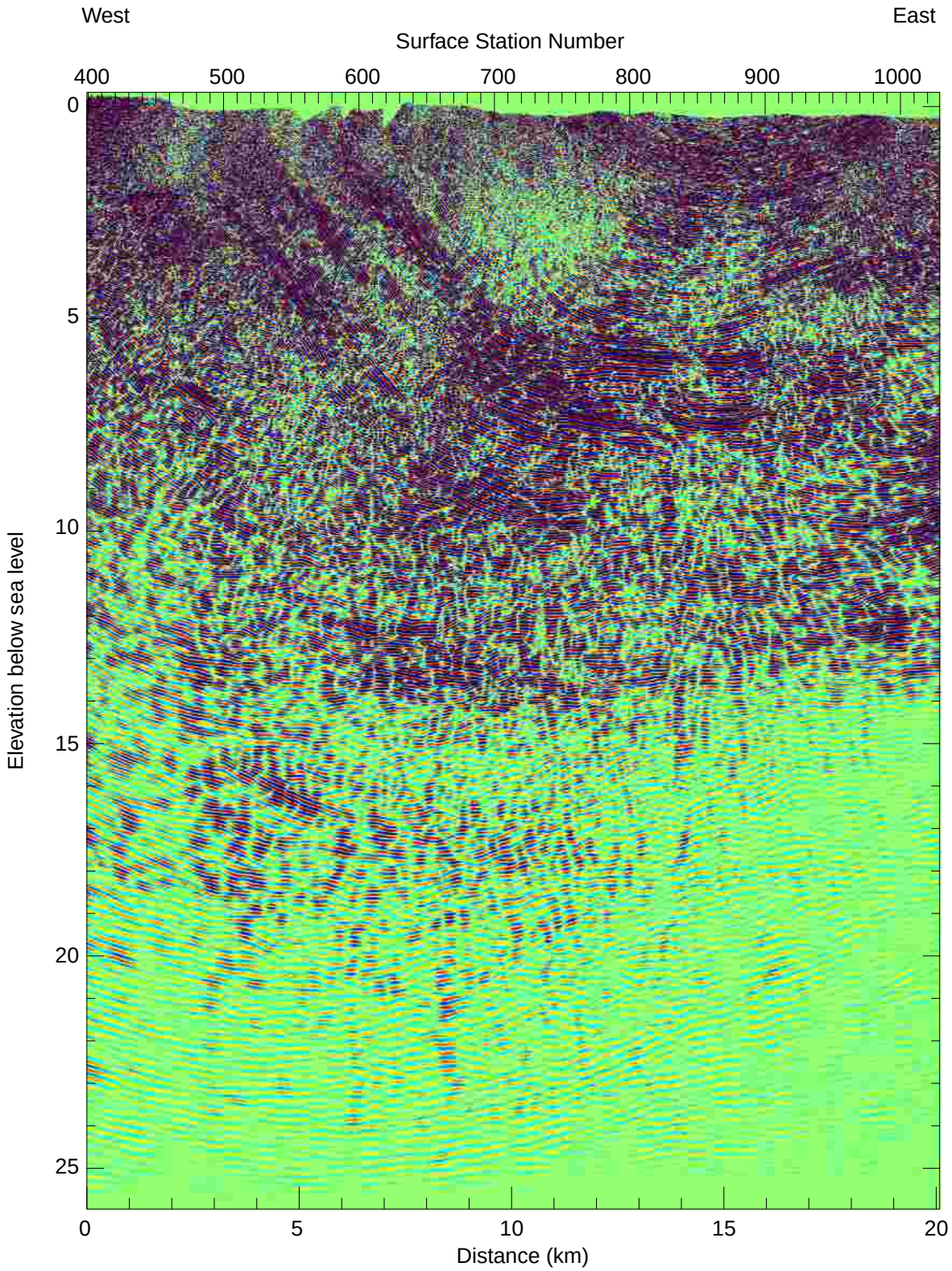


Figure A-5. Seismic line 781.

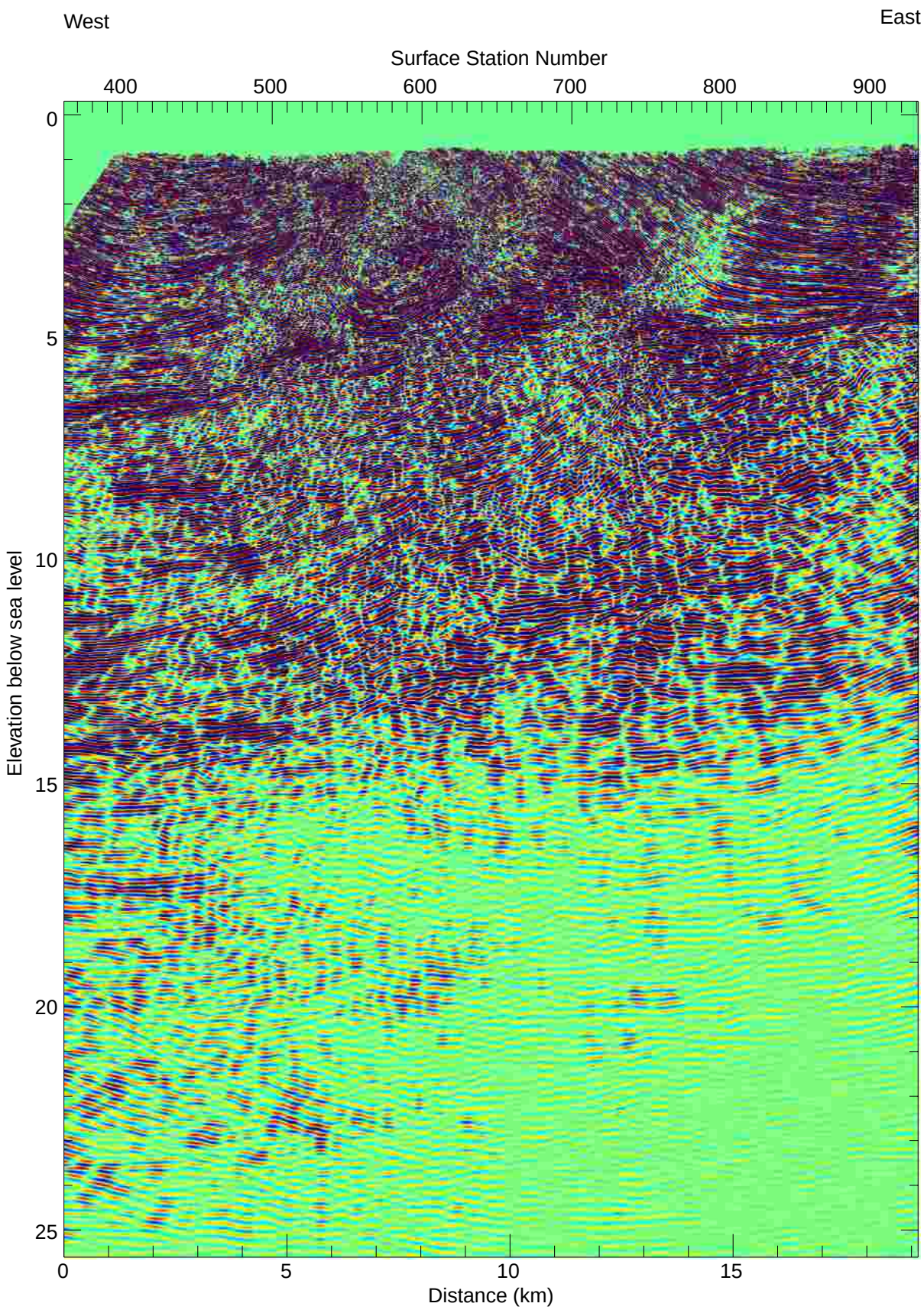


Figure A-6. Seismic line 805.

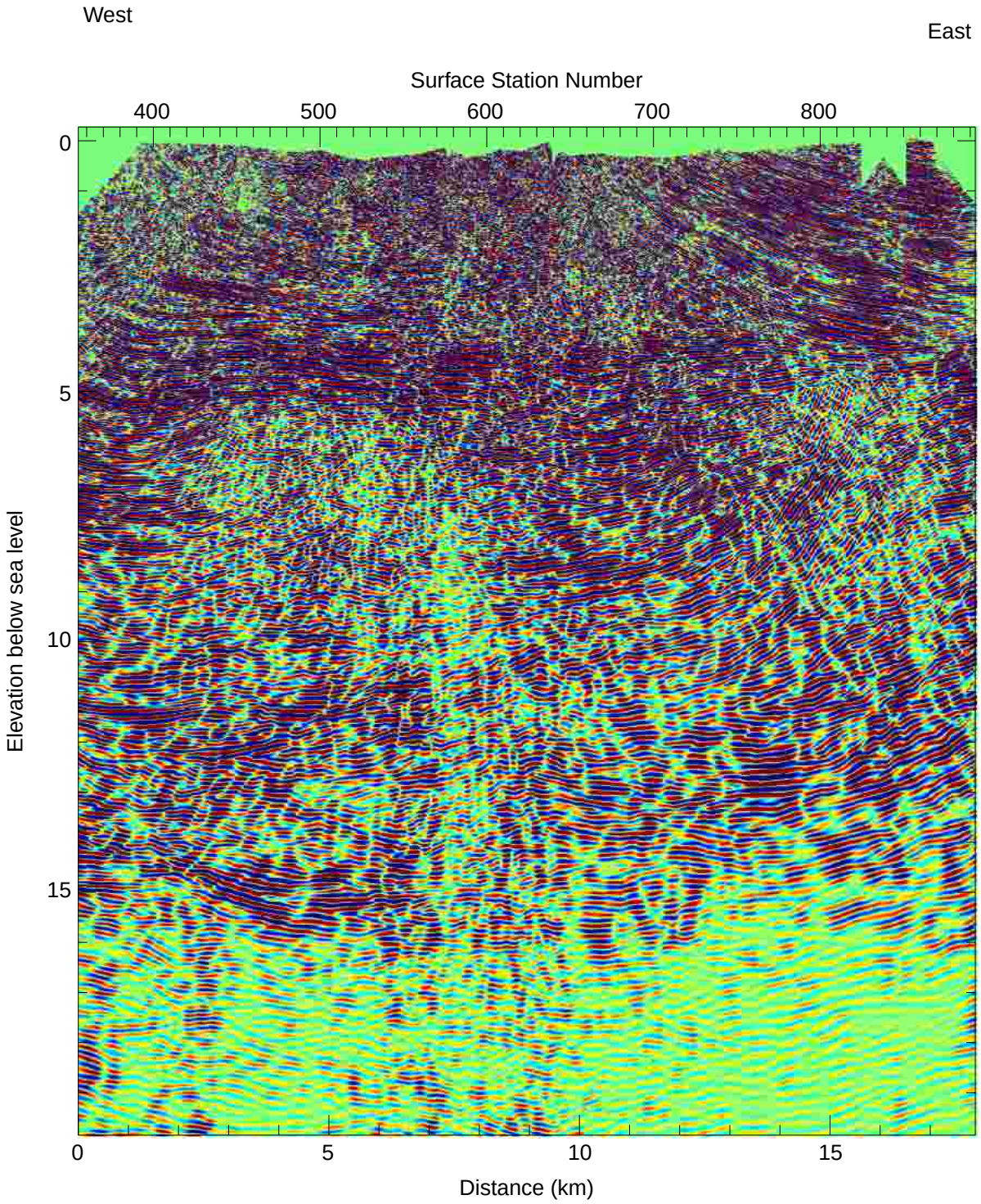


Figure A-7. Seismic line 808.

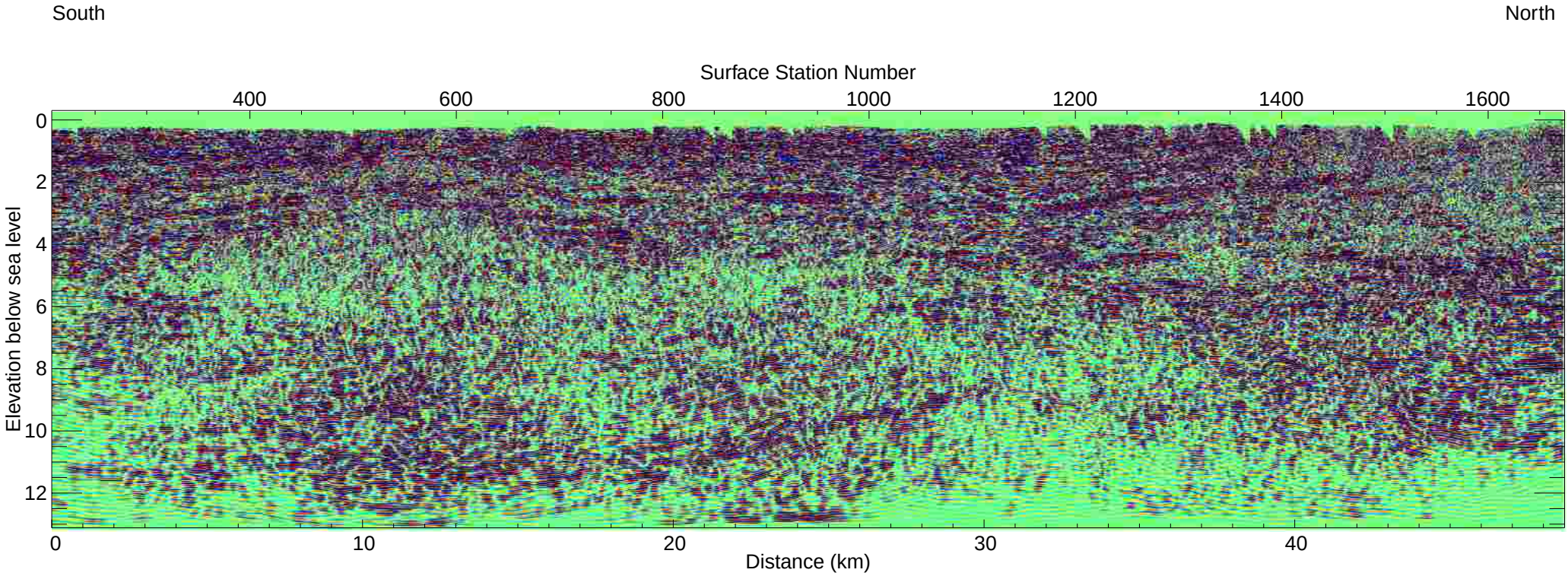


Figure A-8. Seismic line 011.

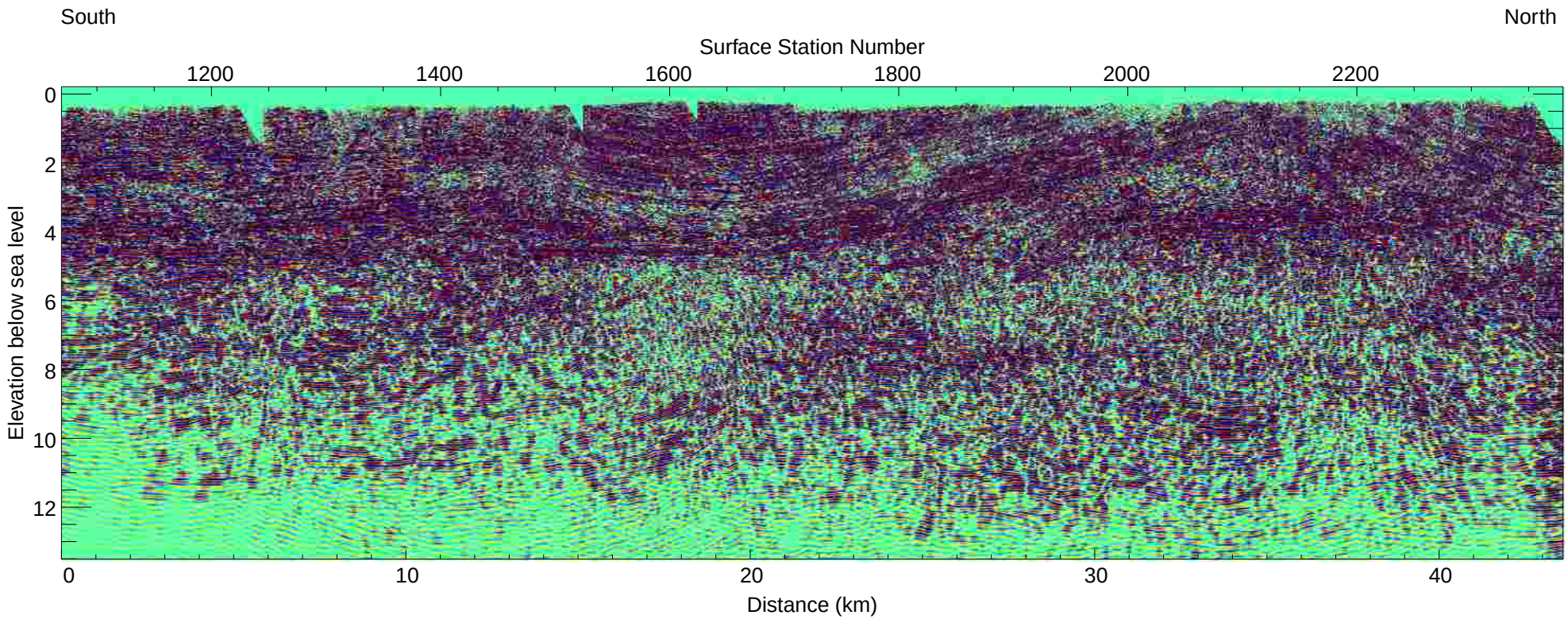


Figure A-9. Seismic line 783.

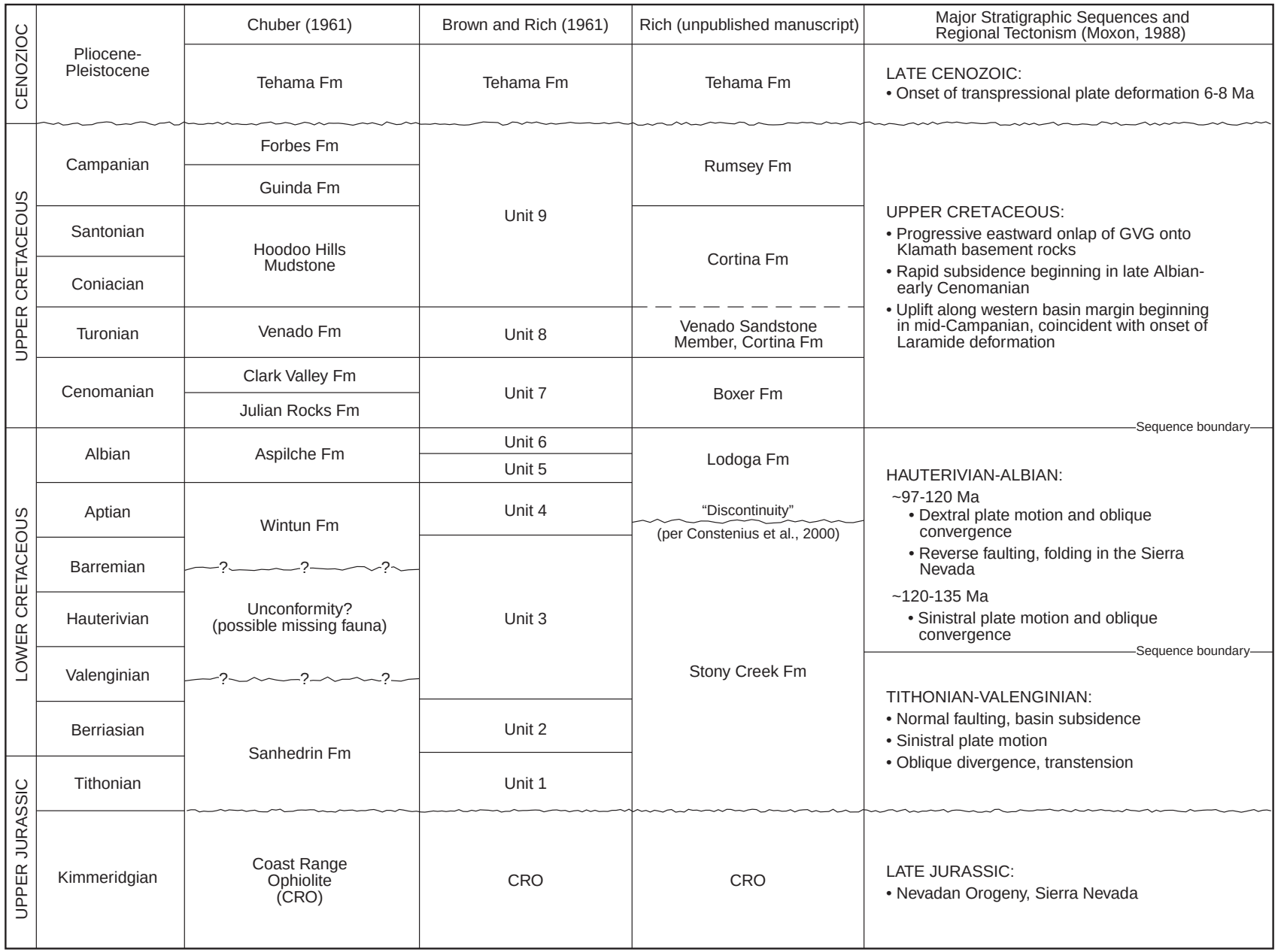


Figure A-10. Stratigraphic correlation chart for the study region.

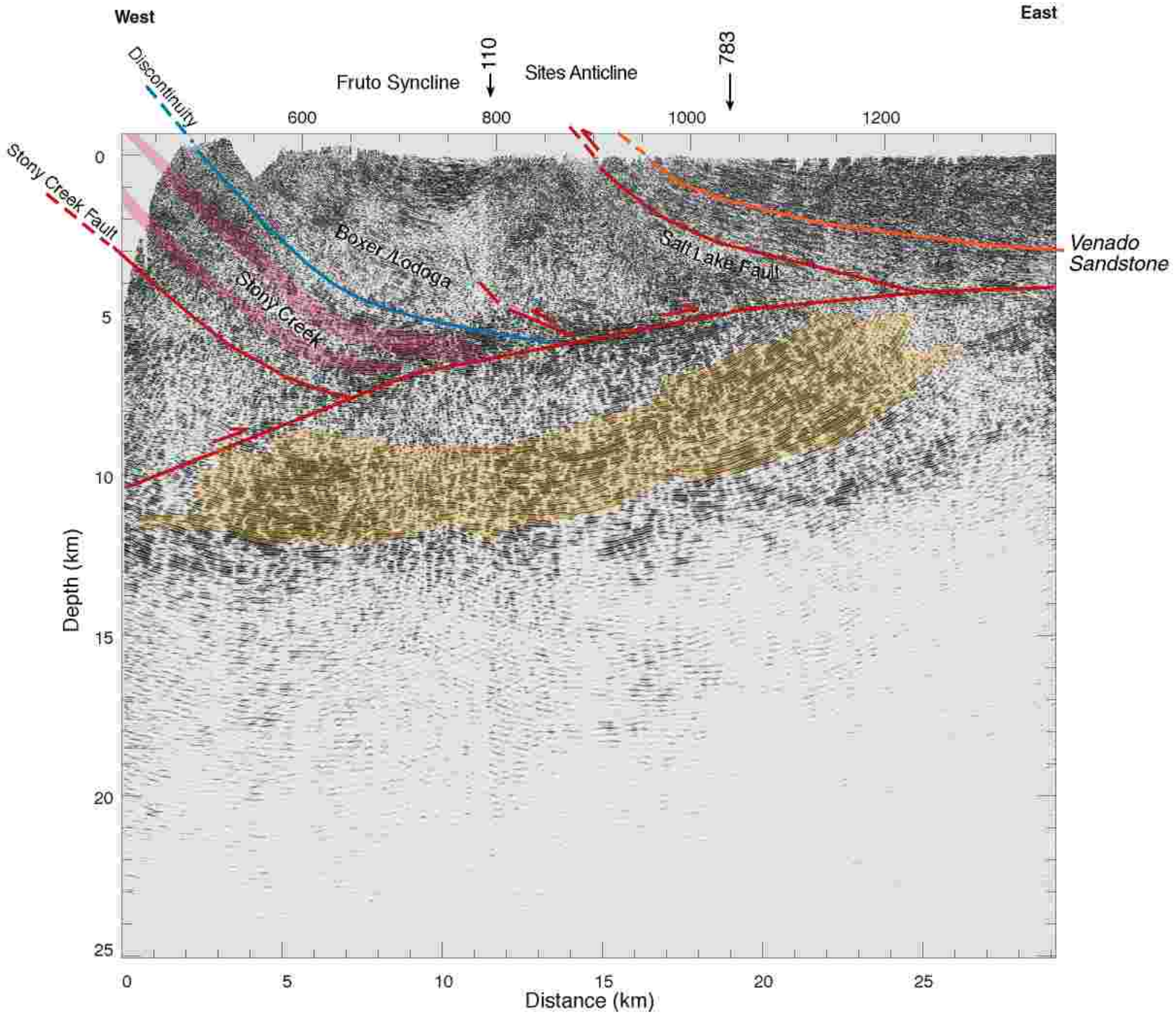


Figure A-11. Interpretation of seismic line 798.

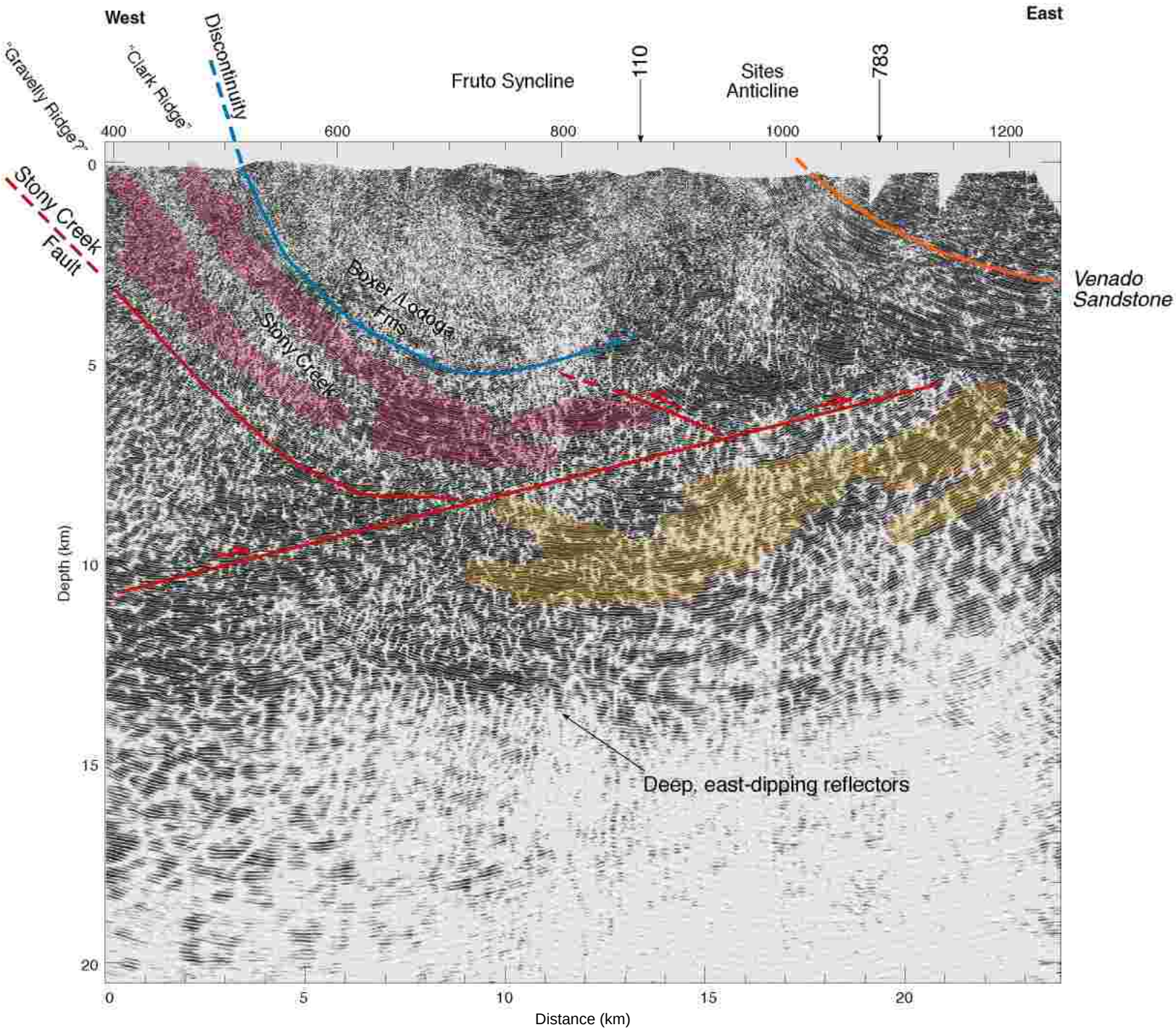


Figure A-12. Interpretation of seismic line 782.

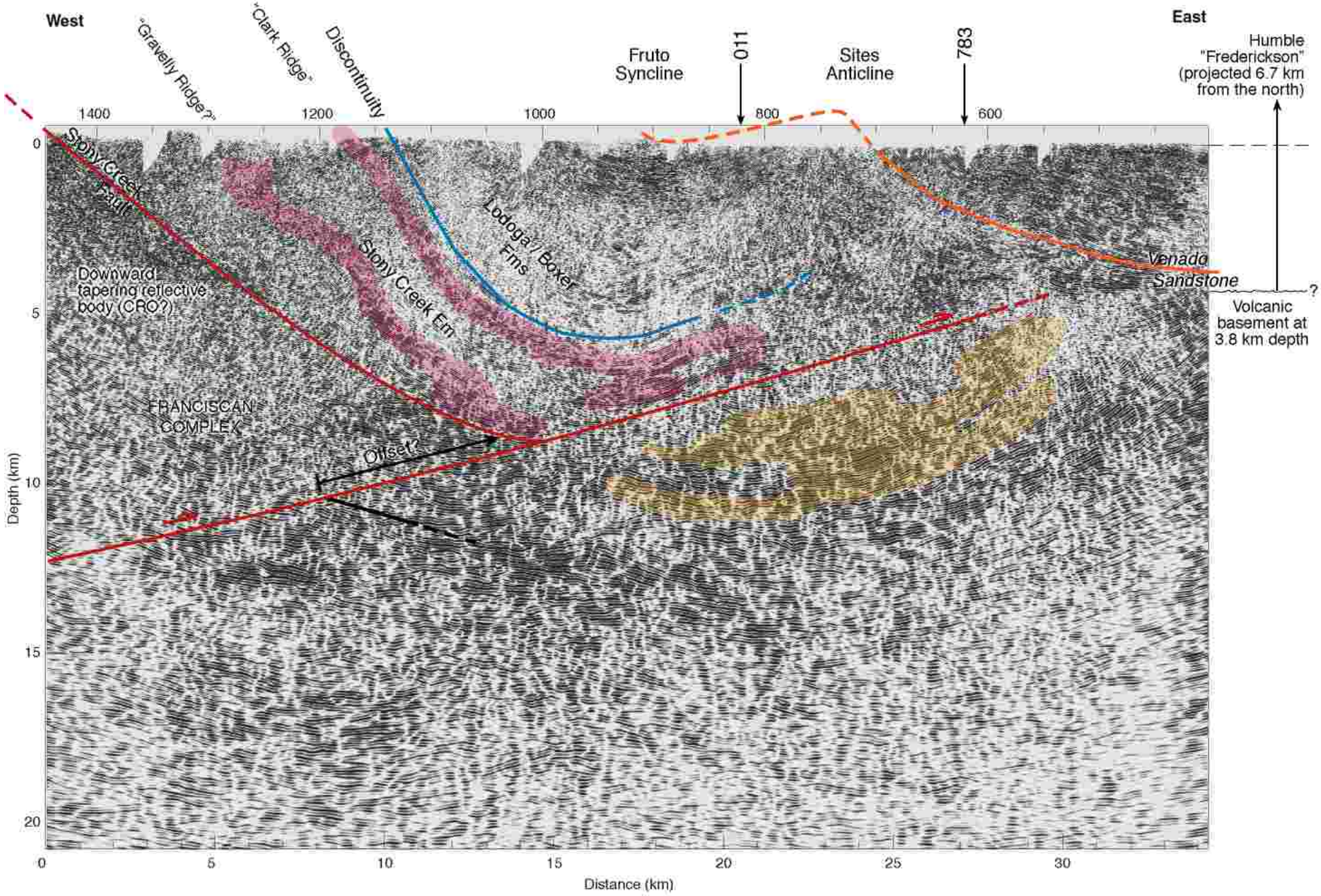


Figure A-13. Interpretation of seismic line 001.

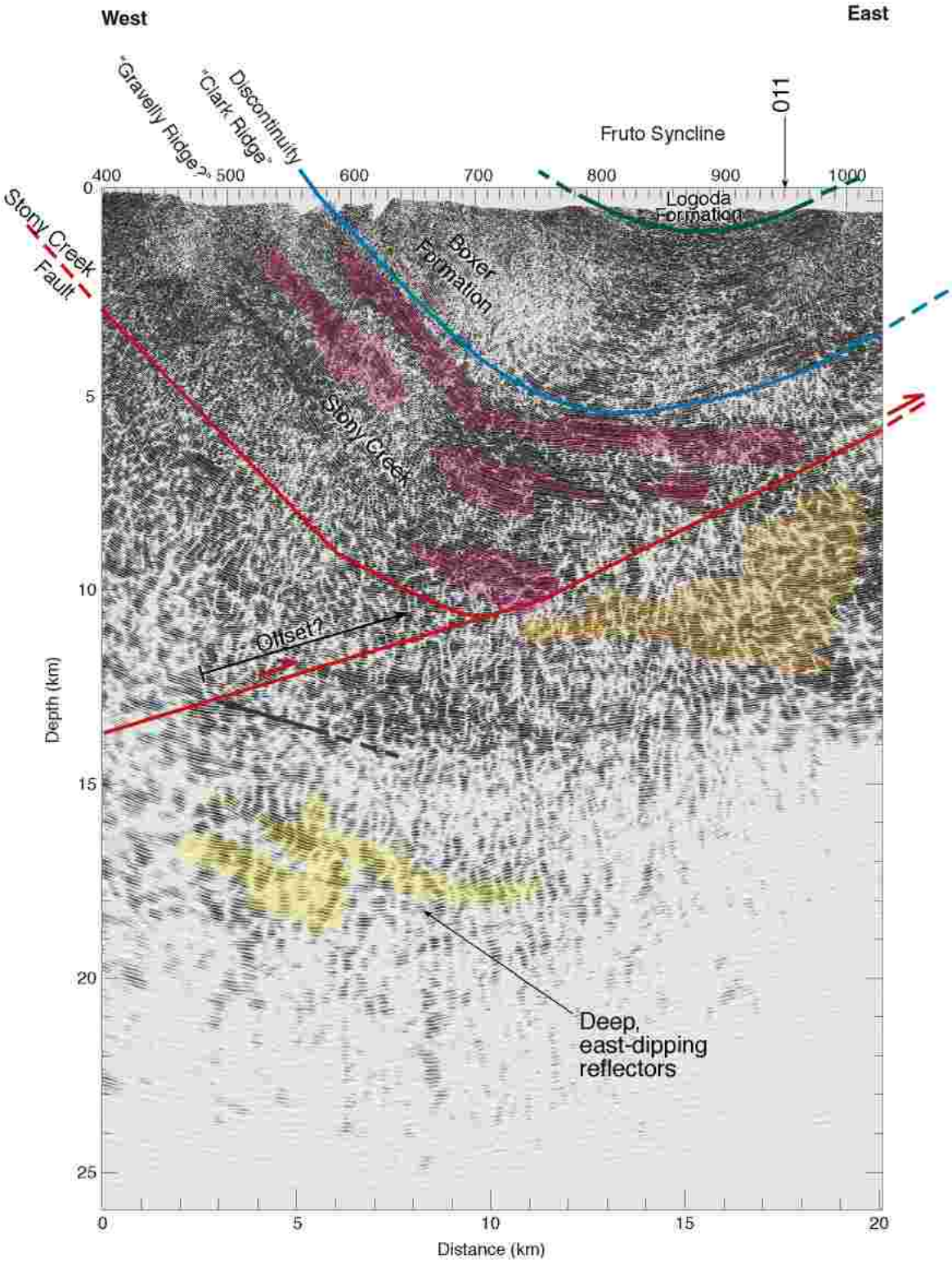


Figure A-14. Interpretation of seismic line 781.

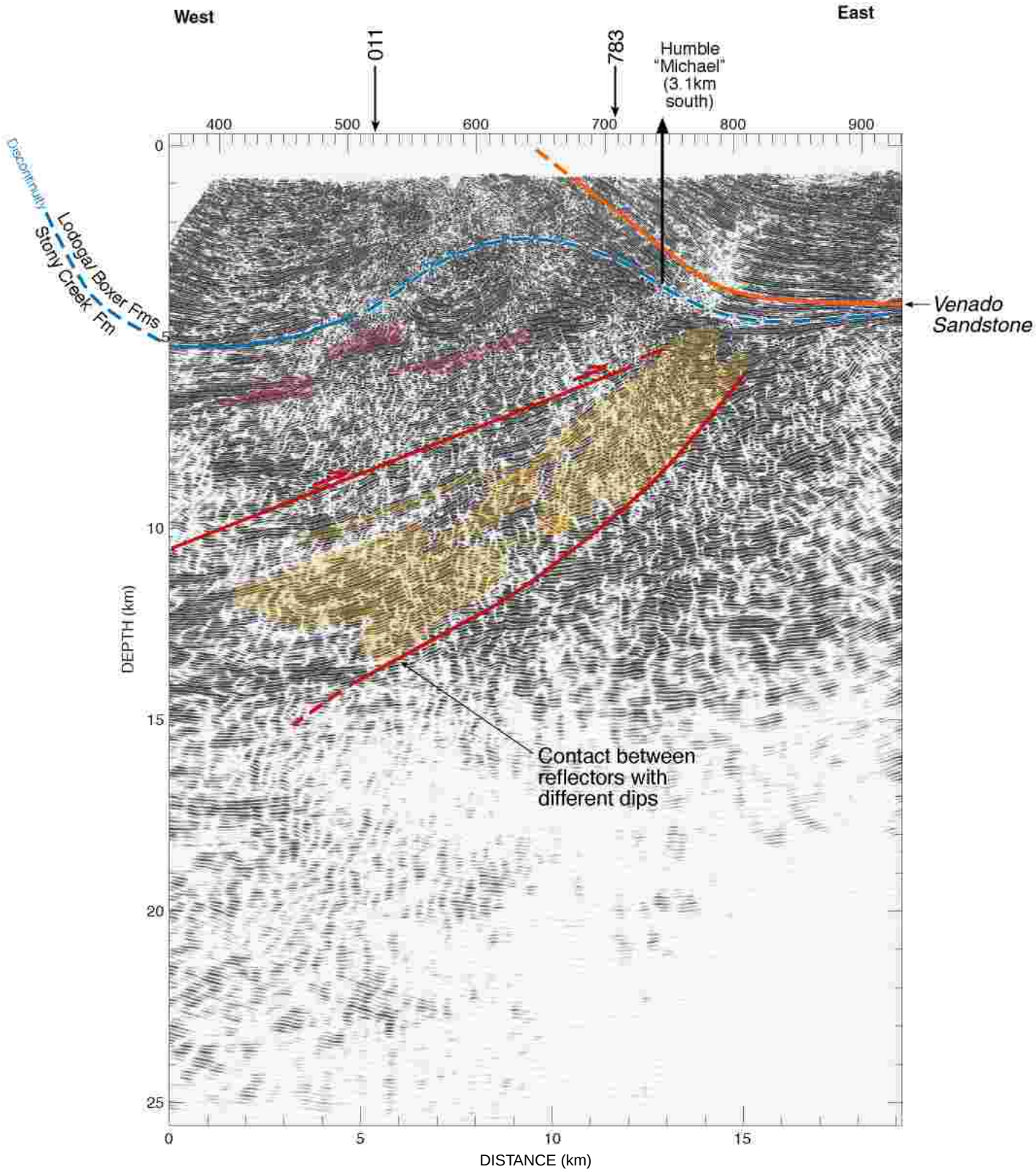


Figure A-15. Interpretation of seismic line 805.

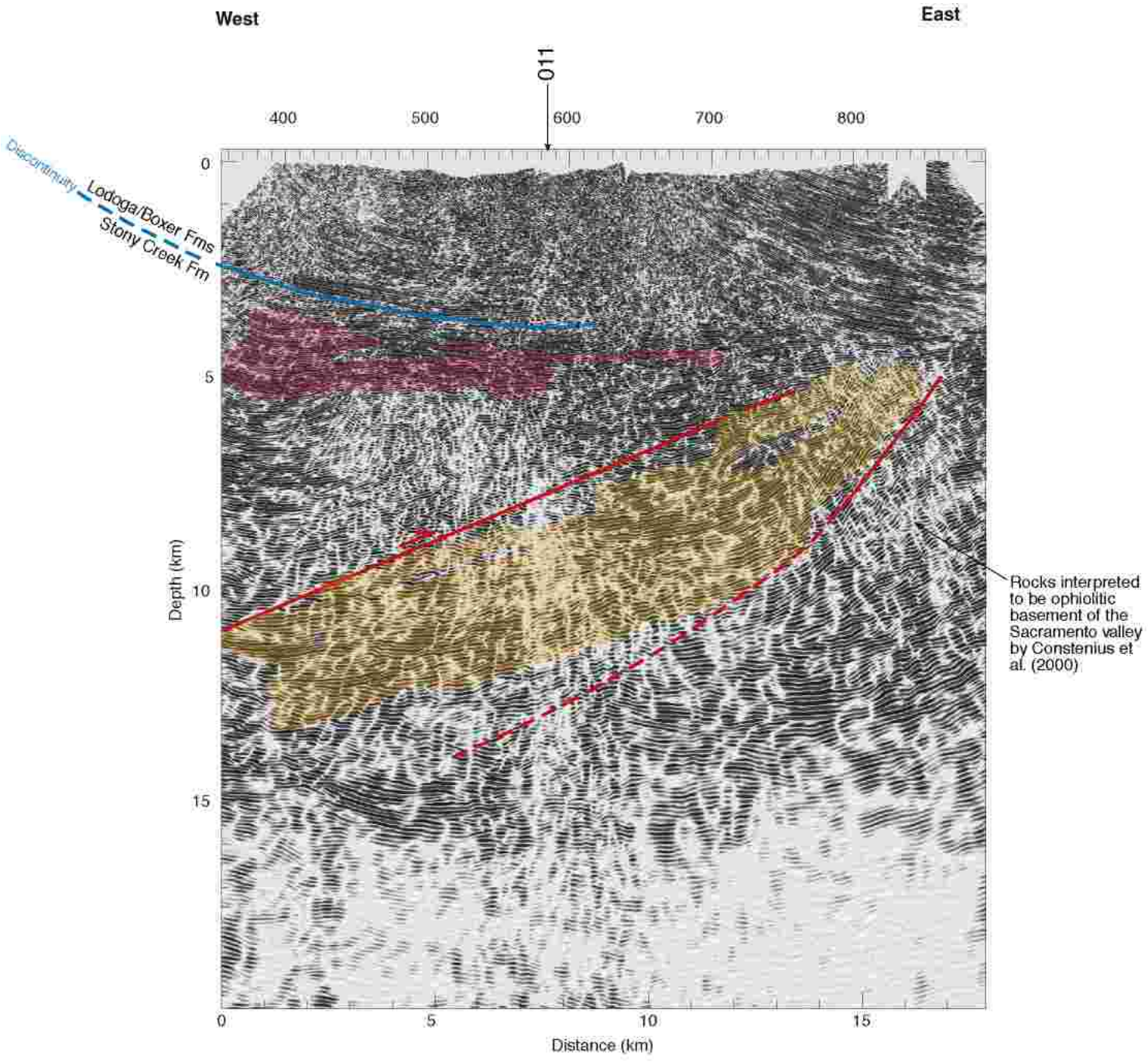


Figure A-16. Interpretation of seismic line 808

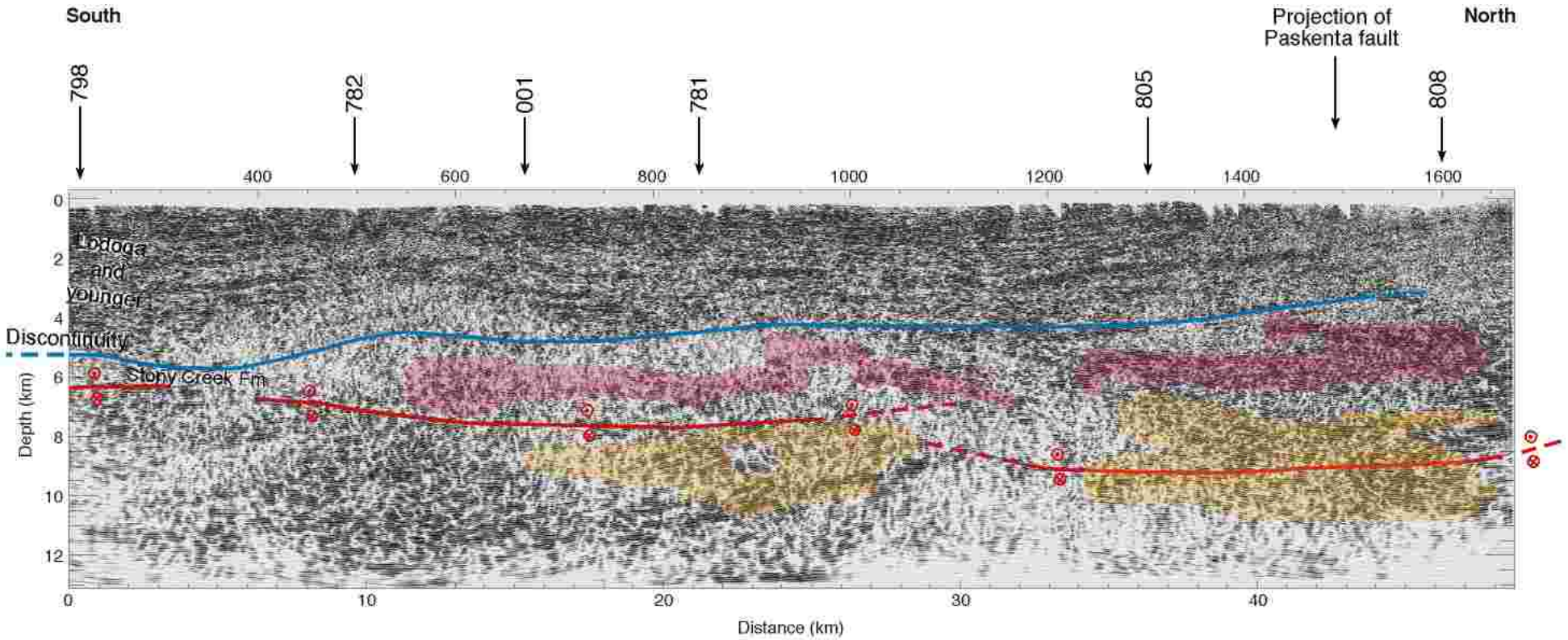


Figure A-17. Interpretation of seismic line 11.

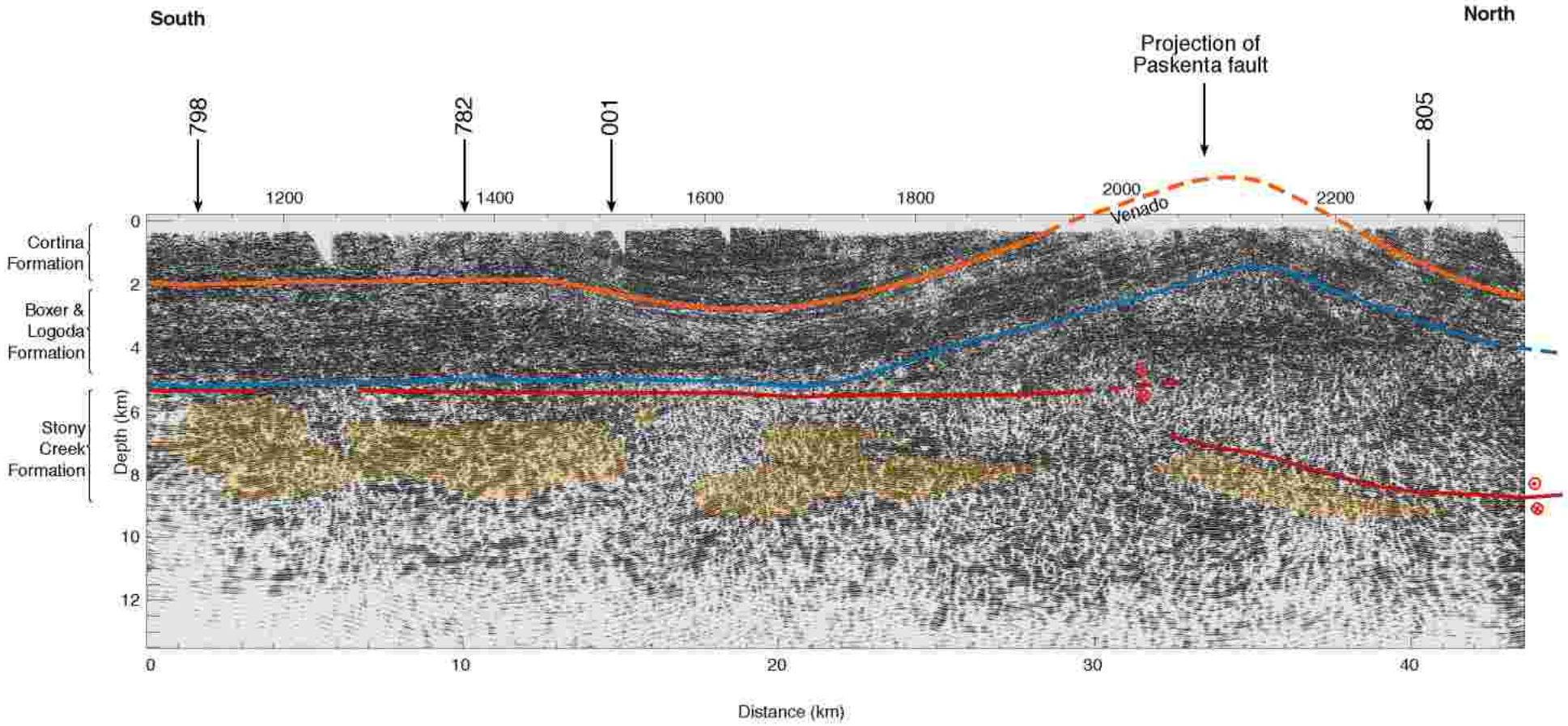


Figure A-18. Interpretation of seismic line 783.

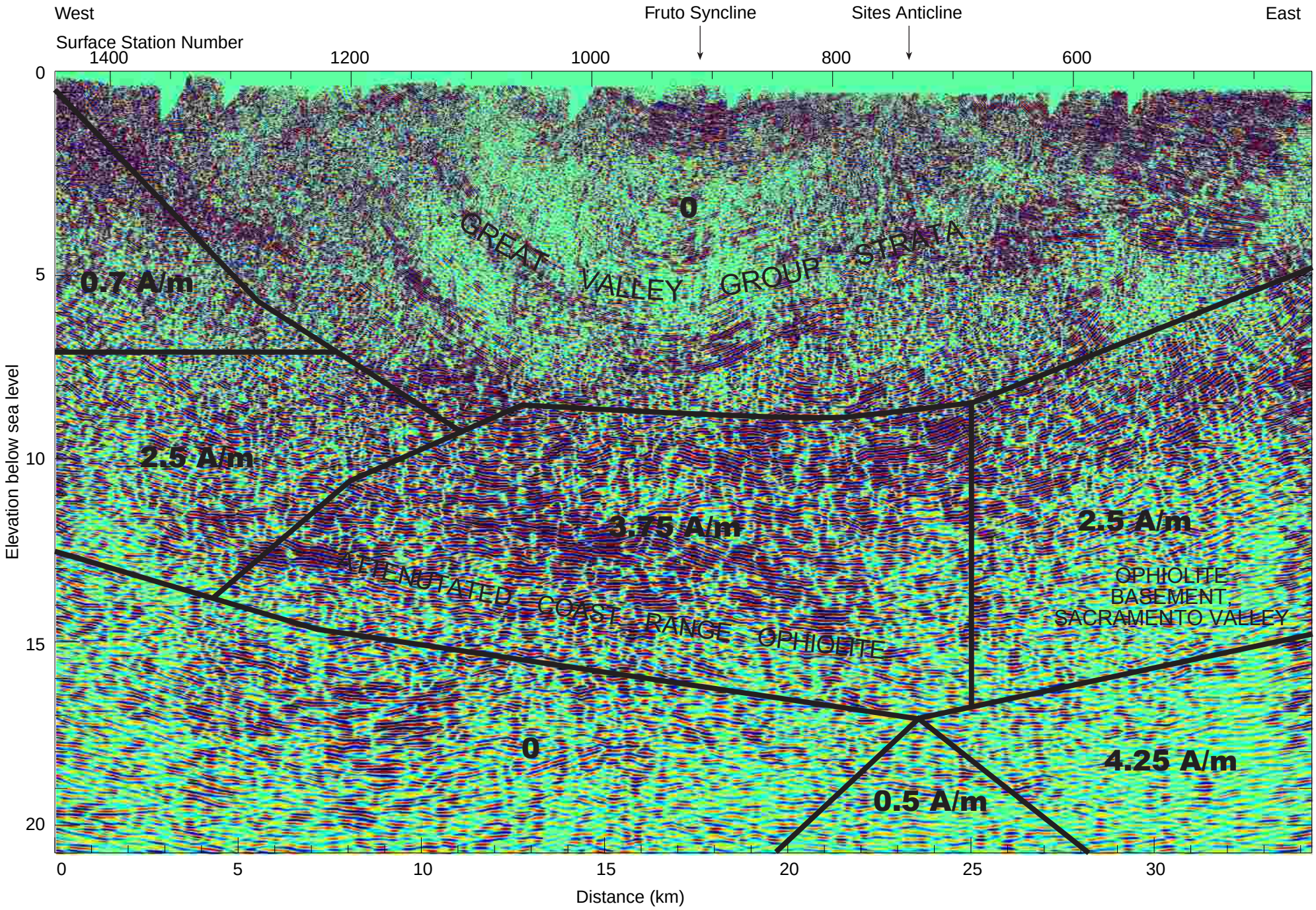


Figure A-19. Boundaries of magnetic bodies modeled by Godfrey et al. (1997; magnetism in A/m), projected onto seismic line 001.

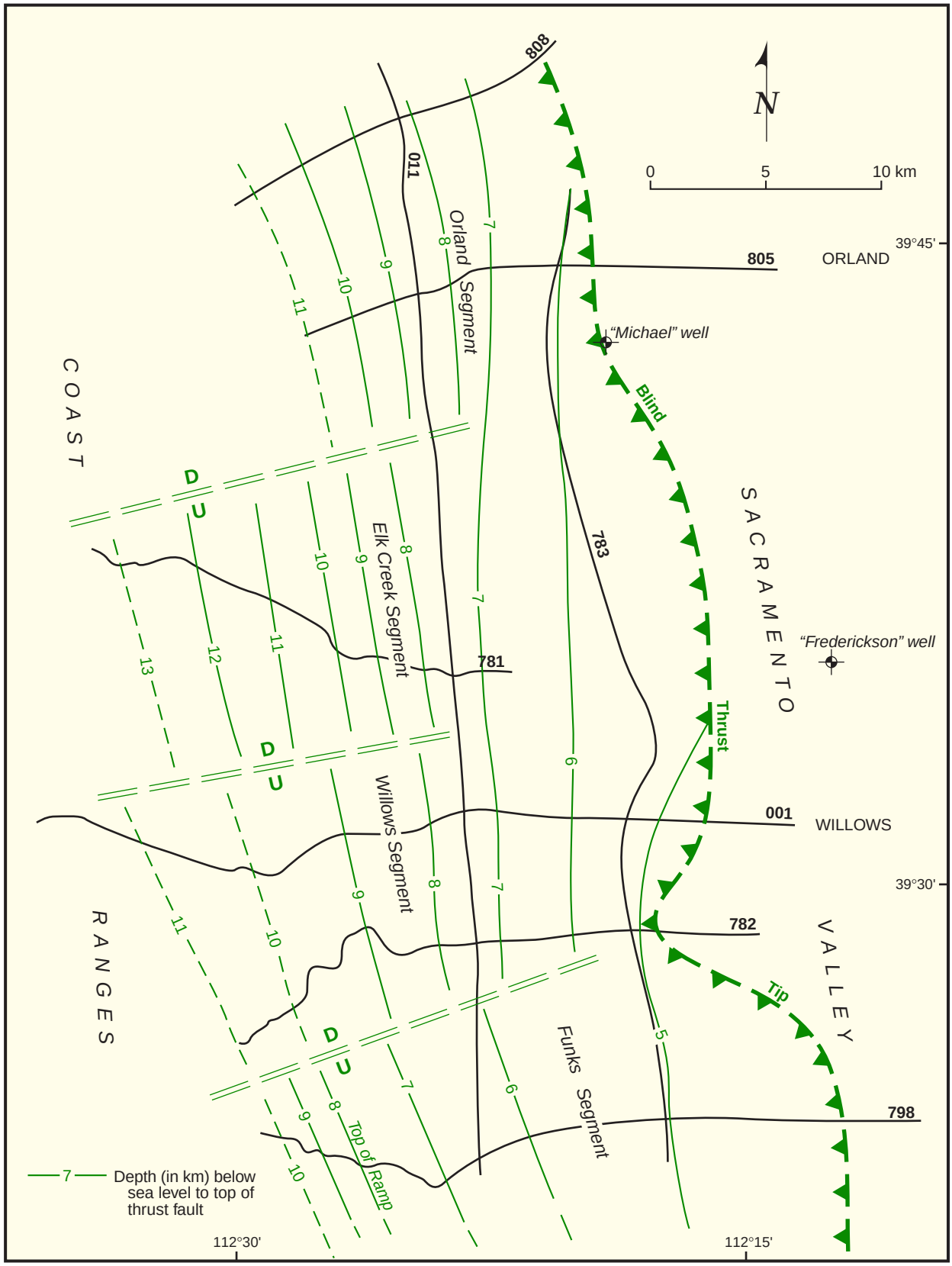


Figure A-20. Structure conture map of blind, west-dipping thrust faults.

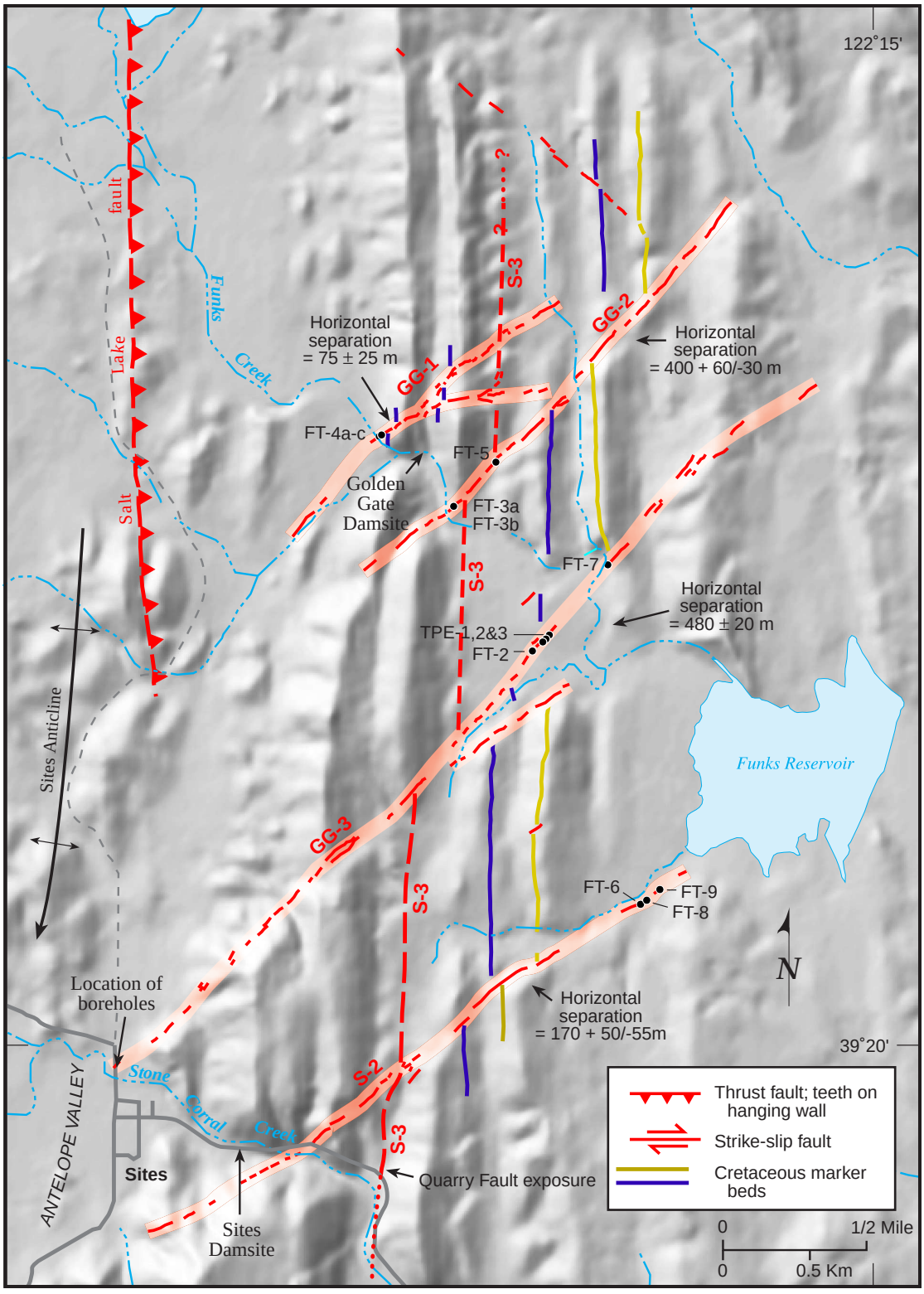


PHASE 2 FAULT AND SEISMIC HAZARDS INVESTIGATION
NORTH OF DELTA OFFSTREAM STORAGE
DWR-INTEGRATED STORAGE INVESTIGATION

**Shaded Relief Map Showing Faults in the Vicinity of the Sites and Golden Gate Dam Sites**

WLA William Lettis & Associates, Inc. | Figure B-1

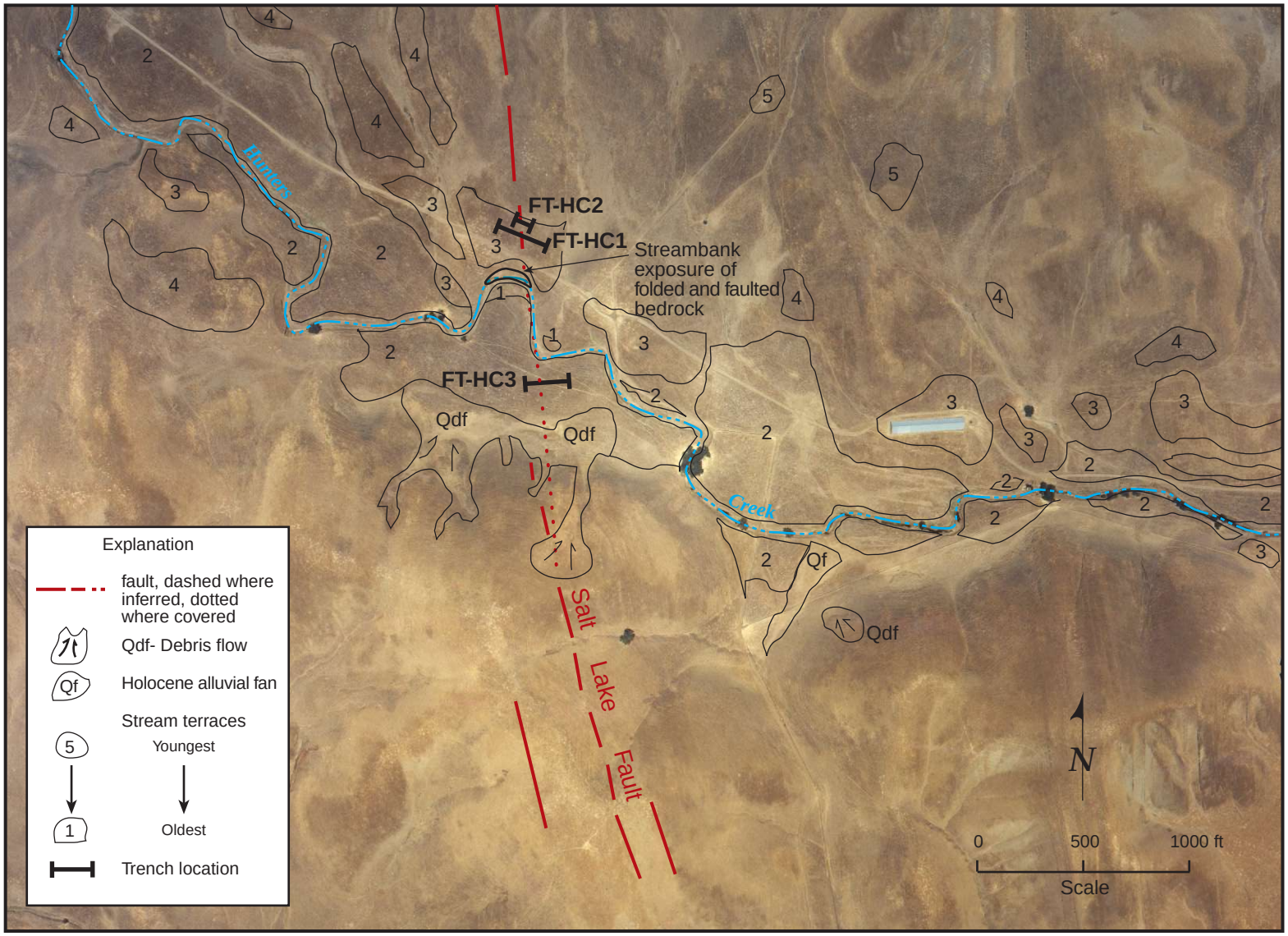


Color photograph taken in June, 1999

PHASE 2 FAULT AND SEISMIC HAZARDS INVESTIGATION
NORTH OF DELTA OFFSTREAM STORAGE
DWR-INTEGRATED STORAGE INVESTIGATION

**Map of Geologic Deposits, Stream Terraces, and Salt Lake Fault at the Hunters Creek Trench Site**

WLA William Lettis & Associates, Inc. | Figure B-2

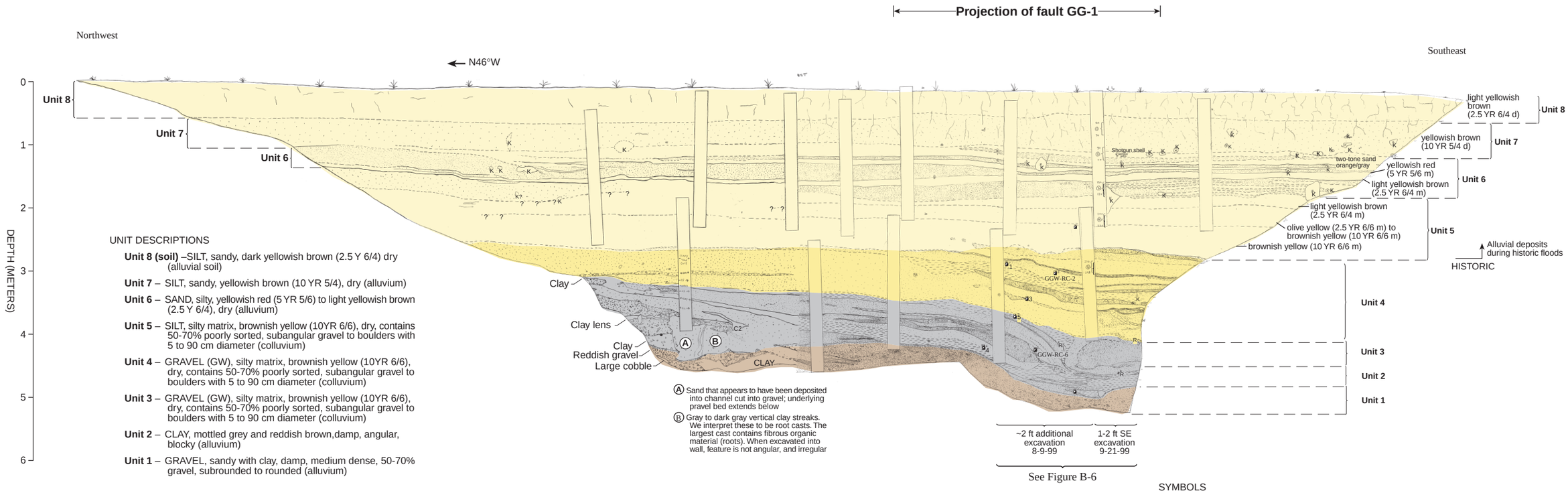


UNIT DESCRIPTIONS

**Unit 8 (soil)** –SILT, sandy, dark yellowish brown (2.5 Y 6/4) dry (alluvial soil)

**Unit 7** – SILT, sandy, yellowish brown (10 YR 5/4), dry (alluvium)

**Unit 6** – SAND, silty, yellowish red (5 YR 5/6) to light yellowish brown (2.5 Y 6/4), dry (alluvium)

**Unit 5** – SILT, silty matrix, brownish yellow (10YR 6/6), dry, contains 50-70% poorly sorted, subangular gravel to boulders with 5 to 90 cm diameter (colluvium)

**Unit 4** – GRAVEL (GW), silty matrix, brownish yellow (10YR 6/6), dry, contains 50-70% poorly sorted, subangular gravel to boulders with 5 to 90 cm diameter (colluvium)

**Unit 3** – GRAVEL (GW), silty matrix, brownish yellow (10YR 6/6), dry, contains 50-70% poorly sorted, subangular gravel to boulders with 5 to 90 cm diameter (colluvium)

**Unit 2** – CLAY, mottled grey and reddish brown,damp, angular, blocky (alluvium)

**Unit 1** – GRAVEL, sandy with clay, damp, medium dense, 50-70% gravel, subrounded to rounded (alluvium)

Ⓐ Sand that appears to have been deposited into channel cut into gravel; underlying pravel bed extends below

Ⓑ Gray to dark gray vertical clay streaks. We interpret these to be root casts. The largest cast contains fibrous organic material (roots). When excavated into wall, feature is not angular, and irregular

SYMBOLS

- Radiocarbon sample
- ss – Medium-fine lithic wacke
- sis – Fine lithic wacke, silty sandstone, massive
- ms – Mudstone, thinly bedded
- Disintegrated weathered bedrock

Trench FT-4C, North Wall
Fault GG-1
Golden Gate Site

0 1 2 3 4 5 6 7 8 9 10 11 12 13 14 15 16 17 18 19 21 21 22

DISTANCE (METERS)

PHASE 2 FAULT AND SEISMIC HAZARDS INVESTIGATION
NORTH OF DELTA OFFSTREAM STORAGE
DWR- INTEGRATED STORAGE INVESTIGATION

**Trench FT-4c - North Wall, GG-1 Fault, Golden Gate Damsite**

William Lettis & Associates, Inc. | Figure B-3

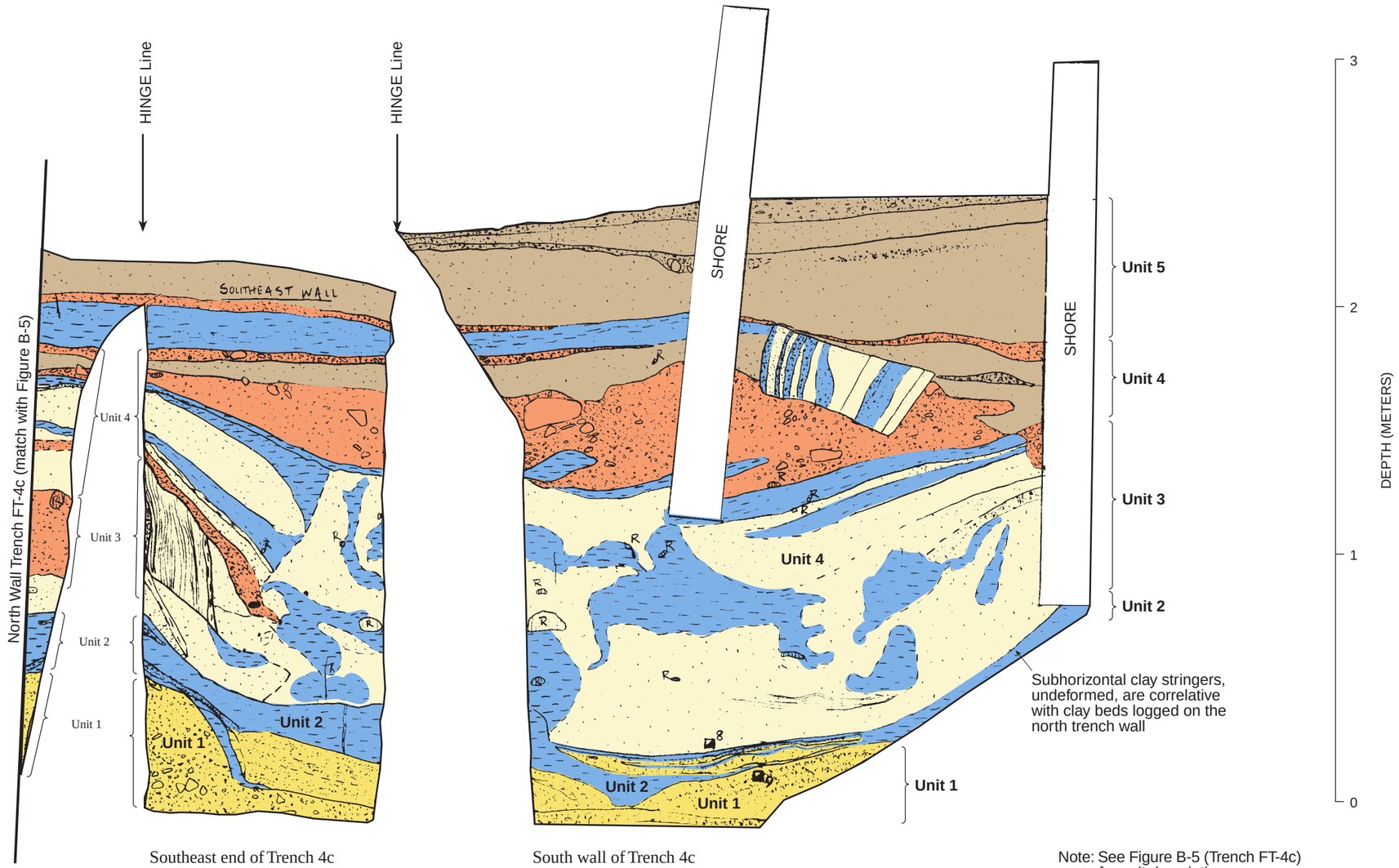


Southeast end of Trench 4c

South wall of Trench 4c

Note: See Figure B-5 (Trench FT-4c) for unit descriptions

PHASE 2 FAULT AND SEISMIC HAZARDS INVESTIGATION
NORTH OF DELTA OFFSTREAM STORAGE
DWR-INTEGRATED STORAGE INVESTIGATION

**Trench FT-4c - Southeat and South Walls, GG-1 Fault, Golden Gate Damsite**

WLA William Lettis & Associates, Inc. | Figure B-4

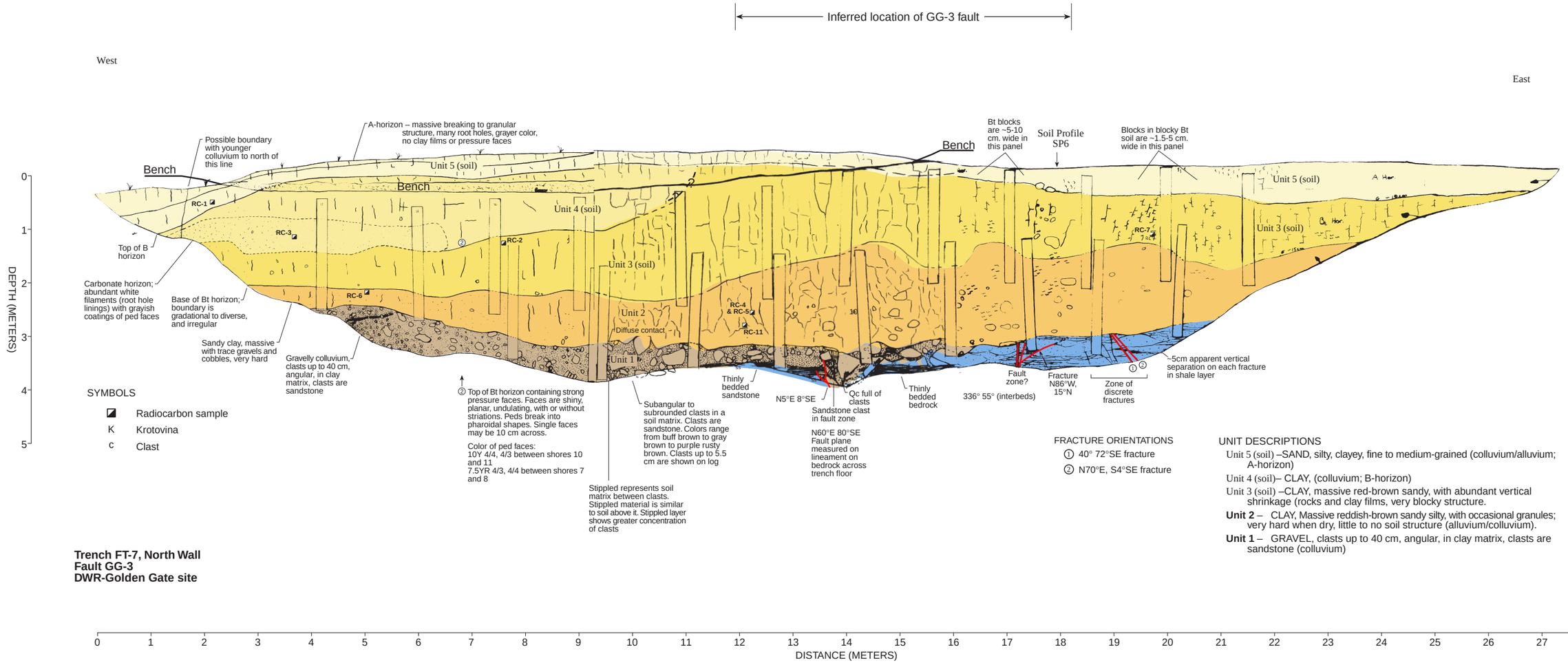


SYMBOLS

- Radiocarbon sample
- K Krotovina
- c Clast

② Top of Bt horizon containing strong pressure faces. Faces are shiny, planar, undulating, with or without striations. Peds break into pharoidal shapes. Single faces may be 10 cm across.

Color of ped faces:
10Y 4/4, 4/3 between shores 10 and 11
7.5YR 4/3, 4/4 between shores 7 and 8

Subangular to subrounded clasts in a soil matrix. Clasts are sandstone. Colors range from buff brown to gray brown to purple rusty brown. Clasts up to 5.5 cm are shown on log

Stippled represents soil matrix between clasts. Stippled material is similar to soil above it. Stippled layer shows greater concentration of clasts

FRACTURE ORIENTATIONS

① 40° 72°SE fracture

② N70°E, S4°SE fracture

UNIT DESCRIPTIONS

Unit 5 (soil) –SAND, silty, clayey, fine to medium-grained (colluvium/alluvium; A-horizon)

Unit 4 (soil)– CLAY, (colluvium; B-horizon)

Unit 3 (soil) –CLAY, massive red-brown sandy, with abundant vertical shrinkage (rocks and clay films, very blocky structure.

**Unit 2** – CLAY, Massive reddish-brown sandy silty, with occasional granules; very hard when dry, little to no soil structure (alluvium/colluvium).

**Unit 1** – GRAVEL, clasts up to 40 cm, angular, in clay matrix, clasts are sandstone (colluvium)

**Trench FT-7, North Wall**
**Fault GG-3**
**DWR-Golden Gate site**

PHASE 2 FAULT AND SEISMIC HAZARDS INVESTIGATION
NORTH OF DELTA OFFSTREAM STORAGE
DWR-INTEGRATED STORAGE INVESTIGATION

# Ternch FT-7 - North Wall, GG-3 Fault, Golden Gate Damsite

William Lettis & Associates, Inc.

Figure B-5

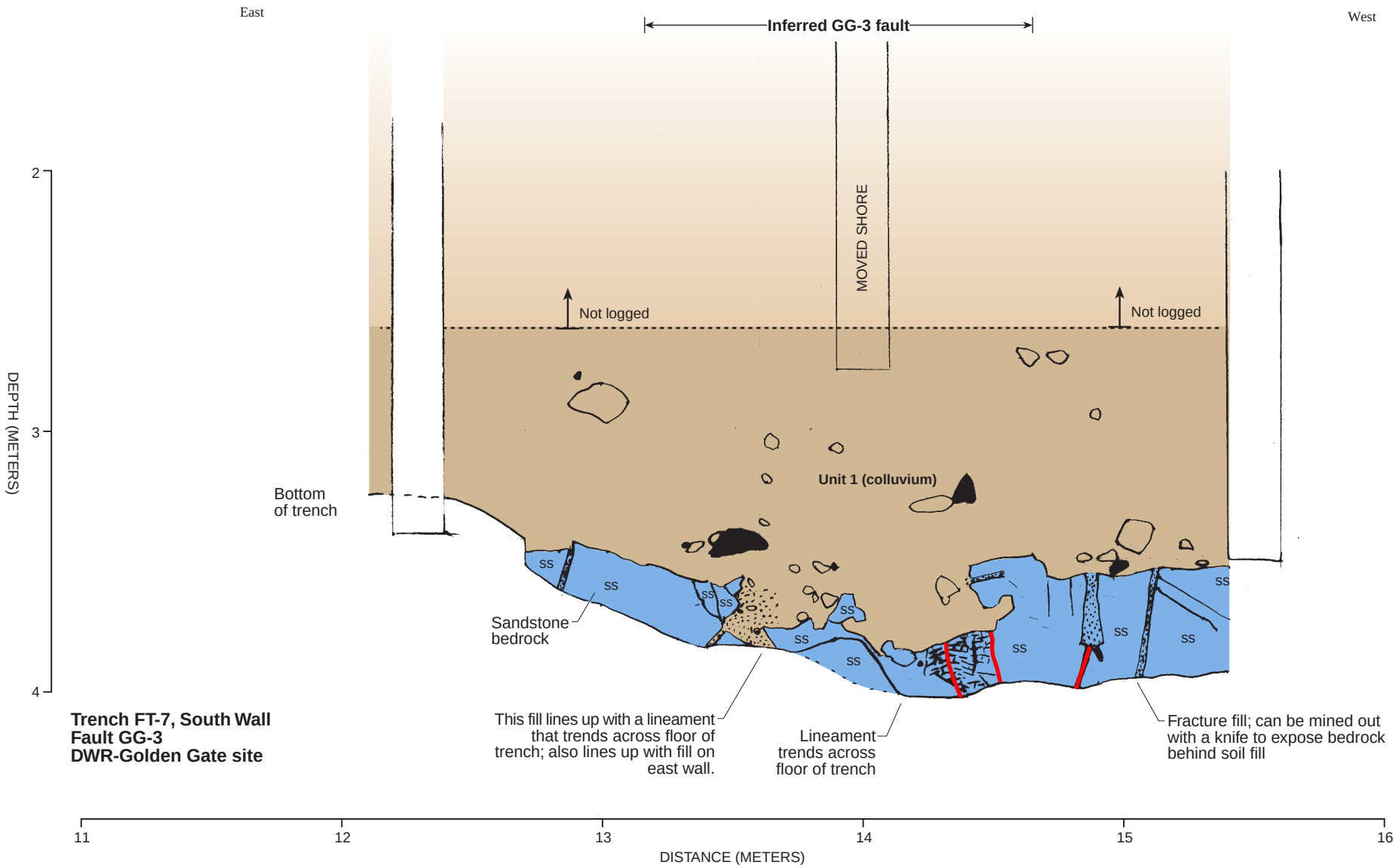


**Trench FT-7, South Wall**
**Fault GG-3**
**DWR-Golden Gate site**

PHASE 2 FAULT AND SEISMIC HAZARDS INVESTIGATION
NORTH OF DELTA OFFSTREAM STORAGE
DWR-INTEGRATED STORAGE INVESTIGATION

# Trench FT-7 - South Wall, GG-3 Fault, Golden Gate Damsite

WLA William Lettis & Associates, Inc.

Figure B-6

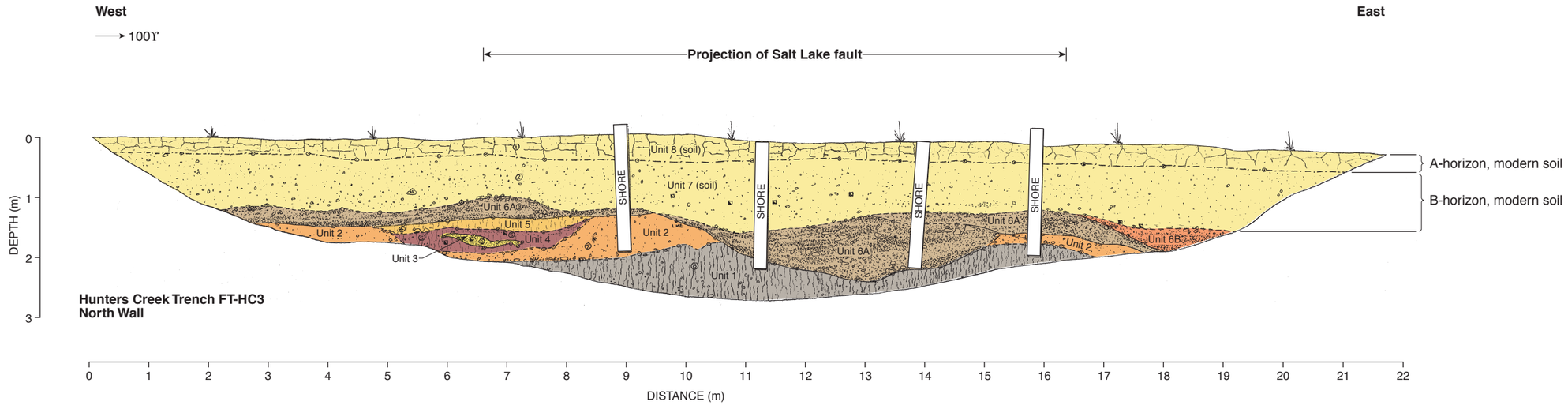


UNIT DESCRIPTIONS

**Unit 8** – SILT; light olive brown (2.5Y 5/4d); dry; hard; slightly sticky, slightly plastic; blocky to platy structure; rare to common subrounded coarse pebbles; vesicular; common roots in upper 3-5 cm; lower contact is clear, smooth (COLLUVIUM - A-soil horizon)

**Unit 7** – pebbly SILT; brownish yellow (10YR 6/6d); dry; stiff; slightly sticky, slightly plastic, commpon subrounded coarse pebbles; lower contact is clear, wavy; reacts to HCl (COLLUVIUM - B-soil horizon)

**Unit 6B** – sandy GRAVEL; brownish yellow (10YR 6/6d); dry; soft; fines upwards; lag is ~90% moderately sorted subrounded cobbles with 10% medium to fine sand; middle is ~90% coarse pebbles with 10% medium to hard sand; top is lens of coarse pebbles and cobbles; fines to the west to medium to coarse sand. Clasts are volcanics, greenstone, blue chist, chert, and pebble conglomerate with red clay matrix; clasts have spatter coatings of $CaCO_3$; base is abrupt, smooth; unit is channelized; reacts to HCl acid (ALLUVIUM)

**Unit 6A** – GRAVEL; light brown; dry; soft; fines upward; ~80% coarse pebbles and 20% very coarse pebbles; common clay (?) coatings on clasts; matrix is very coarse sand; bottom contact is clear, smooth, reacts to HCl acid (ALLUVIUM) (Provenence of clasts similar to Unit 6B)

**Unit 5** – SILT; yellowish brown (10 YR 5/4d); dry; stiff; slightly sticky, slightly plastic (silt loam texture); sparse subrounded pebbles (COLLUVIUM)

**Unit 4** – silty CLAY; light yellowish brown (2.5 YR 6/3d); dry; stiff; sticky, slightly plastic-plastic (silty clay loam); uppermost 2 cm contains abundant snail shells, unbroken, white, <1 cm, and carbonate nodules 2-4 mm in diameter; base is mottled orange with $CaCO_3$ stringers; lower contact is clear, irregular (LACUSTRINE to ALLUVIAL)

**Unit 3** – SAND; strong brown (7.5 YR 5/8d); dry; stiff; slightly sticky to nonsticky, non-plastic (sandy loam); medium sand, coarsens downward; subrounded, moderately sorted, quartz and lithies, no apparent bedding; lower contact is abrupt, irregular (ALLUVIUM)

**Unit 2** – pebbly SILT to SILT LOAM; light, yellowish brown (2.5 YR 6/3d); dry; stiff; slightly sticky-sticky, slightly plastic; common coarse pebbles, subrounded (COLLUVIUM)

**Unit 1** – pebbly CLAY; very dark brown (10 YR 6/6d) to dark yellowish brown (10 YR 4/4d); dry; hard; mottled; sticky, slightly plastic (silty loam to silty clay); common rounded coarse pebbles (COLLUVIUM)

PHASE 2 FAULT AND SEISMIC HAZARDS INVESTIGATION
NORTH OF DELTA OFFSTREAM STORAGE
DWR-INTEGRATED STORAGE INVESTIGATION

**Trench FT-HC3 - North Wall,
Salt Lake Fault, Hunters Creek**

WLA William Lettis & Associates, Inc. | Figure B-7